D 2025

U.PORTO
FEUP FACULDADE DE ENGENHARIA
UNIVERSIDADE DO PORTO

SMART DIAGNOSIS FOR PREVENTING MOISTURE DAMAGE IN BUILDINGS

LETÍCIA CARVALHO MOREIRA DAFICO

DOCTORAL THESIS PRESENTED TO
FACULTY OF ENGINEERING OF UNIVERSITY OF PORTO IN
CIVIL ENGINEERING

U.PORTO

FEUP FACULDADE DE ENGENHARIA
UNIVERSIDADE DO PORTO

SMART DIAGNOSIS FOR PREVENTING MOISTURE DAMAGE IN BUILDINGS

LETÍCIA CARVALHO MOREIRA DAFICO

Master in Civil Engineering - Federal University of Goiás

Doctoral Thesis submitted to obtain the Doctor Degree in Civil Engineering

Supervisor: Prof. Dr. Eva Sofia Botelho Machado Barreira

Cosupervisor: Prof. Dr. Ricardo R. M. S. Almeida, IPV

Cosupervisor: Prof. Dr. Romeu S. Vicente, UA

MARCH 2025

DOCTORAL PROGRAM IN CIVIL ENGINEERING

Phone. +351-22-508 1901

Fax +351-22-508 1446

✉ prodec@fe.up.pt

Edited by

FACULDADE DE ENGENHARIA DA UNIVERSIDADE DO PORTO

Rua Dr. Roberto Frias

4200-465 PORTO

Portugal

Phone. +351-22-508 1400

✉ feup@fe.up.pt

http://www.fe.up.pt

Partial reproduction of this document is allowed provided that credit is given to the author and to Programa Doutoral em Engenharia Civil - Departamento de Engenharia Civil, Faculdade de Engenharia da Universidade do Porto, Porto, Portugal.

The opinions and information included herein solely represent the point of view of the author. The Editor cannot accept any legal liability or otherwise for errors or omissions that may exist.

This document was produced from an electronic version provided by the author.

To my son, Henrique, who came into this world to bring light during this doctoral journey, to my husband, Pedro, who has always supported me, and to my loved family

It always seems impossible until it's done

Nelson Mandela

ACKNOWLEDGEMENTS

This journey has been long and full of challenges, learning, and growth. I could not have reached this milestone without the support and guidance of very important people.

Firstly, I would like to thank Professor Eva Barreira, whose patience, dedication, and assertiveness have been invaluable throughout this process. Her exceptional ability to guide me through the complexities of my research, always encouraging me to improve and refine my work, has made all the difference. Her insights and support were essential.

I extend my sincere thanks to Professor Ricardo Almeida for his valuable contributions. His thoughtful discussions and expertise helped shape the results of this research. I am also grateful to Professor Romeu Vicente for his guidance and support during this journey.

To FCT-Fundação para a Ciência e a Tecnologia, the funding of the Doctoral Grant 2022.11621.BD. This work was financially supported by Base Funding UIDB/04708/2020 of the CONSTRUCT – Instituto de I & D em Estruturas e Construções, funded by national funds through FCT/MCTES (PIDDAC).

My sincere appreciation goes to all the professors of PRODEC for their teaching, especially to Professor Vasco de Freitas and Professor Maria de Lurdes for their guidance, which helped me understand crucial concepts fundamental to this thesis's development.

I sincerely appreciate Eduardo, the laboratory technician, for his assistance and guidance during the numerous laboratory experiments I conducted throughout my PhD.

A very special acknowledgement goes to my son, Henrique, who was born during my doctoral studies and has filled my life with indescribable joy. His arrival brought new meaning and gave me even more motivation to persevere. A sincere thank you to my husband for his support. He moved to another country with me so I could pursue my PhD and continued to support me after we returned to Brazil, ensuring I had the time and space to focus on my research. His encouragement made this achievement possible.

I am also grateful to all my PhD colleagues, especially Amanda, Ahmad, Mohamed, Mohammad, Jean, Amir, Diogo, Andrea, Sofia, and Tereza, who brought joy and light to my daily life at FEUP. Their friendship and support made this journey much more enjoyable.

This achievement was only possible because of the encouragement and support of those around me. To each of them, I extend my deepest gratitude.

ABSTRACT

Moisture is one of the main causes of defects in buildings, leading to degradation. The complexity of moisture phenomena makes it more challenging to interpret the results during building inspections. However, proper diagnosis and prevention of moisture damage are of paramount importance to guarantee the durability of the building, the comfort of the users, and the quality of the indoor environment conditions since high levels of moisture can lead to mould growth, surface condensation, and salt crystallisation, increasing the risk of respiratory-related infections of the users and reducing the thermal performance of the building envelope.

Non-destructive techniques (NDTs) that measure the surface temperature of building materials have good potential for moisture analysis since changes in moisture content relate to changes in surface temperature. In recent years, there has been an increasing number of studies in which building inspection technologies are integrated with computational methods for automatically identifying and classifying building defects. Despite the recent advances in these techniques, their use for moisture diagnosis is not fully exploited, as the lack of quantitative interpretation criteria is still a critical drawback that must be more deeply addressed.

In this context, this work aimed to define reliable criteria indicative of the level of moisture in buildings through Infrared Thermography (IRT) in different environmental conditions and to develop a framework for assessing the moisture evolution during the drying process in building materials, based on machine learning algorithms/models.

The relationship between thermal gradient and moisture content was investigated through laboratory tests and hygrothermal simulations. The results showed how different environmental conditions and the material properties affect the moisture-thermal gradient relationship. The experimental and simulation data were used as training and testing datasets in the development of machine learning models that predict the moisture content based on surface temperature results and transform the thermal images into moisture maps. Additionally, the building physics principles presented in the literature review are used to create algorithms that generate the moisture content curve during the materials drying process.

The results showed that the machine learning models achieved a coefficient of determination (R^2) greater than 0.95 between predicted and real moisture values, providing accurate predictions of the moisture content, especially in highly porous building materials such as mortar, clay brick and limestone. Regarding the algorithm based on building physics principles, it successfully generated moisture curves that closely matched the ones obtained from laboratory tests and simulations. Furthermore, the findings of this study suggest that the drying behaviour of porous building materials can be effectively monitored using IRT, which helps prevent moisture-related degradation in buildings.

KEYWORDS: Infrared Thermography; Moisture; Quantitative Diagnosis; Hygrothermal behaviour; Machine learning models.

RESUMO

A humidade é uma das principais causas de defeitos em edificações, levando à degradação. A complexidade dos fenómenos relacionados à humidade torna mais difícil a interpretação dos resultados durante as inspeções prediais. No entanto, o diagnóstico adequado e a prevenção de danos causados pela humidade são de suma importância para garantir a durabilidade da edificação, o conforto dos usuários e a qualidade das condições do ambiente interno, pois altos níveis de humidade podem levar ao crescimento de mofo, condensação superficial e cristalização de sais, aumentando o risco de infeções respiratórias dos usuários e reduzindo o desempenho térmico da envolvente do edifício.

As técnicas não destrutivas (NDTs) que medem a temperatura superficial dos materiais de construção têm um bom potencial para análise de humidade, uma vez que as mudanças no teor de humidade se relacionam com as mudanças na temperatura da superfície. Nos últimos anos, tem-se verificado um número crescente de estudos em que as tecnologias de inspeção de edifícios são integradas a métodos computacionais para a identificação e classificação automática de defeitos em edifícios. Apesar dos recentes avanços dessas técnicas, seu uso para o diagnóstico de humidade não está totalmente explorado, pois a falta de critérios quantitativos de interpretação continua a ser uma limitação crítica que deve ser abordada com mais profundidade.

Neste contexto, este trabalho teve como objetivo definir critérios fiáveis indicativos do nível de humidade em edifícios através da Termografia de Infravermelhos (TIV) em diferentes condições ambientais e desenvolver uma ferramenta para avaliar a evolução da humidade durante o processo de secagem dos materiais de construção, baseado em algoritmos/modelos de machine learning.

A relação entre o gradiente térmico e o teor de humidade foi investigada através de ensaios laboratoriais e simulações higrotérmicas. Os resultados demonstraram como as diferentes condições ambientais e as propriedades dos materiais afetam a relação entre o gradiente térmico e a humidade. Os dados experimentais e de simulação foram utilizados como conjuntos de dados de treinamento e teste no desenvolvimento de modelos de machine learning que preveem o teor de humidade com base nos resultados da temperatura superficial e convertem as imagens térmicas em mapas de humidade. Além disso, os princípios da física das construções apresentados na revisão da literatura foram utilizados para criar algoritmos que geram a curva do teor de humidade durante a secagem dos materiais.

Os resultados mostraram que os modelos de machine learning alcançaram um coeficiente de determinação (R^2) superior a 0,95 entre os valores previstos e os reais de humidade, fornecendo previsões precisas do teor de humidade, especialmente em materiais de construção altamente porosos, como argamassa, tijolo e pedra calcária. Relativamente ao algoritmo baseado nos princípios da física das construções, este gerou com sucesso curvas de humidade que coincidiram de forma precisa com as obtidas nos ensaios laboratoriais e nas simulações. Além disso, os resultados deste estudo sugerem que o comportamento

de secagem dos materiais de construção porosos pode ser monitorizado de forma eficaz utilizando TIV, o que ajuda a prevenir a degradação relacionada à humidade nos edifícios.

PALAVRAS-CHAVE: Termografia de Infravermelhos; Humidade; Machine learning; Comportamento higrotérmico; Diagnóstico quantitativo.

CONTENTS

1 INTRODUCTION 1

1.1. CONTEXT 1

1.2. OBJECTIVES 2

1.3. METHODOLOGY 3

1.4. THESIS STRUCTURE 5

2 MOISTURE IN POROUS BUILDING MATERIALS: FUNDAMENTALS, DIAGNOSIS AND CHALLENGES 9

2.1. MOISTURE DAMAGE 9

2.2. MOISTURE AND HEAT TRANSFER 12

2.2.1. MOISTURE TRANSFER IN POROUS MATERIALS 13

2.2.1.1. The moisture content of building materials 13

2.2.1.2. Moisture transfer by diffusion 14

2.2.1.3. Moisture transfer by capillarity 15

2.2.1.4. Moisture transfer during the drying process 18

2.2.2. HEAT TRANSFER IN POROUS MATERIALS 20

2.2.2.1 Heat transfer by conduction 20

2.2.2.2 Heat transfer by convection 21

2.2.2.3 Heat transfer by radiation 22

2.2.3. COMBINED HEAT AND MOISTURE PHENOMENA 24

2.2.3.1. Combined moisture transport in building physics 24

2.2.3.2. Combined heat transport in building physics 25

2.2.3.3. Combined moisture and heat transport 26

2.3. HYGROTHERMAL BEHAVIOUR SIMULATION 28

2.4. MOISTURE DIAGNOSIS 29

2.5. INFRARED THERMOGRAPHY – IRT 33

2.5.1. PRINCIPLES AND HISTORY 33

2.5.2. MEASUREMENT APPROACHES AND RESULTS TREATMENT 35

2.5.3. APPLICATIONS IN DEFECT DIAGNOSIS 36

2.5.4. APPLICATIONS IN MOISTURE ANALYSIS 40

2.5.4.1. Laboratory tests 43

2.5.4.2. In situ tests 44
2.6. MACHINE LEARNING AND AUTOMATION FOR MOISTURE ANALYSIS 47
2.6.1. PRINCIPLES 47
2.6.2. METAMODELS 48
2.6.3. APPLICATIONS FOR DEFECT DETECTION 49
3 EXPERIMENTAL ANALYSIS OF THE THERMAL GRADIENT AND MOISTURE CONTENT 53
3.1 INITIAL REMARKS 53
3.2 TESTS UNDER FREE-RUNNING CONDITIONS 53
3.2.1 MATERIALS AND METHODS 53
3.2.1.1 Framework 53
3.2.1.2 Materials 54
3.2.1.3 Equipment 56
3.2.1.4 Preliminary measurements and procedures 57
3.2.1.5 Environmental conditions 60
3.2.1.6 Procedure 61
3.2.2 RESULTS 63
3.2.2.1 Qualitative analysis 63
3.2.2.2 Influence of artificial lighting on the results 66
3.2.2.3 Thermal gradient and moisture content over time 67
3.2.2.4 Surface Moisture Meter Results over time 69
3.2.2.5 Correlation analysis – thermal gradient vs moisture content 71
3.2.2.6 Cluster Analysis 76
3.2.2.7 Correlation analysis – thermal gradient vs surface moisture meter results 81
3.2.2.8 Evaporation rate 83
3.3 TESTS UNDER CONTROLLED CONDITIONS 85
3.3.1 CHARACTERISATION OF THE PRE-DOSED MORTAR 87
3.3.1.1. Emissivity test 88
3.3.1.2. Water vapour permeability 88
3.3.1.3. Absorption coefficient of water 91
3.3.1.4. Moisture storage function 92

3.3.1.5. Thermal conductivity 93
3.3.1.6. Pore size distribution 95
3.3.2 SPECIMENS PREPARATION AND PROCEDURES 95
3.3.3 RESULTS 97
3.3.3.1 Qualitative analyses 97
3.3.3.2 Quantitative analysis 98
3.3.3.3 Evaporation rate 101
3.4 FINAL REMARKS 104
4 HYGROTHERMAL SIMULATIONS 107
4.1 SIMULATIONS WITH WUFI 107
4.2 DRYING PROCESS UNDER VARYING INITIAL CONDITIONS OF MOISTURE CONTENT 107
4.2.1 FRAMEWORK 107
4.2.2 RESULTS 109
4.2.2.1 Variables evolution over time 109
4.2.2.2 Evolution of the maximum thermal gradient as a function of the moisture content 113
4.2.2.3 Correlation analysis 115
4.2.2.4 Comparison with the laboratory results 118
4.3 DRYING PROCESS UNDER DIFFERENT ENVIRONMENTAL CONDITIONS 120
4.3.1 FRAMEWORK 120
4.3.2 RESULTS 122
4.4 INPUT DATA FOR THE PREDICTION MODELS OF MOISTURE CONTENT 128
4.4.1 FRAMEWORK 128
4.4.2 RESULTS 128
4.4.2.1 Data distribution 128
4.4.2.2 Correlation between thermal gradient and moisture content 129
4.4.2.3 Evolution of the thermal gradient and the moisture content 131
4.4.2.4 Evaporation rate 132
4.4.2.5 Relationship between the evaporation capacity and the maximum thermal gradient 134
4.5 FINAL REMARKS 135
5 MOISTURE PREDICTION MODELS 137
5.1. PRELIMINARY MACHINE LEARNING MODELS 137
5.1.1. FRAMEWORK 137
5.1.2. MODEL CREATION 138

5.1.3. MODEL TRAINING, EVALUATION AND APPLICATION 141
5.1.4. RESULTS 142
5.1.4.1. Neural Network's architecture and performance 142
5.1.4.2. Applications of the developed models 146
5.1.5. DISCUSSION 149
5.2. FINAL ALGORITHMS 150
5.3. MOISTURE PREDICTION MODEL WITH MACHINE LEARNING 152
5.3.1. FRAMEWORK 152
5.3.2. RESULTS 154
5.4. MOISTURE PREDICTION MODEL BASED ON BUILDING PHYSICS CONCEPTS 158
5.4.1 FRAMEWORK 158
5.4.2 RESULTS 161
5.5. GUIDELINES FOR APPLYING THE MOISTURE PREDICTION MODELS 163
5.6. FINAL REMARKS 167
6 CONCLUSIONS 169
REFERENCES 174

FIGURE INDEX

Figure 1 – Thesis flowchart 3

Figure 2 – Equilibrium RH of different soluble salts [2], [29] 10

Figure 3 – Schematic representation of the durability of a stone wall with salt damage [30], [31] 11

Figure 4 – Moisture storage function [4] 14

Figure 5 – Vapour permeability coefficient of building materials [37] 15

Figure 6 – (a) Phenomenon involved in wall humidification by capillary rise. (b) Height of the wet source, which depends on water absorption at the base and evaporation at the surface [46] 16

Figure 7 – Different phases of drying in a porous material ([50]) 18

Figure 8 – Evaporation flux rate at a fixed relative humidity (50%) and temperature (25°C) for a sample of plaster [4] 19

Figure 9 – Blackbody spectral radiance [55] adapted from [37] 23

Figure 10 – Schematic diagram showing the moisture transport in porous hygroscopic building material with the gradients of vapour pressure and relative humidity running in opposite directions (winter conditions). Adapted from [40] 24

Figure 11 – Classification of methods for assessing the moisture content [57] 30

Figure 12 – Classification of the moisture content of brick walls [57] 31

Figure 13 – Comparison of the feasibility of IRT, EFD, NMR, holographic radar, gravimetric test, and fixed points [59] 31

Figure 14 – Historic building façade moisture map [16] 33

Figure 15 – Measurement field of view [70] 34

Figure 16 – Thermograms captured to assess cracks in a wall. (a) Inspection 8:00; (b) Inspection 10:00; (c) Inspection 15:00 [91] 37

Figure 17 – Thermal contrast in concrete block over a 24-hour period [84] 39

Figure 18 – Use of IRT to identify detachments in façades [82] 39

Figure 19 – External wall of a basement of a residential building: a) thermal image b) moisture meter results [1] 45

Figure 20 – Workflow of the laboratory tests under free-running conditions 54

Figure 21 – Clay brick specimens partially immersed in water 55

Figure 22 – Limestone specimens partially immersed in water 55

Figure 23 – Emissometer 58

Figure 24 –Measurement of the clay brick emissivity 58

Figure 25 – Preparation of granite for measuring the emissivity 58

Figure 26 – MIP results for the materials under study 59

Figure 27 – Calibration of the precision balance used in the tests 60

Figure 28 – Procedure to calculate the reflected apparent temperature 60

Figure 29 –Temperature and relative humidity sensor used in tests (HOBO) 61

Figure 30 – Room temperature and relative humidity during the tests with brick and limestone 61

Figure 31 – Room temperature and relative humidity during the tests with granite, mortar, and concrete 61

Figure 32 – Specimens at the beginning of the test (a) brick; (b) limestone; (c) granite; (d) mortar; and (e) concrete 62

Figure 33 – Selected boxes in InfRec Analyser software to calculate the surface average temperature (limestone: A – HMC; B – IMC; C – LMC; D – HYEQ; brick: E – HYEQ; F – LMC; G – IMC; H – HMC) 63

Figure 34 – Infrared images of the drying process of clay brick, limestone, mortar, concrete, and granite 65

Figure 35 – ΔT of each specimen with lights off (LOFF) and lights on (LON) 66

Figure 36 – Time-variation of the thermal gradient (ΔT) and moisture content (u) of each specimen during the drying process, for: (a) brick; (b) limestone; (c) granite; (d) mortar; and (e) concrete 68

Figure 37 – Values of the moisture content (u) and SMM of the specimens: (a) granite; (b) mortar; and (c) concrete 70

Figure 38 – ΔT and SMM values of the specimens: (a) mortar; (b) concrete 71

Figure 39 – Curves of regression models for: (a) clay brick; (b) limestone; (c) granite; (d) mortar; (e) concrete 73

Figure 40 – Curves of quadratic model for (a) clay brick; (b) limestone; (c) granite; (d) mortar; and (e) concrete 75

Figure 41 – Scatter chart with clusters label - clay brick 76

Figure 42 – Scatter chart with clusters label – limestone 78

Figure 43 – Scatter chart with clusters label – granite 79

Figure 44 – Scatter chart with clusters label – mortar 80

Figure 45 – Scatter chart with clusters label – concrete 81

Figure 46 – Curves of regression models for: (a) granite; (b) mortar; and (c) concrete 82

Figure 47 – Evaporation rate and thermal gradient over time for (a) clay brick; (b) limestone; (c) granite; (d) mortar; and (e) concrete 84

Figure 48 – Correlation in the second drying phase - for (a) clay brick; (b) limestone; and (c) mortar. 85

Figure 49 – Workflow of the laboratory tests under controlled conditions 86

Figure 50 – Samples of dimensions of 90 mm x 20 mm (diameter x thickness) 87

Figure 51 – Samples of dimensions of 210 mm x 210 x 20 mm 87

Figure 52 – Test cup assembly for the water vapour permeability test 89

Figure 53 – Test cup assembly inside the climatic chamber 89

Figure 54 - Water vapour permeability test of the mortar under study – mass of the assembly over time 90

Figure 55 – Mass variation in relation to the square root of time of the mortar 92

Figure 56 – Sorption curve of the mortar under study 93

Figure 57 – ISOMET 2114 equipment 94

Figure 58 – Weight of a specimen during the thermal conductivity test 94

Figure 59 – Area selected for the analyses 97

Figure 60 – Thermal images: a) environment I (20ºC / 70%), b) environment II (25ºC / 60%), and c) environment III (15ºC / 80%). 98

Figure 61 – Thermal gradient, ΔT (ºC), and moisture content, u (%): a) environment I (20ºC / 70%), b) environment II (25ºC / 60%), and c) environment III (15ºC / 80%) 99

Figure 62 – Difference in surface temperature between the wet specimen and the dry specimen and moisture content for Scenario I (T=20°C and RH=70%): (a) Point cloud; (b) Regression Curves 100

Figure 63 – Difference in surface temperature between the wet specimen and the dry specimen and moisture content for Scenario II (T=25°C and RH=60%): (a) Point cloud; (b) Regression Curves 100

Figure 64 – Difference in surface temperature between the wet specimen and the dry specimen and moisture content for Scenario III (T=15°C and RH=80%): (a) Point cloud; (b) Regression Curves ... 101

Figure 65 – Comparison between the evaporation rate density and the thermal gradient for: (a) scenario I; (b) scenario II; and (c) scenario III 103

Figure 66 – Correlation between the thermal gradient and the moisture content after the first drying phase for scenario I (a); scenario II (b); and scenario III (c) 104

Figure 67 – Brick hygroscopic curve 108

Figure 68 – Limestone hygroscopic curve 108

Figure 69 – Surface temperature during drying of clay brick specimens with different initial moisture content 110

Figure 70 –Relative humidity variation relative to the surface of the clay brick specimens 110

Figure 71 – Variation of moisture content on the surface of clay brick for different initial moisture content [in kg/m³] 111

Figure 72 – Variation of moisture content on the surface of clay brick for different initial moisture content [in %] 111

Figure 73 – Surface temperature during drying of limestone specimens for different initial moisture content 112

Figure 74 – Relative humidity variation relative to the surface of the limestone specimens 112

Figure 75 – Variation of moisture content on the surface of limestone for different initial moisture content [in kg/m³] 113

Figure 76 – Variation of moisture content on the surface of limestone for different initial moisture content [in %] 113

Figure 77 – Maximum thermal gradient identified in the drying phase for different initial moisture content - clay brick 114

Figure 78 – Maximum thermal gradient identified in the drying phase of each specimen - limestone 114

Figure 79 – Correlation between thermal gradient and moisture content - clay brick 115

Figure 80 – Correlation between thermal gradient and moisture content separated by initial moisture content - clay brick 116

Figure 81 – Drying phases in the correlation graph – Brick specimen with initial moisture content of 100% 116

Figure 82 – Drying phases in the correlation graph – Brick specimen with initial moisture content of 10% 117

Figure 83 – Correlation between thermal gradient and moisture content – limestone 118

Figure 84 – Correlation between thermal gradient and moisture content separated by specimen – limestone 118

Figure 85 – Correlation between thermal gradient and moisture content – clay brick laboratory tests 119

Figure 86 – Correlation separated by initial moisture content – clay brick laboratory tests..... 119

Figure 87 – Correlation chart - comparison of LFC (experimental) and WUFI (numerical) results 120

Figure 88 – Data simulated in the hygrothermal software and data selected for the analysis 122

Figure 89 – Data distribution of (a) $\Delta T_{surfacemax}$ clay brick (ºC), (b) $\Delta T_{surface}$ clay brick (ºC), (c) Moisture content (kg/m³) clay brick, (d) $\Delta T_{surfacemax}$ concrete (ºC), (e) $\Delta T_{surface}$ concrete (ºC), (f) Moisture content (kg/m³) concrete, (g) $\Delta T_{surfacemax}$ granite (ºC), (h) $\Delta T_{surface}$ granite (ºC), (i) Moisture content (kg/m³) granite, (j) $\Delta T_{surfacemax}$ limestone (ºC), (k) $\Delta T_{surface}$ limestone (ºC), (l) Moisture content (kg/m³) limestone 124

Figure 90 – Drying behaviour of concrete, clay brick, granite, and limestone regarding the (a) Moisture Content [kg/m³], and (b) $\Delta T_{surface}$ 125

Figure 91 – Variation of the $\Delta T_{surface}$ according to the moisture content for different materials 125

Figure 92 – Variation of $\Delta T_{surfacemax}$ with ambient the air temperature and relative humidity for (a) Brick; (b) Concrete; (c) Granite; and (d) Limestone 127

Figure 93 – Evaporation rate density for an air temperature of 7°C and relative humidity of 53.73% 127

Figure 94 – Histograms (a) $\Delta T_{surface}$ [°C] – simulations; (b) $\Delta T_{surface}$ [°C] – laboratory; (c) Moisture content [kg/m³] – simulations; (d) Moisture content [kg/m³] – laboratory 129

Figure 95 – Relationship between moisture content and thermal gradient ($\Delta T_{surface}$ [°C]) - simulation results 130

Figure 96 – Comparison of the relationship between moisture content and thermal gradient ($\Delta T_{surface}$ [°C]) for simulation and experimental results – scenario I..... 130

Figure 97 – Comparison of the relationship between moisture content and thermal gradient ($\Delta T_{surface}$ [°C]) for simulation and experimental results – scenario II..... 131

Figure 98 – Comparison of the relationship between moisture content and thermal gradient ($\Delta T_{surface}$ [°C]) for simulation and experimental results – scenario III..... 131

Figure 99 – Evolution of the thermal gradient ($\Delta T_{surface}$ [°C]) and moisture content over time for simulation and experimental results: (a) $\Delta T_{surface}$ [°C] x Time for scenario I; (b) Moisture Content [kg/m³] x Time for

scenario I; (c); (d) $\Delta T_{surface}$ [°C] x Time for scenario II; (e) Moisture Content [kg/m³] x Time for scenario II; (f); (g) $\Delta T_{surface}$ [°C] x Time for scenario III; (h) Moisture Content [kg/m³] x Time for scenario III 132

Figure 100 – Comparison between the evaporation rate density and $\Delta T_{surface}$ – scenario I..... 133

Figure 101 – Comparison between the evaporation rate density and $\Delta T_{surface}$ – scenario II..... 133

Figure 102 – Comparison between the evaporation rate density and $\Delta T_{surface}$ – scenario III..... 134

Figure 103 – Relationship between the vapour pressure and the $\Delta T_{surfacemax}$ (Saturation vapour pressure subtracted from the vapour pressure of the air and $\Delta T_{surfacemax}$ [°C]) 134

Figure 104 – Framework of the development of the machine learning models to predict the moisture content 137

Figure 105 – Adjustment time of the temperature of moist areas at the beginning of the evaporation 138

Figure 106 – Architecture of the NN developed to predict the moisture content..... 139

Figure 107 – Weights applied to the first neuron in the first layer 140

Figure 108 – Example of the point at which the model starts overfitting 142

Figure 109 - Training and validation according to each epoch (a) Model I – Loss (b) Model I – MAE (c) Model II - Loss (d) Model II- MAE (e) Model III – Loss (f) Model III - MAE 144

Figure 110 – Correlation between predicted and true values and coefficient of determination (R^2) score for (a) Model I – training set; (b) Model I – testing set; (c) Model II – training set; (d) Model II – testing set; (e) Model III – training set; and (f) Model III – testing set 145

Figure 111 – Predictions of the moisture content based on the $\Delta T_{surface}$ in three different environmental conditions for (a) clay brick, (b) concrete, (c) granite, and (d) limestone 148

Figure 112 - Cross section when the $\Delta T_{surface}$ was close to 0°C for (a) concrete (5 days of simulation) and (b) clay brick (60 days of simulation) 149

Figure 113 – Moisture storage function of clay brick and the moisture content (w) corresponding to a $\Delta T_{surface}$ of 2.0°C and 0.2°C 149

Figure 114 – Procedures to develop the final algorithms 151

Figure 115 – Final algorithms developed for moisture prediction..... 152

Figure 116 – Steps to generate the moisture map 153

Figure 117 – Different approaches and framework for algorithm 1 154

Figure 118 – Training and validation according to each epoch: Random Initialisation (a) Model I – Loss (b) Model I – MAE; (c) Model II - Loss (d) Model II- MAE; Soft start (e) Model I – Loss (f) Model I – MAE; (g) Model II - Loss (h) Model II- MAE 156

Figure 119 – Correlation between predicted and true values and coefficient of determination (R^2) score for: Random Initialisation (a) Model I – training (b) Model I – testing; (c) Model II - training (d) Model II- testing; Soft start (e) Model I – training (f) Model I – testing; (g) Model II - training (h) Model II- testing 157

Figure 120 – Moisture map generated by Algorithm 3 158

Figure 121 – Generic evolution of moisture content over time (inputs of algorithm based on building physics concepts) 160

Figure 122 – Comparison between the algorithm results and the simulation and laboratory tests: (a) 25°C, 60% RH simulation; (b) 25°C, 60% laboratory test; (c) 20°C, 70% laboratory test; (d) 15°C, 80% laboratory test 162

Figure 123 – Comparison between the curves plotted by the algorithm and the results from laboratory test in T=25°C and RH of 60% considering 24 hours of duration of the 1st drying phase 163

Figure 124 – Flowchart describing the procedures for conducting an inspection with IRT using the algorithms and methodology presented in this work 165

Figure 125 – Algorithm for selecting a combination of temperature and relative of the air to plot the curve of the ΔTsurface over time 166

TABLE INDEX

Table 1 – Material's properties under assessment 5
Table 2 – Ranges of μ-values for some building materials [37] 15
Table 3 – Convective surface film coefficient for heat transfer – natural convection [54] 21
Table 4 – Convective surface film coefficient for heat transfer – forced convection [54] 22
Table 5 – Characteristics of the use of active and passive thermography for moisture analysis [10] 42
Table 6 – ML models applied to moisture analysis in buildings 51
Table 7 – Dimension of the specimens 54
Table 8 – Initial moisture content of the specimens 56
Table 9 – Infrared Camera Specifications - Thermo Tracer TH9100MR 57
Table 10 – Aquant indicators [152] 57
Table 11 – Emissivity values of the materials analysed 57
Table 12 – Properties of the materials used in the laboratory tests 59
Table 13 – Monitoring time 61
Table 14 – ΔT correlation table with pearson coefficient (r) and p-value 71
Table 15 – R^2 values and parameter estimates for each regression model – clay brick 73
Table 16 – R^2 values and parameter estimates for each regression model - limestone 74
Table 17 – R^2 values and parameter estimates for each regression model - granite 74
Table 18 – R^2 values and parameter estimates for each regression model - mortar 74
Table 19 – R^2 values and parameter estimates for each regression model - concrete 74
Table 20 – Equations for calculating the ΔT (quadratic model) 74
Table 21 – Lower and upper limit of ΔT and moisture content (u) of each cluster - clay brick 77
Table 22 – Lower and upper limit of ΔT and moisture content (u) of each cluster - limestone 78
Table 23 – Lower and upper limit of ΔT and moisture content (u) of each cluster - granite 79
Table 24 – Lower and upper limit of ΔT and moisture content (u) of each cluster - mortar 80
Table 25 – Lower and upper limit of ΔT and moisture content (u) of each cluster - concrete 81
Table 26 – R^2 values and parameter estimates for each regression model - Granite 82

Table 27 – R^2 values and parameter estimates for each regression model - Mortar 82

Table 28 – R^2 values and parameter estimates for each regression model – Concrete 82

Table 29 – Properties of the pre-dosed mortar selected for the laboratory campaign 87

Table 30 – Dimensions and mass of the mortar samples used in the water vapour permeability test . 88

Table 31 – Conditions for the water vapour permeability test 89

Table 32 – Mortar's properties obtained with the water vapour permeability test 90

Table 33 – Absorption coefficient of water of the mortar under study in different units 92

Table 34 –Thermal conductivity of the mortar – dry specimens 94

Table 35 – Results of the thermal conductivity test for the moist specimens 94

Table 36 – Results of the thermal conductivity test for the saturated specimens 95

Table 37 – Mass and moisture content of the specimens 95

Table 38 – Infrared Camera Specifications – Fluke, model TiS60+ 96

Table 39 – Reflected temperature measured for each environment under study 96

Table 40 – Coefficient of determination (R^2) for each regression model for the different scenarios .. 101

Table 41 – Properties of the clay brick and limestone for numerical simulation 108

Table 42 – Initial moisture conditions of the materials simulated in WUFI 109

Table 43 – Properties of concrete and granite for numerical simulation 121

Table 44 – Properties of the mortar for numerical simulation 128

Table 45 – Parameters of the NNs developed 140

Table 46 – Architecture analysis for the NN of Model I 143

Table 47 – Architecture analysis for the NN of Model II 143

Table 48 – Architecture analysis for the NN of Model III 143

Table 49 – Information and performance of the models 154

Table 50 – Coefficient of determination (R^2) between the values predicted by the algorithm and the true values 161

NOMENCLATURE

ROMAN-LETTER NOTATIONS

Symbol	Unit	Meaning
A	m^2	Area
A_w	$kg/(m^2s^{0,5})$	Absorption coefficient of water
b	%/M.-%	Thermal conductivity supplement
c_e	J/kgK	Specific heat capacity of ice
c_s	J/kgK	Specific heat capacity of building material
c_w	J/kgK	Specific heat capacity of liquid water
d	m	Thickness
D_a	m^2/s	Water vapour diffusion coefficient in the air
D_w	m^2/s	Capillary transport coefficient
D_φ	kg/ms	Liquid conduction coefficient
E_b	W/m^2	Total emissive power
g	m/s^2	Acceleration due to gravity
g_v	kg/m^2s	Density of vapour flow rate
g_w	kg/m^2s	Density of liquid flux
g_d	kg/m^2s	Evaporation rate density
H	m	Height of capillary rise
h	W/m^2K	Surface film coefficient for heat transfer
h_c	W/m^2K	Convective surface film coefficient for heat transfer
h_e	J/kg	Specific enthalpy of melting
h_l	J/kg	Phase change latent heat
h_s	J/m^3	Enthalpy of dry building material
h_v	J/kg	Evaporation enthalpy of water
h_w	J/m^3	Enthalpy of moisture in building material
m_d	g	Mass of the dry sample
m_i	Kg	Initial mass
m_s	Kg/m^2	Mass per area of sorbed moisture from a water surface
m_t	Kg	Mass at time t

Symbol	Unit	Meaning
m_w	g	Mass of the wet sample
m_1	kg/m³	Mass at t1
m_2	kg/m³	Mass at t2
p_{sat}	Pa	Water vapour saturation pressure
q	W/m²	Heat flux
Q	W	Total emitted radiation
q_c	W/m²	density of convective heat flow rate
q_h	W/m²	Combined heat flux
r	m	Capillary radius
R	m²K/W	Thermal resistance
R_m	m²K/W	Thermal resistance of the layers
R_{se}	m²K/W	Thermal resistance of the outer surface
R_{si}	m²K/W	Thermal resistance of the inner surface
S_h	J/m³.s	Heat source or heat sink due to condensation/evaporation
t_d	s	Duration of the first drying period
t	s	Time
t_f	s	Total duration of the test
t_1	s	Measurement time 1
t_2	s	Measurement time 2
T	K	Temperature
T_a	K	Air temperature
Te	K	Temperature at the other side of the assembly
Ti	K	Temperature at one side of the assembly
T_s	K	Surface temperature
u	%	Moisture content
w_{cap}	kg/m³	Free water saturation
w_{crit}	kg/m³	Critical moisture content
W	kg/m³	Moisture content
w_e	kg/m³	Frozen water content

GREEK-LETTER NOTATIONS

Symbol	Unit	Meaning
α	-	Part of radiation absorbed
β_p	s/m	Surface film coefficient for vapour diffusion
δ_p	kg/m.s.Pa	Water vapour permeability
δ_v	m²/s	Vapour permeability coefficient
Δm_t	kg/m²	Mass variation
$\Delta m_{,0}$	kg	Mass variation at time t0
$\Delta m_{,tf}$	kg/m²	Value of Δm_t at time t_f
ϵ	-	Emissivity
Φ	W	Heat flow rate
φ	%	Relative humidity
γ	N/m	Surface tension
θ	degrees	Contact angle of the liquid with the glass of the tube
λ	W/mK	Thermal conductivity
λ_0	W/mK	Thermal conductivity of dry building material
$\lambda(w)$	W/mK	Thermal conductivity of moist building material
μ	-	Water vapour resistance factor
ρ	kg/m³	Density of the liquid
ρ_r	-	Part of radiation reflected
ρ_s	kg/m³	Density of dry building material
$\rho_{v,a}$	Pa	Water vapour partial pressure in the ambient air
$\rho_{v,s}$	Pa	Water vapour partial pressure in the ambient surface
σ	W/m²K⁴	Stefan-Boltzmann constant
τ	-	Part of radiation transmitted
υ_1	kg/m³	Vapour concentration on one side of the layer
υ_2	kg/m³	Vapour concentration on the other side of the layer

MATHEMATICAL OPERATORS

Symbol	**Meaning**
d	Operator for total differential
∂	Operator for partial differential
∇	Nabla operator
Δ	Variation operator

ACRONYMS

Symbol	**Meaning**
AI	Artificial Intelligence
ASTM	American Society for Testing and Materials
CNN	Convolutional Neural Networks
DIN	German National Standard
DTT	Dynamic Thermal Tomography
EN	European Standard
ENet	Elastic Net
HMC	High Moisture Content
HYEQ	Hygroscopic Equilibrium
IMC	Intermediate Moisture Content
IRT	Infrared Thermography
ISO	International Organization for Standardization
LARS	Least-Angle Regression
LFC	Building Physics Laboratory
LMC	Low Moisture Content
LOFF	Lights Off
LON	Lights On
LR	Linear Regression
LR - LS	Linear Regression Least Squares
LR – SVM	Linear Regression Support Vector Machine
LSTM	Long Short-Term Memory

Symbol	Meaning
MAE	Mean Absolute Error
MAPE	Mean Absolute Percentage Error
ML	Machine Learning
MLP	Multilayer Perceptrons
MIP	Mercury Intrusion Porosimetry
MSE	Mean-Square Error
NDT	Non-Destructive Techniques
NN	Neural Networks
PATDT	Pixel Algorithm for Time-Derivative of Temperature
PCT	Principal Component Thermography
PT	Pulsed Thermography
RH	Relative Humidity
RNN	Recurrent Neural Networks
SHT	Step Heating Thermography
SMM	Surface Moisture Meter
SVM	Support Vector Machine
T	Temperature
TSR	Thermography Signal Reconstruction

1

INTRODUCTION

1.1. CONTEXT

Moisture-related defects are quite common in masonry walls and hinder the long-term durability of buildings, the quality of the indoor environment, and the comfort of the users since a high amount of moisture in building materials can lead to mould growth, salt crystallisation, surface condensation, and even reduced structural strength [1], [2], [3]. Therefore, an early and proper diagnosis of moisture-related defects is critical to prevent moisture damage.

Infrared Thermography (IRT) is a non-destructive technique that does not require contact with the surface and allows the assessment of the thermal behaviour of building materials, enabling the identification of potential problems. Hence, it has a good potential for moisture analysis, making it possible to identify moisture-related defects [4]. IRT can also be used for the detection of other abnormalities such as detachments and the existence of voids [5], [6]; energy losses in installations and construction details [7]; cracks [8], and for the analysis of the overall thermal performance of a building envelope [9], so IRT results can be integrated to assess several pathologies. However, despite its potential to detect moisture, there is a gap in the literature regarding the identification of quantitative criteria for the interpretation of results due to the complexity and variability of the phenomena involved in the humidification and drying process of materials [4], [10], [11]. Therefore, obtaining surface temperature criteria indicative of the level of moisture is a significant challenge that must be addressed.

The applicability of IRT to detect moisture occurs due to three physical phenomena that influence the surface temperature of building materials based on the changes in their moisture content: evaporative cooling, reduced thermal resistance, and high heat storage capacity. Based on these phenomena, wet areas can be colder than dry areas due to surface evaporation. Moist areas can also be identified as warmer zones due to the high thermal inertia of water when compared to the one of the dry materials. If the moisture accumulates in the inner layer of the building components, it will store more heat during the heating phase, which will take longer to be released during the

cooling phase, and the wet area will appear in the thermal image with higher temperatures. The results can be influenced by environmental conditions (e.g. direct solar radiation, temperature and relative humidity of the air, etc.), moisture content, dirt at the surface, physical-chemical characteristics of the material, thermal conductivity of layers, and soluble salts [4], [10], [11].

Because of the high number of variables influencing the correlation between the moisture content and the surface temperature, most studies presented only qualitative analyses, or a quantitative analysis applied to a specific environment [12], [13], [14], [15], [16], [17], [18], [19]. Recent studies have also used IRT to detect moisture automatically using image processing techniques [20]. However, the moisture content or level was not evaluated in this situation.

In recent years, the construction industry is experiencing a technological revolution driven by digitalisation and automation [21]. This trend is also visible in several studies that have been conducted to integrate the results of building inspection technologies with machine learning techniques, including the development of algorithms that make it possible to automate the identification and classification of defects in buildings, thus reducing the subjectivity in the analysis of the inspection results [22], [23], [24].

Despite the recent advances in image-based techniques and computational methods for building diagnosis, their use for moisture assessment still needs to be more deeply exploited. The combination of laboratory tests and hygrothermal simulation tools with machine learning models to identify the behaviour of moist building materials and correlate their surface temperature with their moisture content has great potential and must be further developed.

Overall, these studies highlight the need to obtain reliable criteria from image-based techniques that indicate the moisture content or the level of moisture in building components and develop a risk assessment framework that enables the identification of the moisture level and its evolution, making it possible to predict when favourable conditions for moisture damage can potentially occur.

1.2. OBJECTIVES

The main objectives of this work are to (i) define reliable criteria indicative of the level of moisture in buildings using IRT in different environmental conditions and (ii) to develop a moisture risk assessment framework. To achieve this, the following specific objectives have been defined:

- Identify the correlation between the moisture content and the surface temperature of various building materials under different environmental conditions.
- Apply machine learning techniques trained and tested with data obtained in laboratory tests and simulations to predict the moisture content in building materials.

- Develop a machine learning model to generate a moisture map based on IRT results.
- Create an algorithm to generate the moisture content curve during the materials drying process.

1.3. METHODOLOGY

According to Figure 1, the work was divided into seven main tasks to achieve the specific objectives stated in § 1.2. The first step of the research (task 1) involved a comprehensive review of the state of the art about wall degradation caused by moisture. This review also covered the hygrothermal behaviour of building materials, techniques used to diagnose moisture, and an analysis of machine learning models applied to moisture analysis in buildings.

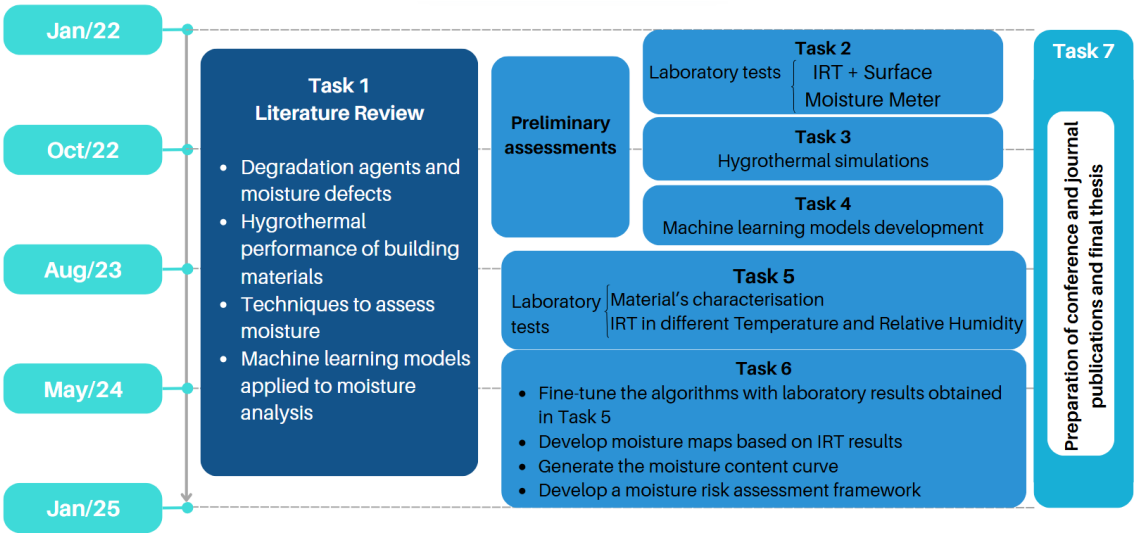


Figure 1 – Thesis flowchart

Task 1 was essential to understand the moisture degradation agents and the damage caused by them, the conditions necessary for superficial condensation to occur, the point at which moisture stains and mould growth potentially initiate and, in extreme cases, when moisture compromises load-bearing capacity.

Additionally, the research focused on the hygrothermal performance of building materials to understand the heat and mass transfer phenomena and the correlation between moisture and temperature changes. A thorough analysis of available techniques for diagnosing moisture, including infrared thermography (IRT), was conducted to check if IRT was a promising tool for providing 2D images that could indicate areas with atypical moisture content.

In the studies with the use of IRT for moisture assessment, it was checked if the various factors influencing surface evaporation were accounted for and if quantitative analyses were carried out.

Complementary non-destructive testing (NDT) techniques, such as the gravimetric and electromagnetic methods, were investigated to check if they could complement the results from IRT.

Finally, in the final stage of task 1, a review of machine learning models applied to moisture and other defect detection was carried out. Machine learning is a field of artificial intelligence that enables learning the relationship between variables of interest. It has presented considerable progress in the last few years due to the increase in computational capacity and available training data. The aim was to use these techniques to learn the relationship between the surface temperature of building materials and their moisture content, which would enable the estimation of moisture content in building components and, consequently, help prevent moisture-related damage.

In task 2, a preliminary experimental campaign was conducted under free-running laboratory conditions to monitor the drying process of samples using IRT, the gravimetric method, and a surface moisture meter. The experimental campaign was carried out at the Building Physics Laboratory (LFC) of the Faculty of Engineering of the University of Porto, which was equipped with the necessary tools for these tests. This step was essential to preliminarily evaluate the thermal gradient of the materials in a specific environmental condition.

During this campaign, samples of five materials commonly used in the construction of walls were tested: clay brick, limestone, granite, concrete, and mortar. Samples with three different initial moisture content were used to assess the influence of the moisture content on the NDT results. The monitoring period was approximately 15 days or until the specimens dried.

Following the preliminary experimental campaign, the same conditions tested in the laboratory were simulated using hygrothermal simulation software to analyse the differences between the laboratory and simulated results. This step corresponds to task 3.

Tasks 2 and 3 were critical for understanding the hygrothermal behaviour of building materials and the correlation between moisture content and surface temperature. However, as these steps were conducted under free-running environmental conditions, task 4 involved additional hygrothermal simulations to analyse the drying phase of materials under various environmental conditions, ranging from 5°C to 25°C air temperature and 50% to 90% relative humidity. After conducting the simulations, machine learning models were developed to predict the moisture content (in any environment in the range of the temperature and relative humidity tested) based on the surface temperature of moist materials. Additionally, a machine learning model was created to predict the maximum thermal gradient identified in each material under varying environmental conditions.

The machine learning model developed in task 4 predicted the moisture content of initially saturated materials based on their surface temperature and the environmental conditions for four types

of materials: clay brick, concrete, granite, and limestone. The material's properties used for the model were those available in the hygrothermal simulation software's database.

Based on the latter, it was necessary to fine-tune the model. Therefore, task 5 consisted of carrying out laboratory tests with a mortar commonly used in Portugal for rendering masonry walls. The material was characterised according to its key properties, such as thermal conductivity, pore size distribution, water vapour permeability, emissivity, capillary water absorption, density, and moisture storage function. Subsequently, the material was subjected to different moisture contents, and its drying process was monitored using the gravimetric method and IRT in three controlled laboratory conditions inside a climatic chamber. Table 1 lists the properties analysed, the standards and manuals followed, and the number and dimensions of the test specimens.

Table 1 – Material's properties under assessment

Material's properties	Standard/ manuals	Number of specimens	Specimens dimensions
Pore size distribution	ISO 15901-1	1	40x40x40 mm
Thermal conductivity	ISOMET 2114	3	90 mm diameter 20 mm thickness
Water vapour permeability	EN ISO 12572	5	90 mm diameter 20 mm thickness
Capillary water absorption	EN ISO 15148	3	210x210x20 mm
Moisture storage function	EN ISO 12571	3	210x210x20 mm
Emissivity	ASTM C1371-04a	3	210x210x20 mm

Finally, in task 6, the laboratory test results were used to fine-tune the machine learning algorithm developed in task 4. An algorithm was developed to create moisture maps based on IRT results, showing moisture risk areas, thereby highlighting the need for preventive and remedial measures regarding the conservation status of building elements. Additionally, a moisture risk assessment framework was created to present guidelines for the identification of the moisture level and its evolution with IRT. In this task, it was also developed an algorithm to generate the moisture content curve during the drying phase with IRT based on building physics principles.

Lastly, task 7 involved the final compilation of the thesis and its dissemination through peer-reviewed journal publications and conference articles.

1.4. THESIS STRUCTURE

This thesis is structured into seven chapters:

-Chapter 1 – This chapter presents the context of the study, highlighting the importance of taking forward research on reliable techniques for moisture diagnosis in buildings. It also defines the main research objectives and methodology and outlines the structure of the research work.

-Chapter 2 – Moisture in Porous Building Materials: This chapter provides a comprehensive literature review on moisture damage, moisture and heat transfer mechanisms in building materials and presents some techniques available for moisture diagnosis. It includes detailed discussions on hygrothermal behaviour, measurement methods, and the application of infrared thermography (IRT) for moisture analysis. Additionally, this chapter presents the developments in machine learning techniques applied to the identification and classification of defects in buildings, specifically focusing on moisture detection. It reviews recent studies integrating computational methods with building inspection technologies.

-Chapter 3 – Experimental analysis of the thermal gradient and moisture content: This chapter discusses the laboratory tests conducted to investigate the drying process of various building materials, including clay brick, limestone, granite, concrete, and mortar. The chapter provides detailed descriptions of the experimental setup, materials tested, and methods used for monitoring moisture content and surface temperature through IRT and other techniques.

-Chapter 4 – Hygrothermal simulations: This chapter presents the results of hygrothermal simulations conducted using the WUFI software. It discusses the drying process of building materials such as clay brick, limestone, concrete, granite, and mortar under varying environmental conditions. The chapter also compares simulation results with experimental data.

-Chapter 5 – Moisture Prediction Models: This chapter presents the development of machine learning models designed to predict the moisture content in building materials and a model to generate the moisture curve during the drying process based on IRT results. The preliminary models were trained using simulation data, with an emphasis on the relationship between thermal gradients, moisture content, and environmental conditions. These models provided insights into the data preparation, model training, and evaluation processes, focusing on the creation of models for different building materials. Building on the preliminary models, refined moisture prediction models are presented. It includes a machine learning model fine-tuned with experimental data for improved moisture content predictions, as well as a model based on building physics principles to generate the moisture curve during the drying process. These models are validated using data from laboratory tests and simulations.

-Chapter 6 – Conclusions: This final chapter summarises the key findings of the research, discusses the implications of the results, and identifies directions and trends for future research in the field of moisture detection and building diagnosis.

-Appendix 1 – Thermal and digital images obtained at each measurement time for the tests under free-running laboratory conditions for: (a) clay brick and limestone; and (b) granite, mortar, and concrete.

-Appendix 2 – Analysis of regression models for measurements taken after the maximum thermal gradient is reached.

-Appendix 3 – Thermal and digital images obtained at each measurement time for the tests under controlled laboratory conditions for: (a) T=20°C and RH=70%; (b) T=25°C and RH=60%; and (c) T=15°C and RH=80%.

-Appendix 4 – Preliminary machine learning models developed with simulation data to predict, for clay brick, limestone, concrete, and granite: (a) the maximum thermal gradient; and (b) the moisture content [kg/m³].

-Appendix 5 – Final machine learning models developed with simulation and experimental data to predict, for mortar: (a) the maximum thermal gradient; and (b) the moisture content [kg/m³].

-Appendix 6 – Algorithms developed to convert a thermal image to a file with $\Delta T_{surface}$ values (a) and to create a moisture map based on the thermal image uploaded (b).

-Appendix 7 – Algorithm developed to plot the moisture content curve during the drying process based on IRT results.

-Appendix 8 – Simulation data for mortar in the thirty environmental conditions selected for training and testing the models.

-Appendix 9 – Algorithm developed to plot the curve of the $\Delta T_{surface}$ over time, according to the environmental condition selected by the user.

2

MOISTURE IN POROUS BUILDING MATERIALS: fundamentals, diagnosis and challenges

2.1. MOISTURE DAMAGE

Moisture in buildings has its origin from rain, contact with soil, inherent in construction materials, manufacturing and production processes, water vapour productive activities inside the building or even from fortuitous causes, such as leaky or faulty piping [2], [25]. It may originate defects, such as salt crystallisation, moisture staining, mould growth, and reduced structural strength [2], [3], [26], besides increasing the U-values of building components [27].

Among moisture transport mechanisms, capillarity is one of the most common that lead to moisture induced defects [28]. As water transported by capillarity has soluble salts originating from rocks, soils, and construction materials, such as mortars and stones, when it evaporates, the aqueous solution becomes more concentrated, and when the supersaturation is reached, crystallisation of salts occurs [2]. Salts may crystallise at the exterior surface as efflorescences, or behind the covering as subflorescences. The depth at which salts crystallise greatly influences the extension and severity of the damage caused to the masonry [25].

In masonries with moisture, there are zones with distinct levels of deterioration according to the type and amount of salt present and the environmental conditions. The different types of salts, such as sulphates, chlorides, and nitrates, may be present at different heights, according to their solubility, and in various forms, either aqueous or crystallised. The more soluble ions percolate to greater heights and accumulate in those zones, while the less soluble salts tend to remain at lower heights. The crystallisation of these salts will depend on the amount of salt, the environmental conditions, and the equilibrium relative humidity (RH) for each salt since they can only crystallise when the ambient RH becomes lower than the equilibrium RH of the saturated solution [25]. Figure 2 shows the equilibrium RH of different soluble salts usually found in walls. Studies

carried out by [25] showed that, when analysing the drying process of two equal samples in different RH conditions, when it occurred at 32% of RH, a relevant amount of crystallised salt was found in the interior of the porous structure, while when drying occurred at 69%, it produced more efflorescences on the surface.

salt	0°C	5°C	10°C	15°C	20°C	25°C	30°C
$CaCl_2 \cdot 6H_2O$	41	37.7	33.7		30.8	28.6	22.4
$MgCl_2 \cdot 6H_2O$	33.7	33.6	33.5	33.3	33.1	32.8	32.4
$K_2CO_3 \cdot 2H_2O$	43.1	43.1	43.1	43.2	43.2	43.2	43.2
$Ca(NO_3)_2 \cdot 4H_2O$	59	59.6	56.5	54	53.6	50.5	46.8
$Mg(NO_3)_2 \cdot 6H_2O$	60.4	58.9	57.4	55.9	54.4	52.9	51.4
NH_4NO_3						61.8	
$NaNO_3$		78.6	77.5	76.5	75.4	74.3	73.1
NaCl	75.5	75.7	75.7	75.6	75.5	75.3	75.1
Na_2SO_4					82	82.8	84.3
KCl	88.6	87.7	86.8	85.9	85.1	84.3	83.6
$MgSO_4 \cdot 7H_2O$			86.9		90.1	88.3	88
$Na_2CO_3 \cdot 10H_2O$				96.5	97.9	88.2	83.2
$Na_2SO_4 \cdot 10H_2O$				95.2	93.6	91.4	87.9
KNO_3	96.3	96.3	96	95.4	94.6	93.6	92.3
K_2SO_4	98.8	98.5	98.2	97.9	97.6	97.3	97

Figure 2 – Equilibrium RH of different soluble salts [2], [29]

In terms of the degradation of walls and their life cycle, the study carried out by [30] has developed a conceptual model that represents the damage rate over time in a stone wall with salts, illustrated in Figure 3. This study uses the concept proposed by [31] to describe concrete's durability. According to this study, for the damage to initiate, it requires an accumulation of salts, so there is an initial phase, named the "accumulation phase", when there is no damage yet. After the "damage threshold", the "propagation stage" starts and the damage will progress at a damage rate until it reaches the limit of an acceptable degree of damage, which means the end of service life.

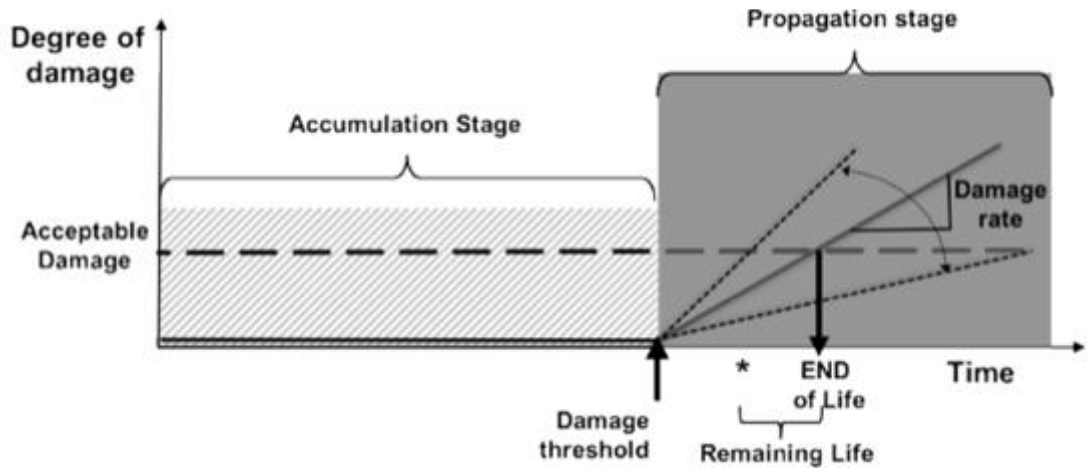


Figure 3 – Schematic representation of the durability of a stone wall with salt damage [30], [31]

Besides the risk of degradation due to salt crystallisation, moisture is also the governing factor affecting mould growth. Mould has an impact on the visual appearance of surfaces and, more importantly, on the health of the occupants of the buildings since occupants of damp or mould-affected compartments in buildings are at increased risk of respiratory symptoms, respiratory infections, and exacerbation of asthma [26]. The occurrence of indoor dampness is estimated to be in the order of 10 to 50% in buildings in the most affluent countries [32].

According to the World Health Organization guidelines [32], the presence of many biological agents indoors is mainly due to high humidity and poor ventilation. The document highlights that the high moisture content in an indoor environment can promote the growth of microorganisms such as mould, fungi, and bacteria. Therefore, moisture is considered a strong indicator of risk for asthma and respiratory symptoms.

The species of microorganisms that grow on the surface of building materials depend on the water activity at their surface, which is the same as the relative humidity above the substrate. When the water activity is less or equal to 0.80, primary colonisers can grow; when it is between 0.80 and 0.90, secondary colonisers grow, and tertiary colonisers require a water activity greater than 0.90 to germinate and start growing. Overall, previous studies show that the critical relative humidity above the substrate for microbiological growth is around 75 to 90%. However, a single limit value is inadequate for the hygrothermal design of building structures since the outdoor climate does not permit the relative humidity at surfaces to be kept below 75%. Therefore, the mould growth prediction might be made using equations that calculate the mould growth index based on the time, the temperature, the relative humidity, and the coefficients related to the type of material [32].

On the other hand, since the relationship between dampness, microbial exposure, and health effects cannot be precisely quantified, quantitative health guidelines values or acceptable limits for

microbial contamination cannot be recommended. Instead, the recommendation is that surface dampness must be prevented, and if it does occur, it should be addressed [32].

Moisture damage is a serious problem that can occur in environments with both high and low RH. Mould growth is more likely to occur in environments with high RH, but even ambiences with lower RH can cause damage to building materials in the form of salts crystallised in the interior of the walls. Hence, an appropriate and timely diagnosis of moisture-related defects is of main importance and must be done to avoid building decay and assure the quality of the indoor environment conditions. According to [33], it is important to monitor not only the existence of moisture but also its evolution over time to prevent damage since the presence of water can decrease in the dry seasons and quickly increase after rainy periods. The monitoring time should vary according to the variability of the environmental changes. The common variables to be monitored are the moisture content and its distribution, the surface temperature, and the air temperature and relative humidity [33].

The most appropriate repair solution should be selected after identifying the condition of the substrate regarding the moisture content and its evolution over time in order to reduce the risk of applying products and methods that are not effective [33]. Additionally, climatic changes are also highlighted by several authors as a factor contributing to the increase in moisture and deterioration of buildings, which highlights the need for adequate solutions for building retrofitting [33], [34], [35]. Measures for reducing the moisture content might include the use of adequate ventilation, heating, and drying in controlled conditions, amongst others [2], [32].

2.2. MOISTURE AND HEAT TRANSFER

The transport of moisture in building materials is influenced by various factors, such as material properties, the surrounding environment, and the nature of the aqueous phase (liquid or vapour), all of them interacting with each other in a complex manner [36]. Therefore, to accurately diagnose moisture-related defects in buildings, it is crucial to understand the hygrothermal behaviour of building materials. This includes, for example, knowledge of how the humidification and drying processes occur and how environmental conditions affect them, how the moisture profile changes along the thickness of the wall, and how the moisture content affects the physical properties of the materials since non-destructive techniques will, in most cases, measure the physical properties of the materials and based on them infer the moisture condition of the substrate.

To analyse the hygrothermal behaviour of buildings, it is essential to consider both heat and mass transfer phenomena, as they are intimately connected. For instance, temperature differences can induce air movements, which, in turn, transfer both heat and moisture from one location to another. Another illustration is the evaporation of water from a surface, which leads to a decrease

in surface temperature. These examples highlight the interdependence of heat and mass transfer in building systems [37].

In this way, the moisture content of building elements will result from the dynamic equilibrium established between the component and the environment. This equilibrium will be influenced by the complex interaction between moisture and the porous structure of the materials, as well as by the existence of several simultaneous moisture transfer phenomena in vapour and liquid phases [38].

2.2.1. MOISTURE TRANSFER IN POROUS MATERIALS

2.2.1.1. The moisture content of building materials

Building materials can be classified according to their hygroscopicity. When the mass is practically constant, whatever the RH of the environment, they are considered non-hygroscopic. If the amount of water fixed by adsorption is relevant, they are considered hygroscopic (such as gypsum and wood) [39].

In hygroscopic porous building materials, for each relative humidity of the air, there will be a corresponding equilibrium moisture content for the material, which can be represented by the moisture storage function of the material. Figure 4 presents the adsorption and desorption curves. The adsorption isotherm follows three stages: (i) the first, monomolecular adsorption, in which a layer of water molecules is attached to the inner surface of the pores; (ii) the second, plurimolecular adsorption, when there is the deposition of several layers of molecules; and (iii) the third, capillary condensation, when the pore diameter is small enough, and the multimolecular layers join together, a phase in which the capacity to store water in the internal structure of the material increases, as can be seen by the increase in the slope of the adsorption isotherm curve [37], [39].

When a capillary-active building material comes into contact with liquid water, it will absorb water until it reaches free water saturation (w_{cap} in Figure 4), which is less than the maximum possible moisture content. Higher moisture contents up to pore saturation or even maximum water saturation (w_{max}) can be reached only with the application of pressure by diffusion of water vapour in a temperature gradient [40].

If a material is immersed in water until w_{max} and then dried at different RHs, the amount of water in the pores is higher than the one stored during the adsorption phase. Hence, the desorption curve is different from the adsorption curve [37], as shown in Figure 4. However, for the sake of simplicity, in some hygrothermal models, the adsorption curve is used for computational simulations since the differences between both curves can be neglected.

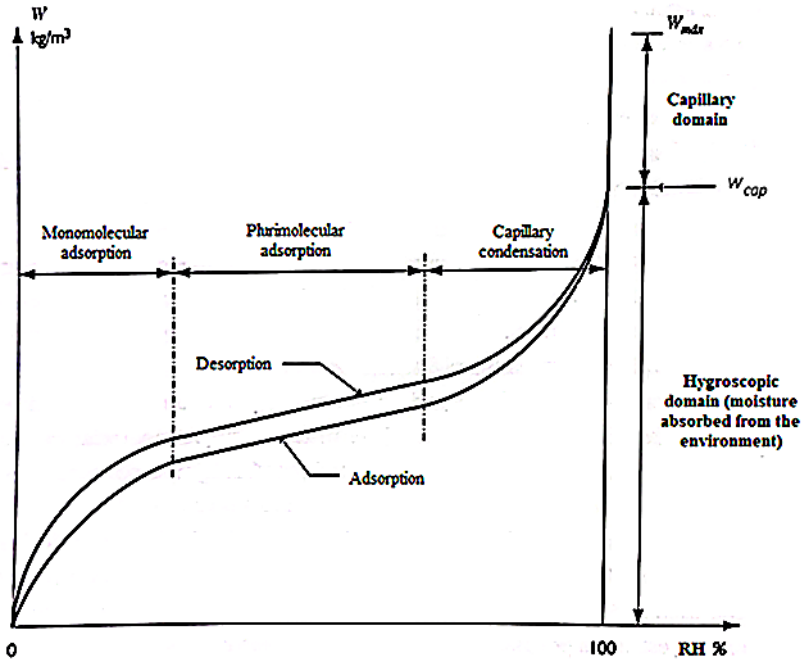


Figure 4 – Moisture storage function [4]

2.2.1.2. Moisture transfer by diffusion

Moisture transfer in porous building materials occurs by different mechanisms in each of the phases, and the primary transport processes are vapour diffusion, vapour convection, capillarity of liquid water through porous materials, and the flow of gravity of liquid water by fissures, openings, and macropores [41]. When transport occurs in the vapour phase, it is conditioned by the mechanisms of diffusion and convection. In contrast, when it occurs in the liquid phase, it is ruled by capillarity, the effect of gravity, and the effect of the pressure gradient [39].

Although moisture transfer in the vapour phase can also occur by convection, the relevant moisture transport mechanisms regarding building physics are water vapour diffusion and liquid transport by capillary forces [40].

Moisture transport by vapour diffusion analysis is important to assess the risk of interstitial condensation and the risk of mould growth on the internal surface of buildings [42]. The transfer of vapour by diffusion occurs according to equation (1) [37].

$$g_v = \frac{D_a}{\mu}\frac{\upsilon_1 - \upsilon_2}{\mathrm{d}} \quad (1)$$

Where:

g_v: density of vapour flow rate [kg/(m².s)]

D_a: water vapour diffusion coefficient in the air [m²/s]

μ: water vapour resistance factor [-]

υ_1: vapour concentration on one side of the layer [kg/m³]

υ_2: vapour concentration on the other side of the layer [kg/m³]

d: thickness [m]

Table 2 contains ranges of μ values for some materials commonly used in buildings. Figure 5 depicts the vapour permeability coefficient of some building materials, which is the ratio between the water vapour diffusion coefficient in the air and the μ factor of each material [37].

Table 2 – Ranges of μ-values for some building materials [37]

Material	μ (-)
Mineral wool, lightweight concrete, brick, lime mortar	1-10
Concrete, wood, cement mortar, and lime	15-100
Linoleum, PVC sheet, polyethylene sheet, glass	10^3-10^6

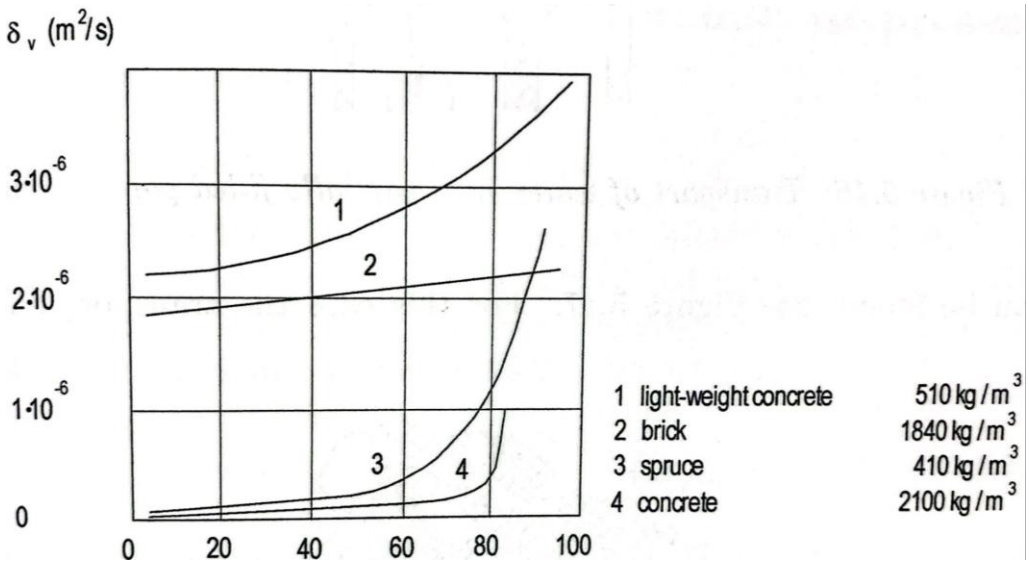


Figure 5 – Vapour permeability coefficient of building materials [37]

2.2.1.3. Moisture transfer by capillarity

When a thin tube is immersed in a container with water, it is possible to verify the phenomenon of capillarity since the water rises inside the tube. According to [43], in this phenomenon, which is the result of surface tension, the molecules close to the surface of the liquid are attracted by the molecules of the glass tube, and there is a curvature of the water along the walls of the tube. The height of capillary rise in a tube can be found using Jurin's Law, according to equation (2).

$$H = \frac{2\gamma\cos\theta}{\rho g r} \tag{2}$$

Where:

H: height of capillary rise [m]

γ: surface tension [N/m]

r: capillary radius [m]

θ: contact angle of the liquid with the glass of the tube [degrees]

ρ: density of the liquid [kg/m³]

g: acceleration due to gravity [m/s²]

However, to estimate the capillary rise in porous materials, it is also important to consider several factors that influence the process [44], such as the evaporation conditions at the surface and the amount of water available at the base of the materials. In the case of rising damp in porous materials, an explanation based solely on the capillary rise is not adequate, as water can evaporate from the wall surface into the atmosphere, and thus, the rise of water by capillary action can be balanced by evaporation. Therefore, the height of the wet front will be determined by the interaction of these variables [45]. [46] presents a physical view of rising damp, as shown in Figure 6.

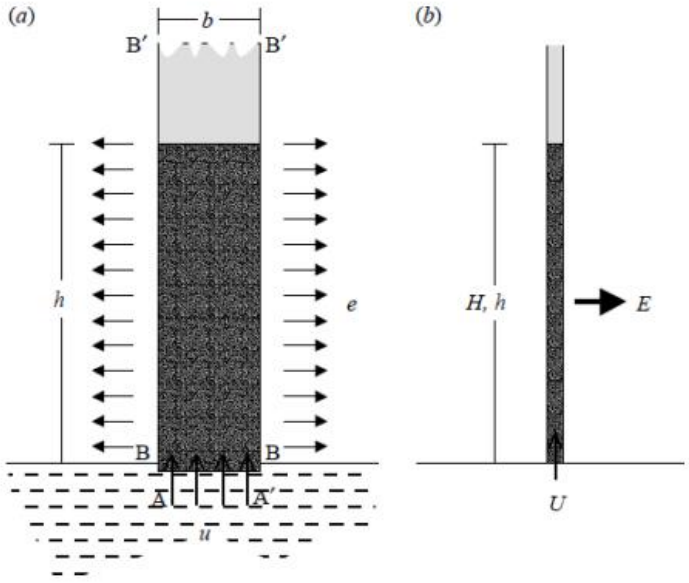


Figure 6 – (a) Phenomenon involved in wall humidification by capillary rise. (b) Height of the wet source, which depends on water absorption at the base and evaporation at the surface [46]

According to [46], Figure 6 depicts a structure composed of a porous material of thickness b and height h, in hydraulic contact with the ground and of unlimited height. The starting point is the proposition that rising damp is the result of competition between capillary absorption of water along the base AA', whose total rate is designated by U, and evaporation of water along the exposed surface BB', whose total rate is denoted by E. When the rising moisture is stabilised, there is a steady state in which U = E, meaning that the incoming water is balanced with the outgoing water.

Sources for capillary rise can be groundwater or surface water. In the first case, the height of the wet front on the interior walls is greater than on the exterior walls since evaporation conditions are less favourable indoors. In contrast, in the second case, the height of the wet front may vary from wall to wall but tends to be higher on the outer walls [39].

The absorption coefficient of water quantifies the amount of water entry into a porous material due to absorption when its surface is in direct contact with liquid water. It can be obtained according to equation (3) [47], [48]. The procedures for obtaining A_w are established by the standard ISO 15148 [49]. This coefficient is used to approximately describe the increase of the liquid transport coefficient with increasing moisture content, as presented in equation (4).

$$m_s = A_w\sqrt{t} \tag{3}$$

Where:

m_s: mass per area of sorbed moisture from a water surface [kg/m²]

A_w: absorption coefficient of water [kg/(m².s$^{1/2}$)]

t: time [s]

$$D_w = 3.8\left(\frac{A_w}{W_{cap}}\right)1000^{\left(\frac{w}{W_{cap}}\right)-1} \tag{4}$$

Where:

D_w: capillary transport coefficient [m²/s]

w_{cap}: free water saturation [kg/m³]

w: moisture content [kg/m³]

The capillary liquid transport in porous materials can be characterised by means of the transport coefficients for suction and redistribution, using equations (5) and (6) [40].

$$g_w = -D_\varphi \nabla_\varphi \tag{5}$$

$$D_\varphi = D_w \frac{\mathrm{d}_w}{d_\varphi} \tag{6}$$

Where:

g_w: density of liquid flux [kg/m².s]

D_φ: liquid conduction coefficient [kg/ms]

φ: relative humidity [-]

$\frac{\mathrm{d}_w}{d_\emptyset}$: derivative of moisture storage function [kg/m³]

2.2.1.4. Moisture transfer during the drying process

The drying process of porous building materials is complex and difficult to analyse. However, the knowledge of this process is important to understand the behaviour of these materials in service [50]. The moisture content will be different at different depths of the constructive element [51].

According to [50], when a saturated porous material is in contact with the environment at constant temperature and relative humidity, it is possible to identify three different drying phases with different drying speeds, as shown in Figure 7. The first phase is characterised by constant moisture content throughout the thickness of the material and constant drying speed. When water on the surface becomes scarce and the wet front is reduced, the drying process occurs by diffusion between the limit of the wet front and the outer surface, which corresponds to the second phase. In this process, the dry layer increases, and the flux is reduced. The third phase begins when the two wet fronts meet, and the drying speed at this stage is extremely slow.

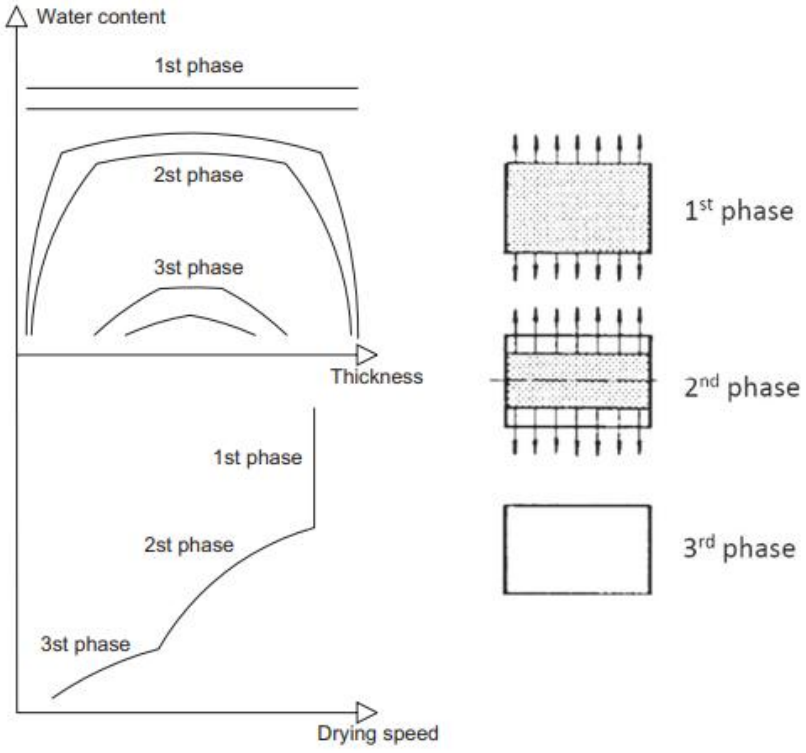


Figure 7 – Different phases of drying in a porous material ([50])

The different drying speeds during the evaporation process in a sample of plaster can be seen in Figure 8. The evaporation flux rate changes according to the moisture content. When the material is very humid (moisture content between 24% to 12%), the evaporative flux rate is high and almost constant, guaranteeing the highest and constant drying speed, as presented in Figure 7; when it is between 12% and 9%, it presents a considerable reduction in the evaporation flux rate, and below 9% of moisture content, the evaporation flux rate decreases sharply [4].

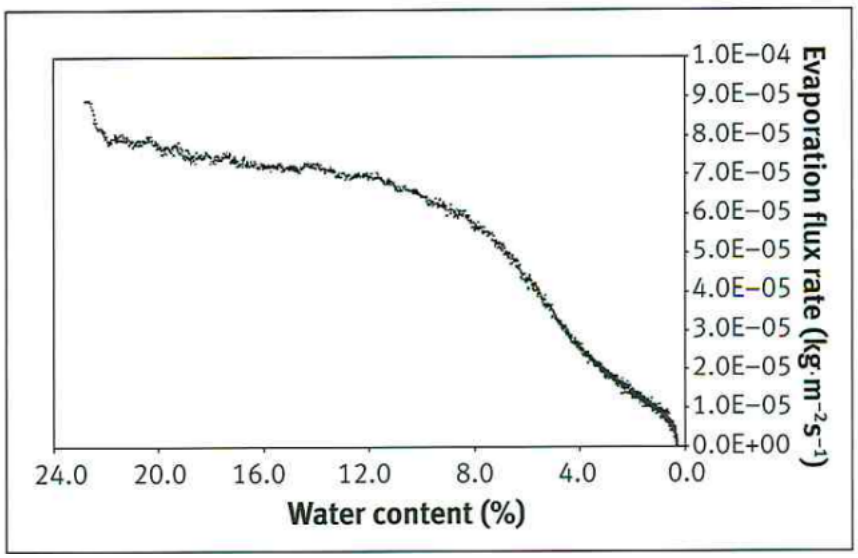


Figure 8 – Evaporation flux rate at a fixed relative humidity (50%) and temperature (25°C) for a sample of plaster [4]

To explain the drying behaviour at the beginning of the process, it is important to highlight two important moisture contents. The first one is called capillary saturation or free water saturation (w_{cap}), presented in Figure 4, and corresponds to the saturated state obtained when a material is in contact with water at atmospheric pressure. Secondly, there is the moisture content above which liquid moisture transport starts to occur. That is called critical moisture content (w_{crit}) [52]. Below w_{crit}, the main transport mechanisms are vapour diffusion and adsorbed layer diffusion, while above this value, capillary conduction is the main form of transport [52]. According to [38], in this first phase of the drying process, the drying rate can be calculated with equation (7).

$$g_d = \frac{(w_{cap} - w_{crit})\ \frac{d}{2}}{t_d} \tag{7}$$

Where:

w_{cap}: free water saturation [kg/m³]

w_{crit}: critical moisture content [kg/m³]

g_d: evaporation rate density [kg/m².s]

d: thickness [m]

t_d: duration of the first drying period [s]

The critical moisture content and the capillary moisture content are related to the pore size distribution [38]. Hence, the pore size distribution of the materials will influence the evaporation rate and, therefore, the temperature at the surface.

2.2.2. HEAT TRANSFER IN POROUS MATERIALS

Heat transfer occurs when there is a temperature gradient. It is transferred via conduction, convection, and radiation [37]. In conduction, there is heat transfer by collision between atomic particles without mass exchange. That is, energy is transmitted due to internal vibrations of molecules without displacement of the molecules themselves [37]. The transmission between solids at different temperatures occurs by conduction, and according to the second law of thermodynamics, the heat flow always occurs in the direction of lower temperatures [53].

Convection, on the other hand, is the result of the macroscopic movement of liquids and gases in media with temperature differences, including contact with colder or hotter solids [53]. Convection can occur naturally due to differences in fluid density or can be forced by external forces that promote movement [37]. As in the case of conduction, convection also needs a medium to occur [53].

Heat is also transferred due to the emission and absorption of electromagnetic waves by surfaces in a process named radiation. In this case, there is no need for a physical medium for heat transfer. It can occur even when there is a vacuum between the surfaces of two bodies at different temperatures [37], [53].

The thermal system can also be affected by latent heat, which is directly linked to changes in physical state. When water is evaporated from a surface, for example, an amount of sensible heat equal to the heat of evaporation is absorbed, so the reaction acts as a heat sink [53].

2.2.2.1 Heat transfer by conduction

According to Fourier's Law, the rate of heat transfer by conduction in a material follows equation (8) [37]. Equations (9), (10), (11) and (12) represent the relationship between the heat flux, the heat rate, and the thermal resistance of each layer of a material.

$$\Phi = -\lambda A \frac{dT}{dx} \tag{8}$$

$$q = \frac{\Phi}{A} \tag{9}$$

$$q = \lambda \frac{Ti - Te}{d} \tag{10}$$

$$q = \frac{Ti - Te}{R} \tag{11}$$

$$R = \frac{d}{\lambda} \tag{12}$$

Where:

Φ: heat flow rate [W]

λ: thermal conductivity [W/mK]

A: area [m²]

q: heat flux [W/m²]

R: thermal resistance [m²K/W]

T_i: temperature at one side of the assembly [K]

T_e: temperature at the other side of the assembly [K]

d: thickness [d]

2.2.2.2 Heat transfer by convection

The rate and flux related to convective heat transfer can be explained by equation (13) [47].

$$q_c = h_c(T_s - T_a) \tag{13}$$

Where:

q_c: density of convective heat flow rate [W/m²]

h_c: convective surface film coefficient for heat transfer [W/m²K]

T_s: surface temperature [K]

T_a: temperature of a well-chosen spot in the ambient air [K]

The calculation of h_c is complex and involves several factors, including the type of airflow, and the type of convection, amongst others. This coefficient can be calculated using the information in Table 3 and Table 4 [37], [54].

Table 3 – Convective surface film coefficient for heat transfer – natural convection [54]

Natural convection	
$h_c = 2 \cdot \lvert T_a - T_s \rvert^{1/4}$	At interior surfaces
$0.3 \leq h_c \leq 0.8$	Stable air layers horizontal surface
$h_c = a \cdot (\Delta\theta / L)^b$	At ambient temperatures
3.5	Inside vertical surfaces
5.5	Inside horizontal surfaces (heat upwards)
1.2	Inside horizontal surfaces (heat downwards)
2.5	Inside vertical surfaces
5	Inside horizontal surfaces (heat upwards)
0.7	Inside horizontal surfaces (heat downwards)
$3 \leq h_c \leq 10$	-

Table 4 – Convective surface film coefficient for heat transfer – forced convection [54]

Forced convection	
$h_c = 5 + 4.5 \cdot v_v - 0.14 \cdot v_v^2$	Windward side
$h_c = 5 + 1.5 \cdot v_v$	$v_v \leq 10$ m/s
	Leeward side
	$v_v \leq 8$ m/s
$h_c = 5.6 + 3.9 \cdot v_v$	vv ≤ 5 m/s
$h_c = 7.2 \cdot v_v^{0.78}$	vv > 5 m/s
19.0	Outside surfaces
$h_c = 4 + 4 \cdot v_v$	-
$h_c = 4.5 + 1.6 \cdot v_v$	Windward side
$h_c = 4.5 + 0.33 \cdot v_v$	Leeward side
$10 \leq h_c \leq 100$	-

2.2.2.3 Heat transfer by radiation

Radiation can be explained as the propagation of photons or, alternatively, the propagation of electromagnetic waves, independent of a physical medium [37].

A blackbody absorbs all energy incident on it, regardless of wavelength and direction. Planck's Law deals with the radiation emitted by a black body. As shown in Figure 9, the surface of a blackbody emits different amounts of energy at different wavelengths. For a fixed wavelength, radiation increases with increasing temperature [37].

The total emissive power of a black body is obtained with the Stefan-Boltzmann Law, according to equation (14) [37].

$$E_b = \sigma . T^4 \quad (14)$$

Where:

E_b: total emissive power [W/m²]

σ: Stefan-Boltzmann constant [5,67.10^{-8} W/m²K^4]

T: temperature [K]

Real surfaces cannot emit the same amount of energy as a blackbody. The emissivity of a surface is the ratio between the total radiation emitted by a body and the total radiation emitted by a blackbody at the same temperature (equation (15)) [37]. The value of the emissivity is 1 for a blackbody and 0 for a perfect reflector.

$$\epsilon = \frac{E\,(T)}{E_b(T)} \quad (15)$$

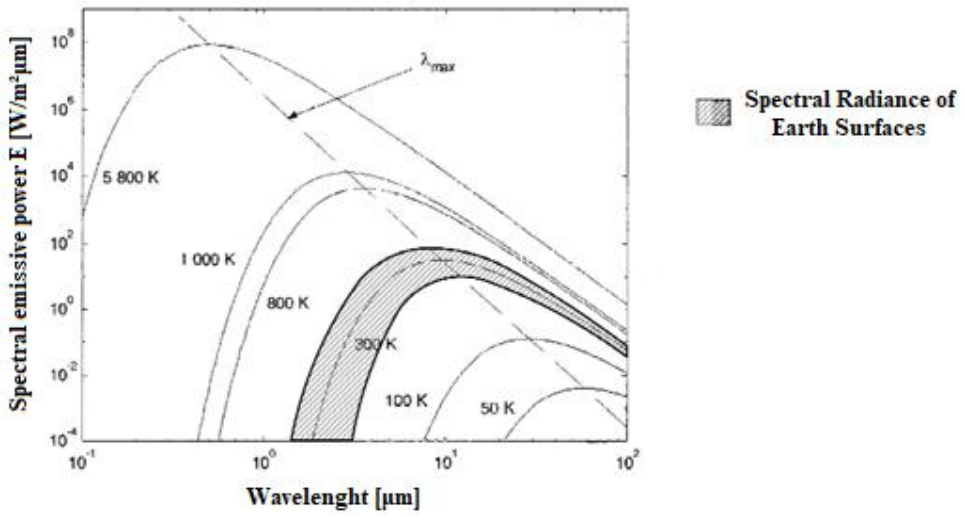


Figure 9 – Blackbody spectral radiance [55] adapted from [37]

The total radiative energy emitted by a surface is described by the Stefan-Boltzmann Law in equation (16).

$$Q = \epsilon \sigma A T^4 \quad (16)$$

Where:

Q: Total emitted radiation [W]

ϵ: emissivity [-]

σ: Stefan-Boltzmann constant [$5{,}67.10^{-8}$ W/m²K⁴]

A: area [m²]

T: temperature [K]

When radiant energy reaches the surface of a material, part of the radiation is reflected (ρ_r), part is absorbed (α), and part is transmitted (τ), according to the constant relationship of equation (17). Most solids used as building materials do not transmit radiation. Therefore, $\tau=0$ [37].

$$\rho + \alpha + \tau = 1 \quad (17)$$

Since building components absorb longwave radiation emitted by other objects and by the atmosphere and also emit this type of radiation, there is always an exchange of longwave radiation with the surroundings. Regarding radiative exchange in an indoor environment, for two close, parallel, flat, and non-metallic surfaces at approximately room temperature, the radiative heat transfer coefficient has values around 3 to 5 W/m²K [54].

2.2.3. COMBINED HEAT AND MOISTURE PHENOMENA

2.2.3.1. Combined moisture transport in building physics

In building physics, the relevant moisture transport mechanisms of vapour diffusion and liquid transport through capillary forces occur according to the schematic diagram shown in Figure 10 [40]. It represents the interaction of water vapour diffusion and liquid transport in building components that separate the indoor environment (higher vapour pressure) from the outdoor environment (higher relative humidity) in winter conditions. In low moisture contents (Figure 10a), vapour diffusion flows from inside to outside since the temperature (and consequently the vapour pressure) indoors is higher than outdoors. When the moisture content rises (Figure 10b), a sorbate film covers the pore walls (which are thicker on the outside than on the inside due to the higher RH outdoors), and the water molecules move from the thicker film sections to the thinner sections in a process called surface diffusion, which moves in the opposite direction to vapour diffusion. When the total moisture increases (Figure 10c), the moisture transport is reversed, and the transport becomes from the outside to the inside by capillary conduction.

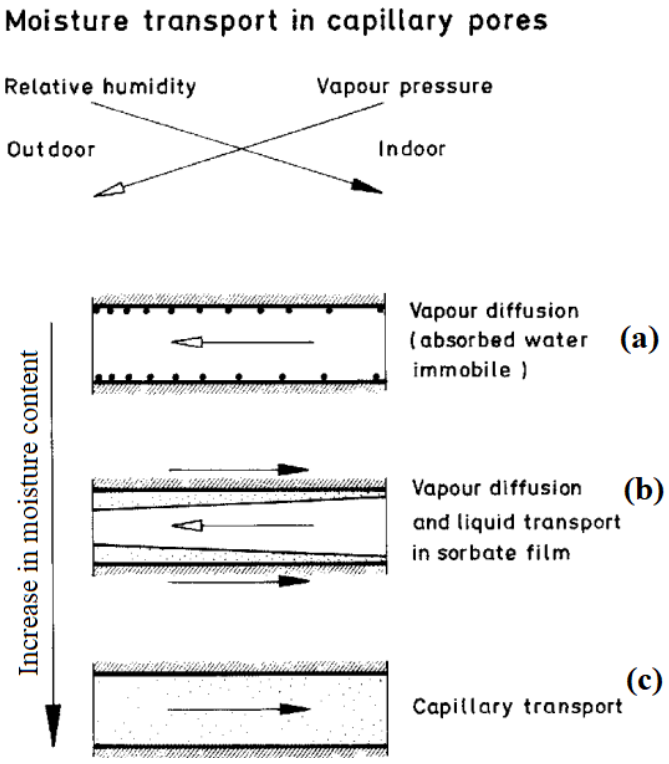


Figure 10 – Schematic diagram showing the moisture transport in porous hygroscopic building material with the gradients of vapour pressure and relative humidity running in opposite directions (winter conditions). Adapted from [40]

In the sorption moisture region of most building materials (between 0 and 95% of RH in the moisture storage function), vapour and liquid transport do not influence each other because liquid transport happens via the micropores, while vapour diffusion occurs mainly in the larger pores [40].

2.2.3.2. Combined heat transport in building physics

When there is heat transfer in a material, there will be conduction phenomenon happening inside. However, on the outer and inner surfaces, there will be convection and radiation. In these cases, the heat flux will consider a sum of the thermal resistance of the material (R_m) with the thermal resistance of the outer (R_{se}) and inner (R_{si}) surfaces [37]. Equations (18), (19) and (20) contain the calculation of the heat flux for a material.

$$q_h = \frac{Ti - Te}{Rse + Rm + Rsi} \tag{18}$$

$$R_m = \frac{d}{\lambda} \tag{19}$$

$$q_h = \frac{Ti - Te}{Rse + \frac{d1}{\lambda 1} + \frac{d2}{\lambda 2} + \cdots + Rsi} \tag{20}$$

Where:

q_h: combined heat flux [W/m²]

Ti: temperature at one side of the assembly [K]

Te: temperature at the other side of the assembly [K]

R_{se}: thermal resistance of the outer surface [m²K/W]

R_m: thermal resistance of the layers [m²K/W]

R_{si}: thermal resistance of the inner surface [m²K/W]

d: thickness [m]

λ: thermal conductivity [W/mK]

The detailed modelling of heat transfer phenomena due to conduction by air adjacent to the surface, convective transport by air flows, and emission of longwave radiation is complex. However, it is possible to carry out simplifications that are adequate in the context of building physics [40]. Equation (21) contains the simplification of heat flux on surfaces of building materials:

$$q = h\ (T_a - T_s) \tag{21}$$

Where:

q: heat flux [W/m²]

h: surface film coefficient for heat transfer (sum of convective and radiative heat transfer coefficient) [W/m²K]

Ta : air temperature [K]

Ts: surface temperature [K]

In building physics, it is usual to adopt standard values for the thermal resistance of the interior and exterior surfaces of buildings. According to [40], the mean values of h for calculating the heat and moisture exchange between outdoor and indoor building component surfaces and the surrounding is 0.125 m²K/W for internal surfaces and 0.059 m²K/W for external surfaces. Values for other situations, according to the position of the surface and the direction of the heat flow can be found in [53].

2.2.3.3. Combined moisture and heat transport

The principles for calculating the thermal behaviour of building materials in dry conditions are known, however, as moisture transport affects heat transport, these must be analysed together. The heat and moisture transfer governing equations proposed by [40] are presented in equations (22) and (23), respectively.

$$\frac{\partial w}{\partial \varphi}\frac{\partial \varphi}{\partial t} = \nabla(D_\varphi \nabla_\varphi + \delta_p \nabla(\varphi p_{sat})) \quad (22)$$

$$\frac{\partial H}{\partial T}\frac{\partial T}{\partial t} = \nabla(\lambda \nabla \mathrm{T}) + h_v \nabla(\delta_p \nabla(\varphi p_{sat})) \quad (23)$$

Where:

∂w/dφ: moisture storage capacity [kg/m³]

∂H/dT: heat storage capacity of the moist building material [J/kg]

w: moisture content [kg/m³]

φ: relative humidity [%]

D_φ: liquid conduction coefficient [kg/m.s]

δ_p: water vapour permeability [kg/m.s.Pa]

p_{sat}: water vapour saturation pressure [Pa]

T: temperature [K]

λ: thermal conductivity [W/m.K]

h_v: evaporation enthalpy of water [J/kg]

In building physics, there is an approximately linear relationship between the enthalpy of a material and its temperature. The enthalpy of a dry material, related to the enthalpy at 0°C, is described according to equation (24) [56]. However, in the case of wet building materials, the enthalpy of the water contained in the material must be added. Equation (25) can be used to determine the enthalpy of water in a building material [40].

$$H_s = \rho_s c_s T \quad (24)$$

Where:

h_s: dry building material enthalpy [J/m³]

ρ_s: density of dry building material [kg/m³]

c_s: specific heat capacity of building material [J/kg.K]

T: temperature [K]

$$h_w = \left[(w - w_e)c_w + w_e c_e - h_e \frac{dw_e}{d\vartheta}\right]\vartheta \quad (25)$$

Where:

h_w: enthalpy of moisture in building material [J/m³]

c_w: specific heat capacity of liquid water [J/kg.K]

c_e: specific heat capacity of ice [J/kg.K]

h_e: specific enthalpy of melting [J/kg]

w: moisture content [kg/m³]

w_e: frozen water content [kg/m³]

The moisture content also influences the thermal conductivity of building materials. Equation (26) can be used to calculate this influence [40].

$$\lambda(w) = \lambda_0(1 + b.\frac{w}{\rho_s}) \quad (26)$$

Where:

$\lambda(w)$: thermal conductivity of moist building material [W/m.K]

λ_0: thermal conductivity of dry building material [W/m.K]

ρ_s: density of dry building material [kg/m³]

b: thermal conductivity supplement [%/M.-%]

Supplement b indicates how much % the thermal conductivity increases per mass percentage of moisture. Its value is determined according to the type of construction material.

The interaction of vapour diffusion and phase change is considered as a source or a sink of heat in the heat balancing equation (27) [56].

$$S_h = h_v \nabla g_v \quad (27)$$

Where:

S_h: heat source or heat sink due to condensation/evaporation [J/m³.s]

h_l: phase change latent heat [J/kg]

g_v: density of vapour flow rate [kg/m².s]

2.3. HYGROTHERMAL BEHAVIOUR SIMULATION

The analytical calculation of mass and heat transfer phenomena is complex, and, many times, it cannot be carried out manually. There are tools for computational simulations of such phenomena that make it possible to identify the hygrothermal behaviour of buildings. In the field of building physics, hygrothermal models are widely used to simulate the combined transport of heat and moisture and can be applied to a single component or to the entire building [54].

The difference between the models depends on the level at which each one considers parameters such as: moisture transfer dimension; flow type (steady, semi-steady, or transient state); quality and availability of information, and stochastic nature of data (material properties, time, construction quality), amongst others. [54] presented fourteen heat, air, and moisture transport simulation models available to the public outside the organisation where they were developed: 1D-HAM; BSim; Delphin 5; EMPTIED; GLASS; HygIRC; HAMLab; HAM-Tools; IDA-ICE 4.5; MATCH; MOIST 3.0; MOISTURE-EXPERT; UMIDUS; and WUFI.

The hygrothermal balance usually considers: (i) heat fluxes by conduction, convection, and radiation; (ii) moisture fluxes by vapour diffusion, convection, and liquid transport; and (iii) air fluxes driven by natural, external, or mechanical forces [54].

The simulation in the software requires inputs about the interior and exterior environment, the properties of the materials, and the boundary conditions. Normally, climate data that must be inputted are temperature and relative humidity of outdoor and indoor air, barometric pressure, incident solar radiation on the surface (direct and diffuse), incidence of rain on the outdoor surface, wind speed and direction, and, in some software, longwave atmospheric radiation and cloud index. Data can be obtained from a meteorological station nearby or measured with equipment or simulated with specific software [54].

Overall, the required material properties are density, porosity, specific heat capacity, thermal conductivity, water vapour permeability, absorption coefficient of water, and data from the moisture storage function [54]. The theoretical basis presented in § 2.2 enables guidance for identifying the required inputs, including the necessary laboratory tests and the identification of the surface transfer coefficients, among others.

The simulations performed in this work were run in the WUFI Pro software, which allows the simulation of the transient hygrothermal behaviour of constructive elements exposed to climatic conditions. The WUFI family of software was developed by the Fraunhofer Institute for Building Physics. WUFI Pro and WUFI 2D are intended for building component simulations, focused on

the analysis of one or more layers of walls and roofs. The WUFI Pro software allows one-dimensional analysis, while the WUFI 2D allows two-dimensional analysis with the possibility of simulations of corner angles and thermal bridges. The WUFI Plus and WUFI Passive versions allow the analysis of the entire building, focusing on the indoor climate and the energy required to maintain comfortable and healthy indoor conditions.

WUFI Pro only focuses on elements such as walls and roofs with one or more layers, subject to specific external and internal weather conditions. The software enables analyses related to one-dimensional cross-sections to assess the hygrothermal behaviour of building elements. In addition, it is also possible to incorporate post-processing modules into the software to allow the assessment of the risk of mould growth or corrosion development in steel.

In calculating heat transport, WUFI considers thermal conduction, enthalpy fluxes by phase-change of water, shortwave solar radiation, and longwave radiation. Regarding moisture transfer, the effects of convection due to differences in total pressure were disregarded, and the only means considered were diffusion of water vapour or movement of liquid water by capillarity [40].

With WUFI software, the following results can be achieved:

- Densities of heat flux through the interior and exterior surface.
- Temperatures and relative humidity at monitoring points.
- The moisture content of each layer and of the entire building component.
- Temperature, relative humidity, and moisture content profiles.
- Limiting isopleths for assessing mould growth.

Limiting isopleths show the limit below which no mould growth is expected. If conditions are at a threshold above isopleths for an extended period, mould growth may be possible, but additional criteria may be needed for an accurate statement, according to the WUFI Pro database.

2.4. MOISTURE DIAGNOSIS

Since moisture plays a crucial role in the durability of building components, there is a need for accurate ways of assessing it. Both destructive and non-destructive tests are available for the diagnosis of moisture in building components. [57] presented a classification of the methods that can be used for moisture measurement (Figure 11), highlighting that the use of destructive tests has the disadvantage of not being applicable to all situations due to restrictions on the level of damage to the elements, but that the use of non-destructive tests also requires attention due to the conditions of use, since it is necessary to guarantee reliable results.

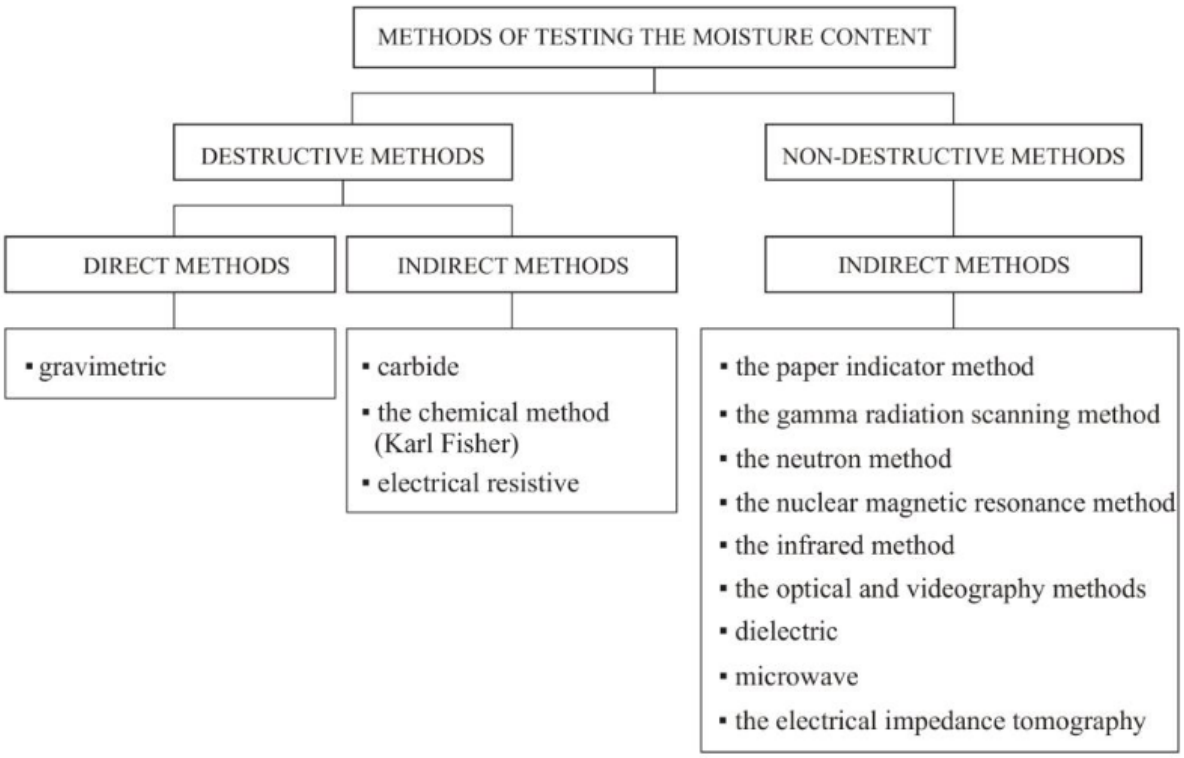


Figure 11 – Classification of methods for assessing the moisture content [57]

Techniques for measuring moisture in porous materials have undergone great development in recent years, from traditional techniques, such as the gravimetric method, to more modern techniques, such as nuclear magnetic resonance, microwave reflection, infrared thermography, and the use of electrical properties of the material [44].

According to [57], the direct gravimetric method provides the most reliable results of the moisture content of all known methods. However, it is necessary to take samples of the material for its use. This method consists of collecting samples and sending them to the laboratory to determine their mass before and after drying at a temperature of 105°C. The moisture content (u) in percentage is calculated according to equation (28), in which m_w is the mass of the wet sample in kg and m_d is the mass of the dry sample in kg [58]:

$$u = \frac{m_w - m_d}{m_d} 100\% \quad (28)$$

[57] also highlights that the classification of the moisture content of brick walls can be done according to Figure 12, which shows that moisture content above 3% is already considered high and that higher than 8% is already considered very wet/damp.

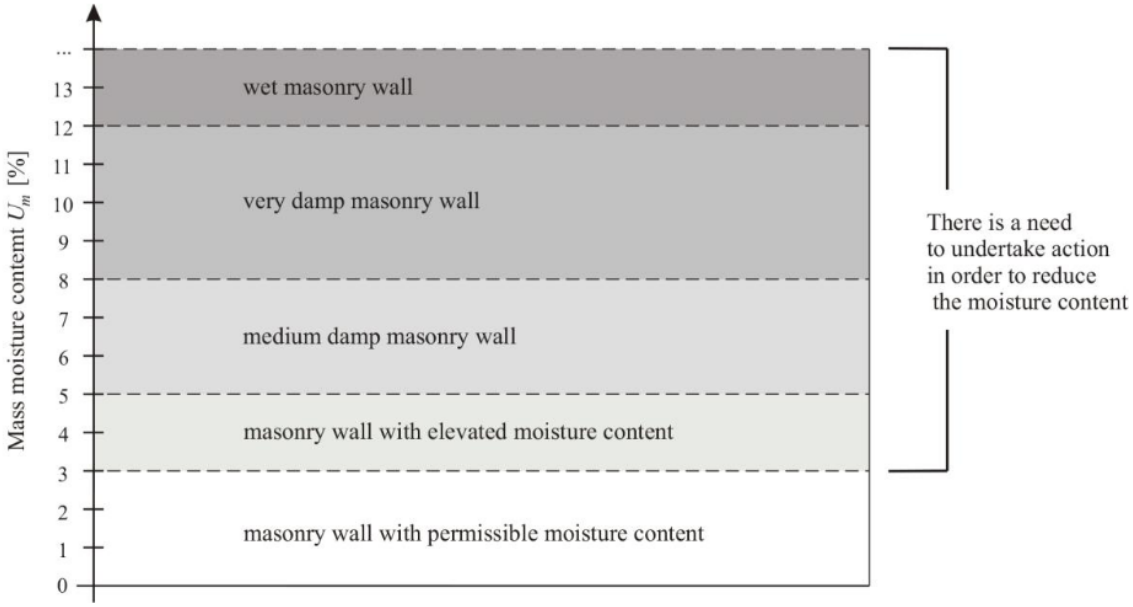


Figure 12 – Classification of the moisture content of brick walls [57]

Figure 13 presents a comparison between different moisture measurement techniques that were used by [59] to assess moisture content in a church in Italy. The authors found that the techniques used to evaluate moisture in a more superficial layer (up to 20 mm deep) were in line with each other, while the data obtained with the techniques used to investigate the masonry more deeply showed great variability.

	IRT	EFD	NMR	Holographic radar	Gravimetric test	Fixed points
Depth	Surface	20 mm	Surface – 5 mm	50 – 200 mm, depending on the chosen frequency	Up to 200 – 300 mm	Up to 200 mm
Feasibility	Portable, noncontact, non invasive	Portable, contact meas., non invasive	Portable, contact meas., non invasive	Portable, contact meas., non invasive	Collection of samples and laboratory meas., invasive	Collection of samples and laboratory meas., invasive
Surface features for the application	Any surface with low specular reflectivity	Flat surface	Any flat surface (dimensions of the investigated area: 20×50 mm^2)	Flat surface	Any surface	Any surface
Best work condition	RH < 70% T > 6 – 7°C	Any condition	Flat surface (affected by iron)	Any condition	Any condition	Any condition

Figure 13 – Comparison of the feasibility of IRT, EFD, NMR, holographic radar, gravimetric test, and fixed points [59]

Regarding the commonly applied measurement methods, [58] highlights that the gravimetric or carbide methods provide only discrete measurements of moisture content, and the lack of a method that determines the spatial distribution of moisture that does not require drilling and sampling is still a challenge. Additionally, the study points out that indirect methods need scale, and their accuracy may depend on chemical composition, density, pore structure, type of salt and its concentration, amongst others.

For the monitoring and inspection of buildings, non-destructive tests are more suitable than destructive ones, as they do not cause damage to the structure and systems, allowing to check the current situation of the building immediately and classifying the degree of deterioration of each part, and, in this way, plan the necessary maintenance and/or repair measures.

Electromagnetic methods are valuable tools for monitoring moisture and its distribution in building components. In addition to moisture-sensitive dielectric properties, building materials mainly reveal electrolytic conductivity, which depends on the moisture content. Therefore, specific electrical conductivity can also be used to estimate moisture. Since various phenomena affect the conductivity of materials, making it difficult to process this value, the potential of conductivity was overlooked for a long time. However, recent advances are promising for the use of this technique for moisture analysis [60]. The electrical resistance measurement can also be used to estimate moisture content indirectly by measuring the resistance to the passage of an electric current between two electrodes in contact with the surface of the material [61].

The moisture detector used by [11] operates according to the principle that the electrical impedance of the material varies proportionally to its moisture content. Hence, the equipment measures this impedance by creating a low-frequency electric field alternating between the electrodes and displays on the screen a value on a relative scale, in percentage, which indicates the dimension of the signal, that is, higher values represent a higher moisture content.

[62] analysed a moisture-related defect in a concrete column structure using non-destructive tests based on electrical resistivity and found that the electrical resistivity was lower at the base, which indicated that there was more moisture in that area. [63] studied in the laboratory the influence of the moisture content on the properties of an industrialised mortar coating. To assess the surface moisture of the coatings, an electrical resistivity hygrometer was used. Tests carried out with wet or saturated coatings showed much lower adhesion and surface resistance than when they are in the air-dried condition.

The moisture meter was also used by [64] in a study of rising damp in masonry walls made of ceramic blocks with different waterproofing solutions for the beams, subfloor positioning and paint age of mortar coatings. Through the dielectric constant of the material, it was possible to verify that flexible waterproofing was more efficient than rigid waterproofing to mitigate moisture transfer from the foundation beam to the wall.

[16] used the electrical resistance measurement test to assess the moisture of the external walls of a historic building. With the data from the moisture meters, moisture maps were made, as shown in Figure 14, thus allowing the identification of the location and size of the affected areas and the corresponding moisture values for these areas. The device provided values on a scale from 0 to 100, by which it was possible to estimate whether the material was wet (blue), intermediate

(yellow) or dry (red). The study emphasises, however, that the results only indicate the level of moisture that the material has and do not traduce the moisture content.

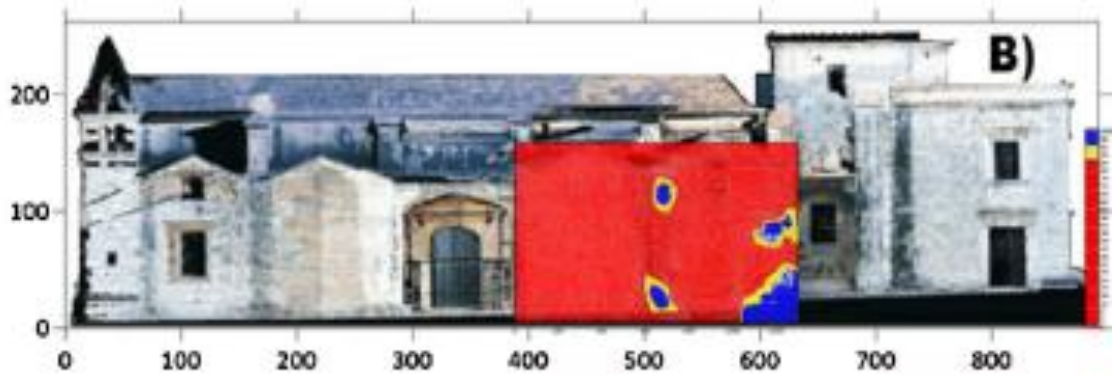


Figure 14 – Historic building façade moisture map [16]

[65] points out the need to pay attention to the results obtained with moisture meters, since dissolved salts can affect the results. Also, according to the authors, sometimes the readings of the percentage of moisture provided by different meters in the same circumstances can differ significantly. Therefore, it is necessary to be careful in the measurements carried out with this technique, evaluating the conditions of the inspected substrate and, also, understanding how to interpret the results provided by the moisture meter used.

2.5. INFRARED THERMOGRAPHY – IRT

2.5.1. PRINCIPLES AND HISTORY

Infrared thermography is a non-destructive testing method that does not require contact with the surface under study and allows evaluating the thermal behaviour of buildings, enabling the identification of potential problems [1].

In the last few decades, this technique was not widespread due to the high cost of equipment and a large number of criteria that must be established to make it possible to identify accurately the anomalies. However, measurements with IRT are gaining more and more popularity in many research areas due to the increasing availability of equipment, the agility of its use, and the large number of applications, which make it a technique with great potential [66], [67].

IRT started being used in 1950 with the first radiometers and evolved in 1960 when the first thermal imagers were created. However, the initial equipment did not measure temperature. From 1970 onwards, temperature measurement was implemented, and, in subsequent years, equipment was improved [68]. This technique is based on the detection of infrared radiation emitted by the surface of bodies, converting this radiation into a thermal image, which portrays the distribution

of the surface temperature of the body, in which each colour expresses a certain temperature range [11].

As real surfaces do not totally absorb incident radiation, nor re-emit it uniformly in all directions [69], it is important to consider the emissivity of the materials for the analysis of surface temperature with this technique [91]. In laboratory tests carried out to evaluate the influence of the emissivity value on the measurements made with infrared thermography in specimens of autoclaved cellular concrete, [55] verified that the choice of the appropriate emissivity value can facilitate the visualization of temperature differences in the thermal image. The choice of the correct emissivity value to be used is essential for quantitative analysis, but it might not be very relevant in the case of qualitative analyses.

Another important factor to be observed in the analysis with IRT is the field of view of the equipment, which determines its total viewing area, depending on the distance to the object under study. Figure 15 depicts the measurement field of view of a thermographic camera, indicating that depending on the size of the object to be measured, it must be located at an ideal measurement distance for the thermal image reading to be accurate.

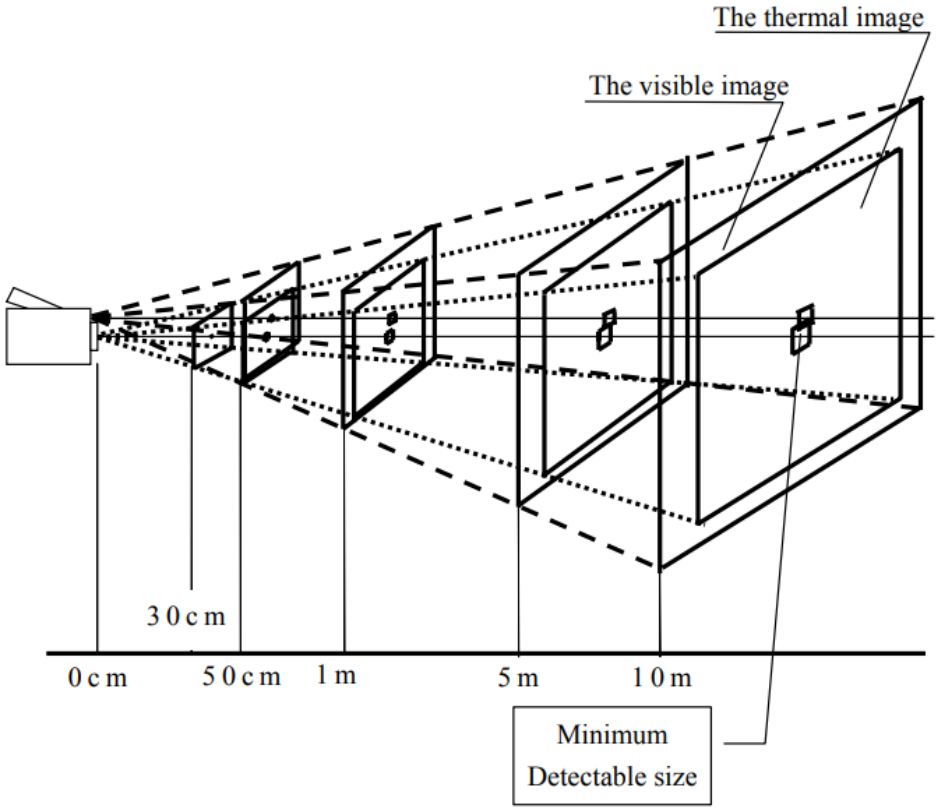


Figure 15 – Measurement field of view [70]

The thermographic inspection methodology consists, firstly, in recognizing and/or measuring the object in situ with the camera and, subsequently, more in-depth analyses can be conducted using

the corresponding software. When using the thermographic camera and software, the image must be corrected, that is, parameters such as emissivity and reflected apparent temperature must be considered [13].

The reflected apparent temperature is related to the radiation emitted by other objects and reflected by the surface under study, which is detected by thermographic cameras. This must be corrected to ensure accurate measurements and the methods presented in [71] can be used.

The standards [72], [73] specify how the detection of thermal irregularities in the envelope of buildings should be carried out. According to these standards, the principle of thermographic inspection comprises the determination of the surface temperature distribution in a part of the building envelope, followed by the verification of areas with abnormal surface temperature distribution and, finally, analysis of the type and extent of the defects.

2.5.2. MEASUREMENT APPROACHES AND RESULTS TREATMENT

Infrared thermography is a technique that can be used with two approaches: passive and active. In the passive approach, the heat flux in the inspected material is generated by the natural boundary conditions [74], which means no energy source is needed for the anomaly to become detectable by the camera. Active thermographic inspection, on the other hand, consists of using an external heat source to stimulate the materials to be inspected and measuring the increase in temperature of the heated surface, according to the supplied flow [10]. This approach is necessary when the defects to be studied are in thermal equilibrium, with all points at room temperature, thus, it is necessary to generate a heat flow so that the structural and thermophysical properties of the material in the damaged area can increase or prevent this flow [75].

According to [76], in active thermography, the behaviour of a building component can be studied with thermal stimulation, which can be applied at intervals, by Pulsed Thermography (PT), or in a more prolonged form, by means of Thermography Continuous Heating (Step Heating Thermography – SHT). The Modulated Thermography technique (Lock-in Thermography – LT) uses periodic heating instead of pulsed heating [75].

In active thermography with external stimulation, optical systems are usually used, such as halogen lamps (periodic heating), or photographic flashes (modelled impulse heating) [45]. In the PT technique, energy is applied to the specimen using pulsed excitation by a rapid burst of thermal energy, and in the LT technique a modulated laser source is used to periodically illuminate the object's surface point by point, and this technique requires longer inspection times [75].

The comparison between the LT and PT techniques was carried out by [77], in the quantitative analysis of defects below the surface of acrylic samples. With the study, it was verified that the LT technique provides quantitative information about the size, depth, and thermal resistance of

the defects. The PT technique is, in principle, faster than the LT. However, it has limitations since to show deeper defects it is necessary to heat more the surface, which can damage the materials. The authors also verified that the techniques allowed the depth of the defect to be defined with a combined standard uncertainty of around 5% for thicknesses of up to 3.6 mm.

Active thermography was used to locate defects in building elements [78]. A 7.2 kW infrared radiator was used for 30 minutes, and, as a result, defects were detected at a depth of up to 22 mm from the surface. The authors identified that to locate defects in building components, it is enough to heat the surface to a temperature of approximately 60° C, with which the test does not lose its non-destructive character. They also verified that the greater temperature contrast between the defective and non-defective sections appear in an interval of 15 to 40 minutes from the beginning of cooling down phase.

The analysis of results obtained with IRT can be carried out qualitatively or quantitatively. Qualitative analyses involve looking for any sign of non-uniformity in the thermal patterns. The heterogeneities are caused by different thermal properties between the region with anomalies and the region without problems. Therefore, the areas with defects will be visualised by the difference of colours in the thermal images [75].

Although some problems can be identified and analysed using qualitative inspections, there are some applications that require using quantitative techniques, such as the analysis used to characterise the different types of existing defects in buildings and assess their severity [69], [79]. In quantitative inspection, specific temperature values are used.

2.5.3. Applications in defect diagnosis

IRT can be used for the detection of abnormalities such as moisture (more detailed discussion on this topic can be found in § 2.5.4), detachments and voids [5], [6], [80], [81], [82], [83], [84], [85], [86], [87]; energy loss and thermal performance [7], [9], [88], [89]; and cracks [8], [90], [91]. In this way, IRT results can be integrated to assess several pathologies.

In the research carried out in situ for the analysis of cracks in coatings, results showed that inspections are more accurate in the afternoon and in the dry season [90]. On the other hand, other authors identified that measurements taken in the morning allow a greater difference in temperature between the region with cracks and the region without cracks, providing clearer thermal images [91]. Figure 16 depicts the thermograms captured in the inspection carried out by [91] at three different times of the day in the analysis of cracks on a façade.

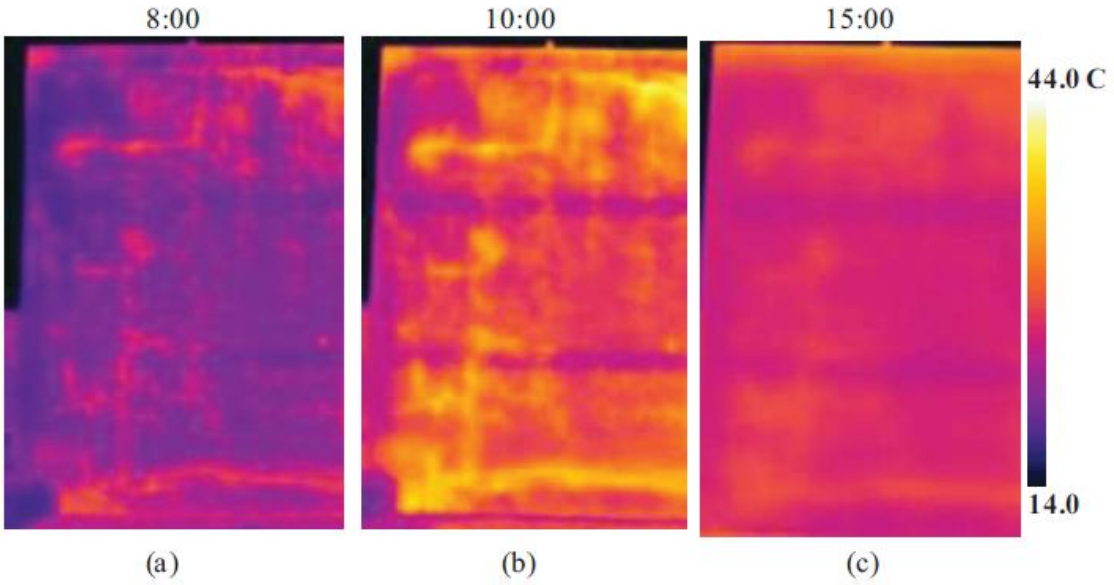


Figure 16 – Thermograms captured to assess cracks in a wall. (a) Inspection 8:00; (b) Inspection 10:00; (c) Inspection 15:00 [91]

Still, [90] identified cracks with a temperature lower than the temperature of the region without defects in measurements taken in the afternoon, while [91] identified higher temperatures in the region of the cracks both in the morning and in the afternoon. [92] found that thermograms taken in the morning show a higher temperature in the regions of cracks, while measurements taken in the afternoon and evening indicate the area with cracks at a lower temperature.

In addition to the time of measurement, it was possible to verify that the temperature difference also depends on other factors, such as the depth of the crack and the level of degradation of the coating. [91] found a temperature difference of up to 9.4°C in linear cracks with higher solar incidence, while, in the late afternoon, when there was no direct solar radiation, this variation was 1°C. In measurements made by [90], the maximum variation found was also 1°C.

Although it is possible to use infrared thermography to analyse cracks, it was found that: (i) not all cracks visually detected were identified in thermal images [90]; (ii) it was only possible to detect microcracks with IRT in materials in tests carried out in the laboratory, but only in one of the samples under study, where the microcracks were also visible to the naked eye [8]; (iii) and in situ analyses are complex and strongly depend on climatic conditions, such as temperature and incident solar radiation [8], [91]. Furthermore, the analysis of the literature on this topic showed great differences on the ideal moment stated by the authors for the measurements to be carried out and also on the period of the day in which the temperature of the crack was higher than the region with no defects. Therefore, for a good diagnosis, it is necessary to understand the physical phenomena related to the use of the technique, as well as the climatic conditions and characteristics of the substrate of the situation under study.

Thermography can also be used to identify and analyse defects in concrete structures, such as voids, delamination, and displacement, especially in areas where access is difficult, considering that, during the day, when the sun and the ambient temperature are heating the material, the surface area above the delamination heats up at a faster rate than surface areas where the concrete is intact, whereas during the night when the ambient temperature is decreasing and the material is cooling, the surface area above the delamination cools at a faster rate than the defect-free area of the concrete.

According to [85] in a research carried out to detect defects in reinforced concrete structures, there are some contradictions regarding the best period of the day for the measurements since some researchers recommend measurements at daytime, from 5 to 9 hours after sunrise, for solar heating [86], while there are also reports that the thermal image produced after 40 minutes of sunrise yielded a much clearer image than that recorded at noon [93]. However, [94] concluded that for this application, the inspection should be carried out during periods of the day or night when solar radiation or its absence produces the fastest heating or cooling of the concrete surface.

[84] carried out tests with a concrete block, in which styrofoam plates were inserted at depths of 25, 51, 76, and 127 mm to evaluate the thermal contrast on the defects, at different moments of the day. Figure 17 portrays the results found, through which it is possible to verify that the maximum contrast occurred with the styrofoam at a depth of 25 mm at approximately 12:00.

As an advantage of analysing delamination in concrete, it is highlighted that thermography provides fast and accurate images and can be applied at distance. However, some limitations are also pointed: dependence on environmental conditions to create thermal gradients in concrete that are necessary to detect inner voids or delaminations [84]; the lack of homogeneity of the concrete due to irregular distribution of the grains and the incorporation of different materials make it difficult to obtain accurate images [87]; the lack of information regarding the depth of the defect; and the fact that the technique must be used in conjunction with other techniques, such as ground penetration radar, to obtain more reliable results [87], [94].

In laboratory analyses carried out to verify the applicability of thermography to identify detachments in coatings, it was found that regions with detachments produce higher temperatures during heating and lower temperatures during cooling, which occurs because the defects create an air layer between the coating and the substrate, increasing the thermal resistance and changing the distribution of temperatures in the areas that present problems [81], [82], [83].

In situ tests [82] showed that heating the surface with direct sunlight allowed adequate identification of hidden defects on the façade, as shown in Figure 18. However, there are restrictions on certain periods of the day. Therefore, it is necessary to plan the inspection and consider the weather conditions. [81] proved to be possible to identify detachments in situ, both on cloudy and sunny days, but on cloudy days, the thermal contrast was lower, and detection was more difficult.

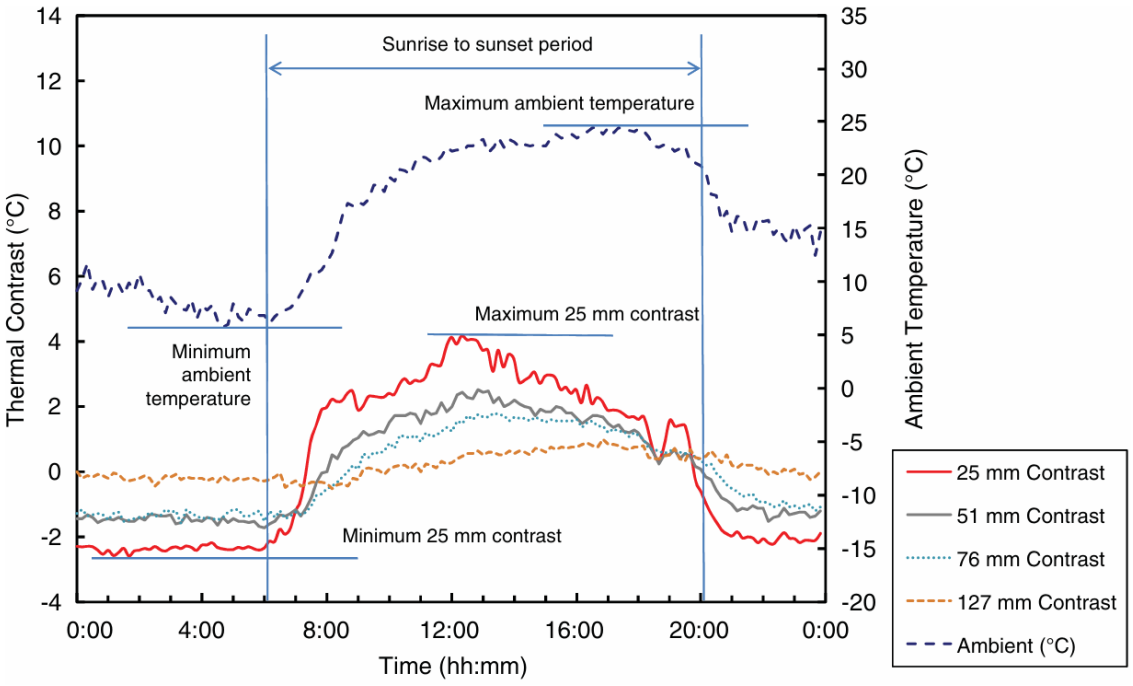


Figure 17 – Thermal contrast in concrete block over a 24-hour period [84]

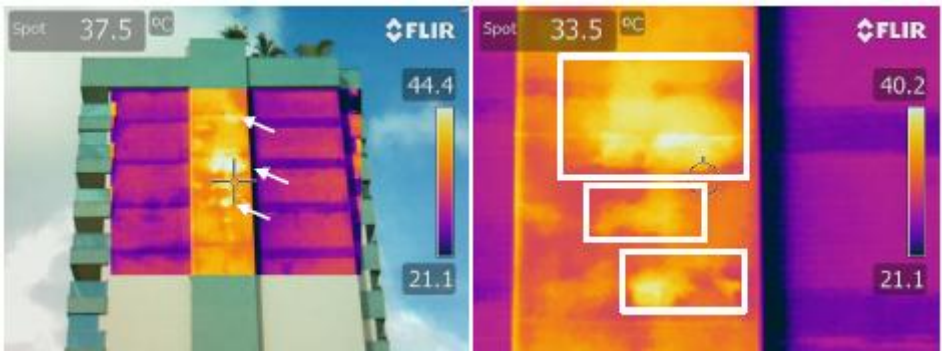


Figure 18 – Use of IRT to identify detachments in façades [82]

Some authors stated that at the beginning of the cooling phase, the regions with detachments undergo an inversion of the thermal contrast, in which they change from a warmer condition to a colder one in relation to the areas without defects. Therefore, there will be a point in time where the temperatures of the two regions will be similar and the defects will be little or not visible in thermograms [14,46,47]. This inversion in the thermal contrast during the heating and cooling phases was also investigated by [95] when assessing surfaces of bonded and unbonded tiles. The authors found that in the state between the cooling and heating phases, almost no thermal difference could be seen, showing the limitation of applying IRT during the equilibrium phase.

The analysis of the published results shows that the change in ambient temperature is a factor of great importance in the thermal contrast between the areas with and without defects. However, thermography can also be affected by parameters such as solar radiation, surface emissivity, wind speed [87], surface colour, infrared reflections from metal or glazed surfaces, distance between

camera and object, camera characteristics, and calibration procedures [96]. Other factors should be considered for the accuracy of the measurements, such as not carrying out inspections in rainy conditions or with wind speeds higher than 25 km/h [60].

Regarding the analysis of the thermal performance, [88] used IRT for the diagnosis of thermal bridges in buildings through inspections at different moments of the day, with and without solar radiation and with and without a heating source. Through this study, it was possible to verify that IRT cannot be used to study zones in thermal equilibrium since it is the heat flux through the building element that allows highlighting the areas with lower thermal resistance.

This technique coupled with the blower door apparatus to depressurise the indoor environment was also used to detect air infiltrations [89]. Simultaneously, the corresponding airflow was measured. The authors verified that the active approach increased the thermal contrast in the areas near the leakage points, proving that IRT combined with the blower door apparatus is an effective method to detect air infiltrations.

[97] used infrared scanning in fourteen residential buildings with different construction characteristics in order to verify whether the technique allows estimating, indirectly, the thermal transmittance of external walls. The authors verified that the technique is not very reliable for buildings with external walls with thermal insulation (cavity and insulating material), while the results were reliable for walls made of solid bricks and mortar.

Recent studies showed that using IRT to estimate the U-value of buildings is possible, as long as there is a minimum of 10°C of temperature differences between indoor and outdoor environments and low wind speed to minimise errors [96], [98], [99].

2.5.4. APPLICATIONS IN MOISTURE ANALYSIS

According to [1], changes in moisture content can be detected by infrared thermography because they are related to changes in surface temperature according to three physical phenomena: evaporative cooling, reduced thermal resistance and high heat storage capacity.

The evaporative flow is a very important measure for analysing the effects of moisture on the degradation of building materials [4]. Evaporation on the surface is an endothermic reaction which induces a decrease in surface temperature [1]. According to [100], if a material has a moisture content higher than the humidity of the surrounding environment, the moisture inside the material will begin to evaporate, and this will lead to a decrease in the surface temperature of the material so that the higher the moisture content, the greater the loss of heat by evaporation and, consequently, there will be a drop in the measured temperature. Therefore, regions with high moisture content, subject to evaporation, will appear in thermal images with a lower temperature than drier regions.

The factors that most influence superficial evaporation are the relative humidity of the air close to the surface, the air temperature, the moisture content of the material, the physicochemical characteristics of the material and the content of soluble salts [4], [10], [101].

In terms of surface degradation, [4] point out that more intense surface evaporation reduces the risk to the material because under saturated conditions, the salts remain in soluble form, and their deposit will occur on the surface, while in lower moisture contents and, consequently, lower evaporation rates, there will be favourable conditions for crystallisation of salts inside the material.

The specific heat and thermal conductivity of water are higher than those of ordinary building materials. Therefore, when water is present in these materials, their density, specific heat, and thermal conductivity will increase [10]. Since thermal resistance is inversely proportional to thermal conductivity, the thermal resistance of wet materials is lower than that of dry materials. So, as the heat flow through these wet materials is greater, a heterogeneous thermal pattern will be created, with different surface temperatures between the dry and wet region [1].

When the surface evaporation is restricted due to the presence of a more vapour impermeable superficial layer, the temperature variations on the surface will be caused by heat storage capacity of the wet material or by reduced thermal resistance of the moist region [102].

The principle of high heat storage capacity is related to the fact that a wet material will respond more slowly to a change in air temperature than a dry material. Based on this principle, during surface heating, dry areas will heat up faster than wet areas and with surface cooling, dry areas will also cool faster [1]. Therefore, the high heat storage capacity of the wet material will create different thermal patterns at the surface under heating or cooling phases, which are detected by infrared thermography.

Although IRT can be used for moisture analysis in buildings, its application requires more studies because wet areas can be colder than dry ones, but they can also be warmer [10]. The temperature of the wet areas will be lower than the temperature of the dry areas due to superficial evaporation. When there is surface heating, the temperature of the wet areas will also be lower during heating due to the reduced thermal resistance and the high heat storage capacity of the wet material. However, when cooling occurs, the temperature of the wet areas will be higher due to the high thermal capacity of water compared to dry materials [4].

Still, difficulties in applying IRT also occur due to the complex and variable relationship between evaporative flow and surface temperature [4] and the strong influence of radiation from the surroundings and the optical properties of the inspected surface [51].

Several studies in the past years have highlighted the need to conduct studies to analyse the influence of environmental conditions [10] in order to find a direct correlation between the variables and obtain a valid measure to assess evaporative flow through IRT. Currently, despite the numerous advances in the use of thermography for moisture analysis, establishing a criterion for

quantitative analyses is still an obscure item. The criteria that can be found in the literature are suitable for specific cases and cannot be generalised [1], as also highlighted by [102], when pointed out that IRT applied to assess moisture is not yet fully standardised.

Thermal images for moisture analysis are very useful, as they portray the spatial distribution of wet areas [4]. A homogeneous dry wall without defects will present an almost homogeneous thermal image, but if it is affected by moisture, the thermogram will portray the moist areas with a different thermal pattern [13]. The authors in the study carried out by [4] points out, however, that the technique only investigates the existence of water in a thin surface layer.

Both active and passive infrared thermography can be used to assess moisture. With the passive approach, a large surface can be mapped, performing an early diagnosis in areas with greater risks of degradation. However, it has the disadvantage of depending on environmental conditions and microclimate [10].

Generally, the detection of defects in dynamic thermal regimes seems to be more appropriate than in the steady state, and the detection of defects in materials can be improved by a thermal stimulus, either by solar irradiation, by air flow, or by radiation from an artificial source. One way to improve moisture detection, for example, is to increase water evaporation from the surface of the material, by increasing the air flow, exposing the material to continuously modulated ventilation [4], [79]. Table 5, presented by [10], depicts the characteristics of using active and passive thermography for moisture analysis.

Table 5 – Characteristics of the use of active and passive thermography for moisture analysis [10]

	Active Method (Detection of major inertia areas)	Passive Method (Detection of surface interested by evaporative flux)
Advantages	Direct measurement of moisture content (in laboratory samples)	Direct relationship between evaporative flow and surface damage. No heating required. Applicable on large surfaces
Limitations	Difficulty in obtaining high and homogeneous heating. Reference method: measurements are relative to a dry area	Dependence on the environment and microclimatic conditions
Dependence on soluble salts	Yes; Soluble salts can change surface absorption	Yes; evaporative flow decreases where soluble salts are present
Speed of the test	Fast measurements in the field, quantitative results require a post-processing phase	Fast measurements in the field, quantitative results require a post-processing phase
Sensibility to the moisture content	Low-medium: 10% for porous materials	Low-medium: 10% for porous materials
Dependence on environmental conditions	No	Yes
Cost	Low	Low

2.5.4.1. Laboratory tests

In the works carried out by [11] and [13], the results of thermography were compared with the ones obtained with a surface moisture meter and, in the case of [12], a RH sensor placed inside the masonry was used for comparison. In [103] and [55] the water absorption during the test was also monitored, by weighing the specimens. In [12], water absorption was not monitored during the humidification process, however, after the stabilization of the wet front, the wall was demolished for weighing and verification of the actual moisture content in different location in the masonry.

The maximum temperature difference (ΔT) between the dry and moist regions throughout the humidification or drying strongly depends on the properties of the material tested and the environmental conditions, since high maximum values of ΔT were found, above 10°C, in the case of porous stones [103] and maximum ΔT values slightly higher than 1°C were found for limestone walls [11], [104], lightweight concrete blocks [104], and concrete blocks [13]. Intermediate values of maximum ΔT were found by [12], between 2.2°C and 2.3°C, in the case of brick walls and 4°C, in the case of prismatic specimens of autoclaved cellular concrete [55]. [12] concluded that thermography results quickly and accurately portray the areas of the wall with high moisture content and [103] highlighted that IRT is an effective tool for analysing the behaviour of water percolation in materials untreated and treated with various consolidants.

The porosity and permeability of the materials were not presented in all these studies. Hence, there is no way to accurately assess the influence of these properties on the ΔT. However, it appears that there is a trend for the more porous materials to present a ΔT higher than the ΔT of materials with lower porosity. This situation can be explained by the fact that the moisture content will be higher in these materials and, therefore, there will be greater surface evaporation in the moist region, sharply decreasing the temperature in these areas.

[105] explored active IRT for estimating soil moisture content and found a strong correlation between soil surface temperature and moisture levels, validating thermography as a non-invasive tool for assessing moisture.

Other relevant contributions of previous studies on moisture analysis through IRT can also be highlighted:

- The comparison of the thermal images with the data from the moisture meter showed that the thermography results were not completely in line with the results obtained by the moisture meter since this device detects moisture at deeper levels than thermography. Therefore, it was verified that, at the end of the test, in the thermal images the maximum level of moisture obtained with IRT was much lower than the level indicated by the moisture meter. This can be explained by the evaporation at the surface being more preponderant than the capillarity, which allows stabilization of the level of superficial moisture,

while inside the specimen the capillarity is the main force and the moisture level continues to rise [11];

- In thermal images, an intermediate moisture range, not visible to the human eye, can be identified [11], [13];
- The correlation between the maximum visible height of the wet front, the ΔT and the maximum height detected by the moisture meter showed that there is not a good linear correlation between the variables, especially when comparing the ΔT and the levels of the wet front visually detectable and assessed by the moisture meter. Still, the authors found that the complexity of the phenomenon is confirmed by the best approximation found with a polynomial correlation, highlighting the need for further studies under controlled environmental conditions [11].

Despite obtaining promising results for the use of IRT for moisture analysis in the laboratory, some needs for improvements are printed in [104]:

i. Separate the cooling effect due to the presence of water from the adjustment of the surface temperature to room temperature.
ii. Analyse different moisture contents to understand their influence on the results.
iii. Correlate the results with the properties of the materials.
iv. Develop a way to model this phenomenon to correlate the decrease in surface temperature with moisture evaporation.

2.5.4.2. In situ tests

By analysing the available literature, it appears that all studies implemented the passive approach to assess moisture in situ using IRT, that is, no artificial source of heat is used. However, in some situations, part of the monitoring was carried out during the period of solar incidence [14], [15], which means that a passive approach with a natural source of heat was used.

Regarding the maximum ΔT detected between dry and moist regions, it is noteworthy that in the measurements conducted by [14] and by [15] in the rainy season, the maximum ΔT of 3.9°C was found at 10:00 am and 2.4°C at 2:00 pm. The difference in the amplitude of the thermal gradient in the two situations may be due to moisture content and the environmental conditions (temperature, relative humidity, wind, and solar radiation).

According to [79], the observation of wet areas in thermal images can be improved by heating the surface due to the high heat storage capacity of water and the fact that high moisture contents increase the thermal conductivity. However, attention must be paid to the balance of different

effects acting at the same time. Therefore, cases with incident solar radiation are more complex and require greater attention since new variables must be considered in the analysis.

The measurements carried out by [1] also took place after a rainy week, but the authors found a maximum ΔT lower than 1°C. The small amplitude of ΔT may be due to the moisture content of the substrate, the temperature and relative humidity of the air, and the lack of sunlight on the wall under study.

In the comparison of measurements carried out during sunny and rainy periods [15] printed that in the sunny period, the ΔT was only 1.4°C and 1°C lower than in the same region in the rainy period. According to the authors, this difference may have occurred due to the drying provided by the sunny period, which decreases the moisture content. However, it was not possible to verify if the measurements were taken in the beginning of the drying process or after a while, which will influence the thermal gradient.

[73] also compared the results of the measurements performed with the thermographic camera positioned 3 m and 4 m from the wall under study, but no relevant differences were observed in the measurements.

[1], [11], [16] compared the results of thermography with a moisture meter. The thermal images and the moisture maps generated based on the measurements with the moisture meter were not in complete agreement since thermography only detects superficial evaporation, while the meter detects moisture at greater depths. In [1], the level of capillary rise identified in the thermal image was lower than the one obtained with the moisture detector, as depicted in Figure 19. As a result, [16] point out that, to reduce the risk of error and to provide a more detailed diagnosis, the two techniques should be combined.

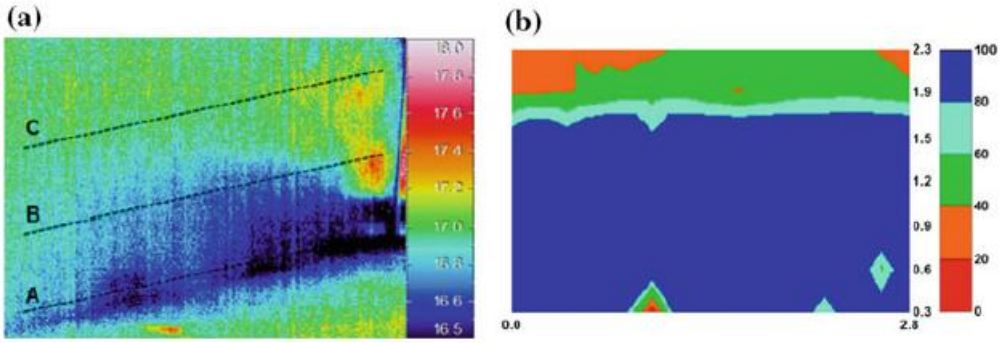


Figure 19 – External wall of a basement of a residential building: a) thermal image b) moisture meter results [1]

The results presented by [100], which used a thermographic camera with lower resolution than the ones used in other studies, showed that even with equipment with lower resolution it is

possible to detect moisture, as temperature differences between the wet and the dry areas were also identified.

[4], [10] also carried out in situ tests with thermography for moisture analysis in conditions of high relative humidity, noting that this condition is critical for inspections due to the lower effects of evaporative cooling. [4] verified that thermograms obtained on the internal side of external walls did not provide useful information on surface water distribution. However, in inspections carried out on the external side, which was never directly exposed to solar radiation, colder temperatures were observed in areas closer to the ground. Therefore, the authors concluded that, in general, conditions of high humidity and low ventilation make the evaporation rate very low, so these conditions are not suitable for passive detection of evaporative flow.

A study carried out by [106] assessed the drying process of external walls for 6 days using thermography and a moisture detector. The authors concluded that the thermal images obtained were not very useful regarding the drying process, due to the following factors that affected the results: dirt on the surface; the different thermal conductivity of interior wall layers; and difficulties in isolating the effect of solar radiation, wind, and air temperature. [107] explored the applicability of IRT for diagnosing historical buildings and highlighted the difficulty of measuring the water content only by thermography because: the presence of plaster detachment and stains may affect the results; the winter heating active inside the building can prevent a correct moisture detection; the heating tends to dry the wall surface, masking the moisture map in case of low to medium water content; and existence thermal bridges may cause false alarms.

[108] assessed the effectiveness of IRT for detecting capillary moisture in buildings and pointed that IRT detected areas affected by humidity. However, it did not provide information about the problem severity, and it presented limitations as it is influenced by environmental conditions.

The results obtained from in situ tests proved that the thermal amplitude between the dry and moist regions is influenced by the environmental conditions, the properties of the materials, and the degradation status of the substrate. Regarding in situ measurements, [51] point out that although solar radiation or the wind make the surface temperature highly variable, thermal patterns can be used as an indication of moisture.

The studies pointed to several factors affecting the use of IRT for moisture analysis. However, they also presented that IRT has a great feasibility for diagnosing defects in buildings and if environmental conditions and other external factors are properly investigated, IRT can be a valuable tool for moisture analysis.

2.6. MACHINE LEARNING AND AUTOMATION FOR MOISTURE ANALYSIS

2.6.1. PRINCIPLES

Machine learning (ML) is a part of the field of artificial intelligence (AI) that enables learning the relationships between quantities of interest based on data, intending to obtain information on how a system works and make predictions for unobserved quantities [109]. The choice of the most adequate machine learning model for each problem depends on the nature of the data and the information that is to be predicted. If the training data used to feed the algorithm is labelled with the desired solution, the learning process can be supervised, and models such as K-Nearest Neighbour, Linear Regression (LR), Logistic Regression, Support Vector Machine (SVMs), Decision Tree, Random Forest, and Neural Network (NN) can be used. On the other hand, if no labels are set in the training data, and the objective is to discover structures, patterns, or even anomalies without knowing the answer, the learning process is unsupervised, such as in clustering algorithms [110].

Neural Networks exists since the 1950s. However, it was only in the last years that this technique presented remarkable progress due to rise in available training data, increased computational capacity, and improved methods that allow training deep neural networks [109]. In this context, the term deep stands for the idea of successive layers of representations [111].

Numerous architectures can be used in NN applied to building diagnosis, such as Multilayer Perceptrons (MLPs), Convolutional Neural Networks (CNN) [23], [98], [112], [113], [114], [115], [116], [117], [118], and Recurrent Neural Networks (RNN) of the Long Short-Term Memory (LSTM) type [119], [120]. CNNs are a successful deep-learning model for image classification and other computer vision applications. The model takes as input tensors of a three-dimensional shape, with the image height, width, and channels [111], and enables achieving feature extraction and learning through the multiple arrays of data [121]. In the convolutional layer, instead of having a large and dense linear layer with a connection from every input to every output, many small linear layers are used in every input position [122]. If the task to be performed is related to time-series input data or if sequential inputs are relevant, it is usually recommended to use RNNs in the model [111], [121], [122]. This model processes the input data of each element at a time and saves all the memory from the history for every single unit of the sequence [111].

The MLPs aim to define a function by learning the value of the parameters that result in the best approximation function. A typical MLP usually has a single input layer, a single output layer, and multiple hidden layers. In each layer, there are neurons connected to neurons in the anterior and posterior layers. Each neuron receives the weighted outputs of other neurons of a previous layer, then a bias is added. After that, an activation function is applied to obtain the output of this neuron. Equation (29) shows the output of a neuron [123]:

$$\hat{y} = f((\sum_{i=1}^{n} W_i\, x_i) + \mathrm{b}) \tag{29}$$

Where x_i is the i_{th} input of the neuron, W_i is the weight of the i_{th} input, b is the bias of the neuron, and f is the activation function [123], which is a nonlinear transformation applied to data in each neuron [109]. One common activation function used for regression problems is the rectified linear unit (ReLU), which makes easier the training of models because it reduces the problems with vanishing gradients [109].

2.6.2. METAMODELS

In some civil engineering applications, it might be interesting to replace finite element models (FEM) that are time-consuming tools for regression models built from a set of simulated situations, which are known as metamodels [109]. In the hygrothermal simulations, specifically, performing these simulations of building components may be computationally inhibitive, with multiple uncertain input parameters, so the metamodel can be useful by replacing the hygrothermal model and representing the original model with a strongly reduced calculation time [124].

Several studies were found in the literature where computational simulation tools were combined with machine learning models to predict the behaviour of building materials. The studies were applied to predict the hygrothermal behaviour of walls [124], to analyse heat conduction in solid materials [125], and to predict mould growth risk [126]. The results showed that neural networks could capture accurately the complex patterns of the hygrothermal response [124]. Additionally, a proper selection of training datasets can enable effective prediction of the hygrothermal performance of wall assemblies [126].

Therefore, data generated by simulation software tools is a widely considered data source to predict building performance [127] and can present good results. In the case of IRT, the relevant gap for quantitative moisture analysis can be addressed with the use of simulation and experimental data and ML models to predict the moisture content of materials based on the surface temperature and other input data, such as the properties of the building material and environmental conditions.

The hybrid models, which combines the use of simulation and experimental data for training and testing machine learning models, offers a promising approach that can significantly improve the prediction of building hygrothermal behaviour, especially in complex systems. Transfer learning, an important technique for this combination, involves pre-training a machine learning model on simulated data to learn core relationships and then fine-tuning it with a small amount of real experimental data. This method has been shown to be effective in overcoming the challenge of sparse real data, as simulations generally provide a good approximation of reality, although with some offset between simulated and real outcomes [128], [129].

Using this hybrid approach, simulations can identify regularities and patterns that are not always visible in raw experimental data. When the model is trained using both real and simulated data, it

becomes more robust, and the predictions become more accurate, effectively bridging the gap between the limited data available and the need for precise moisture analysis in building materials [128], [129].

2.6.3. APPLICATIONS FOR DEFECT DETECTION

In the last decade, the use of machine learning techniques to assess the performance of buildings has grown considerably [130]. The algorithms developed include applications regarding image processing [121], in which deep learning is combined with computer vision to identify defects or characteristics in images, and the use of models to improve building assessment procedures, developed with the results from non-destructive techniques and computational simulation [131]. Despite the increase in publications, there are still barriers in this field, such as limited data access, the quality of datasets, and the processing time [121], [132]. In addition, most studies are still at the experimental or testing stage, and limited number of studies have implemented machine and deep learning strategies in actual buildings [130].

In the field of cultural heritage and structural health monitoring, machine learning models have been applied in the detection of several defects in building materials, such as cracks [112], [133], [134], [135], [136], detachments [137], voids under the surface [23], moisture [20], [138], [139], [140], [141], [142], [143], and also to assess the energy efficiency of buildings [127], [130], [131], [144]. Regarding the assessment of building performance, machine learning models are also being applied in the prediction of mould growth risk [126], [145], indoor airflow [123], [146], and hygrothermal behaviour [119], [124].

[117] reviewed the application of AI techniques in inspecting cultural heritage structures. The deep learning techniques identified in the study for the detection of defects in buildings with CNN were: YOLOv5, faster R-CNN, Mask R-CNN, Inception-ResNet-v2, among others.

Table 6 contains the results from the ML models applied to moisture analysis. The models used to identify the moisture content were mainly NNs of MLP type. In some situations, these models were compared with other ML models, such as linear regression least squares (LR-LS), linear regression support vector machine (LR – SVM) [138], least-angle regression (LARS), and elastic net (ENet) [147]. The studies used as datasets the results from non-destructive techniques, such as dielectric, microwave, and electrical impedance tomography methods carried out in laboratory and in historic buildings. The results pointed out that NNs of MLP type are better than other machine learning algorithms, such as linear regression. However, for some applications, LSTM and ENet might present better results. The linear determination coefficient between the values predicted by the NNs and the actual values of moisture were higher than 0,98 in most situations.

Additionally, moisture detection was also carried out using IRT and image processing techniques in an automatic way [20], [148]. The procedure consisted of raising the difference in the value of

the pixel between moist areas and unaltered surroundings (thresholding technique); removing noise (bilateral filtering); and then implementing filters to detect the contours of moisture areas [20], [148]. Other authors [115], [116] also applied deep learning to IRT images to automate the identification of moisture. However, in all these situations found in the literature, the moisture content was never assessed.

As for the thermal images obtained with IRT, the development of data processing algorithms is of fundamental importance to mitigate the image noise and enable the extraction of accurate information that highlights the existing defects [23]. Algorithms can be based on both thermal parameters and physical heat transfer principles (such as Pixel Algorithm for Time-Derivative of Temperature (PATDT), Partial Least Square Thermography (PLST), Pulse Phase Thermography (PPT) and Thermography Signal Reconstruction (TSR)), as well as mathematical and analytical procedures (such as Principal Component Thermography (PCT) and Dynamic Thermal Tomography (DTT)) [23]. However, despite the good results obtained with these algorithms, not all of them can be automated. The possibility of conducting inspections online and with automated data interpretation is of great interest, as it eliminates subjectivity and dependence on the operator's experience [23], [149].

1 Table 6 – ML models applied to moisture analysis in buildings

Reference/Author	Type of ML model	Objective	Dataset	Results	Main conclusions
[150]	• NN - MLP	Identify the moisture content in saline brick walls.	Based on the results of NDT (dielectric and microwave) and the gravimetric method carried out in the laboratory.	$R_{testing}$ = 0.9871 $R_{validation}$ = 0.9864	Reliable assessment, but with the need for validation on historic buildings.
[151],	• NN – MLP	Identify the moisture content in saline brick walls.	Based on the results of NDT (dielectric and microwave) and gravimetric method carried out in 5 historic buildings.	$R_{testing}$ = 0.928 $R_{experimental}$ = 0.906	Positive results but still requires verification on other historic buildings.
[138],	• LR - LS • LR - SVM • NN - MLP	Identify the moisture content in a wall.	Based on the results of NDT (electrical impedance tomography – EIT, dielectric, and microwave) and the gravimetric method carried out in historic buildings.	PE_{LR-LS} = 34% PE_{LR-SVM} =31% PE_{NN} =14% *PE = percentage error	NN performed better. The selection of the ML model considerably impacts the quality of the results.
[120],	• NN – LSTM • NN - MLP	Identify the moisture content in a wall.	Based on the results of simulation data for training and data from NDT (IRT, Dielectric, and microwave) in a historic cathedral to obtain validation measurements.	$RIE_{NN-LSTM}$ = 0.244 RIE_{NN-MLP} = 0.299 *RIE = relative image error	The LSTM method performed better in all cases and had less reconstruction time than MLP.

[147],	• LARS • ENet • NN - MLP	Compare the efficiency of machine learning methods in applications related to tomographic moisture detection in walls.	Based on the results of simulation data and NDT (electrical impedance tomography – EIT, dielectric, and microwave) and the gravimetric method carried out in historic buildings.	RIE_{LARS} = 0.373 RIE_{EN} = 0.270 RIE_{NN} = 0.401	The best results were obtained with Elastic Net.
[141],	• NN - MLP	Identify the moisture content in a wall.	Based on the results of NDT (electrical tomography, dielectric, and microwave) and gravimetric method carried out in 10 historic buildings.	Whole dataset: $R_{testing}$ = 0.771 $R_{experimental}$ = 0.88 Set of data covering the moisture content from 8% upwards: $R_{testing}$ = 0.918 $R_{experimental}$ = 0.878	The algorithms may be helpful in construction practice for the neural non-destructive assessment of moisture content of brick walls in other historic buildings. Further studies should utilise advanced NN models.

3

EXPERIMENTAL ANALYSIS OF THE THERMAL GRADIENT AND MOISTURE CONTENT

3.1 INITIAL REMARKS

The experimental campaign was carried out at the Laboratory of Building Physics of the Faculty of Engineering of the University of Porto and was divided into two steps. The first consisted of preliminary tests under free-running laboratory conditions, performed to monitor the drying process of samples of five different materials with IRT, the gravimetric method, and the surface moisture meter. This step allows a better understanding of the thermal pattern obtained with IRT for different materials and provides valuable information for the laboratory tests carried out in the second stage, under controlled conditions.

The second step consisted of an experimental campaign in three controlled environmental conditions, inside climatic chambers, to monitor the drying process with IRT and the gravimetric method. In this step, additional tests were performed to characterise the material. These tests under controlled conditions were necessary to improve the performance of machine learning algorithms initially trained with simulation data.

This Chapter presents the materials and methods and the results for both steps.

3.2 TESTS UNDER FREE-RUNNING CONDITIONS

3.2.1 MATERIALS AND METHODS

3.2.1.1 Framework

Figure 20 presents the procedures adopted to perform the preliminary experimental campaign to monitor the drying process of specimens of five materials. Due to the test layout, the tests with clay brick and limestone were carried out prior to the tests with granite, mortar, and concrete. In

the latest, besides IRT and the gravimetric method, the surface moisture meter was also used to assess the moisture content in the building materials.

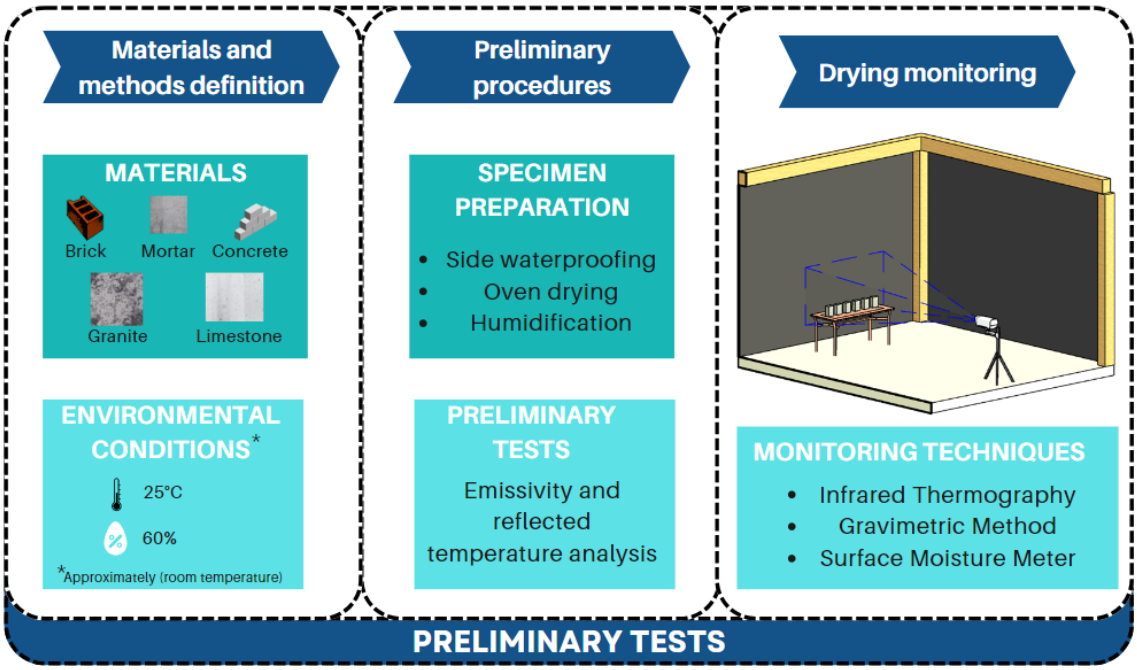


Figure 20 – Workflow of the laboratory tests under free-running conditions

3.2.1.2 Materials

The materials chosen for the analysis were solid clay brick, mortar, concrete, limestone and granite. Four specimens for each material were assessed, with the average dimensions shown in Table 7.

Table 7 – Dimension of the specimens

	Clay brick	Limestone	Granite	Mortar	Concrete
Dimension [cmxcmxcm]	20.5x9.5x6.4	15.0x15.0x2.0	20.0x10.0x5.0	20.0x20.0x4.2	21.1x21.1x2.5

All specimens were initially waterproofed on the lateral sides to prevent evaporation from these surfaces during the drying phase. After this procedure, the specimens were dried in the oven until the mass difference between two 24-hour subsequent weightings was less than 0.1% of the total mass [49]. For each material, three of the four specimens were then humidified by partial immersion in water until different moisture contents were achieved, and the remaining one was maintained dry during the monitoring phase. Figure 21 and Figure 22 portray the clay brick and limestone specimens the humidification process, respectively.

The three wet specimens for each material were kept partially immersed in water until three different water contents were reached: (i) one specimen was fully saturated (HMC) until mass stabilisation was guaranteed, (ii) one specimen had intermediate moisture content (IMC)

(approximately 50-70% of the moisture content of the saturated specimen), and (iii) one specimen had low moisture content (LMC) (approximately 30-50% of the moisture content of the saturated specimen).



Figure 21 – Clay brick specimens partially immersed in water



Figure 22 – Limestone specimens partially immersed in water

After the humidification, the specimens were fully wrapped with plastic film and stored until inner moisture homogenisation. The fourth specimen was left at room temperature and relative humidity until mass stabilisation to ensure the hygroscopic equilibrium. Table 8 contains the moisture content after the humidification of each specimen, corresponding to the beginning of the drying process. One can state that the higher value of moisture content varies considerably for different materials, mainly due to distinct hygric properties. This is also shown by the value of the moisture content of the specimens that were not humidified (HYEQ - hygroscopic equilibrium), as only clay brick, the material with a clear hygroscopic behaviour, presents a value above 0.0%. The calculation of the initial moisture content in percentage of the specimen was performed using equation (28).

Table 8 – Initial moisture content of the specimens

Material	Specimen	Moisture content [kg/m³]	Moisture content [kg/kg x 100]
Clay brick	HMC[1]	337.0	21.3
	IMC[1]	201.5	12.5
	LMC[1]	108.4	6.9
	HYEQ[2]	7.5	0.5
Limestone	HMC[1]	155.6	7.1
	IMC[1]	112.7	5.3
	LMC[1]	50.2	2.3
	HYEQ[2]	0.22	0.0
Granite	HMC[1]	7.30	0.29
	IMC[1]	5.93	0.27
	LMC[1]	4.84	0.22
	HYEQ[2]	0.52	0.0
Mortar	HMC[1]	211.50	13.6
	IMC[1]	141.75	9.1
	LMC[1]	96.19	6.4
	HYEQ[2]	0.00	0.0
Concrete	HMC[1]	117.28	5.0
	IMC[1]	81.45	3.5
	LMC[1]	34.56	1.5
	HYEQ[2]	0.00	0.0

[1]HMC: High Moisture Content (Saturated), IMC: Intermediate Moisture Content, LMC: Low Moisture Content
[2]HYEQ: Hygroscopic equilibrium – sample not humidified was left at room temperature and relative humidity until mass stabilisation

3.2.1.3 Equipment

The infrared camera and the surface moisture meter used in the preliminary laboratory tests were the following:

- Infrared camera: Thermo Tracer TH9100MR from NEC Avio Infrared Technologies Co., Ltd. The main specifications are presented in Table 9 [70].
- Surface moisture meter: Protimeter MMS2. The device can be used to take relative moisture readings, ranging from 60 to 999. Lower values correspond to lower moisture contents. The LCD screen indicates whether the material is in a dry, at risk or wet condition, according to
- Table 10 [152].

Table 9 – Infrared Camera Specifications - Thermo Tracer TH9100MR

Parameter	Value / Interval
Infrared spectral range	8 µm to 14 µm
Sensitivity setup	0.1~20°C / 0.2~30°C
Infrared resolution	320 x 240 (76800 pixels)
Focus range	30 cm to ∞
Field of view	21.7° H x 16.4° V

Table 10 – Aquant indicators [152]

Aquant	Indication	Progress Bar
<60	-	-
>60 but <170	DRY	Green
>170 but <200	RISK	Yellow
>200 but <999	WET	Red
>999	WET	Red

3.2.1.4 Preliminary measurements and procedures

The emissivity of the specimens was measured with an emissometer from the Devices & Services Company, model AE1, whose specifications are fully described in [153]. The procedure for the measurement of the emissivity was performed in accordance with the ASTM C1371 standard [154] and with the guidelines provided by the equipment manufacturer [153]. Figure 23, Figure 24, and Figure 25 show parts of the test to measure the emissivity of the specimens.

The emissivity measurements were performed using a detector, a heat sink, a voltmeter to digitally read the emissivity, a high emittance standard, a low emittance standard, and a fan. After calibrating the equipment, the detector was put on the flat surface of the mortar sample, and several measurements were carried out until the stabilization of the emissivity value.

The emissivity values measured for the materials under study are shown in Table 11. All the values are in line with the ones found in the literature, confirming the representativity of the specimens.

Table 11 – Emissivity values of the materials analysed

Material	Emissivity
Brick	0.89
Limestone	0.87
Granite	0.90
Mortar	0.92
Concrete	0.92

The pore size distribution of the materials was also assessed with Mercury Intrusion Porosimetry (MIP), which is a technique that can be used to characterise the porous structure of building materials. This technique involves subjecting a previously dried sample to increasing pressures of mercury (non-wetting liquid), which progressively penetrates the material [155]. The MIP

provides several key parameters that are important for understanding the pore structure of a material, such as pore size distribution, total pore volume, porosity, bulk density, and average pore diameter.

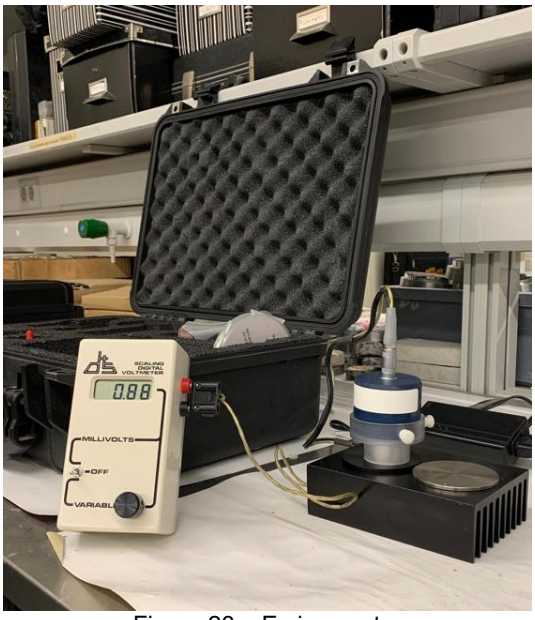


Figure 23 – Emissometer

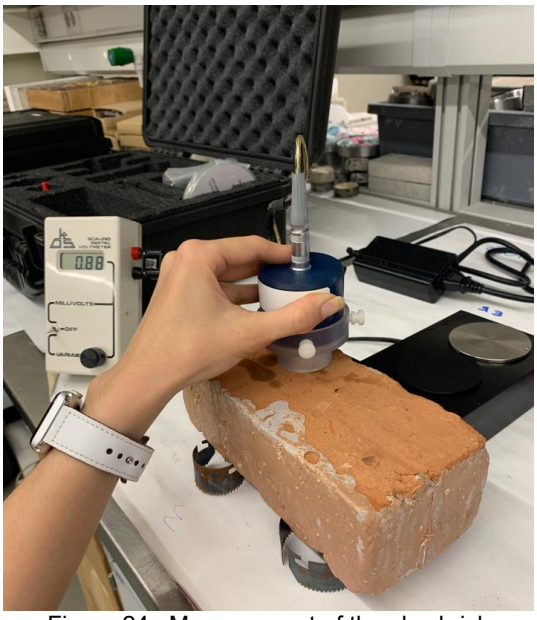


Figure 24 –Measurement of the clay brick emissivity


Figure 25 – Preparation of granite for measuring the emissivity

The results of the MIP tests shown in Figure 26 and the properties displayed in Table 12 also highlight the different characteristics of the materials. Clay brick and mortar present the highest porosity, in contrast to granite. Concrete and granite present a high amount of very small pores, while clay brick and mortar present bigger ones. Limestone presents most of the pores with an

intermediate size, and its curve resembles a normal distribution, with a minimal variation in the pore size.

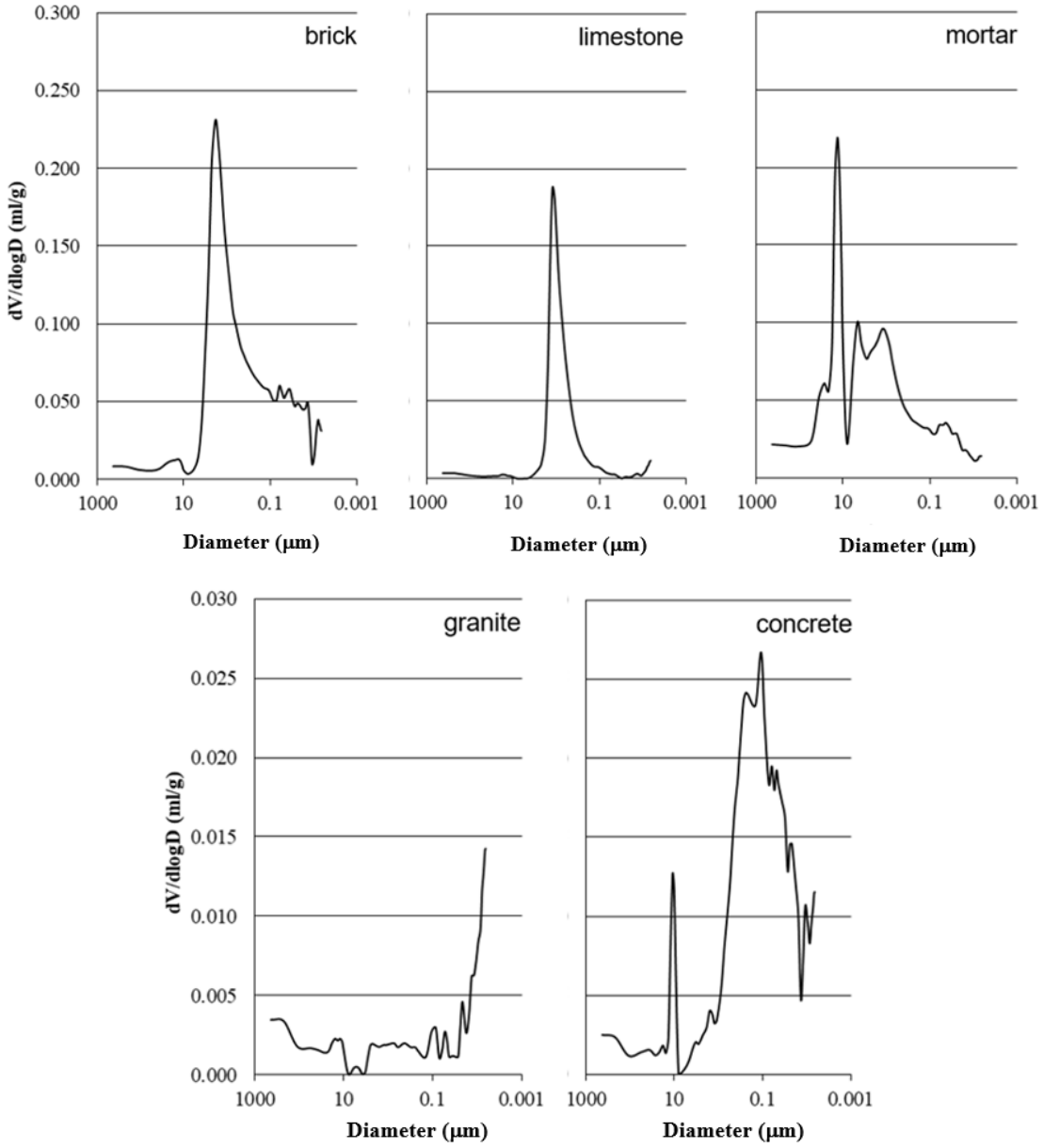


Figure 26 – MIP results for the materials under study

Table 12 – Properties of the materials used in the laboratory tests

Material	Bulk density [g/cm³]	Average pore diameter [4V/A (µm)]	Skeletal density [g/cm³]	Porosity [%]
Clay brick	1.595	0.091	2.629	39.33
Limestone	2.191	0.232	2.707	19.07
Granite	2.615	0.026	2.693	2.92
Mortar	1.567	0.177	2.513	37.57
Concrete	2.336	0.051	2.581	9.52

After carrying out the preliminary measurements, the precision balance that would be used for weighing the specimens for the gravimetric method was calibrated, as shown in Figure 27. Then, the infrared camera was positioned at the test site and all the required calibration procedures were conducted:

- Calculation of reflected apparent temperature according to ASTM E1862 [71] (Figure 28).
- Calibration procedure for the infrared camera, following the recommendations of the manufacturer.



Figure 27 – Calibration of the precision balance used in the tests


Figure 28 – Procedure to calculate the reflected apparent temperature

3.2.1.5 Environmental conditions

A temperature and relative humidity sensor (HOBO) was used to monitor the ambient temperature and relative humidity throughout the test (see Figure 29). The sensor is portable and has an accuracy rate of ±0.024 ºC and a resolution rate of 0.21 ºC for the temperature and an accuracy rate of ±2.5% and a resolution rate of 0.01% for the relative humidity. Figure 30 and Figure 31 show the data obtained regarding the room temperature (T) and relative humidity (HR) during the test. The results confirm a uniform environment as only small variations in temperature and relative humidity are identified throughout the tests. The average temperature and relative humidity were, respectively, approximately 25°C and 60%.



Figure 29 –Temperature and relative humidity sensor used in tests (HOBO)

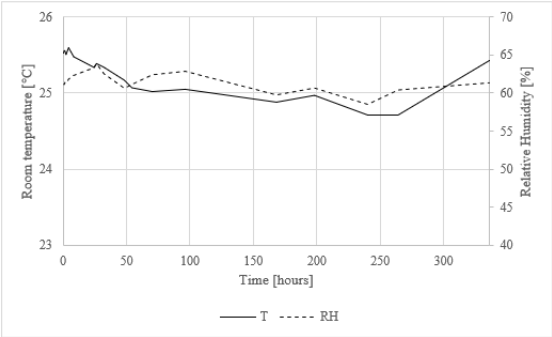


Figure 30 – Room temperature and relative humidity during the tests with brick and limestone

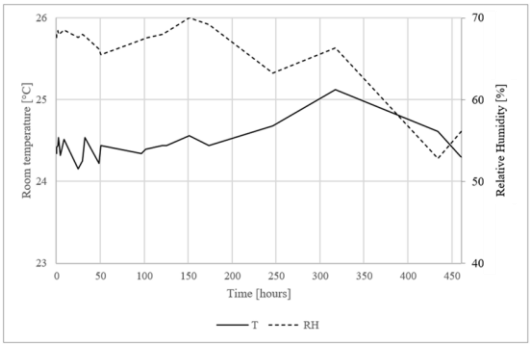


Figure 31 – Room temperature and relative humidity during the tests with granite, mortar, and concrete

3.2.1.6 Procedure

Since the drying process is different for each material, the measurements and data collection were set case-by-case based on the surface temperature variation. In each measurement, a thermal image of the specimens was taken, and the thermal gradient (average temperature of the wet specimen subtracted from the average temperature of the specimen in hygroscopic equilibrium) was calculated. Simultaneously, the specimens were weighed to obtain the moisture content by the gravimetric method. The total monitoring period for each material ended when the thermal gradient became equal to 0°C, i.e., when the temperature of the initially wet specimens equals the one of the HYEQ specimen. Table 13 shows the total monitoring time for each material.

Table 13 – Monitoring time

Material	Monitoring time [hours]
Clay brick	0, 0.5, 1, 2, 4, 8, 24, 26, 32, 48, 54, 70, 96, 168, 198, 240, 264, 336
Limestone	0, 0.5, 1, 2, 4, 8, 24, 26, 32, 48, 54, 70, 96
Granite	0, 0.5, 1, 2, 3, 4, 5, 8.5, 22, 26
Mortar	0, 0.5, 1, 2, 4, 8, 24, 29, 32, 48, 50, 96, 101, 120, 125, 151, 173, 246.5, 317, 434, 460
Concrete	0, 0.5, 1, 2, 4, 8, 24, 29, 32, 48, 50, 96, 101, 120, 125, 151, 173, 246.5, 317, 434, 460

In each monitoring time, two measurements were performed with the infrared camera: one with the lights on and another with the lights off. Figure 32 depicts the specimens at the beginning of the test. The data analysis included a qualitative and quantitative approach to assess eventual correlations between the thermal gradient and the moisture content, as well as their evolution over time. Additionally, the different phases of the drying process were identified either by the calculation of the evaporation rate and the results of IRT.

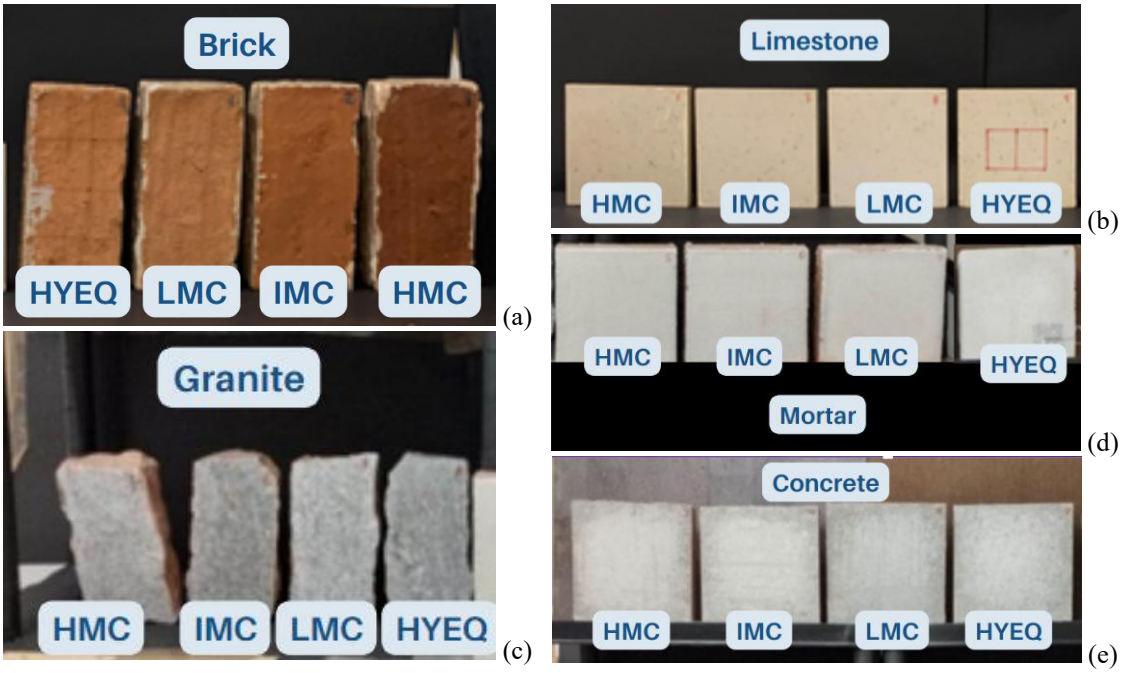


Figure 32 – Specimens at the beginning of the test (a) brick; (b) limestone; (c) granite; (d) mortar; and (e) concrete

The results obtained with IRT were then processed using the InfRec Analyser software. For each thermal image, the average temperature of the specimen was calculated. The thermal gradient between each wet specimen and the corresponding HYEQ specimen was also calculated. As an example, the regions selected in the brick and limestone are depicted in Figure 33. Boxes A, B, C and D refer, respectively, to limestone specimens HMC, IMC, LMC, and HYEQ. Clay brick specimens HYEQ, LMC, IMC, and HMC are indicated by boxes E, F, G, and H, respectively. The temperature results were then analysed in Microsoft Office Excel and IBM SPSS Statistics software for further statistical analysis.

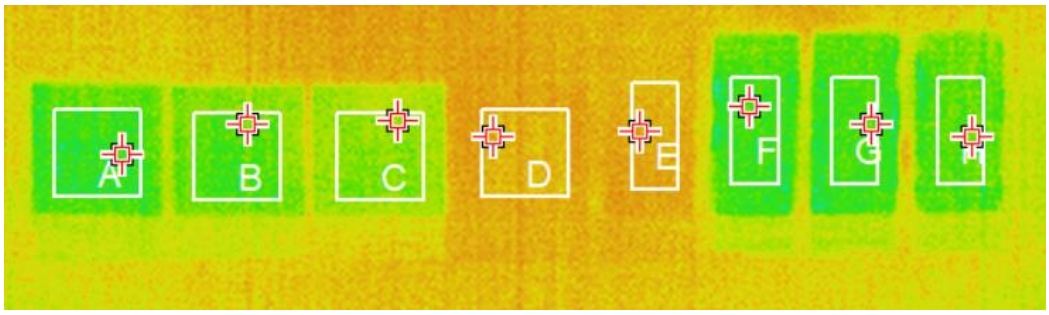


Figure 33 – Selected boxes in InfRec Analyser software to calculate the surface average temperature (limestone: A – HMC; B – IMC; C – LMC; D – HYEQ; brick: E – HYEQ; F – LMC; G – IMC; H – HMC)

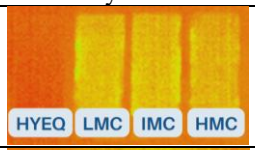
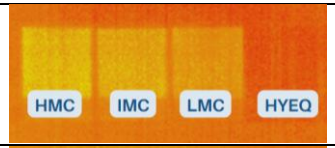
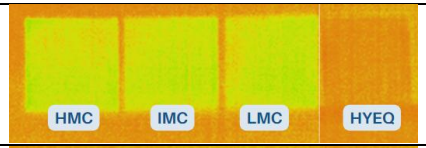
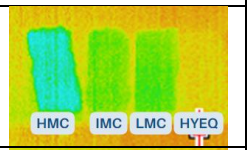
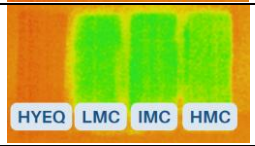
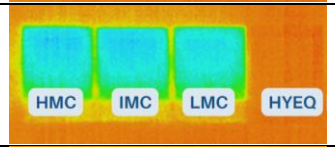
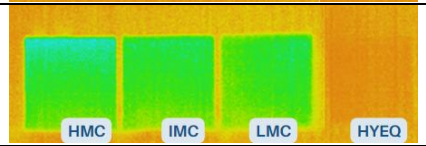
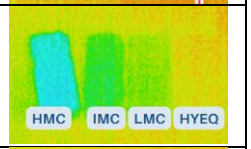
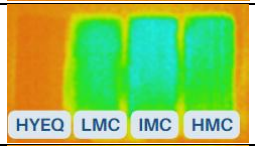
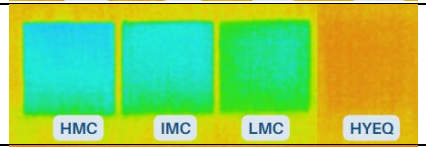
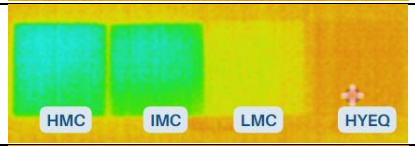
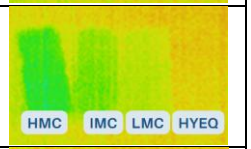
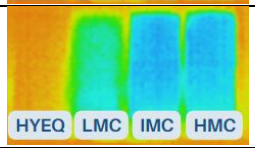
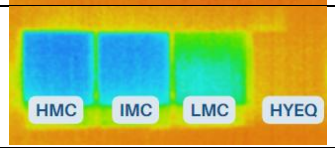
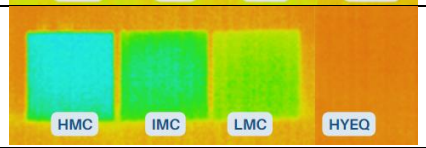
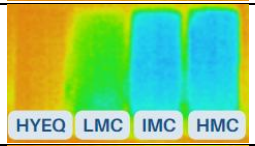
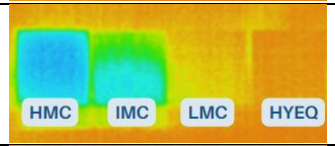
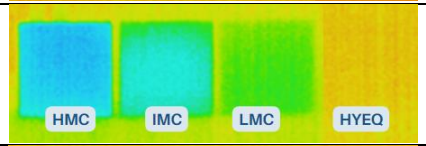
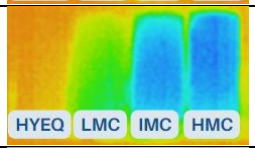
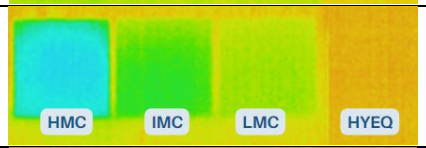
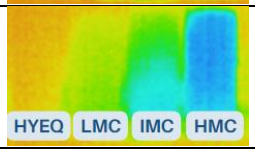
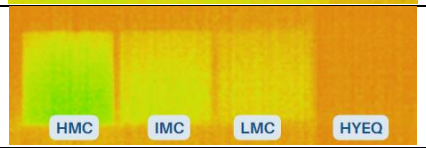
3.2.2 RESULTS

3.2.2.1 Qualitative analysis

Some of the infrared images of the drying process of the materials are shown in Figure 34. The thermal and digital images obtained at each measurement time are presented in appendix 1. The qualitative analysis indicates higher evaporation in all situations at the beginning of the test. However, the temperature difference between the dry and the wet specimens is not the highest at the very beginning of the drying process, as it continues to increase until it reaches a maximum value in the first 48 hours (darker blue areas in the images), depending on the material.

Thereafter, even though evaporation is still occurring over time, the adjustment of the wet specimens' temperature to the one of the HYEQ specimen due to a reduction in the drying flow, leads to a decrease in the temperature differences until no thermal contrasts can be observed between specimens. At that moment, the measurements were stopped. This point in time was different for each material due to the different material's properties, such as thickness and porosity, which influence the drying phenomena in porous materials.

The total monitoring time was 26, 96, 336, 460 and 460 hours for granite, limestone, brick, mortar, and concrete, respectively. Granite and limestone presented the shortest drying times. In the case of granite, this can be explained by its very small porosity, as shown in Table 12, which restricts the absorption of water during the humidification period, and consequently, facilitates the drying process. Regarding limestone, the drying period was shorter due to the smaller thickness of the specimens, when compared to the other materials.

Time	Clay brick[2]	Limestone[2]	Mortar[3]	Concrete[3]	Granite[4]
0h					
1h					
2h					
8h					
24h					
48h					
96h					



[1] Final measurement: 26, 96, 336, 460 and 460 hours for granite, limestone, brick, mortar, and concrete, respectively.

[2] Temperature range: 17.4°C - 27.2°C

[3] Temperature range: 16.9°C – 27.0°C

[4] Temperature range: 18.7°C – 26.7°C

Figure 34 – Infrared images of the drying process of clay brick, limestone, mortar, concrete, and granite

3.2.2.2 Influence of artificial lighting on the results

The influence of the room artificial light on the measurements with the infrared camera was analysed, and the results are shown in Figure 35 for brick, limestone, granite, mortar, and concrete. The solid lines indicated by LOFF refer to the thermal gradient obtained with the lights turned off and the dotted lines indicated by LON refer to the results of the measurements carried out with the lights turned on. In both situations, a very small difference was observed between the results obtained with the lights on and the lights off, without any identifiable trend. According to the literature, measurements should be carried out with the lights turned off and with the entrances of external light blocked to avoid reflections [22]. However, in this case the influence of the light was not relevant. This may be due to the positioning of the samples and the lights. The following sections present the results of the measurements carried out with lights off.

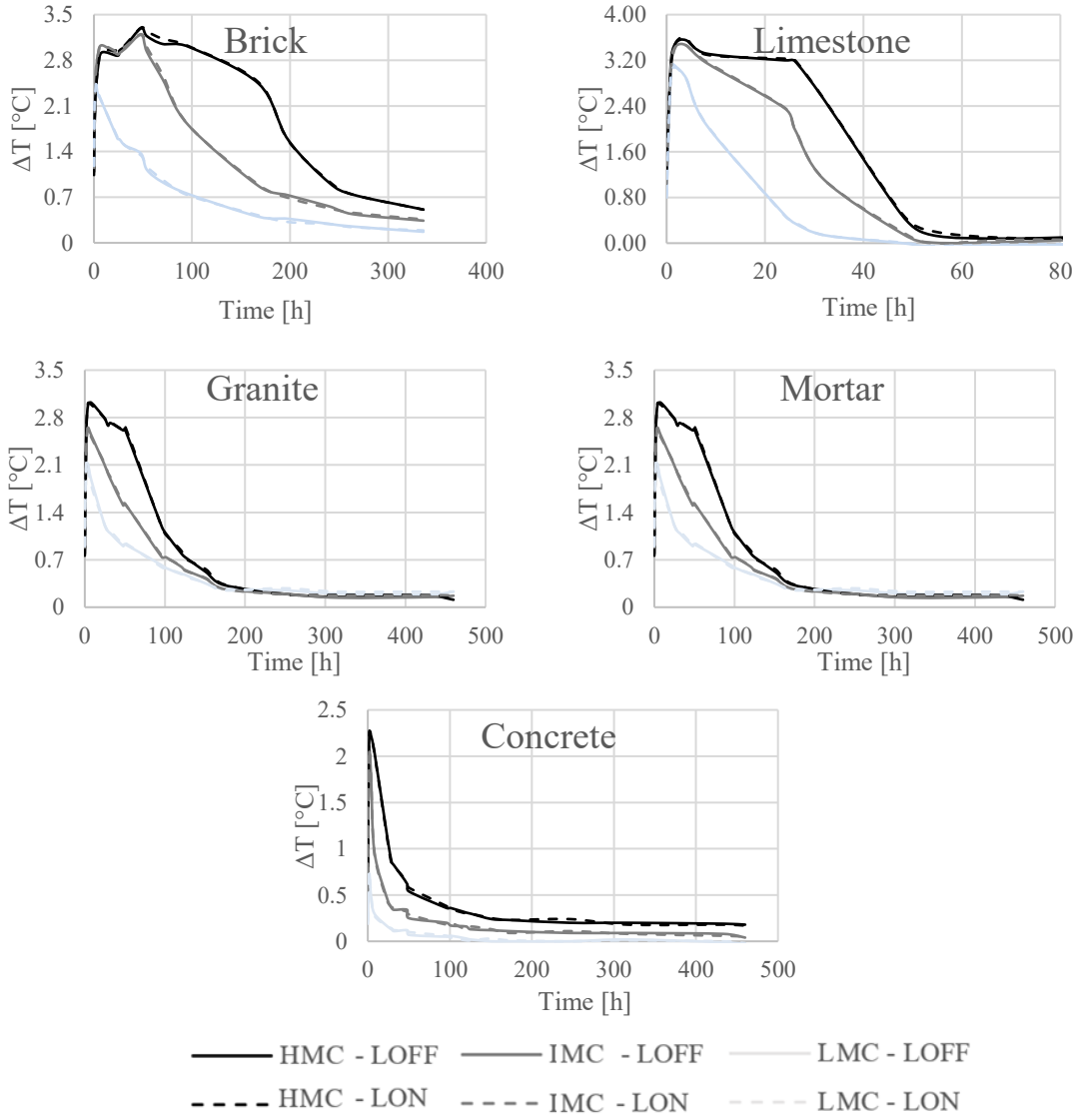
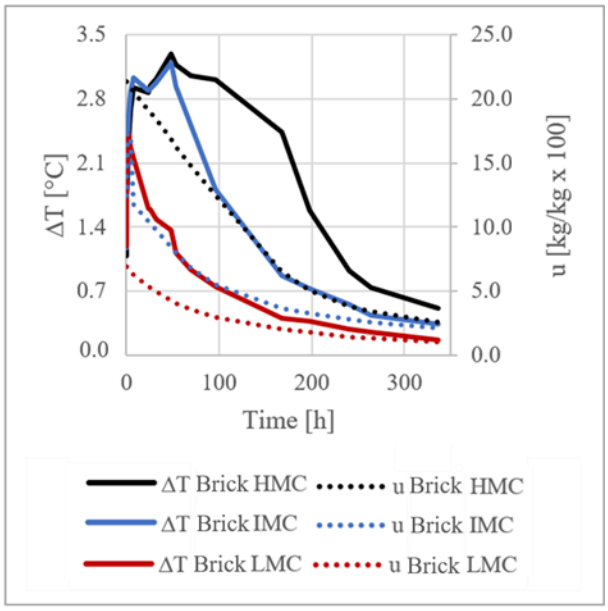


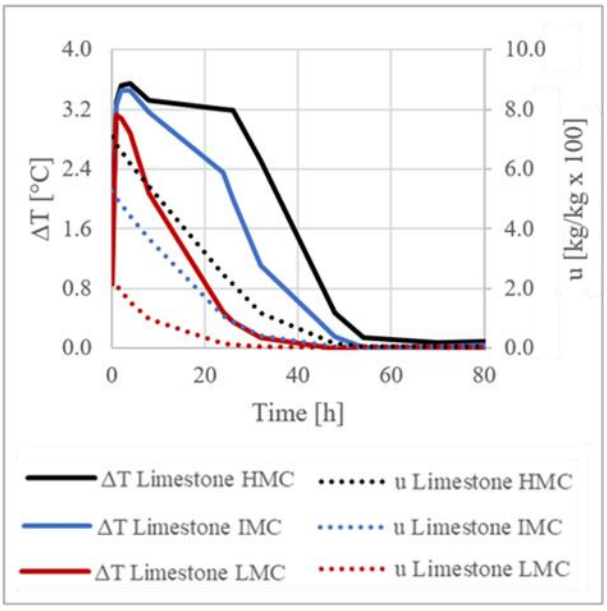
Figure 35 – ΔT of each specimen with lights off (LOFF) and lights on (LON)

3.2.2.3 Thermal gradient and moisture content over time

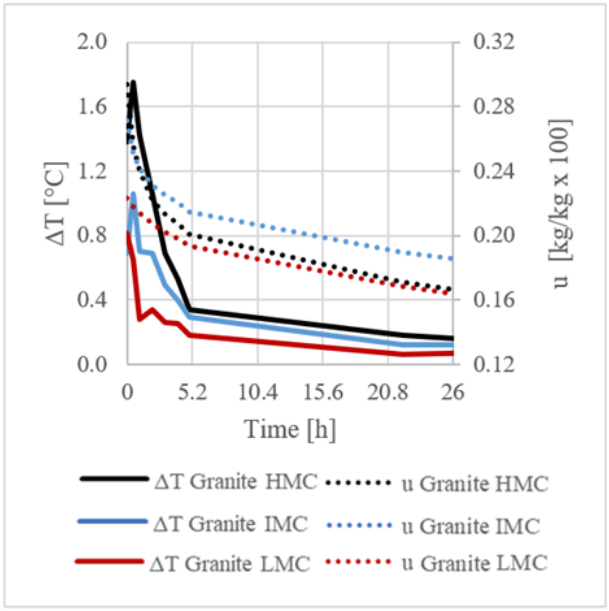
The time-variation of the thermal gradient (ΔT) and the moisture content obtained with the gravimetric method (u) during the test in each specimen (clay brick, limestone, granite, mortar, and concrete) is shown in Figure 36. The solid lines represent the thermal gradient and the dotted lines the moisture content. The black, blue and red colours represent the initial humidification level of the specimens, from the highest to the lowest.



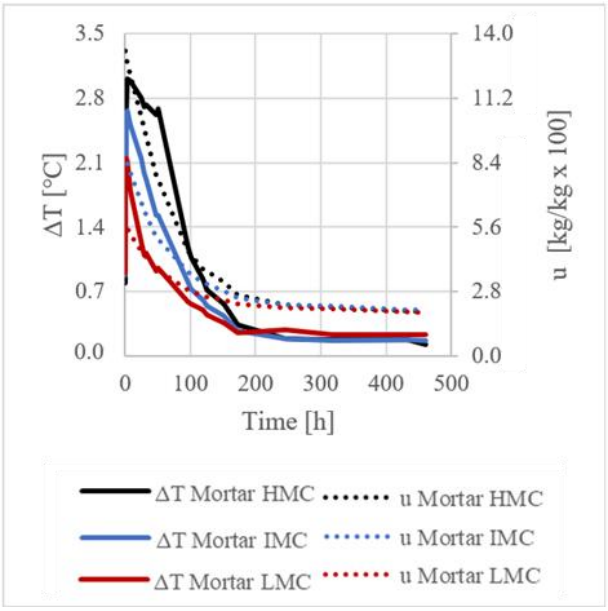
(a)



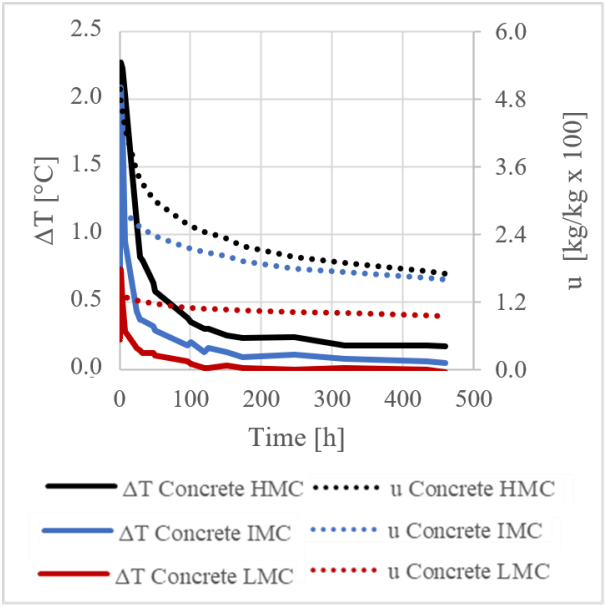
(b)



(c)



(d)



(e)

Figure 36 – Time-variation of the thermal gradient (ΔT) and moisture content (u) of each specimen during the drying process, for: (a) brick; (b) limestone; (c) granite; (d) mortar; and (e) concrete

Figure 36 shows that in specimen HMC of brick, initially saturated, the ΔT at the beginning of the drying process was close to 1,0°C and increased until more than 3,0°C. After that, the ΔT began to reduce. For specimen IMC, the behaviour was similar. However, the thermal gradient reduced more sharply than specimen HMC. Regarding the specimen LMC, which had the lowest initial moisture content, the maximum ΔT was slightly above 2.0°C, and the thermal gradient reduced more rapidly.

The maximum thermal gradient achieved is related to the difference between the vapour pressure of the air and the vapour pressure at the surface. Despite initially different, the moisture content of the HMC and IMC specimens is considerably high, which probably led to a saturated surface in both specimens, resulting in similar maximum thermal gradients. However, since the HMC specimen had a higher initial moisture content, it presented a longer duration of the first phase of the drying process. This reason also justifies the more time it required for the reduction of the thermal gradient, ΔT.

The main difference between the variation of the thermal gradient, ΔT, and the moisture content, u, is that the moisture content in all specimens began with a maximum value and immediately started reducing, while the thermal gradient rose during the first hours and only then started to decrease. That increase in the thermal gradient at the beginning of the drying process is related to the intensification of the evaporative flow at the surface that occurs in the first hours, which enhances the evaporative cooling and, consequently, the temperature differences between the dry and the wet specimens.

For the limestone, the curves of all three specimens were analogous to the ones for brick. However, the maximum values of ΔT were achieved faster than in clay brick. Furthermore, the ΔT values were slightly higher for all specimens of limestone than for the corresponding ones for brick. Regarding the drying

time, it was much shorter for limestone than for brick due to its different properties and smaller thickness.

Granite specimen with the highest moisture content at the beginning of the drying process (HMC) presented a maximum ΔT close to 1.7°C, achieved in less than 1 hour. In the granite specimens, ΔT reduced very quickly. Very few points of ΔT above 1,0°C were obtained. This indicates that the surface evaporation detectable by IRT ceased very rapidly. The different behaviour of granite is due to its extremely low porosity and the high quantity of pores of small size.

Regarding the mortar specimens, the maximum ΔT was reached with 8 hours of measurement, with a value of 3.0°C. Its curves resembled the ones for brick and limestone. Lastly, in concrete specimens, the maximum ΔT occurred in approximately 4 hours of measurement with a value slightly higher than 2.2°C. Like granite, the thermal gradient in concrete specimens decreased rapidly, probably also due to the small porosity and high number of tiny pores, as shown in Figure 26.

To summarise, all materials presented similar patterns but with some differences. The specimens presented an initial ΔT that increased until a maximum value and then started to decrease. The maximum ΔT achieved in the specimens with the highest and intermediate initial moisture content was almost the same in the case of brick, concrete, mortar, and limestone. The main difference between the curves of these specimens (HMC and IMC) in each material was the time necessary for ΔT to sharply reduce since the specimens with higher initial moisture content took more time to dry. The moisture content at the beginning of the tests had the maximum values and gradually reduced throughout the test. Generally, after the thermal gradient reaches the maximum value, ΔT and moisture content follow the same trend.

3.2.2.4 Surface Moisture Meter Results over time

The results of the measurements with the surface moisture meter (SMM) and the gravimetric method are shown in Figure 37. There is not a clear relation between the SMM results and the moisture content in granite. All specimens presented SMM values equal to or lower than 200, which means that there is a risk of moisture presence, according to indicators set in

Table 10, which is not in accordance with the results of the gravimetric method.

About the use of SMM in mortar, there is a sharp decrease in the values for the specimen LMC, while for specimens IMC and HMC a greater number of hours is needed for values start to decrease. This was expected since the specimens IMC and HMC have a higher moisture content and will take longer to dry. However, both SMM and the gravimetric methods tend to stabilise at a similar moment during the drying process, pointing to a good relation between the results of SMM and the moisture content.

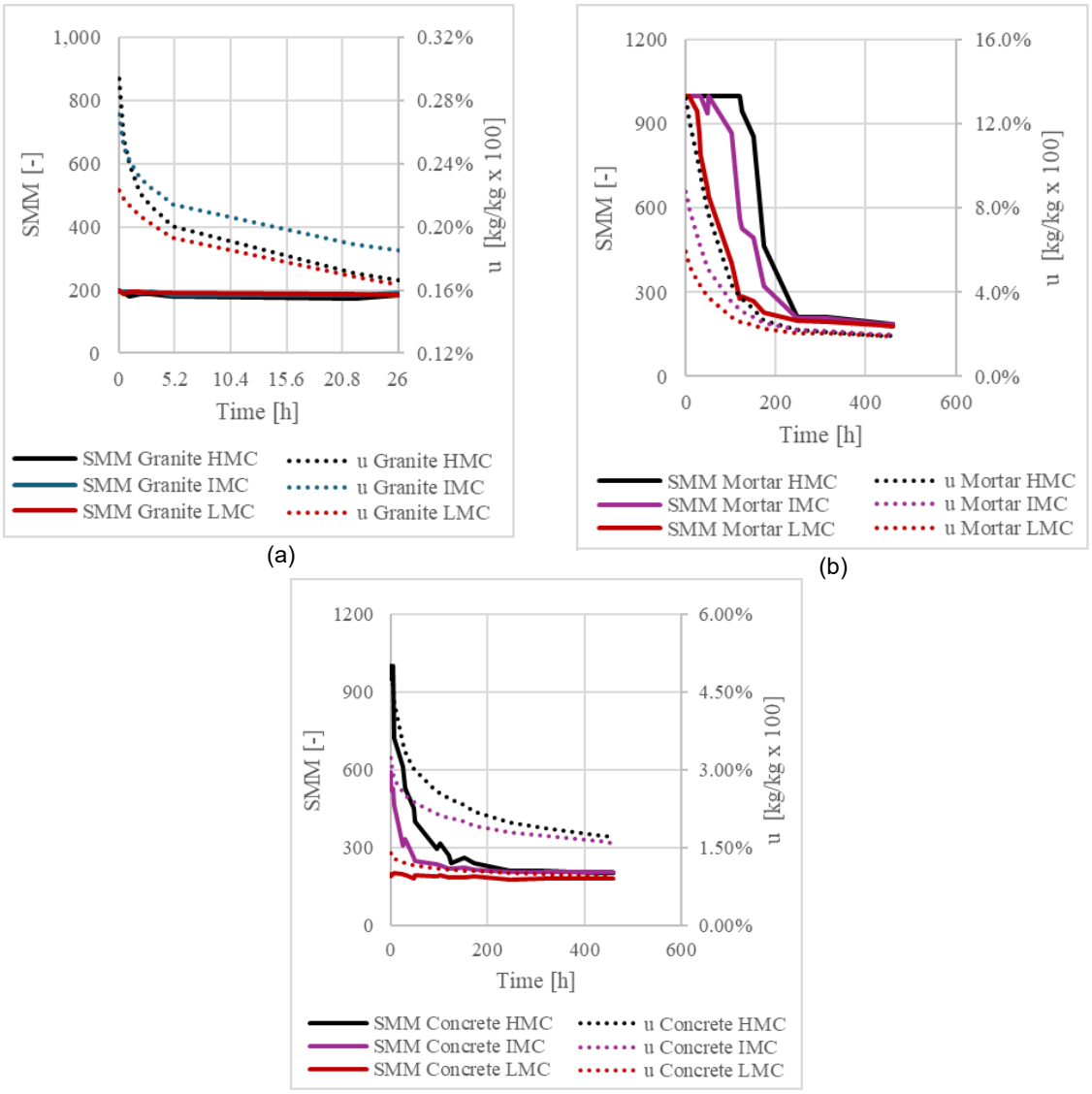
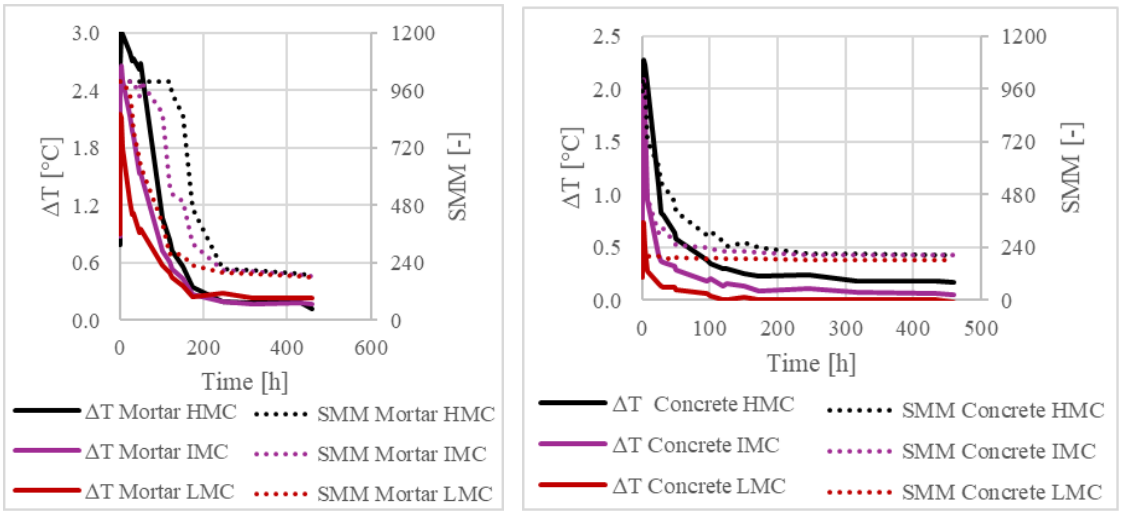


Figure 37 – Values of the moisture content (u) and SMM of the specimens: (a) granite; (b) mortar; and (c) concrete

Regarding concrete, the graph shows a very good relation between the measurements with SMM and the gravimetric method results in all specimens.

The results of the SMM and infrared thermography were compared for mortar and concrete since for granite the SMM values did not change over time. The results are shown in Figure 38. Regarding the measurements in mortar, the thermal gradient starts reducing its values faster than the values of the SMM for specimens IMC and HMC. For the values obtained with the SMM for concrete, the graph shows a clear tendency between the measurements with the SMM and infrared thermography results for all three specimens.



(a) (b)

Figure 38 – ΔT and SMM values of the specimens: (a) mortar; (b) concrete

3.2.2.5 Correlation analysis – thermal gradient vs moisture content

To assess an eventual correlation between the thermal gradient (ΔT) and the moisture content (u), a bivariate correlation analysis was performed using all the results for the five materials. The results of this analysis are shown in Table 14. Table 14 shows that ΔT has statistically significant correlations with the time, the moisture content (u), the ambient temperature (T), and with the type of material. The statistically significant correlation of ΔT with time at a negative level was expected, as the tendency is that the longer the time duration, the lower the ΔT will be due to the drying of the specimens and the lower evaporation flux. Pearson's correlation coefficient obtained between ΔT and light was insignificant, which confirms that the artificial lighting has no considerable influence on ΔT in the conditions of these measurements.

Table 14 – ΔT correlation table with pearson coefficient (r) and p-value

		ΔT	Time	Light	u	T	HR	Material
ΔT	r	1	-0.388**	-0.003	0.703**	0.461**	0.057	-0.358**
	p-value		<0.001	0.941	<0.001	<0.001	0.140	<0.001

** statistically significant correlation

The correlation between ΔT and the ambient temperature was expected to be significant. However, it was quite unexpected that no significant correlation was found between ΔT and RH. This may be related to the fact that the temperature and relative humidity of the environment did not present great variations during the test, pointing to the need of further analyses. Indeed, it is known that under equal moisture conditions of the specimen, high temperatures associated with low ambient relative humidity provide greater ΔT than low temperatures and high ambient relative humidity due to the higher drying capacity of the materials [156]. Hence, the absence of a statistically significant correlation between ΔT and RH appears to go in the opposite way to what would be expectable and must be further explored.

Finally, it should be noted that the ΔT has a statistically significant correlation with the material. Since each material presented a very different variation of ΔT, this correlation was expected. There is also a good correlation coefficient between ΔT and the moisture content of the specimens (u), which shows that IRT has potential for assessing moisture content in building materials. However, further investigation is needed to better understand these correlations. So, an in-depth analysis of the data for each material was carried out separately.

Figure 39 shows the regression analysis performed in the SPSS software to evaluate the correlation between ΔT and moisture content in clay brick, limestone, granite, mortar and concrete. Generally, the quadratic model presented better results, according to the values of the coefficient of determination (R^2) shown in Table 15, Table 16, Table 17, Table 18, and Table 19. Table 20 synthetises the equations for calculating the ΔT based on the value of the moisture content with the quadratic model.

The coefficient of determination (R^2) for the quadratic model (considering all the measurements of the specimens HMC, IMC, and LMC) was 0.88 for clay brick, 0.82 for limestone, 0.63 for granite, 0.79 for mortar, and 0.63 for concrete, which shows a strong correlation between the variables for brick, limestone, and mortar. The weaker correlation for granite and concrete is probably due to the pore size distribution, as presented in § 3.2.1, meaning that additional data is needed to fine-tune the models. Similar results were obtained in [157] regarding the better suitability of IRT for moisture analysis in more porous building materials.

According to the literature [24, 25], in brick masonry, moisture contents above 3% are considered high, and contents above 5% indicate wet masonry. Based on this criterion, if the quadratic model for brick is used, a ΔT above 0.8°C would indicate moist masonry and above 1.5°C would indicate wet masonry. However, it is important to highlight that this regression model was predicted only for the specific conditions of this experimental campaign and, therefore, further studies are needed to define reliable criteria that correlates ΔT with the moisture content, which consider other factors such as ambient temperature and relative humidity, among others. Regarding the other materials, no classification based on the moisture content was found.

Figure 40 presents the correlation curves and the coefficient of determination separated according to the specimen. The ΔT values obtained at the beginning of the tests were not maximum values, despite the maximum moisture contents, since the specimens were waterproofed with plastic wrap before the test started and the surface temperature had not yet begun to decrease. Then, the high levels of evaporation occurring at the beginning of the test, resulting from the drying of the water on the surface of the specimen, enhances evaporative cooling and, consequently, increases the thermal gradient, without having a corresponding relevant variation in the moisture content. Thus, ΔT increases rapidly to a certain value, which varies for the different scenarios, and then progressively decreases until thermal contrast is no

longer visible. At this stage, the moisture content corresponds to the hygroscopic equilibrium with the environment.

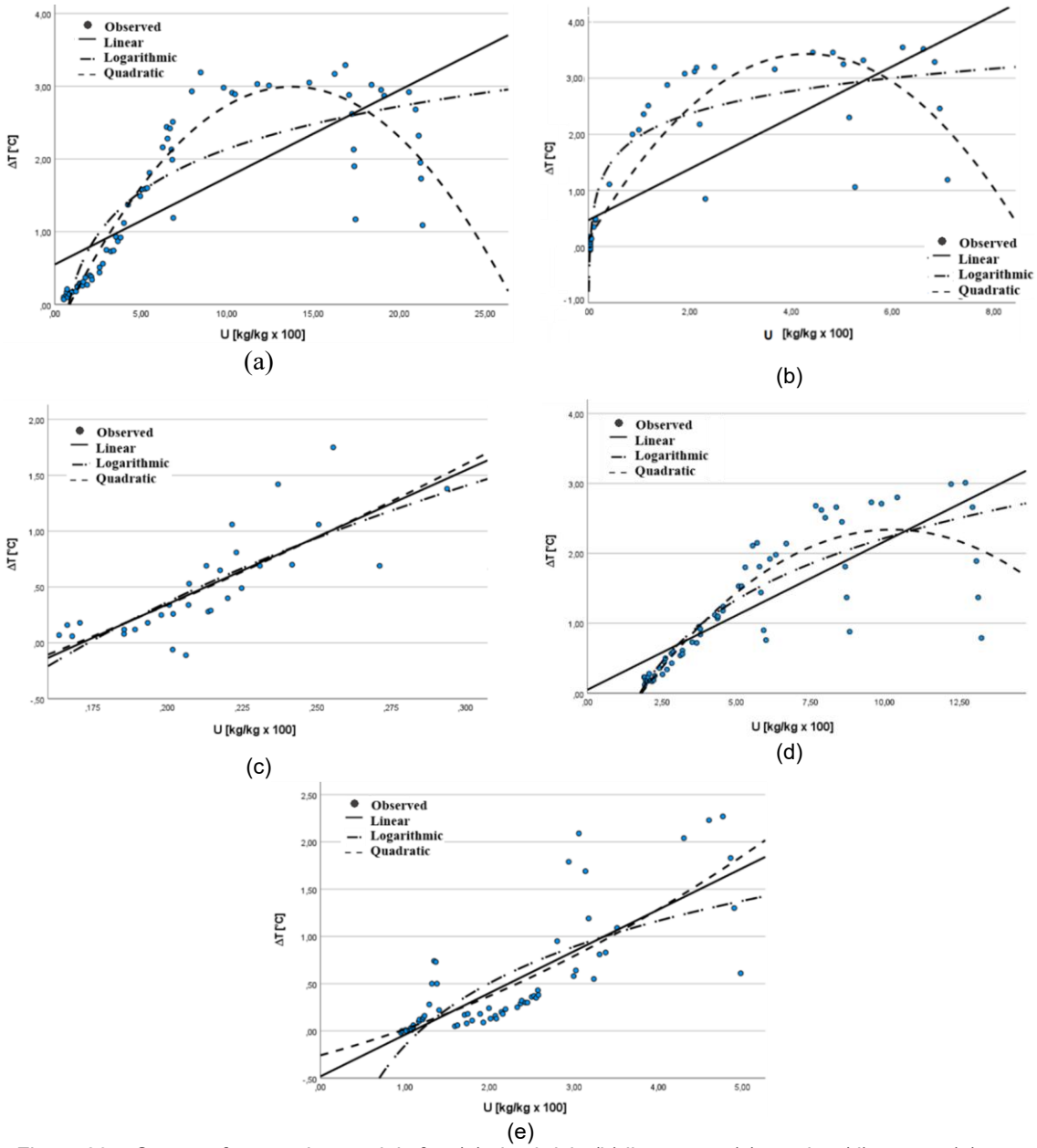


Figure 39 – Curves of regression models for: (a) clay brick; (b) limestone; (c) granite; (d) mortar; (e) concrete

Table 15 – R² values and parameter estimates for each regression model – clay brick

		Parameters estimation		
Model	R²	Constant	b1	b2
Linear	0.567	0.551	0.120	
Logarithmic	0.750	0.188	0.847	
Quadratic	0.881	-0.409	0.494	-0.018

Table 16 – R² values and parameter estimates for each regression model - limestone

		Parameters estimation		
Model	R²	Constant	b1	b2
Linear	0.588	0.47	0.457	
Logarithmic	0.842	1.965	0.58	
Quadratic	0.824	0.122	1.532	-0.177

Table 17 – R² values and parameter estimates for each regression model - granite

		Parameters estimation		
Model	R²	Constant	b1	b2
Linear	0.624	-2.054	12.000	
Logarithmic	0.610	4.497	2.567	
Quadratic	0.625	-1.543	7.292	10.629

Table 18 – R² values and parameter estimates for each regression model - mortar

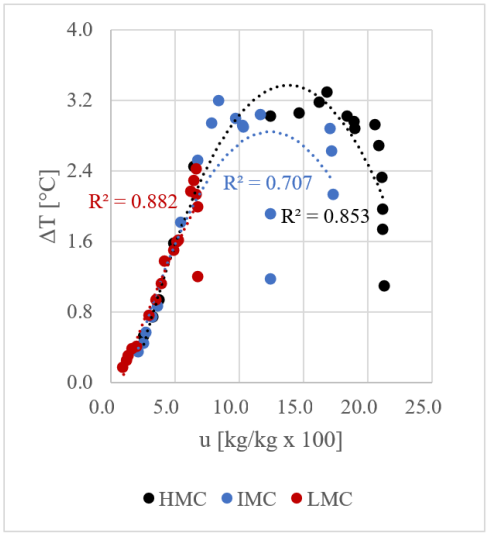
		Parameters estimation		
Model	R²	Constant	b1	b2
Linear	0.626	0.050	0.212	
Logarithmic	0.737	-0.723	1.278	
Quadratic	0.789	-1.115	0.675	-0.033

Table 19 – R² values and parameter estimates for each regression model - concrete

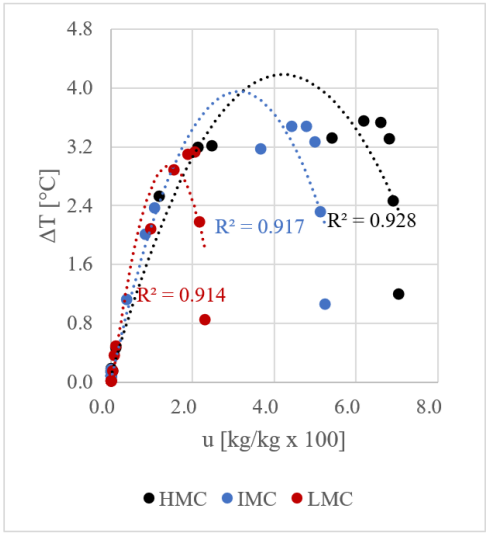
		Parameters estimation		
Model	R²	Constant	b1	b2
Linear	0.621	-0.481	0.441	
Logarithmic	0.541	-0.154	0.952	
Quadratic	0.627	-0.258	0.241	0.036

Table 20 – Equations for calculating the ΔT (quadratic model)

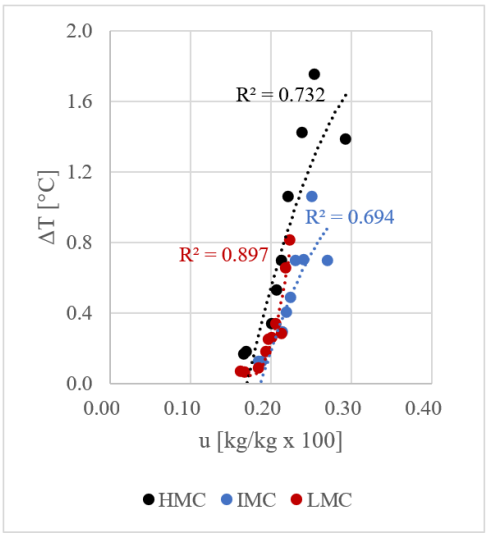
Material	Equation
Brick	$\Delta T = -0.018\ u^2 + 0.494\ u - 0.409$
Limestone	$\Delta T = -0.177\ u^2 + 1.532\ u + 0.122$
Granite	$\Delta T = 10.629\ u^2 - 7.292\ u - 1.543$
Mortar	$\Delta T = -0.033\ u^2 + 0.675\ u - 1.115$
Concrete	$\Delta T = 0.036\ u^2 + 0.241\ u - 0.258$



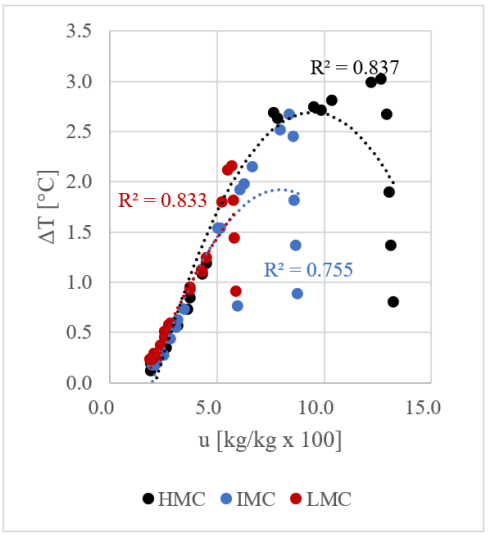
(a)



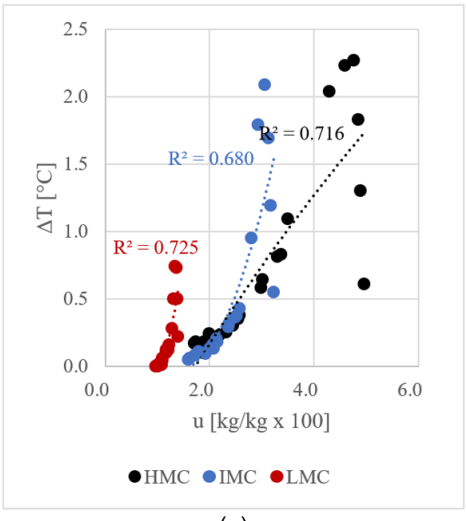
(b)



(c)



(d)



(e)

Figure 40 – Curves of quadratic model for (a) clay brick; (b) limestone; (c) granite; (d) mortar; and (e) concrete

During the initial phase in which the thermal gradient increases until the surface temperature reaches its minimum value, the thermal gradient (ΔT) values are low, but the moisture content is high. This initial period can be seen in Figure 36 and Figure 40, and was also reported by [156].

If this initial phase of adjustment to the environment is disregarded in the regression analysis to evaluate the correlation between ΔT and moisture content considering the quadratic model, the values of the coefficient of determination are 0.96, 0.98, 0.75, 0.95, and 0.78 for clay brick, limestone, granite, mortar, and concrete, respectively, increasing the fitting of the model. The results obtained in this situation are presented in the appendix 2.

3.2.2.6 Cluster Analysis

Since the understanding of the thermal gradient corresponding to abnormal moisture content is of fundamental importance, a cluster analysis was carried out to group the results and try to identify which values of thermal gradient were indicative of high moisture content in each material.

Initially, a hierarchical cluster analysis was conducted to verify the best way to group the data, and then, a k-means cluster analysis was performed to identify the centre of the final clusters. The analysis of the dendogram and the final cluster centre made it possible to identify the ideal number of clusters. The analysis of the ANOVA table showed that the selected variables are statistically significant, considering the p-value ("Sig.") less than 0.001. Figure 41 depicts, for clay brick, the variation of ΔT according to the moisture content (u), labelled per cluster, allowing identifying the location of the data in each cluster.

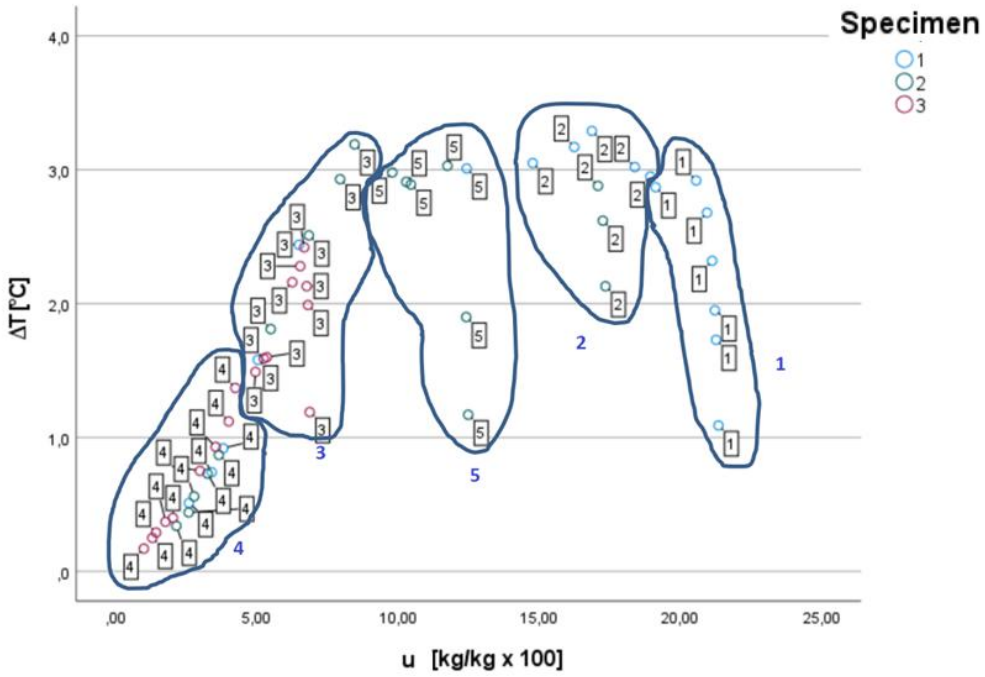


Figure 41 – Scatter chart with clusters label - clay brick

Cluster 1 refers to the points obtained at the beginning of the drying process, that is, with high values of moisture content, but with still intermediate values of ΔT, since the surface temperature had not reduced to its minimum. Cluster 2 predominantly contains the maximum values of ΔT, obtained around 50 hours of testing, a period in which the moisture content was around 17%. Clusters 3 and 5 refer to measurements with intermediate moisture content and, finally, cluster 4 contains the points obtained referring to low values of moisture content.

A descriptive analysis of clusters 1 to 5 was also performed. Table 21 summarises the results for the lower and upper limits of ΔT and moisture content for each cluster. Values shaded in green indicate the measurements with low moisture content and values shaded in red indicate measurements with an elevated moisture content. The results show that, for a 95% confidence interval, points with low moisture content, between 2.20 and 3.30%, will present ΔT values of up to 0.8°C, in accordance with the value defined by the regression analysis presented in Figure 39.

Table 21 – Lower and upper limit of ΔT and moisture content (u) of each cluster - clay brick

Cluster		Inferior limit	Superior limit
1	ΔT	1.40	2.80
	u	20.70	21.40
2	ΔT	2.90	3.10
	u	9.00	12.00
3	ΔT	2.90	3.20
	u	15.50	18.60
4	ΔT	0.50	0.80
	u	2.20	3.30
5	ΔT	1.70	2.30
	u	5.70	6.70

Figure 42 depicts the scatter plot with cluster label for the limestone specimens. Cluster 1 refers to the beginning of the drying process, in which the ΔT has intermediate values, and maximum moisture content values. Cluster 2 corresponds to intermediate values of ΔT and moisture contents. Cluster 3 contains all measurements with the lower moisture contents values and, finally, cluster 4 contains the maximum ΔT values and high moisture content values.

A descriptive analysis of clusters 1 to 4 was also carried out. Table 22 indicates the lower and upper limits of ΔT and moisture content of each cluster for limestone. Although few measurements were obtained for this analysis, due to the rapid drying of the specimens, by analysing the results it can be stated that ΔTs of up to 0.27°C refer to the lowest levels of moisture content (cluster 3).

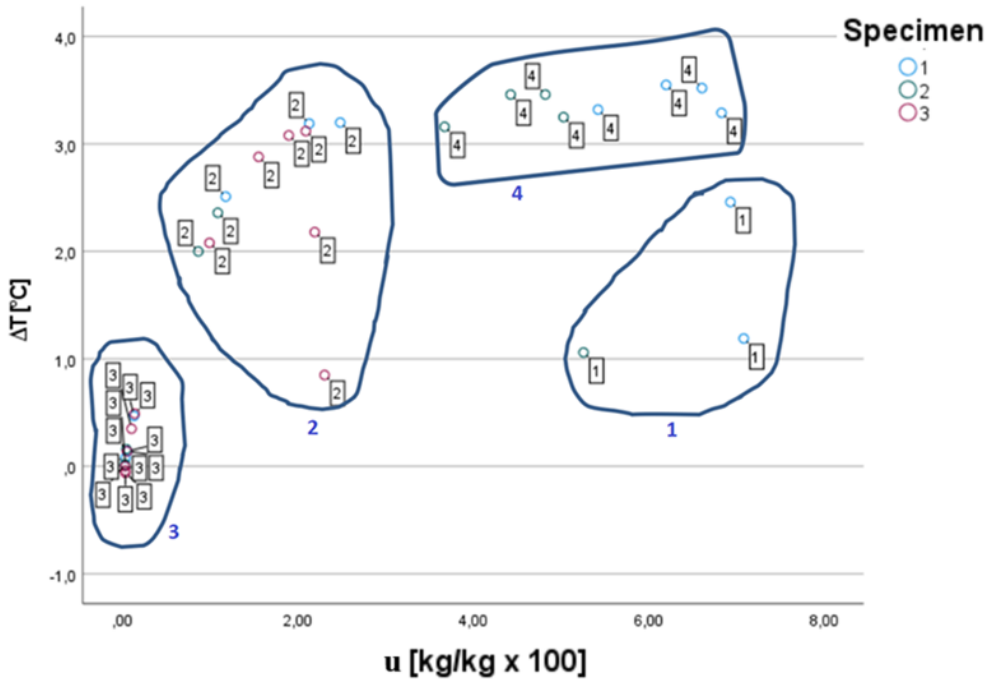


Figure 42 – Scatter chart with clusters label – limestone

Table 22 – Lower and upper limit of ΔT and moisture content (u) of each cluster - limestone

Cluster		Inferior limit	Superior limit
1	ΔT	-0.35	3.50
	u	3.90	8.90
2	ΔT	2.00	3.00
	u	1.31	2.10
3	ΔT	0.03	0.27
	u	0.04	0.09
4	ΔT	3.30	3.50
	u	4.50	6.30

For granite specimens, four clusters were defined. The labels of each cluster is shown in Figure 43. Cluster 3 refers to the points in the beginning of the test, with high moisture content and thermal gradient, while clusters 2 and 4 refer to the middle of the test, with intermediate moisture content, and cluster 1 refers to the points with the lowest moisture contents and thermal gradients. The lower and upper limits of ΔT and moisture content values of each cluster for granite are shown in Table 23, pointing that ΔTs of up to 0.23°C refer to the lowest level of moisture (cluster 1).

In the mortar specimens, three clusters divided the results according to different moisture contents, as shown in Figure 44. The first cluster shows the points with high levels of moisture. The second one refers to points with intermediate moisture content and the third cluster refers to points with lower moisture levels. The descriptive analysis is shown in Table 24. ΔTs of up to 0.64°C refer to the lowest levels of moisture (cluster 3).

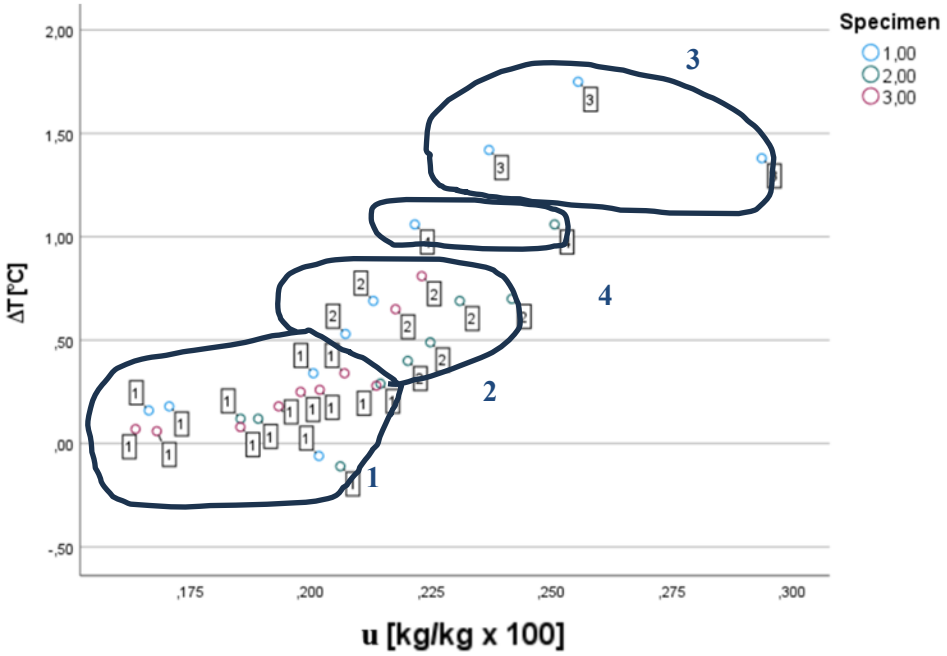


Figure 43 – Scatter chart with clusters label – granite

Table 23 – Lower and upper limit of ΔT and moisture content (u) of each cluster - granite

Cluster		Inferior limit	Superior limit
1	ΔT	0.09	0.23
	U	0.18	0.20
2	ΔT	0.51	0.73
	U	0.21	0.23
3	ΔT	1.01	2.02
	U	0.19	0.33
4	ΔT	1.06	1.06
	u	0.05	0.42

Regarding concrete, Figure 45 shows the variation of the ΔT in relation to the moisture content with the labels of each cluster. Table 25 shows that ΔTs of only up to 0.13°C refer to points with the lowest levels of moisture (cluster 3).

This cluster analysis showed that the thermal gradient which indicates high moisture content varies greatly according to the material being analysed. While in concrete values of ΔT above 0.13°C indicate an abnormal moisture content, in clay brick the moisture content is only considered high for ΔT values above 0.80°C.

It was also possible to define criteria for high moisture content in masonry composed by clay brick, limestone, granite, mortar, and concrete. However, they only apply to the environmental conditions tested. As explained in Chapter 2, the surrounding conditions have considerable effect in thermal gradient since they influence the evaporation. Therefore, further analysis should be carried out to identify the

correlation between the thermal gradient and the moisture content in different scenarios of temperature and relative humidity and for materials with different initial moisture content.

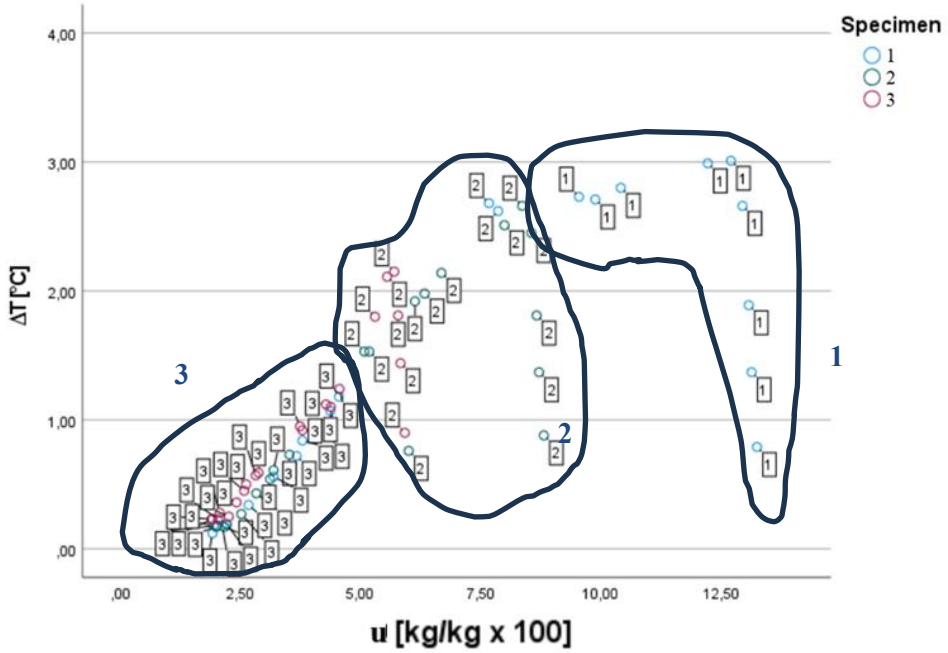


Figure 44 – Scatter chart with clusters label – mortar

Table 24 – Lower and upper limit of ΔT and moisture content (u) of each cluster - mortar

Cluster		Inferior limit	Superior limit
1	ΔT	1.72	2.94
	u	10.74	13.07
2	ΔT	1.58	2.13
	u	6.17	7.44
3	ΔT	0.40	0.64
	u	2.59	3.20

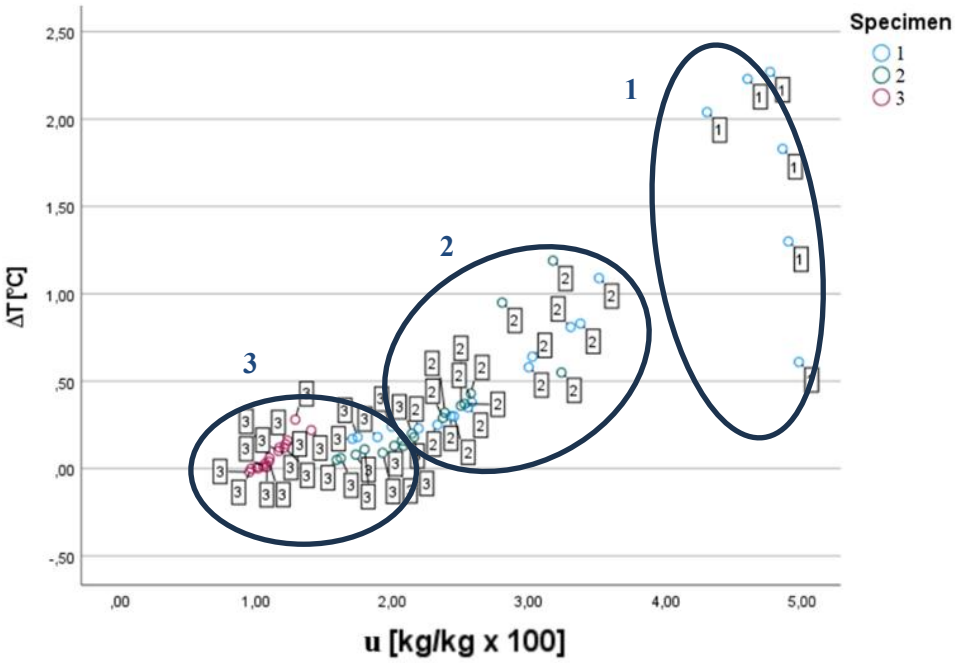


Figure 45 – Scatter chart with clusters label – concrete

Table 25 – Lower and upper limit of ΔT and moisture content (u) of each cluster - concrete

Cluster		Inferior limit	Superior limit
1	ΔT	1.04	2.39
	u	4.47	4.99
2	ΔT	0.39	0.68
	u	2.55	2.95
3	ΔT	0.08	0.13
	u	1.32	1.62

3.2.2.7 Correlation analysis – thermal gradient vs surface moisture meter results

The regression analysis carried out in the SPSS software to evaluate the correlation between the SMM results and the ΔT in granite, mortar, and concrete is shown in Figure 46. Table 26, Table 27, and Table 28 show the coefficient of determination (R^2) and parameter estimates for each regression model. This analysis was not performed for clay brick and limestone since measurements with SMM were not carried out for these materials. In all the situations, the quadratic model presented better results, as in the case of the analysis between thermal gradient and the gravimetric method, although the distribution of points is rather different. Also, the coefficient of determination for the quadratic model points to a correlation for mortar ($R^2 = 0.656$) and concrete ($R^2 = 0.733$), but no correlation was found for granite ($R^2 = 0.046$). These results indicate that the use of SMM, although very useful in practice for moisture assessment, may bring some difficulties in its implementation when combined with IRT.

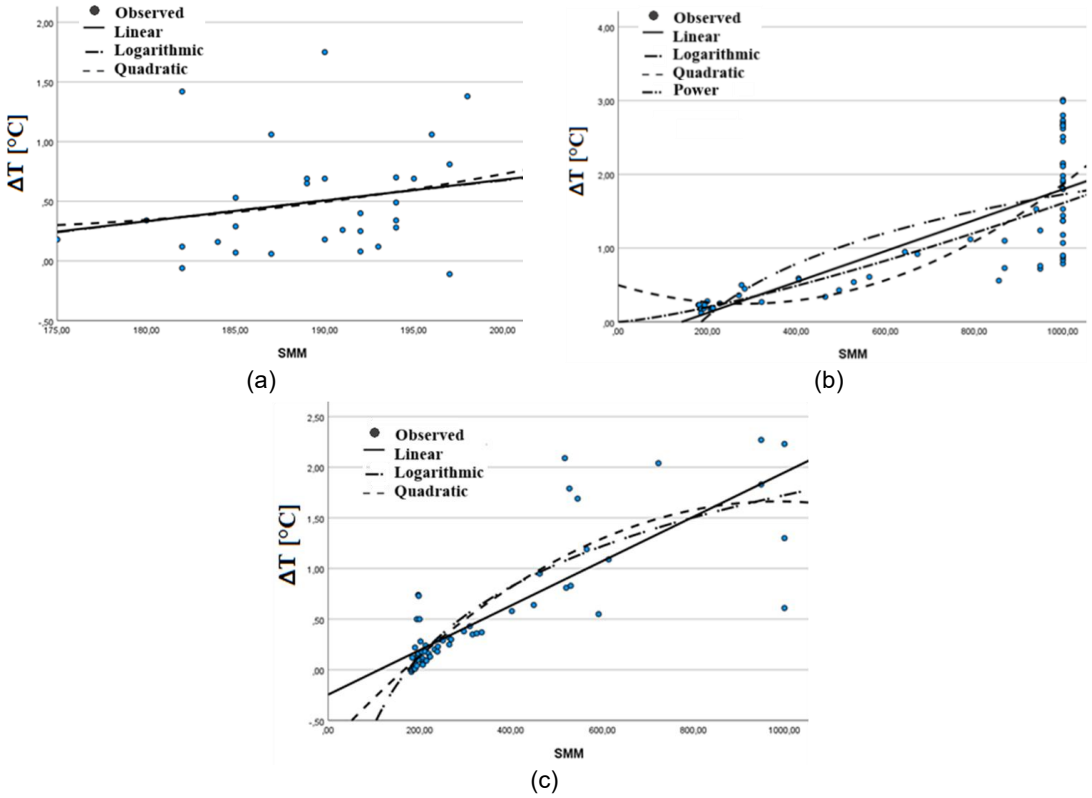


Figure 46 – Curves of regression models for: (a) granite; (b) mortar; and (c) concrete

Table 26 – R² values and parameter estimates for each regression model - Granite

		Parameters estimation		
Model	R²	Constant	b1	b2
Linear	0.046	-2.799	0.017	
Logarithmic	0.046	-16.582	3.257	
Quadratic	0.047	11.932	-0.140	0.00

Table 27 – R² values and parameter estimates for each regression model - Mortar

		Parameters estimation		
Model	R²	Constant	b1	b2
Linear	0.624	-0.298	0.002	
Logarithmic	0.574	-5.376	1.029	
Quadratic	0.656	0.498	-0.002	3.156E-6
Power	0.835	0.0	1.301	

Table 28 – R² values and parameter estimates for each regression model – Concrete

		Parameters estimation		
Model	R²	Constant	b1	b2
Linear	0.687	-0.245	0.002	
Logarithmic	0.718	-5.095	0.987	
Quadratic	0.733	-0.745	0.005	-2.488E-6

3.2.2.8 Evaporation rate

The different moisture transport mechanisms in each drying phase led to a very distinct behaviour of the evaporation rate. While in the first drying phase the evaporation rate presents high values and is almost constant, after a certain moment (w_{crit}), it sharply reduces [4], [38], [52]. Since the values of the thermal gradient are related to the surface evaporation, the relationship between the evaporation rate and the thermal gradient must be explored.

As the gravimetric method was performed simultaneously with the capture of the thermal images, the evaporation rate was calculated considering the subtraction of mass at different measurement times, according to equation (30).

$$g_d = \frac{(m_2 - m_1)}{(t_t - t_1).A} \quad (30)$$

Where:

g_d: evaporation rate density [kg/m².s]

t_2: measurement time 2 [s]

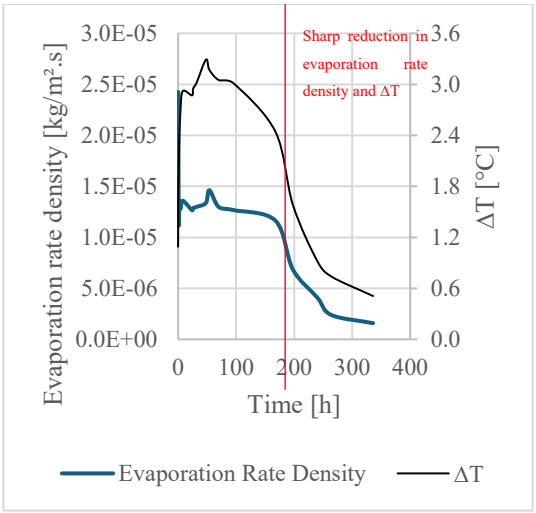
t_1: measurement time 1, previous to t_2 [s]

m_2: mass at t_2 [kg]

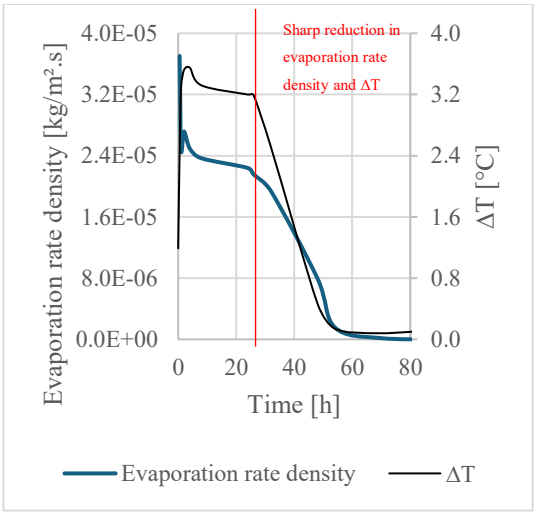
m_1: mass at t_1 [kg]

A: area [m²]

The evaporation rate density and the thermal gradient are shown in Figure 47 for the specimens HMC (saturated) of clay brick, limestone, granite, mortar, and concrete. The black lines show the variation of the thermal gradient during the drying phase and the blue lines present the variation of the evaporation rate.



(a)



(b)

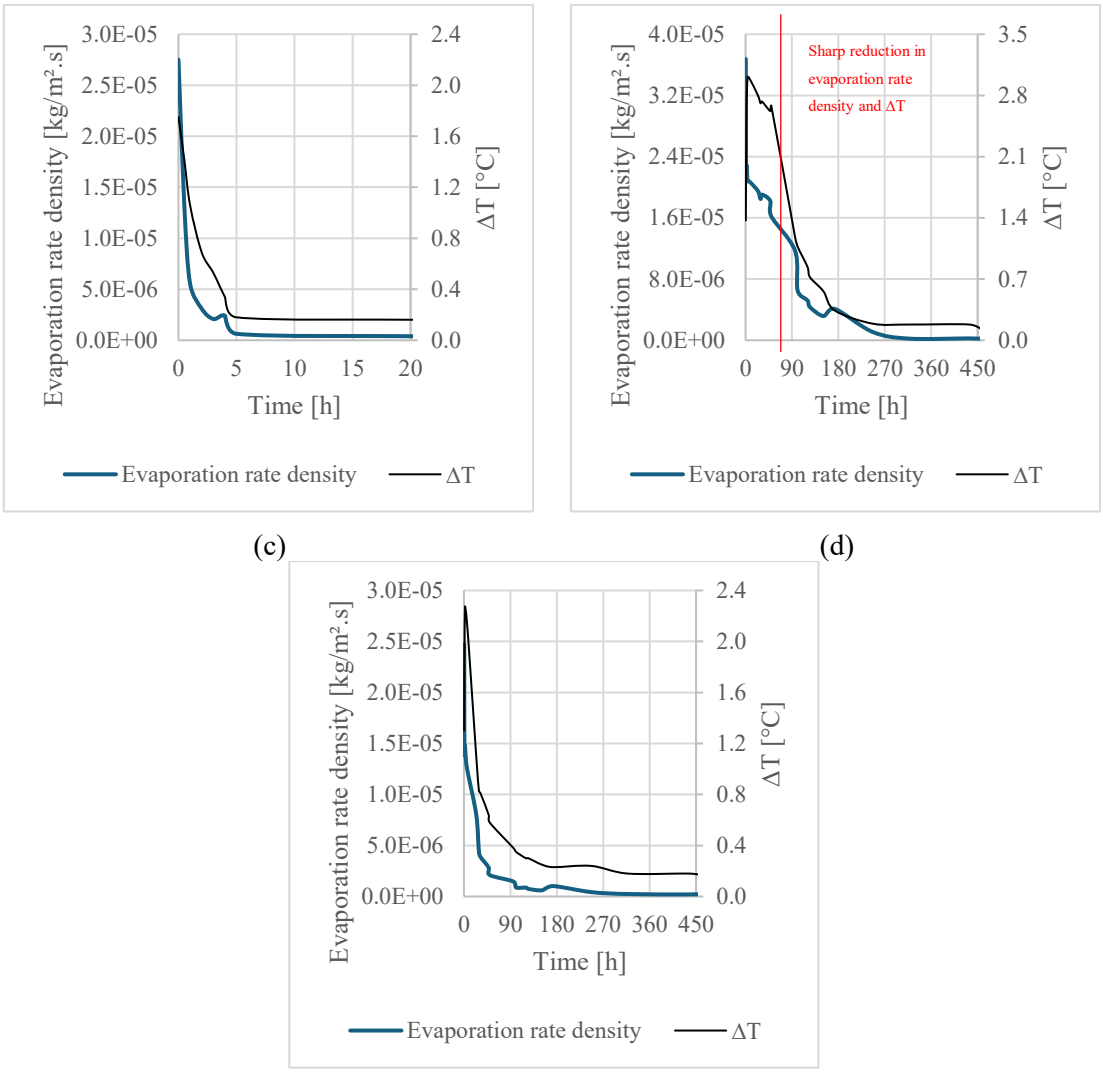


Figure 47 – Evaporation rate and thermal gradient over time for (a) clay brick; (b) limestone; (c) granite; (d) mortar; and (e) concrete

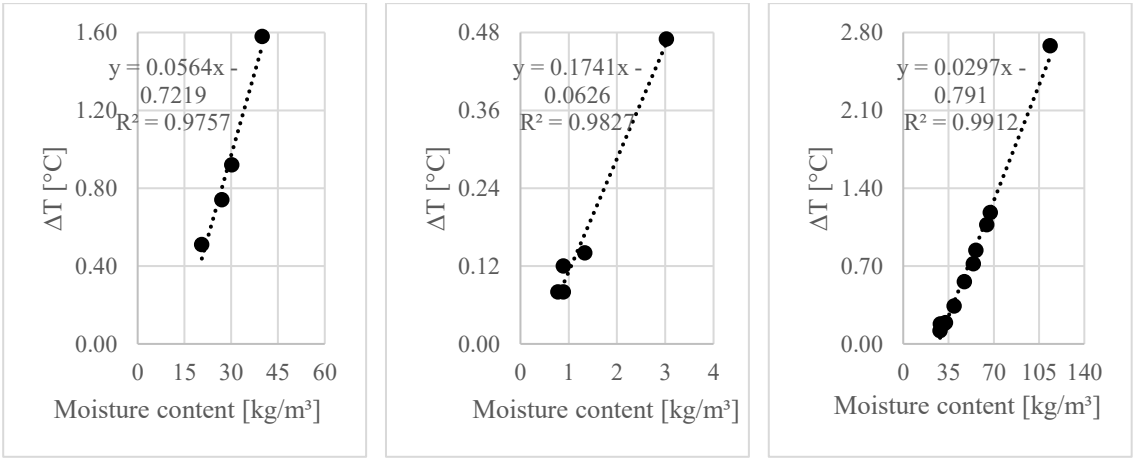
The first drying period mentioned in Chapter 2, in which capillary conduction is the main mechanism of moisture transport, can be clearly identified in clay brick, limestone, and mortar. This period, with an almost constant evaporation rate density, is followed by a second phase in the drying process, in which a sharp decrease in this value can be observed. The first phase of drying matches the period identified by IRT, when the thermal gradient decreases less markedly, before a sharp reduction occurs, confirming the potential of IRT to detect the phenomenon.

In the case of granite, this first drying phase could not be identified, and for concrete, it was for a very short period. The short duration or the absence of this phase probably happened because of the proximity between the values of w_{cap} and $w_{crit.}$, which, in turn, are influenced by the pore size distribution of these materials. Based on the material's properties determined with the MIP, presented in § 3.2.1.4, granite had the lowest porosity and average pore diameter. This might have led to a lower evaporation rate and

the absence of the first phase. Concrete also presented low porosity values and average pore diameter, which explain a similar behaviour.

These results show that IRT has a good potential to identify the duration of the first drying phase for some building materials. According to equation (7), if the properties of the material (w_{cap} and w_{crit}) and the duration of the first drying period are known, it is possible to identify the evaporation rate density and, therefore, the moisture content at any moment of this drying phase. Therefore, for practical application purposes and for certain building materials, IRT can already be applied to quantify moisture content in laboratory conditions, opening the discussion on future in situ applications.

As presented in §3.2.2.3 and §3.2.2.5, the correlation between the moisture content and the thermal gradient at the beginning of the drying process is not very strong since in the first hours the thermal gradient rises but the moisture content starts with its maximum value and then decreases. However, if the correlation between these variables is assessed only for the period after w_{crit} is reached, the results show a much stronger correlation, as presented in Figure 48 for clay brick, limestone, and mortar.



(a) (b) (c)

Figure 48 – Correlation in the second drying phase - for (a) clay brick; (b) limestone; and (c) mortar

3.3 TESTS UNDER CONTROLLED CONDITIONS

Figure 49 presents a structured workflow of the laboratory campaign for monitoring moisture in mortar samples under controlled environmental conditions with Infrared Thermography (IRT) and the gravimetric method. In the first stage, the material to be studied and the environmental conditions were defined. A pre-dosed cement mortar was chosen for the analysis. Also, three different environmental conditions were selected for the tests in the climatic chambers.

Secondly, preliminary procedures were performed to characterise the material and prepare the specimens. The third and final step consists of monitoring the drying process of the samples using IRT and the gravimetric method. This Section presents the materials characterisation and methods as well as the results of these tests.

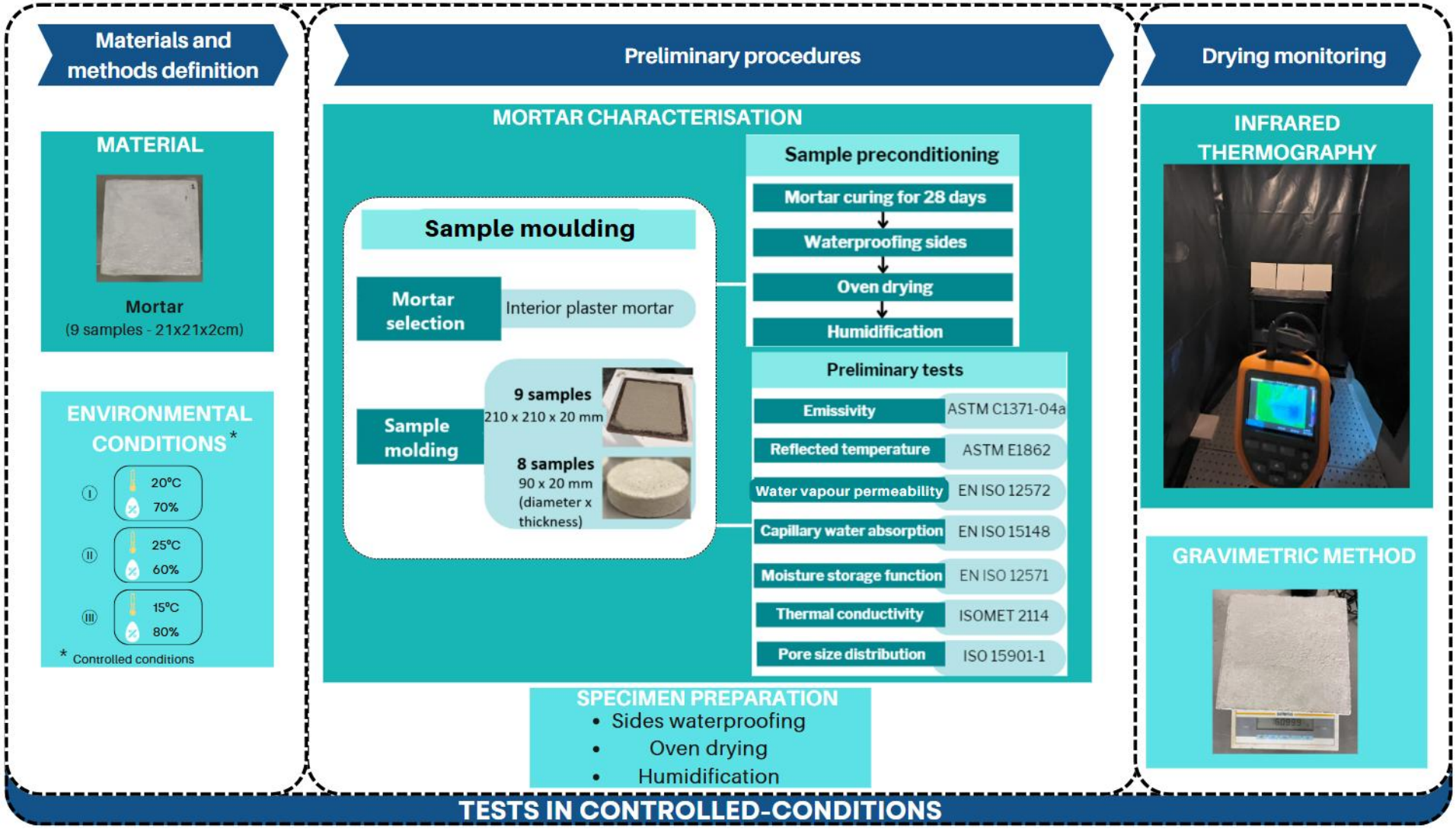


Figure 49 – Workflow of the laboratory tests under controlled conditions

3.3.1 CHARACTERISATION OF THE PRE-DOSED MORTAR

The first step was to select the type of mortar that would be used in the laboratory tests. The objective was to select a material widely used for rendering walls. Additionally, measurements would be carried out in the laboratory to simulate the internal wall conditions. Therefore, a common pre-dosed mortar specific for rendering internal sides of walls (indoors) was chosen for the analysis. The properties described in the technical sheet of the product are shown in Table 29.

Table 29 – Properties of the pre-dosed mortar selected for the laboratory campaign

Property	Value
Density (powder)	1500 ± 200 kg/m³
Density (paste)	1750 ± 200 kg/m³
Compressive strength (28 days)	≥ 6 N/mm^2
Capillarity (28 days)	> 0,40 kg/m^{2}min$^{0.5}$
Water vapour permeability (28 days)	μ ≤ 15
Thermal conductivity (λ_{10},dry)	0,8 W/mK

Nine samples of 210 x 210 x 20 mm³ were moulded for the tests to be carried out inside a climatic chamber. Three samples were used for each of the three different environments. One sample was kept in hygric equilibrium during the whole test, while the two other samples were humidified, one until the saturation water content and the other one with an intermediate value of water content. Eight other samples of 90 mm in diameter and 20 mm in thickness were moulded to carry out preliminary tests. Figure 50 and Figure 51 show the samples.



Figure 50 – Samples of dimensions of 90 mm x 20 mm (diameter x thickness)

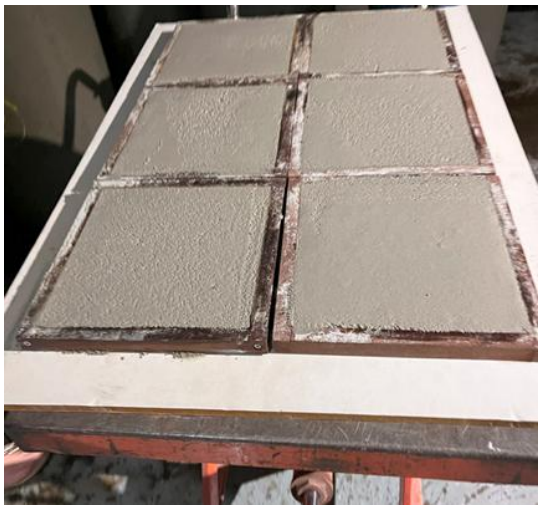


Figure 51 – Samples of dimensions of 210 mm x 210 x 20 mm

After moulding the bigger samples, they were cured for 28 days, waterproofed on all sides but the one faced to the infrared camera, and dried in the oven until mass stabilization. Following the drying, the samples were humidified by partial immersion.

The preliminary tests to assess the properties of the mortar consisted of measuring the emissivity, water vapour permeability, absorption coefficient of water, moisture storage function, thermal conductivity, and pore size distribution. The tests were performed according to the standards listed in Figure 49.

3.3.1.1. Emissivity test

The emissivity of the mortar was defined according to the same procedures described in § 3.2.1. The average emissivity value measured for the mortar specimens was 0.92. In the study conducted by [158], the emissivity of a mortar sample was tested with an emissometer and with IRT. The values obtained with the emissometer and IRT were, respectively, 0.93 and 0.92. In the work presented by [16], the authors used an emissivity value for mortar of 0.92. Therefore, the value obtained in this work is in line with the ones found in the literature, confirming the representativity of the specimens.

3.3.1.2. Water vapour permeability

The water vapour permeability test was carried out according to EN ISO 12572 [159]. Five specimens of the mortar were tested. Table 30 shows the dimensions and mass of the specimens.

Table 30 – Dimensions and mass of the mortar samples used in the water vapour permeability test

Specimen	Diameter [mm]	Thickness [mm]	Mass [g]	Total mass (cups and aqueous solution) [g]
1	86.7	21.8	214.21	545.75
2	86.5	21.5	214.54	538.05
3	86.9	21.5	212.3	520.32
4	86.8	21.5	222.94	530.1
5	86.4	20.4	211.98	515.32

The mortar samples were stored at 23°C of temperature and 50% of relative humidity for their weight to stabilise. Then, the samples were sealed with paraffin to the open side of a stainless cup containing a saturated aqueous solution which guarantees 93% of relative humidity at the bottom of the sample. The assemblies were weighed and placed in a controlled test chamber with a temperature of 23°C and 50% relative humidity of the air. Table 31 displays the test conditions.

Table 31 – Conditions for the water vapour permeability test

Temperature [°C]	Relative humidity [%]			
	Dry state (top of the specimen)		Wet State (bottom of the specimen)	
	Setpoint	Tolerance	Setpoint	Tolerance
23 ± 0.5	50	± 3	93	± 3

Figure 52 and Figure 53 show the test cup assembly and the assembly inside the climatic chamber. A temperature and relative humidity sensor (HOBO) was placed inside the chamber to monitor the conditions constantly.



Figure 52 – Test cup assembly for the water vapour permeability test



Figure 53 – Test cup assembly inside the climatic chamber

The different partial vapour pressure between the test cup and the climatic chamber leads to a vapour flow through the specimens. Therefore, periodic weighing of the assemblies was made to identify the rate of water vapour transmission according to the following time intervals: 0h, 24h, 96h, 120h, 144h, 168h, 192h, 216h, 264h, 288h, 312h, 336h, 360h, 434h, 458h, 482h, 533h, 604h, and 647h.

The variation of the mass of the assembly over time, excluding the earlier, non-linear stage of the test, is shown in Figure 54. The properties calculated based on the water vapour permeability test are presented in Table 32.

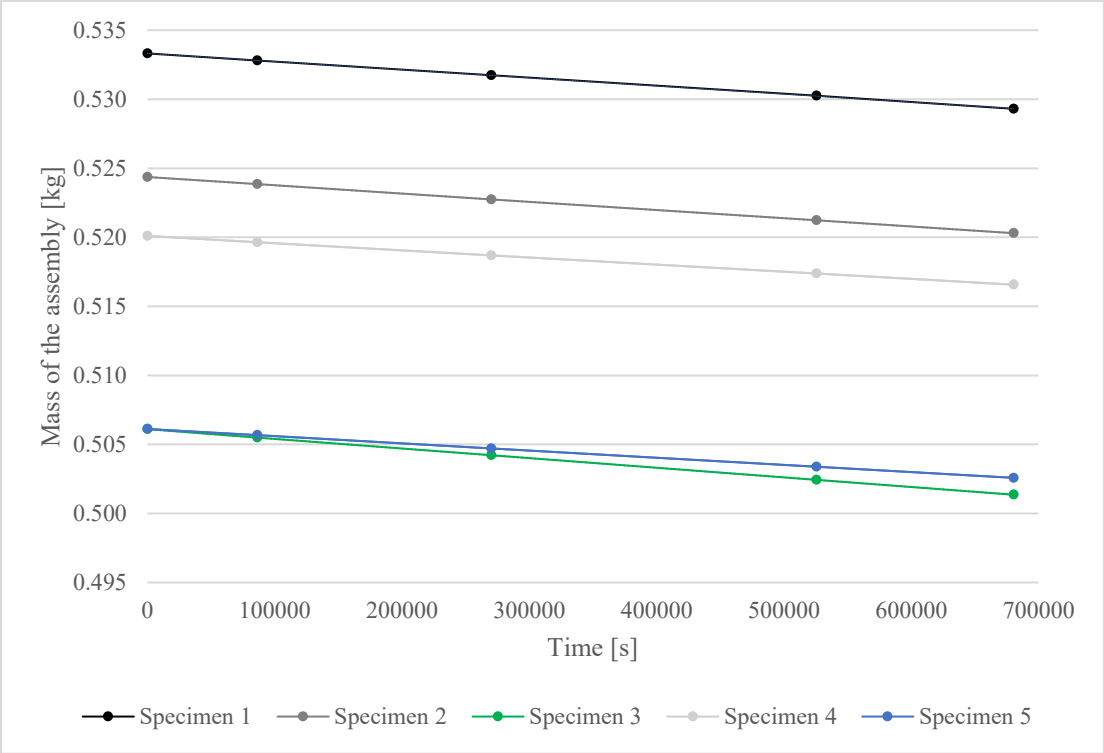


Figure 54 - Water vapour permeability test of the mortar under study – mass of the assembly over time

Table 32 – Mortar's properties obtained with the water vapour permeability test

Mortar's properties	
Water vapour flow rate (G) – kg/s	5.84×10^{-9}
Density of water vapour flow rate (g) – kg/(m².s)	9.91×10^{-7}
Water vapour permeance (W_p) – kg/(m².s.Pa)	8.20×10^{-10}
Water vapour permeability (δ_p) – kg/(m.s.Pa)	1.75×10^{-11}
Water vapour resistance factor (μ) – dimensionless	11.27
Water vapour diffusion-equivalent air layer thickness (s_d) – m	0.24

The water vapour resistance factor (μ) obtained in this work is aligned with the specifications of the technical sheet of the pre-dosed mortar since it is lower than 15. In other work carried out to assess the water vapour diffusion resistance factor, [160] found the value of 17.9 for cement mortar and 12.8 for lime mortar in the wet cup test carried out according to EN 12572, which shows that the values obtained are in line with the ones found in the literature. The value available on WUFI material database for a cement mortar is between 14.8 and 15.5, which also indicates values close to the ones measured.

3.3.1.3. Absorption coefficient of water

The absorption coefficient of water was calculated according to the standard ISO 15148 [49]. Prior to the test, the specimens were sealed on the lateral sides with epoxy resin. Absorption coefficient of water was then measured by partial immersion by measuring the change in mass of the specimens over time. ISO 15148 specifies that the change in mass should be monitored over time, at least 24 hours. However, after 3 hours of measurements, the water appeared on the top surface of the specimens. In this way, the test was terminated within 3 hours. The water depth at the base of the specimens was 5 ± 2 mm, and the mass measurement times were 0h, 5 minutes, 20 minutes, 1 hour, 2 hours, and 3 hours.

To calculate the absorption coefficient of water (A_w), it must first be calculated the difference in mass between each weighing (m_t) and the initial mass (m_i), in relation to the base area (A), according to equation (31). The absorption coefficient of water was calculated according to equation (32).

$$\Delta m_t = \frac{m_t - m_i}{A} \tag{31}$$

$$A_w = \frac{\Delta m'_{tf} - \Delta m'_0}{\sqrt{t_f}} \tag{32}$$

Where:

A_w: absorption coefficient of water [kg/(m²s^{0,5})]

A: area [m²]

Δm_t: mass variation [kg/m²]

t_f: total duration of the test [s]

$\Delta m'_0$: mass variation at time t0 [kg]

$\Delta m'_{tf}$: value of Δm_t at time t_f [kg/m²]

The graph with the result of the mass variation (Δm_t) in relation to the square root of time is shown in Figure 55. The average absorption coefficient of water obtained for the mortar specimen is presented in Table 33.

The technical sheet specifies that the absorption coefficient of water must be higher than 0.40 kg/(m².min^{0,5}), so the values obtained are aligned with the specifications of the technical sheet. According to the German Standard DIN 52617 [161], the materials can be classified by a function of the capillary absorption coefficient of water as the following:

- $A_w > 2.0$ kg/(m².h^{0,5}) – fast suction
- $A_w < 2.0$ kg/(m².h^{0,5}) – preventive water
- $A_w < 0.5$ kg/(m².h^{0,5}) – quasi-waterproof
- $A_w < 0.001$ kg/(m².h^{0,5}) –waterproof

Therefore, the value obtained in this work shows that the mortar is classified as fast suction. The mortar used is specified for indoor environments, so this high value is acceptable.

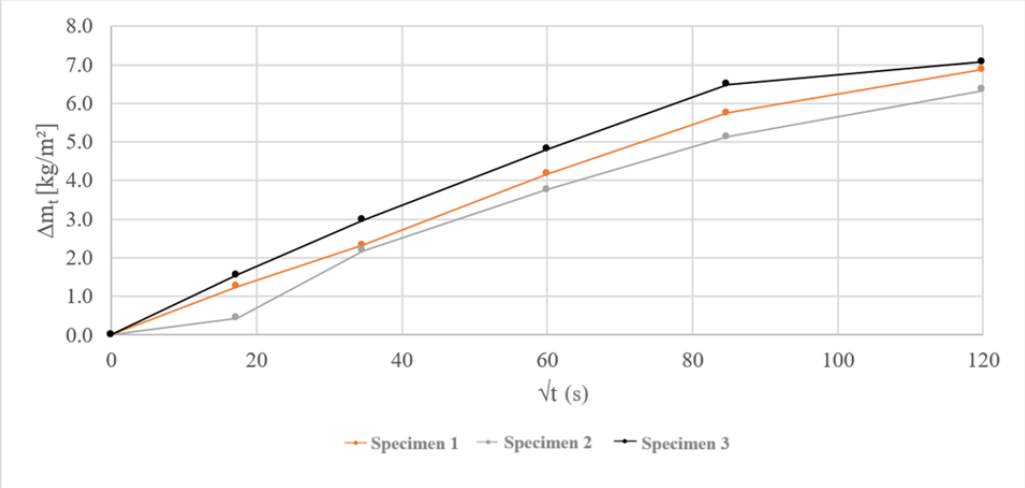


Figure 55 – Mass variation in relation to the square root of time of the mortar

Table 33 – Absorption coefficient of water of the mortar under study in different units

Absorption coefficient of water	
A_w (kg/(m².s^{0,5})	0.056
A_w (kg/(m².min^{0,5})	0.437
A_w (kg/(m².h^{0,5})	3.381

3.3.1.4. Moisture storage function

The moisture storage function of a porous material traduces the equilibrium moisture for a relative humidity of the air. The determination of the moisture storage function of the mortar under study followed the standard ISO 12571:2000 [161]. According to the standard, to obtain the sorption curve, the specimen must initially be dried to constant mass. Then, it should be placed consecutively in different test environments, with increasing relative humidity, until it reaches equilibrium with the environment (when constant mass is reached). In this study, carried out inside a climatic chamber, four relative humidities were considered: 40%, 60%, 80%, and 90%, and the temperature was kept constant during the whole test. Three specimens were tested, and the moisture content was calculated using equation (28). Figure 56 presents the sorption curve of the mortar, with the mean values of the three specimens tested.

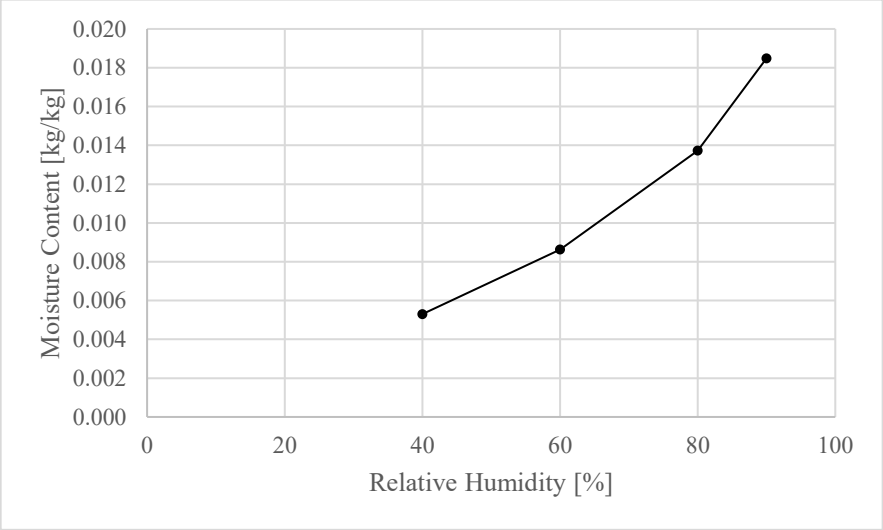


Figure 56 – Sorption curve of the mortar under study

3.3.1.5. Thermal conductivity

The thermal conductivity of the mortar used in the laboratory tests was evaluated using the ISOMET 2114 [162] in samples in the dry state and samples with two different moisture contents.

The principle of operation of ISOMET 2114 consists of providing a heat flow through electrical heating of a resistor heater inserted into the surface probe that is put in direct contact with the specimens. Then, the temperature response of the specimens to heat flow impulses is analysed. For this test, a sensor was used to monitor the temperature and relative humidity of the air during the whole test. The dimensions of the specimens were measured with a pachymeter.

At first, three samples were dried in the oven until their mass was stable so that it was possible to measure the thermal conductivity in the dry state. After removing from the oven, the specimens were wrapped in plastic film to avoid adsorbing moisture from the air and left to cool down for 24 hours to achieve thermal equilibrium with the ambiance of the room. After that, three measurements were performed in each sample with ISOMET 2114 to assess the thermal conductivity. Figure 57 and Figure 58 contain, respectively, the equipment ISOMET 2114 and the weighing of a specimen during the thermal conductivity test.

To determine the variation of the thermal conductivity with the moisture content, the specimens were partially immersed in water for 10 minutes and then wrapped with plastic film to avoid losing water during the measurement, and the thermal conductivity was assessed. Then, the specimens were immersed in water until saturation and then wrapped with plastic film again for a new measurement of the thermal conductivity.



Figure 57 – ISOMET 2114 equipment



Figure 58 – Weight of a specimen during the thermal conductivity test

Table 34, Table 35, and Table 36 – Results of the thermal conductivity test for the saturated specimens

Specimen	Moisture content	λ [W/m.K]	c.ρ [J/m³.K]	a [m²/s]	Tmean [°C]	ΔT [K]
1	202,90	1,4240	1,7978E+06	7,9200E-07	30,3160	9,8942
2	196,97	1,3854	1,8235E+06	7,5970E-07	30,6860	9,8251
3	206,55	1,5547	1,7838E+06	8,7200E-07	30,6850	9,7750

show, respectively, the results of the thermal conductivity test for the dry specimens, moist specimens, and saturated specimens. The technical sheet of the pre-dosed mortar specifies a thermal conductivity of 0,8 W/mK, which is similar to the average obtained for the dry specimens tested. The thermal conductivity increases considerably with the increase in the water content.

Table 34 –Thermal conductivity of the mortar – dry specimens

Specimen	λ [W/m.K]	c.ρ [J/m³.K]	a [m²/s]	T_{mean} [°C]	ΔT [K]
1	0,7838	1,6243E+06	4,8250E-07	30,7990	9,8722
2	0,7573	1,6311E+06	4,6430E-07	31,2480	9,8304
3	0,8687	1,5990E+06	5,4330E-07	31,2880	9,8298
Average	0,8033	1,6181E+06	4,9670E-07	31,1117	9,8441

Table 35 – Results of the thermal conductivity test for the moist specimens

Specimen	Moisture content [kg/m³]	λ [W/m.K]	c.ρ [J/m³.K]	a [m²/s]	T_{mean} [°C]	ΔT [K]
1	182,84	1,3737	1,7282E+06	7,9490E-07	31,4030	9,8502
2	101,64	1,0371	1,6256E+06	6,3800E-07	31,8500	9,8022

3	111,16	1,2366	1,6151E+06	7,6560E-07	31,6850	9,6830

Table 36 – Results of the thermal conductivity test for the saturated specimens

Speci-men	Moisture con-tent	λ [W/m.K]	c.ρ [J/m³.K]	a [m²/s]	T_{mean} [°C]	ΔT [K]
1	202,90	1,4240	1,7978E+06	7,9200E-07	30,3160	9,8942
2	196,97	1,3854	1,8235E+06	7,5970E-07	30,6860	9,8251
3	206,55	1,5547	1,7838E+06	8,7200E-07	30,6850	9,7750

3.3.1.6. Pore size distribution

The pore size distribution of the mortar used in the laboratory tests in controlled conditions is presented in § 3.2.1.4.

3.3.2 SPECIMENS PREPARATION AND PROCEDURES

After characterising the mortar, the specimens were prepared for the monitoring of the drying process with IRT and the gravimetric method. Nine specimens were moulded, three for each different environmental condition, with dimensions of 21 x 21 x 2 (cm x cm x cm). The specimens were waterproofed on their faces (all faces except the one facing to the infrared camera, with 21x21 cm²), dried in the oven until mass stabilization and then humidified with different water contents: one 100% saturated (HMC), one with an intermediate moisture content (IMC) and one in equilibrium with the environmental conditions of the climatic chamber (HYEQ). The information regarding dimensions, dry mass, final mass, and moisture content are shown in Table 37.

Table 37 – Mass and moisture content of the specimens

Scenario	Specimen	Dry mass (g)	Mass after humidification (g)	Moisture content (kg/m³)	Initial specimen's moisture content (%)
Scenario I	HMC[1]	1460.6	1636.9	199.9	12.1
	IMC[1]	1498.7	1615.9	132.9	7.8
	HYEQ[2]	1475.2	1494.7	22.2	1.3
Scenario II	HMC[1]	1547.5	1731.8	209.0	11.9
	IMC[1]	1594.0	1710.3	131.8	7.3
	HYEQ[2]	1507.2	1537.6	34.4	2.0
Scenario III	HMC[1]	1573.8	1769.0	221.3	12.4
	IMC[1]	1507.2	1614.4	121.5	7.1
	HYEQ[2]	1578.6	1593.5	16.9	0.9

[1]HMC: High Moisture Content (100% saturated), IMC: Intermediate Moisture Content
[2]HYEQ: hygroscopic equilibrium: sample was not humidified, just left for one week at room temperature and relative humidity

Each set of 3 specimens (HMC, IMC, and HYEQ)) was placed inside a climatic chamber, considering three scenarios of ambient temperature and relative humidity: (i) Scenario I – 20°C and 70%, (ii) Scenario II – 25°C and 60%, (iii) Scenario III – 15°C and 80%.

The specimens and the water used for their humidification were placed inside the climatic chamber before the tests began to ensure thermal equilibrium. The inner surface of the climatic chamber was lined with black cardboard to avoid reflections during the measurements, and the position of the specimens on the support was marked to ensure they were placed in the same position after weighing.

The main characteristics of the thermographic camera used in the tests are indicated in Table 38. All thermal images were corrected using the camera software, considering the emissivity of the mortar, previously measured, and the reflected temperature, measured according to ASTM E1862 [71].

Table 38 – Infrared Camera Specifications – Fluke, model TiS60+

Infrared Camera Specifications	
Spectral band	7,5~14 µm
Thermal sensitivity	≤ 0.045 °C at 30 °C
Minimum focus length	46 cm
Field of View	Horizontal 34° x Vertical 25°
Spatial resolution (IFOV)	1.86 mRad, D:S 532:1
Number of pixels	320 (H) x 240 (V)

The reflector method was adopted in the test to measure the reflected temperature. This method uses an infrared reflector with an assumed reflectance of 1.0 (a crumpled and re-flattened piece of aluminium foil placed with the shiny side up on a piece of cardboard was used). A thermal image of the infrared reflector, placed in front of the specimen under study, was captured, considering an emissitivy of 1.0. The reflected temperature was the average of the temperature of a square centred in the infrared reflector. The procedure was repeated three times for the three environments under study, and the average temperature was assumed as the reflected temperature for each environment (Table 39).

Table 39 – Reflected temperature measured for each environment under study

Environment	Reflected Temperature
Temperature = 15°C Relative Humidity = 80%	15.3°C
Temperature = 20°C Relative Humidity = 70%	20.6°C
Temperature = 25°C Relative Humidity = 60%	26.1°C

For each specimen, the surface temperature used for the quantitative treatment of the thermal images was the average of the values belonging to a central square of 60 x 60 pixels, as shown in Figure 59.

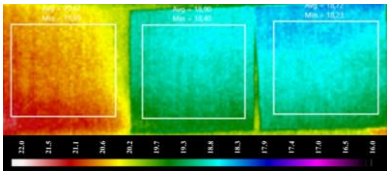


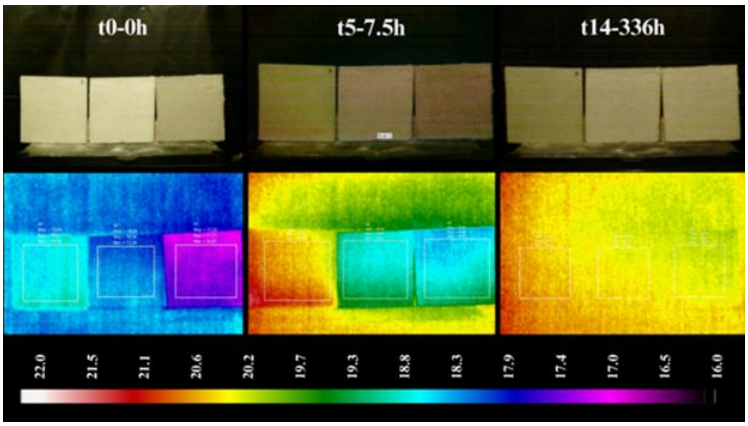
Figure 59 – Area selected for the analyses

Between 15 to 17 measurements were performed (thermal image capture and specimen weighing), depending on the ambient conditions. The temperature gradient (average temperature of the wet specimen subtracted from the average temperature of the dry specimen) and the moisture content were defined for each measurement.

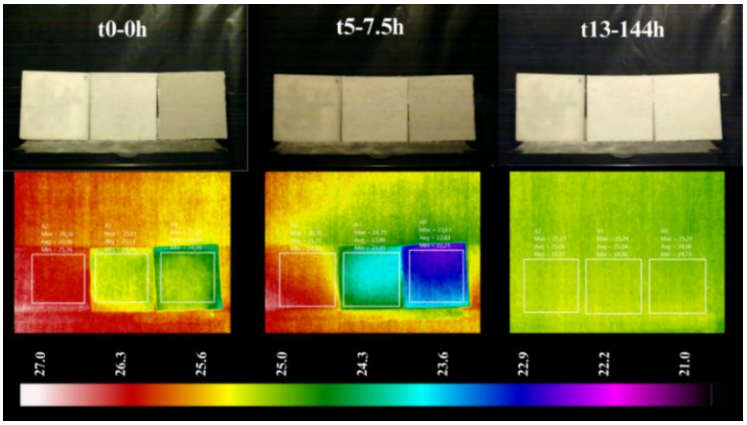
3.3.3 RESULTS

3.3.3.1 Qualitative analyses

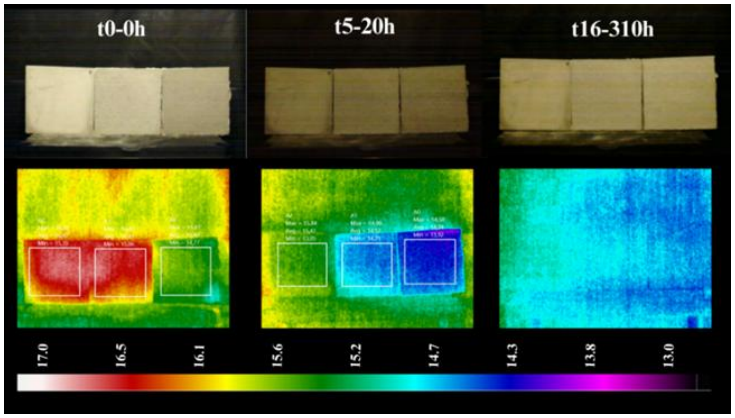
Figure 60 depicts the thermal images taken at three different moments (beginning of the drying, end of drying and in between), for scenarios I, II and III, with the specimens positioned, from left to right, from the driest to most saturated (HYEQ, IMC, HMC). All the thermal images are presented in Appendix 3.



(a)



(b)



(c)

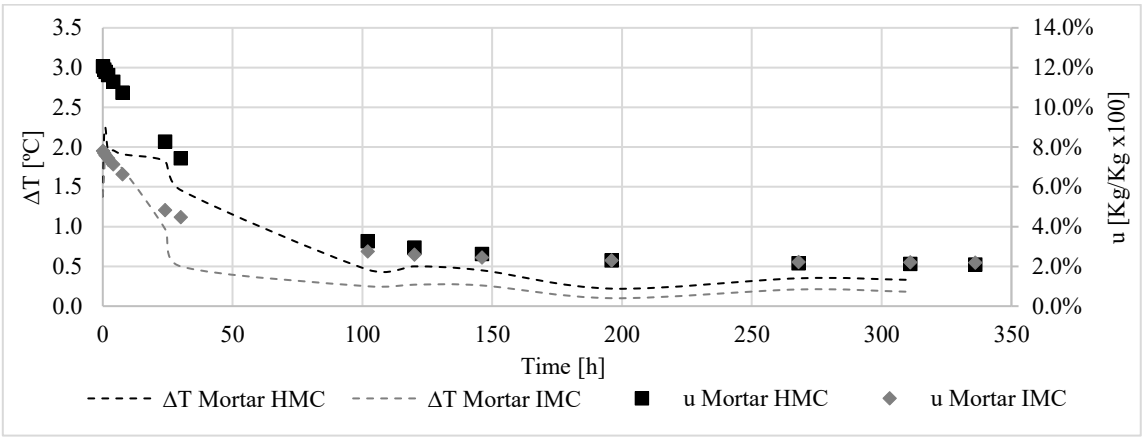
Figure 60 – Thermal images: a) environment I (20ºC / 70%), b) environment II (25ºC / 60%), and c) environment III (15ºC / 80%).

There is a clear temperature gradient between the dry specimen and the specimens with higher moisture content. The greater the evaporation capacity, the greater is the thermal gradient, so in environment II, with a higher temperature and lower relative humidity, the differences between the moisture contents are more evident. The temperature gradient in the three environments gradually reduces with the drying, as expected.

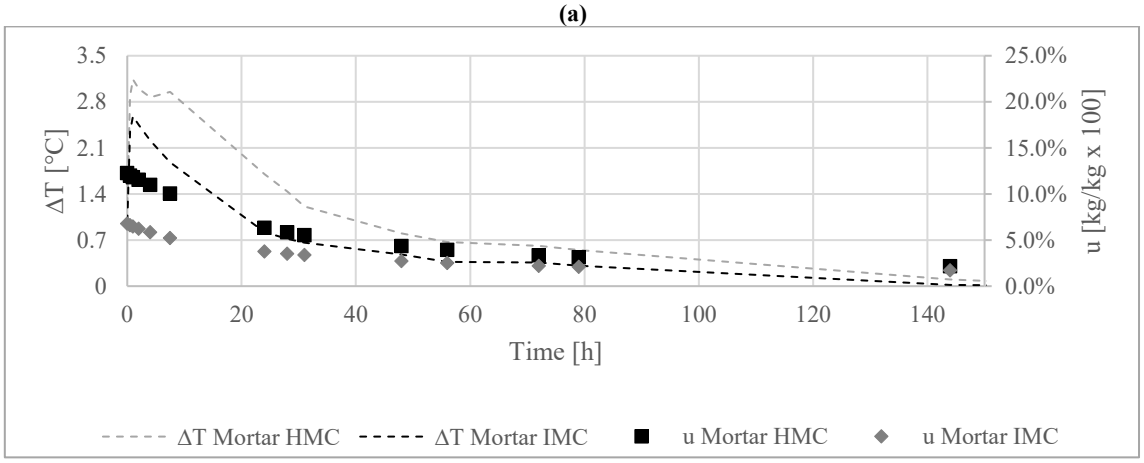
Analysing the thermal images, it can be stated that for environment I, the thermal gradient between specimens with different moisture contents is no longer perceptible after 96 hours. In environment II, something similar occurs earlier, after 56h, and in environment III differences are no longer detectable after 262h, highlighting and confirming that the drying process is strongly dependent on the ambient conditions.

3.3.3.2 Quantitative analysis

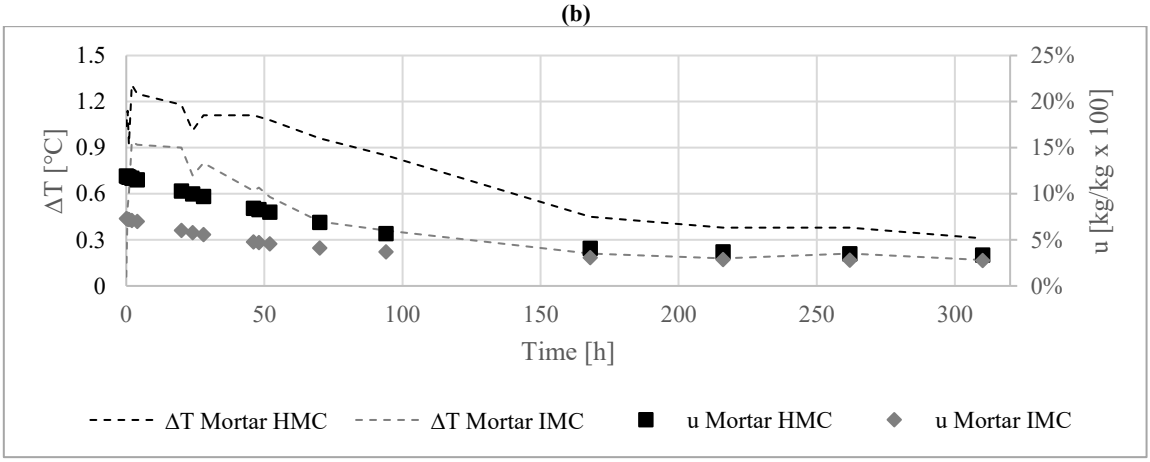
The relationship between thermal gradients, ΔT (ºC), and moisture contents, u (%), is shown in Figure 61. For each environment, lower moisture contents (dots) are related to lower thermal gradients (lines). On the other hand, higher degree of initial saturation, corresponds to higher values of ΔT, since the black elements (dots and lines), corresponding to specimens 100% saturated, are always above the grey elements, corresponding to specimens approximately 50% saturated. It can also be seen that, in the first hours of the drying period, the evolution of the moisture content diverges from the temperature gradient. However, as the drying continues, the two variables follow the same trend: in all environments, the moisture content decreases throughout the drying process and the temperature gradient follows this decrease.



(a)



(b)



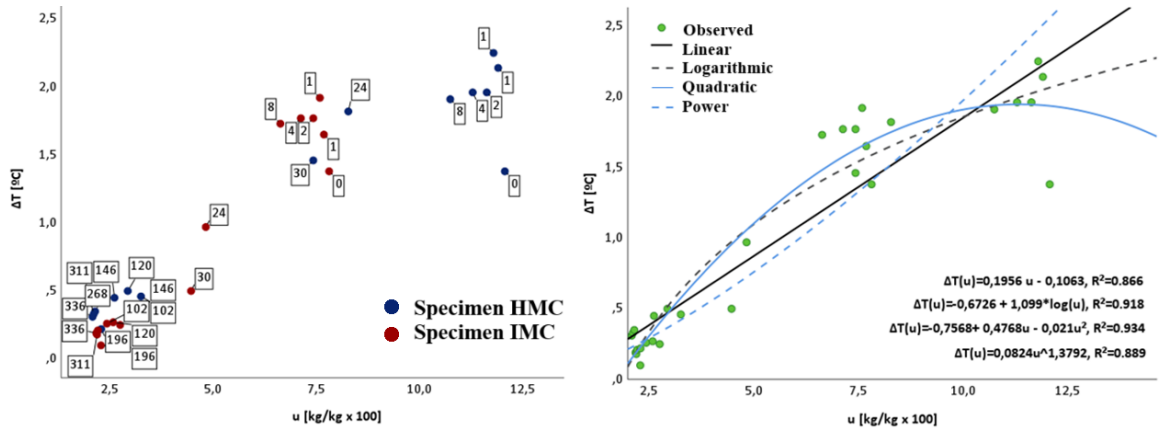
(c)

Figure 61 – Thermal gradient, ΔT (ºC), and moisture content, u (%): a) environment I (20ºC / 70%), b) environment II (25ºC / 60%), and c) environment III (15ºC / 80%)

In the first hours, the temperature of the wet specimens drops sharply as evaporation is enhanced in the beginning of the drying process and, due to evaporative cooling, the thermal gradient increases rapidly up to a specific surface moisture content. After this point in time, which is not clearly defined, the ΔT gradually decreases until it is no longer visible in the thermal images. This decrease is sharper under more favourable drying conditions (higher air temperature and lower relative humidity). In these cases,

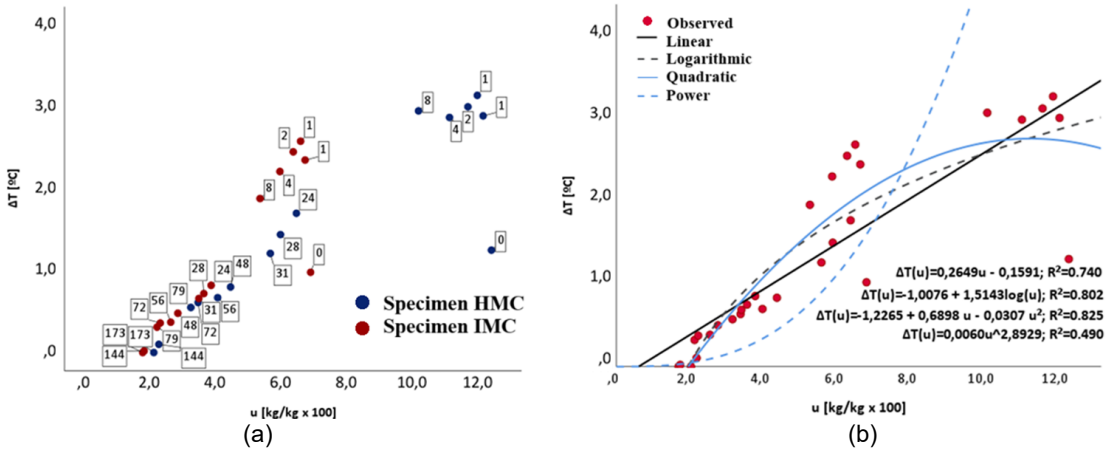
the 2-stages of the drying process is more evident, both in the u and ΔT values, which can be an added value in future applications of using IRT to assess moisture.

The correlation between the thermal gradient, ΔT (°C), and the moisture content, u (%), in the three scenarios is shown in Figure 62, Figure 63, and Figure 64, with the figures (a) representing the scatter plots, where the data labels indicate the measurement times in hours, and (b) representing the regression analysis. For each environment, the lower the moisture content of the specimen, the lower the recorded thermal gradient.



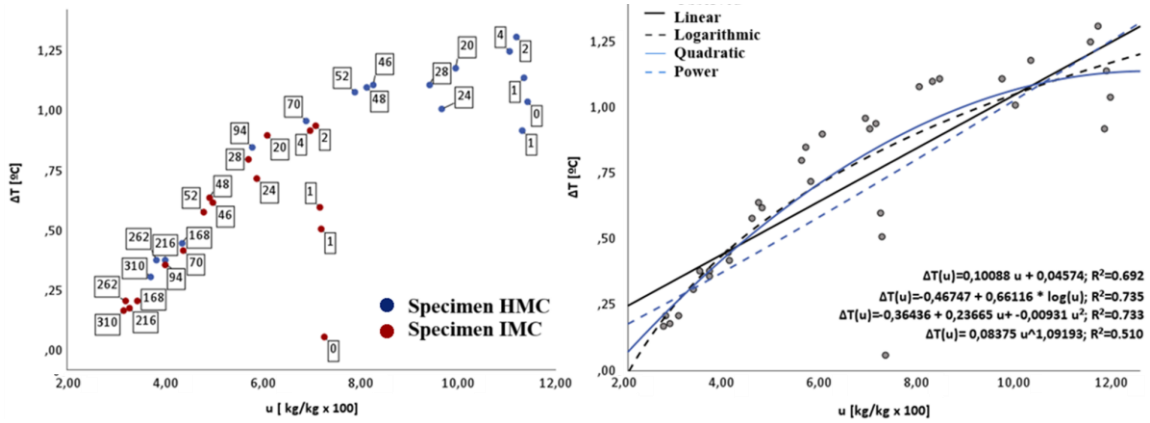
(a) (b)

Figure 62 – Difference in surface temperature between the wet specimen and the dry specimen and moisture content for Scenario I (T=20°C and RH=70%): (a) Point cloud; (b) Regression Curves



(a) (b)

Figure 63 – Difference in surface temperature between the wet specimen and the dry specimen and moisture content for Scenario II (T=25°C and RH=60%): (a) Point cloud; (b) Regression Curves



(a) (b)

Figure 64 – Difference in surface temperature between the wet specimen and the dry specimen and moisture content for Scenario III (T=15°C and RH=80%): (a) Point cloud; (b) Regression Curves

A regression analysis was also carried out to test the best correlation between the variables ΔT (°C) and u (%) for the three studied scenarios (Figure 62b, Figure 63b, and Figure 64b, and Table 40). The results show that the values in the first hours of drying influence the models that best fit the phenomenon. Indeed, considering the value of the correlation coefficient, R^2, it is observed that the quadratic regression model generally fits better the scatter plot, with a good correlation also found with the logarithmic model. This was also found in the free-running tests presented at § 3.2. The best fit is always observed for Scenario I, which may indicate that it is not influenced by the drying conditions, as Scenario II corresponds to the most favourable environment for the drying process.

Table 40 – Coefficient of determination (R^2) for each regression model for the different scenarios

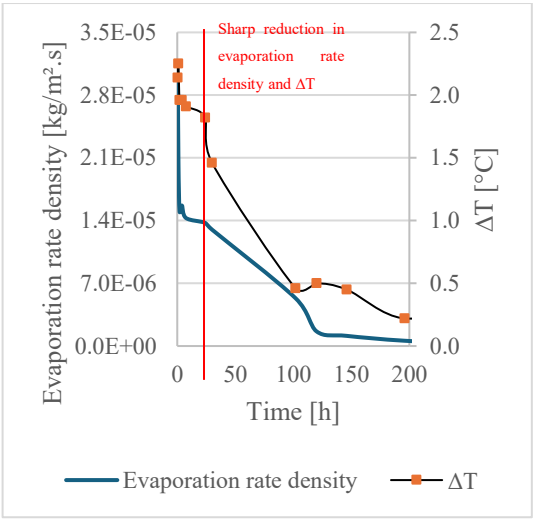
Regression model	Scenario I (20°C e 70%)	Scenario II (25°C e 60%)	Scenario III (15°C e 80%)
Linear	0.866	0.740	0.692
Logarithmic	0.918	0.802	0.735
Quadratic	0.934	0.825	0.733
Power	0.889	0.490	0.510

3.3.3.3 Evaporation rate

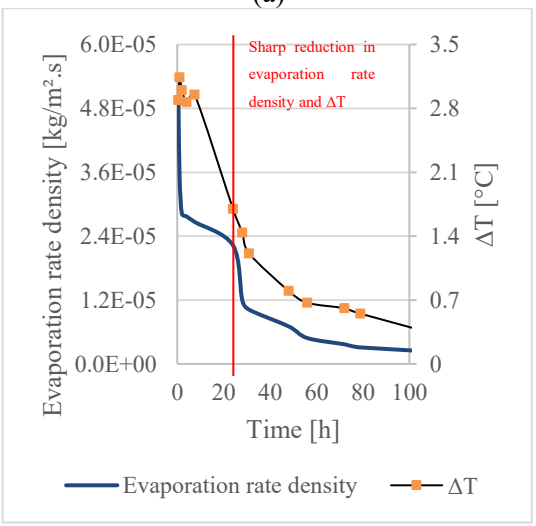
The comparison between the evaporation rate density and the thermal gradient is presented in Figure 65. In all scenarios, the evaporation rate density follows the same trend as the ΔT, exhibiting a sharp reduction in values at nearly the same time. As previously stated, the first drying phase of porous materials is characterised by an approximately constant evaporation rate density followed by a sharp decrease. In scenario II, ΔT starts reducing sharply several hours before the evaporation rate. This can be due to a lack of measurements between 8h and 24h, which means that the thermal gradient may have started decreasing anytime in this period. After this period, there is a second phase of drying with a higher drop of the evaporation rate density. Lastly, there is a third drying phase with a lower drop in the

evaporation rate density. Therefore, for higher moisture contents, the evaporation rate density is approximately constant, but at a certain point it starts to decline at a high rate. As the process continues, the rate of reduction becomes more stable, and the evaporation rate density decreases at a nearly constant rate, albeit with lower values.

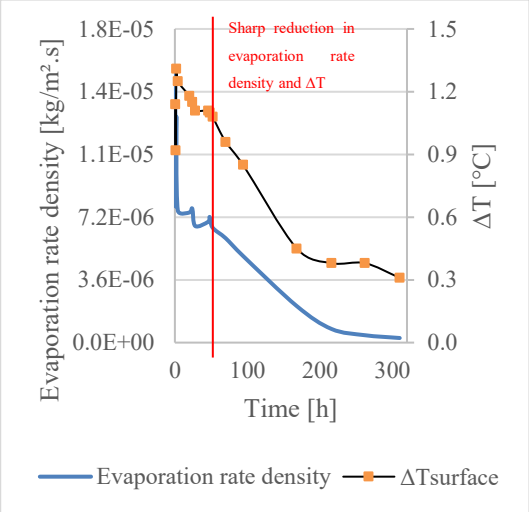
As was expected, the evaporation rate density is higher in scenario II, with higher air temperature and lower relative humidity of the air, intermediate in scenario I (intermediate air temperature and relative humidity) and lower in scenario III, with a lower temperature and higher relative humidity of the air. These results highlight the ability of IRT in detecting the different drying phases in porous materials.



(a)



(b)



(c)

Figure 65 – Comparison between the evaporation rate density and the thermal gradient for: (a) scenario I; (b) scenario II; and (c) scenario III

The correlation between the thermal gradient and the moisture content after the first drying phase is finished is presented in Figure 66. The very strong coefficient of determination (R^2) in the second drying phase can be identified in all scenarios. The R^2 identified in the regression analysis carried out in § 3.3.3.2 is smaller than the coefficient of determination identified in this analysis. Therefore, IRT can be applied to identify the duration of the first phase, and, in the second drying phase, these regression models can be applied to estimate the moisture content with a high accuracy.

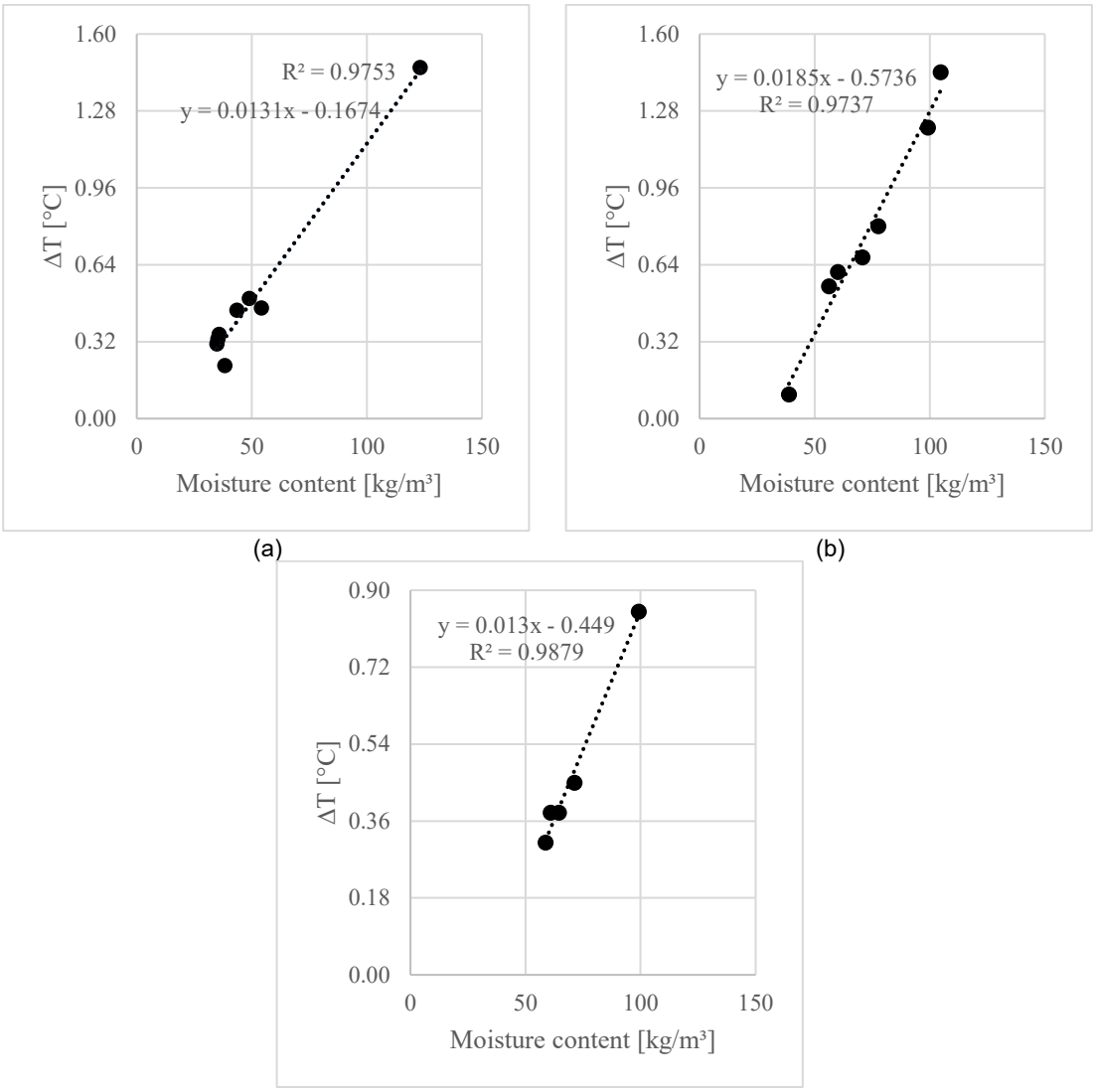


Figure 66 – Correlation between the thermal gradient and the moisture content after the first drying phase for scenario I (a); scenario II (b); and scenario III (c)

3.4 FINAL REMARKS

The laboratory tests provided a comprehensive analysis of the correlation between thermal gradient and moisture content for different materials and different environments. It was possible to identify general correlation patterns, demonstrating the relationship between temperature variations and hygric behaviour in various building materials. These initial results laid the foundation for a deeper understanding of the phenomena. They revealed that each material exhibited unique thermal behaviour during the drying process, confirming that the drying characteristics are strongly dependent on the specific properties of each material, such as porosity. Materials with lower porosity, such as concrete and granite, demonstrated weaker correlation between thermal gradient and moisture content.

It was observed that the regression models are specific to each material and environmental condition since there are relevant differences in the equations found for different materials and environments. Although the quadratic model presented the best fit in all scenarios tested, it cannot be extended to other materials, thicknesses or environmental conditions without further research.

Distinct drying phases were observed through the analysis of the thermal gradient and moisture content. In all scenarios, the evaporation rate density exhibited a sharp decline at roughly the same moment in time that the thermal gradient began to reduce. The first drying phase in porous materials is characterised by an evaporation rate density that remains nearly constant, followed by a significant drop. This transition approximates the moment when the thermal gradient reaches its peak and then begins to fall. After this initial phase, a second drying phase is observed, where the evaporation rate density decreases progressively. At this phase, the thermal gradient follows the same trend.

With the use of IRT, it is possible to identify the duration of the first phase of drying. Then, it is possible to calculate the evaporation rate density and, therefore, identify the moisture content at any time during the first drying phase. During the second drying phase, the moisture content presented a very strong coefficient of determination with the thermal gradient, which means it can also be calculated based on thermal gradient values.

The analysis of the hygrothermal behaviour of saturated materials using IRT was more suitable for materials with higher porosity, which in the case of this work were clay brick, limestone, and mortar. Similar results were obtained in [157] regarding the better suitability of IRT for moisture analysis in more porous building materials.

The use of data from experimental campaigns to train machine learning algorithms enables the algorithm to learn patterns and correlations to predict the behaviour in different scenarios, so the results obtained in the laboratory campaign are of key importance for the development of algorithms to predict the moisture content of different materials in different environmental conditions and algorithms to better understand the drying process in porous building materials.

4

HYGROTHERMAL SIMULATIONS

4.1 SIMULATIONS WITH WUFI

Hygrothermal simulation is a crucial method for understanding the drying behaviour of building materials, enabling the analysis of surface temperature and moisture content during the drying process. Through simulations, it is possible to compare different moisture levels, materials, and environmental conditions, contributing to a more detailed understanding of the factors that influence material performance under different moisture conditions.

WUFI simulations were conducted in three distinct phases. Initially, the drying of clay brick and limestone with varying initial moisture levels under a single environmental condition was evaluated and compared with laboratory results. This step aimed to understand the characteristics of these two materials under controlled conditions. Subsequently, hygrothermal simulations were extended to assess the drying behaviour of clay brick, limestone, concrete, and granite under 30 different environmental conditions. This dataset was the basis for the development of an algorithm that predicts moisture content using IRT data. Lastly, simulations were performed for a fully characterised mortar under the same 30 environmental conditions, aiming to fine-tune the previous model using a combination of simulation and real data for training. Also in this step, simulation data was compared with the results obtained in laboratory for mortar.

These three phases of simulation provided comprehensive insights into the behaviour of different materials during the drying process, contributing to the development of predictive models with practical applications in building diagnosis.

4.2 DRYING PROCESS UNDER VARYING INITIAL CONDITIONS OF MOISTURE CONTENT

4.2.1 FRAMEWORK

The hygrothermal properties of the clay brick and limestone used in the laboratory tests under free-running conditions (§ 3.2) were not measured. Therefore, WUFI Pro material's database was used to define the required input properties of the building materials for the simulation. Regarding geometry, the thickness of the models was 6.4 cm for clay brick and 2.0 cm for limestone, the same as the specimens used in the experimental campaign. Table 41 contains the values of bulk density, porosity, specific heat, heat conductivity of the dry material, and water vapour resistance factor of the dry material for

clay brick and limestone. Figure 67 and Figure 68 depicts the hygroscopic curves for clay brick and limestone, respectively. In both cases, the moisture content starts to increase considerably after the RH exceeds 80%. Regarding the surface transfer coefficients and the related parameters, the following data were defined:

- Internal and external heat resistance: 0.125 m²K/W.
- No dependence of the wind.
- No external and internal coating.
- No shortwave radiation absorption.
- No ground short-wave reflectivity.

Table 41 – Properties of the clay brick and limestone for numerical simulation

Material	Bulk density [kg/m³]	Porosity [kg/m³]	Specific heat [J/kgK]	Heat conductivity dry [W/mK]	Water vapour resistance factor dry [-]	Practical moisture content (equilibrium moisture at a RH of 0.8) [kg/m³]
Solid clay brick	1900.0	0.24	850.0	0.6	10.0	18.0
Limestone	2650.0	0.03	2600.0	3.0	35.7	-

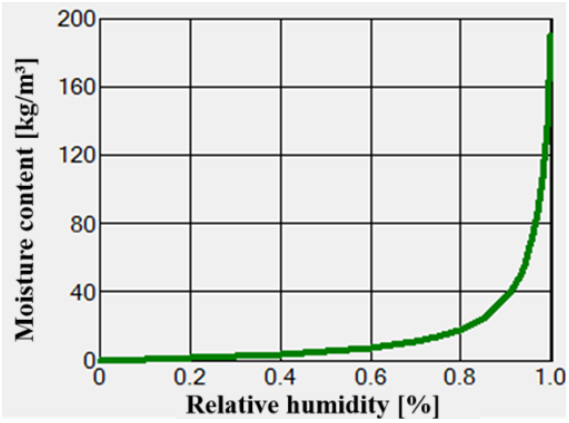


Figure 67 – Brick hygroscopic curve

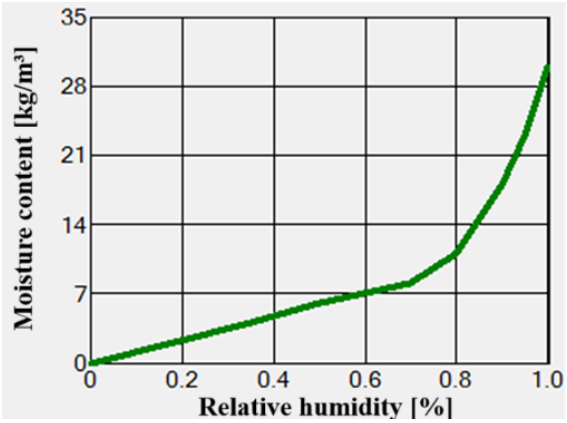


Figure 68 – Limestone hygroscopic curve

In the beginning of the simulation, the temperature of the material was set as 25.0°C and the air relative humidity was set as 60%, approximately the same environmental conditions of the experimental campaign under free-running conditions. Ten different initial moisture content were simulated. For brick, the hygroscopic moisture content at 60% of RH is 7 kg/m³and the maximum moisture content is 240 kg/m³. Therefore, ten different values of moisture content between 7 and 240 kg/m³ equally divided in this range were selected. The moisture content of 7 kg/m³ was not selected since in this condition the material does not have any additional moisture. Similar procedure was implemented for limestone. Table 42 shows the moisture conditions of the materials at the beginning of the simulation.

Table 42 – Initial moisture conditions of the materials simulated in WUFI

Material	Simulation	Bulk density [kg/m³]	Moisture content [kg/m³]	Moisture [kg/kg x 100]	Initial moisture content [%]*
Solid clay brick	1	1900,0	240,0	12,6	100
	2		216,7	11,4	90
	3		193,4	10,1	80
	4		170,1	8,8	70
	5		146,8	7,6	60
	6		123,5	6,3	50
	7		100,2	5,1	40
	8		76,9	3,8	30
	9		53,6	2,5	20
	10		30,3	1,3	10
Lime-stone	1	2650,0	30,0	1,13	100
	2		27,7	1,05	90
	3		25,4	0,96	80
	4		23,1	0,87	70
	5		20,8	0,78	60
	6		18,5	0,70	50
	7		16,2	0,61	40
	8		13,9	0,52	30
	9		11,6	0,44	20
	10		9,3	0,35	10

*Percentage in relation to the maximum moisture content

The simulation period considered for the clay brick was of 46 days. This period was defined considering the average time required for the surface temperature of a wet specimen to achieve the same surface temperature as a dry specimen. As for the limestone, it was observed that they require less time to achieve the initial dry conditions, therefore, the simulation period was shorter, of 32 days.

Regarding boundary conditions, the simulations were run considering an indoor environment in both sides of the material as the aim was to evaluate the variation of moisture and surface temperature under constant climate conditions. In this way, it was defined a constant air temperature and RH of 25 °C and 60%, respectively. The same values were defined both for the “outdoor climate” and the “indoor climate”. After defining all the necessary input parameters, the twenty simulations were performed.

4.2.2 RESULTS

4.2.2.1 Variables evolution over time

Figure 69 depicts the surface temperature variation of the clay brick specimens with initial moisture content from 10 to 100% (specimen characteristics detailed in Table 41). As expected, the higher the initial moisture content, the longer the surface temperature of the specimen took to return to the ambient temperature (25°C). In the first hours of the test, the different specimens had very different temperatures, however, with time the surface temperature of all specimens approximated to each other.

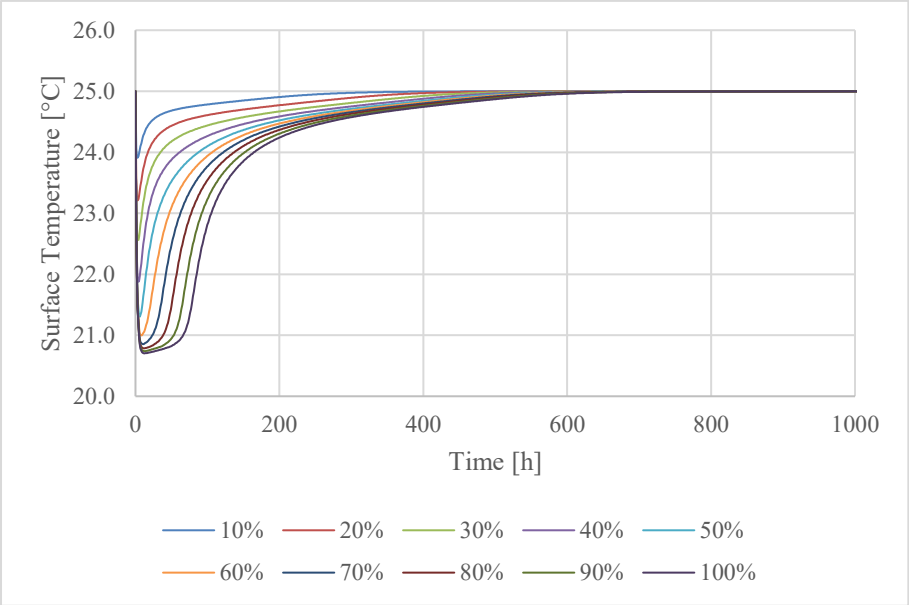


Figure 69 – Surface temperature during drying of clay brick specimens with different initial moisture content

The variation in surface relative humidity [%] and moisture content in [kg/m³] and in [kg/kg x 100] is shown in Figure 70, Figure 71, and Figure 72, respectively. It is observed that the initially saturated specimen took approximately 600 hours for total drying. The specimen with only 10% of initial humidity took approximately 400 hours for total drying. However, after 100 hours of testing it already had very low moisture contents, below 1.0%.

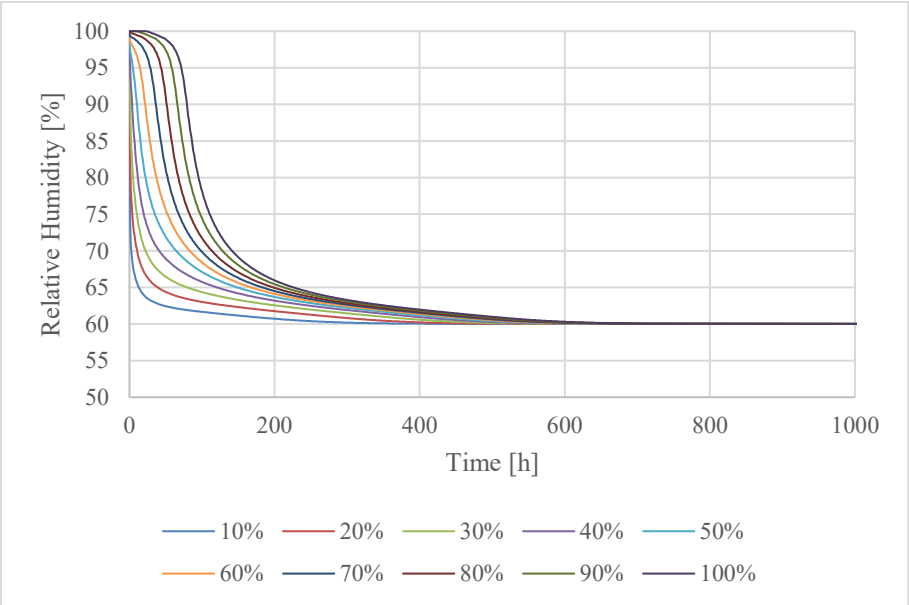


Figure 70 –Relative humidity variation relative to the surface of the clay brick specimens

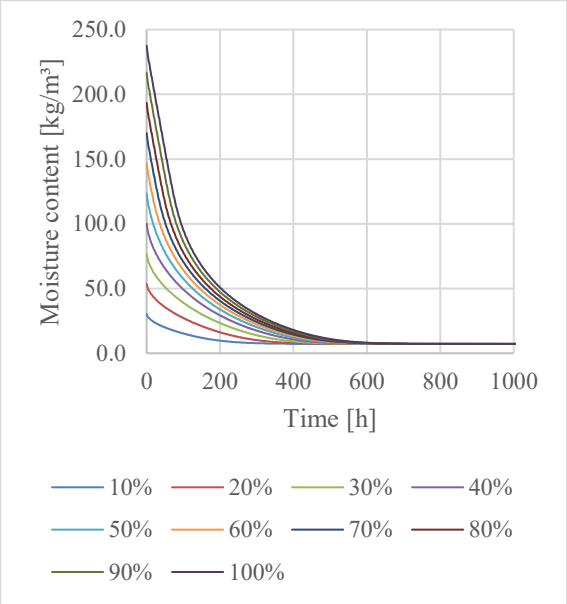


Figure 71 – Variation of moisture content on the surface of clay brick for different initial moisture content [in kg/m³]

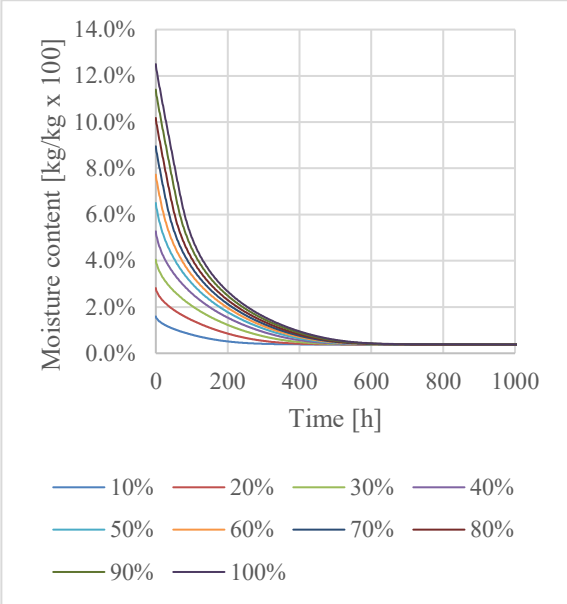


Figure 72 – Variation of moisture content on the surface of clay brick for different initial moisture content [in %]

The graphs showed that specimens with a higher initial moisture content show a sharp drop in humidity at the beginning and, as the test progresses, the drying speed decreases, showing a reduction in the evaporative flow as the moisture content decreases, as pointed out by [4].

The reduction in the surface temperature observed in the limestone specimens was considerably lower than that observed in the clay brick specimens, although with a similar pattern, as depicted in Figure 73. In addition, it is also observed that the time taken for the surface temperature of the limestone specimens to return to the initial temperature was only 60 hours, while in the clay bricks it was approximately 600 hours.

The microstructure of materials has a great influence on their drying capacity, and the porosity is one of the characteristics of the microstructure with greater influence. The porosity of the clay brick available in the database of materials of WUFI is 0.24, while the porosity of the limestone is 0.03, which leads to a great difference in the results obtained. Also, the thickness of the limestone specimens (2 cm) was more than three times smaller than the thickness of the clay brick specimens (6.4 cm). Therefore, such factors have a big impact on the rapid drying speed of the limestone specimens compared to clay brick.

The surface relative humidity variation in the specimens during the test is shown in Figure 74. The graphs that depict the moisture content of the specimens in kg/m³ and in % are shown in Figure 75 and Figure 76, respectively.

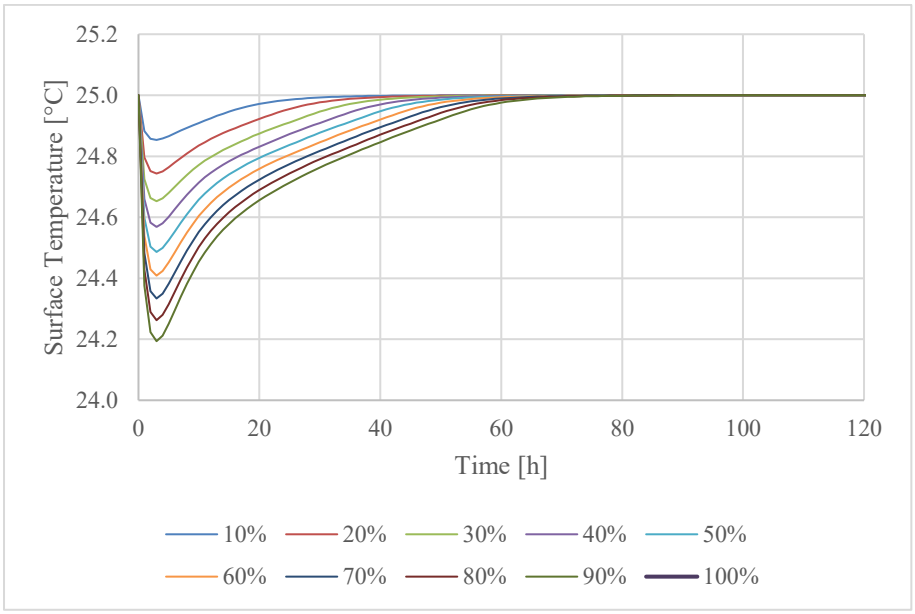


Figure 73 – Surface temperature during drying of limestone specimens for different initial moisture content

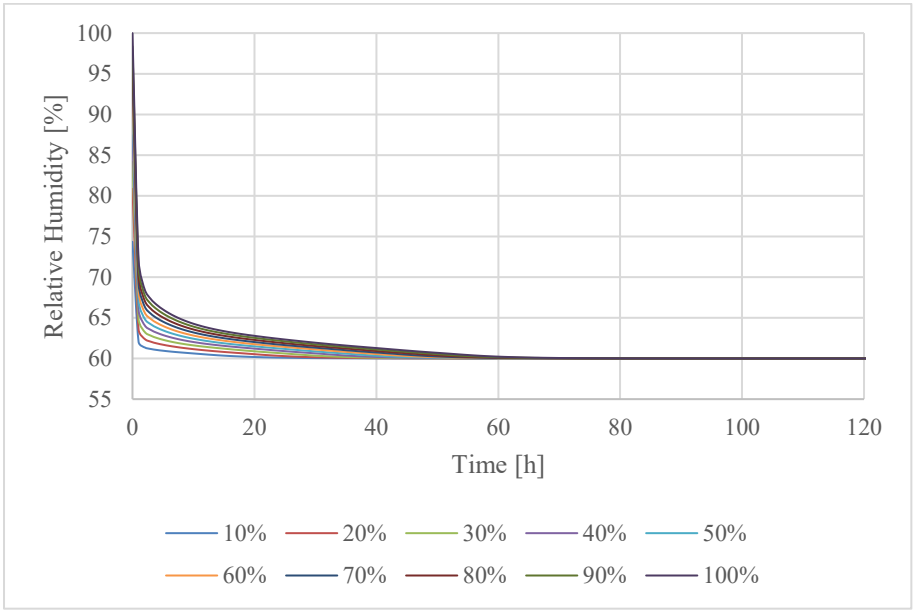


Figure 74 – Relative humidity variation relative to the surface of the limestone specimens

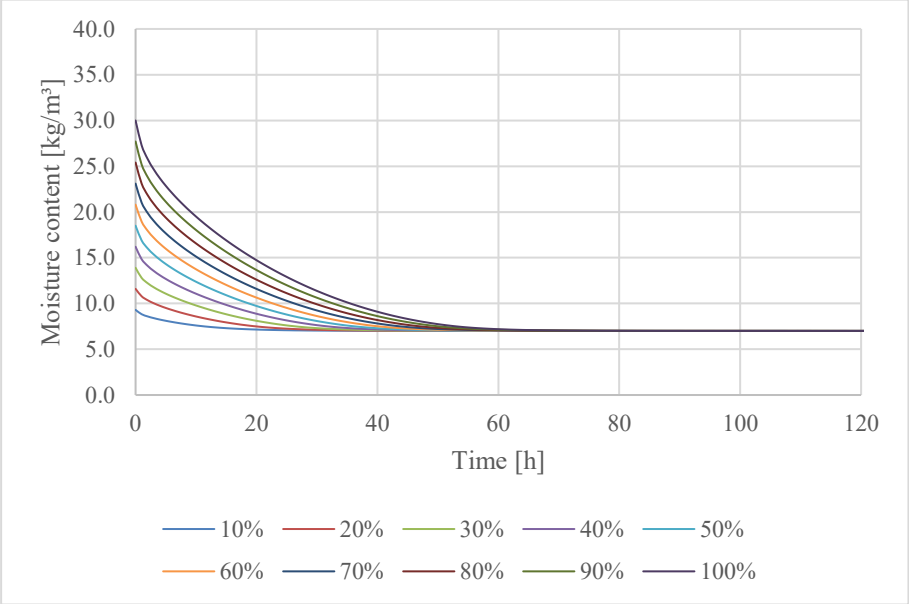


Figure 75 – Variation of moisture content on the surface of limestone for different initial moisture content [in kg/m³]

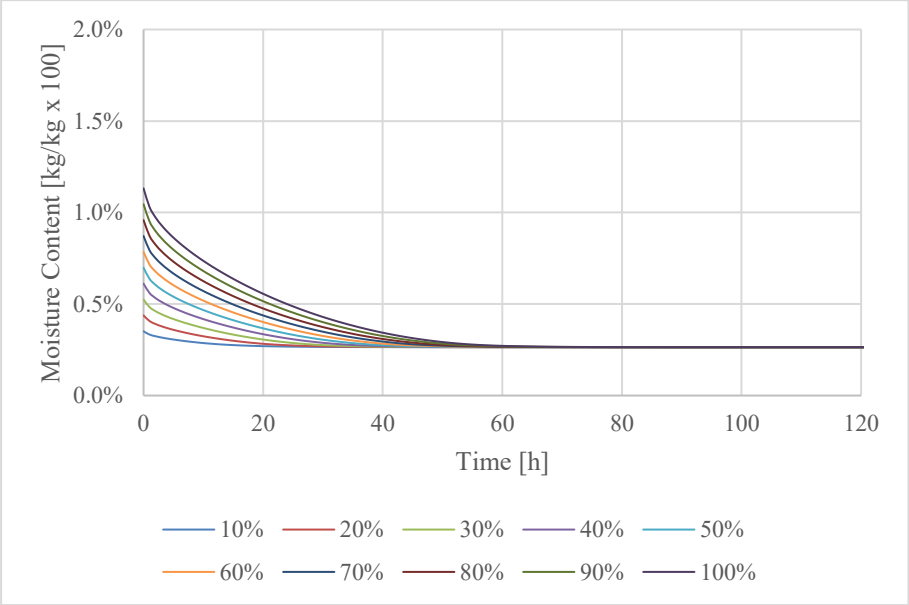


Figure 76 – Variation of moisture content on the surface of limestone for different initial moisture content [in %]

4.2.2.2 Evolution of the maximum thermal gradient as a function of the moisture content

The graph in Figure 77 depicts the maximum thermal gradient identified during the entire drying phase of each clay brick specimen. The maximum thermal gradient increases significantly up to the initial moisture content of 50%, but it tends to stabilise after that. It is possible to observe a trend line for a quadratic regression model indicating a R^2 near 1.

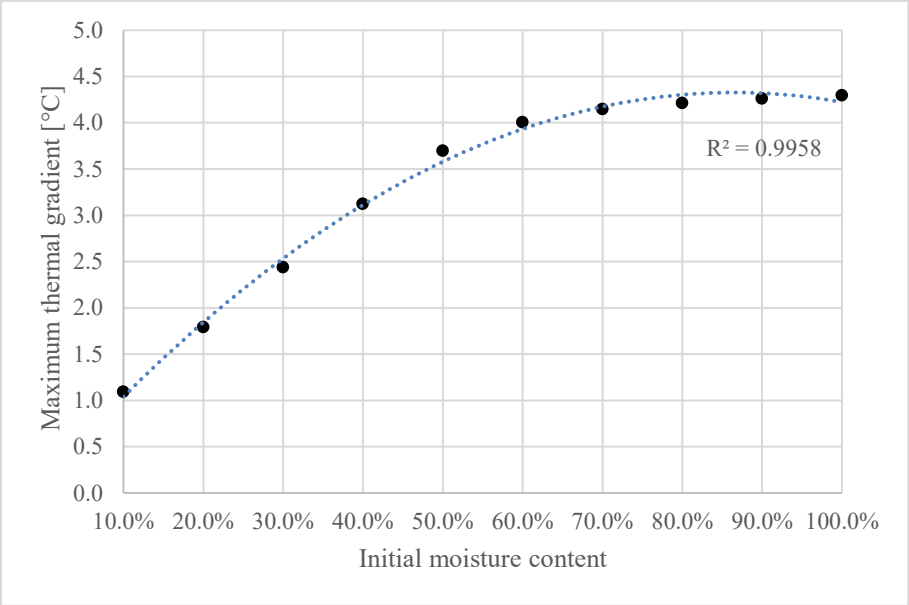


Figure 77 – Maximum thermal gradient identified in the drying phase for different initial moisture content - clay brick

Figure 78 depicts a graph with the maximum thermal gradient identified during the drying phase of the limestone specimens. For the quadratic regression model (which presented the best adjustment to the points) a R^2 near 1 is observed. While for clay brick the maximum gradient identified for the 10% moisture content is greater than 1.0 °C, in the case of limestone the maximum gradient identified for the 10% moisture content is just 0.15 °C.

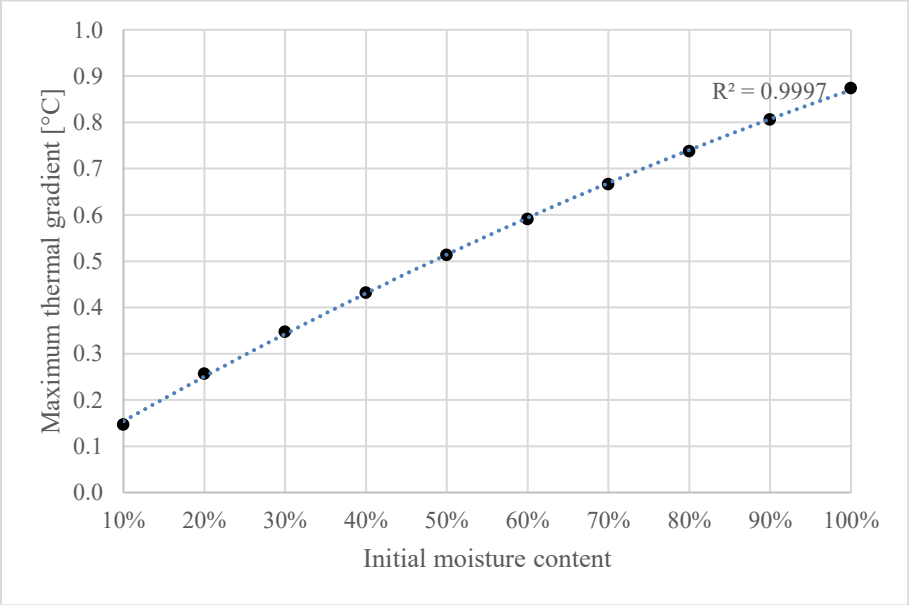


Figure 78 – Maximum thermal gradient identified in the drying phase of each specimen - limestone

4.2.2.3 Correlation analysis

With the aim of analysing the relationship between the variables “thermal gradient” and “moisture content”, the graph in Figure 79 was generated, which includes the results of all the simulations for clay brick. The coefficient of determination (R^2) found for the quadratic model was 0.92. Although the coefficient shows a strong correlation between the variables, this curve does not capture the correlation in the beginning of the tests when the thermal gradient and the moisture content are high.

To facilitate the understanding of the pattern identified in each of the specimens, the data was separated according to the initial moisture content of each specimen, as depicted in Figure 80. For each of the specimens, there is a clear downward curve between the thermal gradient and the moisture content.

The specimens with higher initial moisture content presented a phase in which the thermal gradient varied in a narrow range while the moisture content varied more widely. Figure 81 shows this phase for the specimen with initial moisture content of 100%, which is called “2nd phase”. The first phase refers to the beginning of the test, which is the time that the surface temperature takes to reach its minimum value. The third phase refers to a significant decrease in the thermal gradient until it tends to zero. For smaller initial moisture content, the second phase does not exist, as it can be seen in Figure 82.

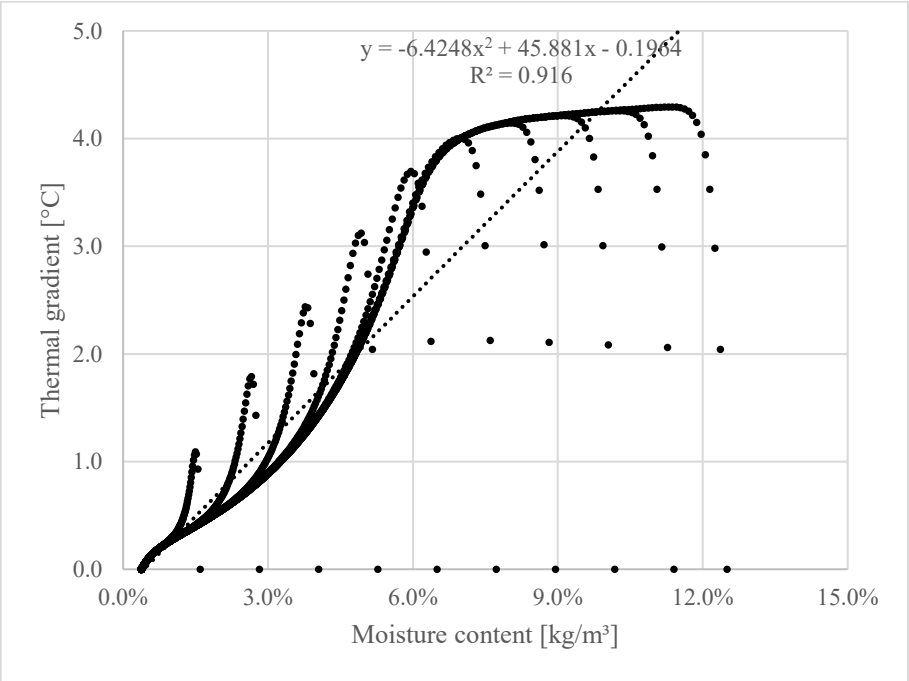


Figure 79 – Correlation between thermal gradient and moisture content - clay brick

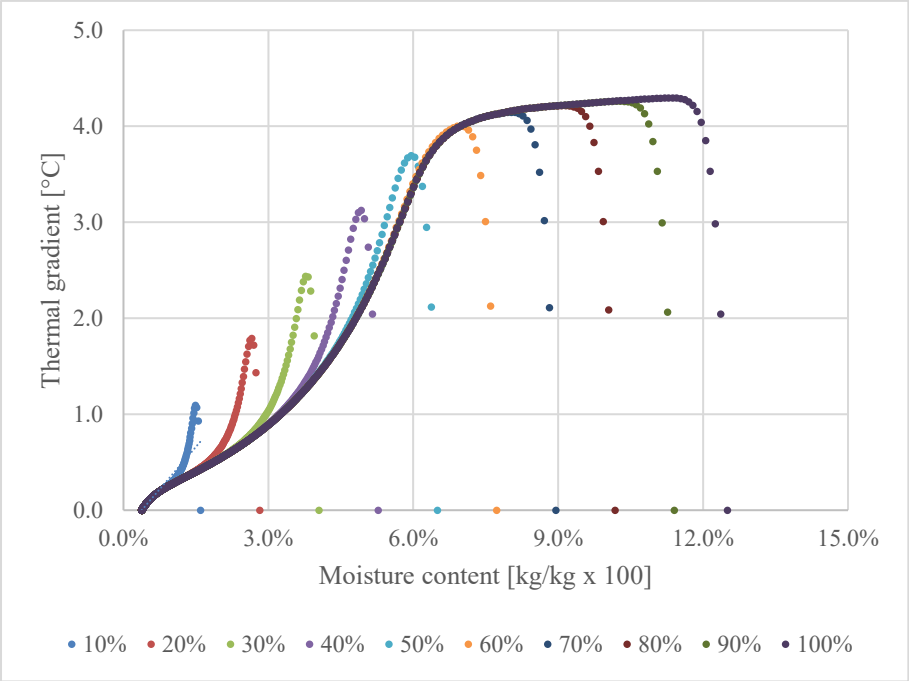


Figure 80 – Correlation between thermal gradient and moisture content separated by initial moisture content - clay brick

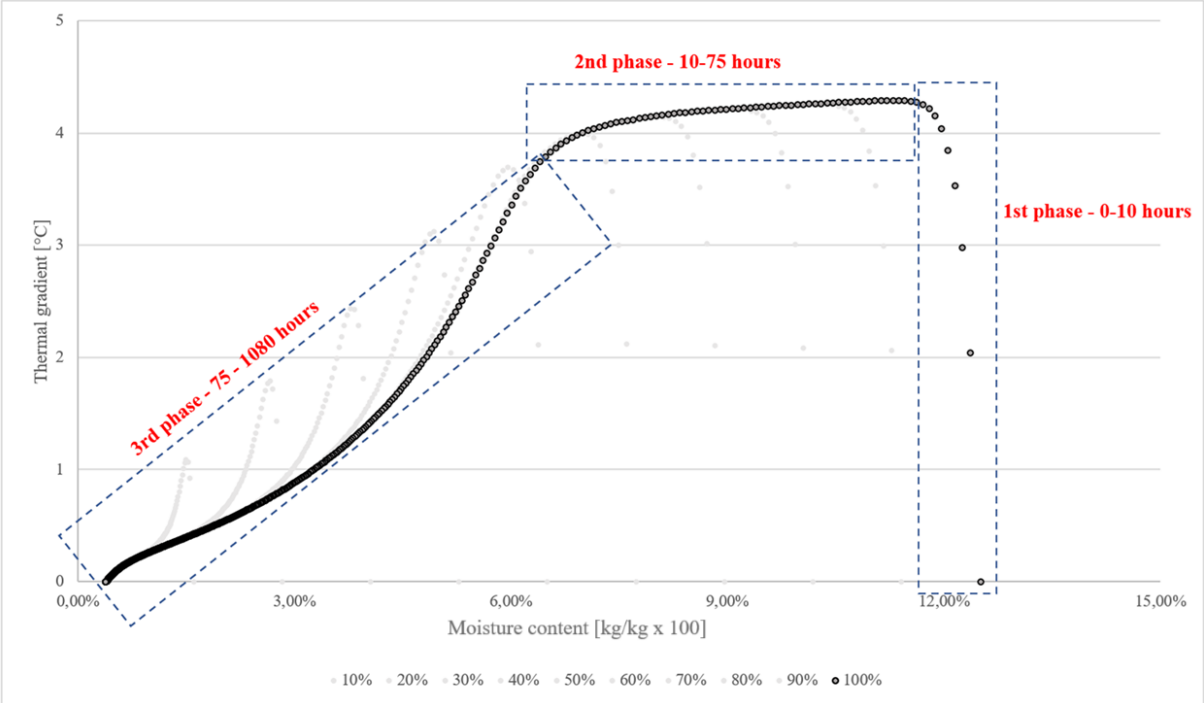


Figure 81 – Drying phases in the correlation graph – Brick specimen with initial moisture content of 100%



Figure 82 – Drying phases in the correlation graph – Brick specimen with initial moisture content of 10%

The graphs in Figure 83 and Figure 84 indicate the correlation between thermal gradient and moisture content [%] for limestone. In Figure 83, all values are presented without distinction according to the initial moisture content of the specimen, while in Figure 84 there is a distinction between moisture contents. As in the case of clay bricks, it is observed a pattern in the results obtained and a high coefficient of determination of 0.91 for the quadratic regression model. Unlike the results of clay bricks, even the specimen with 100% of initial moisture content did not present the “2nd phase”. Only two phases were identified in all the simulations. This might be related to the low porosity and low moisture content of the limestone specimens analysed.

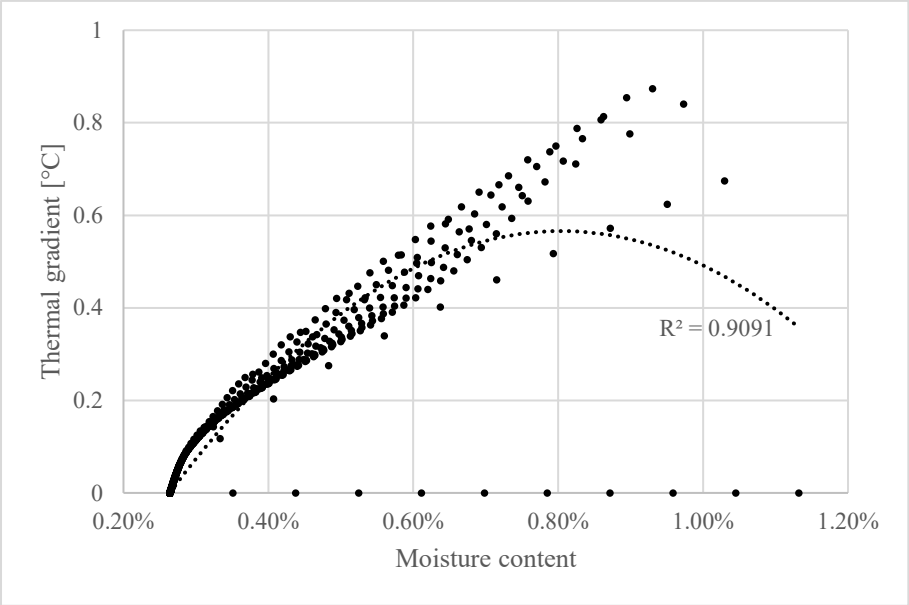


Figure 83 – Correlation between thermal gradient and moisture content – limestone

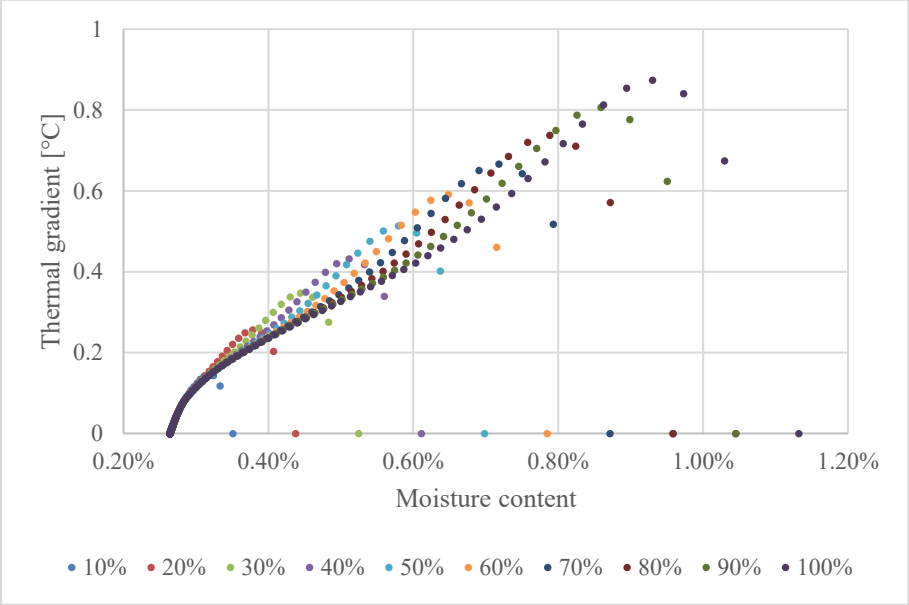


Figure 84 – Correlation between thermal gradient and moisture content separated by specimen – limestone

4.2.2.4 Comparison with the laboratory results

The specimens used in the laboratory had very different characteristics from the materials selected for simulation, as verified by the difference in porosity and density values. Hence, it is not possible to carry out a quantitative analysis to compare them. However, a qualitative analysis of the obtained results was conducted.

Figure 85 shows the relationship between the thermal gradient and the moisture content for all data obtained in the laboratory tests with the clay brick specimens. The relationship between the thermal gradient and the moisture content with the data separated according to the initial moisture content of each specimen is depicted in Figure 86. The comparison with the results shown in Figure 80 highlights some similarities in the behaviour of the clay brick specimens in relation to that identified in the simulations. However, the maximum thermal gradient identified in the simulations was almost 1.0 °C higher than the one observed in the laboratory tests.

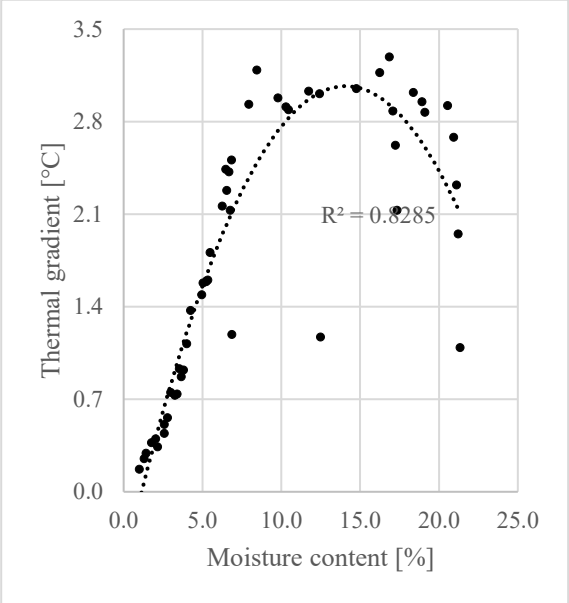


Figure 85 – Correlation between thermal gradient and moisture content – clay brick laboratory tests

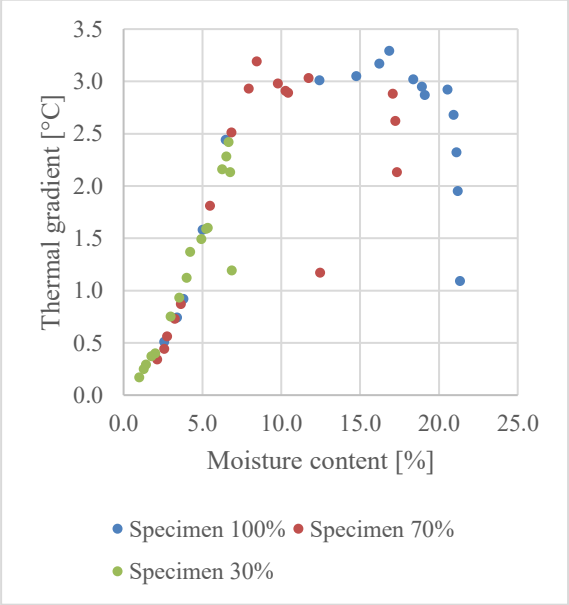


Figure 86 – Correlation separated by initial moisture content – clay brick laboratory tests

To enable a better comparison, the porosity and the apparent density of the clay brick were adjusted in WUFI Pro software. With this adjustment it was possible to make a simulation with an initial moisture content similar to the one measured in the test specimens in laboratory conditions. With a porosity of 0.24 (pre-defined value for the clay brick from the WUFI database), the maximum initial moisture content is 240 kg/m³, and the saturated clay brick specimen from the LFC test showed an initial moisture content of 336 kg/m³. The graph in Figure 87 shows the curves of the three specimens with the mentioned adjustment. A very similar shape of the curves can now be identified for each specimen, but the maximum thermal gradient identified remains considerably higher in the simulation results.

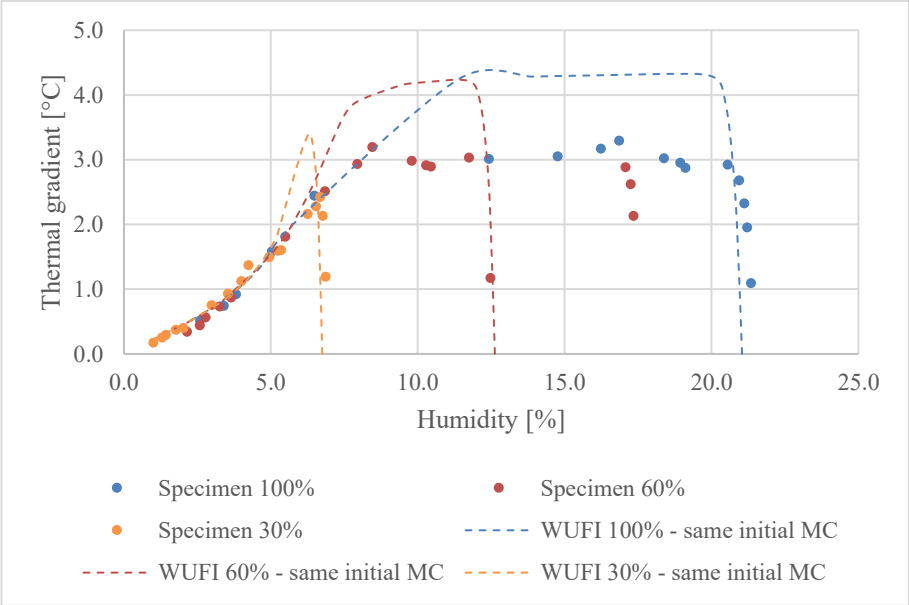


Figure 87 – Correlation chart - comparison of LFC (experimental) and WUFI (numerical) results

It is important to note that the infrared camera showed surface temperature results lower than the air temperature, as presented in Chapter 3. If the same procedure adopted by [163] is adopted in this analysis, that is, adjusting the air temperature in WUFI according to the temperature provided by the infrared camera for the dry specimens (22 ºC), the maximum thermal gradient obtained in WUFI is 3.9 ºC. With this approach, the difference between the predicted results in WUFI and those measured in the laboratory tests for the maximum thermal gradient would reduce to 0.7 °C.

As verified in EN 12524:2000 [164], limestone is a material with a wide range of variation of its properties. There are stones with a density of 1600 kg/m^3 and a water vapour resistance factor of 20, and stones with a density of 2600 kg/m^3 and a resistance factor of 200. In the experimental campaign conducted with limestone, it was observed that it reached saturation at approximately 30 minutes of measurement, indicating a high porosity of this stone and a great divergence with the limestone available in WUFI. Therefore, it was decided not to carry out comparison analyses between the results predicted with WUFI and the laboratory tests for limestone.

4.3 DRYING PROCESS UNDER DIFFERENT ENVIRONMENTAL CONDITIONS

4.3.1 FRAMEWORK

For these simulations, it was defined the air temperature ranging between 5 to 25°C and the air relative humidity from 50 to 90% since these are common values in the building context. The Latin Hypercube Sampling method was used to randomly generate a set of 30 combinations between these parameters. The materials chosen for the analysis were clay brick, concrete, granite, and limestone, which are

building materials usually applied in walls. A reference thickness of 0.10 m was considered for the simulations.

The software WUFI Pro was used to simulate the surface temperature and moisture content during the drying phase of initially saturated building materials. The heat and moisture transfer equations used by the software were previously presented in Chapter 2.

To simulate the drying of wet building materials, the software requires the following input: material's properties, moisture condition, simulation period, and climate conditions. Regarding the material's properties, the predefined materials and their properties available in the software's database were used. The properties of solid clay brick and limestone were presented in Table 41 and of concrete and granite are presented in Table 43.

Table 43 – Properties of concrete and granite for numerical simulation

Material	Bulk density [kg/m³]	Porosity [kg/m³]	Specific heat [J/kgK]	Heat conductivity dry [W/mK]	Water vapour resistance factor dry [-]	Practical moisture content (equilibrium moisture at a RH of 0.8) [kg/m³]
Concrete	2104.0	0.22	776.0	1.373	76.0	101.0
Granite	2453.0	0.095	702.0	1.66	54.0	7.3

Since the simulation was run considering indoor environment in both sides of the material, the surface film coefficient for heat transfer on both boundaries was set at 0.125 m²K/W [40]. The material was initially considered saturated, with the moisture content [kg/m³] at the beginning of the simulation set to the maximum possible value for each material.

Figure 88 shows the total data simulated with the hygrothermal tool and selected for developing the machine learning models. Concerning the environmental conditions, the 30 combinations of air temperature and relative humidity were defined as input and set as constant during the simulation period. Since four types of materials were simulated for each combination of air temperature and relative humidity, a total of 120 simulation scenarios were obtained.

The simulation period in each scenario was set as 65000 hours, and the time step was 1 hour. For computational effort purposes, it was necessary to reduce the data for the next steps, so approximately 40 sets of data (inputs and outputs) were selected among the 65000, using the maximum thermal gradient identified during the drying phase ($\Delta T_{surfacemax}$). At the beginning of the drying process, the thermal gradient (ΔT) is 0°C; then, it rises until it reaches $\Delta T_{surfacemax}$. Two sets of data were selected in this initial phase. The remaining sets of data were selected in the period from the $\Delta T_{surfacemax}$ until the ΔT returned to 0°C. Hence, a total of 4800 sets of data were selected for the analysis (Figure 88).

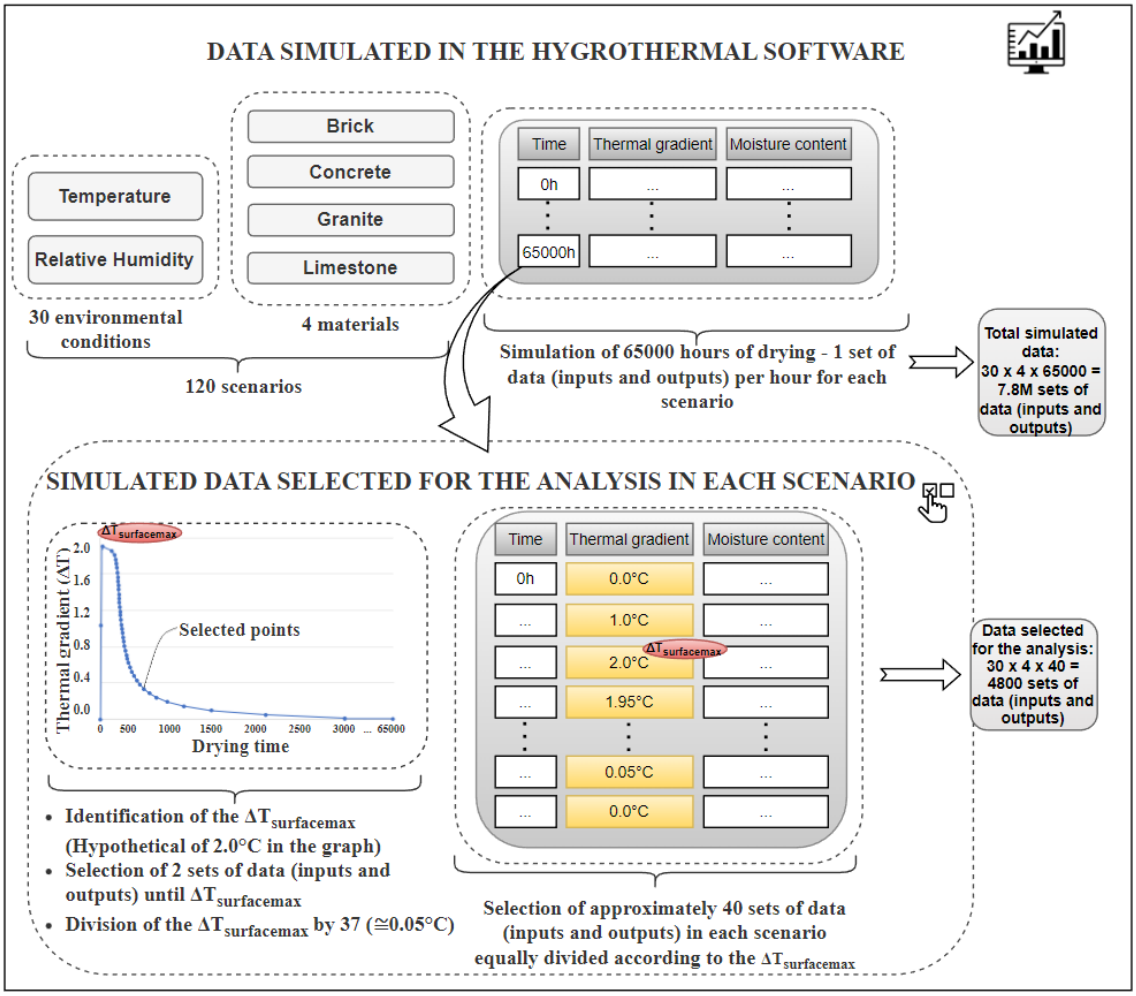


Figure 88 – Data simulated in the hygrothermal software and data selected for the analysis

4.3.2 RESULTS

The assessment of the data generated in the hygrothermal simulation software is presented in this Section. The models developed are presented in Chapter 5.

Figure 89 shows the data distribution of the simulation outputs ($\Delta T_{surfacemax}$, $\Delta T_{surface}$, and moisture content). There are 30 values of $\Delta T_{surfacemax}$ for each material since there were 30 different environmental conditions that influenced these values. For the clay brick and granite, the values of $\Delta T_{surfacemax}$ were similar, ranging from approximately 0.5 to 4.5°C. For concrete, the $\Delta T_{surfacemax}$ ranged from about 0.3 to 0.9°C. Lastly, for limestone, the maximum thermal gradient identified between the wet and dry surfaces varied from 0.10 to 0.45°C.

Regarding the $\Delta T_{surface}$, there are approximately 1200 values for each material, as explained in the previous section. All materials presented a high number of low $\Delta T_{surface}$ values. This can be explained by the fact that building materials have different drying phases, which directly impact their surface temperature. At the beginning of the drying process, the surface evaporation rate is very high, so the $\Delta T_{surface}$

presents high values. However, this initial drying phase does not last long, and the $\Delta T_{surface}$ quickly reduces to low values due to a sharp reduction in the drying rate. Then, it takes a long time until the $\Delta T_{surface}$ reaches 0°C because the drying rate is very low. The different evaporation rates during the drying process are also explained in [4], [50].

The histograms presented very different formats for all materials in relation to the moisture content. The clay brick's histogram resembled a normal distribution, in which most values were concentrated around the mean moisture content. Figure 90 shows the drying behaviour of the four materials regarding the values of moisture content and $\Delta T_{surface}$ in the environment with an air temperature of 7°C and relative humidity of 53.73%. Results reveal that, in the case of clay brick, the moisture content sharply decreases in the beginning, but it then takes a long time to return to values near to 0 kg/m³, justifying the high number of intermediate values.

Regarding the concrete's moisture content, there are only a few values below 180 kg/m³. According to Figure 90 (a) and (b), its $\Delta T_{surface}$ quickly reduces to values close to 0°C, but the moisture content remains high when $\Delta T_{surface}$ tends to 0. Despite no thermal gradient, the concrete was still very humid, and the evaporation was low. For granite, the moisture content decreases more sharply than in the case of clay brick, attaining to very low values sooner. This explains why there are a bigger number of small values in this histogram. Lastly, limestone's behaviour was similar to concrete since there was no sharp decrease in moisture content at the beginning of the drying process.

The variation of the $\Delta T_{surface}$ according to the moisture content of the materials is shown in Figure 91. The graph shows that the correlation between the thermal gradient at the surface and the moisture content depends substantially on the type of material, as limestone and concrete present a much narrower variation than clay brick and granite. Besides that, it is possible to see in Figure 91 several downward curves for each material, each corresponding to a different environmental condition.

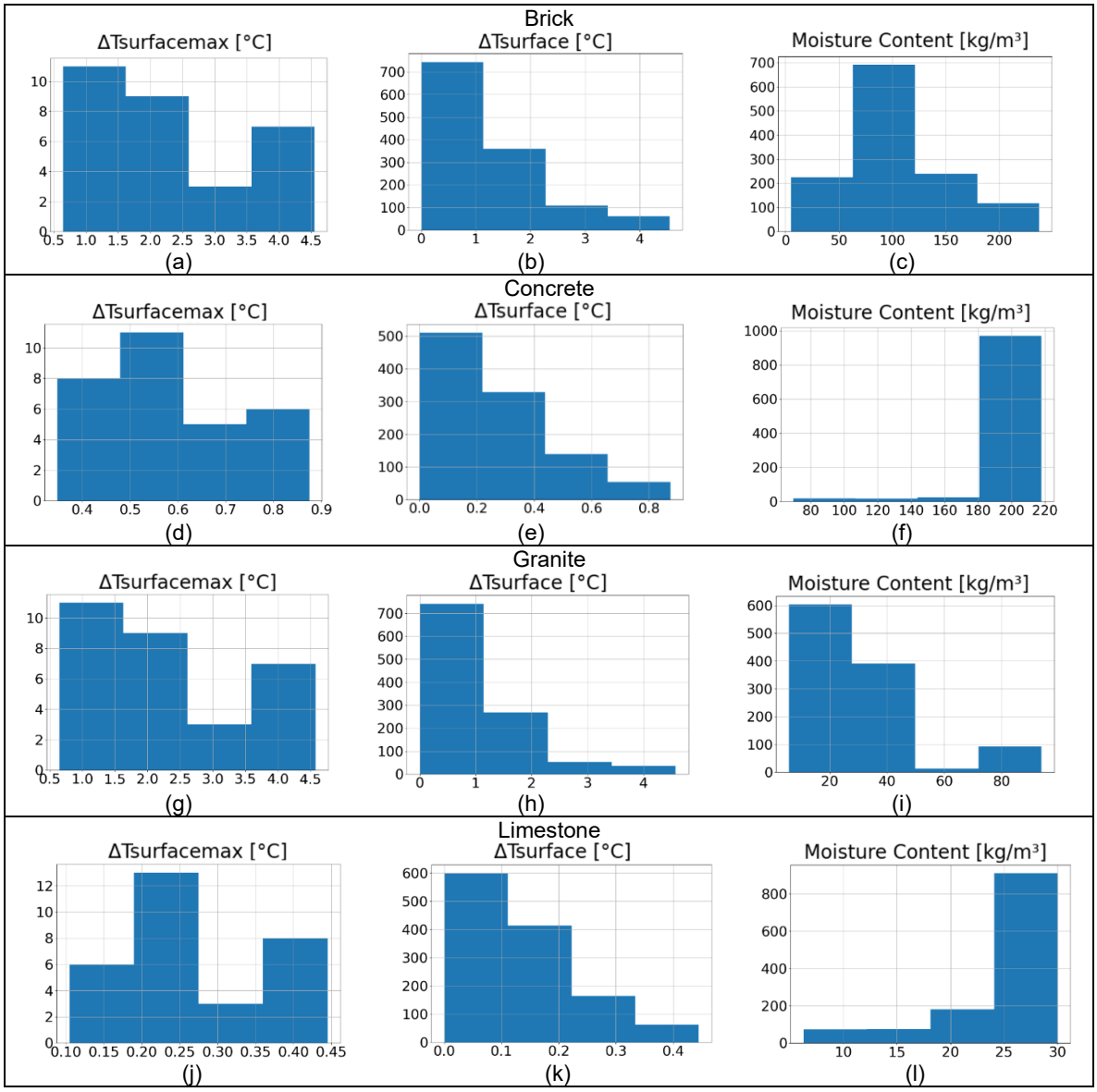
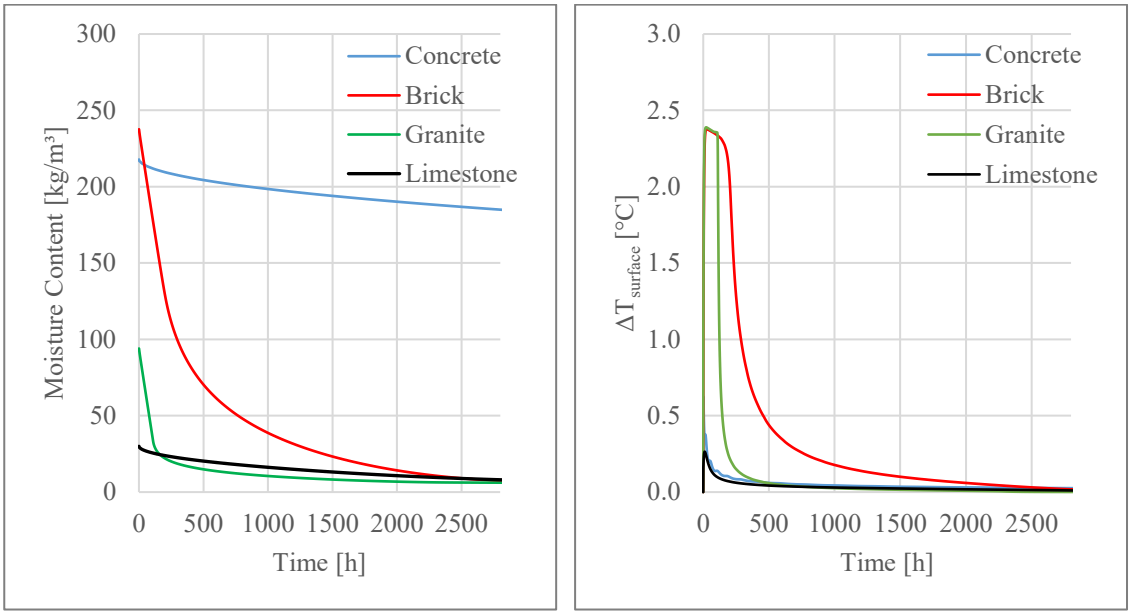


Figure 89 – Data distribution of (a) $\Delta T_{surfacemax}$ clay brick (ºC), (b) $\Delta T_{surface}$ clay brick (ºC), (c) Moisture content (kg/m³) clay brick, (d) $\Delta T_{surfacemax}$ concrete (ºC), (e) $\Delta T_{surface}$ concrete (ºC), (f) Moisture content (kg/m³) concrete, (g) $\Delta T_{surfacemax}$ granite (ºC), (h) $\Delta T_{surface}$ granite (ºC), (i) Moisture content (kg/m³) granite, (j) $\Delta T_{surfacemax}$ limestone (ºC), (k) $\Delta T_{surface}$ limestone (ºC), (l) Moisture content (kg/m³) limestone



(a) (b)

Figure 90 – Drying behaviour of concrete, clay brick, granite, and limestone regarding the (a) Moisture Content [kg/m³], and (b) $\Delta T_{surface}$

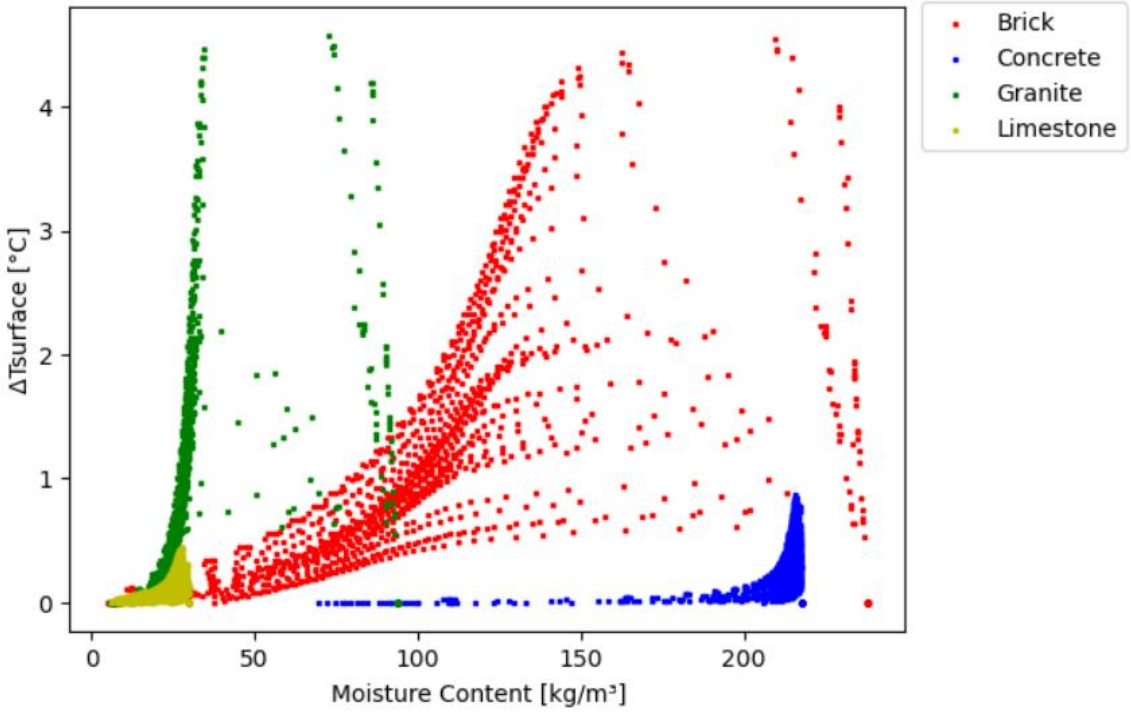


Figure 91 – Variation of the $\Delta T_{surface}$ according to the moisture content for different materials

To further understand the impact of the environmental conditions, the graphs in Figure 92 show the variation of the maximum thermal gradient with the temperature and relative humidity of the ambient air in the case of each material. Although each material presented a different $\Delta T_{surfacemax}$, it is possible to

see a common pattern as the greater thermal gradients occur for a combination of high temperature and low relative humidity for all four materials assessed.

The density of the vapour flow rate can be obtained according to equation (33), so the evaporation at the surface will be influenced by the subtraction of the water vapour partial pressure in the ambient air from the water vapour partial pressure at the surface, which, on its turn, will be influenced by the temperature and relative humidity of the ambient air [47]. Since the density of the flow rate affects the surface temperature [4], the difference in the water vapour pressure of the ambient air and the surface is expected to influence the thermal gradient. For this reason, in environments with high air temperature and low air relative humidity, the evaporation capacity and, therefore, the thermal gradient, will be higher than in environments with low temperature and high relative humidity of the air [47].

$$g_v = \beta_p \,.(\rho_{v,a} - \rho_{v,s}) \tag{33}$$

Where:

g_v: density of vapour flow rate [kg/(m².s)]

β_p: surface film coefficient for vapour diffusion [s/m]

$\rho_{v,a}$: water vapour partial pressure in the ambient air [Pa]

$\rho_{v,s}$: water vapour partial pressure in the surface [Pa]

The similar results between clay brick and granite might be explained by their similar evaporation rate density identified at the beginning of the simulation, the period when the $\Delta T_{surfacemax}$ is detected. Figure 93 contains the evaporation rate density of the materials in the same environment presented in Figure 90. The density of the evaporation rate density of the clay brick and granite is very similar until 109 hours of simulation, when they both reach approximately 99.3% of surface relative humidity.

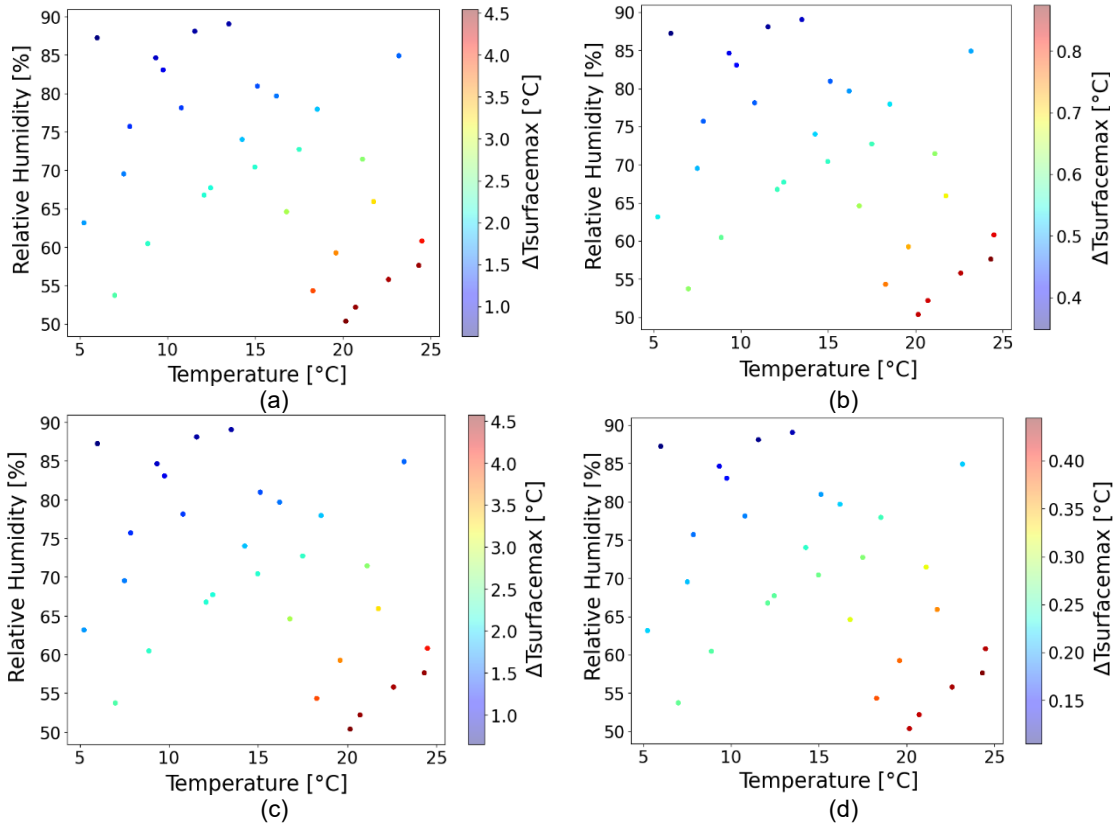


Figure 92 – Variation of $\Delta T_{surfacemax}$ with ambient the air temperature and relative humidity for (a) Brick; (b) Concrete; (c) Granite; and (d) Limestone

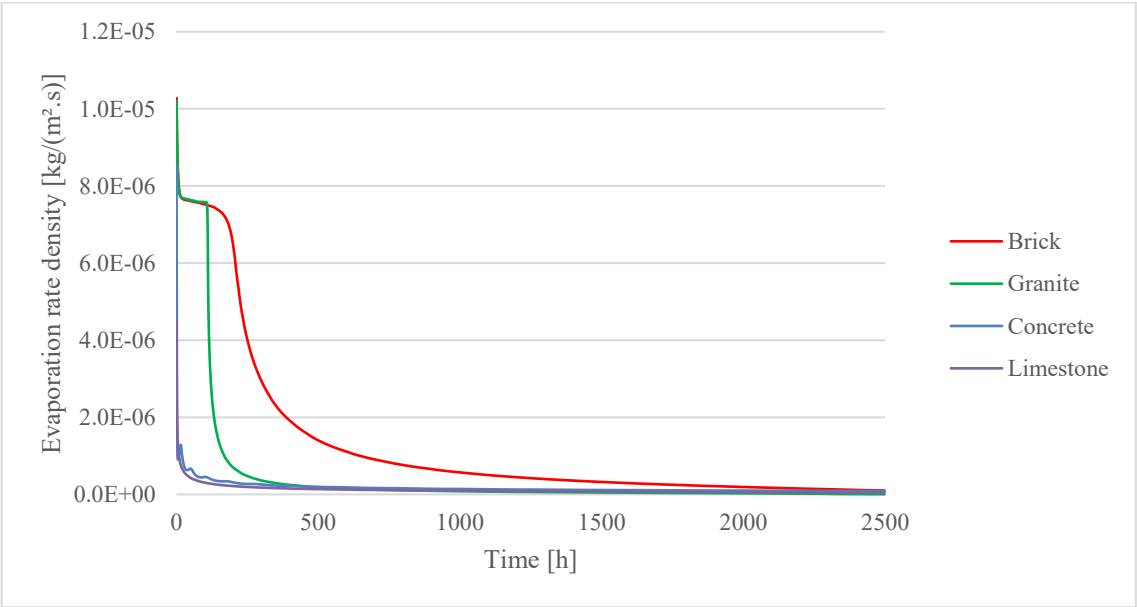


Figure 93 – Evaporation rate density for an air temperature of 7°C and relative humidity of 53.73%

The explanation of the drying behaviour at the beginning of the drying process was presented in § 2.2.1.4, where it is presented the influence of the free water saturation (w_{cap}) and critical moisture content

(w_{crit}) in the evaporation rate density in the first drying phase. For concrete and limestone, this initial drying phase that is approximately constant could not be identified in the simulations.

4.4 INPUT DATA FOR THE PREDICTION MODELS OF MOISTURE CONTENT

4.4.1 FRAMEWORK

For this step, the same environmental conditions presented in § 4.3 were adopted and a thickness of 0.02 m of mortar was considered. An additional layer of a waterproofing material with 0.001 m was used since the specimens used in the laboratory tests were waterproofed to simulate evaporation only for one surface of the material. The properties of the mortar used as inputs for the simulations were assessed through laboratory tests (§ 3.3.1) and are presented in Table 44. A similar procedure to the one presented in Figure 88 was performed. A total of 1200 sets of data were selected for the analysis of the mortar. This data was combined with the 4800 sets of data generated in § 4.3.

Table 44 – Properties of the mortar for numerical simulation

Material	Bulk density [kg/m³]	Porosity [kg/m³]	Specific heat [J/kgK]	Thermal conductivity dry [W/mK]	Water vapour resistance factor dry [-]	Reference water content (equilibrium moisture at a RH of 0.8) [kg/m³]
Mortar	1569.0	0.38	850.0	0.803	11.3	22.36

4.4.2 RESULTS

4.4.2.1 Data distribution

The distribution of the values of thermal gradient ($\Delta T_{surface}$ [°C]) and moisture content [kg/m³] are shown in Figure 94 (a). The values obtained in the experimental tests (laboratory) with the same mortar used in the simulations is presented in Figure 94 (b).

In the simulations, which had 30 environmental conditions, the $\Delta T_{surface}$ varied from 0°C to 3.10°C and the moisture content varied from 0 to 202 kg/m². In laboratory conditions, the $\Delta T_{surface}$ also varied from 0°C to 3.10°C, but the moisture content varied from 0 to 220 kg/m². As previously explained in this Chapter, the drying behaviour of the porous building materials explain the high number of low $\Delta T_{surface}$ values and the small number of higher $\Delta T_{surface}$ values (long period of time with a low evaporation rate).

In the simulations, a longer period was simulated compared to the monitored period in the laboratory. This explains why the simulations led to much smaller values of moisture content in comparison to experimental laboratory results where the results of moisture content are higher.

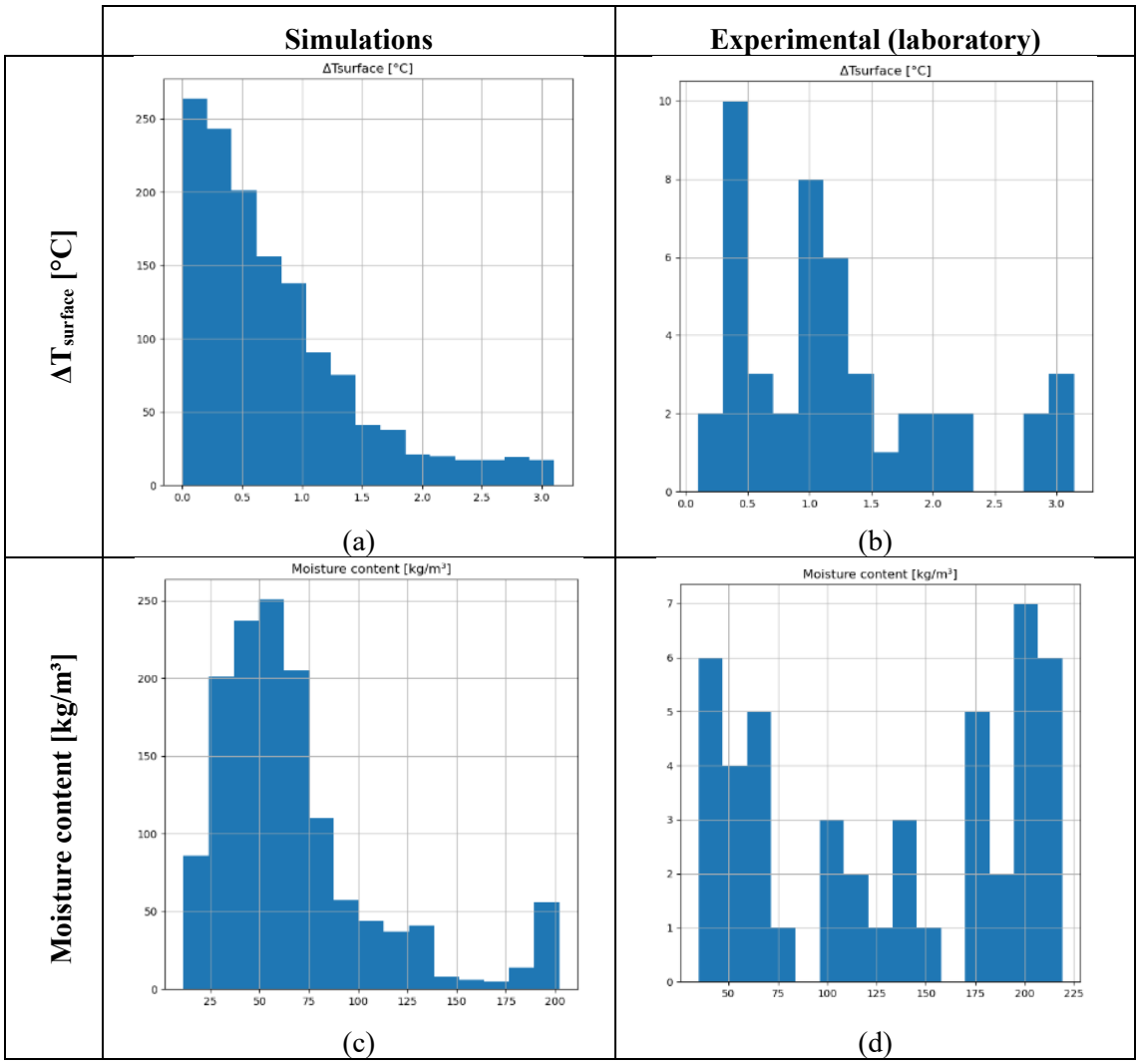


Figure 94 – Histograms (a) $\Delta T_{surface}$ [°C] – simulations; (b) $\Delta T_{surface}$ [°C] – laboratory; (c) Moisture content [kg/m³] – simulations; (d) Moisture content [kg/m³] – laboratory

4.4.2.2 Correlation between thermal gradient and moisture content

The relationship between the moisture content and the $\Delta T_{surface}$ for the simulation results are shown in Figure 95. Each simulation in which the environmental condition is defined led to a curve, observing that the higher the evaporation capacity, the higher the $\Delta T_{surface}$ reached.

The three scenarios tested in laboratory conditions were simulated in WUFI. In the first, the temperature was 20°C and the relative humidity 70%. In the second, the temperature was 25°C and 60% of relative humidity. In the last, the temperature was 15°C and the relative humidity was 80%.

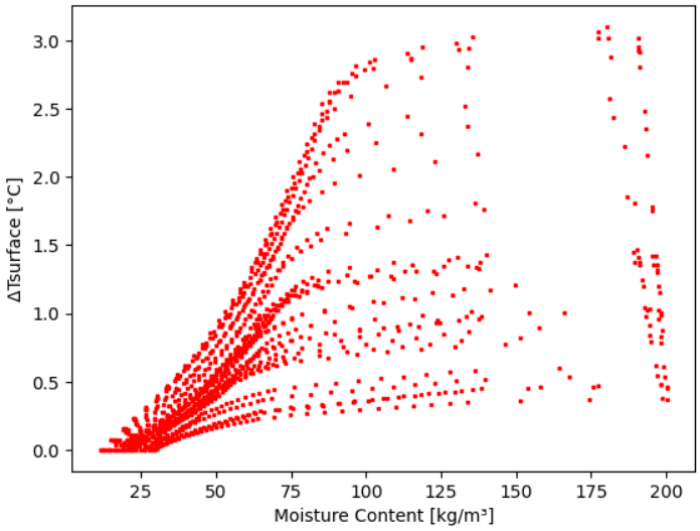


Figure 95 – Relationship between moisture content and thermal gradient ($\Delta T_{surface}$ [°C]) - simulation results

The comparison between the experimental and simulation results is shown in Figure 96, Figure 97, and Figure 98 for scenarios I, II, and III, respectively. Similar profiles of curves were obtained. However, in all scenarios the maximum thermal gradient achieved in laboratory conditions was slightly higher than in simulations.

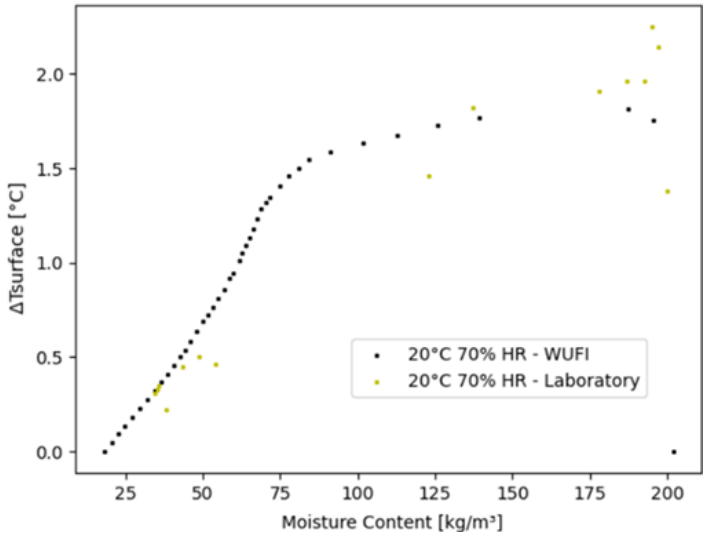


Figure 96 – Comparison of the relationship between moisture content and thermal gradient ($\Delta T_{surface}$ [°C]) for simulation and experimental results – scenario I

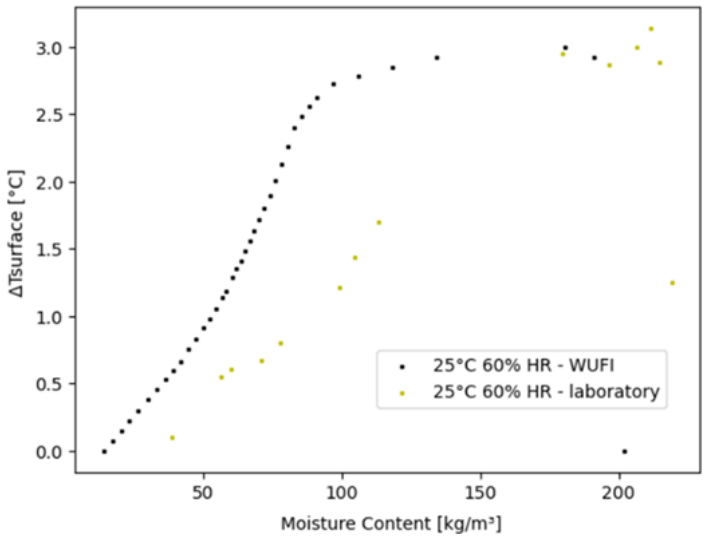


Figure 97 – Comparison of the relationship between moisture content and thermal gradient ($\Delta T_{surface}$ [°C]) for simulation and experimental results – scenario II

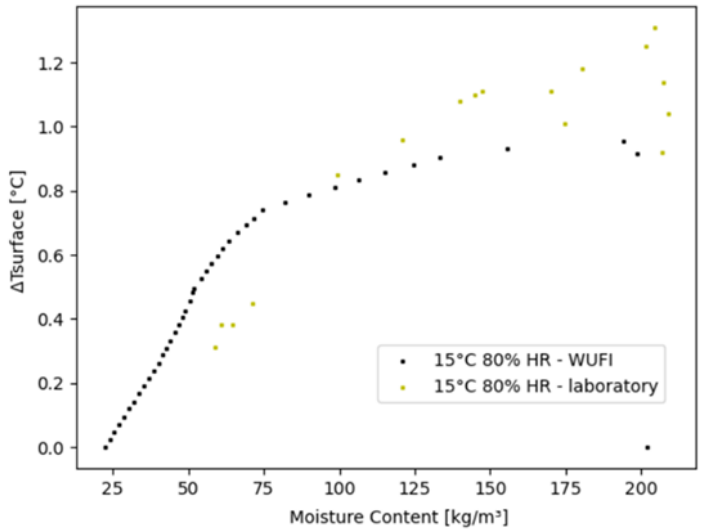


Figure 98 – Comparison of the relationship between moisture content and thermal gradient ($\Delta T_{surface}$ [°C]) for simulation and experimental results – scenario III

4.4.2.3 Evolution of the thermal gradient and the moisture content

The evolution of the thermal gradient and the moisture content over time for experimental and simulation results is shown in Figure 99.

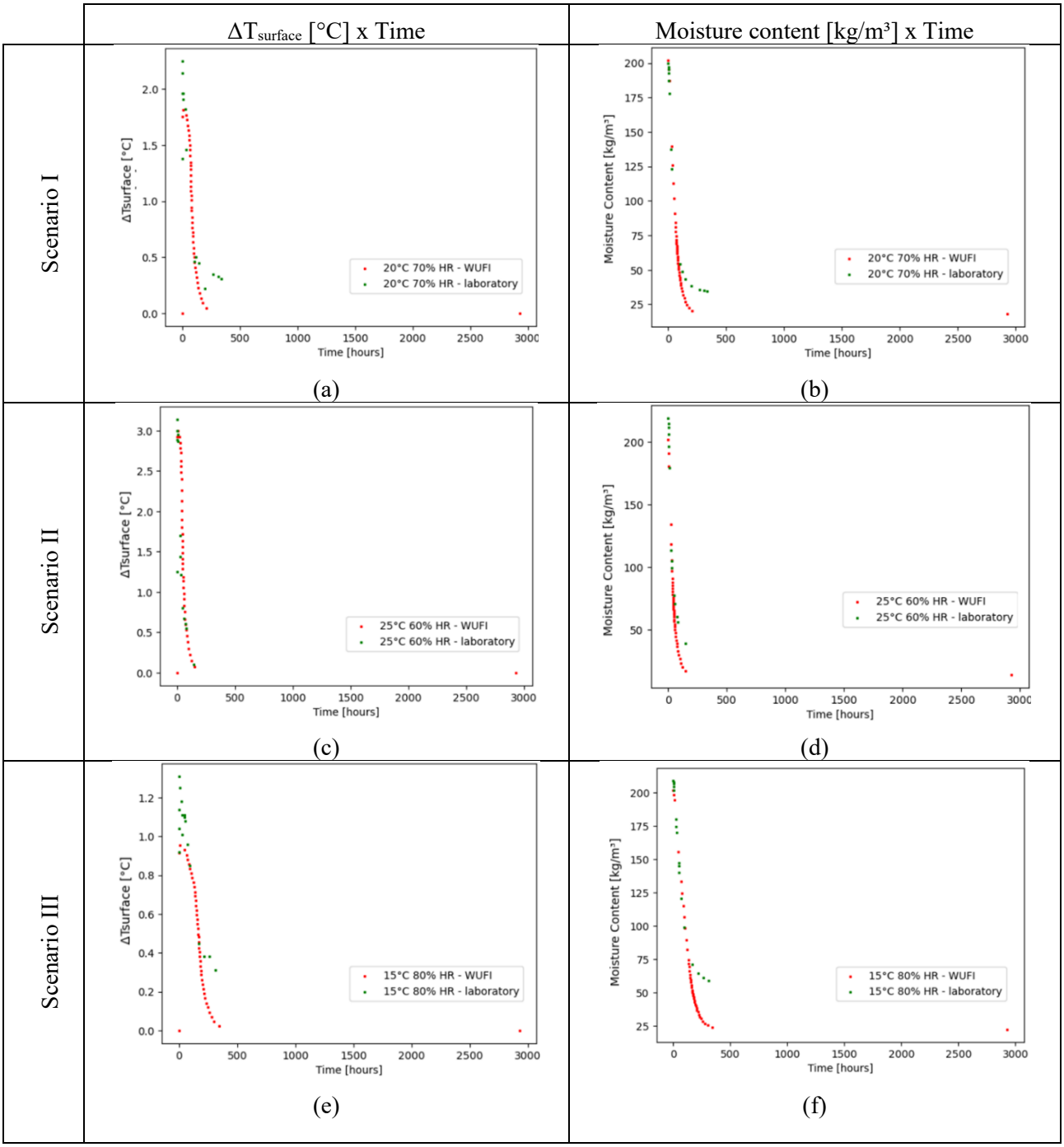


Figure 99 – Evolution of the thermal gradient ($\Delta T_{surface}$ [°C]) and moisture content over time for simulation and experimental results: (a) $\Delta T_{surface}$ [°C] x Time for scenario I; (b) Moisture Content [kg/m³] x Time for scenario I; (c); (d) $\Delta T_{surface}$ [°C] x Time for scenario II; (e) Moisture Content [kg/m³] x Time for scenario II; (f); (g) $\Delta T_{surface}$ [°C] x Time for scenario III; (h) Moisture Content [kg/m³] x Time for scenario III

4.4.2.4 Evaporation rate

The comparison between the evaporation rate density and the thermal gradient for the simulation results are presented in Figure 100, Figure 101, and Figure 102. The thermal gradient of the surface reduces at

the same time of the evaporation rate density and the slope of the reduction curves is similar. As presented in Chapter 3, this fact shows that IRT can be applied to identify the duration of the first drying phase and, therefore, in the context of practical inspections, calculate the evaporation rate density with the use of equation (7).

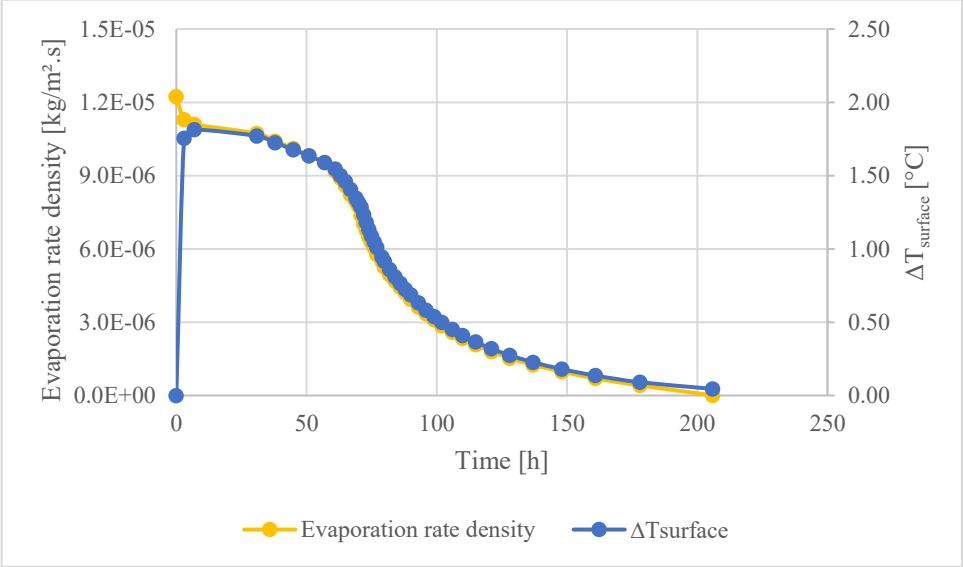


Figure 100 – Comparison between the evaporation rate density and $\Delta T_{surface}$ – scenario I

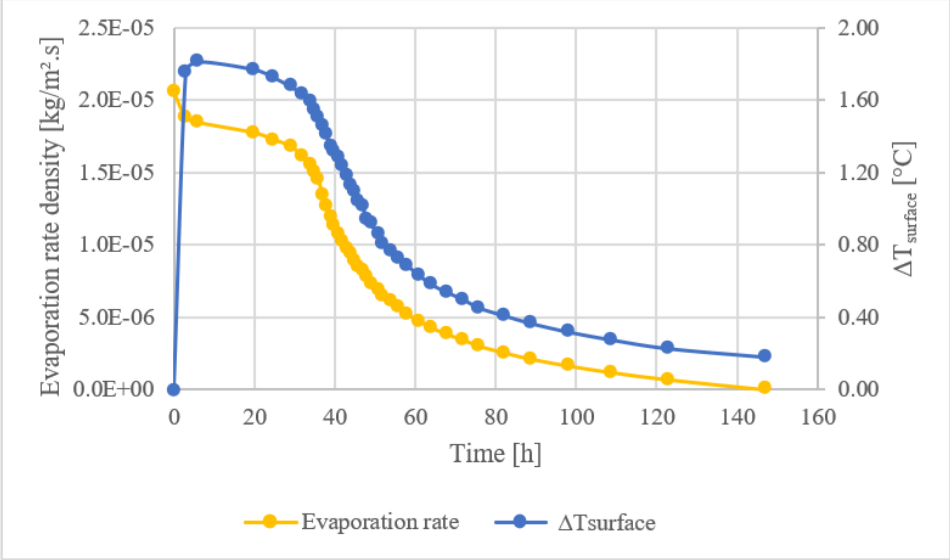


Figure 101 – Comparison between the evaporation rate density and $\Delta T_{surface}$ – scenario II

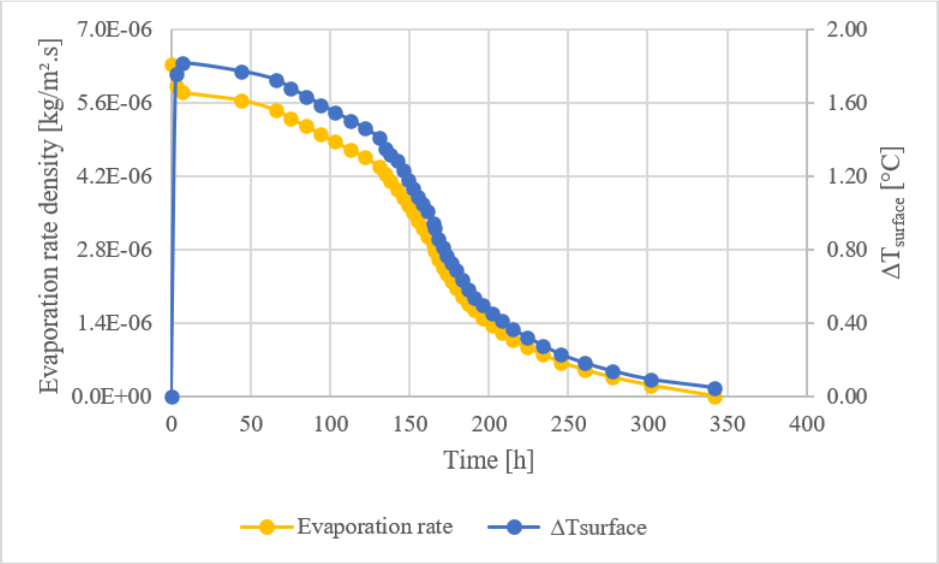


Figure 102 – Comparison between the evaporation rate density and $\Delta T_{surface}$ – scenario III

4.4.2.5 Relationship between the evaporation capacity and the maximum thermal gradient

The difference between the saturation vapour pressure and the vapour pressure of the air is compared with the maximum thermal gradient for all the 30 simulated scenarios, according to Figure 103. The coefficient of determination (R^2) is close to 1, indicating that the identification of the $\Delta T_{surfacemax}$ [°C] can be identified based on the environmental conditions if the linear curve of the material behaviour is previously known.

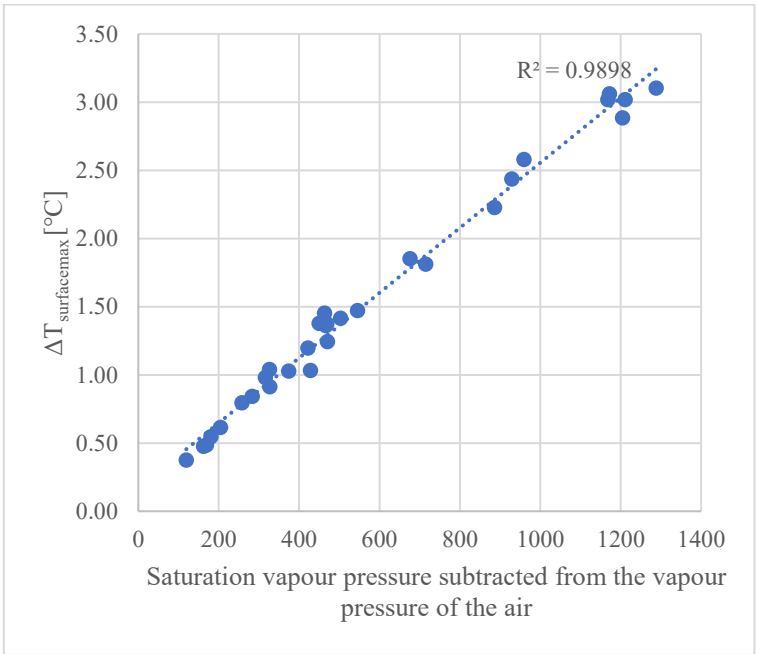


Figure 103 – Relationship between the vapour pressure and the $\Delta T_{surfacemax}$ (Saturation vapour pressure subtracted from the vapour pressure of the air and $\Delta T_{surfacemax}$ [°C])

4.5 FINAL REMARKS

The comparison between experimental and simulation data pointed out to a good agreement between the results predicted by computer simulation software for hygrothermal behaviour and the results identified in practice, through laboratory tests. The shape of the correlation curve between thermal gradient and moisture content was similar for experimental and simulation data. However, the maximum thermal gradient identified in simulation was slightly different than the one identified in laboratory.

The results obtained from the WUFI software show that the maximum thermal gradient varies according to the initial moisture content of the material. The maximum thermal gradient is similar for specimens with the initial moisture content higher than 60% of the maximum moisture content in the case of clay brick. For values above 60%, the relative humidity of the surface is 100% (Figure 70). As the maximum thermal gradient is related to the difference between the saturated vapour pressure at the surface and the vapour pressure of the air, materials with initial moisture content 60% above of the maximum value (saturated surface) will have the same maximum thermal gradient. Below this value, the maximum thermal gradient reduces in a linearly trend according to the initial moisture content.

For the clay bricks, in the simulations with an initial moisture content of 10% (of the maximum moisture content), a maximum thermal gradient of 1.1 °C was found, while for the simulation with an initial moisture content of 100%, the maximum gradient increased to 4.3 °C. The evolution of the maximum gradient according to the initial moisture content could be adjusted by a quadratic regression model, with a coefficient of determination (R^2) of 0.99. As for limestone, much smaller temperature gradients were identified, 0.15 °C for the initial moisture content of 10% and 0.9°C for the initial moisture content of 100%.

The time needed in the drying period for the thermal gradient to return to values near to 0 was around 600 hours for clay bricks and 60 hours for limestone, approximately. The big difference between the results found for the two materials is due to different properties and layer thickness. The clay brick presents a porosity eight times greater than the limestone and a thickness more than three times greater, thus justifying the longer drying time and the greater thermal gradients identified, in line with the information found in the literature and presented in Chapter 2.

It was identified that the evaporative flux in clay brick is very high for moisture contents above 6.0%. In other words, between 12.0% and 6.0%, the moisture content decreased rapidly (see Figure 72) and the thermal gradient was almost constant (see Figure 80), but below 6.0% the speed of moisture reduction decreased considerably. As for limestone, a high evaporative flow was observed for values above 1.0% (Figure 76).

Regarding the correlation between the thermal gradient and the moisture content, it was observed a clear pattern in the results and a high coefficient of determination, of 0.92 for clay brick and 0.91 for limestone.

The data analysis of the simulations of the drying process under different environmental conditions (§ 4.3) revealed that each environmental condition and material presented a specific downward curve for the correlation between the moisture content of the material and the thermal gradient. The downward curves resemble the shape of a quadratic regression model. The different curves occurs because the $\Delta T_{surface}$ is influenced by the evaporation at the surface, and the evaporation is influenced by the properties of the materials, such as the pore size distribution, and the surrounding environmental conditions.

Computer simulation software are very efficient for identifying the hygrothermal behaviour of materials, systems and building components, as well as revealing a great potential for aiding in the automated identification of defects related to moisture in buildings since they allow to predict the behaviour of different materials under different environmental conditions. The knowledge of the whole drying process of each material is crucial in the quantification of the moisture content of the material.

Overall, the use of computational tools, such as WUFI, has proven to be valuable in predicting the hygrothermal behaviour of building materials, putting forward a sound approach for applications in building diagnosis and moisture related defects, especially when combined with advanced techniques such as machine learning. The use of these simulations with real-world data will be essential for developing the algorithms that enables the identification of the moisture content of porous building materials.

5

MOISTURE PREDICTION MODELS

5.1. PRELIMINARY MACHINE LEARNING MODELS

5.1.1. FRAMEWORK

Figure 104 contains the framework for developing the preliminary model to predict the moisture content of building materials based on the surface temperature and other input data obtained from simulations. The complete analysis can be divided into three main steps. The first involves data collection and preparation, the second is the creation of the machine learning model, and the last comprises training, evaluating, and application of the model. This Section presents the detailed description of each step.

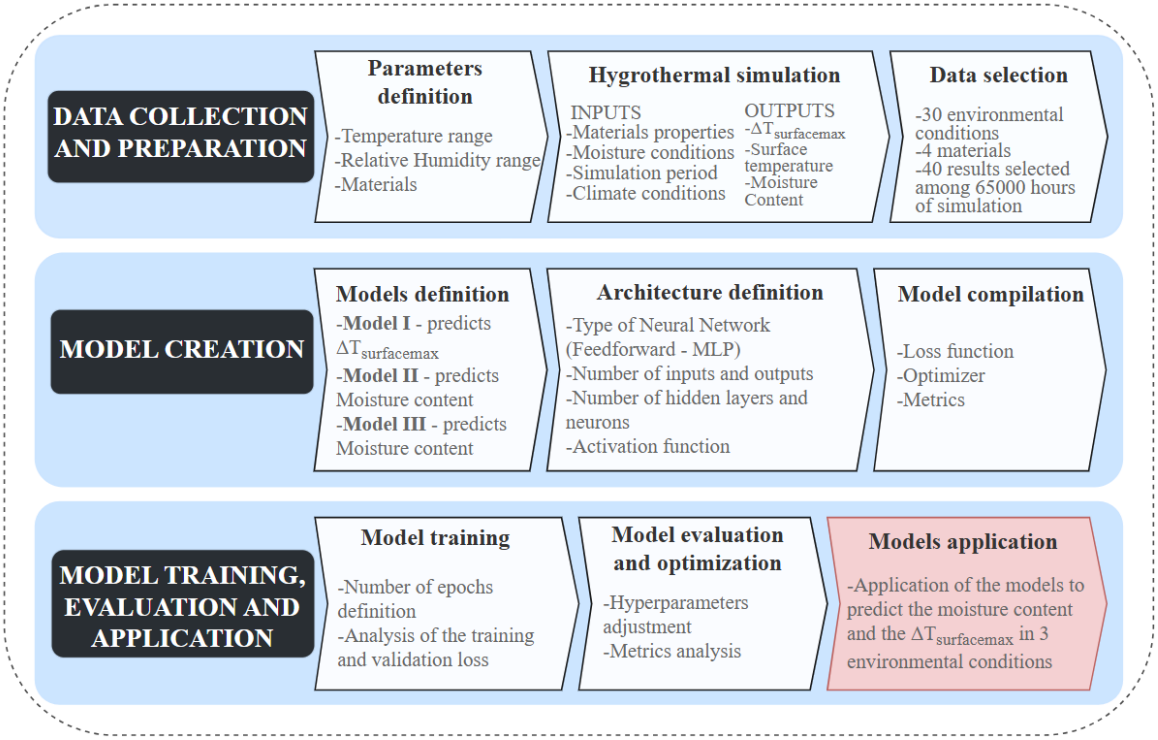


Figure 104 – Framework of the development of the machine learning models to predict the moisture content

The data collection and preparation comprises the definition of the parameters necessary as input for the simulation with the hygrothermal software. The details about this step are presented in Chapter 4 and § 4.3.2 presents the results of the simulation data used as dataset for training and testing the algorithms developed in this Section. Complete information about the algorithms developed at this stage is presented in Appendix 4.

5.1.2. MODEL CREATION

Three models were developed in this step. Model I predicts the maximum thermal gradient ($\Delta T_{surfacemax}$) in the drying phase of an initially saturated material. The thermal gradient of the surface at an instant *i* ($\Delta T_{surface}$) was obtained by subtracting the surface temperature of the dry material from the surface temperature of the moist material at the time *i*. This model had as inputs the type of material and the temperature and relative humidity of the air. In terms of practical applications, during a building moisture inspection, it is useful to know the maximum thermal gradient of saturated materials to compare it with the thermal gradient identified at the moment of the inspection. In this way, it is possible to estimate how moist the material is.

An analysis of the moisture condition of the selected building materials was possible using Models II and III, which were developed to identify the moisture content of the materials, in kg/m³. Both models considered as inputs: material, environmental conditions (air temperature and relative humidity), and thermal gradient of the surface ($\Delta T_{surface}$). Model II was developed with all the values in the selected dataset. However, for accuracy purposes, Model III disregarded the data from the initial phase of the simulation, when the surface temperature of the moist material has not yet reached its minimum value, but the moisture content is very high. This adjustment period usually takes 1 to 30 hours, depending on the material (Figure 105).

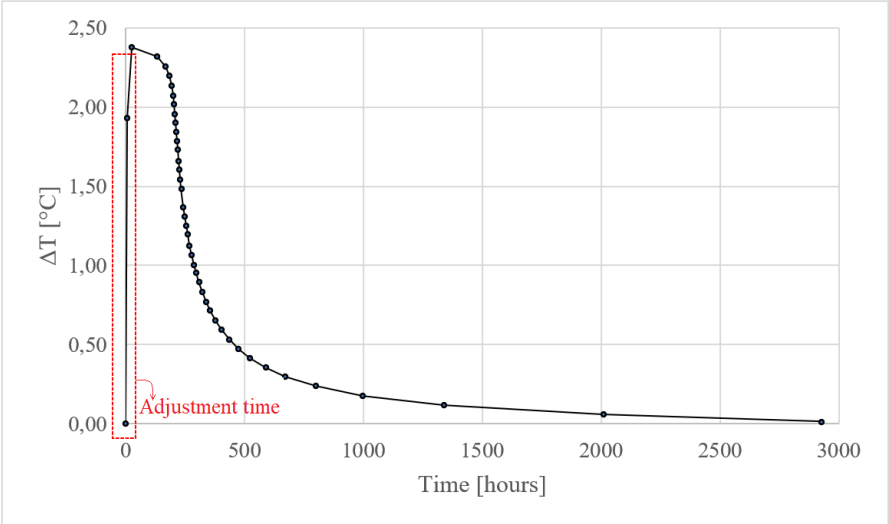


Figure 105 – Adjustment time of the temperature of moist areas at the beginning of the evaporation

After defining the inputs and outputs of each model, the data was divided into subsets for training and testing purposes. Preliminary simulations with different training and testing sizes showed that 80% of the values should be used for training and 20% for testing. These values are in agreement with the references found in the literature.

A critical step before training the models is to preprocess the data through methods such as standardisation and normalisation [123]. The data must be transformed by applying feature scaling to put the values in the same scale since machine learning algorithms do not perform well with values of very different scales [111], [124]. The scaling method adopted was normalisation due to the nature of the dataset. Data preparation, model creation, and evaluation were performed using Jupyter Notebook in Python.

This work used a regression type of task and supervised learning, in which a labelled training set was used to feed the algorithm to predict a target numeric value. Many researchers have used the Neural Networks (NN) of the Multilayer Perceptrons (MLPs) type to deal with tabular data [150], [151], [147], [141]. Therefore, this type was selected for this analysis. Several tests were performed to define the ideal number of hidden layers and neurons. As an example, the generic architecture of the NN Models II and III is represented in Figure 106. Table 45 contains information regarding the parameters of the NNs models developed.

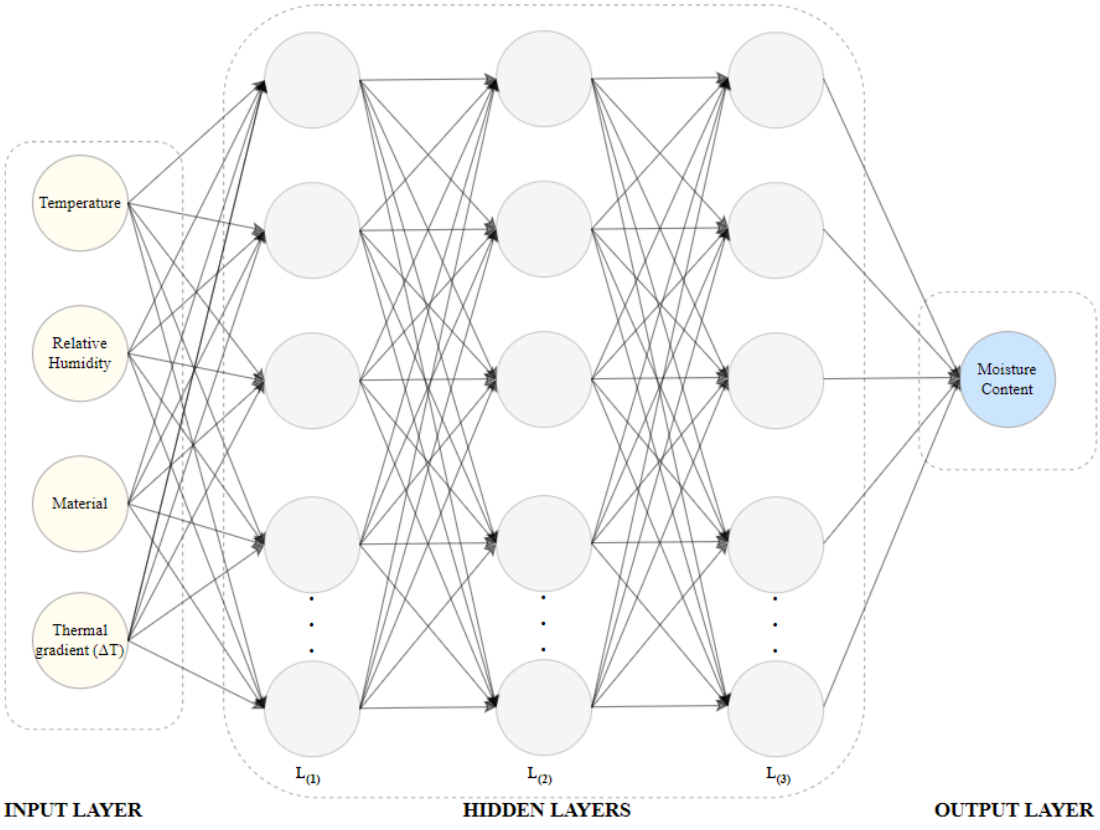


Figure 106 – Architecture of the NN developed to predict the moisture content

Table 45 – Parameters of the NNs developed

Parameters	Model I	Model II	Model III
Inputs	Material, Air temperature, Air relative humidity	Material, Air temperature, Air relative humidity, Surface thermal gradient ($\Delta T_{surface}$)	Material, Air temperature, Air relative humidity, Surface thermal gradient ($\Delta T_{surface}$)
Output	Maximum surface thermal gradient ($\Delta T_{surface-max}$)	Moisture content (kg/m³)	Moisture content (kg/m³)
Activation function	Rectified Linear Units (ReLU)	Rectified Linear Units (ReLU)	Rectified Linear Units (ReLU)
Optimiser	Adam	Adam	Adam
Metrics	MSE, MAE, MAPE	MSE, MAE, MAPE	MSE, MAE, MAPE

The output of each neuron in the NN was calculated according to equations (34) and (35), which represents the neuron shown in Figure 107, where the values of $w_{1,1}$, $w_{1,2}$, $w_{1,3}$, and $w_{1,4}$ are the weights applied to each of the neurons in the input layer regarding the grey highlighted neuron; b_1 is the bias of the grey highlighted neuron; and σ is the activation function applied to the value of $z_1^{[1]}$ to obtain the output $a_1^{[1]}$ of the grey highlighted neuron. These operations are applied to every neuron in every layer of the model. The output of a neuron will become the input of the neurons in the following layer.

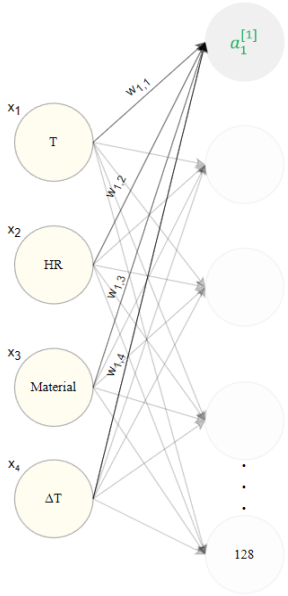


Figure 107 – Weights applied to the first neuron in the first layer

$$z_1^{[1]} = w_{1,1}x_1 + w_{1,2}x_2 + w_{1,3}x_3 + w_{1,4}x_4 + b_1 \quad (34)$$

$$a_1^{[1]} = \sigma(z_1^{[1]}) \quad (35)$$

To compile the model, it was necessary to select the cost function, the optimizer, and the metrics to analyse its performance. The cost function of a machine learning model takes the prediction

made by the model and the true value and computes a distance score, measuring how well the network has predicted that value. Training a NN means learning the model parameters of weights and biases that minimise this cost function. In the training process, the parameters are initialised randomly. Then, the loss function is calculated, and the gradient of the loss function with respect to the weight and the bias is obtained with the backpropagation method, which employs the chain rule of derivative. In the beginning, the model performs poorly at fitting the observations in the training set. Then, the optimal values are obtained using a gradient-descent algorithm that updates the parameters in each iteration according to the defined learning rate, improving the fitting ability of the model [109], [111].

In all the NN presented in this preliminary model, the loss function selected was the mean-square error (MSE). Thus, the optimal set of parameters is the one which minimise the MSE. The optimizer and the metric to analyse the model were Adam and the mean absolute error (MAE), respectively, the most suitable for this type of regression problem. Equations (36), (37) and (38) presents how the MSE, MAE and mean absolute percentage error (MAPE) are calculated, where $\widehat{y_i}$ represents the predicted value and y_i the true value.

$$MSE = \frac{1}{n}\sum_{i=1}^{n}(y_i - \widehat{y_i})^2 \quad (36)$$

$$MAE = \frac{1}{n}\sum_{i=1}^{n}|y_i - \widehat{y_i}| \quad (37)$$

$$MAPE = \frac{1}{n}\sum_{i=1}^{n}\left|\frac{y_i - \widehat{y_i}}{y_i}\right| x\ 100\% \quad (38)$$

5.1.3. MODEL TRAINING, EVALUATION AND APPLICATION

During the training phase, an early stopping function was applied to prevent the model from overfitting the data. The objective was to find the exact point during training where it reached the most generalizable fit, which means the moment between an underfit and an overfit curve [109]. In this way, the iterations (epochs) stop when the model starts to overfit, and the value of the performance metrics for the training and validation data will be closer to each other. If the early stopping function was not applied, the performance of the training set would continue to improve, while the performance of the validation set would reduce, according to the example illustrated in Figure 108, which presents the training and validation loss curves for a test conducted in this study where no early stopping function was used.

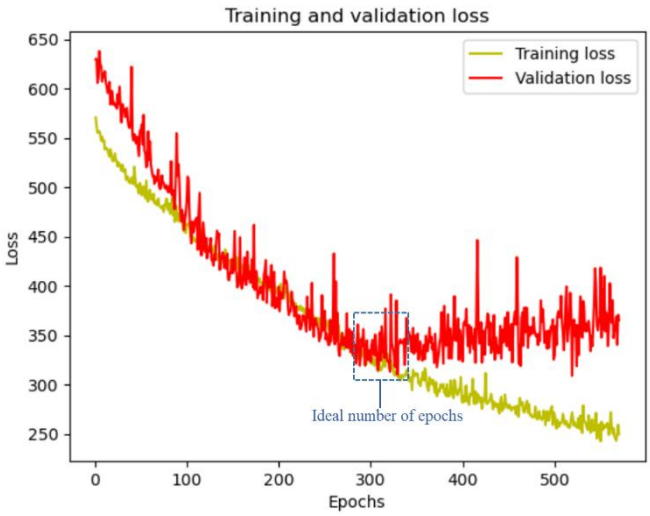


Figure 108 – Example of the point at which the model starts overfitting

The loss and the MAE for the training and validation sets were computed at each epoch. The graphs plotting these values were analysed for different architectures of the NN models, and the hyperparameters were adjusted. Another important metric to analyse the performance of a machine learning model is the coefficient of determination (R^2) between the predicted values and the true values for the test set. The R^2s of the NNs were computed and compared.

After the training and evaluation steps, the best models were chosen to be applied in three hypothetical environmental conditions to predict the moisture content and the maximum thermal gradient.

5.1.4. RESULTS

5.1.4.1. Neural Network's architecture and performance

The results of the evaluation of the most appropriate architecture for the NN Models I, II, and III are shown in Table 46,

Table 47, and Table 48, respectively. Regarding Model I, the best architecture was two hidden layers, the first with 128 neurons and the second with 64. For Model II, it is possible to see that the architecture leading to the smaller error is the one with three hidden layers: the first with 128 neurons and the second and the third with 64 neurons each. The latter finding also applies to Model III.

The best architecture in Model I converged to an optimal solution with only 35 epochs. The smaller number of layers and epochs in Model I can be explained by its lower complexity. This model presented minor errors, indicating high accuracy in predicting the maximum thermal gradient. The complexity of the model can also explain the architecture and the performance of

Models II and III. Model II comprised a larger amount of data with a more complex pattern, as explained in § 5.1.2. In this way, it required more epochs to reach the optimal solution and presented more considerable errors than Model III. The predictions of Model II are off, on average, by 21% of the actual value, more than five times the value found for Model III, which shows the higher accuracy of Model III.

Table 46 – Architecture analysis for the NN of Model I

Number of hidden layers	Number of neurons on each hidden layer	Epochs	MSE	MAE	MAPE
1	128	93	0.011	0.067	21.7
2	**1st: 128; 2nd: 64**	**35**	**0.0072**	**0.018**	**2.7**
3	1st: 128; 2nd: 64; 3rd: 64	27	0.00085	0.022	3.7

Table 47 – Architecture analysis for the NN of Model II

Number of hidden layers	Number of neurons on each hidden layer	Epochs	MSE	MAE	MAPE
2	1st: 128; 2nd: 64	684	412.43	9.18	22.0
3	**1st: 128; 2nd: 64; 3rd: 64**	**444**	**300.69**	**7.83**	**21.0**
4	1st: 128; 2nd: 64; 3rd: 64; 4th: 64	165	390.86	8.37	21.0

Table 48 – Architecture analysis for the NN of Model III

Number of hidden layers	Number of neurons on each hidden layer	Epochs	MSE	MAE	MAPE
2	1st: 128; 2nd: 64	258	148.15	6.27	10.4
3	**1st: 128; 2nd: 64; 3rd: 64**	**230**	**40.30**	**2.56**	**4.1**
4	1st: 128; 2nd: 64; 3rd: 64; 4th: 64	156	57.17	2.96	4.4

The loss and the MAE in the training and validation sets for Models I, II, and III are shown in Figure 109. In Model I, the loss had low values since the beginning of the training process, which was expected due to its lower complexity. The errors obtained after finding the optimal solution in this model were close to 0. In Models II and III, a zoom of the MAE values at the end of the training process is presented. It indicates that in Model II, the MAE ranged from approximately 6.0 to 8.0 in the last epochs, while in Model III, the MAE ranged from about 2.0 to 4.0. In the last epochs of all the Models, the validation loss is close to the training loss, which shows that the model does not underfit or overfit the data.

The correlation between the predicted and the true values and the coefficient of determination (R^2) are shown in Figure 110 for Models I, II, and III. Models I and III presented a very strong correlation between the predicted and the true values in the training and testing sets, close to 1, showing an excellent performance of the models. As for Model II (containing all data, including that from the adjustment period), it presented a strong correlation (R^2=0.96). Still, the MSE, MAE, and MAPE metrics showed error values much higher than Model III due to the large dispersion of data, as seen in Figure 110 (c) and (d).

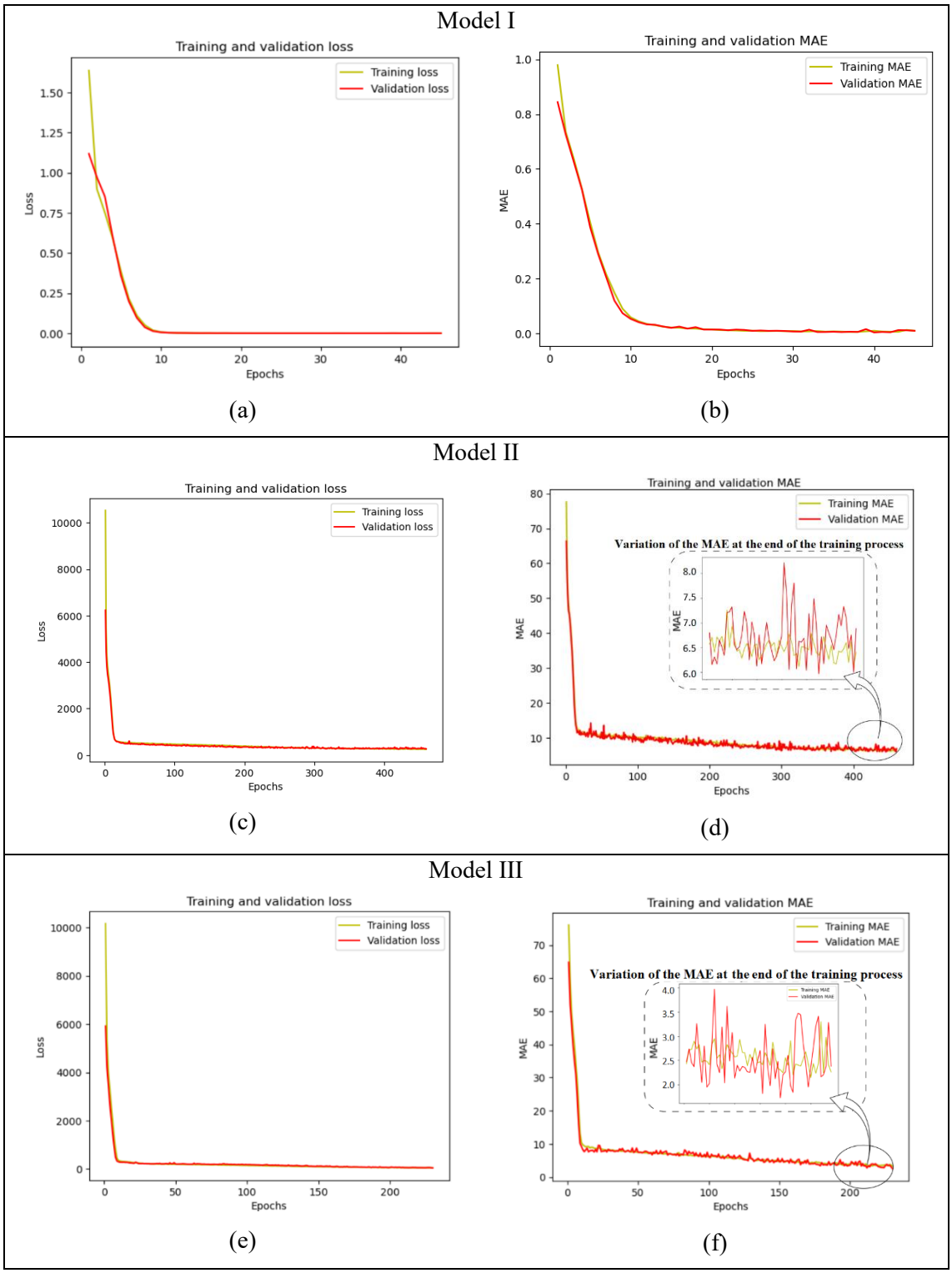


Figure 109 - Training and validation according to each epoch (a) Model I – Loss (b) Model I – MAE (c) Model II - Loss (d) Model II- MAE (e) Model III – Loss (f) Model III - MAE

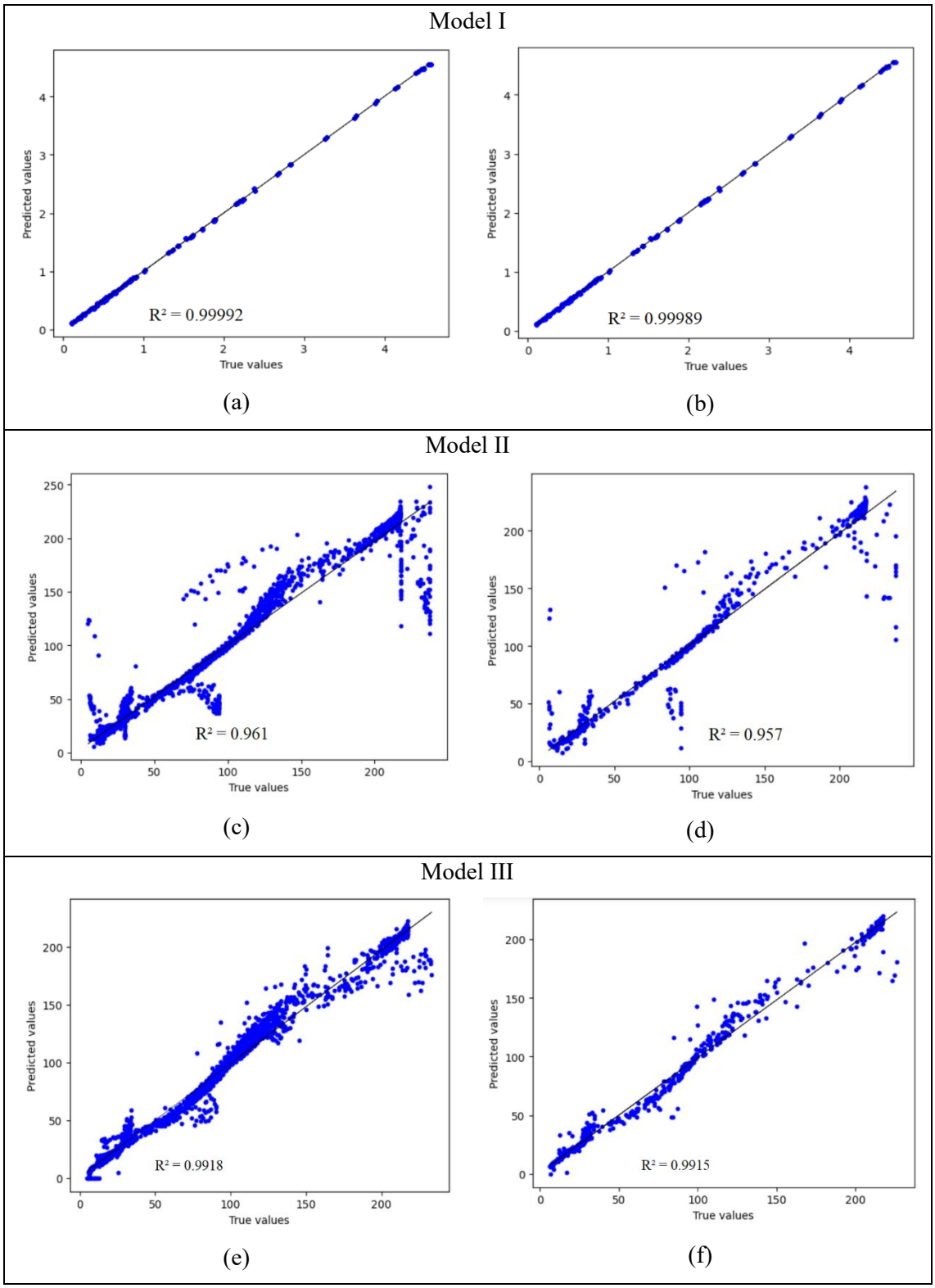


Figure 110 – Correlation between predicted and true values and coefficient of determination (R^2) score for (a) Model I – training set; (b) Model I – testing set; (c) Model II – training set; (d) Model II – testing set; (e) Model III – training set; and (f) Model III – testing set

5.1.4.2. Applications of the developed models

Model III presented the best performance for predicting the moisture content in the building materials analysed. For this reason, this model was applied to predict the moisture content in three hypothetical environmental conditions that are common in real applications: (i) Temperature (T) of 15°C and Relative Humidity (RH) of 80%; (ii) T = 20°C and RH = 70%; and (iii) T=25°C and RH=60%. The predictions were based on the thermal gradient between the surface of the moist material and the dry surface ($\Delta T_{surface}$). Figure 111 shows the results obtained for clay brick, concrete, granite and limestone in the three environmental conditions. It is also highlighted in Figure 111 the maximum thermal gradient ($\Delta T_{surfacemax}$) that can be identified in each case, predicted by Model I.

In the first environment (T = 15°C and RH = 80%), which had the lowest evaporation capacity, the $\Delta T_{surfacemax}$. was 1.45°C in clay brick, 0.47°C in concrete, 1.47°C in granite, and 0.20°C in limestone. Regarding the second environment (T = 20°C and RH = 70%), the maximum thermal gradient reached 2,64°C in clay brick, 0.61°C in concrete, 2.70°C in granite, and 0.27°C in limestone. Lastly, in the third environment (T = 25°C and RH = 60%), the $\Delta T_{surfacemax}$ was 4.27°C in clay brick, 0.83°C in concrete, 4.25°C in granite, and 0.47°C in limestone.

In clay brick and granite, there is a clear variation in the moisture content according to the variation in the $\Delta T_{surface}$ (Figure 111(a) and Figure 111(c)). The moisture content is very low when the $\Delta T_{surface}$ reaches 0°C, especially in the third environment. In limestone, in the third environment, it is possible to see changes in the moisture content with changes in $\Delta T_{surface}$. However, in the first environment, very little difference is noticeable. For limestone, the moisture content does not reach lower values in any of the three environments even when the $\Delta T_{surface}$ tends to 0°C.

As to concrete, the variations in the $\Delta T_{surface}$ do not reflect considerable changes in the moisture content in any of the three environments. Even when the $\Delta T_{surface}$ was almost 0°C, the moisture content of concrete was still very high. This can be explained by the drying behaviour of concrete. The drying simulation of concrete in the first environment showed that with five days of simulation, the $\Delta T_{surface}$ was already lower than 0.1°C, and, at this point, only approximately 2.5 mm out of the 100 mm of thickness was dry, as shown in Figure 112(a), which contains the cross-section of concrete when $\Delta T_{surface}$ was close to 0°C. The whole thickness of concrete took approximately eight years to dry. As mentioned in Chapter 3, this behaviour can be explained by the pore size distribution of the materials. On the other hand, in clay brick, when the $\Delta T_{surface}$ approaches 0°C, the value of the moisture content inside the clay brick is already very low, as shown in Figure 112 (b).

Additionally, two important considerations must be highlighted regarding the application of Models I and III to practical cases. The first one is that some infrared cameras present a thermal

sensitivity of around 0.1°C, which means that they are not so effective in evaluating temperature differences lower than 0.1°C. Therefore, in environments where the thermal gradient presents very low values, it might be difficult to identify differences in the moisture content. Secondly, the developed models only can be applied for the conditions set for the simulation step: 0.10 m thickness, no heat source or wind, initially saturated materials, and constant temperature and relative humidity of the air.

Overall, the results indicate that the machine learning model enables the identification of the moisture content in clay brick, granite, and limestone in all the tested environments. However, in environments with very high relative humidities and low temperatures, it might be challenging to identify the exact moisture content when the values are below 30 kg/m³ for clay brick, 15 kg/m³ for granite, and 25 kg/m³ for limestone (minimum values of the green lines in Figure 111) since when the materials reach these values, there is no thermal gradient or the thermal gradient is very small. Also, for limestone, the low values of the thermal gradient and the mentioned thermal sensitivity of some equipment might make it difficult to identify the moisture content based on slight differences in the thermal gradient. Lastly, for concrete, considering its pore size distribution, it might be possible to identify the moisture content only down to a few millimetres below the surface since the drying of the internal moisture content happens at a very low drying rate which cannot be identified by the available infrared cameras.

In a practical application, it is also important to analyse the moisture storage function of the material to understand the real meaning of the value of the moisture content predicted by the model, as shown in Figure 113. For example, for clay brick in an environment with a relative humidity of 70% and a $\Delta T_{surface}$ of 2.0°C, Model III predicted a moisture content of 113 kg/m³, which represents a very wet material since the equilibrium moisture content for a relative humidity of 70% is around 10.0 kg/m³. In this environment, if the $\Delta T_{surface}$ were 0.2°C, it would represent a material with an amount of moisture higher than usual, but not critical.

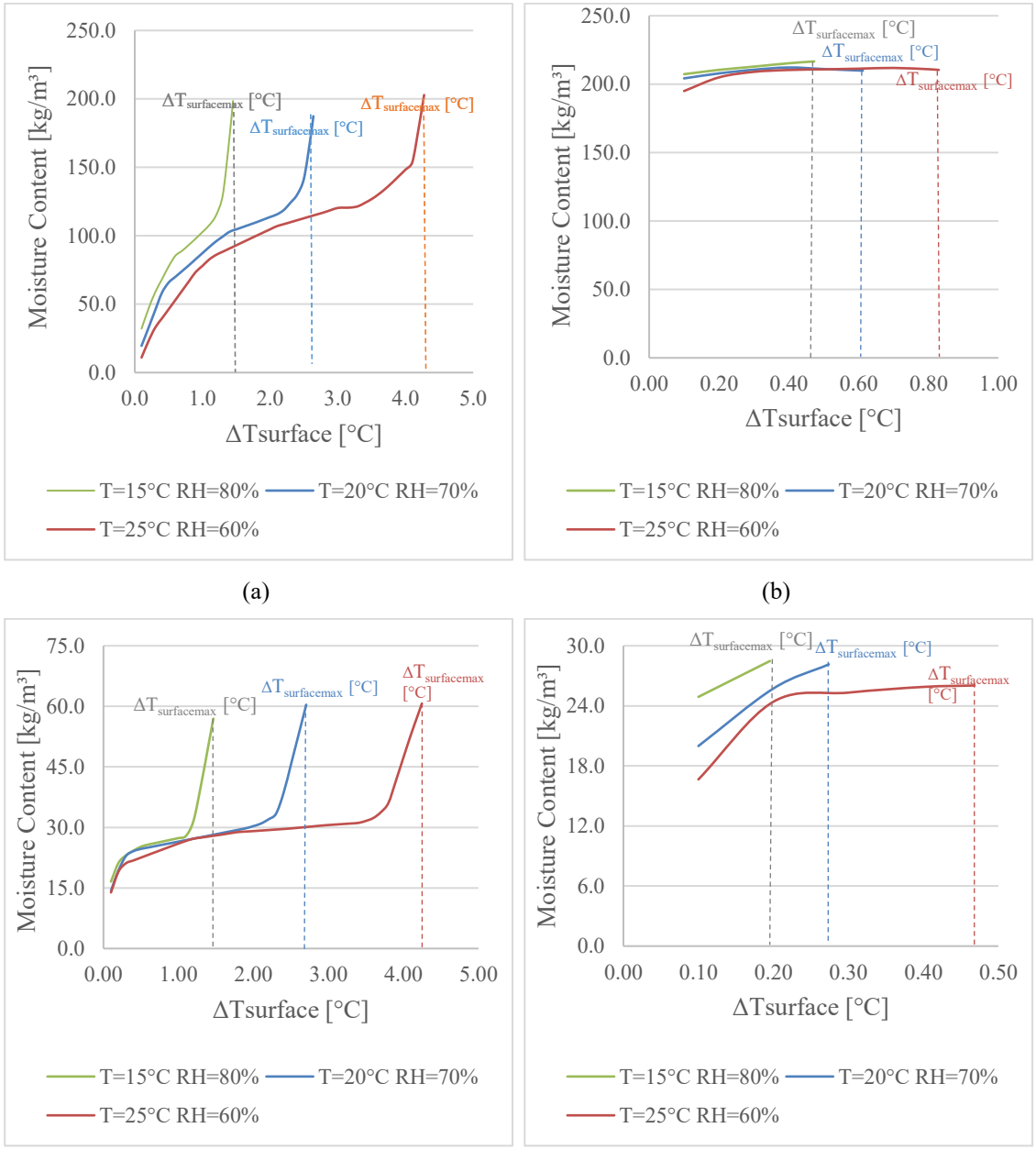
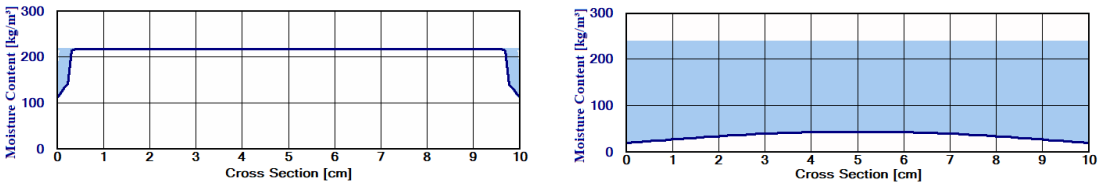


Figure 111 – Predictions of the moisture content based on the $\Delta T_{surface}$ in three different environmental conditions for (a) clay brick, (b) concrete, (c) granite, and (d) limestone



(a) (b)

Figure 112 - Cross section when the $\Delta T_{surface}$ was close to 0°C for (a) concrete (5 days of simulation) and (b) clay brick (60 days of simulation)

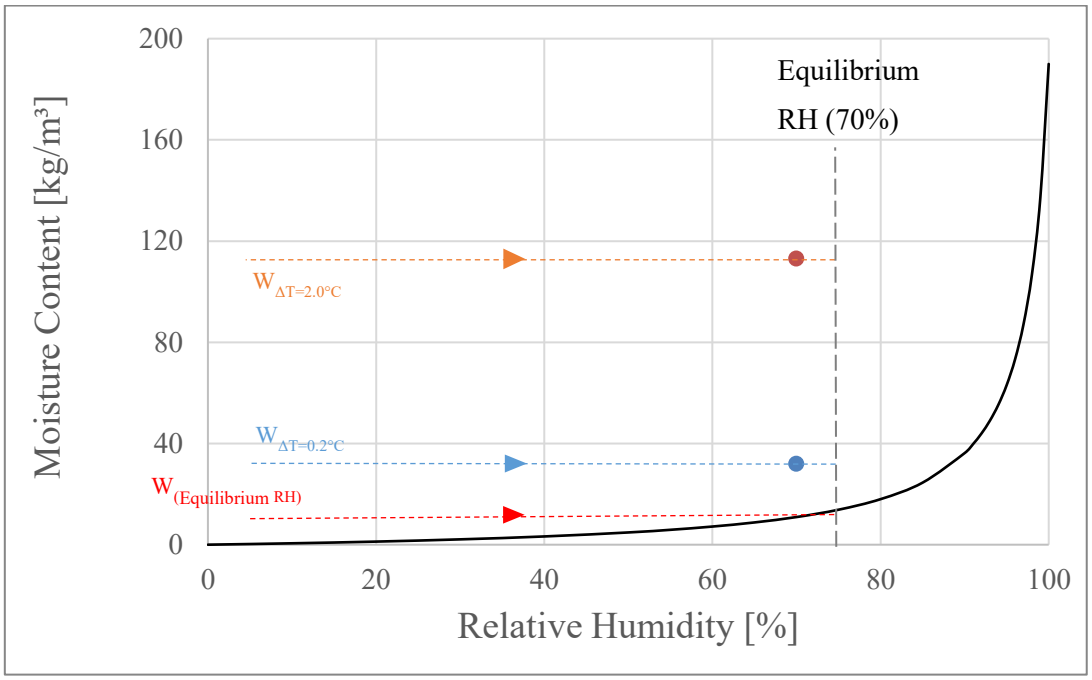


Figure 113 – Moisture storage function of clay brick and the moisture content (w) corresponding to a $\Delta T_{surface}$ of 2.0°C and 0.2°C

5.1.5. Discussion

Algorithms were developed to predict: (i) the moisture content of moist materials based on the thermal gradient between areas with and without moisture ($\Delta T_{surface}$) and (ii) the maximum thermal gradient ($\Delta T_{surfacemax}$) for saturated materials. The inputs considered were the type of material, the temperature and relative humidity of the air, and the $\Delta T_{surface}$. All data used to create and test the models were generated by hygrothermal simulation.

It was found that computational tools combined with machine learning models enabled the creation of models with a very strong correlation between the predicted and the true values of moisture content and $\Delta T_{surfacemax}$. The NN developed to predict the $\Delta T_{surfacemax}$ (Model I) showed the coefficient of determination (R^2) of 0.99. A R^2 value of 0.96 was found for the NN model that predicts

the moisture content using all the data generated by simulation (Model II). Still, the model disregarding the adjustment period (Model III) presented a higher coefficient of determination, about 0.99.

The applications of the developed models in environmental conditions that are common in real applications demonstrated how they could be used in building inspection and their limitations. In clay brick and granite, the model presented excellent results in identifying the moisture content from saturation until the material reached low values of moisture content. In concrete, the model enabled the identification of the moisture content only at surface, since when the material was dry at surface but still wet at internal layers no thermal gradient was identified. For limestone, the model could identify high and intermediate moisture content values.

5.2. FINAL ALGORITHMS

In the previous chapters, the relationship between thermal gradients and moisture content in building materials was investigated through laboratory tests and hygrothermal simulations. Chapters 3 and 4 presented the results of these tests and simulations, which aimed to identify how various environmental conditions and different materials affect the moisture-thermal gradient relationship. These procedures were crucial for understanding moisture transport in materials such as clay brick, concrete, limestone, granite, and mortar.

Based on these insights, § 5.1 introduced the preliminary results of a machine learning model developed to predict moisture content in building materials. This initial model was trained with simulation data to provide a foundational approach to predict moisture content based on surface temperature. Although this preliminary model is an important step towards non-destructive moisture diagnosis in buildings, it is still necessary to fine-tune it to achieve more accurate results.

To this end, two new moisture prediction models were developed based on what was developed and identified previously. The first is a machine-learning model built on the model introduced in § 5.1. This new model incorporates additional data from laboratory tests performed on mortar and simulations using as input data measured properties of samples used in the experimental campaign. Through a fine-tuning process using experimental data, this machine-learning model achieves more accurate predictions of moisture content in building materials.

The second model is based on building physics principles. It focuses on generating the moisture content curve during the drying phase of mortar coatings, using infrared thermography to detect the different drying stages and assess the moisture content. This model integrates both linear and exponential drying phases to capture the full range of moisture behaviour during the drying process.

Figure 114 illustrates the framework of these two models. In the first one, which employs machine learning, simulation data is combined with laboratory test data to train a neural network for predicting moisture content in materials like clay brick, concrete, limestone, and granite under various environmental conditions. The process begins with preliminary tests on different materials (presented in § 5.1), followed by new simulations and laboratory tests on mortar. The inputs for this model include the material, air temperature and relative humidity, slope (rising or decreasing $\Delta T_{surface}$ during the drying process) and surface temperatures (wet and dry material), with the output being a moisture map. Meanwhile, the second algorithm based on building physics principles uses the evaporation rate and thermal gradient to determine the moisture content during the two drying phases of mortar, providing equations that traduces them. The inputs presented in Figure 114 can be obtained from laboratory tests and with IRT. While the first model predicts the moisture content based on a specific thermal gradient, the second one traces the moisture content curve during the whole drying process, based the duration of the different drying phases identified with infrared thermography.

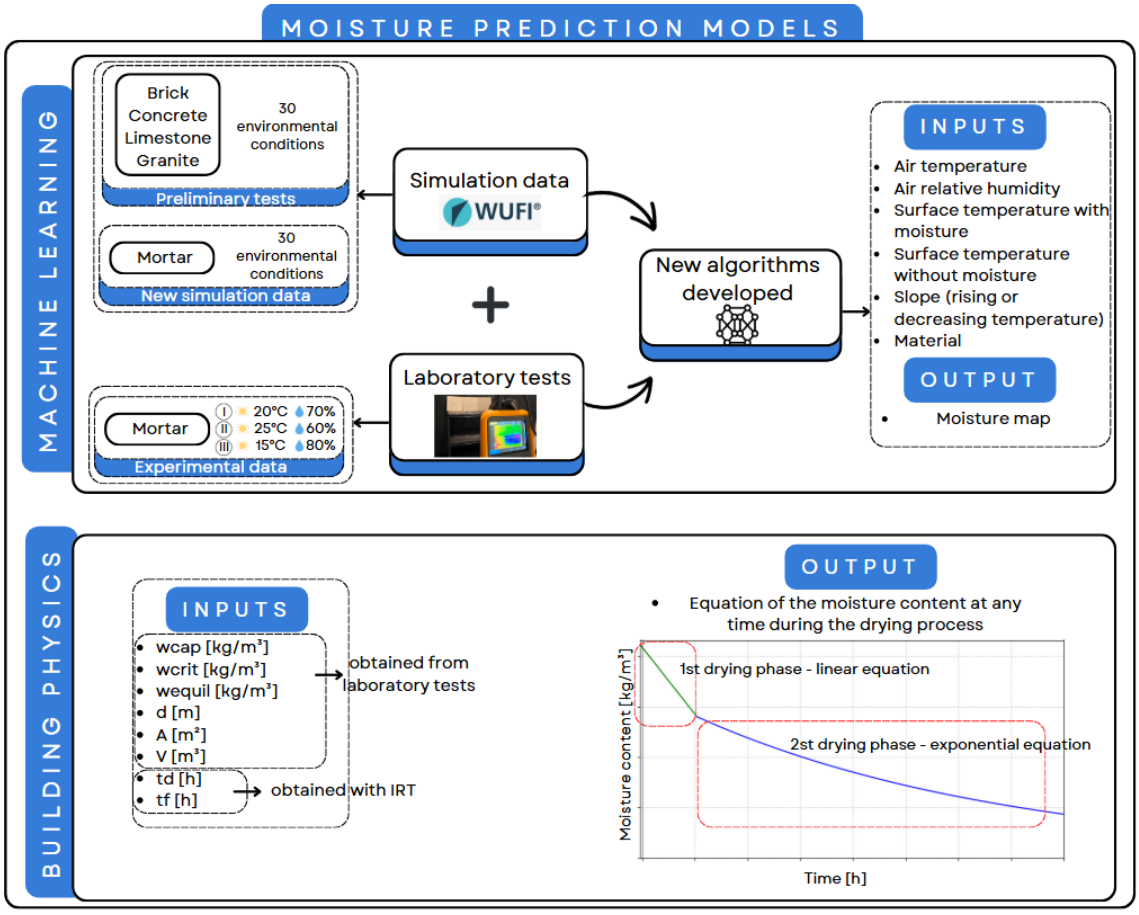


Figure 114 – Procedures to develop the final algorithms

5.3. MOISTURE PREDICTION MODEL WITH MACHINE LEARNING

5.3.1. FRAMEWORK

Figure 115 shows the three algorithms developed to create this final moisture prediction model. The procedures adopted to develop Algorithm 1 with machine learning were similar to the ones presented in § 5.1. New simulation data were generated using the results of hygrothermal simulation for mortar. This data was combined with the one previously generated for clay brick, concrete, limestone, and granite. Additionally, experimental data collected in the laboratory tests were combined with the simulation data. The developed algorithm is presented in Appendix 5.

After that, a new algorithm that converts a thermal image to a file with $\Delta T_{surface}$ values was developed (Algorithm 2). Finally, Algorithm 3 intended to create a moisture map based on the thermal image uploaded. Algorithms 2 and 3 are presented in Appendix 6. The inputs of this last algorithm were the file with the ΔT values, the file with the neural network developed in algorithm 1, and information regarding the material, slope (rising or decreasing $\Delta T_{surface}$ during the drying process) and air temperature and relative humidity. Figure 116 shows the steps to obtain the moisture maps based on the results of infrared thermography.

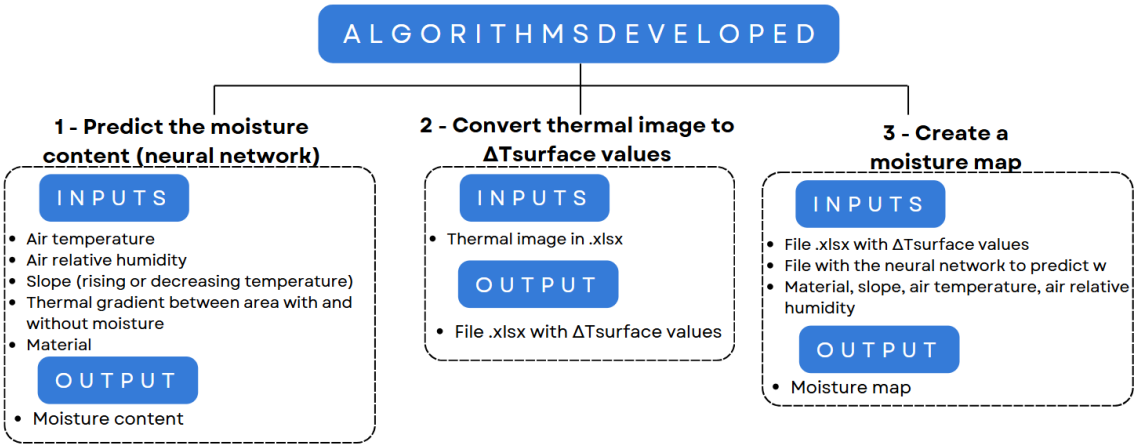


Figure 115 – Final algorithms developed for moisture prediction

Two different approaches were adopted to develop algorithm 1: random initialisation and soft start. The first one consisted of training a neural network with all data (laboratory and simulation), while the second one consisted of training the neural network with the simulation data and then fine-tuning the algorithm with the laboratory data.

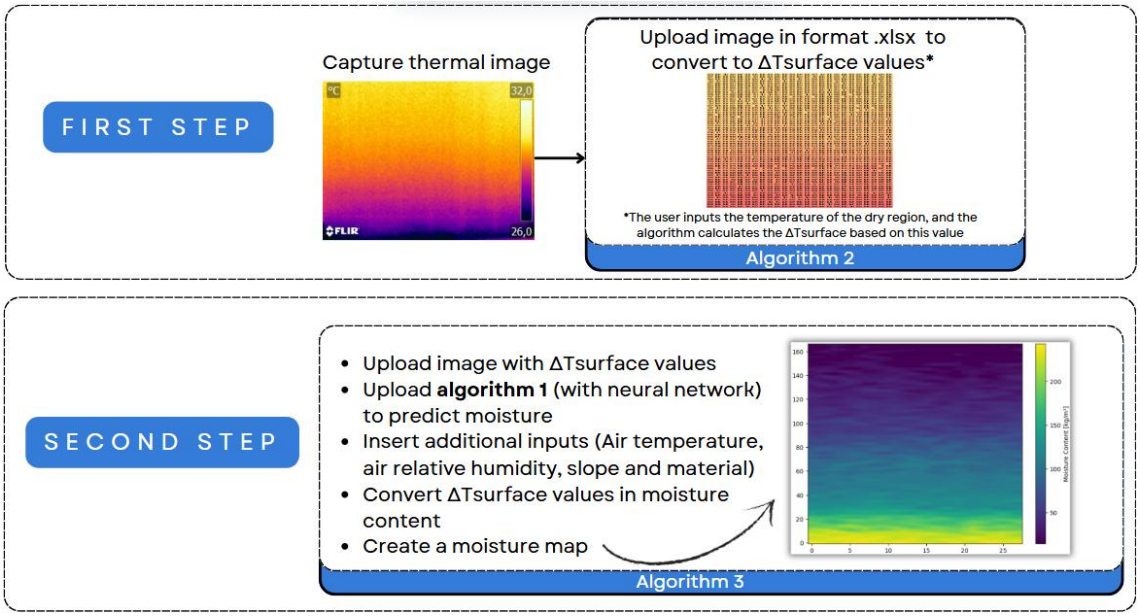


Figure 116 – Steps to generate the moisture map

Figure 117 shows the approaches adopted and the models developed. Besides the model to predict the moisture content in kg/m³ (Model II), it was also developed a model to predict the maximum thermal gradient ($\Delta T_{surfacemax}$) in the drying phase of an initially saturated material (Model I). The inputs of model I were the type of material, air temperature and relative humidity, and the output was the $\Delta T_{surfacemax}$. Model II was developed with all the values obtained in simulation (like Model II presented in § 5.1, it did not disregard the data from the initial phase of the simulation). It had as inputs the air temperature, air relative humidity, slope (showing if the surface temperature is rising or decreasing), surface temperature at the moist area, surface temperature if the dry area, and the material. The output was the moisture content. This final algorithm is better suited for mortar since it was adjusted with experimental data from mortar samples. Similarly to the algorithms developed in the preliminary tests, Neural Networks of the MLP type were used.

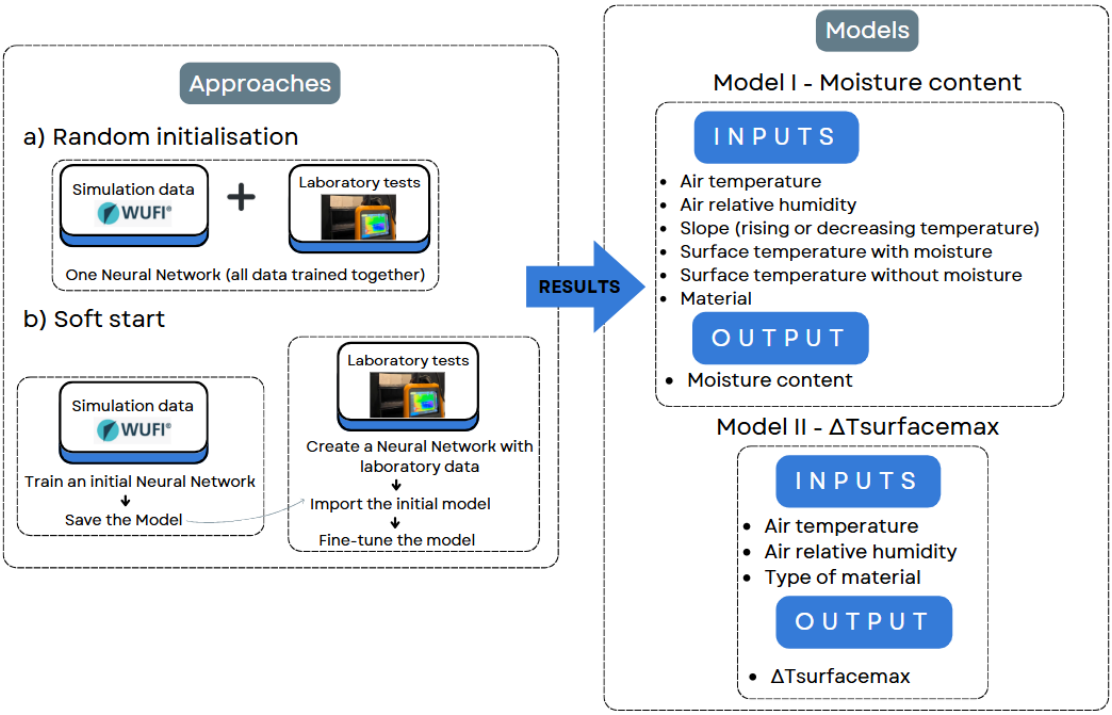


Figure 117 – Different approaches and framework for algorithm 1

5.3.2. RESULTS

Different architectures were assessed in random initialisation, with different numbers of hidden layers and neurons. In soft start, it was also evaluated the effect of dropping and adding different layers. However, only the architectures that presented the best performance, selected based on higher values of the coefficient of determination (R^2) between the predicted and the true values, were chosen for the analysis (Table 49).

Table 49 – Information and performance of the models

		Random initialisation	Soft start
Model I	Layers	1st: 128; 2nd: 64; 3rd: 64	Added layers: 1st: 128; 2nd: 128
	Epochs	37	218
	R^2 (training)	0.999	0.976
	R^2 (testing)	0.999	0.964
Model II	Layers	1st: 128; 2nd: 64; 3rd: 64	Added layers: 1st: 128; 2nd: 128
	Epochs	210	721
	R^2 (training)	0.995	0.355
	R^2 (testing)	0.994	0.494

The graphs with the metrics of loss and MAE are shown in Figure 118. Model I performed well in both situations (random initialisation and soft start). However, for Model II, which presented a higher complexity, random initialisation performed better since, with soft start, the model presented lower coefficient of determination (R^2), and the MAE graph showed signs of overfitting.

Figure 119 shows the correlation between the predicted and the true values as well as the coefficient of determination (R^2) when using random initialisation and soft start for developing Model I and II. The number of scenarios obtained with the laboratory campaign was too small to use the soft start technique, as can be seen in Figures 135 (e), (f), (g) and (h), pointing to unsatisfactory results. The superior performance of random initialisation can be clearly seen when comparing Figure 119 (c) and (g), where Figure 119 (g) exhibits greater data dispersion.

The algorithms developed in §5.1 have limitations, as they do not incorporate experimental data. Additionally, Model III (from §5.1) disregarded initial data from the training and testing datasets, preventing it from accurately predicting moisture content during the early stages of the drying process. The algorithms presented in this Section aim to improve upon those in §5.1 by integrating experimental data and considering the entire values of the dataset. As a result, the updated Model II in this Section achieved an R^2 value of 0.994 for the testing dataset, compared to 0.957 for Model II in §5.1, confirming its higher accuracy.

Algorithm 2 was developed to process a thermal image of a wall with regions with and without moisture. Each pixel corresponds to a specific temperature value. This algorithm requires the user to input the temperature of a dry region, which can be obtained by averaging values from an area without moisture. Once this information is provided, the algorithm generates a file containing thermal gradient ($\Delta T_{surface}$) values. This file, along with the neural network from Algorithm 1, must then be uploaded into Algorithm 3, which will generate a moisture map displaying the moisture content of the wall, according to Figure 120.

Based on the obtained results, the new machine learning model demonstrated the ability to predict the moisture content in building materials, specifically focused on mortar, with improved accuracy. By combining simulation data with laboratory results, the model achieved a high degree of precision in estimating moisture content using the random initialisation approach.

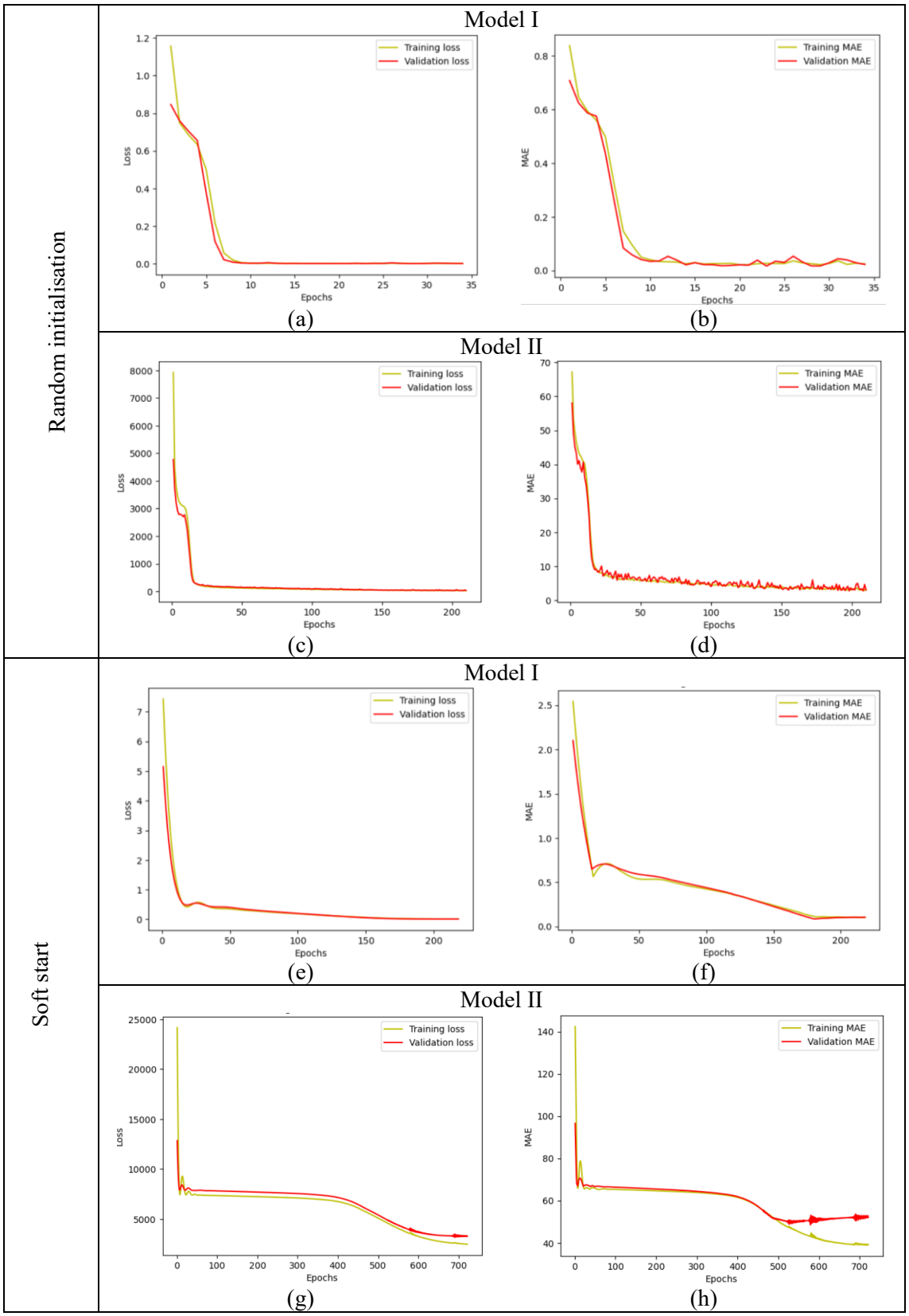


Figure 118 – Training and validation according to each epoch: Random Initialisation (a) Model I – Loss (b) Model I – MAE; (c) Model II - Loss (d) Model II- MAE; Soft start (e) Model I – Loss (f) Model I – MAE; (g) Model II - Loss (h) Model II- MAE

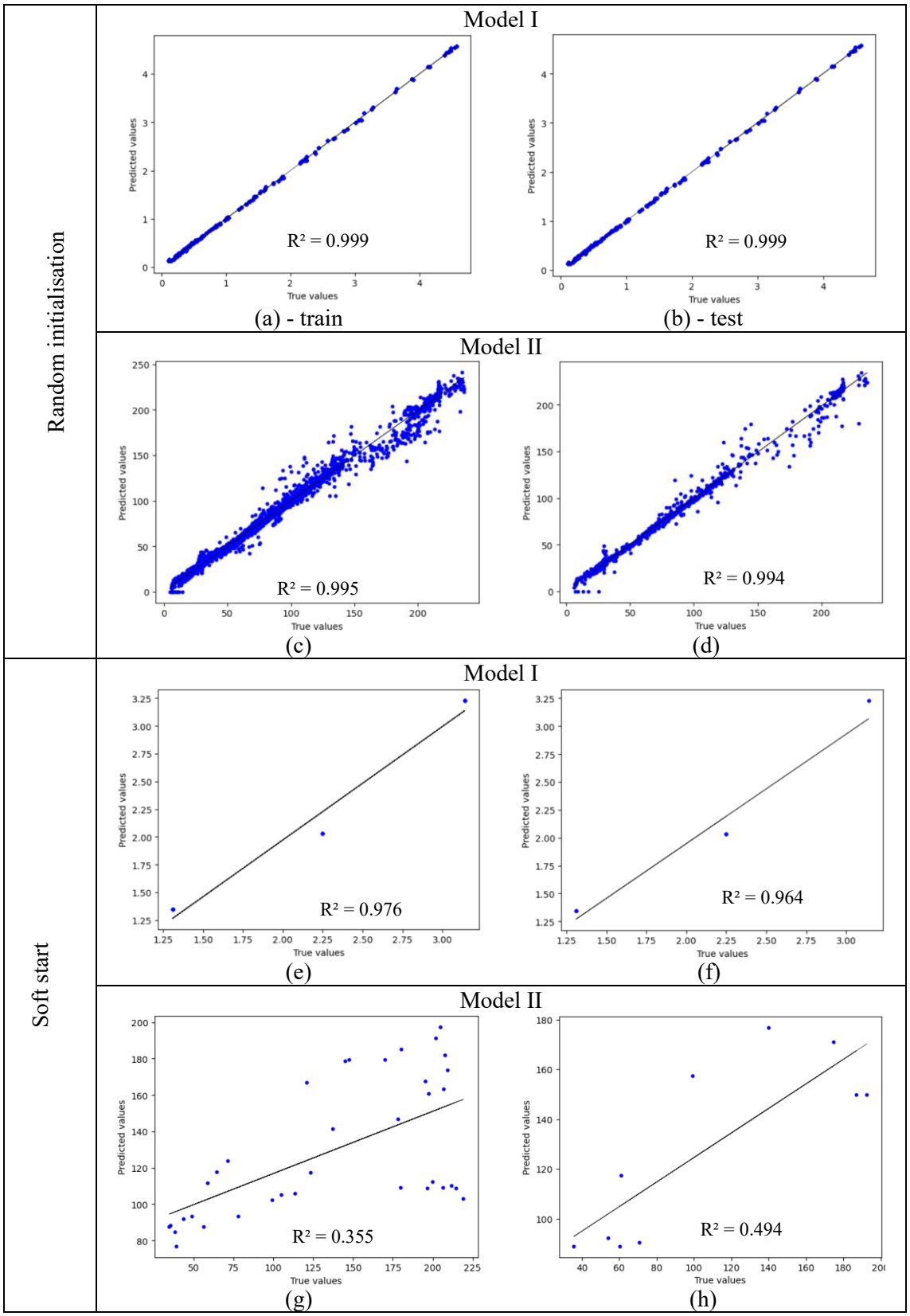


Figure 119 – Correlation between predicted and true values and coefficient of determination (R^2) score for: Random Initialisation (a) Model I – training (b) Model I – testing; (c) Model II - training (d) Model II- testing; Soft start (e) Model I – training (f) Model I – testing; (g) Model II - training (h) Model II- testing

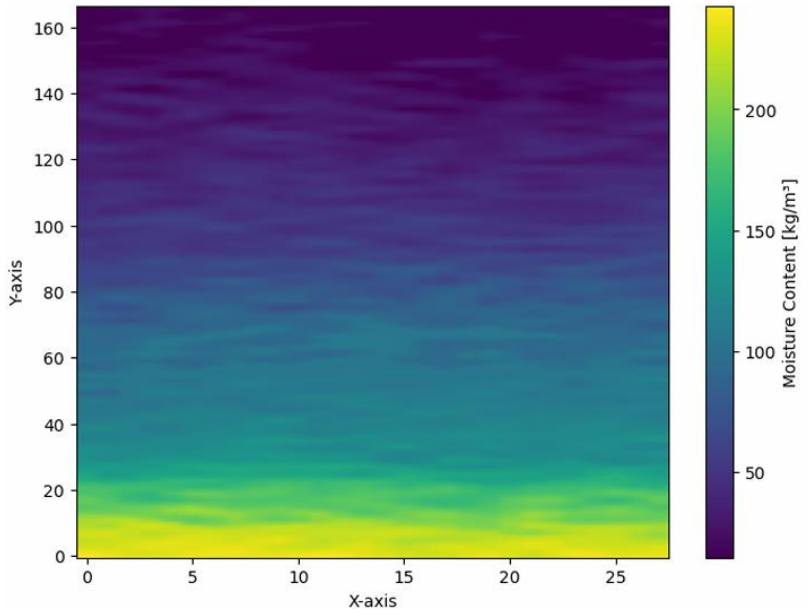


Figure 120 – Moisture map generated by Algorithm 3

5.4. MOISTURE PREDICTION MODEL BASED ON BUILDING PHYSICS CONCEPTS

5.4.1 FRAMEWORK

Building materials undergo two distinct drying phases, each are characterised by different evaporation rates. In the initial phase, the evaporation rate remains approximately constant. However, as drying progresses, it gradually decreases [38]. Consequently, the moisture content decreases linearly during the early stages and follows an exponential decay as the material approaches equilibrium. This behaviour is heavily influenced by the specific properties of the material, such as porosity, permeability, and others, as discussed in Chapter 2, where the physical phenomena governing heat and moisture transport were outlined.

In Chapter 2, Figure 7 and Figure 8 illustrate the different drying phases and the correlation between the evaporation rate and the moisture content in a plaster. Those concepts are the basis for using infrared thermography (IRT) to monitor and predict moisture during the drying process. Chapters 3 and 4 further validated the correlation between moisture and thermal gradient through laboratory tests and hygrothermal simulations and confirmed that the evaporation rate is closely related to the thermal gradient on the material's surface. With the use of IRT, the duration of the drying phases can be identified (as presented in § 3.2.2.8, § 3.3.3.3 and § 4.4.2.4 when comparing IRT results with the evaporation rate density), providing critical information about the moisture profile throughout the drying process of building materials.

In a practical application, if a small sample of the material is collected to identify the free water saturation (w_{cap}) and critical moisture content (w_{crit}), IRT can then provide insights about the duration of each drying phase and equation (7) can be used to predict the evaporation rate density.

Based on that, the algorithm developed in this work generates a moisture content curve over the entire drying period, facilitating a comprehensive understanding of its evolution. This approach can be particularly useful for monitoring multiple walls made of the same material. Once the first wall is observed, the moisture evolution during the drying process can be estimated for the others. Furthermore, if a destructive test is conducted at a specific point during the second drying phase, the algorithm can be applied to define the equation of the exponential curve, allowing for an accurate estimation of the total drying time.

The model developed and tested in this Section focuses on the mortar tested in the laboratory (§ 3.3). However, this methodology is versatile enough to be adapted for other building materials. The potential to generalise this method makes it a valuable tool for non-destructive moisture diagnostics and risk assessment in building materials, providing actionable data that supports better-informed decisions in building maintenance and preservation.

The algorithm developed to generate the moisture content curve of materials during the drying process was based on experimental and theoretical foundation and is presented in Appendix 7. The inputs necessary for running the algorithm, as shown in Figure 114, included parameters obtained from laboratory tests and infrared thermography (IRT). The laboratory-derived parameters, presented in Chapter 2, are:

- w_{cap} [kg/m³].
- w_{crit} [kg/m³].
- w_{equil} [kg/m³].
- d (thickness of the material) [m].
- A (exposed surface area) [m²].
- V (volume of the material) [m³].

Time intervals (t_d, t_f), marking the drying phases, are obtained using IRT: t_d represents the period of time until the thermal gradient sharply drops and t_f is the period time until the thermal gradient is no longer visible. The evaporation rate in the first drying phase was calculated according to equation (7). Figure 121 presents the evolution of moisture content over time and the values needed as input of the algorithm.

In the first phase, the drying process followed a linear relationship. The equation that traduces it is calculated using the known points (0 [h], w_{cap} [kg/m³]) and (td [h], w_{crit} [kg/m³]) to define its slope (m). The variation of moisture content over time is given by equation (39), where m and c are determined using equations (40) and (41), respectively.

$$y = mx + c \tag{39}$$

$$m = \frac{w_{cap} - w_{crit}}{t_d} \tag{40}$$

$$c = w_{cap} \tag{41}$$

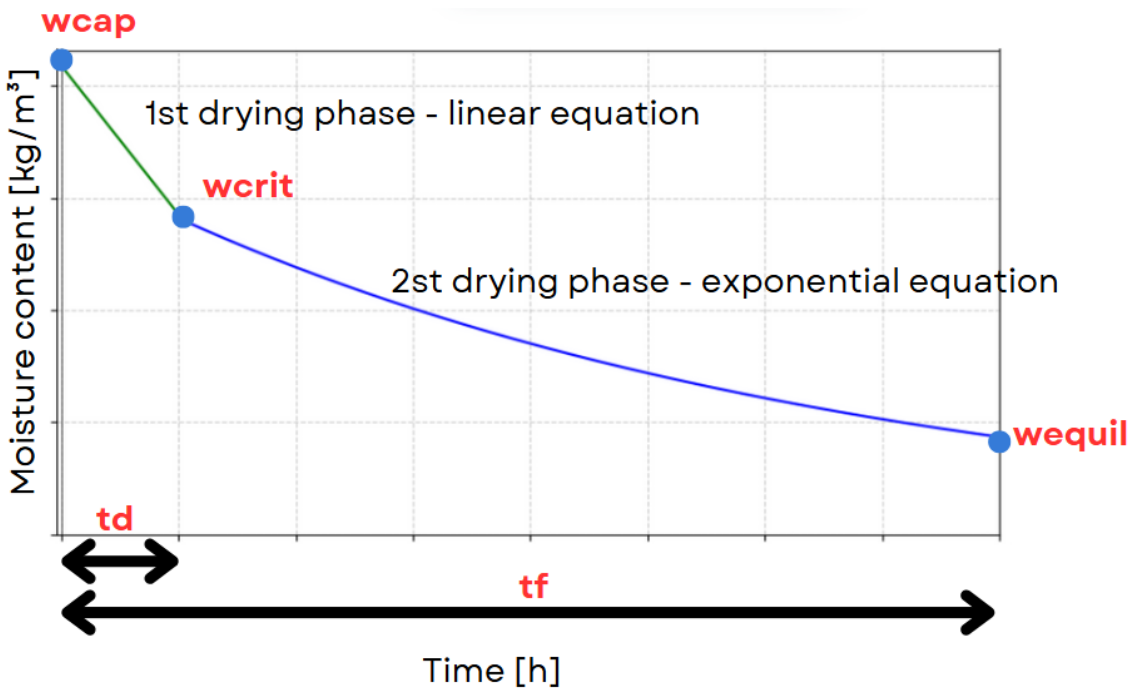


Figure 121 – Generic evolution of moisture content over time (inputs of algorithm based on building physics concepts)

During the second drying phase, after the critical moisture content is reached, the drying process exhibits exponential behaviour. The equation is modelled using the points (t_d [h], w_{crit} [kg/m³]) and (t_f [h], w_{equil} [kg/m³]), as shown in equation (42).

$$y = a \,.\, e^{bx} \tag{42}$$

The coefficients a and b are calculated using equations (43) and (44).

$$b = \frac{\ln \frac{w_{equil}}{w_{crit}}}{t_f - t_d} \tag{43}$$

$$a = \frac{w_{crit}}{e^{b.tf}} \tag{44}$$

The developed algorithm incorporated these equations and generated the moisture content curve in the drying process. Below there is a summary of the implementation:

- Definition of the linear and exponential equations based on the experimental and simulation information (w_{cap}, w_{crit}, t_d, and t_f),
- Application of the algorithm to test its applicability under four scenarios:
    1. Simulation results for 25°C, 60% RH.
    2. Laboratory tests at three different climatic conditions:
        - 25°C, 60% RH.
        - 15°C, 80% RH.
        - 20°C, 70% RH.

- Comparison between the curves predicted by the algorithm and the curves identified in the experimental campaign and simulation.

5.4.2 RESULTS

The results obtained by the algorithm were compared with the experimental data from laboratory tests under three different climatic conditions and with the simulation data for the environment T = 25°C and RH = 60%. This comparison aimed to evaluate the accuracy of the algorithm in predicting the drying curves. Figure 122 shows the results of the algorithm (the green line represents the linear phase of the drying process, the blue curve represents the exponential phase, and the red points represent the true data, obtained in the laboratory tests and by simulation).

Table 50 presents the coefficient of determination (R^2) between the values predicted by the algorithm and the true values. Regarding the comparison of the moisture content obtained from the simulation data in WUFI (25°C and 60%), the curves generated by the algorithm showed excellent agreement with them with a high R^2 value. The linear phase accurately captured the initial drying behaviour, while the exponential phase effectively described the approach to equilibrium moisture content. Minor discrepancies were identified.

The comparison of the algorithm with the results from the laboratory tests (25°C and 60%) also showed a good correlation, though with a slightly lower R^2 than the simulation data. In the linear phase, the experimental points are closely aligned with the predicted straight line. In the exponential phase, the predicted curve follows the same trend as the measurements, but it deviates more than the simulation results. This probably occurred because, in the laboratory tests, the exact duration of the first drying phase could not be identified with high precision since no measurements were made between the 8^{th} and the 24^{th} hour of the drying process (at night/dawn). In the example of Figure 122 (b), it was assumed that the first drying phase ended within 8 hours, but if the duration of the first drying phase was set as 24 hours, the algorithm would plot the curve shown in Figure 123, presenting a better adjustment regarding the real measurements (the R^2 value would be 0.985).

Table 50 – Coefficient of determination (R^2) between the values predicted by the algorithm and the true values

Scenario	R^2
25°C, 60% RH simulation	0.959
25°C, 60% laboratory test	0.868
20°C, 70% laboratory test	0.925
15°C, 80% laboratory test	0.970

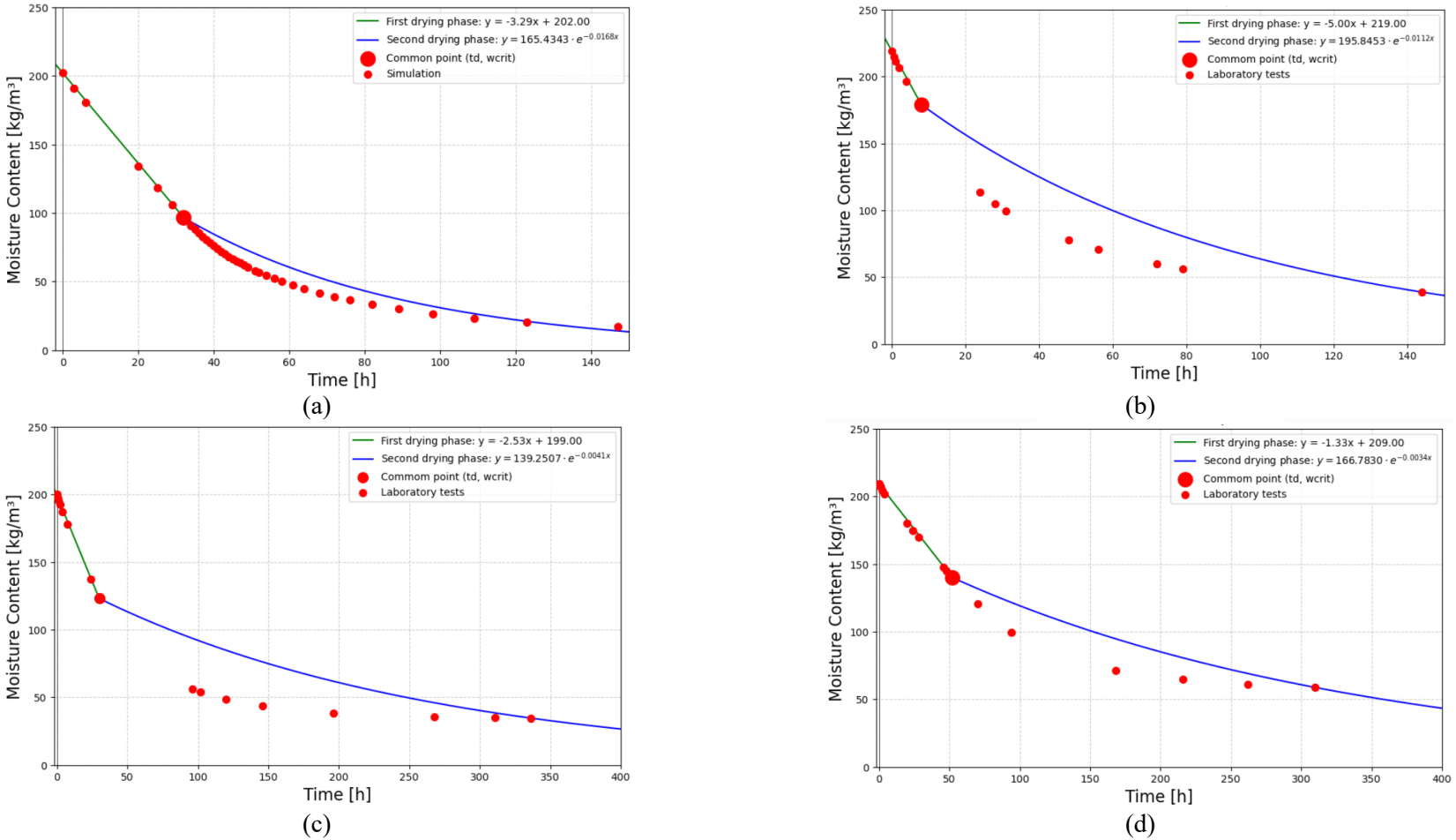


Figure 122 – Comparison between the algorithm results and the simulation and laboratory tests: (a) 25°C, 60% RH simulation; (b) 25°C, 60% laboratory test; (c) 20°C, 70% laboratory test; (d) 15°C, 80% laboratory test

The comparison between the results of the algorithm and the data from the laboratory tests with 20°C and 70% Figure 122 (c) showed that the algorithm presents a slower drying behaviour, as the moisture content reduced faster in the laboratory test, but the R^2 value showed a strong correlation. The difference between the algorithm's predictions and the moisture content values measured in the laboratory tests also might have happened due to the lack of measurements between 30 and 102 hours. Under the coldest and most humid condition (15°C and 80%), the algorithm's predictions closely followed the experimental points, with an R^2 value close to 1.

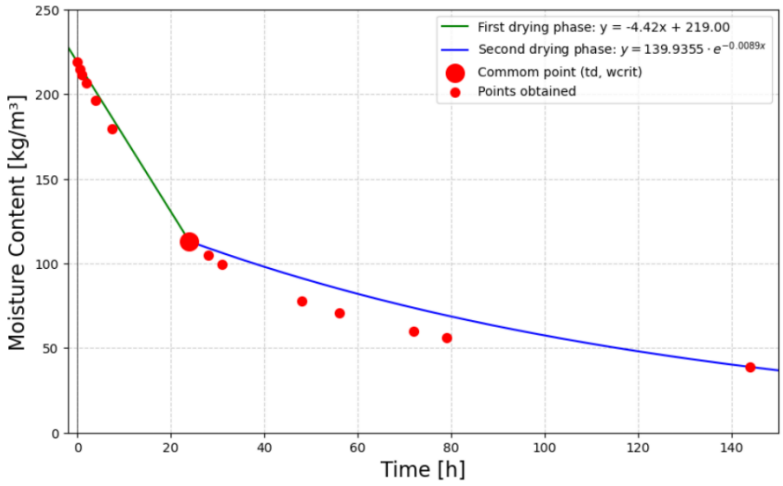


Figure 123 – Comparison between the curves plotted by the algorithm and the results from laboratory test in T=25°C and RH of 60% considering 24 hours of duration of the 1st drying phase

In general, the algorithm consistently provided curves that closely matched the experimental and simulated data across all scenarios. The linear phase was perfectly represented in the algorithm, and the exponential phase presented some discrepancies but, nevertheless, represented accurately the moisture content curve. The algorithm traduces the physical behaviour of the drying process across different phases and environmental conditions. Future enhancements, such expanding tested materials and experimental datasets, could further improve its performance. The guidelines for applying the models and the methodology presented in this work in a practical moisture diagnosis situation is presented in the following Section.

5.5. GUIDELINES FOR APPLYING THE MOISTURE PREDICTION MODELS

Infrared thermography (IRT) has proven to be an effective, non-destructive tool for assessing moisture content in building elements. This Section provides guidelines for applying the moisture prediction models developed in this work to a practical situation of moisture inspection with IRT. The methodology presented in Figure 124 follows a structured decision-making process, ensuring that the obtained results are reliable and applicable under different conditions.

The first step in conducting an inspection using IRT is to capture a thermal image of the target wall. If the material composition is similar to the mortar analysed in this study and the environmental conditions are stable, the algorithms presented in this thesis can be directly applied. These algorithms correlate the thermal gradient with the corresponding moisture content, allowing the identification of moisture distribution across the inspected wall.

The algorithms were developed for a material initially saturated. In some building inspection situations, it is not possible to know if the material was initially saturated. However, as shown in Figure 40, Figure 80, and Figure 84, the correlation curve between $\Delta T_{surface}$ and the moisture content for the materials that are not initially saturated does not deviate much from the ones initially saturated (especially for mortar – see Figure 40 (d)), except for concrete. For this reason, it might be reasonable to apply the algorithm to predict the moisture content even for materials initially non-saturated.

An example of the application of the algorithms is shown in Figure 124. For an inspection of masonry rendered with mortar in an environment with a temperature of 25°C and a relative humidity of 60% in which the maximum thermal gradient identified with IRT is 2.0°C, the application of Algorithm 1 – Model I will show that the maximum possible thermal gradient for that environment and that material is 2.8°C. Additionally, Algorithm 1 – Model II will calculate that the moisture content for the thermal gradient of 2.0°C (considering that the thermal gradient has a decreasing curve at the moment of the inspection) is 75 kg/m³. Based on the moisture storage function, it is possible to compare the moisture content of 75 kg/m³ with the equilibrium moisture content for that environment (14 kg/m³) to understand how moist the wall is. After that, Algorithms 2 and 3 can also be applied to generate a moisture map to identify the moisture content of each pixel of the wall.

The drying process can also be monitored with IRT to analyse the evolution of the thermal gradient over time. This data should be compared to the results from the simulation (Appendix 8) to identify in which part of the drying process the material is. The algorithm presented in Appendix 9 enables the user to select one of the combinations of temperature and relative humidity of the air used in the simulations to visualise the curve of the $\Delta T_{surface}$ over time (Figure 125). This approach enables the estimation of the drying time under specific environmental conditions.

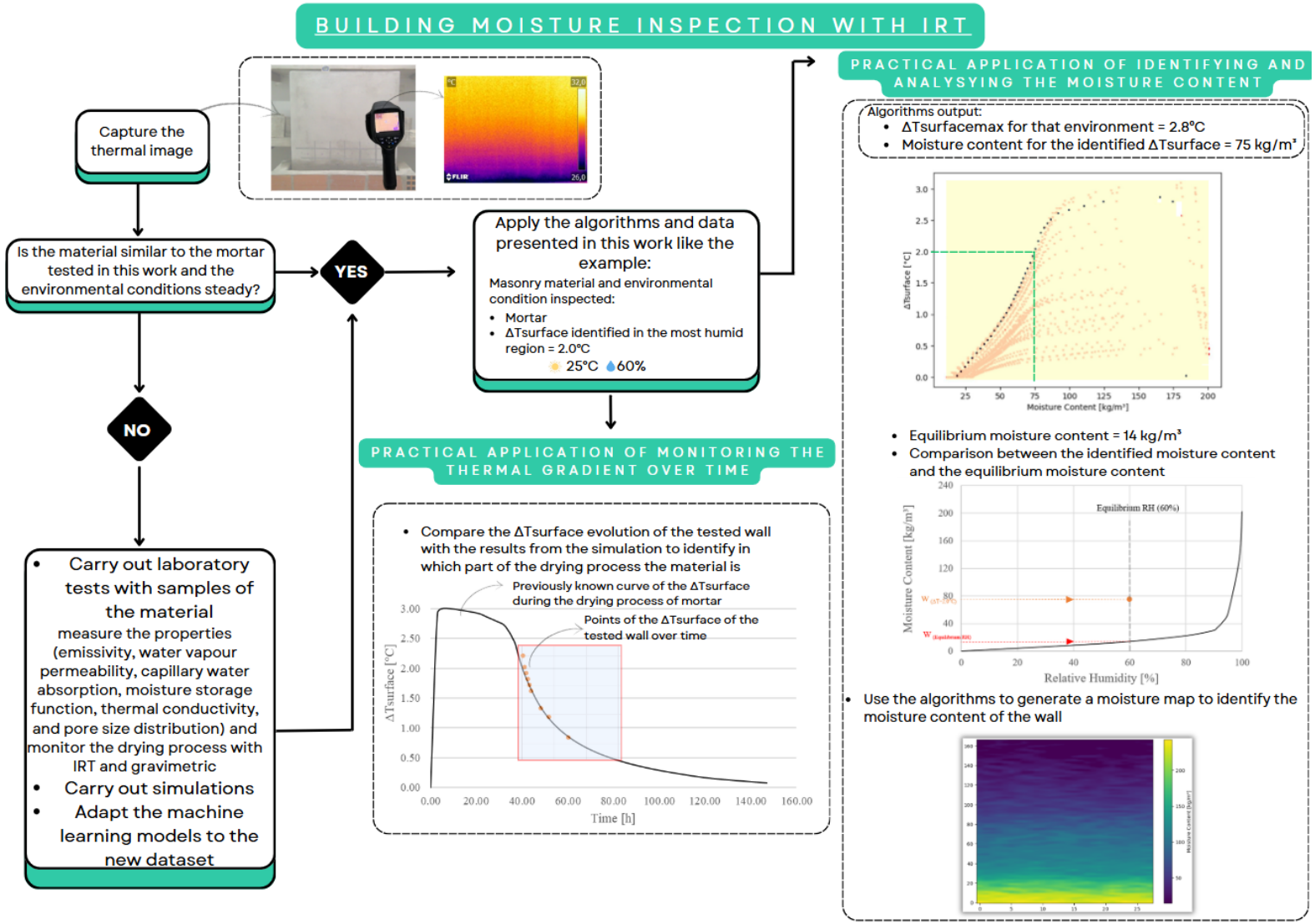


Figure 124 – Flowchart describing the procedures for conducting an inspection with IRT using the algorithms and methodology presented in this work

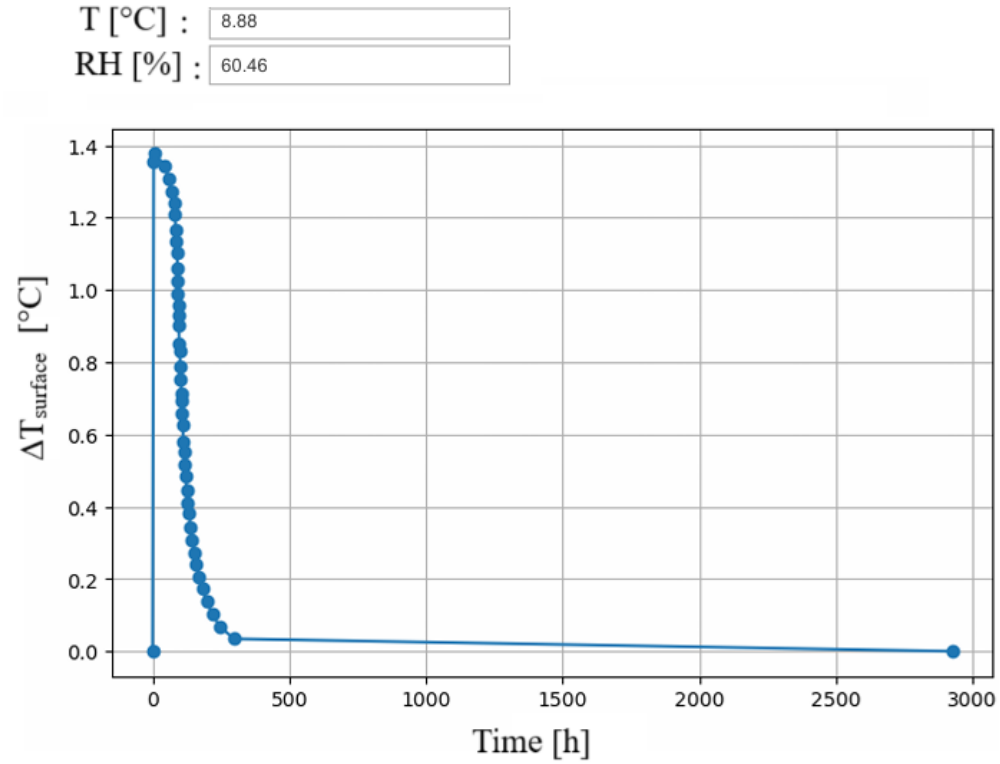


Figure 125 – Algorithm for selecting a combination of temperature and relative of the air to plot the curve of the ΔTsurface over time

Additionally, for an initially saturated wall scenario, it is possible to use IRT to monitor the whole drying process and identify the duration of the different drying phases. With these values, the algorithm based on the building physics principles can be applied to plot the moisture profile throughout the drying process. This might be useful for visualising the moisture behaviour during the drying process after the wall is dry. However, it can also be used to monitor multiple walls made of the same material (since the drying behaviour will already be known) or to use a destructive test to identify the moisture content at some point in the second drying phase and then predict the drying time.

If the material of the wall under study is not a mortar similar to the one analysed in this work or the environmental conditions vary during the drying process, additional steps must be undertaken before applying the developed models. This involves conducting laboratory tests with samples of the material to determine key material properties such as emissivity, water vapour permeability, capillary water absorption, moisture storage function, thermal conductivity, and pore size distribution. Additionally, the drying process should be monitored using both IRT and gravimetric methods. These data should then be used to perform numerical simulations replicating the moisture transfer process in the specific material under study.

Once the material properties and drying behaviour are well understood, the obtained data can be integrated into the machine learning models to retrain them for the new dataset. This ensures that the prediction algorithms remain accurate for different materials and environmental conditions. Following this adaptation, the step-by-step methodology established for mortar walls can be applied to the newly

studied material, enabling the generation of moisture maps and the identification of the drying behaviour in a reliable manner. Through this approach, the use of IRT for moisture inspection becomes adaptable and applicable to a wide range of building materials and scenarios.

It is worth noting that the application of IRT for monitoring moisture is more suited for highly porous building materials, as presented in this thesis. In materials such as concrete, it will be possible to identify the moisture content only down to a few millimetres below the surface since IRT cannot identify a very low drying rate of the internal moisture.

5.6. FINAL REMARKS

The development and testing of the moisture prediction models using of machine learning techniques and building physics principles proved to be a step forward in understanding and predicting the drying behaviour of building materials using IRT. The final algorithms were designed and refined based on findings from previous steps, culminating in robust and reliable tools for diagnosing moisture behaviour under different conditions.

The machine learning-based moisture prediction model used hygrothermal simulation data and experimental results to provide accurate predictions of moisture content, fine-tuned for mortar. Despite some limitations, such as the small size of experimental datasets, the machine learning model successfully predicted moisture content and maximum thermal gradients during the drying process. This model shows promise for further refinement and applications to a broader range of materials, contributing to an advance in non-destructive testing methods and more effective diagnostics in moisture-related defects.

The algorithm based on building physics principles proved to be an effective tool for modelling the two drying phases—linear and exponential—of mortar. This algorithm requires some material properties (capillary moisture content, critical moisture content, and equilibrium moisture content) and the observation of the drying process with IRT. Comparisons with experimental and simulated data validated the algorithm's reliability. The linear phase was accurately predicted, and while minor discrepancies were observed in the exponential phase, they did not compromise the model's overall performance. The methodology shows potential applications beyond mortar to a variety of building materials.

Future work should focus on enhancing the algorithm based on machine learning by incorporating dynamic environmental boundary conditions and expanding its application to other material types and wall thicknesses. Regarding the model based on the building physics principle, it should be tested for different materials in more environmental conditions. Additionally, reducing the time intervals between measurements of the experimental tests, especially between drying phases, would further improve the analysis of the model's performance.

Furthermore, continued efforts are needed to explore other machine learning models, such as Recurrent Neural Networks of the LSTM type, which are appropriate for analysing time-series data and can be used to deal with data of surface temperature variation according to time. This way, it may facilitate the model's generalised use in different scenarios and enable an assertive diagnosis of the moisture content in walls. Future perspectives also include using computer vision techniques with machine learning models to automate the identification of moisture and classify the walls based on the risk of moisture damage.

6

CONCLUSIONS

This thesis advances the understanding of how infrared thermography (IRT) can be used to diagnose moisture in building materials by correlating surface temperature variations with moisture content. The developed algorithms are a reliable way of identifying the moisture content of certain building materials in different steady environmental conditions. Additionally, future studies can extend this methodology to other materials and explore its applicability in dynamic environmental conditions, considering factors such as solar incidence and wind.

The state-of-the-art review enabled an understanding of the complexities involved in moisture transport and its implications for the durability and comfort of building materials and structures. The review highlighted critical aspects of the hygrothermal behaviour, presenting the different phases in the humidification and drying process and how the changes in the moisture content affect the surface temperature of the materials. Chapter 2 presented that moisture may cause anomalies mainly due to salt crystallisation and mould growth, and the damage caused by them will be influenced by environmental conditions, such as temperature and relative of the air, the existence and type of salts, and the amount of moisture and its evolution over time. Therefore, it is important to identify the level of moisture and the moisture evolution over time to analyse the drying process and check if there is a risk of moisture-related damage. In this way, the review provided a comprehensive analysis of NDT and machine learning applications for defect diagnosis, presenting the most suited approach for studying the correlation between the thermal gradient and the moisture content.

The main results obtained from laboratory tests and simulation are summarised below:

- The regression analysis performed to understand the correlation between the thermal gradient and the moisture content showed better performance in the quadratic model. The following coefficients of determination (R^2) were obtained in the laboratory tests under free-running conditions: 0.881, 0.824, 0.625, 0.789, and 0.627 for clay brick, limestone, granite, mortar, and concrete. Under controlled laboratory conditions, the coefficient of determination for mortar varied from 0.733 to 0.934 in the three scenarios tested.

- The maximum thermal gradient ($\Delta T_{surfacemax}$) was similar for specimens with the highest and intermediate initial moisture content for clay brick, limestone, mortar and concrete tested in the experimental campaign. The simulation results showed that the $\Delta T_{surfacemax}$ is related to the difference between the saturation vapour pressure at the surface subtracted from the vapour pressure of the air (R^2 close to 1). Despite initially different, the moisture content in both situations (HMC and IMC) is high, and this probably led to a saturated surface, leading to a similar maximum thermal gradient (in clay brick simulation results, the surface was saturated for initial moisture contents higher than 60% of the maximum moisture content and in all these situations the maximum thermal gradient was the same). In this context, the value of the maximum thermal gradient achieved can indicate if the surface is saturated.
- The time required to reduce the thermal gradient shows the moisture content level of the material. Specimens with higher initial moisture content required more time for the thermal gradient to reduce than specimens with intermediate moisture content. This happened because of the longer duration of the first phase of the drying process in specimens with higher moisture content (characterised by an approximately constant evaporation rate density, when capillary conduction is the main form of transport).
- The evaporation rate density exhibited a sharp decline at roughly the same moment that the surface thermal gradient reduced sharply. Hence, the reduction of the thermal gradient indicates that the material is starting the second drying phase (with a lower evaporation rate and an exponentially decreasing moisture content curve).
- The coefficient of determination between the thermal gradient and the moisture content in the second drying phase was 0.975, 0.974, and 0.988 for a linear model in scenario I (20°C and 70% RH), scenario II (25°C and 60% RH), and scenario III (15°C and 80% RH), respectively. These results show that IRT can be used to identify the duration of the first drying phase, after which linear equations can be reliably applied to identify the moisture content due to the strong correlation between the variables.
- The simulations showed that in clay bricks, the thermal gradient remains approximately constant when the moisture content is from 6.0 to 12.0%. Below this value, it sharply reduces. As for limestone, this sharp reduction was observed when the moisture content was below 1.0%.
- The simulations showed a coefficient of determination between the thermal gradient and the moisture content of 0.916 for clay brick and 0.909 for limestone.
- The data analysis of the simulation results showed that each environmental condition and material presented a specific downward curve for the correlation between the moisture content and the thermal gradient during the drying phase (Figure 91). This occurs because the $\Delta T_{surface}$ is affected by the evaporation process at the material's surface, which in turn is shaped by factors such as the material's pore size distribution and the surrounding environmental conditions.

- The comparison between laboratory tests and simulation results portrayed some similarities but with a difference in the maximum thermal gradient achieved.

Laboratory tests and simulations demonstrated a consistent correlation between surface thermal gradients and moisture content. The findings revealed that each material exhibits a distinct thermal behaviour during the drying process, emphasising that drying characteristics are strongly influenced by the specific properties of each material, particularly porosity. Materials with lower porosity, such as concrete and granite, showed weaker correlations between thermal gradients and moisture content, while limestone, clay brick, and mortar presented higher coefficients of correlation. These tests confirmed that each material and environmental condition requires specific regression models, as variations in equations were significant across scenarios. Although quadratic models demonstrated good correlation within environmentally controlled settings and linear models demonstrated good correlation in the second drying phase, their applicability was limited to specific materials, thicknesses, and environmental conditions.

The machine learning (ML) models developed in this thesis significantly expanded the scope of moisture content identification. These innovative models demonstrated the ability to adapt to various environmental conditions, with different air temperature and relative humidity levels, and account for various materials. By integrating datasets obtained with simulation and laboratory tests, the machine learning approach provided a more versatile and robust tool for predicting moisture content in variable scenarios. The summarised main results are presented:

- Preliminary models trained with simulation data predicted the moisture content and $\Delta T_{surfacemax}$ in clay brick, limestone, granite, and concrete. The Neural Network (NN) developed to predict the $\Delta T_{surfacemax}$ (Model I) showed the R^2 of 0.999. The R^2 of 0.957 was found for the NN model that predicts the moisture content (Model II). The application of the developed models in environmental conditions that are common in real applications demonstrated that the preliminary model accurately detected the moisture content in clay brick and granite. For concrete, the models could only identify moisture when the surface was moist, as internal moisture did not produce a detectable thermal gradient. In the case of limestone, the model could identify both high and intermediate moisture levels.
- The final ML models (§ 5.3), trained with simulation and experimental data, incorporated additional algorithms to generate a moisture map based on the upload of a thermal image. These models showed the R^2 of 0.999 for predicting the $\Delta T_{surfacemax}$ and the R^2 of 0.994 for predicting the moisture content using the random initialisation approach.

These models predicted moisture content based on surface thermal gradients, and their application extended to creating moisture maps using thermal images. Specifically, models fine-tuned with experimental data for mortar proved particularly effective, offering a reliable tool for visualising moisture distribution in building materials.

The state-of-the-art review, the laboratory tests and the simulations demonstrated that the drying process follows distinct phases: an initial constant evaporation rate, characterised by a linear trend, followed by a decreasing rate, which adheres to an exponential pattern. The comparison between the evaporation rate density and the thermal gradient variation showed that IRT has a good potential to identify the duration of the different drying phases. Based on that, an algorithm grounded in building physics principles was developed to plot the moisture curve during the drying phase, which was successfully validated with laboratory tests and simulation results, achieving an R^2 varying from 0.868 to 0.959. This model is helpful to visualise the moisture behaviour after the drying process is finished but can also be used to monitor multiple walls made of the same material (since the drying behaviour will already be known) or to predict the drying time if a destructive test is performed to identify the moisture content of some point in the second drying phase (the exponential equation can be found and used to predict the total drying time).

Although several authors highlighted the difficulty of quantitatively diagnosing moisture with IRT, this work helped to fill the research gap by demonstrating that machine learning can be applied to identify the complex patterns of surface temperature and moisture content during the drying process of building materials. The models created account for the different factors that affect the correlation between moisture and IRT results.

This study contributes significantly to the field in several ways. Methodologically, it introduced an innovative combination of destructive and non-destructive techniques, simulations, and machine learning to develop predictive models that reduce subjectivity in moisture diagnosis. These findings offer insights for inspecting moisture in buildings and enable more effective preventive maintenance and rehabilitation strategies.

Nevertheless, the study has some limitations. The models can only be applied to some materials (the preliminary models can be applied to the simulated clay brick, limestone, granite, and concrete, and the final models can be applied to the characterised mortar) since the pore size distribution affects the moisture transport behaviour. In some materials, it will be possible to identify the moisture content only down to a few millimetres below the surface since the drying of the internal moisture content happens at a very low drying rate, which cannot be identified by IRT. On the other hand, in highly porous materials, IRT can identify the existence of moisture until the material is almost completely dry.

Although this work presented the impact of different initial moisture contents through laboratory tests and simulations, the final moisture prediction models only consider materials initially saturated. Therefore, additional studies should be carried out with other materials to explore the identification of the moisture content in materials with different initial moisture contents.

In real-world applications, factors besides temperature and relative humidity may affect surface temperature behaviour. Besides that, the environmental conditions usually happen in a dynamic way, and the models assumed a steady environmental condition. However, the methodology presented in this work can be applied to predict the moisture content in any other scenario, including a dynamic one.

Future research should explore more varied and unpredictable scenarios to enhance model robustness. Additionally, while the focus on materials like clay brick, mortar, and limestone provided significant insights, further investigation is needed for materials such as concrete and granite (high quantity of pores with small size).

Future studies should also focus on exploring alternative machine learning models, such as Long Short-Term Memory (LSTM) Recurrent Neural Networks, which are well-suited for analysing time-series data and could effectively handle variations in surface temperature over time. This approach could enhance the generalizability of the models across diverse scenarios, enabling more accurate moisture content diagnosis in walls. Additionally, future work should consider integrating computer vision techniques with machine learning to automate moisture identification and classify walls based on their risk of moisture damage.

In addition, the research opens avenues for future exploration, particularly in integrating these algorithms into real-time diagnosis, especially with the use of drones or robots equipped with thermal imaging sensors for automated building inspections.

Finally, this research contributes to more precise and sustainable approaches to managing moisture in buildings, supporting enhanced durability, occupant comfort, and overall structural performance. These findings provide a foundation for continued innovation in building diagnosis and preservation.

REFERENCES

[1] E. Barreira and R. M. S. F. Almeida, *Infrared Thermography for Building Moisture Inspection*, vol. 34. 2019. [Online]. Available: http://link.springer.com/10.1007/978-3-319-75386-7

[2] A. Arnold and K. Zehnder, "Salt Weathering on Monuments Conservation of wall paintings View project," Bari. [Online]. Available: https://www.researchgate.net/publication/260552681

[3] N. Sathiparan and U. Rumeshkumar, "Effect of moisture condition on mechanical behavior of low strength brick masonry," *Journal of Building Engineering*, vol. 17, no. November 2017, pp. 23–31, 2018, doi: 10.1016/j.jobe.2018.01.015.

[4] E. Grinzato, N. Ludwig, G. Cadelano, M. Bertucci, M. Gargano, and P. Bison, "Infrared thermography for moisture detection: A laboratory study and in-situ test," *Mater Eval*, vol. 69, no. 1, pp. 97–104, 2011.

[5] I. Garrido, E. Barreira, R. M.S.F. Almeida, and S. Lagüela, "Introduction of active thermography and automatic defect segmentation in the thermographic inspection of specimens of ceramic tiling for building façades," *Infrared Phys Technol*, vol. 121, 2022, doi: 10.1016/j.infrared.2021.104012.

[6] S. Perilli, D. Palumbo, S. Sfarra, and U. Galietti, "Advanced insulation materials for facades: Analyzing detachments using numerical simulations and infrared thermography," *Energies (Basel)*, vol. 14, no. 22, 2021, doi: 10.3390/en14227546.

[7] S. Sfarra, A. Cicone, B. Yousefi, C. Ibarra-Castanedo, S. Perilli, and X. Maldague, "Improving the detection of thermal bridges in buildings via on-site infrared thermography: The potentialities of innovative mathematical tools," *Energy Build*, vol. 182, pp. 159–171, 2019, doi: 10.1016/j.enbuild.2018.10.017.

[8] E. Barreira, S. S. De Freitas, V. P. De Freitas, and J. M. P. Q. Delgado, "Experimental study of micro-cracks in laboratory and in situ using infrared thermography," *Defect and Diffusion Forum*, vol. 353, pp. 17–22, 2014, doi: 10.4028/www.scientific.net/DDF.353.17.

[9] M. Mahmoodzadeh, V. Gretka, I. Lee, and P. Mukhopadhyaya, "Infrared thermography for quantitative thermal performance assessment of wood-framed building envelopes in Canada," *Energy Build*, vol. 258, no. 111807, 2022, doi: 10.1016/j.enbuild.2021.111807.

[10] E. Rosina and N. Ludwig, "Optimal thermographic procedures for moisture analysis in buildings materials," in *EUROPTO Conference on Diagnostic Imaging Technologies and Industrial Applications*, Munich: SPIE, Jun. 1999. [Online]. Available: http://proceedings.spiedigitallibrary.org/

[11] E. Barreira, R. M. S. F. Almeida, and J. M. P. Q. Delgado, "Infrared thermography for assessing moisture related phenomena in building components," *Constr Build Mater*, vol. 110, pp. 251–269, 2016, doi: 10.1016/j.conbuildmat.2016.02.026.

[12] M. S. Camino, F. J. León, A. Llorente, and J. M. Olivar, "Evaluation of the behavior of brick tile masonry and mortar due to capillary rise of moisture," *Materiales de Construccion*, vol. 64, no. 314, pp. 1–7, 2014, doi: 10.3989/mc.2014.02513.

[13] P. Cárdenas-Del Campo, F. Soto-Lara, and M. Marín-Granados, "Description of moisture thermal patterns in concrete for the thermal inspection method by infrared thermography," *Lecture Notes in Mechanical Engineering*, vol. 1, pp. 622–631, 2019, doi: 10.1007/978-3-030-12346-8_60.

[14] J. H. A. Rocha, C. F. Santos, and Y. V. Póvoas, "Detection of precipitation infiltration in buildings by infrared thermography: A case study," *Procedia Structural Integrity*, vol. 11, pp. 99–106, 2018, doi: 10.1016/j.prostr.2018.11.014.

[15] C. F. Santos, J. H. A. Rocha, P. I. B. Batista, and Y. V. P. Tavares, "Potencialidade da termografia infravermelha na detecção de infiltrações em edificações," in *Patorreb 2018*, Rio de Janeiro, Apr. 2018.

[16] L. Ruiz Valero, V. Flores Sasso, and E. Prieto Vicioso, "In situ assessment of superficial moisture condition in façades of historic building using non-destructive techniques," *Case Studies in Construction Materials*, vol. 10, no. e00228, 2019, doi: 10.1016/j.cscm.2019.e00228.

[17] Z. Li, Y. Jin, X. Liang, and J. Zeng, "Thermography evaluation of defect characteristics of building envelopes in urban villages in Guangzhou, China," *Case Studies in Construction Materials*, vol. 17, Dec. 2022, doi: 10.1016/j.cscm.2022.e01373.

[18] M. M. Resende, E. B. Gambare, L. A. Silva, Y. de S. Cordeiro, E. Almeida, and R. P. Salvador, "Infrared thermal imaging to inspect pathologies on façades of historical buildings: A case study on the Municipal Market of São Paulo, Brazil," *Case Studies in Construction Materials*, vol. 16, Jun. 2022, doi: 10.1016/j.cscm.2022.e01122.

[19] M. T. G. Barbosa, V. J. Rosse, and N. G. Laurindo, "Thermography evaluation strategy proposal due moisture damage on building facades," *Journal of Building Engineering*, vol. 43, no. 102555, 2021, doi: 10.1016/j.jobe.2021.102555.

[20] I. Garrido, S. Lagüela, and P. Arias, "Autonomous thermography: towards the automatic detection and classification of building pathologies," in *14th Quantitative InfraRed Thermography Conference*, Berlin, Jun. 2018. doi: 10.21611/qirt.2018.022.

[21] M. Q. Huang, J. Ninić, and Q. B. Zhang, "BIM, machine learning and computer vision techniques in underground construction: Current status and future perspectives," *Tunnelling and Underground Space Technology*, vol. 108, no. 103677, 2021, doi: 10.1016/j.tust.2020.103677.

[22] E. Valero, A. Forster, F. Bosché, E. Hyslop, L. Wilson, and A. Turmel, "Automated defect detection and classification in ashlar masonry walls using machine learning," *Autom Constr*, vol. 106, no. 102846, 2019, doi: 10.1016/j.autcon.2019.102846.

[23] I. Garrido *et al.*, "Introduction of deep learning in thermographic monitoring of cultural heritage and improvement by automatic thermogram pre-processing algorithms," *Sensors (Switzerland)*, vol. 21, no. 3, pp. 1–44, Feb. 2021, doi: 10.3390/s21030750.

[24] A. Hoła and Ł. Sadowski, "A method of the neural identification of the moisture content in brick walls of historic buildings on the basis of non-destructive tests," *Autom Constr*, vol. 106, no. 102850, 2019, doi: 10.1016/j.autcon.2019.102850.

[25] F. M. A. Henriques, *Humidade em paredes*. Lisbon, 1994.

[26] L. Kempton, G. Kokogiannakis, and P. Cooper, "Mould risk evaluations in residential buildings via site audits and longitudinal monitoring," *Build Environ*, vol. 191, no. 107584, 2021, doi: 10.1016/j.buildenv.2020.107584.

[27] F. R. d'Ambrosio Alfano, B. I. Palella, and G. Riccio, "Moisture in historical buildings from causes to the application of specific diagnostic methodologies," *J Cult Herit*, vol. 61, pp. 150–159, May 2023, doi: 10.1016/j.culher.2023.04.001.

[28] E. Franzoni, S. Bandini, and G. Graziani, "Rising moisture, salts and electrokinetic effects in ancient masonries: From laboratory testing to on-site monitoring," *J Cult Herit*, vol. 15, no. 2, pp. 112–120, 2014, doi: 10.1016/j.culher.2013.03.003.

[29] L. Greenspan, "Humidity fixed points of binary saturated aqueous solutions," *J Res Natl Bur Stand Sect A Phys Chem*, vol. 81 A, no. 1, pp. 89–96, 1977, doi: 10.6028/jres.081A.011.

[30] R. J. Flatt *et al.*, "Predicting salt damage in practice: a theoretical insight into laboratory tests," *RILEM Technical Letters*, vol. 2, pp. 108–118, 2017, doi: 10.21809/rilemtechlett.2017.41.

[31] K. Tuutti, "Corrosion of steel in concrete," Doctoral Thesis, Swedish Cement and Concrete Research Institute, Stockholm, 1982.

[32] A. Afshari, E. De, O. Fernandes, M.-R. Hirvonen, and S. Kirchner, "WHO guidelines for indoor air quality: dampness and mould CIRCE-SIGFRIED View project Working Group on Sustainable Construction Methods & Techniques View project," 2009. [Online]. Available: www.euro.who.int

[33] E. Rosina, "When and how reducing moisture content for the conservation of historic building. A problem solving view or monitoring approach?," *J Cult Herit*, vol. 31, pp. S82–S88, 2018, doi: 10.1016/j.culher.2018.03.023.

[34] A. Brás, A. Valença, and P. Faria, "Performance-based methods for masonry building rehabilitation using innovative leaching and hygrothermal risk analyses," *Sustain Cities Soc*, vol. 28, pp. 321–331, 2017, doi: 10.1016/j.scs.2016.09.010.

[35] E. Valero, F. Bosché, and A. Forster, "Automatic segmentation of 3D point clouds of rubble masonry walls, and its application to building surveying, repair and maintenance," *Autom Constr*, vol. 96, pp. 29–39, 2018, doi: 10.1016/j.autcon.2018.08.018.

[36] B. Abraham, J.-L. Salagnac, J. Fontan, D. Quenard, S. Gilliot, and C. Pompéo, "Guide Technique - Transferts d'humidité à travers les parois Évaluer les risques de condensation," Sep. 2009.

[37] C.-E. Hagentoft, *Introduction to building physics*. Lund, Sweden: Studentlitteratur, 2001.

[38] J. M. P. Q. Delgado ed., *Drying and Wetting of Building Materials and Components Drying and Wetting of Building Materials and Components*, vol. 4. 2014. [Online]. Available: http://link.springer.com/10.1007/978-3-319-04531-3

[39] V. P. de Freitas, A. S. Guimarães, and M. I. Torres, *Humidade Ascensional*, 1st ed. Porto: FEUP, 2008.

[40] H. M. Künzel, "Simultaneous heat and moisture transport in building components : one- and two-dimensional calculation using simple parameters," Fraunhofer Institute of Building Physics, 1995.

[41] J. Straube, "Moisture in buildings," *ASHRAE J*, vol. 44, no. 1, pp. 15–19, 2002, [Online]. Available: https://www.researchgate.net/publication/271706272

[42] ISO 13788, *Hygrothermal performance of building components and building elements-Internal surface temperature to avoid critical surface humidity and interstitial condensation-Calculation methods*. 2014.

[43] J. De Brito, "Humidade ascendente em paredes térreas de edifícios," Jan. 2003. doi: 10.13140/RG.2.1.4016.6884.

[44] C. Morón, D. Ferrández, P. Saiz, and E. Yedra, "Measuring system of capillary rising damp in cement mortars," *Measurement (Lond)*, vol. 135, pp. 252–259, 2019, doi: 10.1016/j.measurement.2018.11.071.

[45] G. Mason, "Rising damp," *Building Science*, vol. 9, no. 3, pp. 227–231, 1974, doi: 10.1016/0007-3628(74)90021-8.

[46] C. Hall and W. D. Hoff, "Rising damp: Capillary rise dynamics in walls," *Proceedings of the Royal Society A: Mathematical, Physical and Engineering Sciences*, vol. 463, no. 2084, pp. 1871–1884, 2007, doi: 10.1098/rspa.2007.1855.

[47] V. P. Freitas *et al.*, *Heat, Air and Moisture Transfer Terminology - Parameters and Concepts*, CIB, FEUP, LFC. FEUP edições, 2012.

[48] ISO 9346, *Hygrothermal performance of buildings and building materials-Physical quantities for mass transfer-Vocabulary*. 2007.

[49] ISO 15148, *Hygrothermal performance of building materials and products - Determination of water absorption coefficient by partial immersion*. 2002, pp. 1–19.

[50] A. S. Guimarães, I. M. Ribeiro, and V. P. de Freitas, "Numerical models performance to predict drying liquid water in porous building materials: Comparison of experimental and simulated drying water content profiles," *Cogent Eng*, vol. 4, no. 1, pp. 1–17, 2017, doi: 10.1080/23311916.2017.1365572.

[51] E. Grinzato, G. Cadelano, and P. Bison, "Moisture map by IR thermography," *J Mod Opt*, vol. 57, no. 18, pp. 1770–1778, 2010, doi: 10.1080/09500341003731597.

[52] J. F. Straube, "Moisture Control and Enclosure Wall Systems," PhD Thesis, University of Waterloo, Waterloo, Ontario, 1998.

[53] S. L. C. H. Hens, *Building Physics - Heat, Air and Moisture 3e Fundamentals and Engineering Methods with Examples and Exercises*. Berlin, Germany: Wilhelm Ernst & Sohn, 2017. doi: 10.1002/9783433608548.

[54] J. M. P. Q. Delgado, E. Barreira, N. M. M. Ramos, and V. P. Freitas, *Hygrothermal Numerical Simulation Tools Applied to Building Physics*. Springer, 2013.

[55] E. S. B. M. Barreira, "Aplicação da Termografia ao Estudo do Comportamento Higrotérmico dos Edifícios," Master Dissertation, Faculdade de Engenharia da Universidade do Porto, Porto, 2004.

[56] T. Busser, M. Pailha, A. Piot, and M. Woloszyn, "Simultaneous hygrothermal performance assessment of an air volume and surrounding highly hygroscopic walls," *Build Environ*, vol. 148, pp. 677–688, Jan. 2019, doi: 10.1016/j.buildenv.2018.11.031.

[57] A. Hola, "Measuring of the moisture content in brick walls of historical buildings-the overview of methods," *IOP Conf Ser Mater Sci Eng*, vol. 251, no. 1, 2017, doi: 10.1088/1757-899X/251/1/012067.

[58] J. Hoła, Z. Matkowski, K. Schabowicz, J. Sikora, K. Nita, and S. Wójtowicz, "Identification of moisture content in brick walls by means of impedance tomography," *COMPEL - The International Journal for Computation and Mathematics in Electrical and Electronic Engineering*, vol. 31, no. 6, pp. 1774–1792, 2012, doi: 10.1108/03321641211267119.

[59] P. Bison *et al.*, "Limits and advantages of different techniques for testing moisture content in masonry," *Mater Eval*, vol. 69, no. 1, pp. 111–116, 2011.

[60] C. Hübner and U. Kaatze, *Electromagnetic moisture measurement*. 2017. doi: 10.17875/gup2016-958.

[61] M. G. Luiz and E. Superior, "Medição da umidade no sistema concreto-madeira," Master dissertation, Universidade de São Paulo, Piracicaba, 2005.

[62] J. M. Costa, S. S. Azzi, E. G. de Campos, F. M. de Araújo, and E. B. D. Lage, "Análise patológica através do ensaio não destrutivo utilizando resistividade elétrica superficial do concreto," *Revista Construindo*, vol. 9, pp. 25–35, 2017.

[63] H. Carasek, F. H. Vaz, and O. Cascudo, "Statistical analysis of test methods to evaluate rendering surface properties," *Ambiente Construído*, vol. 18, no. 2, pp. 87–105, 2018, doi: 10.1590/s1678-86212018000200244.

[64] M. C. de F. Salomão, "Estudo da umidade ascendente em painéis de alvenaria de blocos cerâmicos," Master dissertation, Universidade Federal de Uberlândia, Uberlândia, 2012.

[65] William G. Foulks, *Historic Building Façades: The Manual for Maintenance and Rehabilitation*. New York: Wiley, 1997.

[66] E. Bauer and E. Pavon, "Termografia de infravermelho na identificação e avaliação de manifestações patológivas em edifícios," 2015.

[67] A. Marynowicz and A. Kucharczyk, "Determination of the water absorption and water diffusion coefficients by means of infrared thermography measurements," *Measurement (Lond)*, vol. 185, Nov. 2021, doi: 10.1016/j.measurement.2021.110054.

[68] E. C. Cortizo, "Avaliação da Técnica de Termografia Infravermelha para Identificação de Estruturas Ocultas e Diagnóstico de Anomalias em Edificações: Ênfase em Edificações do Patrimônio Histórico," Master dissertation, Universidade Federal de Minas Gerais, Belo Horizonte, 2007.

[69] X. Maldague, "Applications of Infrared Thermography in Nondestructive Evaluation," Quebec.

[70] NEC San-ei Instruments, "Thermo Tracer TH9100PMVI / PWVI PMV / PWV / ML / WL Operation Manual."

[71] ASTM E1862, *Standard Test Methods for Measuring and Compensating for Reflected Temperature Using Infrared Imaging Radiometers*. 1998, pp. 1–3. doi: 10.1520/E1862-97R10.2.

[72] EN 18187, *Thermal performance of buildings - Qualitative detection of thermal irregularities in building envelopes - Infrared method*. 1998, pp. 1–18.

[73] ISO 6781, *Thermal insulation - Qualitative detection of thermal irregularities in building envelopes - Infrared method*. 1983, pp. 1–16.

[74] E. Grinzato, P. G. Bison, and S. Marinetti, "Monitoring of ancient buildings by the thermal method," *J Cult Herit*, vol. 3, no. 1, pp. 21–29, 2002, doi: 10.1016/S1296-2074(02)01159-7.

[75] P. I. Theodorakeas, "Quantitative Analysis and Defect Assessment Using Infrared Thermographic Approaches," PhD Thesis, National Technical University of Athens, Athens, 2013.

[76] Elton. Bauer, E. K. Castro, E. Pavon, and A. H. S. Oliveira, "Criteria for application and identification of anomalies on the facades of buildings with the use of passive infrared thermography," *1st Internacional symposium on building pathology*, pp. 163–172, 2015.

[77] R. Montanini, "Quantitative determination of subsurface defects in a reference specimen made of Plexiglas by means of lock-in and pulse phase infrared thermography," *Infrared Phys Technol*, vol. 53, no. 5, pp. 363–371, 2010, doi: 10.1016/j.infrared.2010.07.002.

[78] P. Noszczyk and H. Nowak, "Inverse contrast in non-destructive materials research by using active thermography," *Materials*, vol. 12, no. 5, 2019, doi: 10.3390/MA12050835.

[79] E. Grinzato, V. Vavilov, and T. Kauppinen, "Quantitative infrared thermography in buildings," *Energy Build*, vol. 29, no. 1, pp. 1–9, 1998, doi: 10.1016/s0378-7788(97)00039-x.

[80] N. N. Kulkarni, K. Raisi, N. A. Valente, J. Benoit, T. Yu, and A. Sabato, "Deep learning augmented infrared thermography for unmanned aerial vehicles structural health monitoring of roadways," *Autom Constr*, vol. 148, 2023, doi: 10.1016/j.autcon.2023.104784.

[81] S. S. De Freitas, V. P. De Freitas, and E. Barreira, "Detection of façade plaster detachments using infrared thermography - A nondestructive technique," *Constr Build Mater*, vol. 70, pp. 80–87, 2014, doi: 10.1016/j.conbuildmat.2014.07.094.

[82] M. C. Israel, "Ensaios não destrutivos aplicados à avaliação de revestimentos de argamassa," Master dissertation, Universidade de São Paulo, São Paulo, 2016.

[83] E. Bauer, V. P. de Freitas, N. Mustelier, E. Barreira, and S. S. de Freitas, "Infrared thermography – evaluation of the results reproducibility," *Structural Survey*, vol. 33, no. 1, pp. 20–35, 2015, doi: 10.1108/SS-05-2014-0021.

[84] G. Washer, N. Bolleni, and R. Fenwick, "Thermographic imaging of subsurface deterioration in concrete bridges," *Transp Res Rec*, no. 2201, pp. 27–33, 2010, doi: 10.3141/2201-04.

[85] B. Milovanović and I. B. Pečur, "Review of active IR thermography for detection and characterization of defects in reinforced concrete," *J Imaging*, vol. 2, no. 2, pp. 1–27, 2016, doi: 10.3390/jimaging2020011.

[86] G. Washer, R. Fenwick, N. Bolleni, and J. Harper, "Effects of environmental variables on infrared imaging of subsurface features of concrete bridges," *Transp Res Rec*, no. 2108, pp. 107–114, 2009, doi: 10.3141/2108-12.

[87] O. Büyüköztürk, "Imaging of concrete structures," *NDT and E International*, vol. 31, no. 4, pp. 233–243, 1998, doi: 10.1016/S0963-8695(98)00012-7.

[88] J. R. R. Garcia, "Potencialidades da Termografia para o Diagnóstico de Patologias em Edifícios," Master thesis, Faculdade de Engenharia da Universidade do Porto, Porto, 2014.

[89] C. Lerma, E. Barreira, and R. M. S. F. Almeida, "A discussion concerning active infrared thermography in the evaluation of buildings air infiltration," *Energy Build*, vol. 168, pp. 56–66, 2018, doi: 10.1016/j.enbuild.2018.02.050.

[90] J. G. de Freitas, H. Carasek, and O. Cascudo, "Utilização de termografia infravermelha para avaliação de fissuras em fachadas com revestimento de argamassa e pintura," *Ambiente Construído*, vol. 14, no. 1, pp. 57–73, 2014, doi: 10.1590/s1678-86212014000100006.

[91] E. Bauer, "Inspeção termográfica de fachadas - Influência da fissuração," in *Anais do Congresso Brasileiro de Patologia das Construções*, Apr. 2016.

[92] J. M. Moresco, F. Bordin, M. Roberto Veronez, and B. Fonseca Tutikian, "Detecção de manifestações patológicas em fachadas com revestimento argamassado por termografia infravermelha," in *Anais XVII Simpósio Brasileiro de Sensoriamento Remoto - SBSR*, João Pessoa - PB, Apr. 2015, pp. 1–8.

[93] N. Gucunski *et al.*, *Nondestructive Testing to Identify Concrete Bridge Deck Deterioration*. Washington D. C.: Transportation Research Board, 2012. doi: 10.17226/22771.

[94] L. V. Mendonça, "Artigo Termografia por Infravermelhos," *Engenharia & Vida*, vol. 16, pp. 53–57, 2005.

[95] S. S. Behbahani, A. J. Golrokh, A. Hafiz, H. Wiggenhauser, and K. Tabrizi, "Utilizing infrared thermography for the condition assessment of tunnel Lining with tiled surface in various temperature conditions," *Tunnelling and Underground Space Technology*, vol. 154, Dec. 2024, doi: 10.1016/j.tust.2024.106093.

[96] F. Tardy, "A review of the use of infrared thermography in building envelope thermal property characterization studies," Sep. 15, 2023, *Elsevier Ltd*. doi: 10.1016/j.jobe.2023.106918.

[97] G. Dall'O', L. Sarto, and A. Panza, "Infrared screening of residential buildings for energy audit purposes: Results of a field test," *Energies (Basel)*, vol. 6, no. 8, pp. 3859–3878, 2013, doi: 10.3390/en6083859.

[98] D. Sadhukhan *et al.*, "Estimating surface temperature from thermal imagery of buildings for accurate thermal transmittance (U-value): A machine learning perspective," *Journal of Building Engineering*, vol. 32, no. 101637, p. 101637, 2020, doi: 10.1016/j.jobe.2020.101637.

[99] B. Tejedor, E. Barreira, R. M. S. F. Almeida, and M. Casals, "Automated data-processing technique: 2D Map for identifying the distribution of the U-value in building elements by quantitative internal thermography," *Autom Constr*, vol. 122, no. 103478, p. 103478, 2021, doi: 10.1016/j.autcon.2020.103478.

[100] T. S. Jing, M. A. Othuman Mydina, and N. Utaberta, "Appraisal of moisture problem of inheritance building envelope assemblies via visible and infrared thermography methods," *J Teknol*, vol. 75, no. 5, pp. 1–6, 2015, doi: 10.11113/jt.v75.4951.

[101] C. Thomachot-Schneider *et al.*, "Thermal response of building stones contaminated with salts," *Constr Build Mater*, vol. 226, pp. 331–344, Nov. 2019, doi: 10.1016/j.conbuildmat.2019.07.127.

[102] E. Edis, I. Flores-Colen, and J. de Brito, "Quasi-quantitative infrared thermographic detection of moisture variation in facades with adhered ceramic cladding using principal component analysis," *Build Environ*, vol. 94, no. P1, pp. 97–108, 2015, doi: 10.1016/j.buildenv.2015.07.027.

[103] N. P. Avdelidis, A. Moropoulou, and P. Theoulakis, "Detection of water deposits and movement in porous materials by infrared imaging," *Infrared Phys Technol*, vol. 44, no. 3, pp. 183–190, 2003, doi: 10.1016/S1350-4495(02)00212-8.

[104] E. Barreira, R. M. S. F. Almeida, and J. P. B. Ferreira, "Assessing the humidification process of lightweight concrete specimens through infrared thermography," *Energy Procedia*, vol. 132, pp. 213–218, 2017, doi: 10.1016/j.egypro.2017.09.757.

[105] N. Almutawa and W. Eid, "Soil moisture content estimation using active infrared thermography technique: An exploratory laboratory study," *Kuwait Journal of Science*, vol. 50, no. 3, pp. 399–404, Jul. 2023, doi: 10.1016/j.kjs.2022.11.001.

[106] E. Barreira and R. M. S. F. Almeida, "Drying evaluation using infrared thermography," *Energy Procedia*, vol. 78, pp. 170–175, 2015, doi: 10.1016/j.egypro.2015.11.135.

[107] E. Rosina, M. Kavuru, and E. I. Parisi, "Advancement of infrared thermography for built heritage," in *Diagnosis of Heritage Buildings by Non-Destructive Techniques*, Elsevier, 2024, pp. 23–47. doi: 10.1016/b978-0-443-16001-1.00002-4.

[108] J. H. A. Rocha, C. F. Santos, and Y. V. Póvoas, "Evaluation of the infrared thermography technique for capillarity moisture detection in buildings," in *Procedia Structural Integrity*, Elsevier B.V., 2018, pp. 107–113. doi: 10.1016/j.prostr.2018.11.015.

[109] James-A. Goulet, "Probabilistic Machine Learning for Civil Engineers," 2020.

[110] A. Géron, *Hands-on Machine Learning with Scikit-Learn, Keras, and TensorFlow Concepts, Tools, and Techniques to Build Intelligent Systems*, 2nd ed. Sebastopol CA: O'Reilly, 2019.

[111] F. Chollet, *Deep Learning with Python*, Second. NY: Manning Shelter Island, 2021.

[112] K. Chen, G. Reichard, X. Xu, and A. Akanmu, "Automated crack segmentation in close-range building façade inspection images using deep learning techniques," *Journal of Building Engineering*, vol. 43, no. 102913, 2021, doi: 10.1016/j.jobe.2021.102913.

[113] G. Park, M. Lee, H. Jang, and C. Kim, "Thermal anomaly detection in walls via CNN-based segmentation," *Autom Constr*, vol. 125, May 2021, doi: 10.1016/j.autcon.2021.103627.

[114] B. Kim, N. Yuvaraj, K. R. Sri Preethaa, and R. Arun Pandian, "Surface crack detection using deep learning with shallow CNN architecture for enhanced computation," *Neural Comput Appl*, vol. 33, no. 15, pp. 9289–9305, Aug. 2021, doi: 10.1007/s00521-021-05690-8.

[115] E. Alexakis, E. T. Delegou, P. Mavrepis, A. Rifios, D. Kyriazis, and A. Moropoulou, "A novel application of deep learning approach over IRT images for the automated detection of rising damp on historical masonries," *Case Studies in Construction Materials*, vol. 20, Jul. 2024, doi: 10.1016/j.cscm.2024.e02889.

[116] P. Wang *et al.*, "An automatic building façade deterioration detection system using infrared-visible image fusion and deep learning," *Journal of Building Engineering*, vol. 95, Oct. 2024, doi: 10.1016/j.jobe.2024.110122.

[117] M. Mishra and P. B. Lourenço, "Artificial intelligence-assisted visual inspection for cultural heritage: State-of-the-art review," Mar. 01, 2024, *Elsevier Masson s.r.l.* doi: 10.1016/j.culher.2024.01.005.

[118] M. R. Islam, S. Azam, B. Shanmugam, and D. Mathur, "Leak detection and localization in underground water supply system using thermal imaging and geophone signals through machine learning," *Intelligent Systems with Applications*, vol. 23, Sep. 2024, doi: 10.1016/j.iswa.2024.200404.

[119] A. Tijskens, S. Roels, and H. Janssen, "Neural networks for metamodelling the hygrothermal behaviour of building components," *Build Environ*, vol. 162, Sep. 2019, doi: 10.1016/j.buildenv.2019.106282.

[120] G. Kłosowski, A. Hoła, T. Rymarczyk, Ł. Skowron, T. Wołowiec, and M. Kowalski, "The concept of using lstm to detect moisture in brick walls by means of electrical impedance tomography," *Energies (Basel)*, vol. 14, no. 22, Nov. 2021, doi: 10.3390/en14227617.

[121] Q. Fang, "Defect detection in infrared thermography by deep learning algorithms," PhD Thesis, Université Laval, Québec, 2021.

[122] A. W. Trask, *Grokking Deep Learning*. NY: Manning Shelter Island, 2019.

[123] Q. Zhou and R. Ooka, "Influence of data preprocessing on neural network performance for reproducing CFD simulations of non-isothermal indoor airflow distribution," *Energy Build*, vol. 230, Jan. 2021, doi: 10.1016/j.enbuild.2020.110525.

[124] A. Tijskens, H. Janssen, and S. Roels, "Optimising convolutional neural networks to predict the hygrothermal performance of building components," *Energies (Basel)*, vol. 12, no. 20, Oct. 2019, doi: 10.3390/en12203966.

[125] Y. Duan *et al.*, "Automated defect classification in infrared thermography based on a neural network," *NDT and E International*, vol. 107, Oct. 2019, doi: 10.1016/j.ndteint.2019.102147.

[126] C. Aggarwal, H. Ge, M. Defo, and M. A. Lacasse, "Hygrothermal performance assessment of wood frame walls under historical and future climates using partial least squares regression," *Build Environ*, vol. 223, Sep. 2022, doi: 10.1016/j.buildenv.2022.109501.

[127] C. Wang, X. Li, and and Hailong Li, "Role of input features in developing data-driven models for building thermal demand forecast," *Energy Build*, vol. 277, no. 112593, Dec. 2022, doi: 10.1016/j.enbuild.2022.112593.

[128] "Transfer-Learning Bridging the Gap between Real and Simulation Data for Machine Learning and Injection Molding".

[129] L. von Rueden, S. Mayer, R. Sifa, C. Bauckhage, and J. Garcke, "Combining Machine Learning and Simulation to a Hybrid Modelling Approach: Current and Future Directions," in *Lecture Notes in Computer Science (including subseries Lecture Notes in Artificial Intelligence and Lecture Notes in Bioinformatics)*, Springer, 2020, pp. 548–560. doi: 10.1007/978-3-030-44584-3_43.

[130] P. W. Tien, S. Wei, J. Darkwa, C. Wood, and J. K. Calautit, "Machine Learning and Deep Learning Methods for Enhancing Building Energy Efficiency and Indoor Environmental Quality – A Review," Nov. 01, 2022, *Elsevier B.V.* doi: 10.1016/j.egyai.2022.100198.

[131] L. Chen, C. Zhan, G. Li, and A. Zhang, "An artificial neural network identification method for thermal resistance of exterior walls of buildings based on numerical experiments," *Build Simul*, vol. 12, no. 3, pp. 425–440, Jun. 2019, doi: 10.1007/s12273-019-0524-6.

[132] B. Tejedor, E. Lucchi, D. Bienvenido-Huertas, and I. Nardi, "Non-destructive techniques (NDT) for the diagnosis of heritage buildings: Traditional procedures and futures perspectives," *Energy Build*, vol. 263, May 2022, doi: 10.1016/j.enbuild.2022.112029.

[133] X. Zhao and S. Li, "A method of crack detection based on convolutional neural networks," in *Structural Health Monitoring 2017: Real-Time Material State Awareness and Data-Driven Safety Assurance - Proceedings of the 11th International Workshop on Structural Health Monitoring, IWSHM 2017*, DEStech Publications, 2017, pp. 978–984. doi: 10.12783/shm2017/13959.

[134] R. S. Adhikari, O. Moselhi, and A. Bagchi, "Image-based retrieval of concrete crack properties for bridge inspection," *Autom Constr*, vol. 39, pp. 180–194, 2014, doi: 10.1016/j.autcon.2013.06.011.

[135] R. Ali, J. H. Chuah, M. S. A. Talip, N. Mokhtar, and M. A. Shoaib, "Structural crack detection using deep convolutional neural networks," *Autom Constr*, vol. 133, 2022, doi: 10.1016/j.autcon.2021.103989.

[136] Y. J. Cha, W. Choi, and O. Büyüköztürk, "Deep Learning-Based Crack Damage Detection Using Convolutional Neural Networks," *Computer-Aided Civil and Infrastructure Engineering*, vol. 32, no. 5, pp. 361–378, May 2017, doi: 10.1111/mice.12263.

[137] T. Dawood, Z. Zhu, and T. Zayed, "Machine vision-based model for spalling detection and quantification in subway networks," *Autom Constr*, vol. 81, pp. 149–160, Sep. 2017, doi: 10.1016/j.autcon.2017.06.008.

[138] T. Rymarczyk *et al.*, "Comparison of machine learning methods in electrical tomography for detecting moisture in building walls," *Energies (Basel)*, vol. 14, no. 10, May 2021, doi: 10.3390/en14102777.

[139] A. Hoła and Ł. Sadowski, "Non-destructive in situ Identification of the Moisture Content in Saline Brick Walls Using Artificial Neural Networks," in *Proceedings of the Creative Construction Conference*, Skibniewski M. J. and M. Hajdu, Eds., 2019, pp. 77–82. doi: 10.3311/ccc2019-012.

[140] T. Rymarczyk *et al.*, "Historical buildings dampness analysis using electrical tomography and machine learning algorithms," *Energies (Basel)*, vol. 14, no. 5, 2021, doi: 10.3390/en14051307.

[141] A. Hoła and S. Czarnecki, "Brick wall moisture evaluation in historic buildings using neural networks," *Autom Constr*, vol. 141, Sep. 2022, doi: 10.1016/j.autcon.2022.104429.

[142] A. Hoła and Ł. Sadowski, "Verification of a nondestructive method for assessing the humidity of saline brick walls in historical buildings," *Applied Sciences (Switzerland)*, vol. 10, no. 19, pp. 1–11, Oct. 2020, doi: 10.3390/app10196926.

[143] A. Goetzke-Pala, A. Hoła, and Ł. Sadowski, "A non-destructive method of the evaluation of the moisture in saline brick walls using artificial neural networks," *Archives of Civil and Mechanical Engineering*, vol. 18, no. 4, pp. 1729–1742, 2018, doi: 10.1016/j.acme.2018.07.004.

[144] M. Chammas, A. Makhoul, and J. Demerjian, "An efficient data model for energy prediction using wireless sensors," *Computers and Electrical Engineering*, vol. 76, pp. 249–257, Jun. 2019, doi: 10.1016/j.compeleceng.2019.04.002.

[145] X. Zhou, D. Derome, and J. Carmeliet, "Analysis of moisture risk in internally insulated masonry walls," *Build Environ*, vol. 212, Mar. 2022, doi: 10.1016/j.buildenv.2021.108734.

[146] A. Royuela-del-Val, M. Á. Padilla-Marcos, A. Meiss, P. Casaseca-de-la-Higuera, and J. Feijó-Muñoz, "Air infiltration monitoring using thermography and neural networks," *Energy Build*, vol. 191, pp. 187–199, May 2019, doi: 10.1016/j.enbuild.2019.03.019.

[147] T. Rymarczyk *et al.*, "Historical buildings dampness analysis using electrical tomography and machine learning algorithms," *Energies (Basel)*, vol. 14, no. 5, Mar. 2021, doi: 10.3390/en14051307.

[148] I. Garrido, S. Lagüela, S. Sfarra, F. J. Madruga, and P. Arias, "Automatic detection of moistures in different construction materials from thermographic images," *J Therm Anal Calorim*, vol. 138, no. 2, pp. 1649–1668, Oct. 2019, doi: 10.1007/s10973-019-08264-y.

[149] I. G. Garrido, "Automation of the Thermographic inspection: Development of thermo-geometric algorithms for detection of pathologies supported by machine learning strategies," PhD Thesis, Universidade Vigo, Vigo, 2021.

[150] A. Goetzke-Pala, A. Hoła, and Ł. Sadowski, "A non-destructive method of the evaluation of the moisture in saline brick walls using artificial neural networks," *Archives of Civil and Mechanical Engineering*, vol. 18, no. 4, pp. 1729–1742, Sep. 2018, doi: 10.1016/j.acme.2018.07.004.

[151] A. Hoła and Ł. Sadowski, "A method of the neural identification of the moisture content in brick walls of historic buildings on the basis of non-destructive tests," *Autom Constr*, vol. 106, Oct. 2019, doi: 10.1016/j.autcon.2019.102850.

[152] Amphenol Corporation, "Protimeter MMS2 Instruction Manual," no. June, 2014, [Online]. Available: https://www.amphenol-sensors.com/microsites/protimeter/MMS2

[153] Devices & Services Company, "AE1 Model - Operating Instructions," Dallas, Tx, USA.

[154] ASTM C1371, "Standard Test Method for Determination of Emittance of Materials Near Room Temperature Using Portable Emissometers," *ASTM International*, vol. 04, no. Reapproved 2010, pp. 1–8, 2004, doi: 10.1520/C1371-04AR10E01.2.

[155] J.-P. Ollivier and A. Vichot, *Durabilidade do Concreto*, 1st ed., vol. 1. São Paulo, 2014.

[156] L. C. M. Dafico, E. Barreira, R. M. S. F. Almeida, and H. Carasek, "Comparison of Infrared Thermography and Other Traditional Techniques to Assess Moisture Content of Wall Specimens," *Sensors*, vol. 22, no. 9, May 2022, doi: 10.3390/s22093182.

[157] L. C. M. Dafico, E. Barreira, R. M. S. F. Almeida, and R. Vicente, "Machine learning models applied to moisture assessment in building materials," *Constr Build Mater*, vol. 405, Nov. 2023, doi: 10.1016/j.conbuildmat.2023.133330.

[158] "Emissivity of Building Materials for Infrared Measurements _ Enhanced Reader."

[159] ISO 12572, "Hygrothermal performance of building materials and products - Determination of water vapour transmission properties - Cup method".

[160] A. Augusto and C. De Azevêdo, "INTERFACE INFLUENCE ON MOISTURE TRANSPORT IN BUILDING COMPONENTS," 2019. [Online]. Available: http://www.fe.up.pt

[161] ISO 12571, *Hygrothermal performance of building materials and products-Determination of hygroscopic sorption properties*. 2021. [Online]. Available: www.iso.org

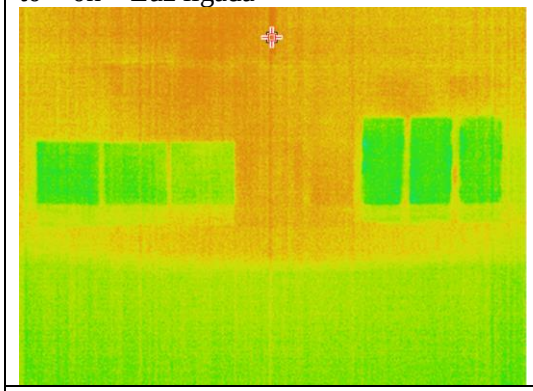
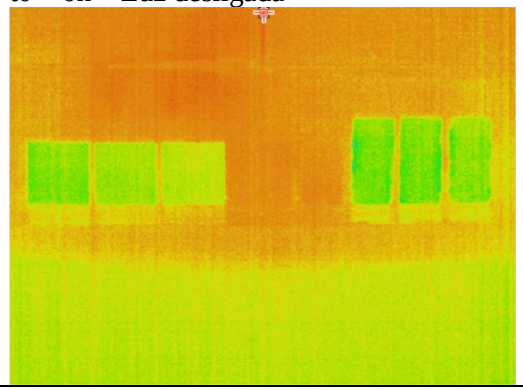
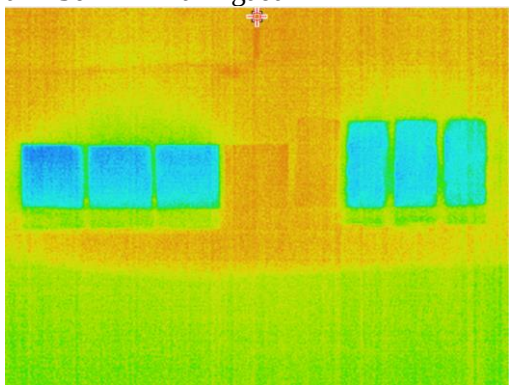
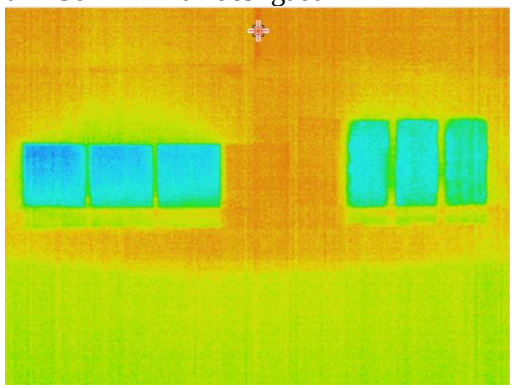
[162] ISOMET 2114, *Thermal properties analyzer User's Guide*. [Online]. Available: www.Manuals-lib.com

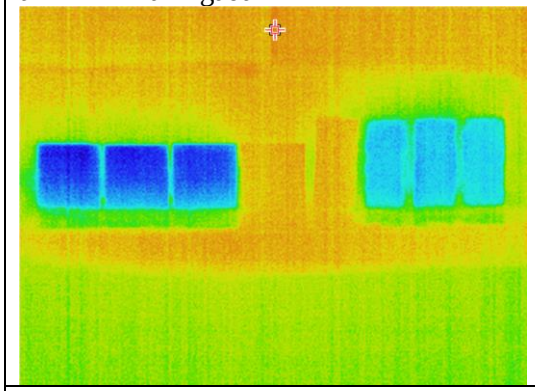
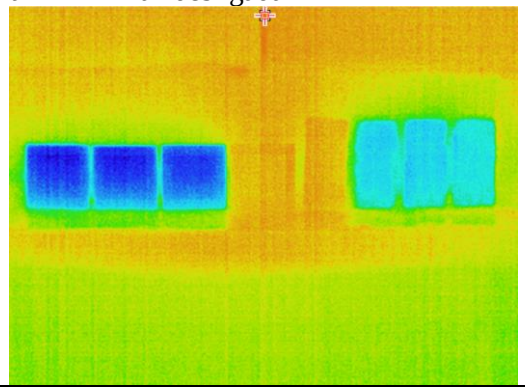
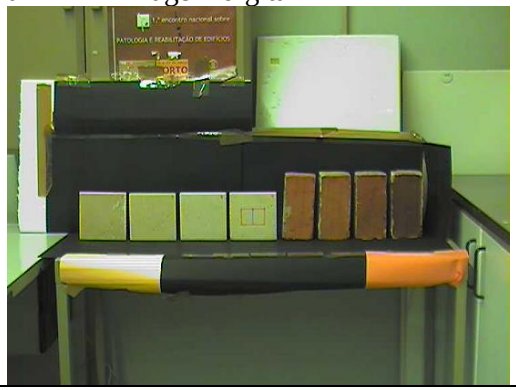
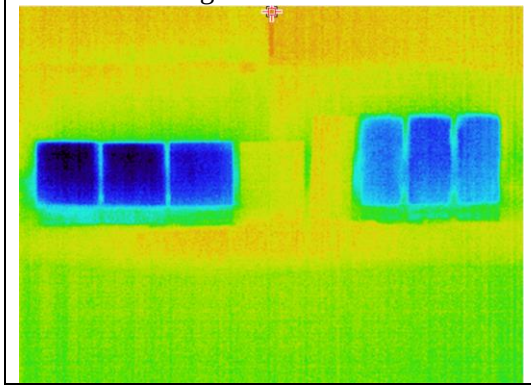
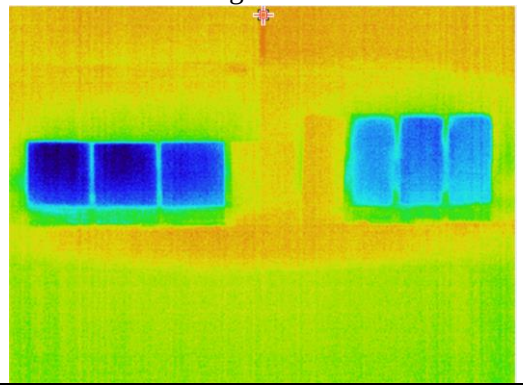
[163] M. T. Pereira, "Avaliação da transferência de calor em fenómenos de humidificação através da simulação higrotérmica 2D," Master dissertation, Faculdade de Engenharia da Universidade do Porto, Porto, 2018.

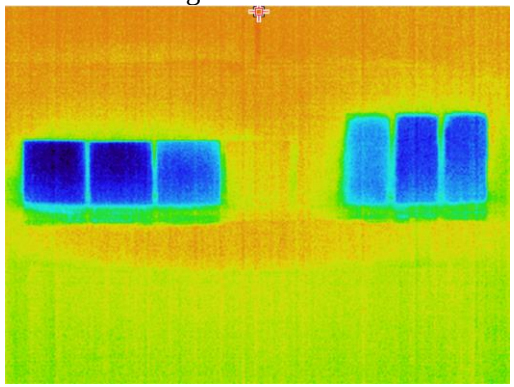
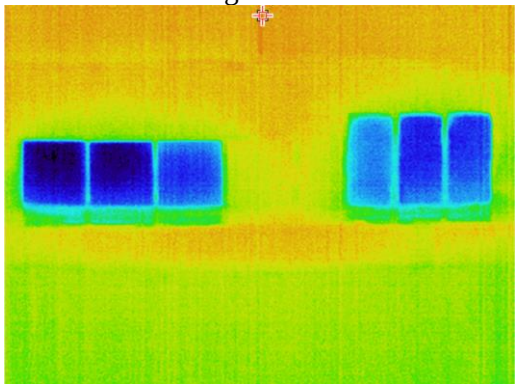
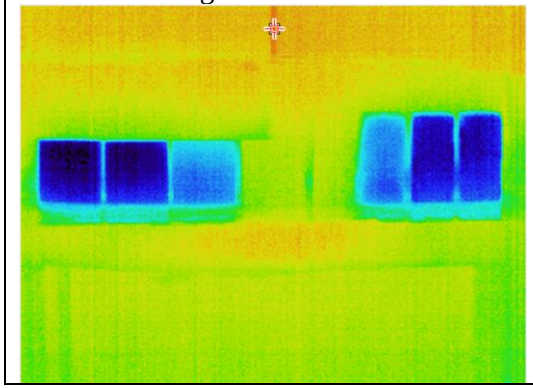
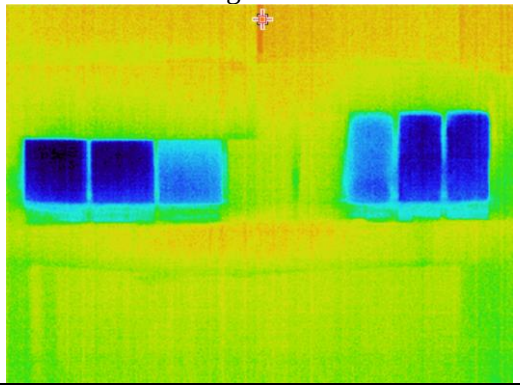
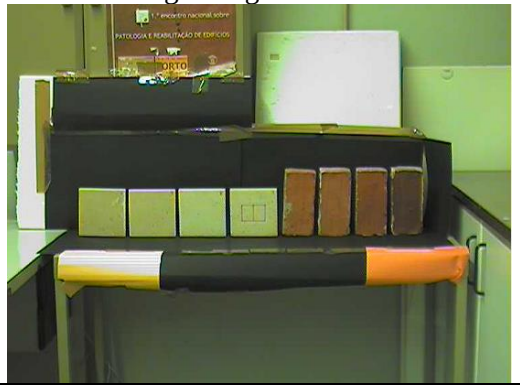
[164] EN 12524, *Building materials and products - Hygrothermal properties - Tabulated design values*. 2000, pp. 1–12.

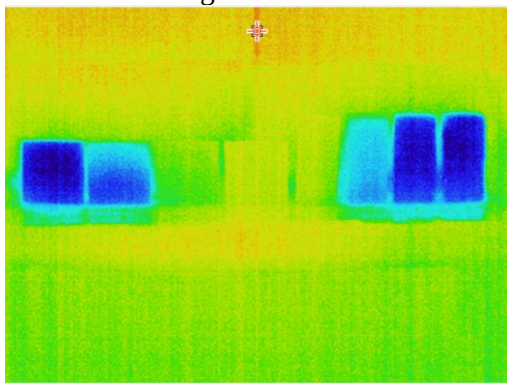
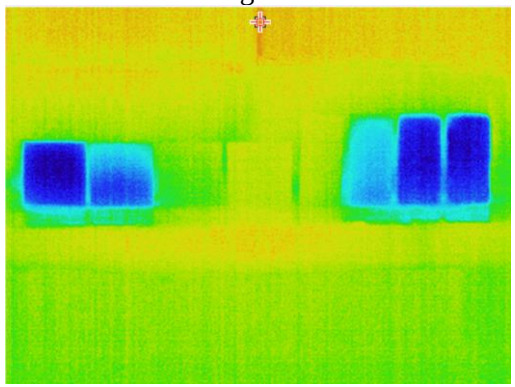
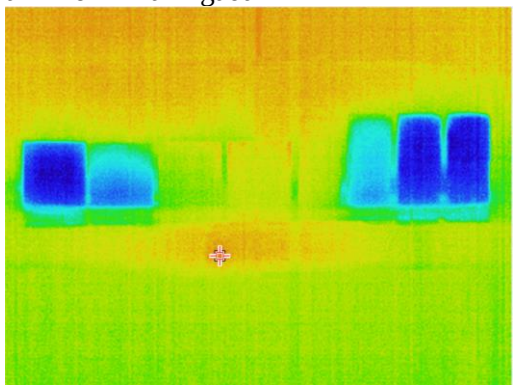
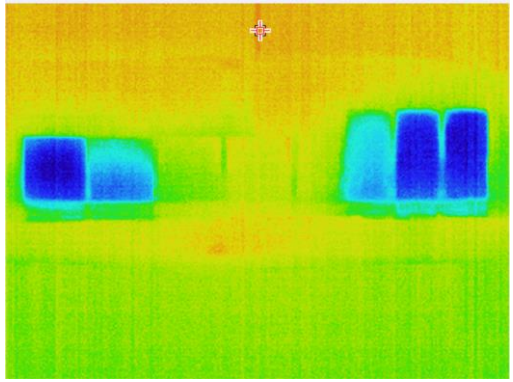
APPENDIX 1 (a)

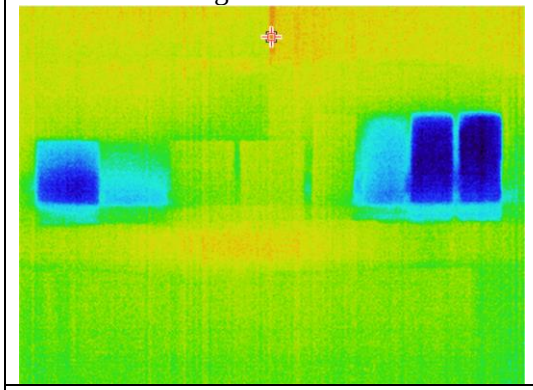
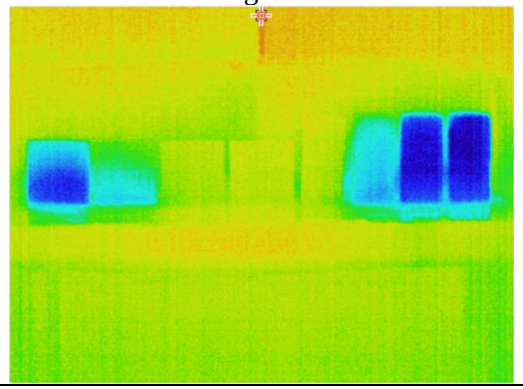
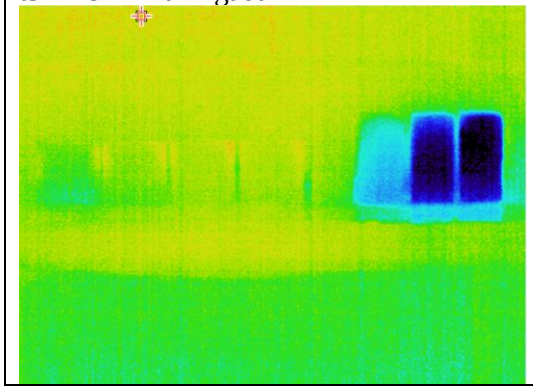
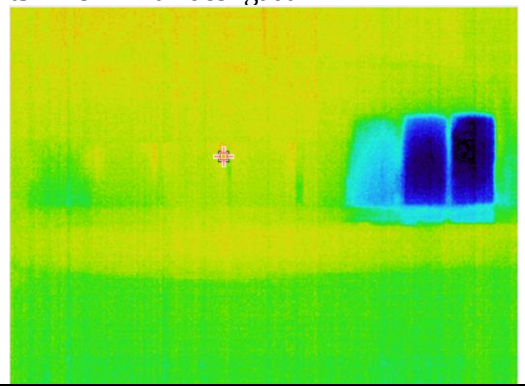
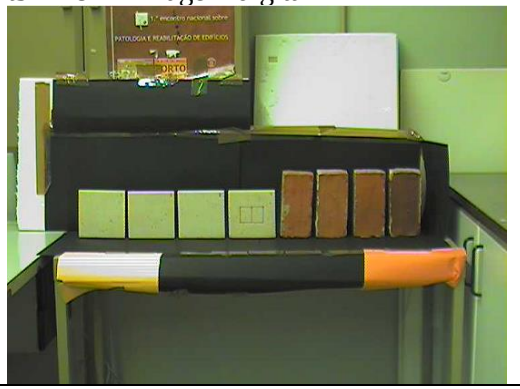
APPENDIX 1

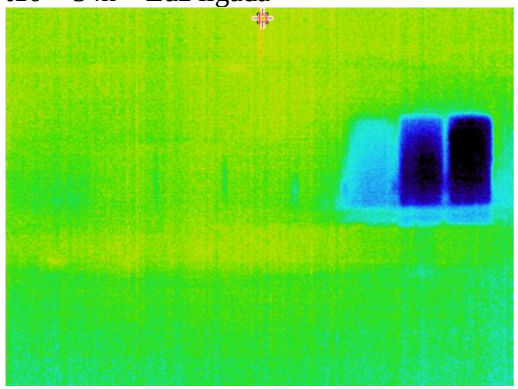
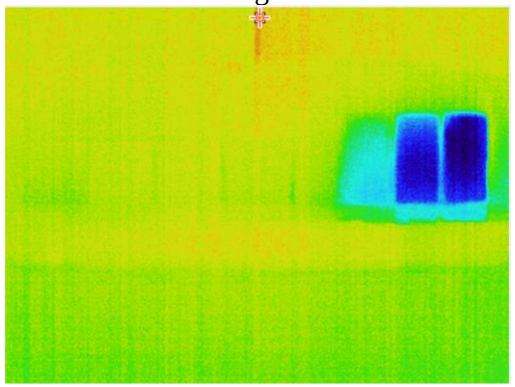
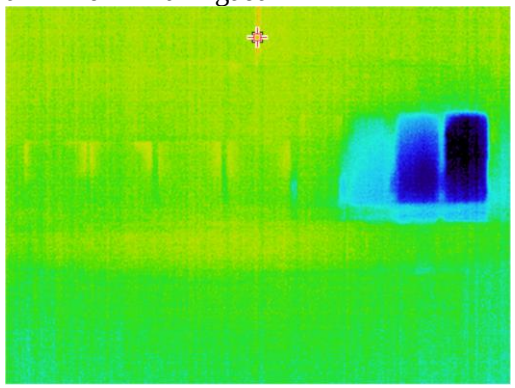
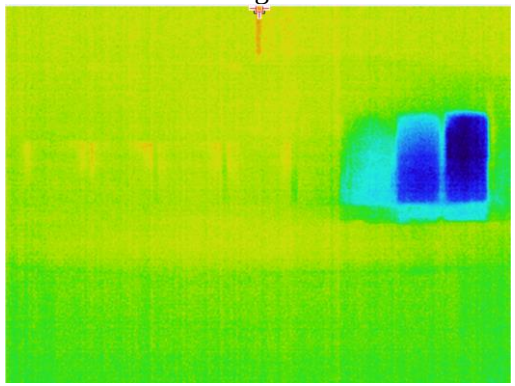
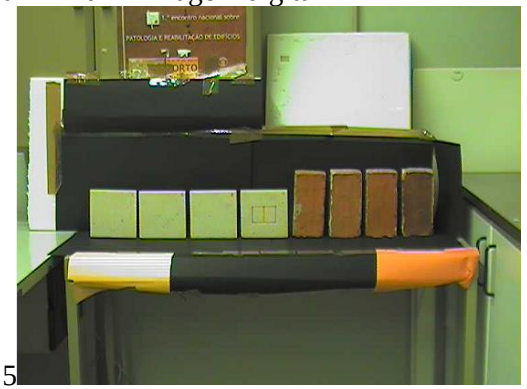
t0 – 0h – Luz ligada 	t0 – 0h – Luz desligada 	t0 – 0h – Imagem digital 
t1 – 30min – Luz ligada 	t1 – 30min – Luz desligada 	t1 – 30min – Imagem digital 

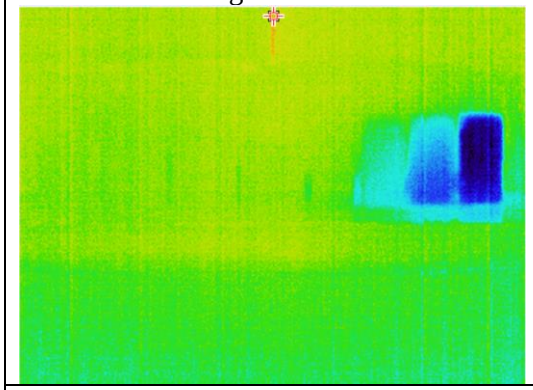
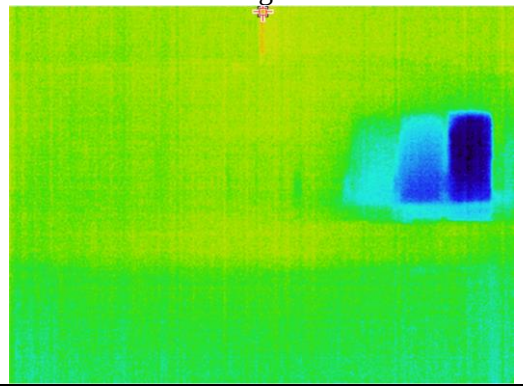
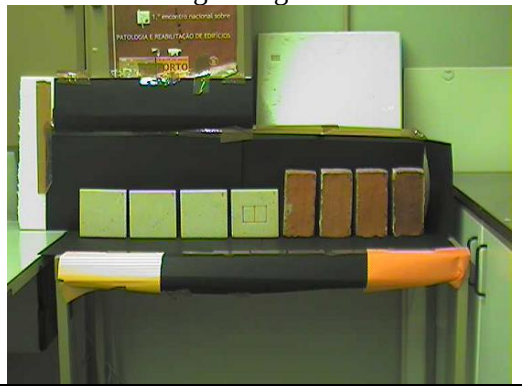
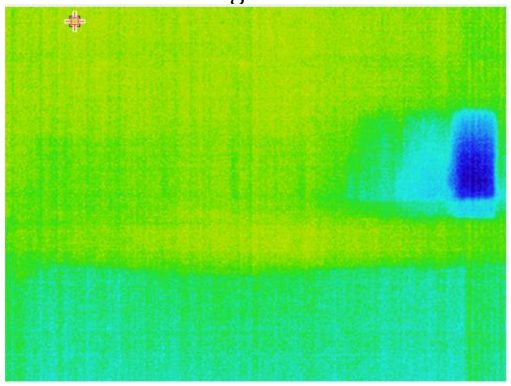
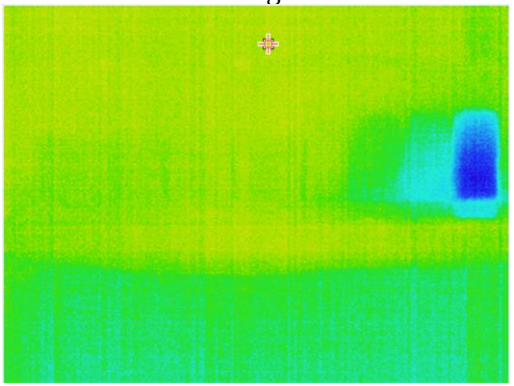
t2 – 1h – Luz ligada 	t2 – 1h – Luz desligada 	t2 – 1h – Imagem digital 
t3 – 2h – Luz ligada 	t3 – 2h – Luz desligada 	t3 – 2h – Imagem digital 

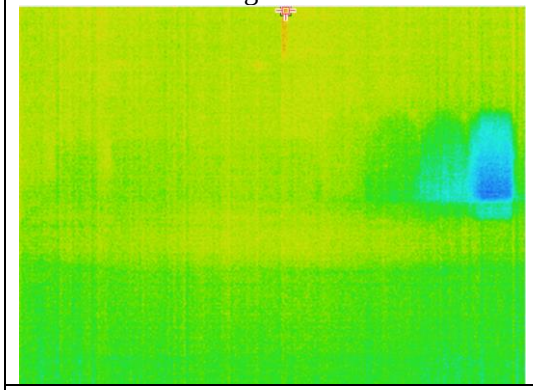
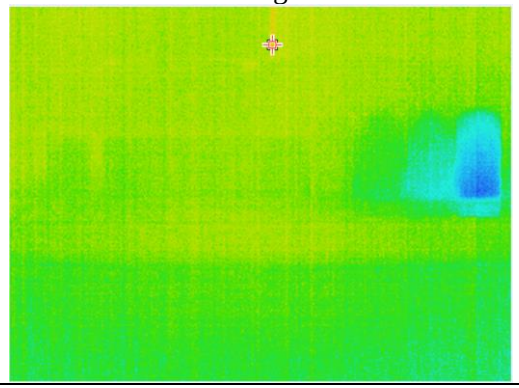
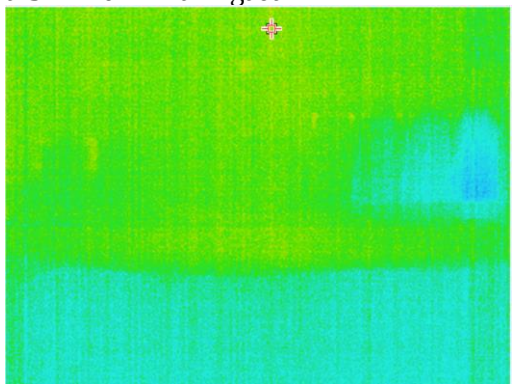
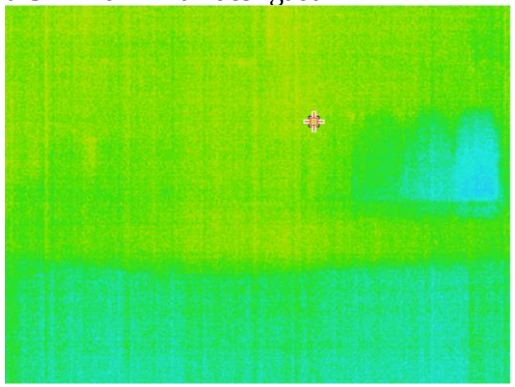
t4 – 4h – Luz ligada 	t4 – 4h – Luz desligada 	t4 – 4h – Imagem digital 
t5 – 8h – Luz ligada 	t5 – 8h – Luz desligada 	t5 – 8h – Imagem digital 

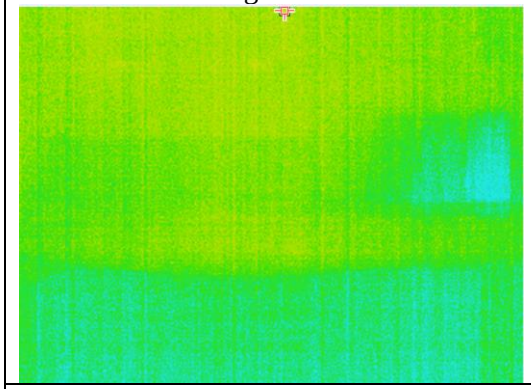
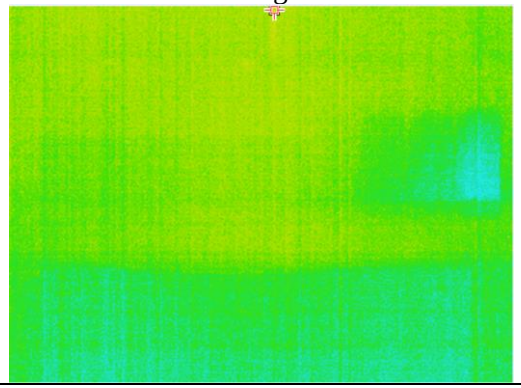
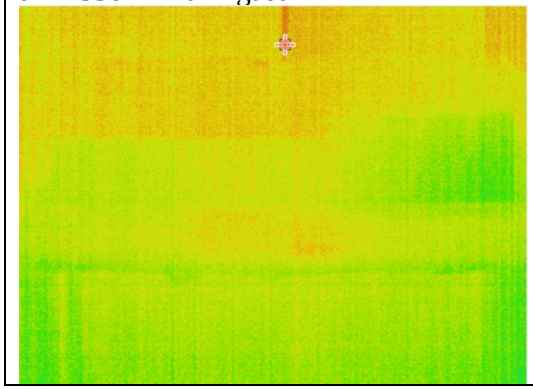
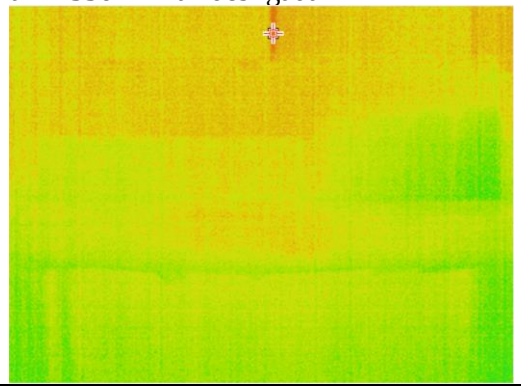
t6 – 24h – Luz ligada 	t6 – 24h – Luz desligada 	t6 – 24h – Imagem digital 
t7 – 26h – Luz ligada 	t7 – 26h – Luz desligada 	t7 – 26h – Imagem digital 

t8 – 32h – Luz ligada 	t8 – 32h – Luz desligada 	t8 – 32h – Imagem digital 
t9 – 48h – Luz ligada 	t9 – 48h – Luz desligada 	t9 – 48h – Imagem digital 

t10 – 54h – Luz ligada 	t10 – 54h – Luz desligada 	t10 – 54h – Imagem digital 
t11 – 70h – Luz ligada 	t11 – 70h – Luz desligada 	t11 – 70h – Imagem digital 

t12 – 96h – Luz ligada 	t12 – 96h – Luz desligada 	t12 – 96h – Imagem digital 
t13 – 168h – Luz ligada 	t13 – 168h – Luz desligada 	t13 – 168h – Imagem digital 

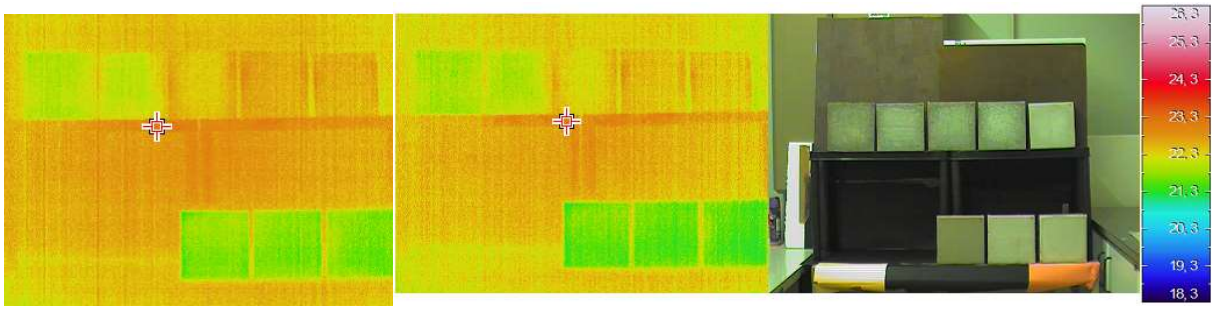
t14 – 198h – Luz ligada 	t14 – 198h – Luz desligada 	t14 – 198h – Imagem digital 
t15 – 240h – Luz ligada 	t15 – 240h – Luz desligada 	t15 – 240h – Imagem digital 

t16 – 264h – Luz ligada	t16 – 264h – Luz desligada	t16 – 264h – Imagem digital
		
t17– 336h – Luz ligada	t17– 336h – Luz desligada	t17– 336h – Imagem digital
		

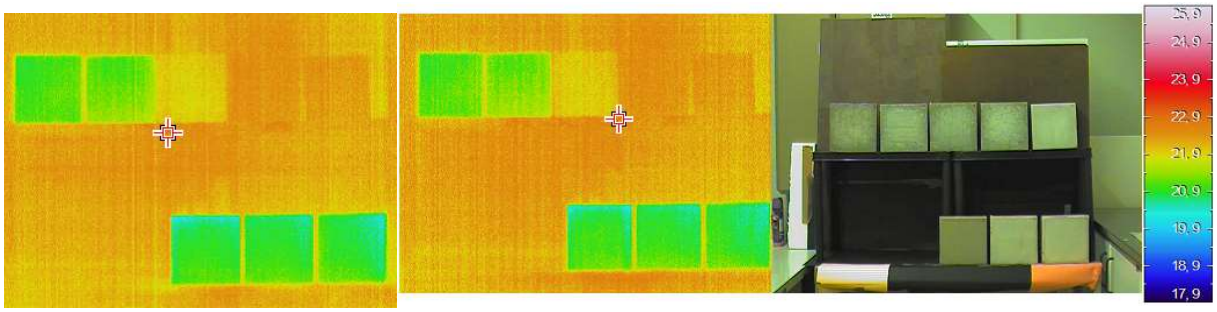
APPENDIX 1 (b)

APPENDIX 1B

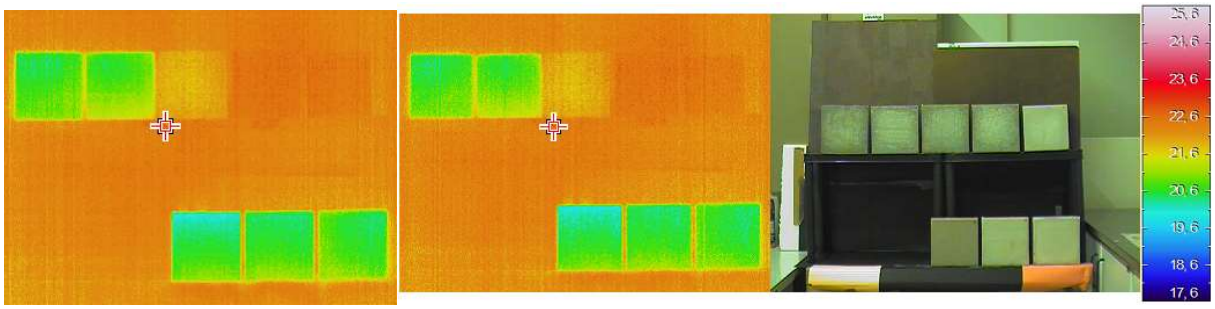
t0 – 0h



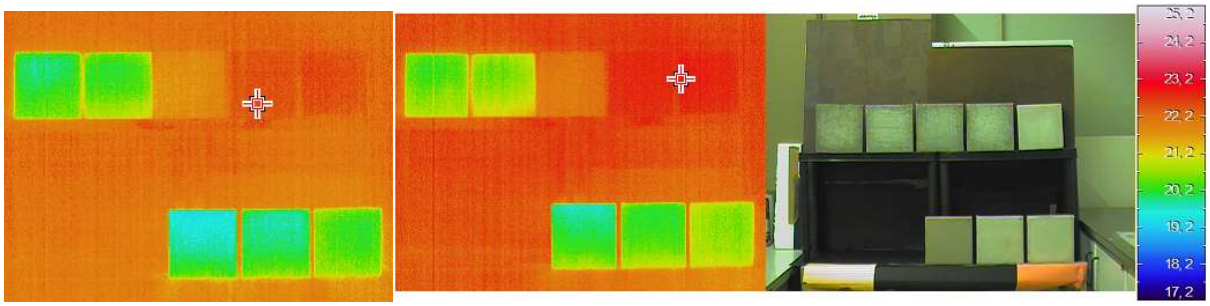
t1 – 0.5h



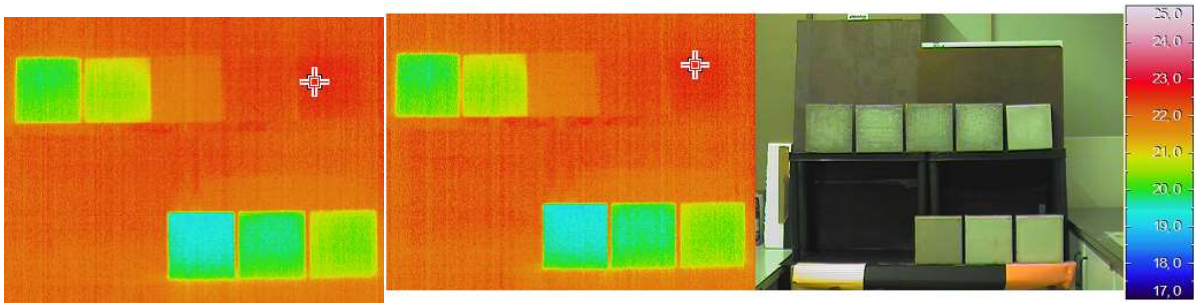
t2 – 1h



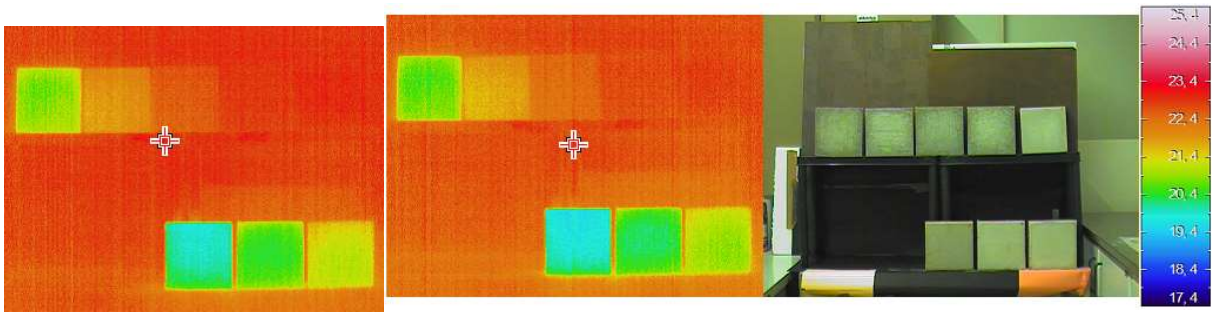
t3 – 2h



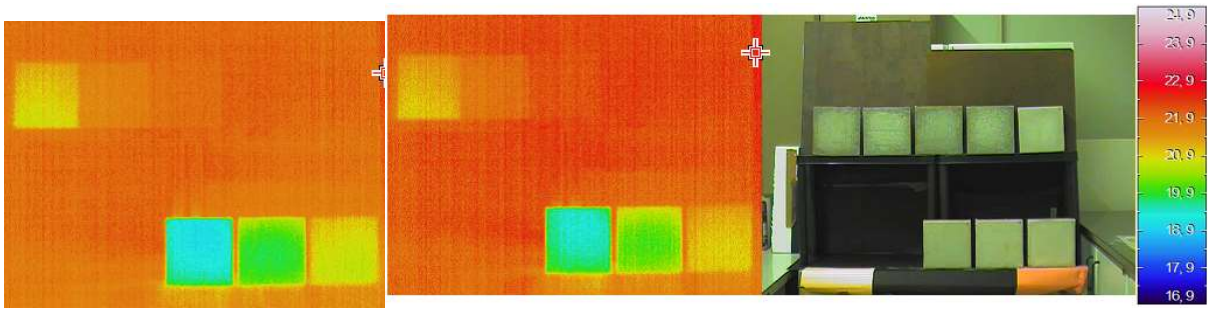
t4 – 4h



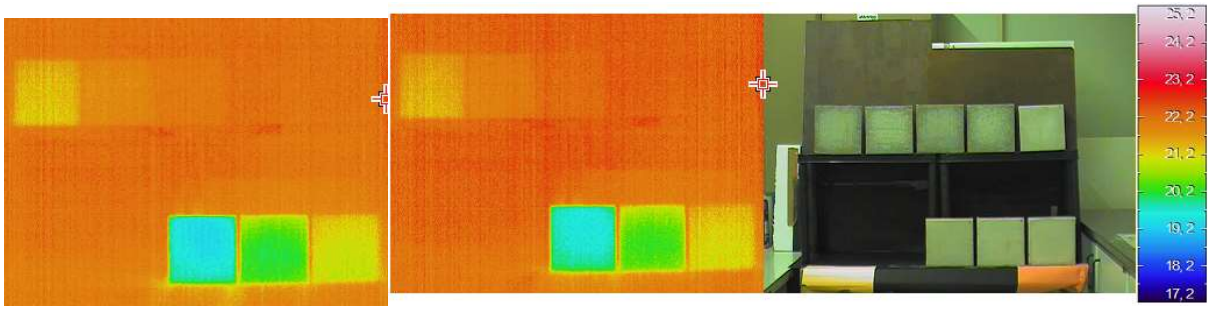
t5 – 8h



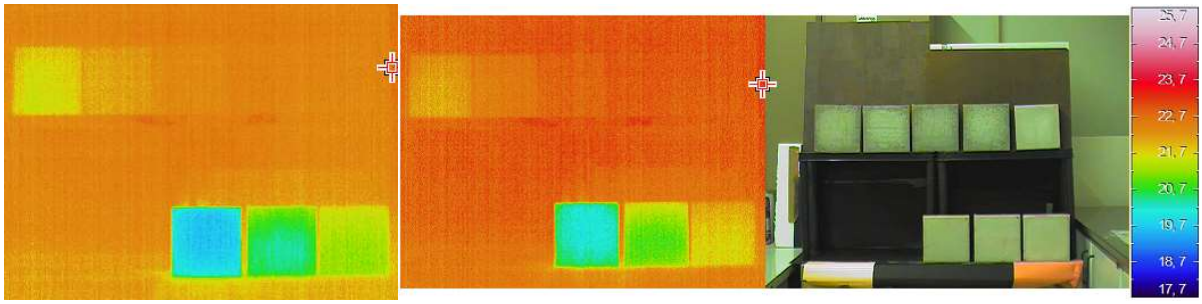
t6 – 24h



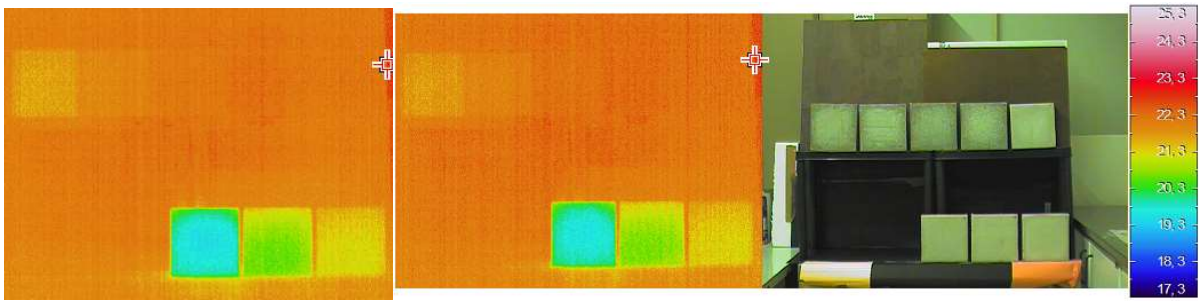
t7 – 29h



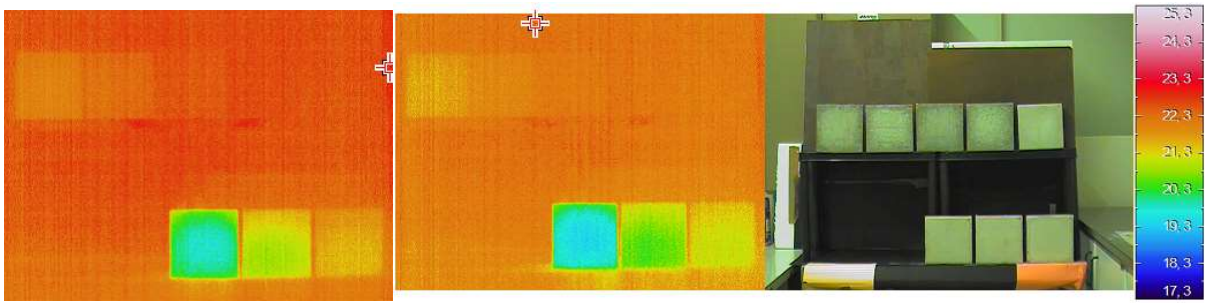
t8 – 32h



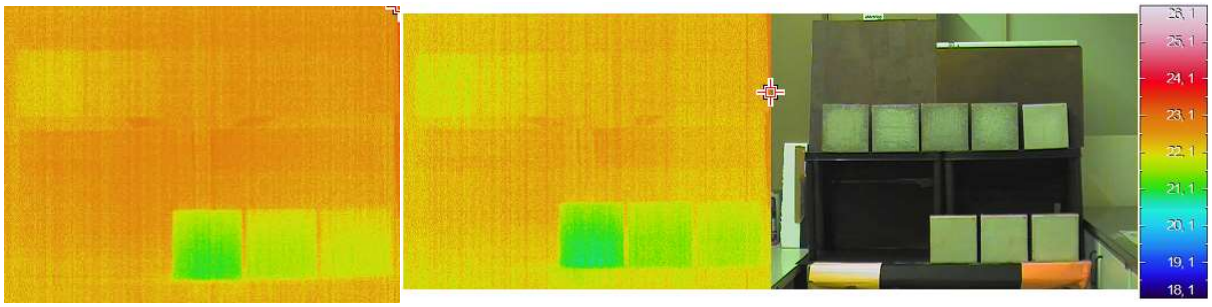
t9 – 48h



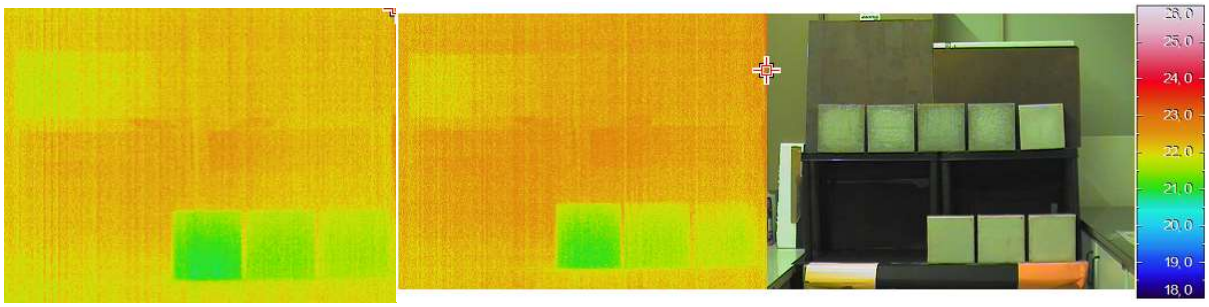
t10 – 50h



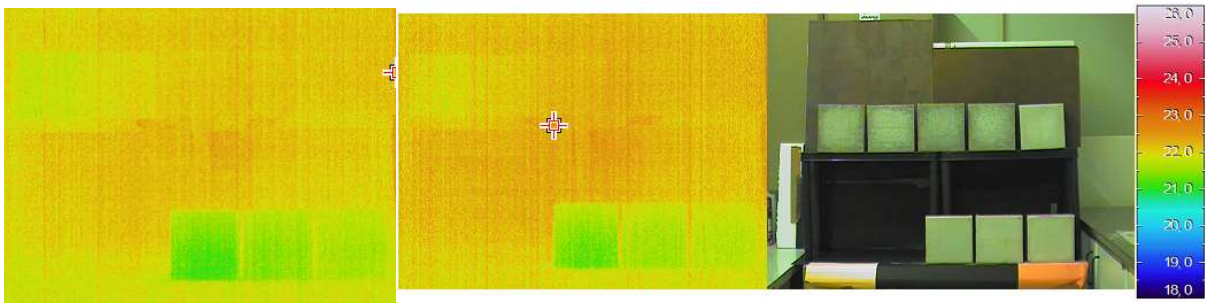
t11 – 96h



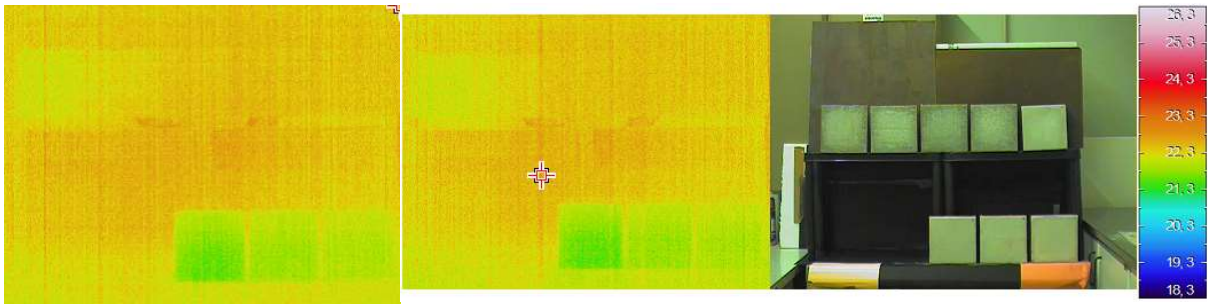
t12 – 101h



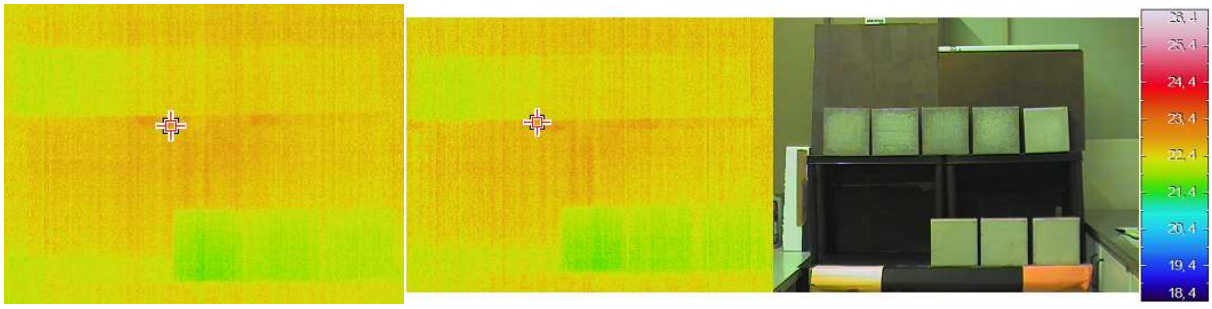
t13 – 120h



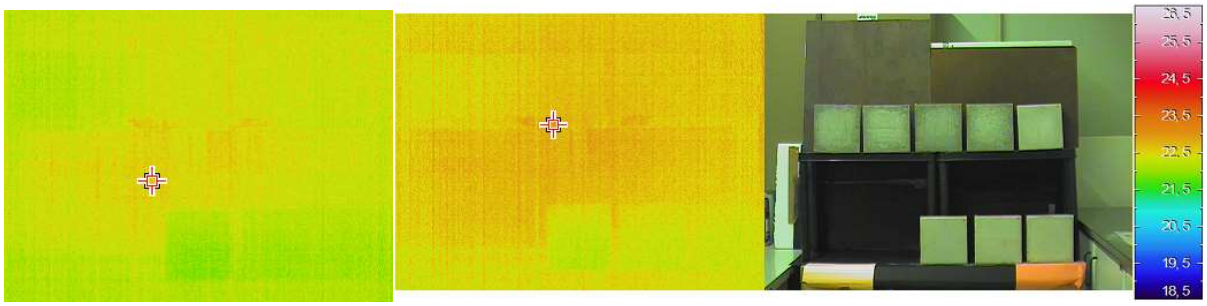
t14 – 125h



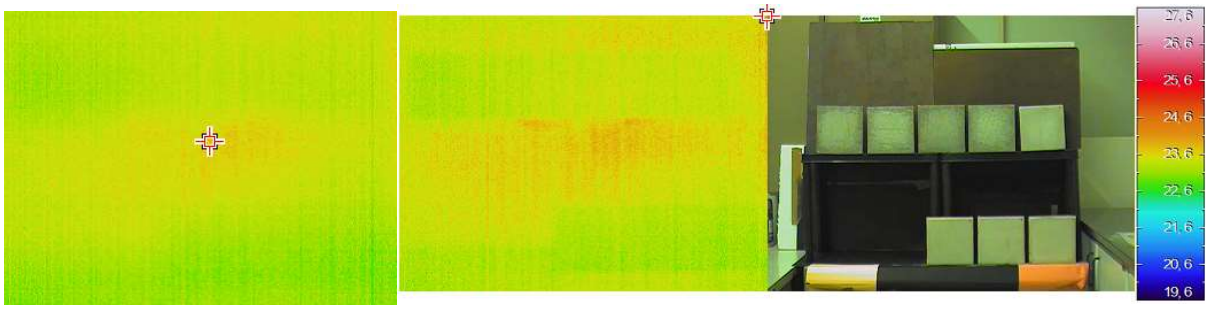
t15 – 151h



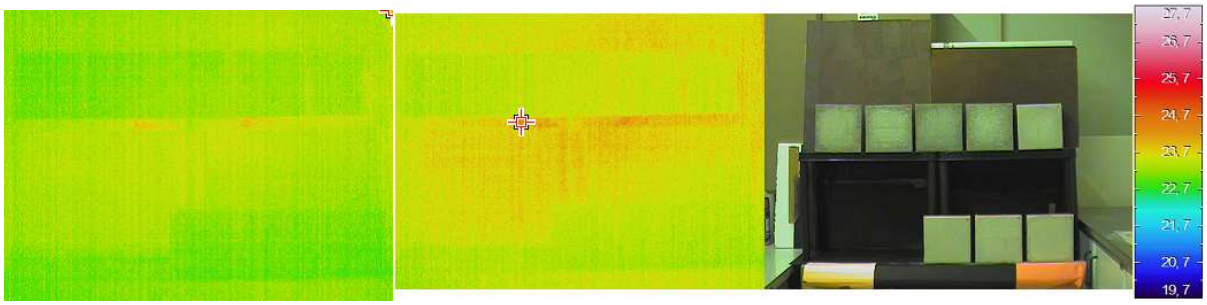
t16 – 173h



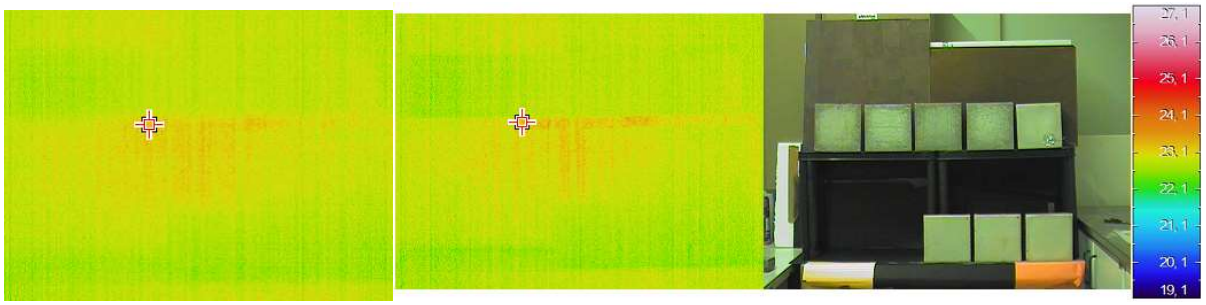
t17 – 246.5h



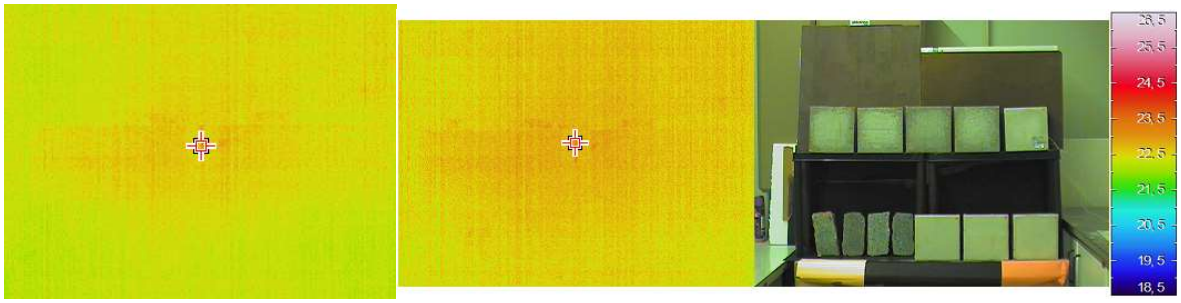
t18 – 317h



t19 – 434h

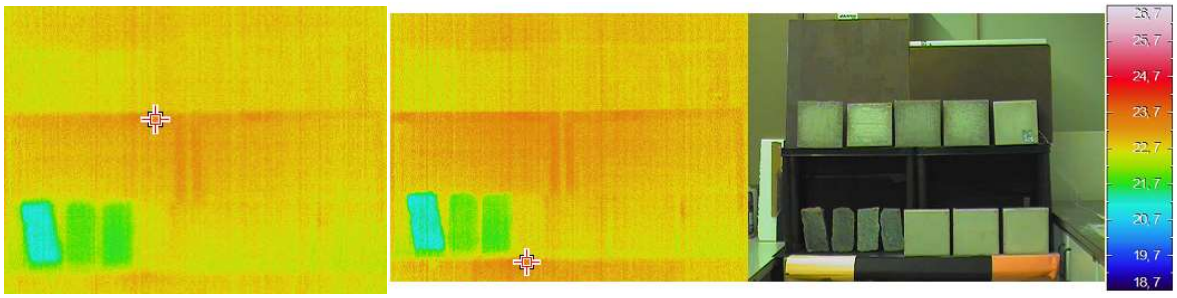


t20 – 460h

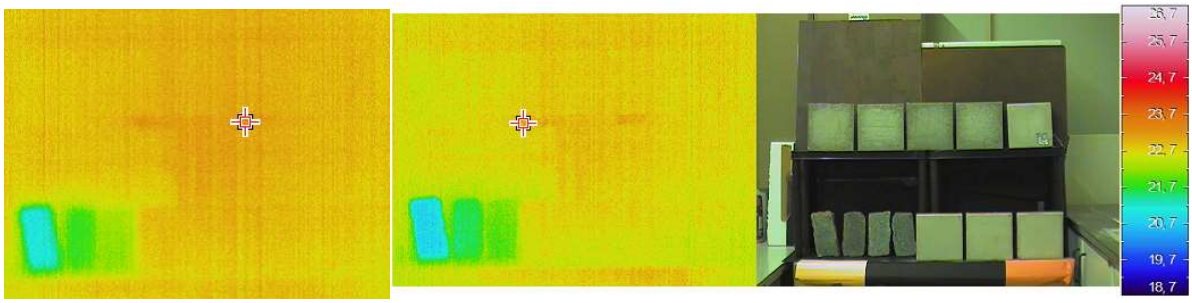


Granito

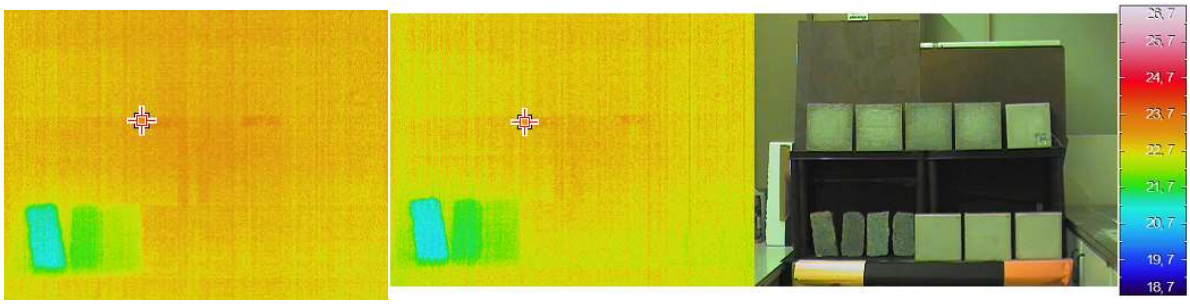
t0 – 0h



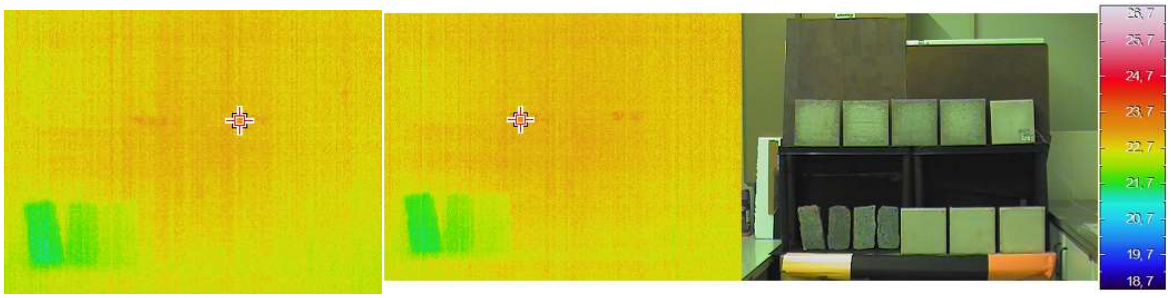
t1 – 0.5h



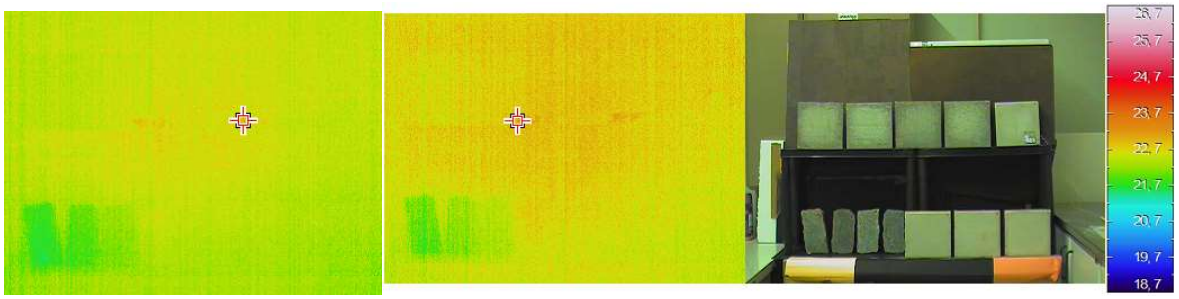
t2 – 1h



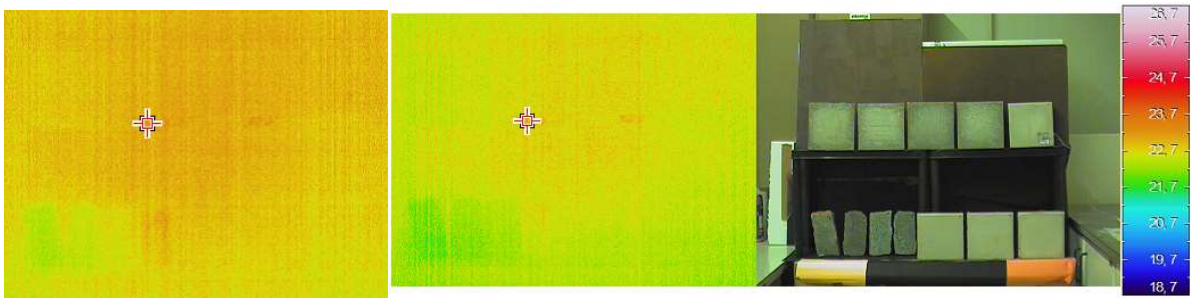
t3 – 2h



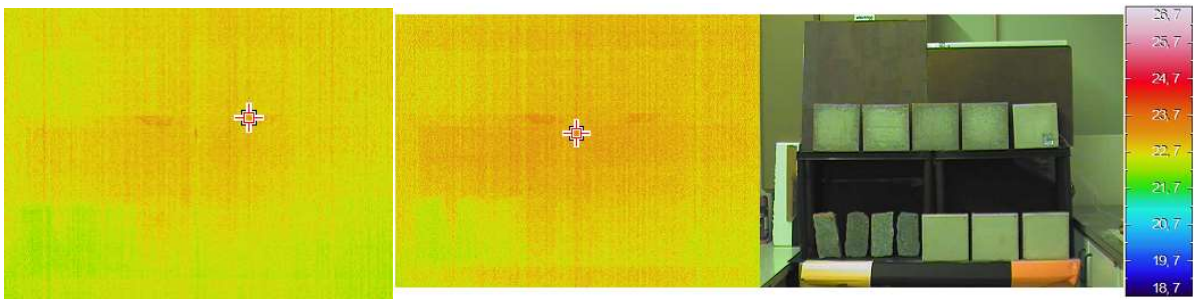
t4 – 3h



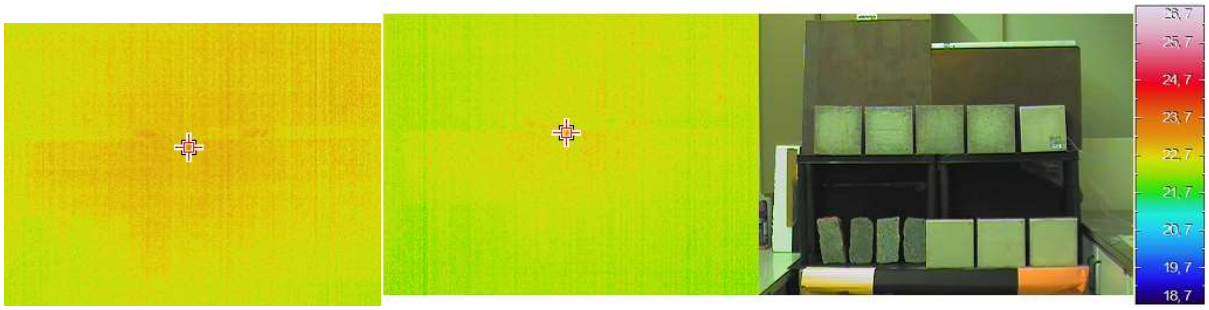
t5 – 4h



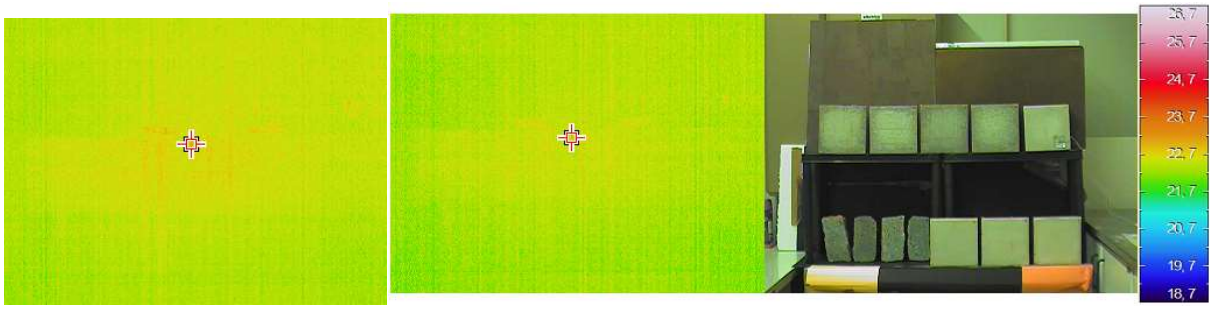
t6 – 5h



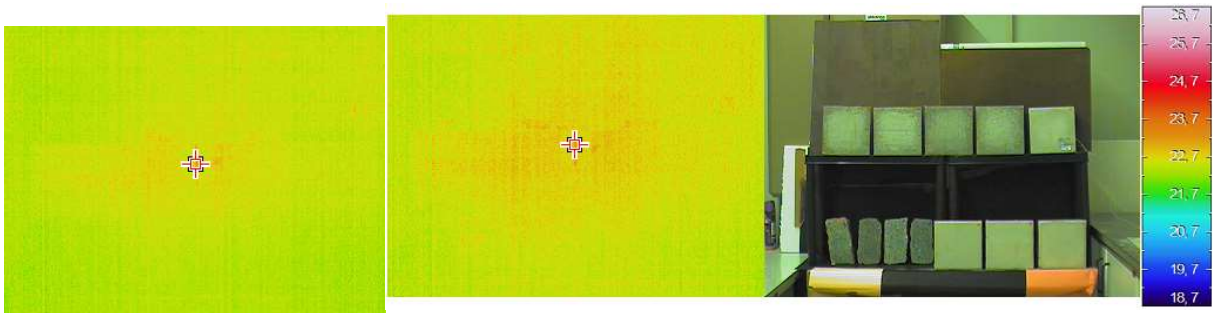
t7- 8.5h



t8 – 22h



t9 – 26h



APPENDIX 2

APPENDIX 2

Analysis of regression models for measurements taken after obtaining the maximum thermal gradient

- **Brick specimens – measurements taken after 48 hours**

Table - R^2 values and parameter estimates for each regression model – brick

		Parameters estimation		
Model	R^2	Constant	b1	b2
Linear	0.827	0.195	0.221	
Logaritmic	0.898	-0.535	1.374	
Quadratic	0.959	-0.757	0.591	-0.021

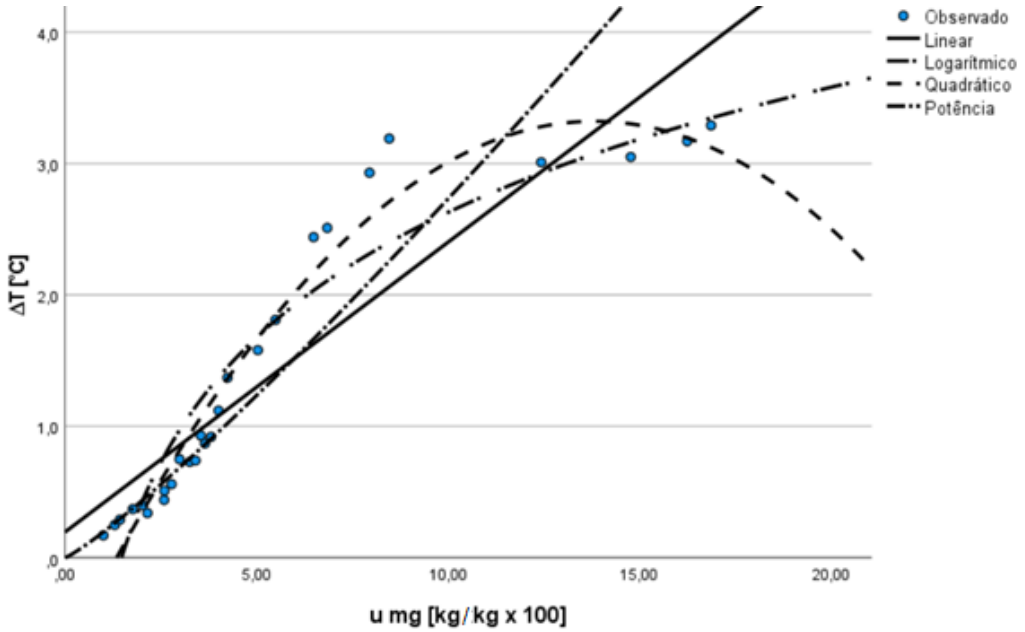


Figure - Curves of regression models - brick

- **Limestone specimens – measurements taken after 2 hours**

Table - R^2 values and parameter estimates for each regression model – limestone

		Parameters estimation		
Model	R^2	Constant	b1	b2
Linear	0.766	0.351	0.667	
Logaritmic	0.978	2.299	0.695	
Quadratic	0.957	0.081	1.820	-0.211

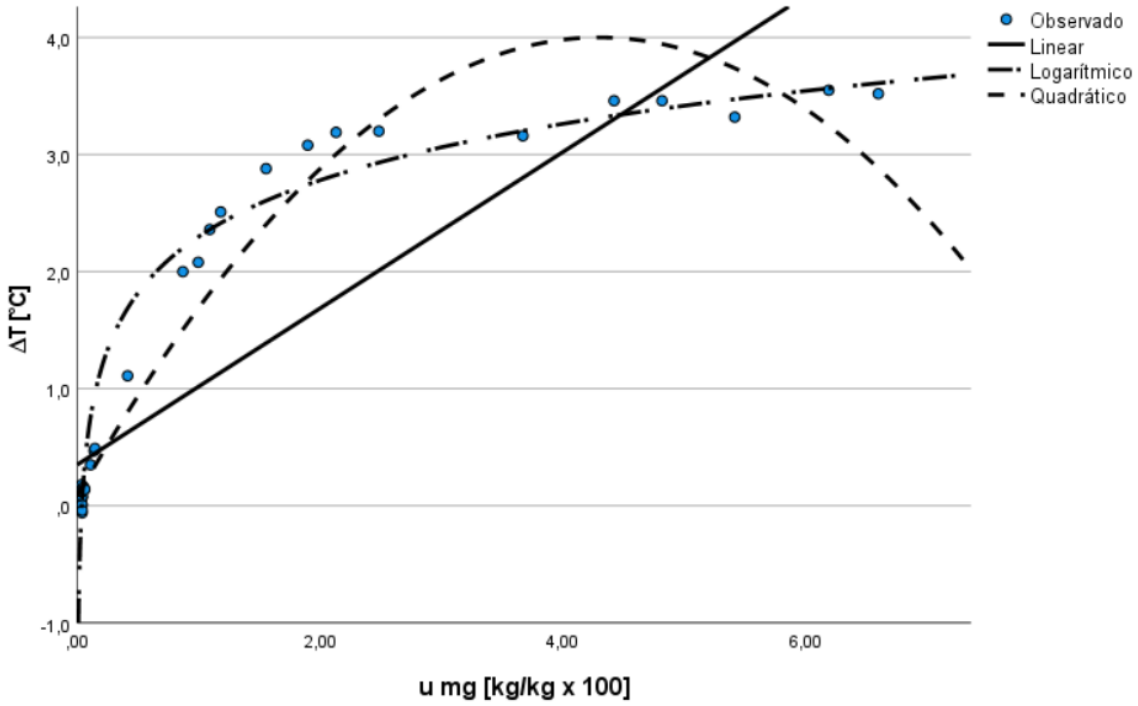
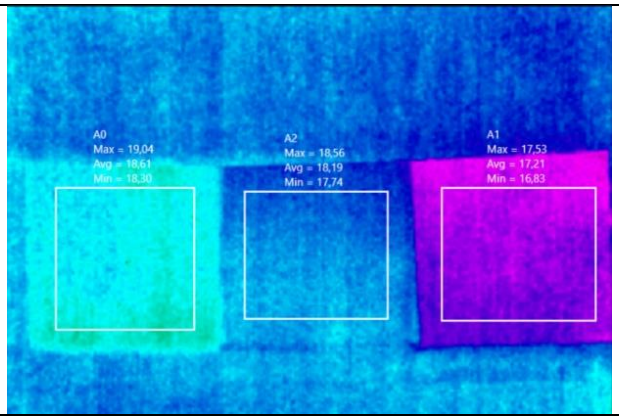
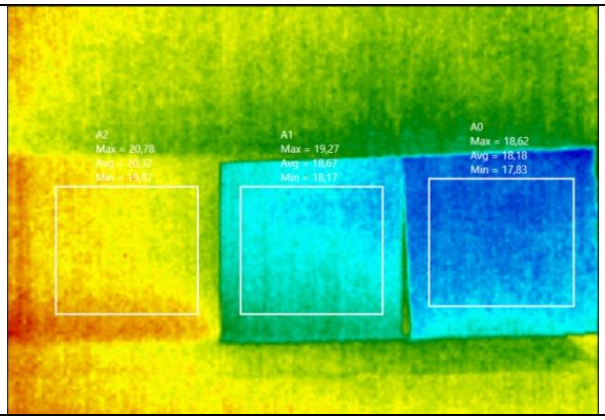
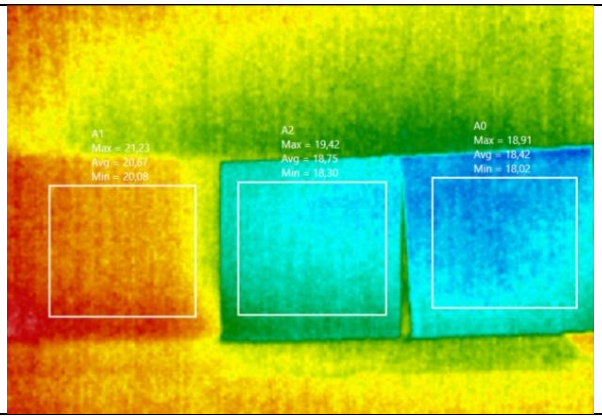
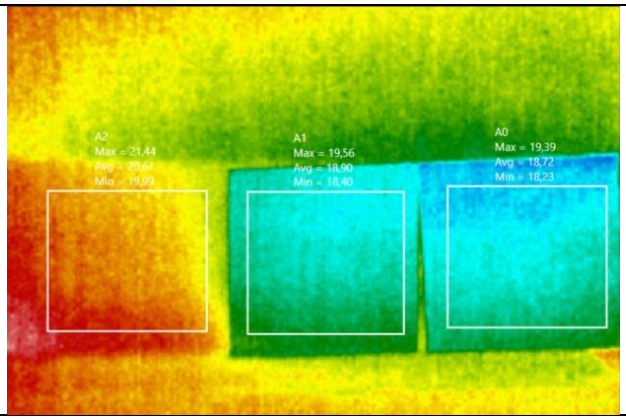


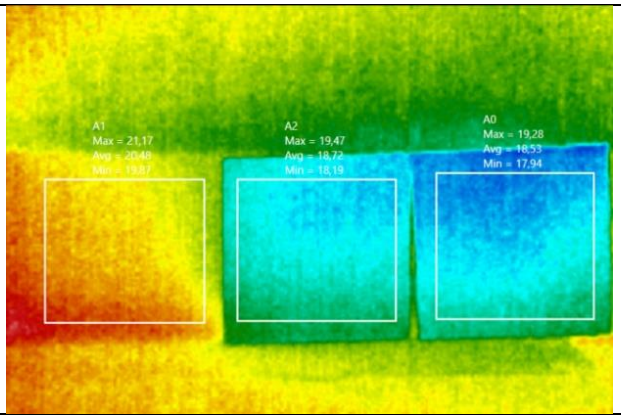
Figure - Curves of regression models - limestone

APPENDIX 3 (a)

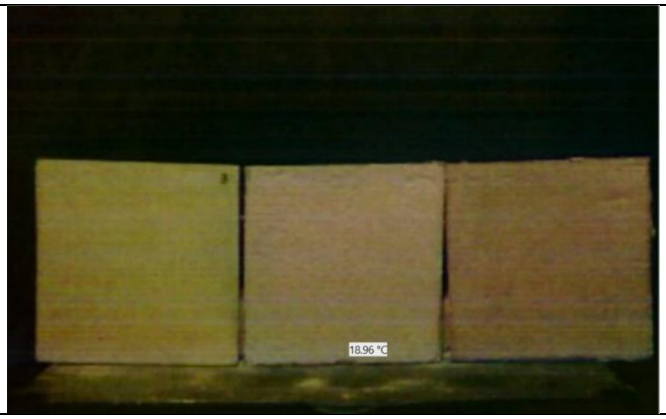
T = 20°C RH=70%	
t0 – 0h	
	
t1 – 0.5h	
	
t2 – 1h	
	
t3 – 2h	
	

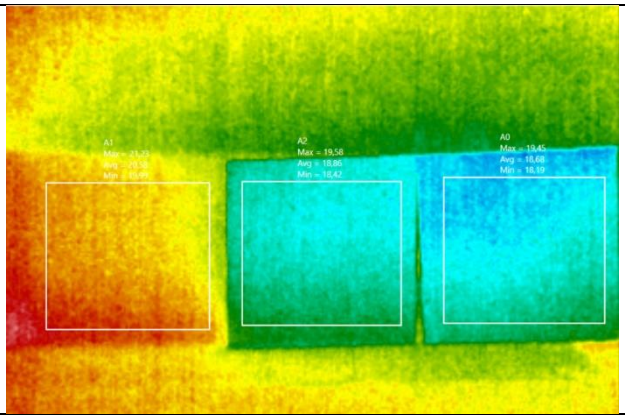
t4 – 4h





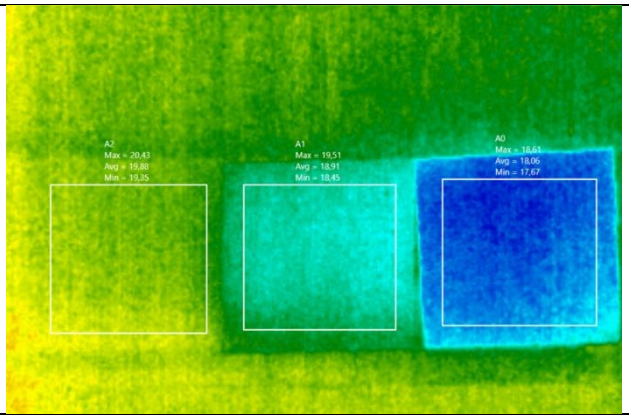
t5 – 7.5h



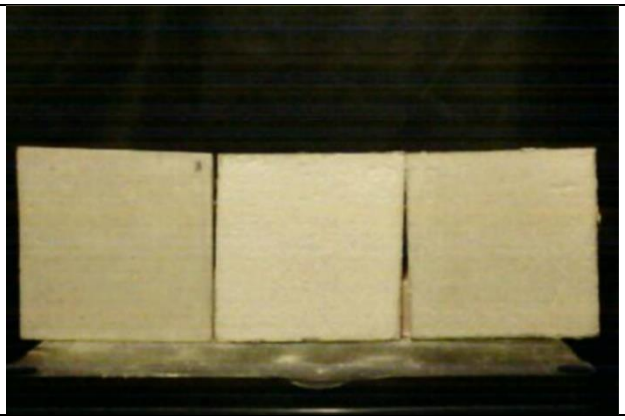


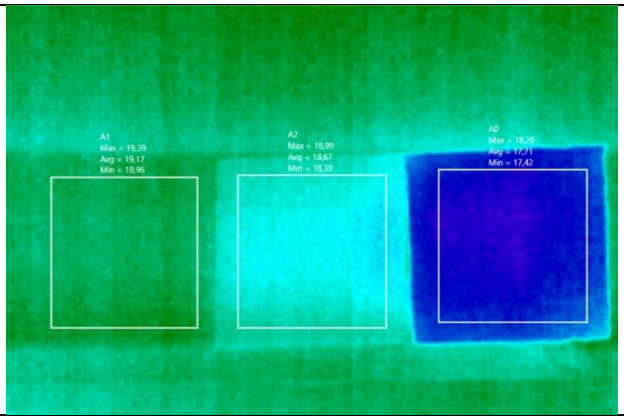
t6 – 24h





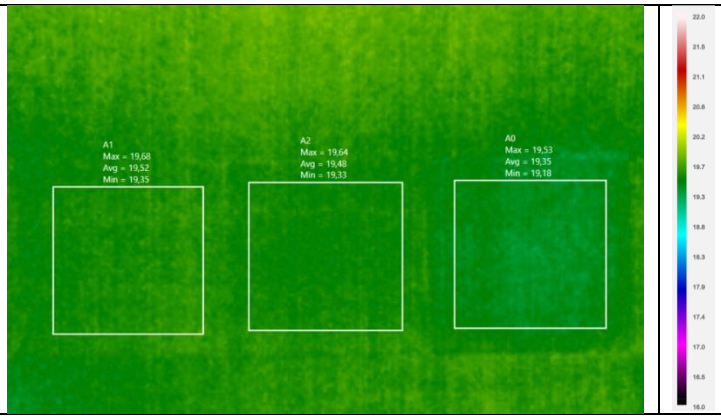
t7 – 30h





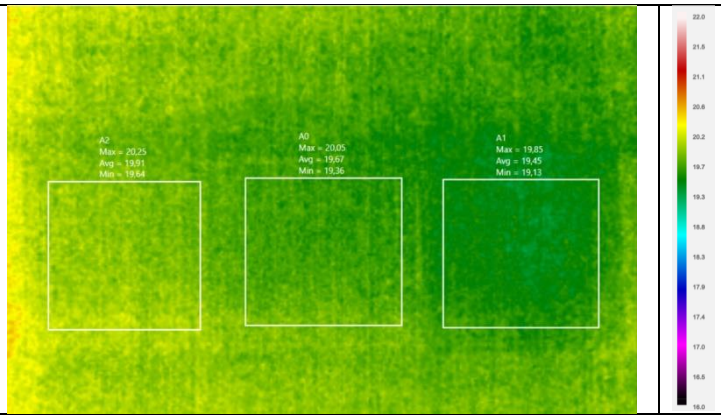
t8 – 96h





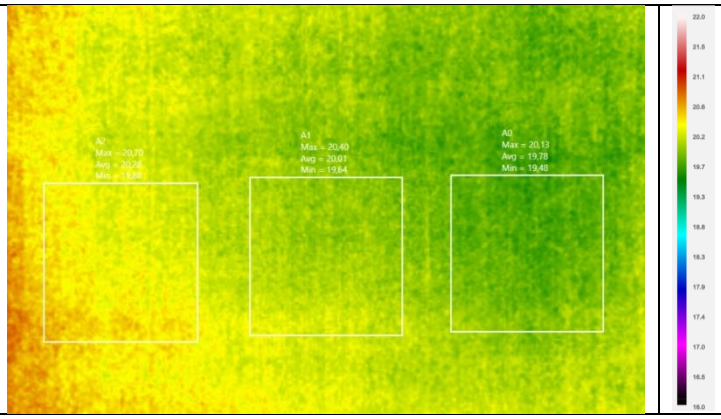
t9 – 102h





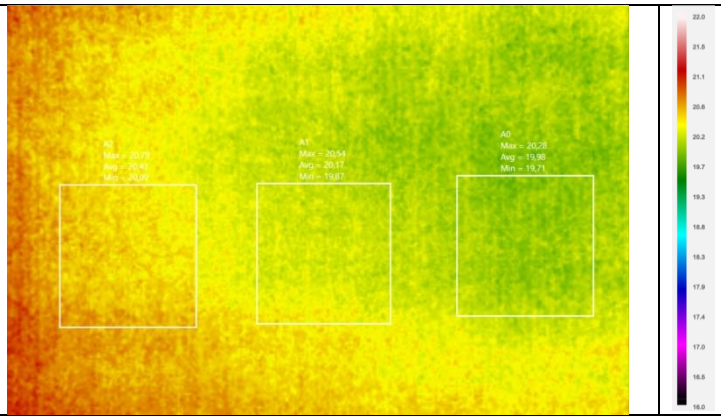
t10 – 120h





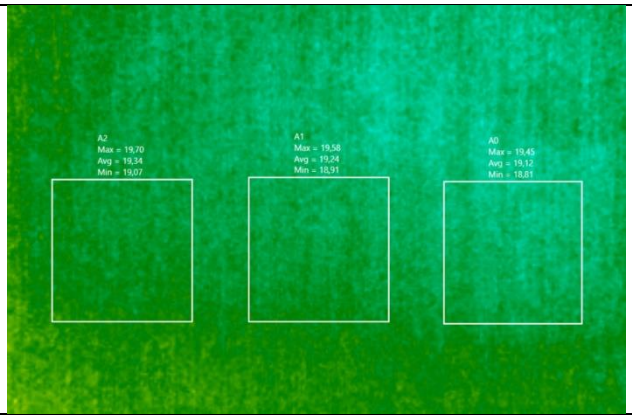
t11 – 146h





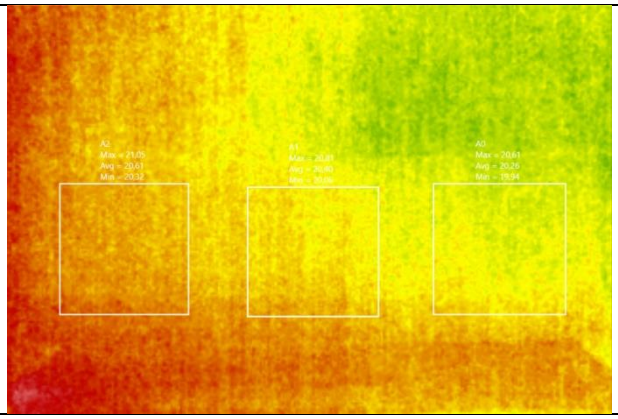
t12 – 196h



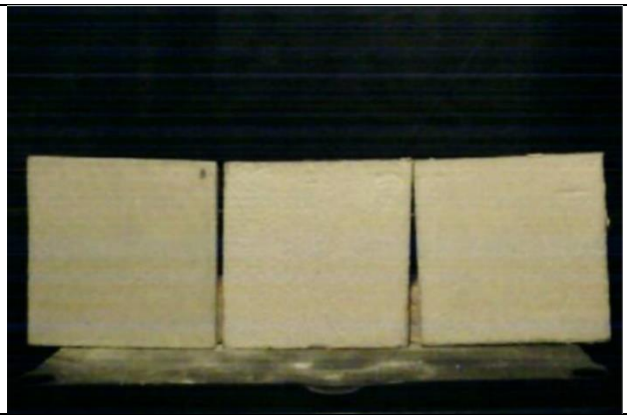


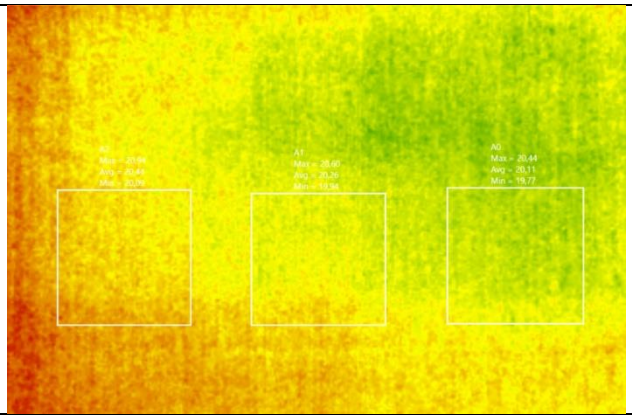
t13 – 268h





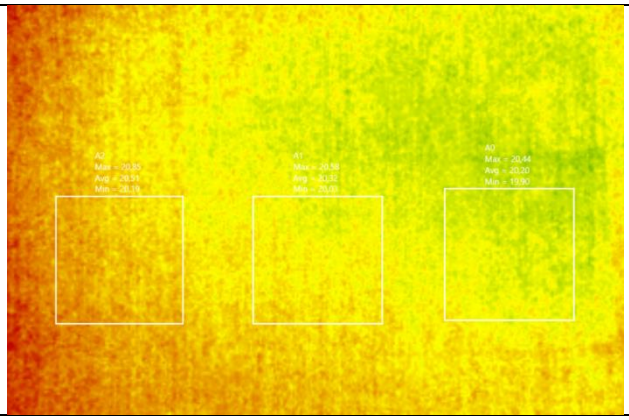
t14 – 311h



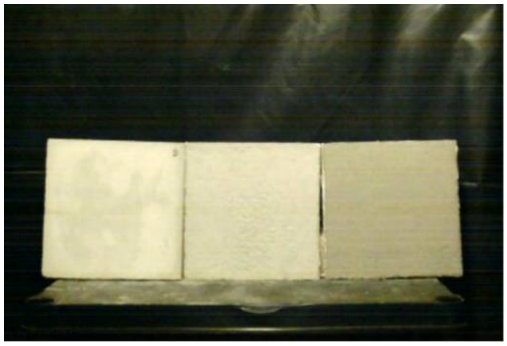
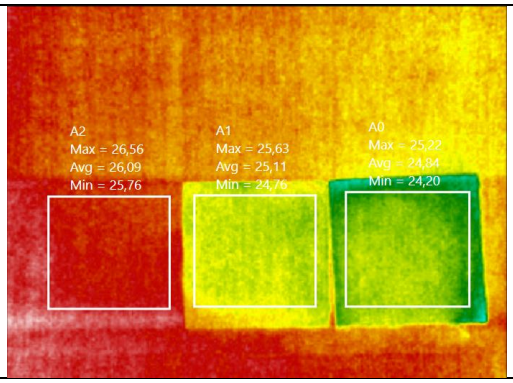
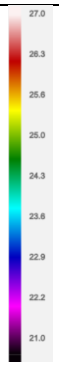
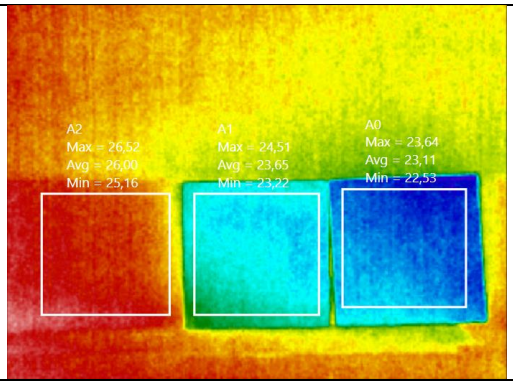
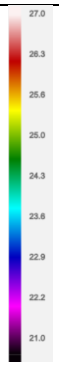
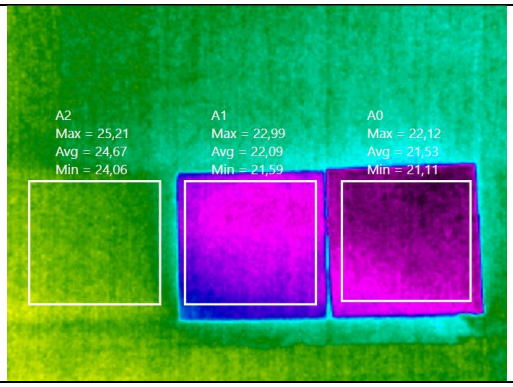
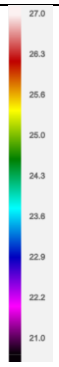
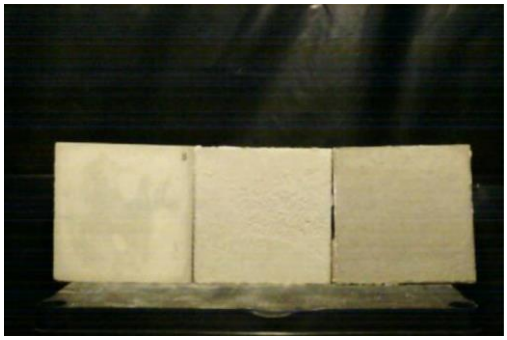
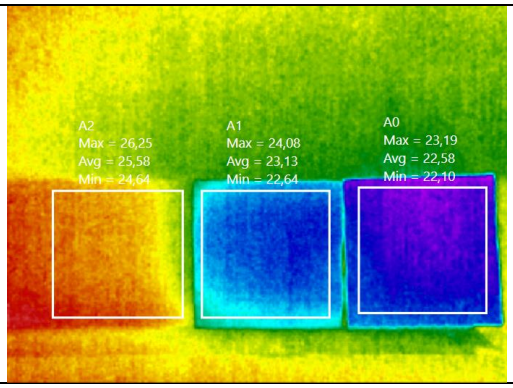
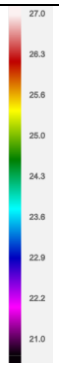


t15 – 336h



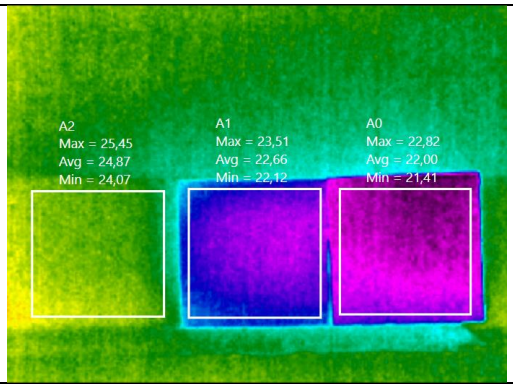


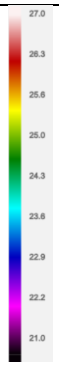
APPENDIX 3 (b)

T = 25°C RH=60%		
t0 – 0h		
		
t1 – 0.5h		
		
t2 – 1h		
		
t3 – 2h		
		

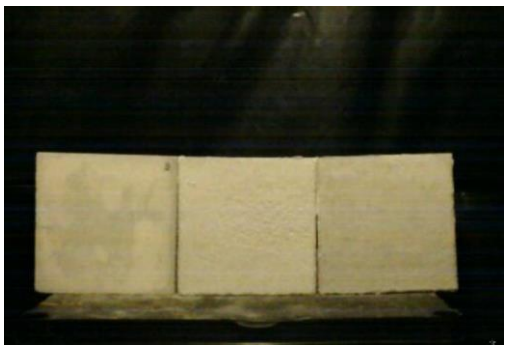
t4 – 4h

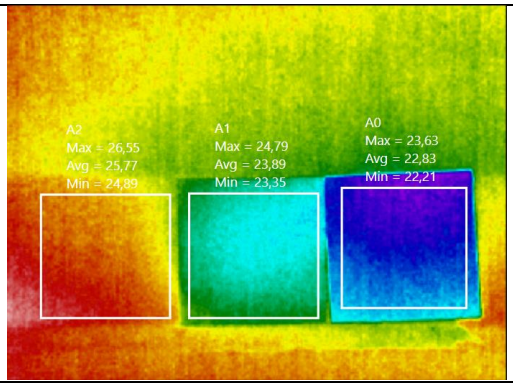


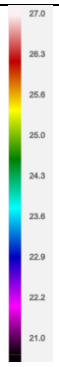




t5 – 7.5h

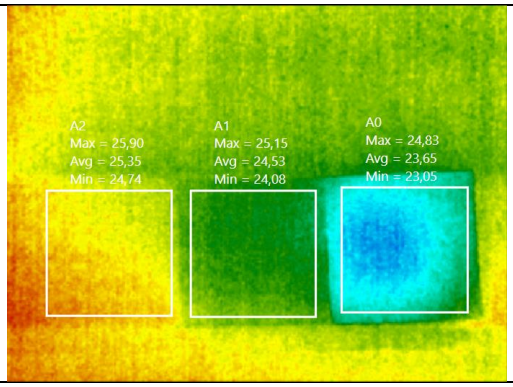


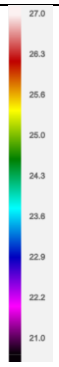




t6 – 24h

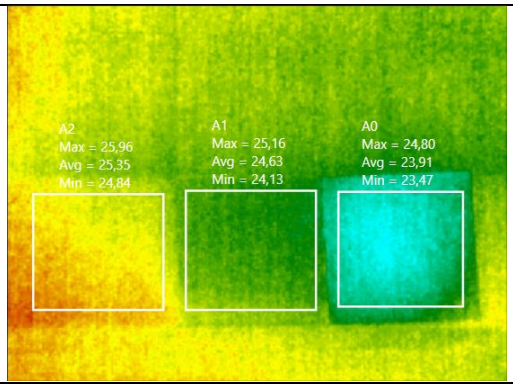


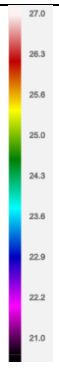


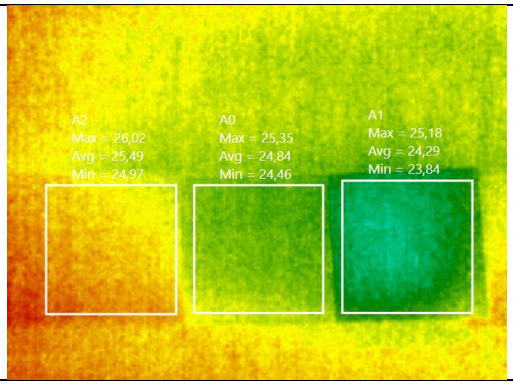
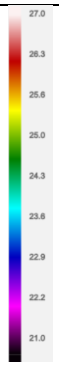
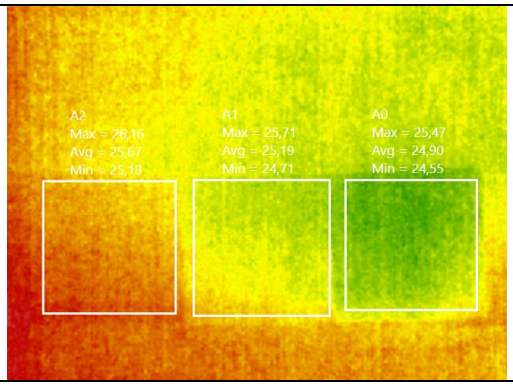
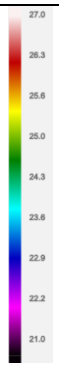
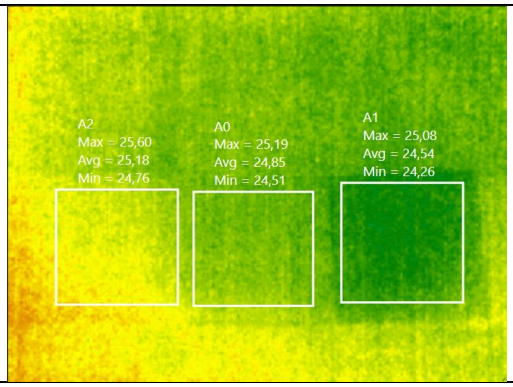
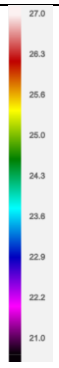
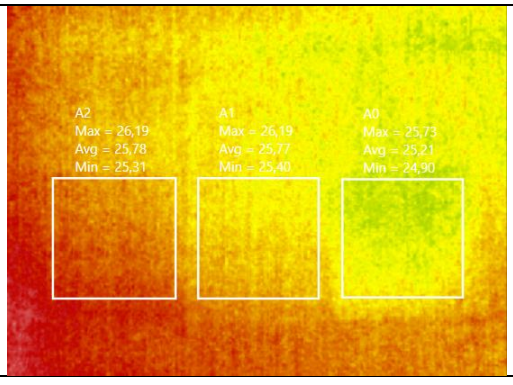
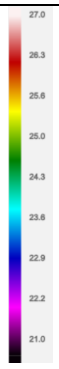


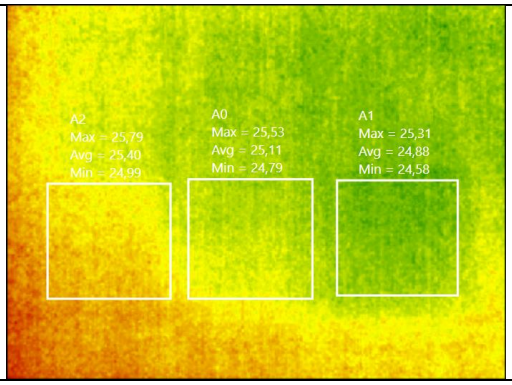
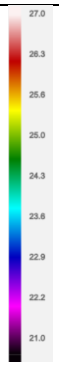
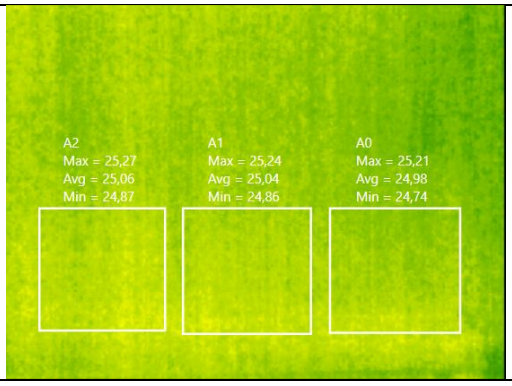
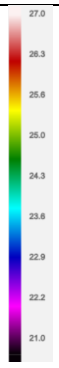
t7 – 28h



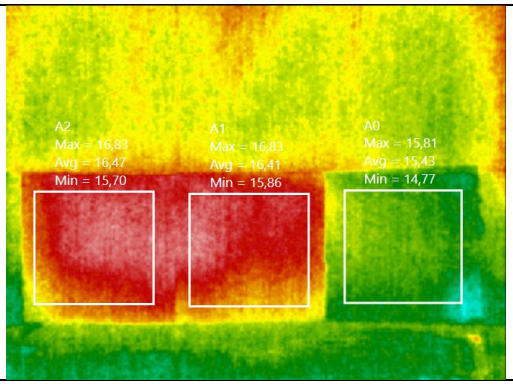
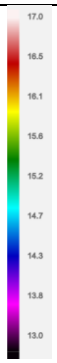
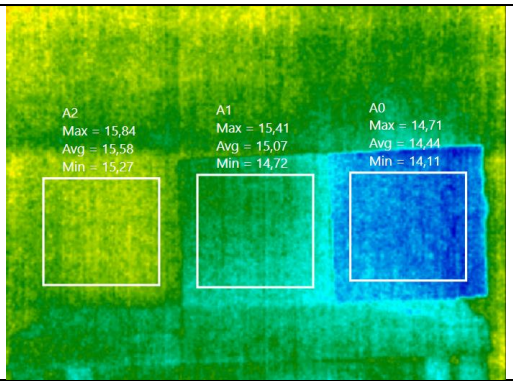
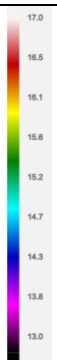
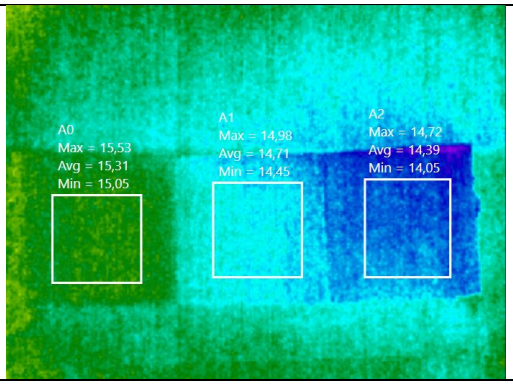
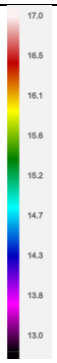
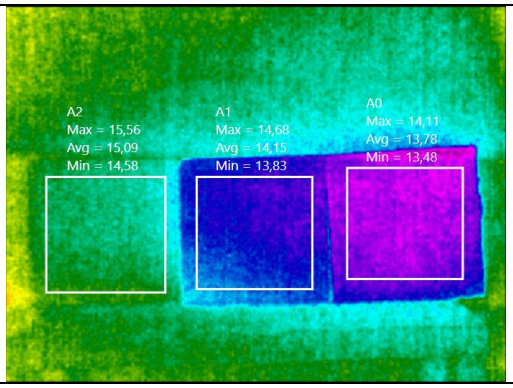
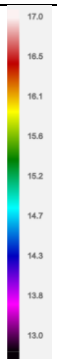




t8 – 31h		
		
t9 – 48h		
		
t10 – 56h		
		
t11 – 72h		
		

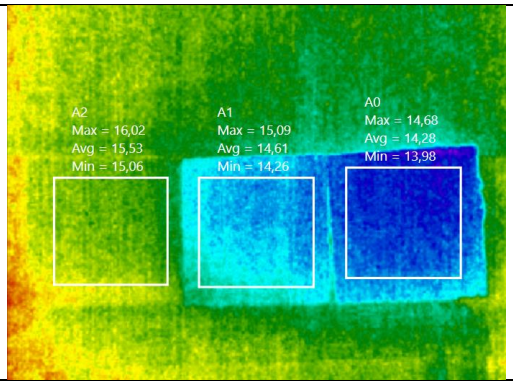
t12 – 79h		
		
t13 – 144h		
		

APPENDIX 3 (c)

T = 15°C RH = 80%		
t0 – 0h		
		
t1 – 0.5h		
		
t2 – 1h		
		
t3 – 2h		
		

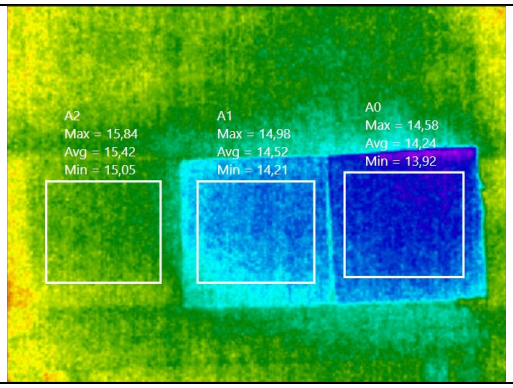
t4 – 4h



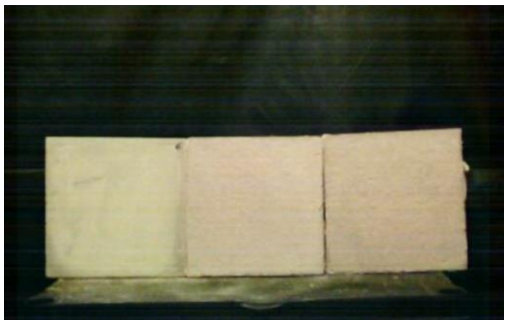


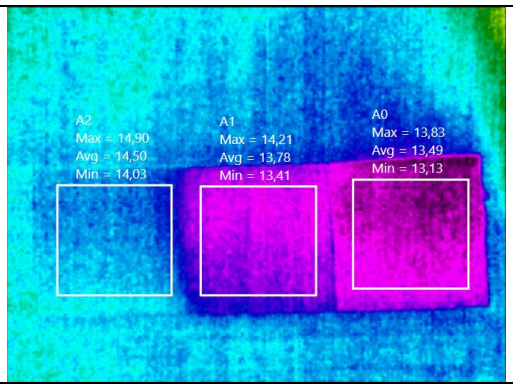
t5 – 20h





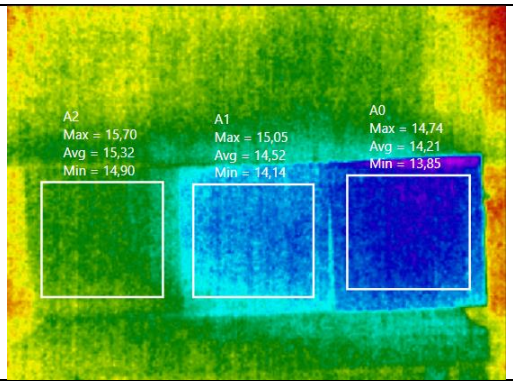
t6 – 24h





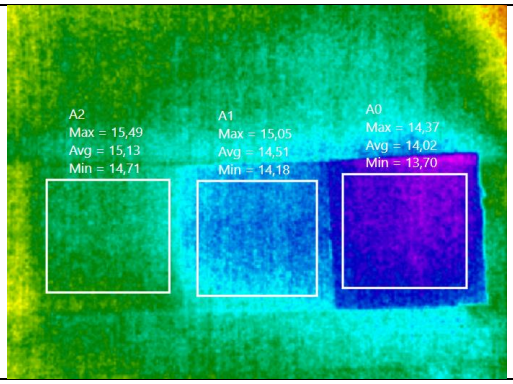
t7 – 28h

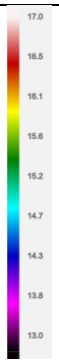




t8 – 46h

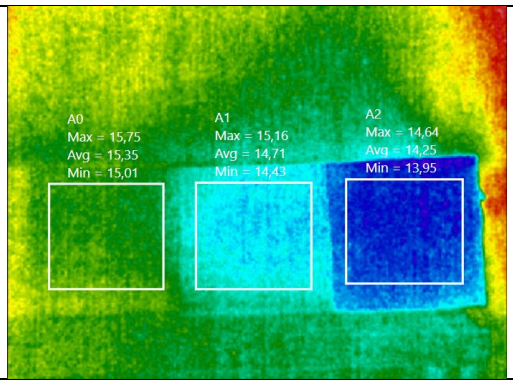


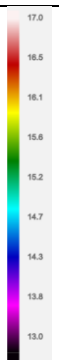




t9 – 48h

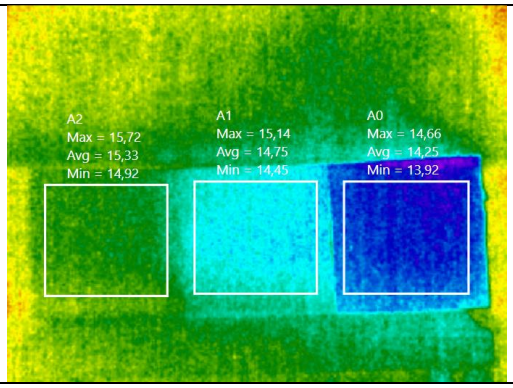


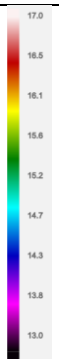




t10 – 52h

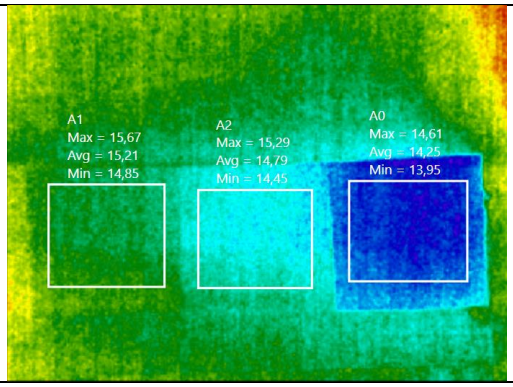


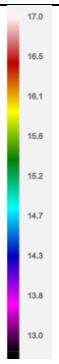




t11 – 70h

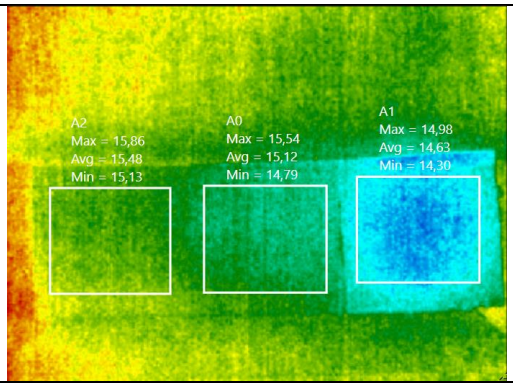


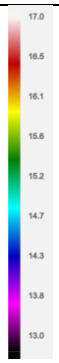




t12 – 94h

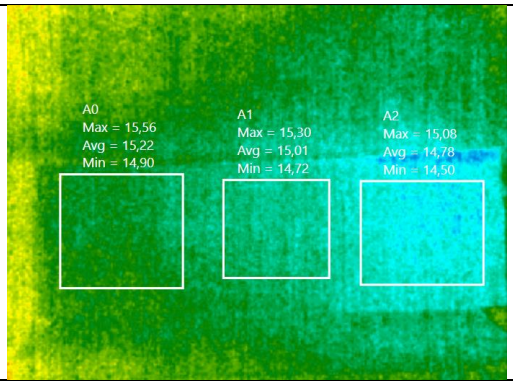


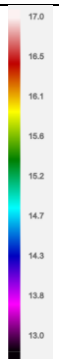




t13 – 168h

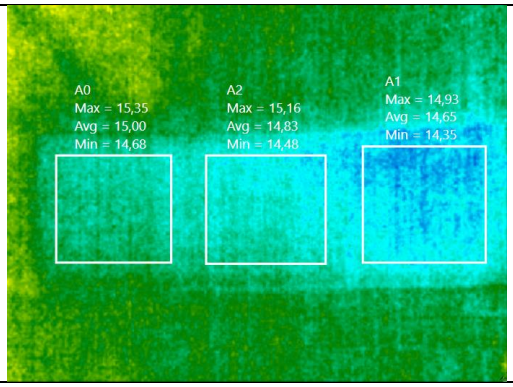


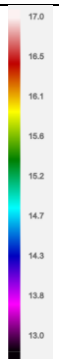




t14 – 216h

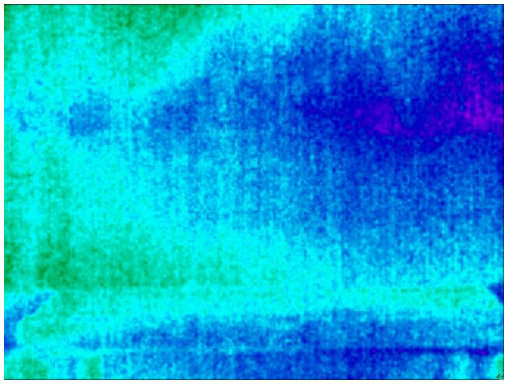


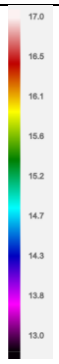


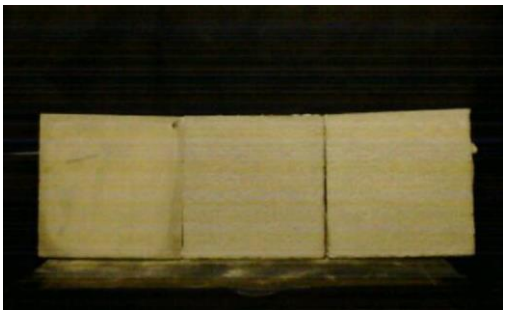
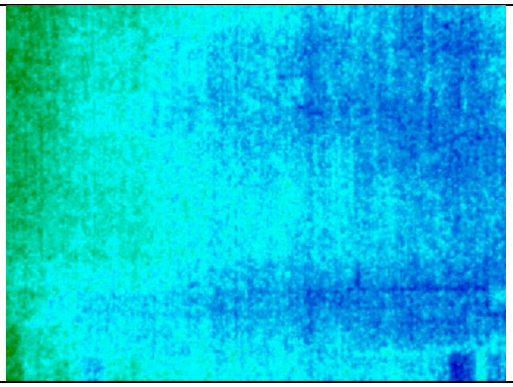
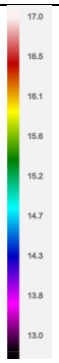


t15 – 262h







t16 – 310h		
		

APPENDIX 4 (a)

In [1]:
```
import numpy as np
import pandas as pd
import seaborn as sns
from matplotlib import pyplot as plt

df = pd.read_excel('datasetneuralnetworks.xlsx')
# VISUALIZAR A DISTRIBUIÇÃO DOS VALORES DE ΔTmax, Humidade, Teor de Humidade e ΔT
df
```

Out[1]:

	Material	Temperature [°C]	Relative Humidity [%]	Δtmax [°C]	ΔT [°C]	Humidity [kg/m³]
0	1	6.99619	53.7301	2.376	0.000000	237.600010
1	1	6.99619	53.7301	2.376	1.929128	233.649250
2	1	6.99619	53.7301	2.376	2.376436	221.900300
3	1	6.99619	53.7301	2.376	2.317941	164.249420
4	1	6.99619	53.7301	2.376	2.256899	145.193510
...	...	...	...	...	...	...
4641	4	19.59770	59.2467	0.376	0.046678	13.039567
4642	4	19.59770	59.2467	0.376	0.036932	11.091906
4643	4	19.59770	59.2467	0.376	0.027231	9.376396
4644	4	19.59770	59.2467	0.376	0.018430	8.182526
4645	4	19.59770	59.2467	0.376	0.010635	7.453972

4646 rows × 6 columns

In [2]:
```
from keras.models import Model
from keras.layers import Dense, Input
from keras.wrappers.scikit_learn import KerasRegressor
from sklearn.model_selection import cross_val_score
from sklearn.model_selection import KFold
from sklearn.pipeline import Pipeline
from sklearn.model_selection import train_test_split
from sklearn.metrics import r2_score
from tensorflow.keras.callbacks import EarlyStopping



# SEPARAR INPUTS DOS OUTPUTS

X = df.drop(['Δtmax [°C]', 'Humidity [kg/m³]', 'ΔT [°C]'], axis=1)
y = df.drop(['Material', 'Temperature [°C]', 'Relative Humidity [%]', 'ΔT [°C]', '
y = y.values

# número de dados de treinamento
m = X.shape[0]
```

In [3]:
```
X_train, X_test, y_train, y_test = train_test_split(X, y, test_size = 0.2, random_
```

In [4]:
```
# Scale data, otherwise model will fail
# Standardize features by removing the mean and scaling to unit variance
from sklearn.preprocessing import MinMaxScaler
scaler = MinMaxScaler()
```

```
scaler.fit(X)

X_train_scaled = scaler.transform(X_train)
X_test_scaled = scaler.transform(X_test)
X_train_scaled
```

Out[4]:
```
array([[1.        , 0.99083513, 0.1878412 ],
       [0.        , 0.09097281, 0.0871127 ],
       [0.66666667, 0.77492025, 0.        ],
       ...,
       [0.66666667, 0.35558569, 0.42422863],
       [1.        , 1.        , 0.26969637],
       [0.        , 0.18888058, 0.26118552]])
```

In [5]:
```
# Define the model
# Experiment with deeper and wider networks

#Start defining the input tensor:
inpTensor = Input(shape= (3,))

#create the layers and pass them the input tensor to get the output tensor:
hidden1Out = Dense(128, activation='relu')(inpTensor)
hidden2Out = Dense(64, activation='relu')(hidden1Out)
finalOut = Dense(1, activation='relu')(hidden2Out)

#define the model's start and end points
model = Model(inpTensor,finalOut)


model.summary()
model.compile(loss='mean_squared_error', optimizer='adam', metrics=['mae'])
```

```
Model: "model"
_________________________________________________________________
 Layer (type)                Output Shape              Param #
=================================================================
 input_1 (InputLayer)        [(None, 3)]               0

 dense (Dense)               (None, 128)               512

 dense_1 (Dense)             (None, 64)                8256

 dense_2 (Dense)             (None, 1)                 65

=================================================================
Total params: 8,833
Trainable params: 8,833
Non-trainable params: 0
_________________________________________________________________
```

In [6]:
```
monitor = EarlyStopping(monitor='val_loss', min_delta=1e-3, patience=20, verbose=1

history = model.fit(X_train_scaled, y_train, validation_split=0.1, epochs=300, cal
```

```
Epoch 1/300
105/105 [==============================] - 1s 3ms/step - loss: 1.4039 - mae: 0.914
1 - val_loss: 1.0588 - val_mae: 0.8120
Epoch 2/300
105/105 [==============================] - 0s 1ms/step - loss: 0.8347 - mae: 0.692
7 - val_loss: 0.9530 - val_mae: 0.6882
Epoch 3/300
105/105 [==============================] - 0s 1ms/step - loss: 0.6691 - mae: 0.584
7 - val_loss: 0.7296 - val_mae: 0.5758
Epoch 4/300
105/105 [==============================] - 0s 1ms/step - loss: 0.4998 - mae: 0.475
1 - val_loss: 0.5078 - val_mae: 0.4509
Epoch 5/300
105/105 [==============================] - 0s 1ms/step - loss: 0.2897 - mae: 0.338
6 - val_loss: 0.2647 - val_mae: 0.3283
Epoch 6/300
105/105 [==============================] - 0s 2ms/step - loss: 0.1416 - mae: 0.246
0 - val_loss: 0.1185 - val_mae: 0.2426
Epoch 7/300
105/105 [==============================] - 0s 1ms/step - loss: 0.0594 - mae: 0.163
5 - val_loss: 0.0461 - val_mae: 0.1486
Epoch 8/300
105/105 [==============================] - 0s 2ms/step - loss: 0.0199 - mae: 0.091
8 - val_loss: 0.0140 - val_mae: 0.0792
Epoch 9/300
105/105 [==============================] - 0s 1ms/step - loss: 0.0075 - mae: 0.058
5 - val_loss: 0.0064 - val_mae: 0.0598
Epoch 10/300
105/105 [==============================] - 0s 2ms/step - loss: 0.0038 - mae: 0.042
9 - val_loss: 0.0031 - val_mae: 0.0380
Epoch 11/300
105/105 [==============================] - 0s 2ms/step - loss: 0.0023 - mae: 0.034
3 - val_loss: 0.0024 - val_mae: 0.0341
Epoch 12/300
105/105 [==============================] - 0s 1ms/step - loss: 0.0016 - mae: 0.028
4 - val_loss: 0.0016 - val_mae: 0.0272
Epoch 13/300
105/105 [==============================] - 0s 2ms/step - loss: 0.0012 - mae: 0.024
6 - val_loss: 0.0012 - val_mae: 0.0242
Epoch 14/300
105/105 [==============================] - 0s 1ms/step - loss: 8.9817e-04 - mae:
0.0216 - val_loss: 8.4393e-04 - val_mae: 0.0212
Epoch 15/300
105/105 [==============================] - 0s 1ms/step - loss: 7.1107e-04 - mae:
0.0191 - val_loss: 6.5599e-04 - val_mae: 0.0187
Epoch 16/300
105/105 [==============================] - 0s 1ms/step - loss: 5.8415e-04 - mae:
0.0176 - val_loss: 8.1581e-04 - val_mae: 0.0208
Epoch 17/300
105/105 [==============================] - 0s 1ms/step - loss: 4.3400e-04 - mae:
0.0150 - val_loss: 5.2807e-04 - val_mae: 0.0169
Epoch 18/300
105/105 [==============================] - 0s 1ms/step - loss: 3.7857e-04 - mae:
0.0139 - val_loss: 4.5092e-04 - val_mae: 0.0167
Epoch 19/300
105/105 [==============================] - 0s 1ms/step - loss: 3.4633e-04 - mae:
0.0136 - val_loss: 4.9801e-04 - val_mae: 0.0174
Epoch 20/300
105/105 [==============================] - 0s 1ms/step - loss: 3.1083e-04 - mae:
0.0131 - val_loss: 3.2733e-04 - val_mae: 0.0136
Epoch 21/300
105/105 [==============================] - 0s 1ms/step - loss: 3.2618e-04 - mae:
0.0138 - val_loss: 4.2823e-04 - val_mae: 0.0158
Epoch 22/300
```

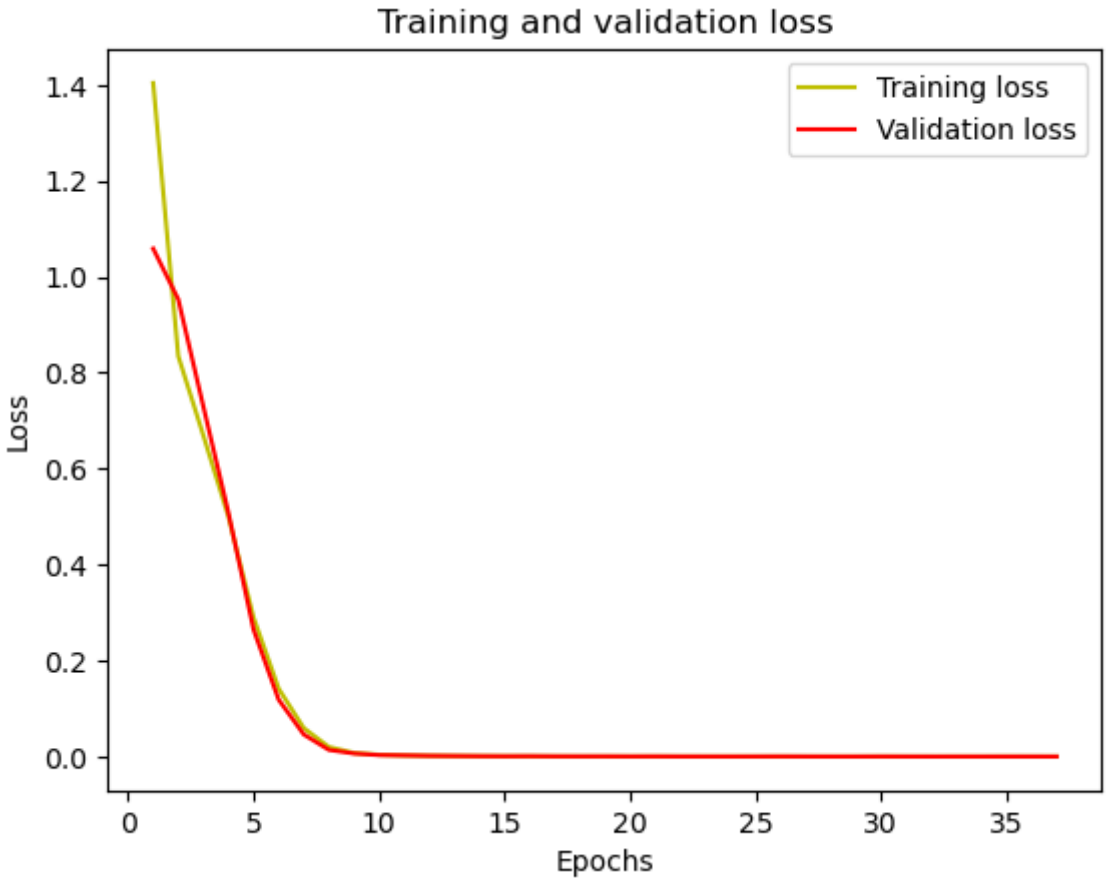
```
105/105 [==============================] - 0s 1ms/step - loss: 2.6729e-04 - mae:
0.0123 - val_loss: 2.3402e-04 - val_mae: 0.0106
Epoch 23/300
105/105 [==============================] - 0s 1ms/step - loss: 2.0177e-04 - mae:
0.0106 - val_loss: 2.2826e-04 - val_mae: 0.0109
Epoch 24/300
105/105 [==============================] - 0s 1ms/step - loss: 2.2862e-04 - mae:
0.0115 - val_loss: 1.8871e-04 - val_mae: 0.0102
Epoch 25/300
105/105 [==============================] - 0s 1ms/step - loss: 2.1175e-04 - mae:
0.0111 - val_loss: 2.5008e-04 - val_mae: 0.0123
Epoch 26/300
105/105 [==============================] - 0s 1ms/step - loss: 2.0913e-04 - mae:
0.0109 - val_loss: 3.4035e-04 - val_mae: 0.0143
Epoch 27/300
105/105 [==============================] - 0s 1ms/step - loss: 1.6727e-04 - mae:
0.0097 - val_loss: 2.2788e-04 - val_mae: 0.0121
Epoch 28/300
105/105 [==============================] - 0s 1ms/step - loss: 1.6017e-04 - mae:
0.0096 - val_loss: 1.4665e-04 - val_mae: 0.0084
Epoch 29/300
105/105 [==============================] - 0s 1ms/step - loss: 1.4350e-04 - mae:
0.0092 - val_loss: 1.4410e-04 - val_mae: 0.0086
Epoch 30/300
105/105 [==============================] - 0s 1ms/step - loss: 2.3465e-04 - mae:
0.0117 - val_loss: 2.4588e-04 - val_mae: 0.0124
Epoch 31/300
105/105 [==============================] - 0s 1ms/step - loss: 1.7634e-04 - mae:
0.0103 - val_loss: 1.5679e-04 - val_mae: 0.0094
Epoch 32/300
105/105 [==============================] - 0s 1ms/step - loss: 1.6043e-04 - mae:
0.0098 - val_loss: 9.0875e-05 - val_mae: 0.0069
Epoch 33/300
105/105 [==============================] - 0s 1ms/step - loss: 1.5783e-04 - mae:
0.0095 - val_loss: 1.3686e-04 - val_mae: 0.0089
Epoch 34/300
105/105 [==============================] - 0s 1ms/step - loss: 1.3170e-04 - mae:
0.0088 - val_loss: 1.3743e-04 - val_mae: 0.0088
Epoch 35/300
105/105 [==============================] - 0s 1ms/step - loss: 2.7627e-04 - mae:
0.0129 - val_loss: 1.2390e-04 - val_mae: 0.0088
Epoch 36/300
105/105 [==============================] - 0s 1ms/step - loss: 1.9347e-04 - mae:
0.0108 - val_loss: 1.5565e-04 - val_mae: 0.0097
Epoch 37/300
 52/105 [=============>................] - ETA: 0s - loss: 1.3549e-04 - mae: 0.009
2Restoring model weights from the end of the best epoch: 17.
105/105 [==============================] - 0s 1ms/step - loss: 1.1437e-04 - mae:
0.0083 - val_loss: 8.8174e-05 - val_mae: 0.0067
Epoch 37: early stopping
```

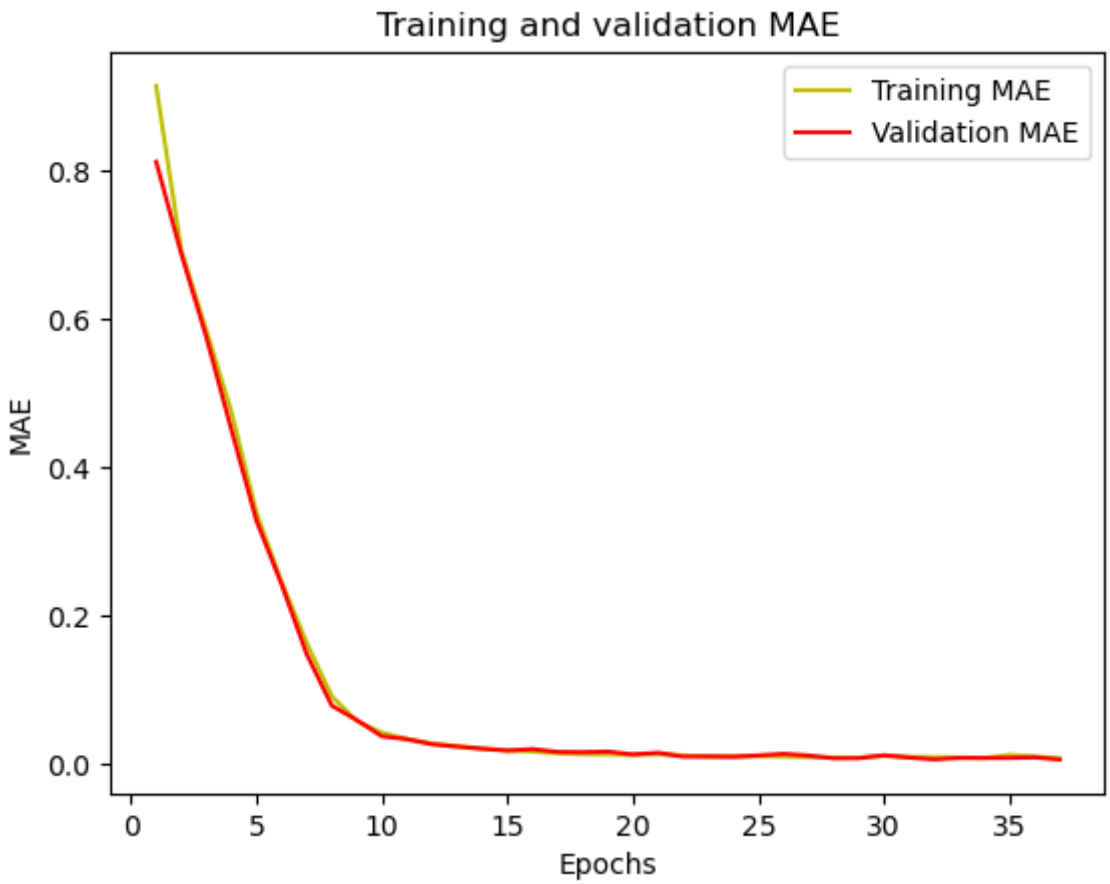
In [7]:

```
# plot the training and validation accuracy and loss at each epoch

loss = history.history['loss']
val_loss = history.history['val_loss']
epochs = range(1, len(loss) + 1)
plt.plot (epochs, loss, 'y', label = 'Training loss')
plt.plot (epochs, val_loss, 'r', label='Validation loss')
plt.title('Training and validation loss')
plt.xlabel ('Epochs')
plt.ylabel('Loss')
plt.legend()
plt.show()
```

```
acc = history.history['mae']
val_acc = history.history['val_mae']
plt.plot (epochs, acc, 'y', label = 'Training MAE')
plt.plot (epochs, val_acc, 'r', label='Validation MAE')
plt.title('Training and validation MAE')
plt.xlabel ('Epochs')
plt.ylabel('MAE')
plt.legend()
plt.show()
```





In [8]:
```
# Predict on test data

predictions = model.predict(X_test_scaled[:])
print("Predicted values are: ", predictions[:5])
print("Real values are: ", y_test[:5])
```

```
30/30 [==============================] - 0s 966us/step
Predicted values are:  [[0.55283284]
 [0.85236317]
 [2.6567783 ]
 [2.1674252 ]
 [0.19885041]]
Real values are:  [[0.563]
 [0.843]
 [2.685]
 [2.19 ]
 [0.2  ]]
```

In [9]:
```
testando = [1, 25.0, 60.0]
testando = np.array(testando)
testando= testando.reshape(1, -1)
testandonormalizado = scaler.transform(testando)

predictions2 = model.predict(testandonormalizado)
print("Predicted: ", predictions2)
print("Real value: Delta T max = 4,13°C")
```

```
1/1 [==============================] - 0s 16ms/step
Predicted:  [[4.279244]]
Real value: Delta T max = 4,13°C
```

```
C:\Users\Lenovo\anaconda3\lib\site-packages\sklearn\base.py:450: UserWarning: X do
es not have valid feature names, but MinMaxScaler was fitted with feature names
  warnings.warn(
```

In [30]:
```
# Runs model with its current weights on the training and testing data

y_train_pred = model.predict(X_train_scaled)
y_test_pred = model.predict(X_test_scaled)

# X_test - input de teste
# X_train - input de treino

# y_test_pred - output de teste previsto
# y test - output de teste real

# Calculates and prints r2 score of training and testing data
print('R2 score train:', r2_score(y_train, y_train_pred))
print('R2 score test:', r2_score(y_test, y_test_pred))
r2nn = r2_score(y_test, y_test_pred)
r2nn
```

```
117/117 [==============================] - 0s 1ms/step
30/30 [==============================] - 0s 1ms/step
R2 score train: 0.9997102862081199
R2 score test: 0.9996388616642997
```

Out[30]:
```
0.9996388616642997
```

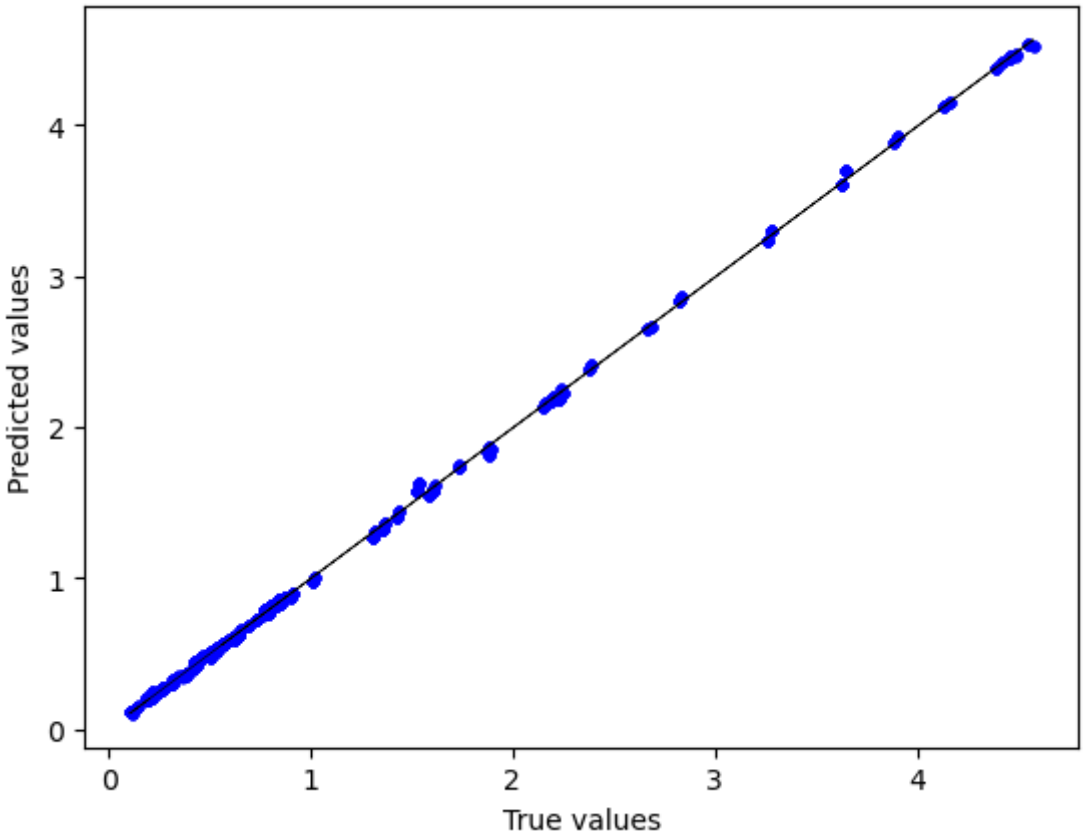
In [11]:
```
x = y_test.flatten()
y = y_test_pred.flatten()

#create scatterplot
plt.scatter(x, y, s=10, color='b')
plt.xlabel('True values')
plt.ylabel('Predicted values')

#calculate equation for trendline
z = np.polyfit(x, y, 1)
p = np.poly1d(z)

#add trendline to plot
plt.plot(x, p(x), color='k', linewidth=0.5)
```

Out[11]:
```
[<matplotlib.lines.Line2D at 0x1e460f86340>]
```



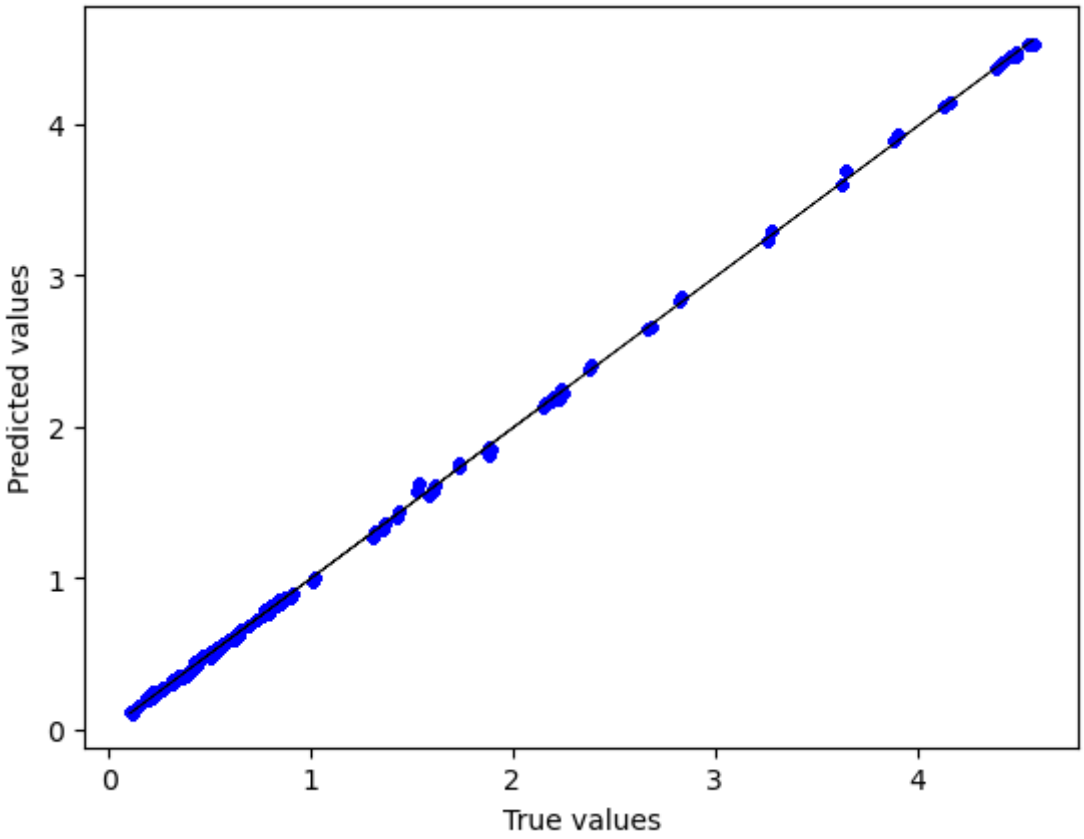
In [12]:
```
x = y_train.flatten()
y = y_train_pred.flatten()

#create scatterplot
plt.scatter(x, y, s=10, color='b')
plt.xlabel('True values')
plt.ylabel('Predicted values')

#calculate equation for trendline
z = np.polyfit(x, y, 1)
p = np.poly1d(z)

#add trendline to plot
plt.plot(x, p(x), color='k', linewidth=0.5)
```

Out[12]:
```
[<matplotlib.lines.Line2D at 0x1e460f5a160>]
```



In [13]:
```
# Comparison with other models
# Neural network - from the current code
from sklearn.metrics import mean_absolute_percentage_error
# outra forma de achar o MAPE com o sklearn: error = mean_absolute_percentage_erro


def mape(y_test, pred):
    y_test, pred = np.array(y_test), np.array(pred)
    mape = np.mean(np.abs((y_test - pred) / y_test))
    return mape


mse_neural, mae_neural = model.evaluate(X_test_scaled, y_test)
mapeNN = mape(y_test, y_test_pred)

print('Mean squared error from neural net: ', mse_neural)
print('Mean absolute error from neural net: ', mae_neural)
print('Mean absolute percentage error from neural net (MAPE): ', mapeNN)
rmse = np.sqrt(mse_neural)
rmse
```

```
30/30 [==============================] - 0s 1ms/step - loss: 5.4357e-04 - mae: 0.0
173
Mean squared error from neural net:  0.0005435676430352032
Mean absolute error from neural net:  0.01732705719769001
Mean absolute percentage error from neural net (MAPE):  0.020773875849882606
```

Out[13]:
```
0.023314537161076204
```

In [14]:
```
# O código da linha de cima também pode ser escrito assim:
from sklearn import metrics

#predict
pred = model.predict(X_test_scaled)
score = metrics.mean_squared_error(pred,y_test)
score
```

```
#quanto menor o mse, melhor
```

```
30/30 [==============================] - 0s 1ms/step
```

Out[14]:
```
0.0005435678846844039
```

In [15]:
```
testando = [1, 25.0, 60.0]
testando = np.array(testando)
testando= testando.reshape(1, -1)
testandonormalizado = scaler.fit_transform(testando)

predictions2 = model.predict(testandonormalizado)
print("Predicted: ", predictions2)
print("Real value: Delta T max = 4,13°C")
```

```
1/1 [==============================] - 0s 25ms/step
Predicted:  [[2.4143262]]
Real value: Delta T max = 4,13°C
```

In [16]:
```
model.save('Neural_Network-DeltaTmax')
```

```
WARNING:absl:Found untraced functions such as _update_step_xla while saving (showi
ng 1 of 1). These functions will not be directly callable after loading.
INFO:tensorflow:Assets written to: Neural_Network-DeltaTmax\assets
INFO:tensorflow:Assets written to: Neural_Network-DeltaTmax\assets
```

In [29]:
```
######################################################################
# Linear regression
from sklearn import linear_model
from sklearn.tree import DecisionTreeRegressor
from sklearn.metrics import mean_squared_error, mean_absolute_error

## Linear Regression
lr_model = linear_model.LinearRegression()
lr_model.fit(X_train_scaled, y_train)
y_pred_lr = lr_model.predict(X_test_scaled)
mse_lr = mean_squared_error(y_test, y_pred_lr)
mae_lr = mean_absolute_error(y_test, y_pred_lr)
print('Mean squared error from linear regression: ', mse_lr)
print('Mean absolute error from linear regression: ', mae_lr)
r2lr = r2_score(y_test, y_pred_lr)
print('R2 score test:', r2lr)

## Decision Tree
tree = DecisionTreeRegressor()
tree.fit(X_train_scaled, y_train)
y_pred_tree = tree.predict(X_test_scaled)
mse_dt = mean_squared_error(y_test, y_pred_tree)
mae_dt = mean_absolute_error(y_test, y_pred_tree)
print('Mean squared error from Decision Tree: ', mse_dt)
print('Mean absolute error from Decision Tree: ', mae_dt)
r2dt=r2_score(y_test, y_pred_tree)
print('R2 score test:', r2dt )
```

```
Mean squared error from linear regression:  0.9073041650691547
Mean absolute error from linear regression:  0.7713692057646364
R2 score test: 0.39720074460020005
Mean squared error from Decision Tree:  5.600929408386973e-31
Mean absolute error from Decision Tree:  4.720387760479513e-16
R2 score test: 1.0
```

In [32]:
```
# Síntese das análises

valores3 = ["NN", "LR", "DT"]
```

```
r2 = [r2nn, r2lr, r2dt]

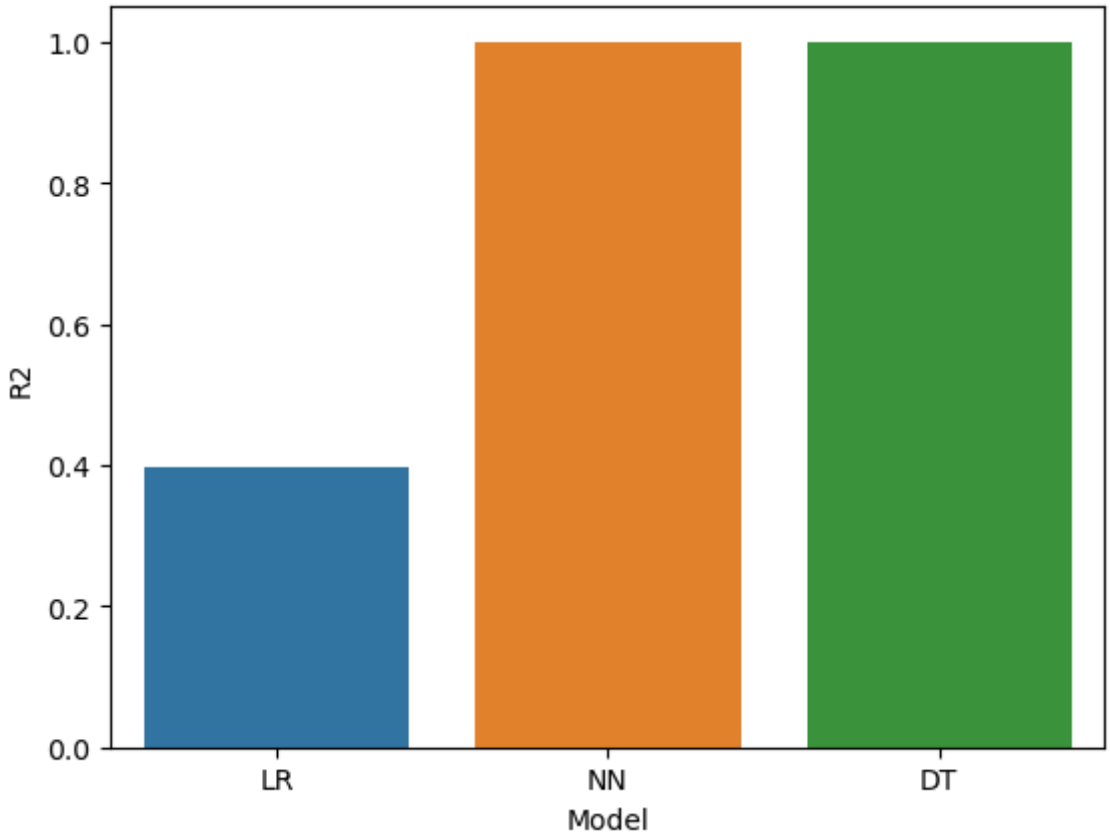
R2 = pd.DataFrame({"Model": valores3, "R2": r2})
R2
```

Out[32]:

	Model	R2
0	NN	0.999639
1	LR	0.397201
2	DT	1.000000

In [33]:
```
sns.barplot(x="Model", y="R2", data=R2, order = R2.sort_values("R2").Model)
```

Out[33]:
```
<AxesSubplot:xlabel='Model', ylabel='R2'>
```



In [23]:
```
# Síntese das análises

valores1 = ["NN", "LR", "DT"]
erros1 = [mse_neural, mse_lr, mse_dt]

MSE = pd.DataFrame({"Model": valores1, "Mean Squared Error - MSE": erros1})
MSE
```

Out[23]:

	Model	Mean Squared Error - MSE
0	NN	5.435676e-04
1	LR	9.073042e-01
2	DT	5.600929e-31

In [24]:
```
valores2 = ["NN", "LR", "DT"]
erros2 = [mae_neural, mae_lr, mae_dt]
```

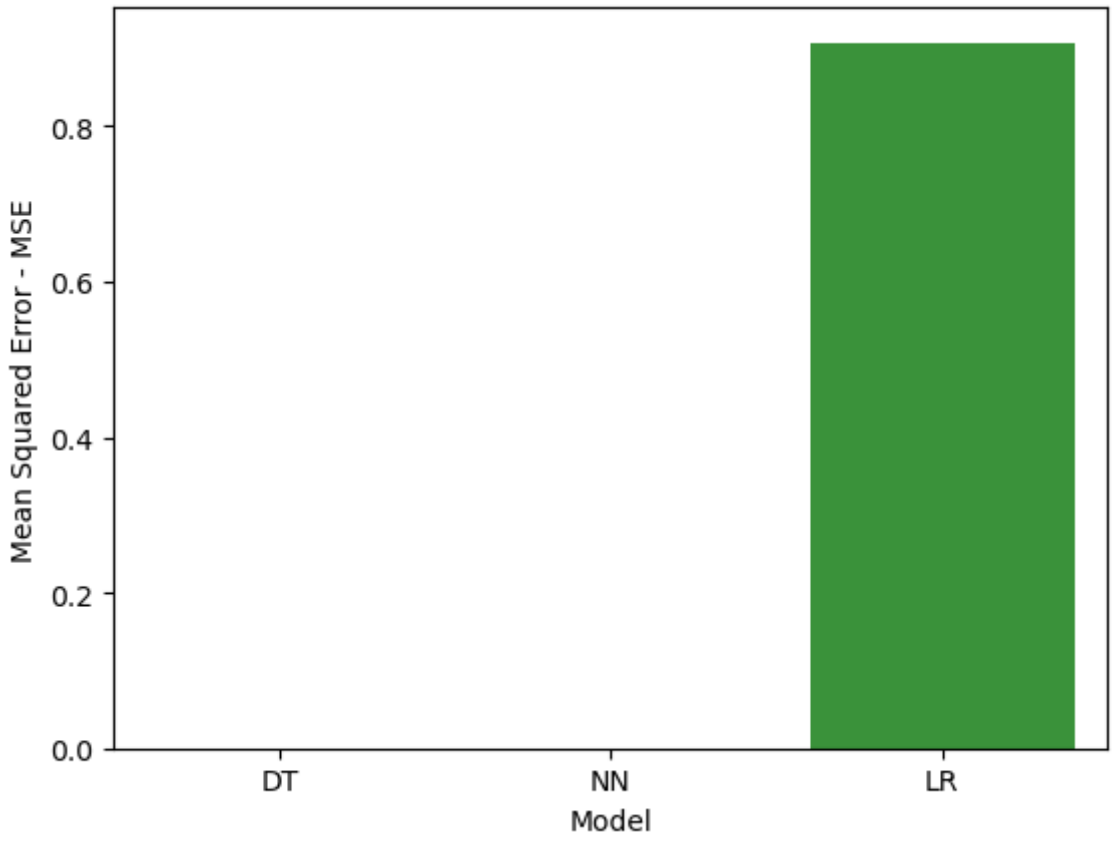
```
MAE = pd.DataFrame({"Model": valores2, "Mean Absolute Error - MAE": erros2})
MAE
```

Out[24]:

	Model	Mean Absolute Error - MAE
0	NN	1.732706e-02
1	LR	7.713692e-01
2	DT	4.720388e-16

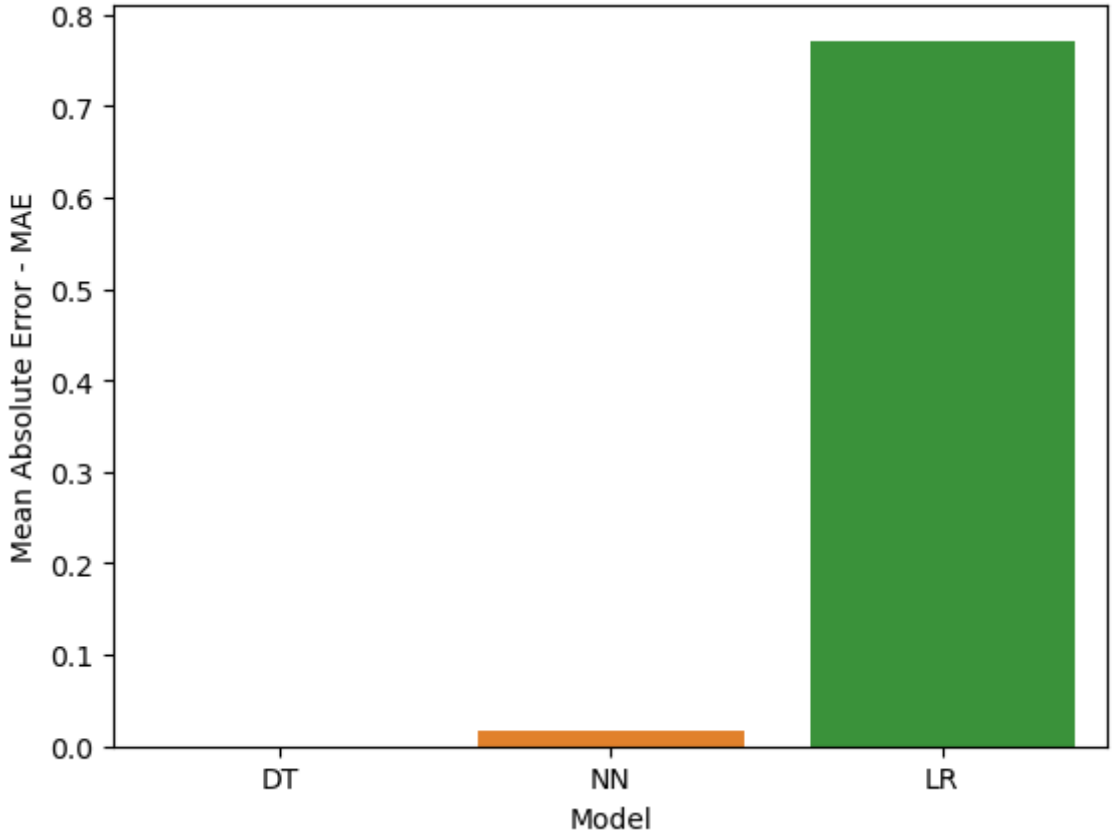
In [25]:
```
sns.barplot(x="Model", y="Mean Squared Error - MSE", data=MSE, order = MSE.sort_va
```

Out[25]:
```
<AxesSubplot:xlabel='Model', ylabel='Mean Squared Error - MSE'>
```



In [27]:
```
sns.barplot(x="Model", y="Mean Absolute Error - MAE", data=MAE, order = MAE.sort_v
```

Out[27]:
```
<AxesSubplot:xlabel='Model', ylabel='Mean Absolute Error - MAE'>
```



In [ ]:

In [ ]:

In [ ]:

APPENDIX 4 (b)

In [28]:

```
import numpy as np
import pandas as pd
import seaborn as sns
from matplotlib import pyplot as plt

df = pd.read_excel('datasetneuralnetworks.xlsx')
# VISUALIZAR A DISTRIBUIÇÃO DOS VALORES DE ΔTmax, Humidade, Teor de Humidade e ΔT PARA C
df
```

Out[28]:

	Material	Temperature [°C]	Relative Humidity [%]	Δtmax [°C]	ΔT [°C]	Humidity [kg/m³]
0	1	6.99619	53.7301	2.376	0.000000	237.600010
1	1	6.99619	53.7301	2.376	1.929128	233.649250
2	1	6.99619	53.7301	2.376	2.376436	221.900300
3	1	6.99619	53.7301	2.376	2.317941	164.249420
4	1	6.99619	53.7301	2.376	2.256899	145.193510
...	...	...	...	...	...	...
4641	4	19.59770	59.2467	0.376	0.046678	13.039567
4642	4	19.59770	59.2467	0.376	0.036932	11.091906
4643	4	19.59770	59.2467	0.376	0.027231	9.376396
4644	4	19.59770	59.2467	0.376	0.018430	8.182526
4645	4	19.59770	59.2467	0.376	0.010635	7.453972

4646 rows × 6 columns

In [29]:

```
from keras.models import Model
from keras.layers import Dense, Input
from keras.wrappers.scikit_learn import KerasRegressor
from sklearn.model_selection import cross_val_score
from sklearn.model_selection import KFold
from sklearn.pipeline import Pipeline
from sklearn.model_selection import train_test_split
from sklearn.metrics import r2_score
from tensorflow.keras.callbacks import EarlyStopping



# SEPARAR INPUTS DOS OUTPUTS

X = df.drop(['Δtmax [°C]', 'Humidity [kg/m³]'], axis=1)
y = df.drop(['Material', 'Temperature [°C]', 'Relative Humidity [%]', 'ΔT [°C]', 'Δtmax
y = y.values

# número de dados de treinamento
m = X.shape[0]

y.shape
```

Out[29]:

```
(4646, 1)
```

In [30]:

```
X_train, X_test, y_train, y_test = train_test_split(X, y, test_size = 0.15, random_state
```

In [31]:

```
# Scale data, otherwise model will fail
# Standardize features by removing the mean and scaling to unit variance
from sklearn.preprocessing import MinMaxScaler
scaler = MinMaxScaler()
scaler.fit(X)

X_train_scaled = scaler.transform(X_train)
X_test_scaled = scaler.transform(X_test)
X_train_scaled
```

Out[31]:

```
array([[0.        , 0.37472074, 0.44893621, 0.35104862],
       [0.33333333, 0.28831427, 0.71788519, 0.03846545],
       [0.33333333, 0.69024388, 0.71333883, 0.06378299],
       ...,
       [0.66666667, 0.35558569, 0.42422863, 0.42431433],
       [1.        , 1.        , 0.26969637, 0.01132252],
       [0.        , 0.18888058, 0.26118552, 0.30565923]])
```

In [32]:

```
# Define the model
# Experiment with deeper and wider networks

#Start defining the input tensor:
inpTensor = Input(shape= (4,))

#create the layers and pass them the input tensor to get the output tensor:
hidden1Out = Dense(128, activation='relu')(inpTensor)
hidden2Out = Dense(64, activation='relu')(hidden1Out)
hidden3Out = Dense(64, activation='relu')(hidden2Out)
finalOut = Dense(1, activation='relu')(hidden3Out)

#define the model's start and end points
model = Model(inpTensor,finalOut)


model.summary()
model.compile(loss='mean_squared_error', optimizer='adam', metrics=['mae'])
```

```
Model: "model_2"
_________________________________________________________________
 Layer (type)                Output Shape              Param #
=================================================================
 input_3 (InputLayer)        [(None, 4)]               0

 dense_8 (Dense)             (None, 128)               640

 dense_9 (Dense)             (None, 64)                8256

 dense_10 (Dense)            (None, 64)                4160

 dense_11 (Dense)            (None, 1)                 65

=================================================================
Total params: 13,121
Trainable params: 13,121
Non-trainable params: 0
_________________________________________________________________
```

In [33]:

```
monitor = EarlyStopping(monitor='val_loss', min_delta=1e-3, patience=40, verbose=1, rest

history = model.fit(X_train_scaled, y_train, validation_split=0.1, epochs=1000, callback
```

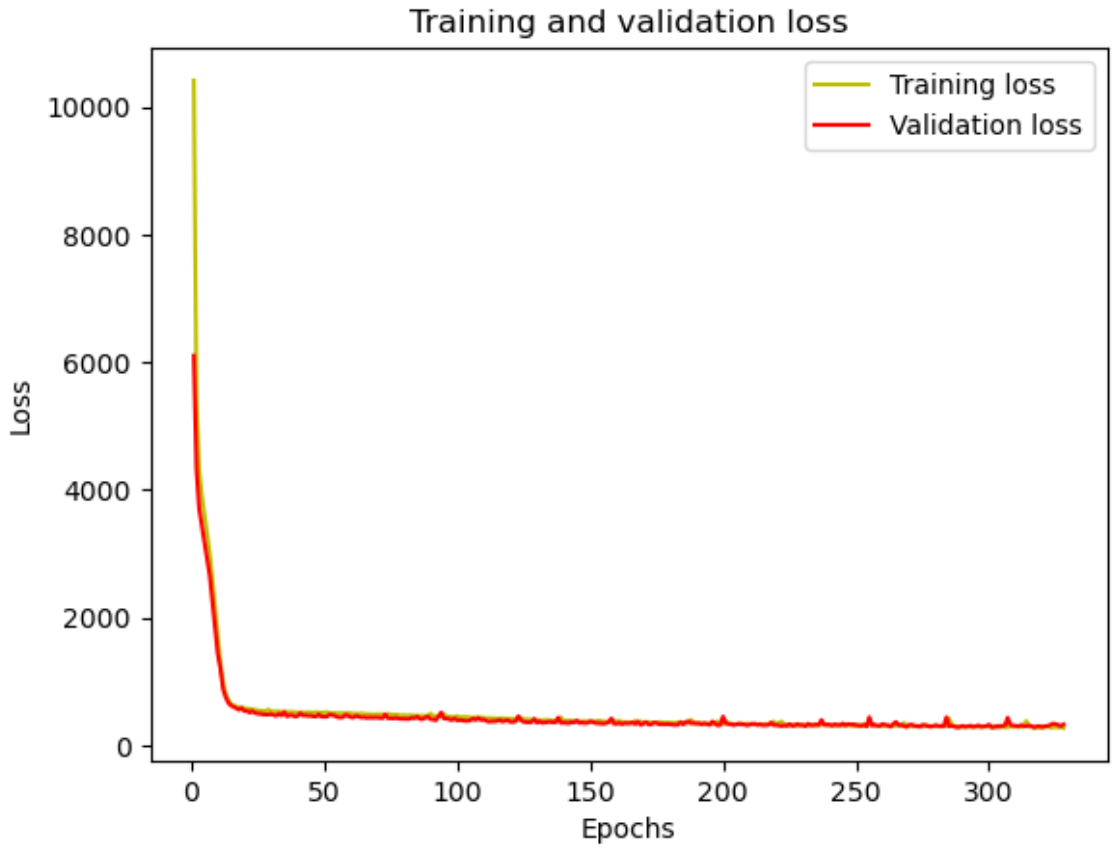
```
Epoch 1/1000
112/112 [==============================] - 1s 2ms/step - loss: 10413.1
172 - mae: 77.6611 - val_loss: 6102.2847 - val_mae: 67.7821
Epoch 2/1000
112/112 [==============================] - 0s 1ms/step - loss: 5452.87
21 - mae: 61.4057 - val_loss: 4333.9805 - val_mae: 54.7417
Epoch 3/1000
112/112 [==============================] - 0s 1ms/step - loss: 4337.26
07 - mae: 52.2654 - val_loss: 3708.4016 - val_mae: 48.2892
Epoch 4/1000
112/112 [==============================] - 0s 1ms/step - loss: 3913.87
38 - mae: 48.6892 - val_loss: 3449.5723 - val_mae: 43.5152
Epoch 5/1000
112/112 [==============================] - 0s 1ms/step - loss: 3614.54
44 - mae: 46.4400 - val_loss: 3171.5344 - val_mae: 43.7014
Epoch 6/1000
112/112 [==============================] - 0s 1ms/step - loss: 3320.80
52 - mae: 44.3718 - val_loss: 2936.4243 - val_mae: 41.3052
Epoch 7/1000
```

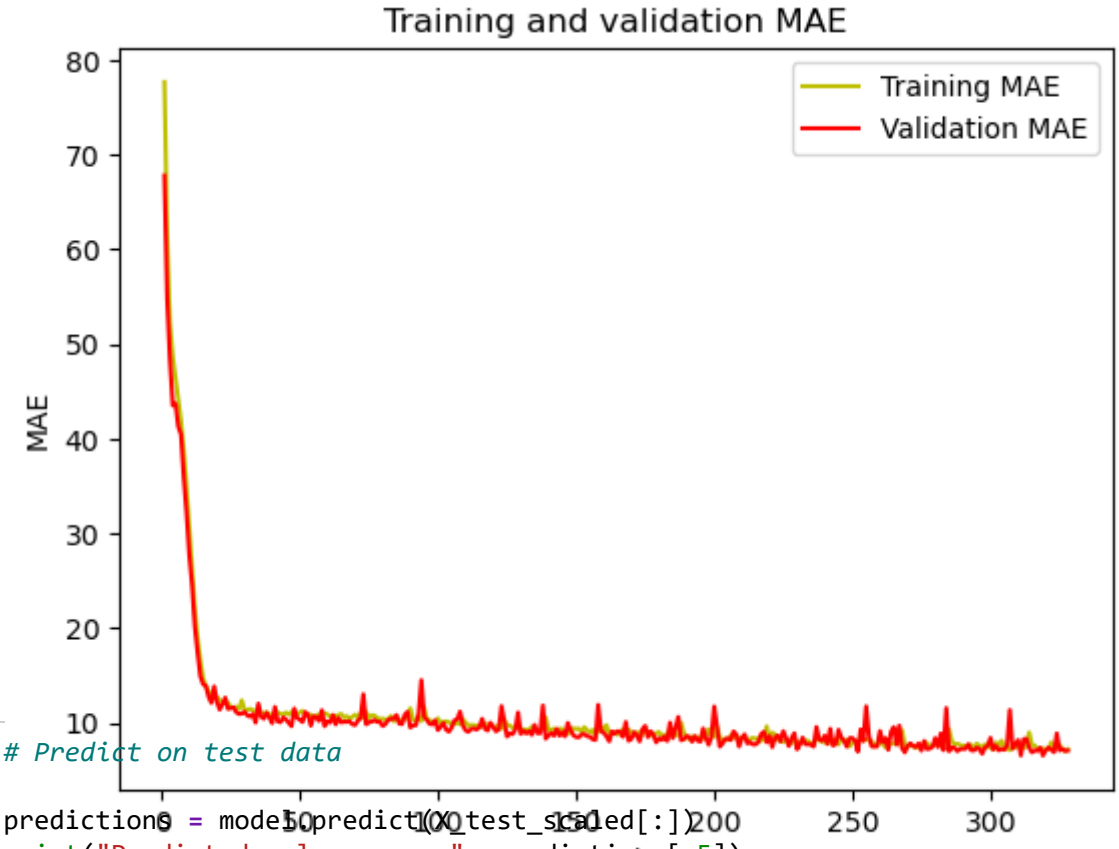
In [34]:

```
# plot the training and validation accuracy and loss at each epoch

loss = history.history['loss']
val_loss = history.history['val_loss']
epochs = range(1, len(loss) + 1)
plt.plot (epochs, loss, 'y', label = 'Training loss')
plt.plot (epochs, val_loss, 'r', label='Validation loss')
plt.title('Training and validation loss')
plt.xlabel ('Epochs')
plt.ylabel('Loss')
plt.legend()
plt.show()

acc = history.history['mae']
val_acc = history.history['val_mae']
plt.plot (epochs, acc, 'y', label = 'Training MAE')
plt.plot (epochs, val_acc, 'r', label='Validation MAE')
plt.title('Training and validation MAE')
plt.xlabel ('Epochs')
plt.ylabel('MAE')
plt.legend()
plt.show()
```






```
# Predict on test data

predictions = model.predict(X_test_scaled[:])
print("Predicted values are: ", predictions[:5])
print("Real values are: ", y_test[:5])
```

```
22/22 [==============================] - 0s 736us/step
Predicted values are:  [[172.97395 ]
 [137.71976 ]
 [ 24.86063 ]
 [ 93.2783  ]
 [ 27.421652]]
Real values are:  [[158.40907 ]
 [217.8     ]
 [ 26.267578]
 [ 93.826157]
 [ 28.193808]]
```

In [36]:

```
testando = [1, 25.0, 60.0, 2.0]
testando = np.array(testando)
testando= testando.reshape(1, -1)
testandonormalizado = scaler.transform(testando)

predictions2 = model.predict(testandonormalizado)
print("Predicted: ", predictions2)
print("Real value: Humidade = 110,27 kg/m³")
```

```
1/1 [==============================] - 0s 17ms/step
Predicted:  [[108.72738]]
Real value: Humidade = 110,27 kg/m³

C:\Users\Lenovo\anaconda3\lib\site-packages\sklearn\base.py:450: UserWarn
ing: X does not have valid feature names, but MinMaxScaler was fitted wit
h feature names
  warnings.warn(
```

In [37]:

```
# Runs model with its current weights on the training and testing data

y_train_pred = model.predict(X_train_scaled)
y_test_pred = model.predict(X_test_scaled)

# X_test - input de teste
# X_train - input de treino

# y_test_pred - output de teste previsto
# y test - output de teste real

r2nn = r2_score(y_test, y_test_pred)

# Calculates and prints r2 score of training and testing data
print('R2 score train:', r2_score(y_train, y_train_pred))
print('R2 score test:', r2_score(y_test, y_test_pred))
```

```
124/124 [==============================] - 0s 642us/step
22/22 [==============================] - 0s 797us/step
R2 score train: 0.9542800062392629
R2 score test: 0.9471472730735905
```

In [38]:

```
x = y_train.flatten()
y = y_train_pred.flatten()

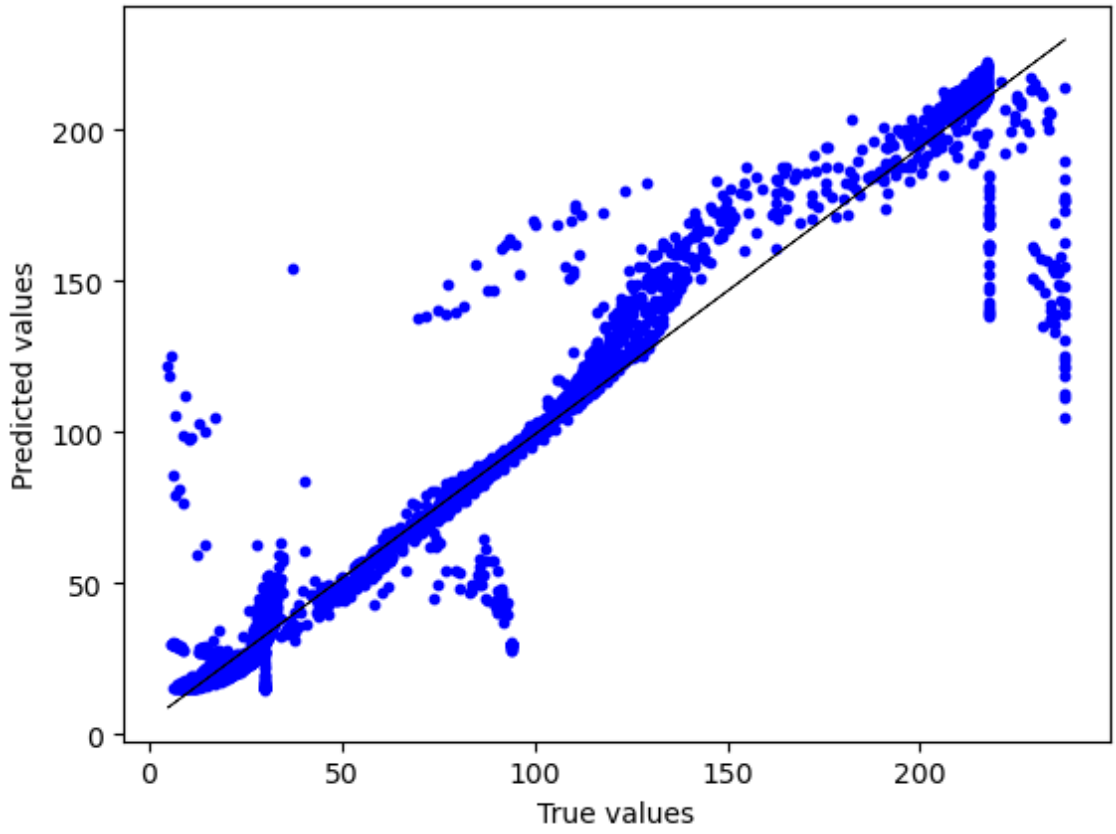
#create scatterplot
plt.scatter(x, y, s=10, color='b')
plt.xlabel('True values')
plt.ylabel('Predicted values')

#calculate equation for trendline
z = np.polyfit(x, y, 1)
p = np.poly1d(z)

#add trendline to plot
plt.plot(x, p(x), color='k', linewidth=0.5)
```

Out[38]:

```
[<matplotlib.lines.Line2D at 0x14564628fa0>]
```



In [39]:

```
x = y_test.flatten()
y = y_test_pred.flatten()

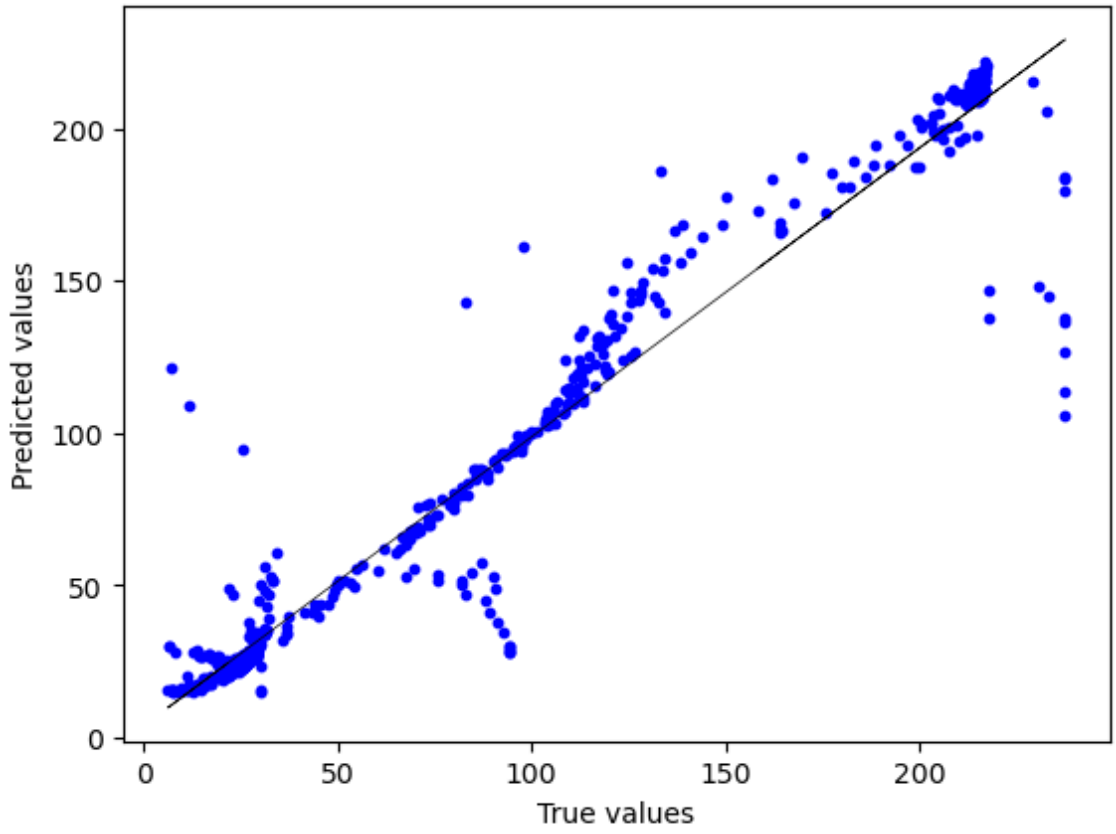
#create scatterplot
plt.scatter(x, y, s=10, color='b')
plt.xlabel('True values')
plt.ylabel('Predicted values')

#calculate equation for trendline
z = np.polyfit(x, y, 1)
p = np.poly1d(z)

#add trendline to plot
plt.plot(x, p(x), color='k', linewidth=0.5)
```

Out[39]:

```
[<matplotlib.lines.Line2D at 0x14564676490>]
```



In [40]:

```
# Comparison with other models
# Neural network - from the current code
from sklearn.metrics import mean_absolute_percentage_error
# outra forma de achar o MAPE com o sklearn: error = mean_absolute_percentage_error(y_te


def mape(y_test, pred):
    y_test, pred = np.array(y_test), np.array(pred)
    mape = np.mean(np.abs((y_test - pred) / y_test))
    return mape


mse_neural, mae_neural = model.evaluate(X_test_scaled, y_test)
mapeNN = mape(y_test, y_test_pred)

print('Mean squared error from neural net: ', mse_neural)
print('Mean absolute error from neural net: ', mae_neural)
print('Mean absolute percentage error from neural net (MAPE): ', mapeNN)
rmse = np.sqrt(mse_neural)
rmse
```

```
22/22 [==============================] - 0s 812us/step - loss: 299.9532 -
mae: 6.9852
Mean squared error from neural net:  299.95318603515625
Mean absolute error from neural net:  6.9851861000061035
Mean absolute percentage error from neural net (MAPE):  0.161551190963421
33
```

Out[40]:

```
17.319156620204005
```

In [41]:

```
# O código da linha de cima também pode ser escrito assim:
from sklearn import metrics

#predict
pred = model.predict(X_test_scaled)
score = metrics.mean_squared_error(pred,y_test)
score

#quanto menor o mse, melhor
```

```
22/22 [==============================] - 0s 527us/step
```

Out[41]:

```
299.95321693775105
```

In [42]:

```
# CROSS VALIDATION
#define the number of folds for cross-validation
num_folds=3

#create the KFold object with the specified number of folds

kf = KFold(n_splits=num_folds, shuffle=True, random_state=42)

performance_mse = []
performance_mae = []

#Loop over each fold and train the model

for fold, (train_index, val_index) in enumerate(kf.split(X_train_scaled, y_train)):
    print(f"Fold: {fold+1}")

    #split the data into training and validation sets for this fold
    X_train_fold, X_val_fold = X_train_scaled[train_index], X_train_scaled[val_index]
    y_train_fold, y_val_fold = y_train[train_index], y_train[val_index]

    #compile and fit the Keras model on the training data for this fold
    model.compile(loss='mean_squared_error', optimizer='adam', metrics=['mae'])
    model.fit(X_train_fold, y_train_fold, epochs=300, batch_size=32, verbose=0)

    #evaluate the model on the validation data for this fold
    mse_neural, mae_neural = model.evaluate(X_val_fold, y_val_fold, verbose=0)
    print(f"Validation loss: {mse_neural}, Validation mae: {mae_neural}")
    performance_mse.append (mse_neural)
    performance_mae.append(mae_neural)
print(performance_mse)
print(performance_mae)

def average(x):
    return sum(x) / len(x)

average_mse = average(performance_mse)
average_mae = average(performance_mae)
print (f"Average loss = {average_mse}")
print (f"Average mae = {average_mae}")
```

```
Fold: 1
Validation loss: 375.2769470214844, Validation mae: 6.9731621742248535
Fold: 2
Validation loss: 268.68621826171875, Validation mae: 6.797024250030518
Fold: 3
Validation loss: 350.0904235839844, Validation mae: 5.90806245803833
[375.2769470214844, 268.68621826171875, 350.0904235839844]
[6.9731621742248535, 6.797024250030518, 5.90806245803833]
Average loss = 331.3511962890625
Average mae = 6.5594162940979
```

In [ ]:

```
#model.save('Neural_Network-Humidity')
```

In [39]:

```
#####################################################################
# Linear regression
from sklearn import linear_model
from sklearn.tree import DecisionTreeRegressor
from sklearn.metrics import mean_squared_error, mean_absolute_error, mean_absolute_perce

def mape(y_test, pred):
    y_test, pred = np.array(y_test), np.array(pred)
    mape = np.mean(np.abs((y_test - pred) / y_test))
    return mape


## Linear Regression
lr_model = linear_model.LinearRegression()
lr_model.fit(X_train_scaled, y_train)
y_pred_lr = lr_model.predict(X_test_scaled)
mse_lr = mean_squared_error(y_test, y_pred_lr)
mae_lr = mean_absolute_error(y_test, y_pred_lr)
mape_lr = mean_absolute_percentage_error(y_test, y_pred_lr)

print('Mean squared error from linear regression: ', mse_lr)
print('Mean absolute error from linear regression: ', mae_lr)
print ('MAPE LR: ', mape_lr)
r2lr = r2_score(y_test, y_pred_lr)
print('R2 score test:', r2lr)
```

```
Mean squared error from linear regression:  3745.0028008914387
Mean absolute error from linear regression:  48.16810187045629
MAPE LR:  1.0283193287175565
R2 score test: 0.3428575430712575
```

In [35]:

```
## Decision Tree
tree = DecisionTreeRegressor()
tree.fit(X_train_scaled, y_train)
y_pred_tree = tree.predict(X_test_scaled)
mse_dt = mean_squared_error(y_test, y_pred_tree)
mae_dt = mean_absolute_error(y_test, y_pred_tree)
print('Mean squared error from Decision Tree: ', mse_dt)
print('Mean absolute error from Decision Tree: ', mae_dt)
mape_tree = mean_absolute_percentage_error(y_test, y_pred_tree)
print ('MAPE Decision Tree: ', mape_tree)
r2dt=r2_score(y_test, y_pred_tree)
print('R2 score test:', r2dt )
```

```
Mean squared error from Decision Tree:  336.80651587864554
Mean absolute error from Decision Tree:  5.417754178870969
MAPE Decision Tree:  0.12437585969262024
R2 score test: 0.9408999477112758
```

In [45]:

```
# Síntese das análises

valores3 = ["NN", "LR", "DT"]
r2 = [r2nn, r2lr, r2dt]

R2 = pd.DataFrame({"Model": valores1, "R2": r2})
R2
```

Out[45]:

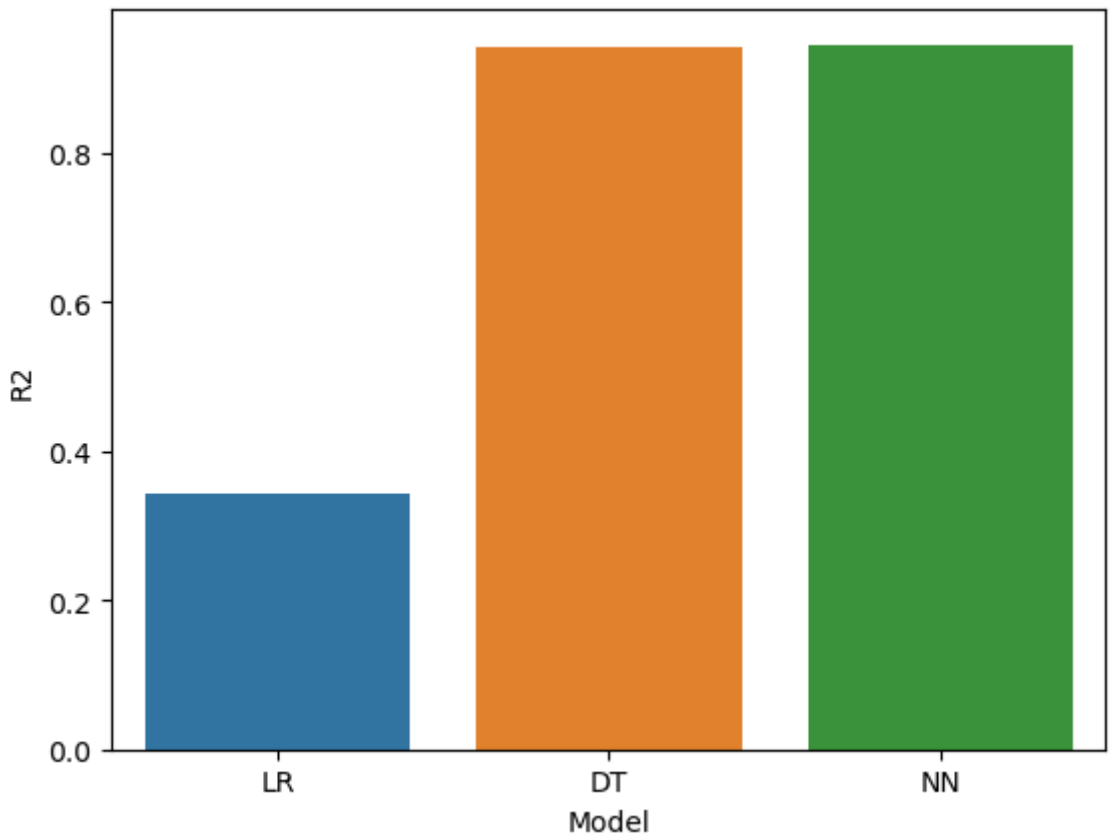
	Model	R2
0	NN	0.944772
1	LR	0.342858
2	DT	0.940900

In [48]:

```
sns.barplot(x="Model", y="R2", data=R2, order = R2.sort_values("R2").Model)
```

Out[48]:

```
<AxesSubplot:xlabel='Model', ylabel='R2'>
```



In [28]:

```
# Síntese das análises

valores1 = ["NN", "LR", "DT"]
erros1 = [mse_neural, mse_lr, mse_dt]

MSE = pd.DataFrame({"Modelo": valores1, "Mean Squared Error - MSE": erros1})
MSE
```

Out[28]:

	Modelo	Mean Squared Error - MSE
0	NN	314.739136
1	LR	3745.002801
2	DT	340.515701

In [29]:

```
valores2 = ["NN", "LR", "DT"]
erros2 = [mae_neural, mae_lr, mae_dt]

MAE = pd.DataFrame({"Modelo": valores2, "Mean Absolute Error - MAE": erros2})
MAE
```

Out[29]:

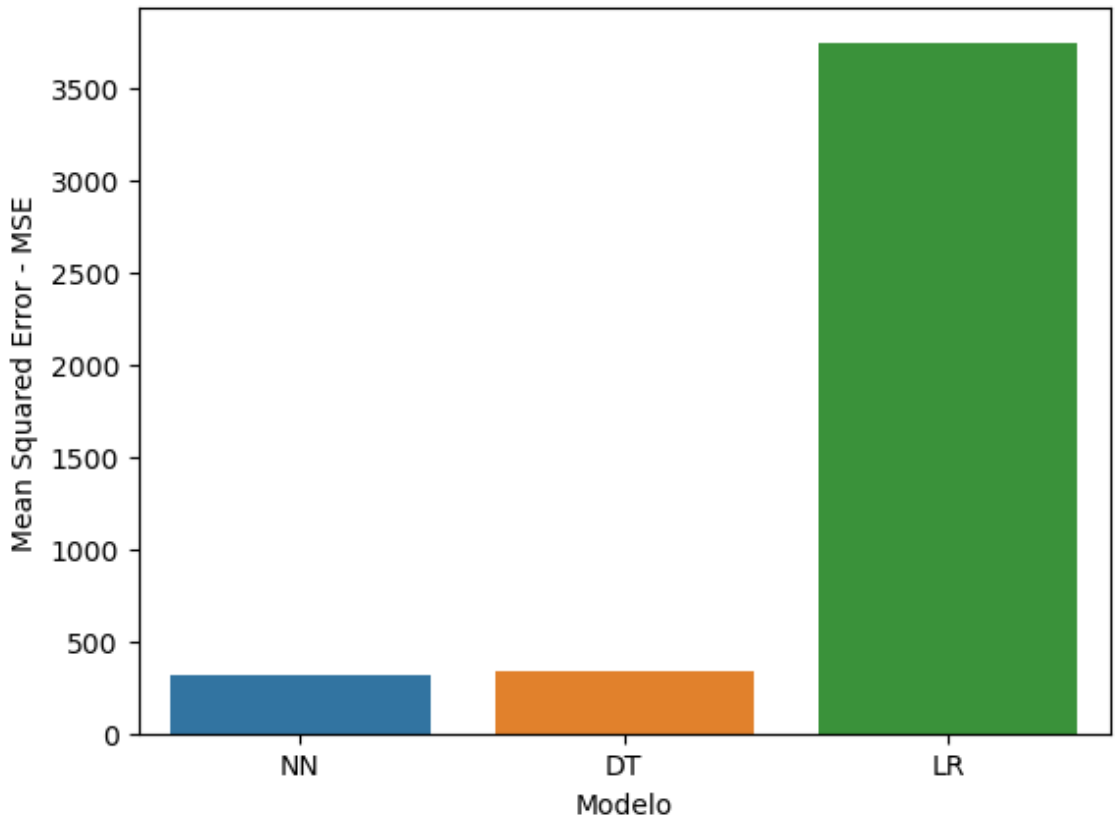
	Modelo	Mean Absolute Error - MAE
0	NN	7.362904
1	LR	48.168102
2	DT	5.436056

In [30]:

```
sns.barplot(x="Modelo", y="Mean Squared Error - MSE", data=MSE, order = MSE.sort_values(
```

Out[30]:

```
<AxesSubplot:xlabel='Modelo', ylabel='Mean Squared Error - MSE'>
```

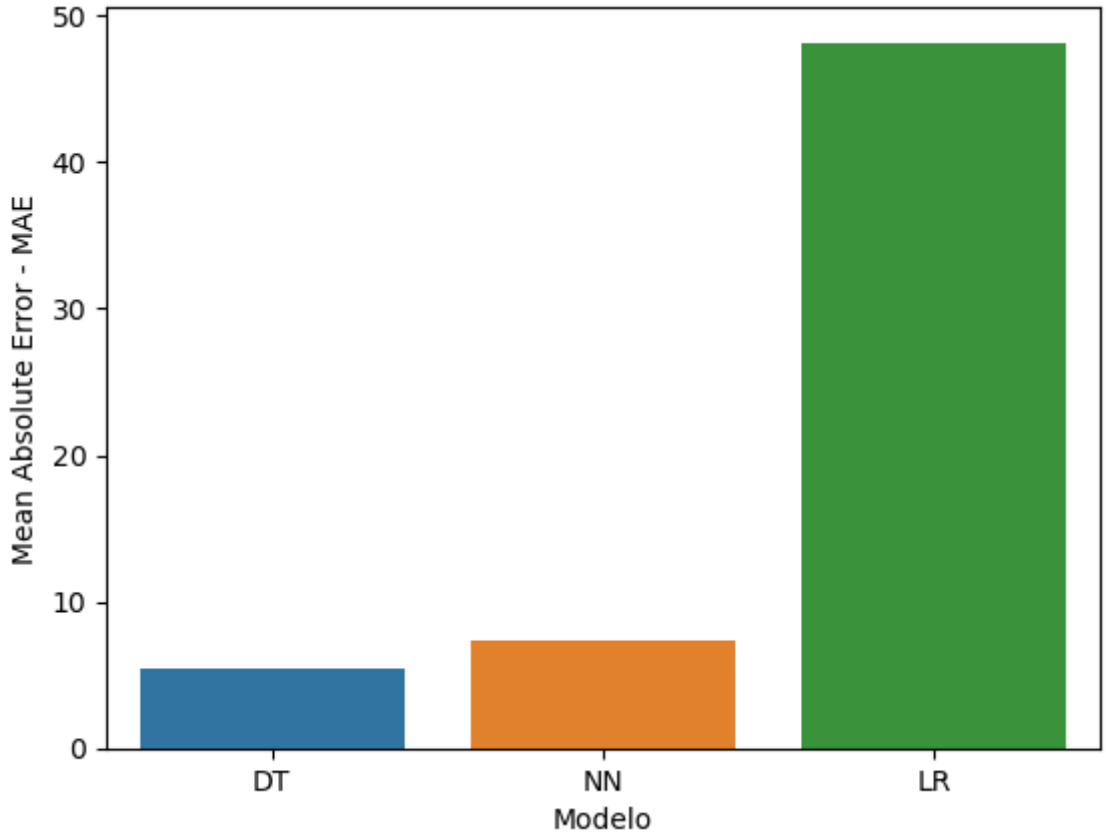


In [31]:

```
sns.barplot(x="Modelo", y="Mean Absolute Error - MAE", data=MAE, order = MAE.sort_values
```

Out[31]:

```
<AxesSubplot:xlabel='Modelo', ylabel='Mean Absolute Error - MAE'>
```



In [ ]:

In [ ]:

In [ ]:

In [1]:
```
import numpy as np
import pandas as pd
import seaborn as sns
from matplotlib import pyplot as plt

df = pd.read_excel('datasetneuralnetworksnoinitialvalues.xlsx')
# VISUALIZAR A DISTRIBUIÇÃO DOS VALORES DE ΔTmax, Humidade, Teor de Humidade e
df
```

Out[1]:

	Material	Temperature [°C]	Relative Humidity [%]	Δtmax [°C]	ΔT [°C]	Humidity [kg/m³]
0	1	6.99619	53.7301	2.376	2.376436	221.900300
1	1	6.99619	53.7301	2.376	2.317941	164.249420
2	1	6.99619	53.7301	2.376	2.256899	145.193510
3	1	6.99619	53.7301	2.376	2.198631	137.497590
4	1	6.99619	53.7301	2.376	2.136100	133.033080
...	...	...	...	...	...	...
4431	4	19.59770	59.2467	0.376	0.046678	13.039567
4432	4	19.59770	59.2467	0.376	0.036932	11.091906
4433	4	19.59770	59.2467	0.376	0.027231	9.376396
4434	4	19.59770	59.2467	0.376	0.018430	8.182526
4435	4	19.59770	59.2467	0.376	0.010635	7.453972

4436 rows × 6 columns

In [2]:
```
from keras.models import Model
from keras.layers import Dense, Input
from keras.wrappers.scikit_learn import KerasRegressor
from sklearn.model_selection import cross_val_score
from sklearn.model_selection import KFold
from sklearn.pipeline import Pipeline
from sklearn.model_selection import train_test_split
from sklearn.metrics import r2_score
from tensorflow.keras.callbacks import EarlyStopping


# SEPARAR INPUTS DOS OUTPUTS

X = df.drop(['Δtmax [°C]', 'Humidity [kg/m³]'], axis=1)
y = df.drop(['Material', 'Temperature [°C]', 'Relative Humidity [%]', 'ΔT [°C
y = y.values

# número de dados de treinamento
m = X.shape[0]

y.shape
```

Out[2]:
```
(4436, 1)
```

In [3]:
```
X_train, X_test, y_train, y_test = train_test_split(X, y, test_size = 0.2, ra
```

In [4]:
```
# Scale data, otherwise model will fail
# Standardize features by removing the mean and scaling to unit variance
from sklearn.preprocessing import MinMaxScaler
scaler = MinMaxScaler()
scaler.fit(X)

X_train_scaled = scaler.transform(X_train)
X_test_scaled = scaler.transform(X_test)
X_train_scaled[3540:3548]
```

Out[4]:
```
array([[0.66666667, 0.28831427, 0.71788519, 0.04470042],
       [0.66666667, 0.1177863 , 0.49563079, 0.21905523],
       [1.        , 0.59942642, 0.36844133, 0.01389536],
       [1.        , 0.74568513, 0.22977736, 0.02066164],
       [0.        , 0.03902761, 0.95329249, 0.03877459],
       [0.66666667, 0.69024388, 0.71333883, 0.39267308],
       [1.        , 0.82436589, 0.54516749, 0.05618227],
       [0.        , 0.35558569, 0.42422863, 0.27262105]])
```

In [5]:
```
# Define the model
# Experiment with deeper and wider networks

#Start defining the input tensor:
inpTensor = Input(shape= (4,))

#create the layers and pass them the input tensor to get the output tensor:
hidden1Out = Dense(128, activation='relu')(inpTensor)
hidden2Out = Dense(64, activation='relu')(hidden1Out)
hidden3Out = Dense(64, activation='relu')(hidden2Out)
finalOut = Dense(1, activation='relu')(hidden3Out)

#define the model's start and end points
model = Model(inpTensor,finalOut)


model.summary()
model.compile(loss='mean_squared_error', optimizer='adam', metrics=['mae'])
```

```
Model: "model"
_________________________________________________________________
 Layer (type)                Output Shape              Param #
=================================================================
 input_1 (InputLayer)        [(None, 4)]               0

 dense (Dense)               (None, 128)               640

 dense_1 (Dense)             (None, 64)                8256

 dense_2 (Dense)             (None, 64)                4160

 dense_3 (Dense)             (None, 1)                 65

=================================================================
Total params: 13,121
Trainable params: 13,121
Non-trainable params: 0
_________________________________________________________________
```

In [6]:
```
# Apply the EarlyStopping function to prevent overfitting
# Train the model

monitor = EarlyStopping(monitor='val_loss', min_delta=1e-3, patience=20, verb

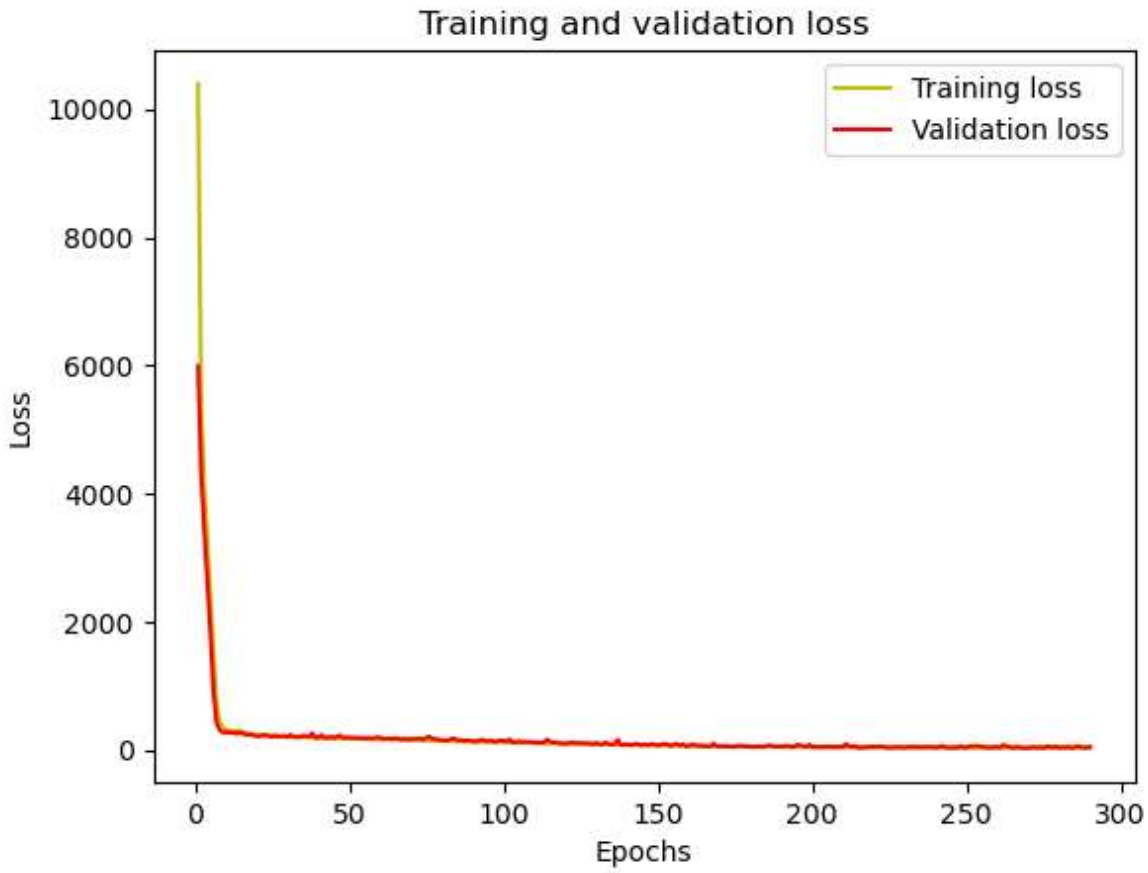
history = model.fit(X_train_scaled, y_train, validation_split=0.1, epochs=500
```

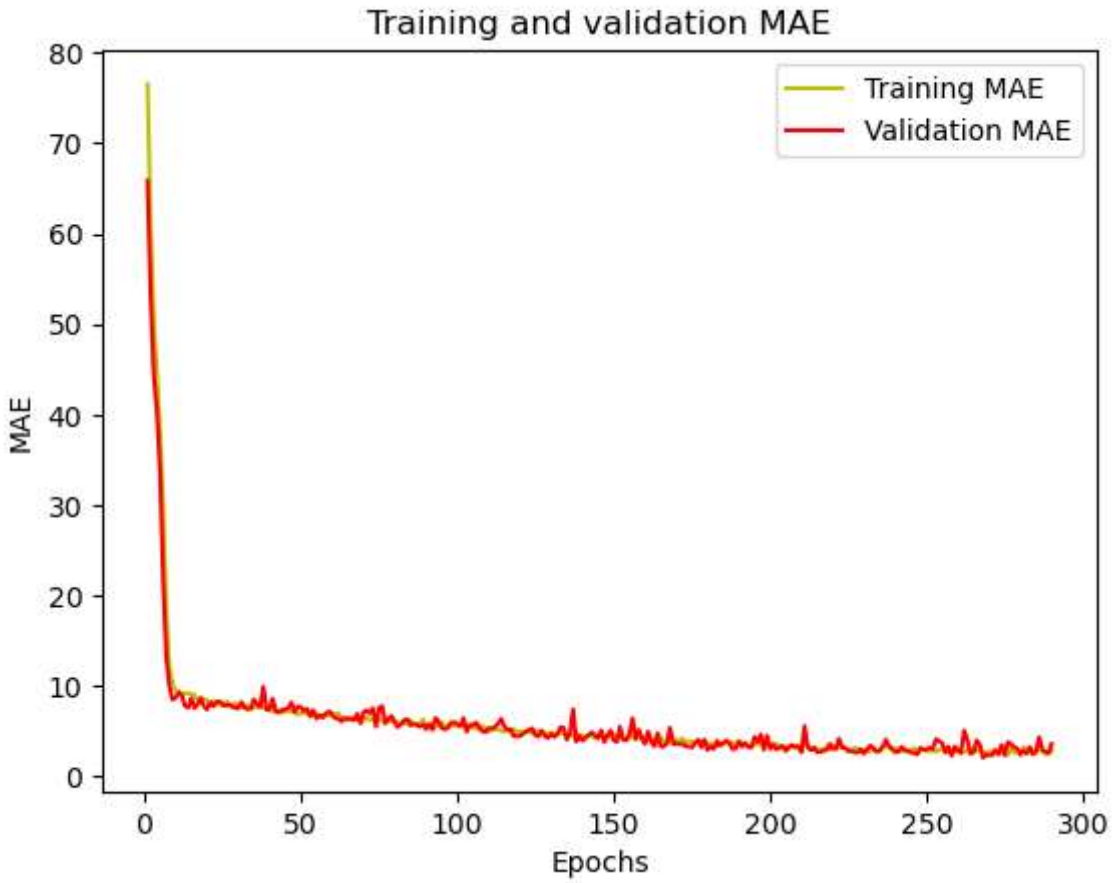
```
Epoch 1/500
100/100 [==============================] - 1s 4ms/step - loss: 10394.0703
- mae: 76.5536 - val_loss: 5987.9951 - val_mae: 65.8683
Epoch 2/500
100/100 [==============================] - 0s 2ms/step - loss: 5391.7251
- mae: 60.8128 - val_loss: 4298.4561 - val_mae: 53.0016
Epoch 3/500
100/100 [==============================] - 0s 2ms/step - loss: 4116.3042
- mae: 50.4960 - val_loss: 3439.9019 - val_mae: 44.3449
Epoch 4/500
100/100 [==============================] - 0s 2ms/step - loss: 3305.8574
- mae: 44.5081 - val_loss: 2647.0122 - val_mae: 40.3623
Epoch 5/500
100/100 [==============================] - 0s 2ms/step - loss: 2451.6780
- mae: 38.4266 - val_loss: 1831.9553 - val_mae: 33.8764
Epoch 6/500
100/100 [==============================] - 0s 2ms/step - loss: 1535.7931
- mae: 29.8232 - val_loss: 900.7150 - val_mae: 21.5721
Epoch 7/500
```

In [7]:
```
# plot the training and validation accuracy and loss at each epoch

loss = history.history['loss']
val_loss = history.history['val_loss']
epochs = range(1, len(loss) + 1)
plt.plot (epochs, loss, 'y', label = 'Training loss')
plt.plot (epochs, val_loss, 'r', label='Validation loss')
plt.title('Training and validation loss')
plt.xlabel ('Epochs')
plt.ylabel('Loss')
plt.legend()
plt.show()

acc = history.history['mae']
val_acc = history.history['val_mae']
plt.plot (epochs, acc, 'y', label = 'Training MAE')
plt.plot (epochs, val_acc, 'r', label='Validation MAE')
plt.title('Training and validation MAE')
plt.xlabel ('Epochs')
plt.ylabel('MAE')
plt.legend()
plt.show()
```





In [8]:
```
# Predict on test data

predictions = model.predict(X_test_scaled[:])
print("Predicted values are: ", predictions[:5])
print("Real values are: ", y_test[:5])
```

```
28/28 [==============================] - 0s 1ms/step
Predicted values are:  [[ 26.972477]
 [ 81.040215]
 [ 27.12572 ]
 [ 28.001616]
 [181.55351 ]]
Real values are:  [[ 27.578331]
 [ 81.648003]
 [ 28.762997]
 [ 28.67828 ]
 [167.63528 ]]
```

In [9]:
```
# Predict on new data
testando = [1, 25.0, 60.0, 2.0]
testando = np.array(testando)
testando= testando.reshape(1, -1)
testandonormalizado = scaler.transform(testando)

predictions2 = model.predict(testandonormalizado)
print("Predicted: ", predictions2)
print("Real value: Humidade = 110,27 kg/m³")
```

```
1/1 [==============================] - 0s 24ms/step
Predicted:  [[110.34043]]
Real value: Humidade = 110,27 kg/m³

C:\Users\Lenovo\anaconda3\lib\site-packages\sklearn\base.py:450: UserWarnin
g: X does not have valid feature names, but MinMaxScaler was fitted with fea
ture names
  warnings.warn(
```

In [38]:
```
# Runs model with its current weights on the training and testing data

y_train_pred = model.predict(X_train_scaled)
y_test_pred = model.predict(X_test_scaled)

# X_test - input de teste
# X_train - input de treino

# y_test_pred - output de teste previsto
# y test - output de teste real

# Calculates and prints r2 score of training and testing data
print('R2 score train:', r2_score(y_train, y_train_pred))
print('R2 score test:', r2_score(y_test, y_test_pred))

r2nn = r2_score(y_test, y_test_pred)
r2nn
```

```
111/111 [==============================] - 0s 2ms/step
28/28 [==============================] - 0s 1ms/step
R2 score train: 0.9989513855046238
R2 score test: 0.9985618264131918
```

Out[38]:
```
0.9985618264131918
```

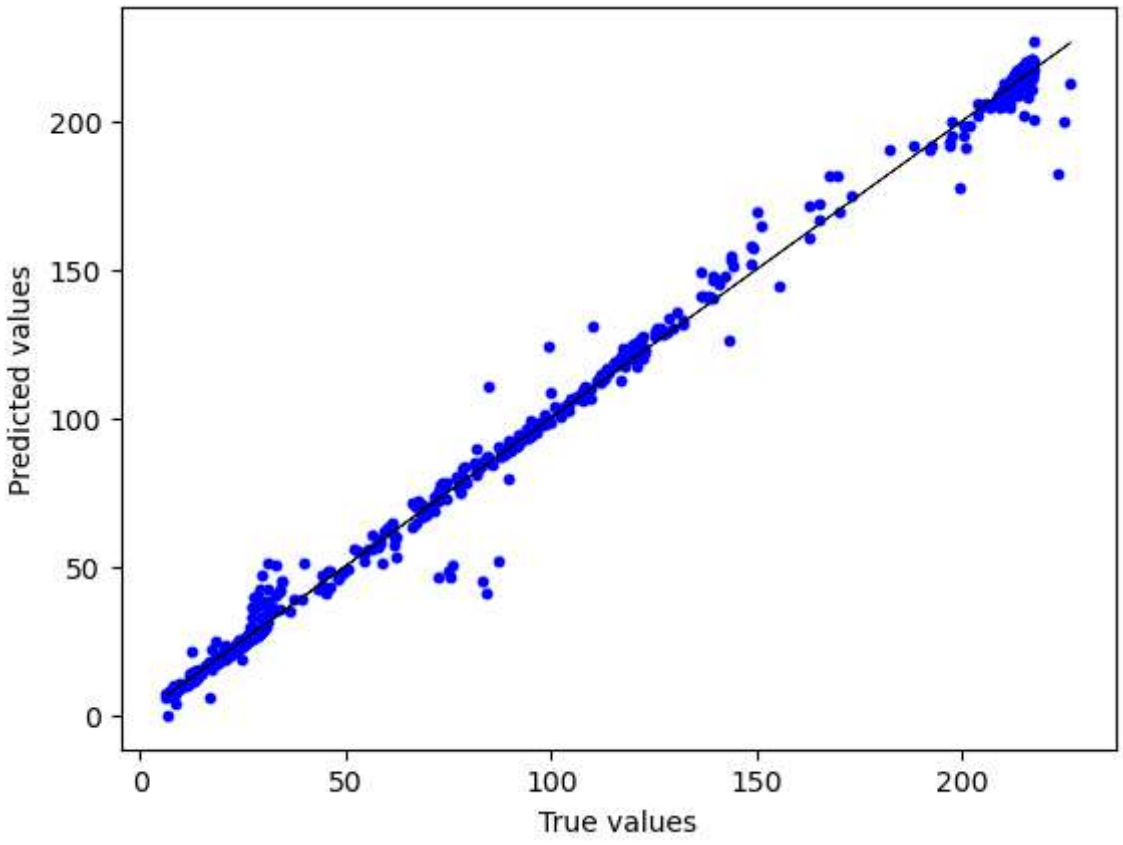
In [11]:
```
x = y_test.flatten()
y = y_test_pred.flatten()

#create scatterplot
plt.scatter(x, y, s=10, color='b')
plt.xlabel('True values')
plt.ylabel('Predicted values')

#calculate equation for trendline
z = np.polyfit(x, y, 1)
p = np.poly1d(z)

#add trendline to plot
plt.plot(x, p(x), color='k', linewidth=0.5)
```

Out[11]:
```
[<matplotlib.lines.Line2D at 0x2f4b089acd0>]
```



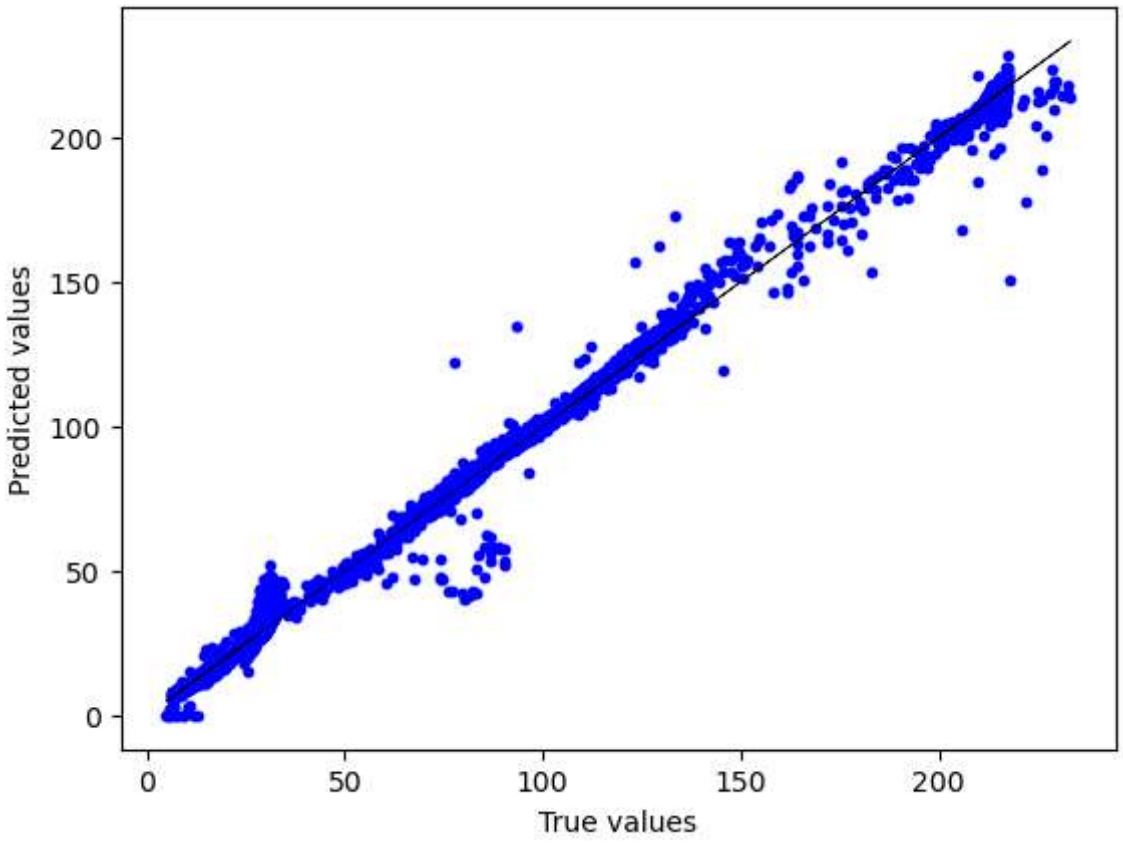
In [12]:
```
x = y_train.flatten()
y = y_train_pred.flatten()

#create scatterplot
plt.scatter(x, y, s=10, color='b')
plt.xlabel('True values')
plt.ylabel('Predicted values')

#calculate equation for trendline
z = np.polyfit(x, y, 1)
p = np.poly1d(z)

#add trendline to plot
plt.plot(x, p(x), color='k', linewidth=0.5)
```

Out[12]:
```
[<matplotlib.lines.Line2D at 0x2f4b088fcd0>]
```



In [13]:
```
# Comparison with other models
# Neural network - from the current code
from sklearn.metrics import mean_absolute_percentage_error
# outra forma de achar o MAPE com o sklearn: error = mean_absolute_percentage_


def mape(y_test, pred):
    y_test, pred = np.array(y_test), np.array(pred)
    mape = np.mean(np.abs((y_test - pred) / y_test))
    return mape


mse_neural, mae_neural = model.evaluate(X_test_scaled, y_test)
mapeNN = mape(y_test, y_test_pred)

print('Mean squared error from neural net: ', mse_neural)
print('Mean absolute error from neural net: ', mae_neural)
print('Mean absolute percentage error from neural net (MAPE): ', mapeNN)
rmse = np.sqrt(mse_neural)
rmse
```

```
28/28 [==============================] - 0s 1ms/step - loss: 23.8059 - mae:
2.3414
Mean squared error from neural net:  23.805892944335938
Mean absolute error from neural net:  2.3413805961608887
Mean absolute percentage error from neural net (MAPE):  0.043251911235235564
```

Out[13]:
```
4.879128297589226
```

O código da linha de cima também pode ser escrito assim:

from sklearn import metrics

#predict pred = model.predict(X_test_scaled) score =
metrics.mean_squared_error(pred,y_test) score

#quanto menor o mse, melhor

In [14]:
```
model.save('Neural_Network-Humidity')
```

```
WARNING:absl:Found untraced functions such as _update_step_xla while saving
(showing 1 of 1). These functions will not be directly callable after loadin
g.

INFO:tensorflow:Assets written to: Neural_Network-Humidity\assets

INFO:tensorflow:Assets written to: Neural_Network-Humidity\assets
```

In [15]:
```
# CROSS VALIDATION
#define the number of folds for cross-validation
num_folds=5

#create the KFold object with the specified number of folds

kf = KFold(n_splits=num_folds, shuffle=True, random_state=42)

performance_mse = []
performance_mae = []

#loop over each fold and train the model

for fold, (train_index, val_index) in enumerate(kf.split(X_train_scaled, y_tr
    print(f"Fold: {fold+1}")

    #split the data into training and validation sets for this fold
    X_train_fold, X_val_fold = X_train_scaled[train_index], X_train_scaled[va
    y_train_fold, y_val_fold = y_train[train_index], y_train[val_index]

    #compile and fit the Keras model on the training data for this fold
    model.compile(loss='mean_squared_error', optimizer='adam', metrics=['mae'
    model.fit(X_train_fold, y_train_fold, epochs=300, batch_size=32, verbose=

    #evaluate the model on the validation data for this fold
    mse_neural, mae_neural = model.evaluate(X_val_fold, y_val_fold, verbose=0
    print(f"Validation loss: {mse_neural}, Validation mae: {mae_neural}")
    performance_mse.append (mse_neural)
    performance_mae.append(mae_neural)
print(performance_mse)
print(performance_mae)

def average(x):
    return sum(x) / len(x)

average_mse = average(performance_mse)
average_mae = average(performance_mae)
print (f"Average loss = {average_mse}")
print (f"Average mae = {average_mae}")
```

```
Fold: 1
Validation loss: 49.11247253417969, Validation mae: 3.501563549041748
Fold: 2
Validation loss: 11.533354759216309, Validation mae: 1.465315341949463
Fold: 3
Validation loss: 21.96905517578125, Validation mae: 1.625471591949463
Fold: 4
Validation loss: 26.00507354736328, Validation mae: 1.8684287071228027
Fold: 5
Validation loss: 5.701254367828369, Validation mae: 1.2670228481292725
[49.11247253417969, 11.533354759216309, 21.96905517578125, 26.0050735473632
8, 5.701254367828369]
[3.501563549041748, 1.465315341949463, 1.625471591949463, 1.868428707122802
7, 1.2670228481292725]
Average loss = 22.86424207687378
Average mae = 1.9455604076385498
```

In [ ]:

In [39]:
```
######################################################################
# Linear regression
from sklearn import linear_model
from sklearn.tree import DecisionTreeRegressor
from sklearn.metrics import mean_squared_error, mean_absolute_error, mean_abs

def mape(y_test, pred):
    y_test, pred = np.array(y_test), np.array(pred)
    mape = np.mean(np.abs((y_test - pred) / y_test))
    return mape


## Linear Regression
lr_model = linear_model.LinearRegression()
lr_model.fit(X_train, y_train)
y_pred_lr = lr_model.predict(X_test)
mse_lr = mean_squared_error(y_test, y_pred_lr)
mae_lr = mean_absolute_error(y_test, y_pred_lr)
mape_lr = mean_absolute_percentage_error(y_test, y_pred_lr)
#mapelr = mape(y_test, y_pred_lr) - ver essa fórmula
print('Mean squared error from linear regression: ', mse_lr)
print('Mean absolute error from linear regression: ', mae_lr)
print ('MAPE LR: ', mape_lr)
r2lr = r2_score(y_test, y_pred_lr)
print('R2 score test:', r2lr)
```

```
Mean squared error from linear regression:  3831.6869267007055
Mean absolute error from linear regression:  48.38035791978404
MAPE LR:  0.985646792908584
R2 score test: 0.33115527261548106
```

In [40]:
```
## Decision Tree
tree = DecisionTreeRegressor()
tree.fit(X_train, y_train)
y_pred_tree = tree.predict(X_test)
mse_dt = mean_squared_error(y_test, y_pred_tree)
mae_dt = mean_absolute_error(y_test, y_pred_tree)
print('Mean squared error from Decision Tree: ', mse_dt)
print('Mean absolute error from Decision Tree: ', mae_dt)
mape_tree = mean_absolute_percentage_error(y_test, y_pred_tree)
#mapetree = mape(y_test, y_pred_tree) - VER
print ('MAPE Decision Tree: ', mape_tree)
r2dt=r2_score(y_test, y_pred_tree)
print('R2 score test:', r2dt )
```

```
Mean squared error from Decision Tree:  53.672580605707765
Mean absolute error from Decision Tree:  2.4724172813063063
MAPE Decision Tree:  0.0425785571021363
R2 score test: 0.9906311180349594
```

In [43]:
```
# Síntese das análises

valores3 = ["NN", "LR", "DT"]
r2 = [r2nn, r2lr, r2dt]

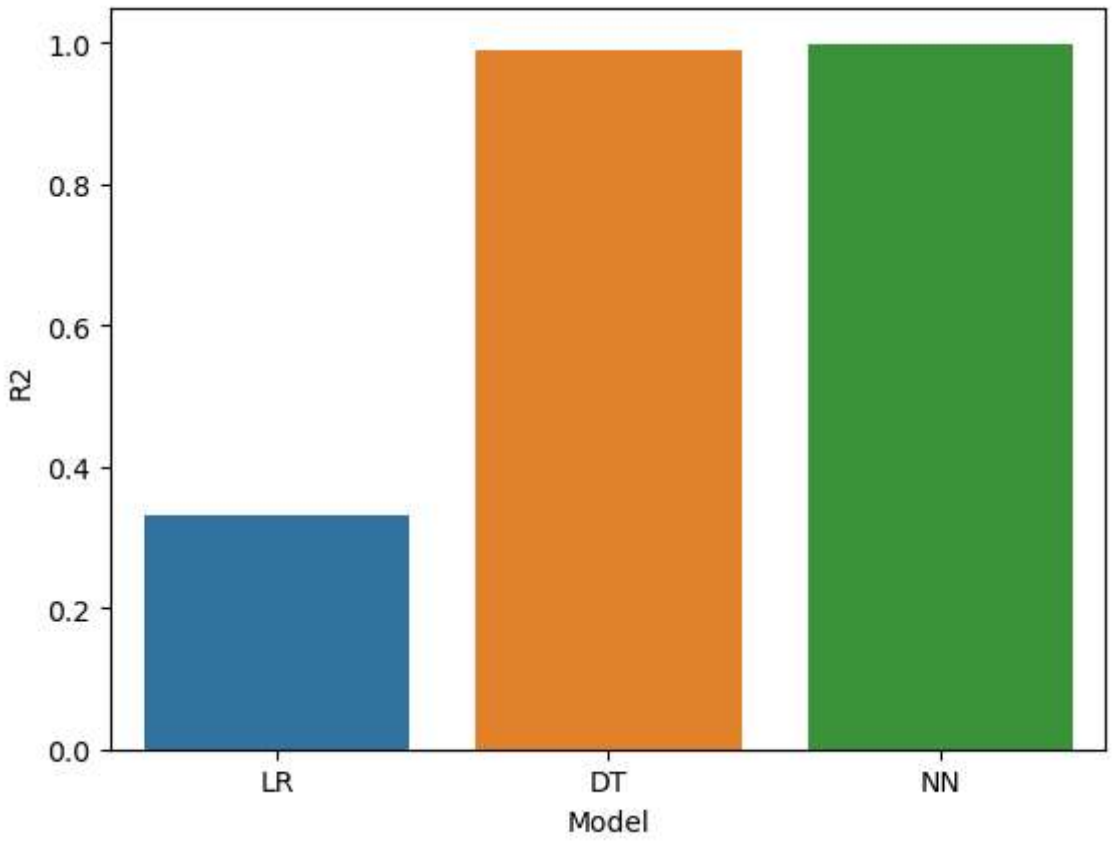
R2 = pd.DataFrame({"Model": valores3, "R2": r2})
R2
```

Out[43]:

	Model	R2
0	NN	0.998562
1	LR	0.331155
2	DT	0.990631

In [44]:
```
sns.barplot(x="Model", y="R2", data=R2, order = R2.sort_values("R2").Model)
```

Out[44]: <AxesSubplot:xlabel='Model', ylabel='R2'>



In [32]:
```
# Síntese das análises

valores1 = ["NN", "LR", "DT"]
erros1 = [23.81, mse_lr, mse_dt]

MSE = pd.DataFrame({"Model": valores1, "Mean Squared Error - MSE": erros1})
MSE
```

Out[32]:

	Model	Mean Squared Error - MSE
0	NN	23.810000
1	LR	3831.686927
2	DT	62.909224

In [33]:
```
valores2 = ["NN", "LR", "DT"]
erros2 = [2.34, mae_lr, mae_dt]

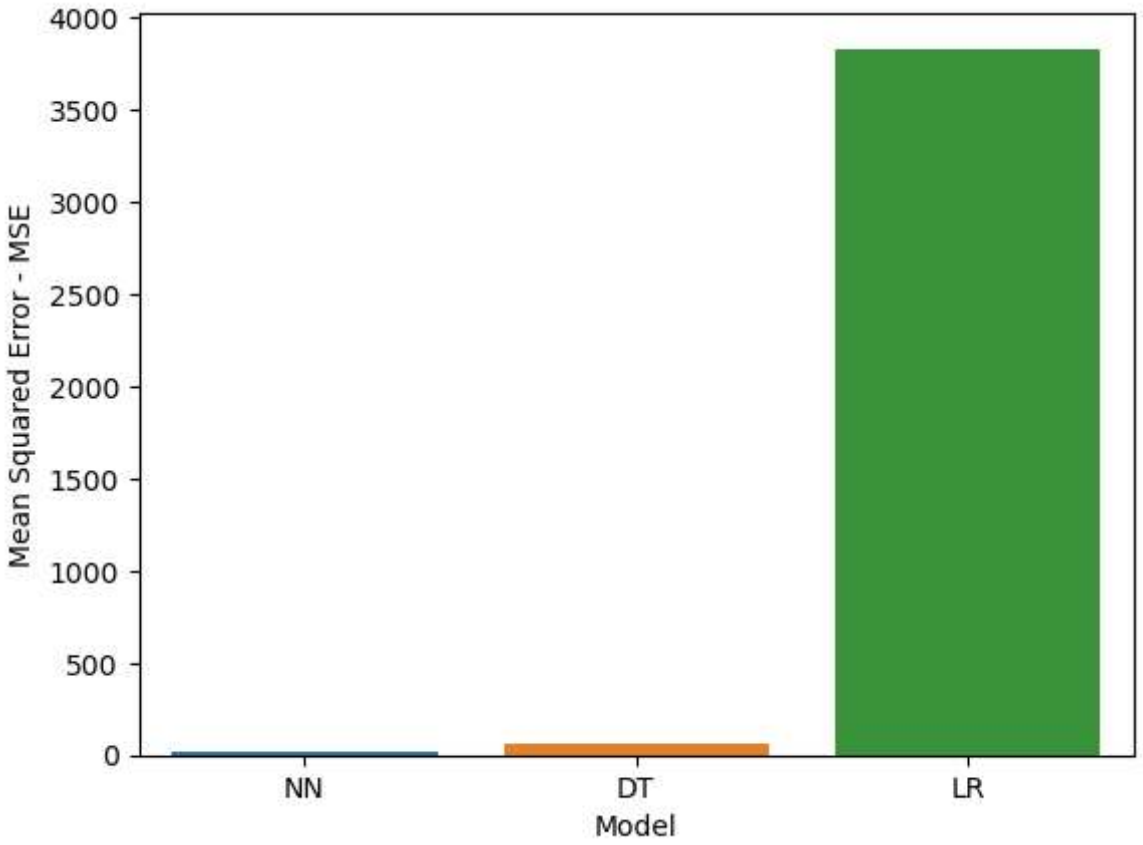
MAE = pd.DataFrame({"Model": valores2, "Mean Absolute Error - MAE": erros2})
MAE
```

Out[33]:

	Model	Mean Absolute Error - MAE
0	NN	2.340000
1	LR	48.380358
2	DT	2.603288

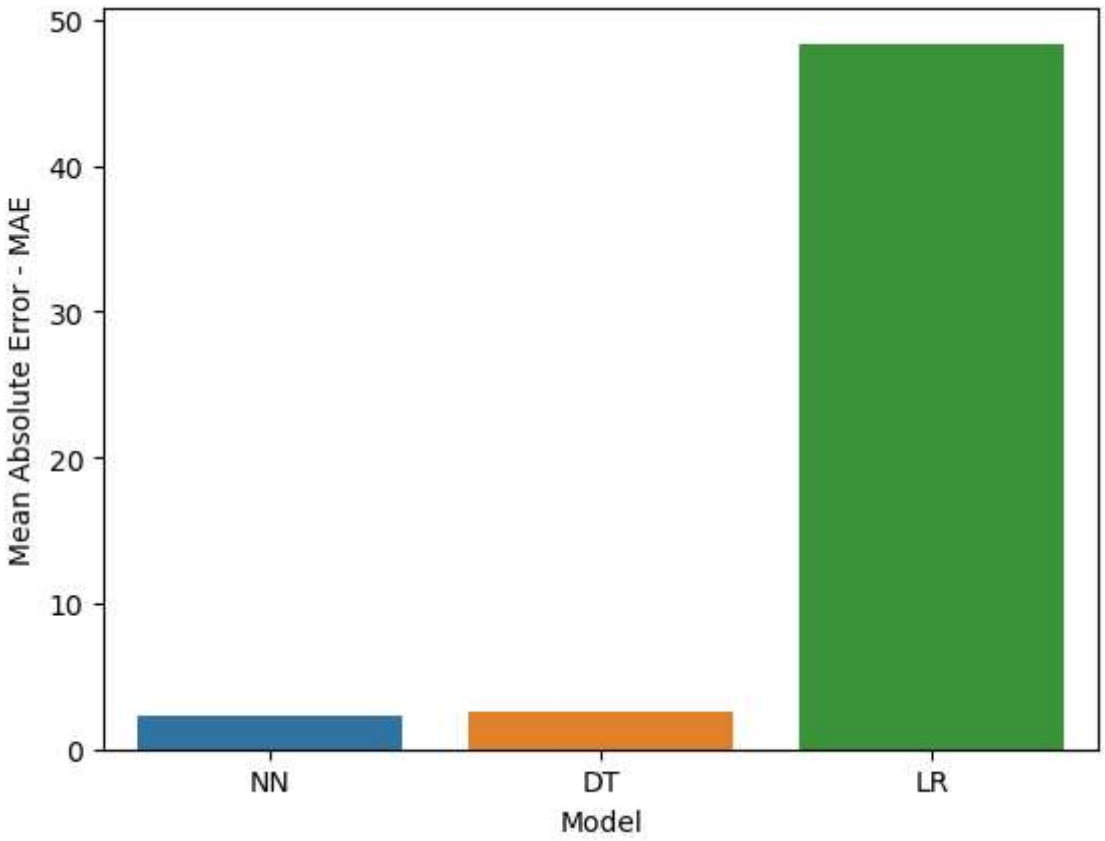
In [34]:
```
sns.barplot(x="Model", y="Mean Squared Error - MSE", data=MSE, order = MSE.so
```

Out[34]:
```
<AxesSubplot:xlabel='Model', ylabel='Mean Squared Error - MSE'>
```



In [35]:
```
sns.barplot(x="Model", y="Mean Absolute Error - MAE", data=MAE, order = MAE.s
```

Out[35]:
```
<AxesSubplot:xlabel='Model', ylabel='Mean Absolute Error - MAE'>
```



In [ ]:

In [ ]:

In [ ]:

APPENDIX 5 (a)

In [11]:
```
import numpy as np
import pandas as pd
import seaborn as sns
from matplotlib import pyplot as plt
from tensorflow.keras.models import load_model, Sequential, Model
from tensorflow.keras.layers import Dense, Dropout, Input
from tensorflow.keras.optimizers import Adam
from tensorflow.keras.regularizers import l1, l2, l1_l2


df = pd.read_excel('dataset.artigo.lab.xlsx')
df
```

Out[11]:

	Material	Temperature [°C]	Relative Humidity [%]	Humidity [kg/m³]	ΔT [°C]
0	5	20	70	199.875283	1.38
1	5	20	70	197.176871	2.14
2	5	20	70	195.328798	2.25
3	5	20	70	192.630385	1.96
4	5	20	70	186.984127	1.96
5	5	20	70	177.981859	1.91
6	5	20	70	137.154195	1.82
7	5	20	70	123.129252	1.46
8	5	20	70	54.104308	0.46
9	5	20	70	48.798186	0.50
10	5	20	70	43.480726	0.45
11	5	20	70	38.163265	0.22
12	5	20	70	35.702948	0.35
13	5	20	70	35.158730	0.33
14	5	20	70	34.693878	0.31
15	5	25	60	219.126984	1.25
16	5	25	60	214.637188	2.89
17	5	25	60	211.473923	3.14
18	5	25	60	206.394558	3.00
19	5	25	60	196.417234	2.87
20	5	25	60	179.614512	2.95
21	5	25	60	113.412698	1.70
22	5	25	60	104.773243	1.44
23	5	25	60	99.274376	1.21
24	5	25	60	77.721088	0.80
25	5	25	60	70.725624	0.67
26	5	25	60	60.102041	0.61
27	5	25	60	56.201814	0.55
28	5	25	60	38.809524	0.10
29	5	15	80	209.002268	1.04
30	5	15	80	207.585034	1.14
31	5	15	80	206.882086	0.92
32	5	15	80	204.546485	1.31
33	5	15	80	201.814059	1.25
34	5	15	80	180.306122	1.18
35	5	15	80	174.773243	1.01
36	5	15	80	169.954649	1.11
37	5	15	80	147.471655	1.11
38	5	15	80	144.875283	1.10
39	5	15	80	140.124717	1.08
40	5	15	80	120.714286	0.96
41	5	15	80	99.240363	0.85
42	5	15	80	71.292517	0.45
43	5	15	80	64.535147	0.38
44	5	15	80	61.020408	0.38
45	5	15	80	58.741497	0.31

In [12]:
```
from keras.models import Model
from keras.layers import Dense, Input
from sklearn.model_selection import cross_val_score
from sklearn.model_selection import KFold
from sklearn.pipeline import Pipeline
from sklearn.model_selection import train_test_split
from sklearn.metrics import r2_score
from tensorflow.keras.callbacks import EarlyStopping
```

```
# SEPARAR INPUTS DOS OUTPUTS

X = df.drop(['Humidity [kg/m³]'], axis=1)
y = df.drop(['Material', 'Temperature [°C]', 'Relative Humidity [%]', 'ΔT [°C]'], axis=1)
y = y.values

# número de dados de treinamento
m = X.shape[0]

X_train, X_test, y_train, y_test = train_test_split(X, y, test_size = 0.2, random_state=42, shuffle=True)

# Scale data, otherwise model will fail
# Standardize features by removing the mean and scaling to unit variance
from sklearn.preprocessing import MinMaxScaler
scaler = MinMaxScaler()
scaler.fit(X)

X_train_scaled = scaler.transform(X_train)
X_test_scaled = scaler.transform(X_test)
```

In [13]:

```
from tensorflow.keras.models import load_model
from tensorflow.keras.layers import Dense, Dropout
from tensorflow.keras.optimizers import Adam

num_classes = 1

# Carregar o modelo treinado com dados de simulação
model_simulation = load_model('C://Users//Leticia Carvalho//Documents//humidity.keras')

# Congelar as primeiras camadas do modelo para preservar os pesos
for layer in model_simulation.layers:
    layer.trainable = False

# Criar a entrada para o novo modelo
input_layer = Input(shape=(4,))

# Passar a entrada pelo modelo pré-treinado
x = model_simulation(input_layer, training=False)


# Adicionar camadas de ajuste
# Adicionando uma camada de dropout
x = Dense(128, activation='relu')(x)
x = Dense(128, activation='relu')(x)

#x = Dropout(0.5)(x)  # Adicionando uma camada de dropout
#x = Dropout(0.5)(x)  # Adicionando uma camada de dropout


#x = Dense(128, activation='relu', kernel_regularizer=regularizers.l2(0.01))(x)

predictions = Dense(1)(x)


# Criar o novo modelo
model = Model(inputs=input_layer, outputs=predictions)

# Compilar o novo modelo
model.compile(optimizer=Adam(learning_rate=0.001), loss='mean_squared_error', metrics=['mae'])

# Treinar o modelo com os dados reais
monitor = EarlyStopping(monitor='val_loss', min_delta=1e-3, patience=30, verbose=1, restore_best_weights=True)
history = model.fit(X_train_scaled, y_train, validation_split=0.2, epochs=2000, callbacks = [monitor], batch_size=32, verbose=1)
```

```
Epoch 1/2000
1/1 [==============================] - 1s 801ms/step - loss: 24155.0879 - mae: 142.3605 - val_loss: 12837.1504 - val_mae: 96.5826
Epoch 2/2000
1/1 [==============================] - 0s 32ms/step - loss: 19153.4277 - mae: 126.4836 - val_loss: 11196.0840 - val_mae: 87.8699
Epoch 3/2000
1/1 [==============================] - 0s 43ms/step - loss: 15065.4746 - mae: 110.7255 - val_loss: 9909.5791 - val_mae: 79.3432
Epoch 4/2000
1/1 [==============================] - 0s 67ms/step - loss: 11910.1006 - mae: 95.3042 - val_loss: 8966.3984 - val_mae: 71.1001
Epoch 5/2000
1/1 [==============================] - 0s 55ms/step - loss: 9654.3193 - mae: 80.3941 - val_loss: 8368.8584 - val_mae: 67.9068
Epoch 6/2000
1/1 [==============================] - 0s 53ms/step - loss: 8289.5361 - mae: 69.3649 - val_loss: 8030.5918 - val_mae: 67.4216
Epoch 7/2000
1/1 [==============================] - 0s 35ms/step - loss: 7594.5122 - mae: 65.9227 - val_loss: 7900.9238 - val_mae: 66.9790
Epoch 8/2000
1/1 [==============================] - 0s 31ms/step - loss: 7433.5542 - mae: 65.9430 - val_loss: 7927.8711 - val_mae: 67.9088
Epoch 9/2000
1/1 [==============================] - 0s 34ms/step - loss: 7666.3438 - mae: 67.6743 - val_loss: 8048.5791 - val_mae: 68.9789
Epoch 10/2000
1/1 [==============================] - 0s 30ms/step - loss: 8117.6289 - mae: 70.4995 - val_loss: 8200.8115 - val_mae: 69.7971
Epoch 11/2000
1/1 [==============================] - 0s 33ms/step - loss: 8621.3076 - mae: 74.1646 - val_loss: 8328.9277 - val_mae: 70.3332
Epoch 12/2000
1/1 [==============================] - 0s 36ms/step - loss: 9027.1045 - mae: 77.0342 - val_loss: 8404.6973 - val_mae: 70.6118
Epoch 13/2000
1/1 [==============================] - 0s 37ms/step - loss: 9263.1094 - mae: 78.5360 - val_loss: 8418.6025 - val_mae: 70.6590
Epoch 14/2000
1/1 [==============================] - 0s 67ms/step - loss: 9307.2490 - mae: 78.8063 - val_loss: 8376.8057 - val_mae: 70.5073
Epoch 15/2000
1/1 [==============================] - 0s 41ms/step - loss: 9179.8760 - mae: 78.0198 - val_loss: 8294.9951 - val_mae: 70.1929
Epoch 16/2000
1/1 [==============================] - 0s 51ms/step - loss: 8926.8838 - mae: 76.3677 - val_loss: 8192.5537 - val_mae: 69.7518
Epoch 17/2000
1/1 [==============================] - 0s 32ms/step - loss: 8603.9404 - mae: 74.0416 - val_loss: 8088.2544 - val_mae: 69.2185
Epoch 18/2000
1/1 [==============================] - 0s 34ms/step - loss: 8264.9404 - mae: 71.3025 - val_loss: 7997.5186 - val_mae: 68.6253
Epoch 19/2000
1/1 [==============================] - 0s 32ms/step - loss: 7954.6143 - mae: 69.6320 - val_loss: 7930.9180 - val_mae: 68.0018
Epoch 20/2000
1/1 [==============================] - 0s 32ms/step - loss: 7704.5503 - mae: 67.9973 - val_loss: 7893.6738 - val_mae: 67.3751
Epoch 21/2000
1/1 [==============================] - 0s 33ms/step - loss: 7531.8584 - mae: 66.4716 - val_loss: 7885.9346 - val_mae: 66.8351
Epoch 22/2000
1/1 [==============================] - 0s 33ms/step - loss: 7439.8555 - mae: 66.0301 - val_loss: 7903.6274 - val_mae: 66.9943
Epoch 23/2000
1/1 [==============================] - 0s 32ms/step - loss: 7420.2998 - mae: 65.6805 - val_loss: 7939.7134 - val_mae: 67.1359
Epoch 24/2000
1/1 [==============================] - 0s 42ms/step - loss: 7456.6665 - mae: 65.4964 - val_loss: 7985.6377 - val_mae: 67.2560
Epoch 25/2000
1/1 [==============================] - 0s 42ms/step - loss: 7527.9526 - mae: 65.7253 - val_loss: 8032.7588 - val_mae: 67.3516
Epoch 26/2000
1/1 [==============================] - 0s 31ms/step - loss: 7612.4429 - mae: 65.9091 - val_loss: 8073.5640 - val_mae: 67.4212
Epoch 27/2000
1/1 [==============================] - 0s 30ms/step - loss: 7690.9180 - mae: 66.0448 - val_loss: 8102.5225 - val_mae: 67.4642
Epoch 28/2000
1/1 [==============================] - 0s 40ms/step - loss: 7748.9409 - mae: 66.1315 - val_loss: 8116.5190 - val_mae: 67.4812
Epoch 29/2000
1/1 [==============================] - 0s 34ms/step - loss: 7778.0381 - mae: 66.1702 - val_loss: 8114.8779 - val_mae: 67.4736
Epoch 30/2000
1/1 [==============================] - 0s 47ms/step - loss: 7775.8154 - mae: 66.1634 - val_loss: 8099.0479 - val_mae: 67.4435
Epoch 31/2000
1/1 [==============================] - 0s 40ms/step - loss: 7745.1968 - mae: 66.1152 - val_loss: 8072.0698 - val_mae: 67.3939
Epoch 32/2000
1/1 [==============================] - 0s 44ms/step - loss: 7693.0601 - mae: 66.0310 - val_loss: 8037.9219 - val_mae: 67.3279
Epoch 33/2000
1/1 [==============================] - 0s 56ms/step - loss: 7628.5713 - mae: 65.9167 - val_loss: 8000.8540 - val_mae: 67.2493
Epoch 34/2000
1/1 [==============================] - 0s 50ms/step - loss: 7561.4790 - mae: 65.7790 - val_loss: 7964.7891 - val_mae: 67.1619
Epoch 35/2000
1/1 [==============================] - 0s 58ms/step - loss: 7500.5894 - mae: 65.6252 - val_loss: 7932.8662 - val_mae: 67.0696
Epoch 36/2000
1/1 [==============================] - 0s 52ms/step - loss: 7452.5859 - mae: 65.4625 - val_loss: 7907.1313 - val_mae: 66.9764
Epoch 37/2000
1/1 [==============================] - 0s 55ms/step - loss: 7421.2944 - mae: 65.4556 - val_loss: 7888.4375 - val_mae: 66.8859
Epoch 38/2000
1/1 [==============================] - 0s 35ms/step - loss: 7407.4585 - mae: 65.6242 - val_loss: 7876.5288 - val_mae: 66.8017
Epoch 39/2000
1/1 [==============================] - 0s 32ms/step - loss: 7409.0073 - mae: 65.7797 - val_loss: 7870.2734 - val_mae: 66.7266
Epoch 40/2000
1/1 [==============================] - 0s 30ms/step - loss: 7421.7456 - mae: 65.9161 - val_loss: 7868.0137 - val_mae: 66.8208
Epoch 41/2000
1/1 [==============================] - 0s 40ms/step - loss: 7440.3271 - mae: 66.0284 - val_loss: 7867.9570 - val_mae: 66.9608
Epoch 42/2000
1/1 [==============================] - 0s 41ms/step - loss: 7459.3135 - mae: 66.1129 - val_loss: 7868.5229 - val_mae: 67.0526
Epoch 43/2000
1/1 [==============================] - 0s 52ms/step - loss: 7474.1416 - mae: 66.1677 - val_loss: 7868.6094 - val_mae: 67.0955
Epoch 44/2000
1/1 [==============================] - 0s 45ms/step - loss: 7481.8032 - mae: 66.1923 - val_loss: 7867.7021 - val_mae: 67.0911
Epoch 45/2000
1/1 [==============================] - 0s 37ms/step - loss: 7481.1538 - mae: 66.1877 - val_loss: 7865.8628 - val_mae: 67.0434
Epoch 46/2000
1/1 [==============================] - 0s 45ms/step - loss: 7472.8291 - mae: 66.1564 - val_loss: 7863.5884 - val_mae: 66.9581
Epoch 47/2000
1/1 [==============================] - 0s 36ms/step - loss: 7458.8481 - mae: 66.1020 - val_loss: 7861.6074 - val_mae: 66.8424
Epoch 48/2000
1/1 [==============================] - 0s 47ms/step - loss: 7441.9976 - mae: 66.0287 - val_loss: 7860.6499 - val_mae: 66.7043
Epoch 49/2000
1/1 [==============================] - 0s 35ms/step - loss: 7425.1909 - mae: 65.9417 - val_loss: 7861.2603 - val_mae: 66.6648
Epoch 50/2000
1/1 [==============================] - 0s 43ms/step - loss: 7410.8906 - mae: 65.8462 - val_loss: 7863.6636 - val_mae: 66.7029
Epoch 51/2000
1/1 [==============================] - 0s 68ms/step - loss: 7400.7188 - mae: 65.7474 - val_loss: 7867.7241 - val_mae: 66.7401
Epoch 52/2000
1/1 [==============================] - 0s 53ms/step - loss: 7395.2847 - mae: 65.6503 - val_loss: 7872.9766 - val_mae: 66.7743
Epoch 53/2000
1/1 [==============================] - 0s 40ms/step - loss: 7394.2334 - mae: 65.5594 - val_loss: 7878.7349 - val_mae: 66.8037
Epoch 54/2000
```

```
1/1 [==============================] - 0s 39ms/step - loss: 7396.4756 - mae: 65.4784 - val_loss: 7884.2080 - val_mae: 66.8268
Epoch 55/2000
1/1 [==============================] - 0s 35ms/step - loss: 7400.5063 - mae: 65.4105 - val_loss: 7888.6577 - val_mae: 66.8426
Epoch 56/2000
1/1 [==============================] - 0s 35ms/step - loss: 7404.7632 - mae: 65.3575 - val_loss: 7891.5029 - val_mae: 66.8505
Epoch 57/2000
1/1 [==============================] - 0s 52ms/step - loss: 7407.9351 - mae: 65.3207 - val_loss: 7892.4062 - val_mae: 66.8505
Epoch 58/2000
1/1 [==============================] - 0s 52ms/step - loss: 7409.1665 - mae: 65.3004 - val_loss: 7891.2983 - val_mae: 66.8429
Epoch 59/2000
1/1 [==============================] - 0s 50ms/step - loss: 7408.1519 - mae: 65.2958 - val_loss: 7888.3633 - val_mae: 66.8282
Epoch 60/2000
1/1 [==============================] - 0s 32ms/step - loss: 7405.1021 - mae: 65.3056 - val_loss: 7883.9800 - val_mae: 66.8075
Epoch 61/2000
1/1 [==============================] - 0s 36ms/step - loss: 7400.6206 - mae: 65.3277 - val_loss: 7878.6377 - val_mae: 66.7820
Epoch 62/2000
1/1 [==============================] - 0s 49ms/step - loss: 7395.5127 - mae: 65.3597 - val_loss: 7872.8550 - val_mae: 66.7531
Epoch 63/2000
1/1 [==============================] - 0s 60ms/step - loss: 7390.5967 - mae: 65.3987 - val_loss: 7867.1045 - val_mae: 66.7222
Epoch 64/2000
1/1 [==============================] - 0s 43ms/step - loss: 7386.5308 - mae: 65.4416 - val_loss: 7861.7515 - val_mae: 66.6908
Epoch 65/2000
1/1 [==============================] - 0s 40ms/step - loss: 7383.7031 - mae: 65.4855 - val_loss: 7857.0327 - val_mae: 66.6603
Epoch 66/2000
1/1 [==============================] - 0s 50ms/step - loss: 7382.1865 - mae: 65.5275 - val_loss: 7853.0581 - val_mae: 66.6319
Epoch 67/2000
1/1 [==============================] - 0s 47ms/step - loss: 7381.7798 - mae: 65.5651 - val_loss: 7849.8262 - val_mae: 66.6066
Epoch 68/2000
1/1 [==============================] - 0s 35ms/step - loss: 7382.0859 - mae: 65.5963 - val_loss: 7847.2734 - val_mae: 66.5852
Epoch 69/2000
1/1 [==============================] - 0s 39ms/step - loss: 7382.6265 - mae: 65.6193 - val_loss: 7845.3027 - val_mae: 66.5682
Epoch 70/2000
1/1 [==============================] - 0s 36ms/step - loss: 7382.9644 - mae: 65.6334 - val_loss: 7843.8232 - val_mae: 66.5558
Epoch 71/2000
1/1 [==============================] - 0s 32ms/step - loss: 7382.7842 - mae: 65.6380 - val_loss: 7842.7656 - val_mae: 66.5477
Epoch 72/2000
1/1 [==============================] - 0s 42ms/step - loss: 7381.9453 - mae: 65.6334 - val_loss: 7842.0874 - val_mae: 66.5438
Epoch 73/2000
1/1 [==============================] - 0s 50ms/step - loss: 7380.4854 - mae: 65.6204 - val_loss: 7841.7695 - val_mae: 66.5434
Epoch 74/2000
1/1 [==============================] - 0s 52ms/step - loss: 7378.5796 - mae: 65.6001 - val_loss: 7841.7959 - val_mae: 66.5458
Epoch 75/2000
1/1 [==============================] - 0s 40ms/step - loss: 7376.4810 - mae: 65.5741 - val_loss: 7842.1348 - val_mae: 66.5502
Epoch 76/2000
1/1 [==============================] - 0s 47ms/step - loss: 7374.4448 - mae: 65.5441 - val_loss: 7842.7266 - val_mae: 66.5555
Epoch 77/2000
1/1 [==============================] - 0s 50ms/step - loss: 7372.6753 - mae: 65.5119 - val_loss: 7843.4810 - val_mae: 66.5611
Epoch 78/2000
1/1 [==============================] - 0s 48ms/step - loss: 7371.2798 - mae: 65.4794 - val_loss: 7844.2778 - val_mae: 66.5659
Epoch 79/2000
1/1 [==============================] - 0s 36ms/step - loss: 7370.2686 - mae: 65.4482 - val_loss: 7844.9814 - val_mae: 66.5694
Epoch 80/2000
1/1 [==============================] - 0s 33ms/step - loss: 7369.5591 - mae: 65.4199 - val_loss: 7845.4556 - val_mae: 66.5709
Epoch 81/2000
1/1 [==============================] - 0s 65ms/step - loss: 7369.0190 - mae: 65.3955 - val_loss: 7845.5859 - val_mae: 66.5701
Epoch 82/2000
1/1 [==============================] - 0s 49ms/step - loss: 7368.4976 - mae: 65.3760 - val_loss: 7845.2935 - val_mae: 66.5666
Epoch 83/2000
1/1 [==============================] - 0s 44ms/step - loss: 7367.8740 - mae: 65.3616 - val_loss: 7844.5405 - val_mae: 66.5606
Epoch 84/2000
1/1 [==============================] - 0s 50ms/step - loss: 7367.0669 - mae: 65.3526 - val_loss: 7843.3428 - val_mae: 66.5521
Epoch 85/2000
1/1 [==============================] - 0s 48ms/step - loss: 7366.0596 - mae: 65.3487 - val_loss: 7841.7568 - val_mae: 66.5413
Epoch 86/2000
1/1 [==============================] - 0s 60ms/step - loss: 7364.8882 - mae: 65.3493 - val_loss: 7839.8633 - val_mae: 66.5287
Epoch 87/2000
1/1 [==============================] - 0s 76ms/step - loss: 7363.6216 - mae: 65.3535 - val_loss: 7837.7676 - val_mae: 66.5148
Epoch 88/2000
1/1 [==============================] - 0s 51ms/step - loss: 7362.3413 - mae: 65.3605 - val_loss: 7835.5747 - val_mae: 66.5001
Epoch 89/2000
1/1 [==============================] - 0s 69ms/step - loss: 7361.1221 - mae: 65.3691 - val_loss: 7833.3813 - val_mae: 66.4851
Epoch 90/2000
1/1 [==============================] - 0s 73ms/step - loss: 7360.0078 - mae: 65.3782 - val_loss: 7831.2690 - val_mae: 66.4702
Epoch 91/2000
1/1 [==============================] - 0s 36ms/step - loss: 7359.0122 - mae: 65.3869 - val_loss: 7829.2969 - val_mae: 66.4561
Epoch 92/2000
1/1 [==============================] - 0s 37ms/step - loss: 7358.1172 - mae: 65.3941 - val_loss: 7827.5020 - val_mae: 66.4430
Epoch 93/2000
1/1 [==============================] - 0s 47ms/step - loss: 7357.2817 - mae: 65.3991 - val_loss: 7825.9082 - val_mae: 66.4313
Epoch 94/2000
1/1 [==============================] - 0s 72ms/step - loss: 7356.4600 - mae: 65.4015 - val_loss: 7824.5225 - val_mae: 66.4209
Epoch 95/2000
1/1 [==============================] - 0s 53ms/step - loss: 7355.6084 - mae: 65.4008 - val_loss: 7823.3374 - val_mae: 66.4121
Epoch 96/2000
1/1 [==============================] - 0s 47ms/step - loss: 7354.6997 - mae: 65.3970 - val_loss: 7822.3418 - val_mae: 66.4048
Epoch 97/2000
1/1 [==============================] - 0s 65ms/step - loss: 7353.7271 - mae: 65.3903 - val_loss: 7821.5151 - val_mae: 66.3987
Epoch 98/2000
1/1 [==============================] - 0s 54ms/step - loss: 7352.7007 - mae: 65.3809 - val_loss: 7820.8311 - val_mae: 66.3937
Epoch 99/2000
1/1 [==============================] - 0s 50ms/step - loss: 7351.6450 - mae: 65.3693 - val_loss: 7820.2549 - val_mae: 66.3894
Epoch 100/2000
1/1 [==============================] - 0s 58ms/step - loss: 7350.5864 - mae: 65.3562 - val_loss: 7819.7529 - val_mae: 66.3855
Epoch 101/2000
1/1 [==============================] - 0s 36ms/step - loss: 7349.5474 - mae: 65.3422 - val_loss: 7819.2769 - val_mae: 66.3818
Epoch 102/2000
1/1 [==============================] - 0s 44ms/step - loss: 7348.5425 - mae: 65.3280 - val_loss: 7818.7866 - val_mae: 66.3778
Epoch 103/2000
1/1 [==============================] - 0s 68ms/step - loss: 7347.5732 - mae: 65.3141 - val_loss: 7818.2383 - val_mae: 66.3734
Epoch 104/2000
1/1 [==============================] - 0s 53ms/step - loss: 7346.6333 - mae: 65.3011 - val_loss: 7817.5991 - val_mae: 66.3683
Epoch 105/2000
1/1 [==============================] - 0s 51ms/step - loss: 7345.7075 - mae: 65.2895 - val_loss: 7816.8384 - val_mae: 66.3624
Epoch 106/2000
1/1 [==============================] - 0s 43ms/step - loss: 7344.7812 - mae: 65.2795 - val_loss: 7815.9424 - val_mae: 66.3556
Epoch 107/2000
1/1 [==============================] - 0s 42ms/step - loss: 7343.8403 - mae: 65.2713 - val_loss: 7814.9087 - val_mae: 66.3480
```

```
Epoch 108/2000
1/1 [==============================] - 0s 62ms/step - loss: 7342.8784 - mae: 65.2648 - val_loss: 7813.7476 - val_mae: 66.3394
Epoch 109/2000
1/1 [==============================] - 0s 39ms/step - loss: 7341.8960 - mae: 65.2601 - val_loss: 7812.4756 - val_mae: 66.3302
Epoch 110/2000
1/1 [==============================] - 0s 43ms/step - loss: 7340.8994 - mae: 65.2567 - val_loss: 7811.1196 - val_mae: 66.3204
Epoch 111/2000
1/1 [==============================] - 0s 52ms/step - loss: 7339.8955 - mae: 65.2544 - val_loss: 7809.7158 - val_mae: 66.3103
Epoch 112/2000
1/1 [==============================] - 0s 54ms/step - loss: 7338.8936 - mae: 65.2529 - val_loss: 7808.2881 - val_mae: 66.3000
Epoch 113/2000
1/1 [==============================] - 0s 68ms/step - loss: 7337.8999 - mae: 65.2517 - val_loss: 7806.8691 - val_mae: 66.2897
Epoch 114/2000
1/1 [==============================] - 0s 53ms/step - loss: 7336.9175 - mae: 65.2504 - val_loss: 7805.4824 - val_mae: 66.2796
Epoch 115/2000
1/1 [==============================] - 0s 41ms/step - loss: 7335.9443 - mae: 65.2488 - val_loss: 7804.1470 - val_mae: 66.2698
Epoch 116/2000
1/1 [==============================] - 0s 34ms/step - loss: 7334.9766 - mae: 65.2464 - val_loss: 7802.8750 - val_mae: 66.2605
Epoch 117/2000
1/1 [==============================] - 0s 40ms/step - loss: 7334.0112 - mae: 65.2431 - val_loss: 7801.6753 - val_mae: 66.2516
Epoch 118/2000
1/1 [==============================] - 0s 68ms/step - loss: 7333.0400 - mae: 65.2387 - val_loss: 7800.5488 - val_mae: 66.2433
Epoch 119/2000
1/1 [==============================] - 0s 47ms/step - loss: 7332.0615 - mae: 65.2333 - val_loss: 7799.4902 - val_mae: 66.2354
Epoch 120/2000
1/1 [==============================] - 0s 38ms/step - loss: 7331.0757 - mae: 65.2269 - val_loss: 7798.4917 - val_mae: 66.2280
Epoch 121/2000
1/1 [==============================] - 0s 42ms/step - loss: 7330.0835 - mae: 65.2195 - val_loss: 7797.5420 - val_mae: 66.2209
Epoch 122/2000
1/1 [==============================] - 0s 36ms/step - loss: 7329.0869 - mae: 65.2115 - val_loss: 7796.6250 - val_mae: 66.2141
Epoch 123/2000
1/1 [==============================] - 0s 39ms/step - loss: 7328.0903 - mae: 65.2029 - val_loss: 7795.7246 - val_mae: 66.2073
Epoch 124/2000
1/1 [==============================] - 0s 42ms/step - loss: 7327.0933 - mae: 65.1941 - val_loss: 7794.8228 - val_mae: 66.2006
Epoch 125/2000
1/1 [==============================] - 0s 42ms/step - loss: 7326.1006 - mae: 65.1853 - val_loss: 7793.9058 - val_mae: 66.1937
Epoch 126/2000
1/1 [==============================] - 0s 37ms/step - loss: 7325.1104 - mae: 65.1767 - val_loss: 7792.9614 - val_mae: 66.1866
Epoch 127/2000
1/1 [==============================] - 0s 44ms/step - loss: 7324.1206 - mae: 65.1685 - val_loss: 7791.9761 - val_mae: 66.1793
Epoch 128/2000
1/1 [==============================] - 0s 58ms/step - loss: 7323.1299 - mae: 65.1608 - val_loss: 7790.9453 - val_mae: 66.1716
Epoch 129/2000
1/1 [==============================] - 0s 59ms/step - loss: 7322.1372 - mae: 65.1537 - val_loss: 7789.8667 - val_mae: 66.1636
Epoch 130/2000
1/1 [==============================] - 0s 75ms/step - loss: 7321.1411 - mae: 65.1473 - val_loss: 7788.7437 - val_mae: 66.1553
Epoch 131/2000
1/1 [==============================] - 0s 73ms/step - loss: 7320.1411 - mae: 65.1414 - val_loss: 7787.5806 - val_mae: 66.1467
Epoch 132/2000
1/1 [==============================] - 0s 48ms/step - loss: 7319.1382 - mae: 65.1360 - val_loss: 7786.3862 - val_mae: 66.1379
Epoch 133/2000
1/1 [==============================] - 0s 53ms/step - loss: 7318.1343 - mae: 65.1311 - val_loss: 7785.1704 - val_mae: 66.1289
Epoch 134/2000
1/1 [==============================] - 0s 50ms/step - loss: 7317.1274 - mae: 65.1264 - val_loss: 7783.9453 - val_mae: 66.1199
Epoch 135/2000
1/1 [==============================] - 0s 48ms/step - loss: 7316.1211 - mae: 65.1218 - val_loss: 7782.7197 - val_mae: 66.1108
Epoch 136/2000
1/1 [==============================] - 0s 45ms/step - loss: 7315.1138 - mae: 65.1173 - val_loss: 7781.5044 - val_mae: 66.1019
Epoch 137/2000
1/1 [==============================] - 0s 48ms/step - loss: 7314.1064 - mae: 65.1125 - val_loss: 7780.3062 - val_mae: 66.0930
Epoch 138/2000
1/1 [==============================] - 0s 39ms/step - loss: 7313.0991 - mae: 65.1075 - val_loss: 7779.1299 - val_mae: 66.0843
Epoch 139/2000
1/1 [==============================] - 0s 44ms/step - loss: 7312.0898 - mae: 65.1021 - val_loss: 7777.9771 - val_mae: 66.0758
Epoch 140/2000
1/1 [==============================] - 0s 68ms/step - loss: 7311.0786 - mae: 65.0964 - val_loss: 7776.8501 - val_mae: 66.0674
Epoch 141/2000
1/1 [==============================] - 0s 75ms/step - loss: 7310.0654 - mae: 65.0903 - val_loss: 7775.7461 - val_mae: 66.0592
Epoch 142/2000
1/1 [==============================] - 0s 41ms/step - loss: 7309.0503 - mae: 65.0838 - val_loss: 7774.6611 - val_mae: 66.0511
Epoch 143/2000
1/1 [==============================] - 0s 65ms/step - loss: 7308.0312 - mae: 65.0770 - val_loss: 7773.5918 - val_mae: 66.0432
Epoch 144/2000
1/1 [==============================] - 0s 38ms/step - loss: 7307.0122 - mae: 65.0699 - val_loss: 7772.5303 - val_mae: 66.0353
Epoch 145/2000
1/1 [==============================] - 0s 51ms/step - loss: 7305.9907 - mae: 65.0627 - val_loss: 7771.4688 - val_mae: 66.0274
Epoch 146/2000
1/1 [==============================] - 0s 64ms/step - loss: 7304.9688 - mae: 65.0555 - val_loss: 7770.4033 - val_mae: 66.0194
Epoch 147/2000
1/1 [==============================] - 0s 37ms/step - loss: 7303.9458 - mae: 65.0483 - val_loss: 7769.3281 - val_mae: 66.0114
Epoch 148/2000
1/1 [==============================] - 0s 40ms/step - loss: 7302.9219 - mae: 65.0412 - val_loss: 7768.2393 - val_mae: 66.0033
Epoch 149/2000
1/1 [==============================] - 0s 46ms/step - loss: 7301.8960 - mae: 65.0343 - val_loss: 7767.1318 - val_mae: 65.9951
Epoch 150/2000
1/1 [==============================] - 0s 48ms/step - loss: 7300.8677 - mae: 65.0276 - val_loss: 7766.0068 - val_mae: 65.9868
Epoch 151/2000
1/1 [==============================] - 0s 48ms/step - loss: 7299.8374 - mae: 65.0211 - val_loss: 7764.8643 - val_mae: 65.9783
Epoch 152/2000
1/1 [==============================] - 0s 53ms/step - loss: 7298.8062 - mae: 65.0148 - val_loss: 7763.7056 - val_mae: 65.9697
Epoch 153/2000
1/1 [==============================] - 0s 43ms/step - loss: 7297.7729 - mae: 65.0087 - val_loss: 7762.5337 - val_mae: 65.9610
Epoch 154/2000
1/1 [==============================] - 0s 39ms/step - loss: 7296.7378 - mae: 65.0027 - val_loss: 7761.3535 - val_mae: 65.9522
Epoch 155/2000
1/1 [==============================] - 0s 32ms/step - loss: 7295.6997 - mae: 64.9968 - val_loss: 7760.1675 - val_mae: 65.9434
Epoch 156/2000
1/1 [==============================] - 0s 31ms/step - loss: 7294.6616 - mae: 64.9910 - val_loss: 7758.9800 - val_mae: 65.9346
Epoch 157/2000
1/1 [==============================] - 0s 47ms/step - loss: 7293.6216 - mae: 64.9852 - val_loss: 7757.7954 - val_mae: 65.9258
Epoch 158/2000
1/1 [==============================] - 0s 35ms/step - loss: 7292.5791 - mae: 64.9793 - val_loss: 7756.6147 - val_mae: 65.9171
Epoch 159/2000
1/1 [==============================] - 0s 30ms/step - loss: 7291.5361 - mae: 64.9732 - val_loss: 7755.4429 - val_mae: 65.9084
Epoch 160/2000
1/1 [==============================] - 0s 43ms/step - loss: 7290.4907 - mae: 64.9671 - val_loss: 7754.2773 - val_mae: 65.8997
Epoch 161/2000
```

```
1/1 [==============================] - 0s 58ms/step - loss: 7289.4443 - mae: 64.9608 - val_loss: 7753.1191 - val_mae: 65.8911
Epoch 162/2000
1/1 [==============================] - 0s 50ms/step - loss: 7288.3940 - mae: 64.9543 - val_loss: 7751.9688 - val_mae: 65.8825
Epoch 163/2000
1/1 [==============================] - 0s 50ms/step - loss: 7287.3428 - mae: 64.9477 - val_loss: 7750.8228 - val_mae: 65.8740
Epoch 164/2000
1/1 [==============================] - 0s 51ms/step - loss: 7286.2900 - mae: 64.9410 - val_loss: 7749.6797 - val_mae: 65.8655
Epoch 165/2000
1/1 [==============================] - 0s 61ms/step - loss: 7285.2349 - mae: 64.9342 - val_loss: 7748.5371 - val_mae: 65.8570
Epoch 166/2000
1/1 [==============================] - 0s 37ms/step - loss: 7284.1772 - mae: 64.9273 - val_loss: 7747.3931 - val_mae: 65.8485
Epoch 167/2000
1/1 [==============================] - 0s 39ms/step - loss: 7283.1187 - mae: 64.9205 - val_loss: 7746.2437 - val_mae: 65.8399
Epoch 168/2000
1/1 [==============================] - 0s 55ms/step - loss: 7282.0581 - mae: 64.9136 - val_loss: 7745.0889 - val_mae: 65.8313
Epoch 169/2000
1/1 [==============================] - 0s 41ms/step - loss: 7280.9956 - mae: 64.9068 - val_loss: 7743.9268 - val_mae: 65.8226
Epoch 170/2000
1/1 [==============================] - 0s 32ms/step - loss: 7279.9302 - mae: 64.9001 - val_loss: 7742.7568 - val_mae: 65.8139
Epoch 171/2000
1/1 [==============================] - 0s 36ms/step - loss: 7278.8638 - mae: 64.8934 - val_loss: 7741.5781 - val_mae: 65.8052
Epoch 172/2000
1/1 [==============================] - 0s 48ms/step - loss: 7277.7959 - mae: 64.8868 - val_loss: 7740.3916 - val_mae: 65.7963
Epoch 173/2000
1/1 [==============================] - 0s 65ms/step - loss: 7276.7241 - mae: 64.8803 - val_loss: 7739.1982 - val_mae: 65.7874
Epoch 174/2000
1/1 [==============================] - 0s 50ms/step - loss: 7275.6509 - mae: 64.8738 - val_loss: 7738.0010 - val_mae: 65.7785
Epoch 175/2000
1/1 [==============================] - 0s 32ms/step - loss: 7274.5767 - mae: 64.8673 - val_loss: 7736.7993 - val_mae: 65.7696
Epoch 176/2000
1/1 [==============================] - 0s 32ms/step - loss: 7273.4995 - mae: 64.8609 - val_loss: 7735.5952 - val_mae: 65.7606
Epoch 177/2000
1/1 [==============================] - 0s 39ms/step - loss: 7272.4204 - mae: 64.8544 - val_loss: 7734.3906 - val_mae: 65.7516
Epoch 178/2000
1/1 [==============================] - 0s 39ms/step - loss: 7271.3384 - mae: 64.8479 - val_loss: 7733.1860 - val_mae: 65.7427
Epoch 179/2000
1/1 [==============================] - 0s 40ms/step - loss: 7270.2549 - mae: 64.8414 - val_loss: 7731.9810 - val_mae: 65.7337
Epoch 180/2000
1/1 [==============================] - 0s 32ms/step - loss: 7269.1694 - mae: 64.8348 - val_loss: 7730.7783 - val_mae: 65.7247
Epoch 181/2000
1/1 [==============================] - 0s 31ms/step - loss: 7268.0811 - mae: 64.8281 - val_loss: 7729.5771 - val_mae: 65.7158
Epoch 182/2000
1/1 [==============================] - 0s 29ms/step - loss: 7266.9912 - mae: 64.8214 - val_loss: 7728.3760 - val_mae: 65.7068
Epoch 183/2000
1/1 [==============================] - 0s 35ms/step - loss: 7265.8979 - mae: 64.8146 - val_loss: 7727.1753 - val_mae: 65.6979
Epoch 184/2000
1/1 [==============================] - 0s 43ms/step - loss: 7264.8032 - mae: 64.8077 - val_loss: 7725.9746 - val_mae: 65.6889
Epoch 185/2000
1/1 [==============================] - 0s 40ms/step - loss: 7263.7056 - mae: 64.8008 - val_loss: 7724.7725 - val_mae: 65.6799
Epoch 186/2000
1/1 [==============================] - 0s 36ms/step - loss: 7262.6079 - mae: 64.7939 - val_loss: 7723.5688 - val_mae: 65.6710
Epoch 187/2000
1/1 [==============================] - 0s 41ms/step - loss: 7261.5054 - mae: 64.7870 - val_loss: 7722.3594 - val_mae: 65.6619
Epoch 188/2000
1/1 [==============================] - 0s 46ms/step - loss: 7260.4023 - mae: 64.7800 - val_loss: 7721.1484 - val_mae: 65.6529
Epoch 189/2000
1/1 [==============================] - 0s 40ms/step - loss: 7259.2969 - mae: 64.7731 - val_loss: 7719.9316 - val_mae: 65.6438
Epoch 190/2000
1/1 [==============================] - 0s 65ms/step - loss: 7258.1875 - mae: 64.7662 - val_loss: 7718.7085 - val_mae: 65.6347
Epoch 191/2000
1/1 [==============================] - 0s 50ms/step - loss: 7257.0767 - mae: 64.7592 - val_loss: 7717.4810 - val_mae: 65.6255
Epoch 192/2000
1/1 [==============================] - 0s 45ms/step - loss: 7255.9624 - mae: 64.7524 - val_loss: 7716.2480 - val_mae: 65.6163
Epoch 193/2000
1/1 [==============================] - 0s 49ms/step - loss: 7254.8472 - mae: 64.7455 - val_loss: 7715.0103 - val_mae: 65.6071
Epoch 194/2000
1/1 [==============================] - 0s 34ms/step - loss: 7253.7290 - mae: 64.7387 - val_loss: 7713.7695 - val_mae: 65.5978
Epoch 195/2000
1/1 [==============================] - 0s 39ms/step - loss: 7252.6069 - mae: 64.7318 - val_loss: 7712.5239 - val_mae: 65.5885
Epoch 196/2000
1/1 [==============================] - 0s 65ms/step - loss: 7251.4844 - mae: 64.7249 - val_loss: 7711.2773 - val_mae: 65.5792
Epoch 197/2000
1/1 [==============================] - 0s 49ms/step - loss: 7250.3584 - mae: 64.7181 - val_loss: 7710.0283 - val_mae: 65.5699
Epoch 198/2000
1/1 [==============================] - 0s 31ms/step - loss: 7249.2280 - mae: 64.7112 - val_loss: 7708.7793 - val_mae: 65.5605
Epoch 199/2000
1/1 [==============================] - 0s 32ms/step - loss: 7248.0962 - mae: 64.7042 - val_loss: 7707.5273 - val_mae: 65.5512
Epoch 200/2000
1/1 [==============================] - 0s 30ms/step - loss: 7246.9619 - mae: 64.6972 - val_loss: 7706.2749 - val_mae: 65.5418
Epoch 201/2000
1/1 [==============================] - 0s 34ms/step - loss: 7245.8257 - mae: 64.6902 - val_loss: 7705.0205 - val_mae: 65.5325
Epoch 202/2000
1/1 [==============================] - 0s 78ms/step - loss: 7244.6851 - mae: 64.6831 - val_loss: 7703.7646 - val_mae: 65.5231
Epoch 203/2000
1/1 [==============================] - 0s 77ms/step - loss: 7243.5425 - mae: 64.6760 - val_loss: 7702.5073 - val_mae: 65.5137
Epoch 204/2000
1/1 [==============================] - 0s 51ms/step - loss: 7242.3975 - mae: 64.6689 - val_loss: 7701.2471 - val_mae: 65.5043
Epoch 205/2000
1/1 [==============================] - 0s 54ms/step - loss: 7241.2490 - mae: 64.6617 - val_loss: 7699.9834 - val_mae: 65.4948
Epoch 206/2000
1/1 [==============================] - 0s 43ms/step - loss: 7240.0972 - mae: 64.6545 - val_loss: 7698.7168 - val_mae: 65.4854
Epoch 207/2000
1/1 [==============================] - 0s 64ms/step - loss: 7238.9429 - mae: 64.6473 - val_loss: 7697.4468 - val_mae: 65.4759
Epoch 208/2000
1/1 [==============================] - 0s 75ms/step - loss: 7237.7856 - mae: 64.6401 - val_loss: 7696.1719 - val_mae: 65.4663
Epoch 209/2000
1/1 [==============================] - 0s 76ms/step - loss: 7236.6255 - mae: 64.6329 - val_loss: 7694.8931 - val_mae: 65.4568
Epoch 210/2000
1/1 [==============================] - 0s 40ms/step - loss: 7235.4619 - mae: 64.6257 - val_loss: 7693.6084 - val_mae: 65.4472
Epoch 211/2000
1/1 [==============================] - 0s 52ms/step - loss: 7234.2969 - mae: 64.6185 - val_loss: 7692.3218 - val_mae: 65.4375
Epoch 212/2000
1/1 [==============================] - 0s 52ms/step - loss: 7233.1274 - mae: 64.6112 - val_loss: 7691.0293 - val_mae: 65.4279
Epoch 213/2000
1/1 [==============================] - 0s 49ms/step - loss: 7231.9556 - mae: 64.6040 - val_loss: 7689.7334 - val_mae: 65.4182
Epoch 214/2000
1/1 [==============================] - 0s 73ms/step - loss: 7230.7788 - mae: 64.5967 - val_loss: 7688.4351 - val_mae: 65.4085
```

```
Epoch 215/2000
1/1 [==============================] - 0s 75ms/step - loss: 7229.6006 - mae: 64.5894 - val_loss: 7687.1328 - val_mae: 65.3987
Epoch 216/2000
1/1 [==============================] - 0s 48ms/step - loss: 7228.4180 - mae: 64.5822 - val_loss: 7685.8281 - val_mae: 65.3890
Epoch 217/2000
1/1 [==============================] - 0s 74ms/step - loss: 7227.2334 - mae: 64.5748 - val_loss: 7684.5200 - val_mae: 65.3792
Epoch 218/2000
1/1 [==============================] - 0s 75ms/step - loss: 7226.0444 - mae: 64.5675 - val_loss: 7683.2095 - val_mae: 65.3694
Epoch 219/2000
1/1 [==============================] - 0s 54ms/step - loss: 7224.8525 - mae: 64.5601 - val_loss: 7681.8955 - val_mae: 65.3595
Epoch 220/2000
1/1 [==============================] - 0s 66ms/step - loss: 7223.6572 - mae: 64.5527 - val_loss: 7680.5786 - val_mae: 65.3497
Epoch 221/2000
1/1 [==============================] - 0s 37ms/step - loss: 7222.4595 - mae: 64.5452 - val_loss: 7679.2583 - val_mae: 65.3398
Epoch 222/2000
1/1 [==============================] - 0s 66ms/step - loss: 7221.2568 - mae: 64.5377 - val_loss: 7677.9346 - val_mae: 65.3299
Epoch 223/2000
1/1 [==============================] - 0s 75ms/step - loss: 7220.0513 - mae: 64.5302 - val_loss: 7676.6069 - val_mae: 65.3199
Epoch 224/2000
1/1 [==============================] - 0s 50ms/step - loss: 7218.8423 - mae: 64.5227 - val_loss: 7675.2769 - val_mae: 65.3100
Epoch 225/2000
1/1 [==============================] - 0s 41ms/step - loss: 7217.6289 - mae: 64.5152 - val_loss: 7673.9404 - val_mae: 65.2999
Epoch 226/2000
1/1 [==============================] - 0s 49ms/step - loss: 7216.4136 - mae: 64.5076 - val_loss: 7672.6011 - val_mae: 65.2899
Epoch 227/2000
1/1 [==============================] - 0s 54ms/step - loss: 7215.1943 - mae: 64.5000 - val_loss: 7671.2568 - val_mae: 65.2798
Epoch 228/2000
1/1 [==============================] - 0s 53ms/step - loss: 7213.9702 - mae: 64.4924 - val_loss: 7669.9097 - val_mae: 65.2697
Epoch 229/2000
1/1 [==============================] - 0s 65ms/step - loss: 7212.7432 - mae: 64.4847 - val_loss: 7668.5571 - val_mae: 65.2596
Epoch 230/2000
1/1 [==============================] - 0s 60ms/step - loss: 7211.5122 - mae: 64.4771 - val_loss: 7667.2002 - val_mae: 65.2494
Epoch 231/2000
1/1 [==============================] - 0s 62ms/step - loss: 7210.2788 - mae: 64.4694 - val_loss: 7665.8389 - val_mae: 65.2392
Epoch 232/2000
1/1 [==============================] - 0s 75ms/step - loss: 7209.0396 - mae: 64.4617 - val_loss: 7664.4736 - val_mae: 65.2290
Epoch 233/2000
1/1 [==============================] - 0s 54ms/step - loss: 7207.7974 - mae: 64.4540 - val_loss: 7663.1035 - val_mae: 65.2187
Epoch 234/2000
1/1 [==============================] - 0s 47ms/step - loss: 7206.5513 - mae: 64.4463 - val_loss: 7661.7305 - val_mae: 65.2084
Epoch 235/2000
1/1 [==============================] - 0s 34ms/step - loss: 7205.3008 - mae: 64.4385 - val_loss: 7660.3525 - val_mae: 65.1981
Epoch 236/2000
1/1 [==============================] - 0s 41ms/step - loss: 7204.0479 - mae: 64.4307 - val_loss: 7658.9707 - val_mae: 65.1877
Epoch 237/2000
1/1 [==============================] - 0s 52ms/step - loss: 7202.7896 - mae: 64.4229 - val_loss: 7657.5859 - val_mae: 65.1773
Epoch 238/2000
1/1 [==============================] - 0s 68ms/step - loss: 7201.5283 - mae: 64.4151 - val_loss: 7656.1973 - val_mae: 65.1669
Epoch 239/2000
1/1 [==============================] - 0s 75ms/step - loss: 7200.2622 - mae: 64.4072 - val_loss: 7654.8047 - val_mae: 65.1565
Epoch 240/2000
1/1 [==============================] - 0s 77ms/step - loss: 7198.9922 - mae: 64.3992 - val_loss: 7653.4111 - val_mae: 65.1460
Epoch 241/2000
1/1 [==============================] - 0s 39ms/step - loss: 7197.7188 - mae: 64.3913 - val_loss: 7652.0112 - val_mae: 65.1355
Epoch 242/2000
1/1 [==============================] - 0s 44ms/step - loss: 7196.4390 - mae: 64.3833 - val_loss: 7650.6069 - val_mae: 65.1250
Epoch 243/2000
1/1 [==============================] - 0s 49ms/step - loss: 7195.1572 - mae: 64.3753 - val_loss: 7649.1978 - val_mae: 65.1145
Epoch 244/2000
1/1 [==============================] - 0s 44ms/step - loss: 7193.8696 - mae: 64.3673 - val_loss: 7647.7832 - val_mae: 65.1039
Epoch 245/2000
1/1 [==============================] - 0s 40ms/step - loss: 7192.5786 - mae: 64.3592 - val_loss: 7646.3643 - val_mae: 65.0932
Epoch 246/2000
1/1 [==============================] - 0s 41ms/step - loss: 7191.2837 - mae: 64.3512 - val_loss: 7644.9385 - val_mae: 65.0825
Epoch 247/2000
1/1 [==============================] - 0s 32ms/step - loss: 7189.9834 - mae: 64.3431 - val_loss: 7643.5088 - val_mae: 65.0718
Epoch 248/2000
1/1 [==============================] - 0s 36ms/step - loss: 7188.6782 - mae: 64.3349 - val_loss: 7642.0742 - val_mae: 65.0611
Epoch 249/2000
1/1 [==============================] - 0s 49ms/step - loss: 7187.3696 - mae: 64.3268 - val_loss: 7640.6348 - val_mae: 65.0503
Epoch 250/2000
1/1 [==============================] - 0s 52ms/step - loss: 7186.0547 - mae: 64.3186 - val_loss: 7639.1899 - val_mae: 65.0394
Epoch 251/2000
1/1 [==============================] - 0s 49ms/step - loss: 7184.7373 - mae: 64.3104 - val_loss: 7637.7432 - val_mae: 65.0286
Epoch 252/2000
1/1 [==============================] - 0s 56ms/step - loss: 7183.4150 - mae: 64.3021 - val_loss: 7636.2920 - val_mae: 65.0177
Epoch 253/2000
1/1 [==============================] - 0s 62ms/step - loss: 7182.0884 - mae: 64.2938 - val_loss: 7634.8359 - val_mae: 65.0068
Epoch 254/2000
1/1 [==============================] - 0s 60ms/step - loss: 7180.7554 - mae: 64.2855 - val_loss: 7633.3760 - val_mae: 64.9958
Epoch 255/2000
1/1 [==============================] - 0s 40ms/step - loss: 7179.4185 - mae: 64.2771 - val_loss: 7631.9111 - val_mae: 64.9848
Epoch 256/2000
1/1 [==============================] - 0s 63ms/step - loss: 7178.0771 - mae: 64.2686 - val_loss: 7630.4395 - val_mae: 64.9738
Epoch 257/2000
1/1 [==============================] - 0s 42ms/step - loss: 7176.7300 - mae: 64.2602 - val_loss: 7628.9619 - val_mae: 64.9627
Epoch 258/2000
1/1 [==============================] - 0s 37ms/step - loss: 7175.3789 - mae: 64.2517 - val_loss: 7627.4775 - val_mae: 64.9515
Epoch 259/2000
1/1 [==============================] - 0s 31ms/step - loss: 7174.0225 - mae: 64.2432 - val_loss: 7625.9863 - val_mae: 64.9403
Epoch 260/2000
1/1 [==============================] - 0s 36ms/step - loss: 7172.6597 - mae: 64.2347 - val_loss: 7624.4883 - val_mae: 64.9291
Epoch 261/2000
1/1 [==============================] - 0s 38ms/step - loss: 7171.2925 - mae: 64.2262 - val_loss: 7622.9849 - val_mae: 64.9177
Epoch 262/2000
1/1 [==============================] - 0s 36ms/step - loss: 7169.9209 - mae: 64.2176 - val_loss: 7621.4746 - val_mae: 64.9064
Epoch 263/2000
1/1 [==============================] - 0s 31ms/step - loss: 7168.5425 - mae: 64.2091 - val_loss: 7619.9565 - val_mae: 64.8950
Epoch 264/2000
1/1 [==============================] - 0s 38ms/step - loss: 7167.1606 - mae: 64.2004 - val_loss: 7618.4351 - val_mae: 64.8835
Epoch 265/2000
1/1 [==============================] - 0s 38ms/step - loss: 7165.7725 - mae: 64.1918 - val_loss: 7616.9062 - val_mae: 64.8720
Epoch 266/2000
1/1 [==============================] - 0s 41ms/step - loss: 7164.3794 - mae: 64.1831 - val_loss: 7615.3740 - val_mae: 64.8605
Epoch 267/2000
1/1 [==============================] - 0s 65ms/step - loss: 7162.9800 - mae: 64.1744 - val_loss: 7613.8364 - val_mae: 64.8489
Epoch 268/2000
```

```
1/1 [==============================] - 0s 76ms/step - loss: 7161.5747 - mae: 64.1656 - val_loss: 7612.2930 - val_mae: 64.8372
Epoch 269/2000
1/1 [==============================] - 0s 59ms/step - loss: 7160.1641 - mae: 64.1568 - val_loss: 7610.7441 - val_mae: 64.8256
Epoch 270/2000
1/1 [==============================] - 0s 47ms/step - loss: 7158.7490 - mae: 64.1479 - val_loss: 7609.1895 - val_mae: 64.8139
Epoch 271/2000
1/1 [==============================] - 0s 44ms/step - loss: 7157.3281 - mae: 64.1390 - val_loss: 7607.6274 - val_mae: 64.8021
Epoch 272/2000
1/1 [==============================] - 0s 35ms/step - loss: 7155.9009 - mae: 64.1300 - val_loss: 7606.0596 - val_mae: 64.7903
Epoch 273/2000
1/1 [==============================] - 0s 34ms/step - loss: 7154.4678 - mae: 64.1211 - val_loss: 7604.4834 - val_mae: 64.7784
Epoch 274/2000
1/1 [==============================] - 0s 44ms/step - loss: 7153.0278 - mae: 64.1121 - val_loss: 7602.8999 - val_mae: 64.7665
Epoch 275/2000
1/1 [==============================] - 0s 48ms/step - loss: 7151.5835 - mae: 64.1031 - val_loss: 7601.3096 - val_mae: 64.7545
Epoch 276/2000
1/1 [==============================] - 0s 59ms/step - loss: 7150.1323 - mae: 64.0940 - val_loss: 7599.7139 - val_mae: 64.7425
Epoch 277/2000
1/1 [==============================] - 0s 60ms/step - loss: 7148.6753 - mae: 64.0849 - val_loss: 7598.1123 - val_mae: 64.7304
Epoch 278/2000
1/1 [==============================] - 0s 42ms/step - loss: 7147.2119 - mae: 64.0758 - val_loss: 7596.5039 - val_mae: 64.7183
Epoch 279/2000
1/1 [==============================] - 0s 49ms/step - loss: 7145.7422 - mae: 64.0666 - val_loss: 7594.8926 - val_mae: 64.7061
Epoch 280/2000
1/1 [==============================] - 0s 44ms/step - loss: 7144.2681 - mae: 64.0573 - val_loss: 7593.2754 - val_mae: 64.6939
Epoch 281/2000
1/1 [==============================] - 0s 37ms/step - loss: 7142.7856 - mae: 64.0480 - val_loss: 7591.6523 - val_mae: 64.6817
Epoch 282/2000
1/1 [==============================] - 0s 50ms/step - loss: 7141.2969 - mae: 64.0386 - val_loss: 7590.0229 - val_mae: 64.6694
Epoch 283/2000
1/1 [==============================] - 0s 48ms/step - loss: 7139.8022 - mae: 64.0291 - val_loss: 7588.3862 - val_mae: 64.6571
Epoch 284/2000
1/1 [==============================] - 0s 52ms/step - loss: 7138.3022 - mae: 64.0196 - val_loss: 7586.7422 - val_mae: 64.6446
Epoch 285/2000
1/1 [==============================] - 0s 41ms/step - loss: 7136.7935 - mae: 64.0101 - val_loss: 7585.0913 - val_mae: 64.6322
Epoch 286/2000
1/1 [==============================] - 0s 72ms/step - loss: 7135.2803 - mae: 64.0006 - val_loss: 7583.4326 - val_mae: 64.6197
Epoch 287/2000
1/1 [==============================] - 0s 49ms/step - loss: 7133.7578 - mae: 63.9910 - val_loss: 7581.7666 - val_mae: 64.6071
Epoch 288/2000
1/1 [==============================] - 0s 38ms/step - loss: 7132.2300 - mae: 63.9814 - val_loss: 7580.0884 - val_mae: 64.5945
Epoch 289/2000
1/1 [==============================] - 0s 62ms/step - loss: 7130.6953 - mae: 63.9718 - val_loss: 7578.4014 - val_mae: 64.5818
Epoch 290/2000
1/1 [==============================] - 0s 48ms/step - loss: 7129.1538 - mae: 63.9622 - val_loss: 7576.7061 - val_mae: 64.5690
Epoch 291/2000
1/1 [==============================] - 0s 49ms/step - loss: 7127.6055 - mae: 63.9526 - val_loss: 7575.0059 - val_mae: 64.5562
Epoch 292/2000
1/1 [==============================] - 0s 48ms/step - loss: 7126.0503 - mae: 63.9429 - val_loss: 7573.2988 - val_mae: 64.5433
Epoch 293/2000
1/1 [==============================] - 0s 34ms/step - loss: 7124.4873 - mae: 63.9331 - val_loss: 7571.5864 - val_mae: 64.5304
Epoch 294/2000
1/1 [==============================] - 0s 59ms/step - loss: 7122.9165 - mae: 63.9232 - val_loss: 7569.8672 - val_mae: 64.5174
Epoch 295/2000
1/1 [==============================] - 0s 47ms/step - loss: 7121.3403 - mae: 63.9133 - val_loss: 7568.1396 - val_mae: 64.5044
Epoch 296/2000
1/1 [==============================] - 0s 34ms/step - loss: 7119.7554 - mae: 63.9033 - val_loss: 7566.4062 - val_mae: 64.4913
Epoch 297/2000
1/1 [==============================] - 0s 36ms/step - loss: 7118.1641 - mae: 63.8933 - val_loss: 7561.9673 - val_mae: 64.4580
Epoch 298/2000
1/1 [==============================] - 0s 46ms/step - loss: 7114.4077 - mae: 63.8758 - val_loss: 7560.0117 - val_mae: 64.4432
Epoch 299/2000
1/1 [==============================] - 0s 46ms/step - loss: 7112.5513 - mae: 63.8630 - val_loss: 7558.5083 - val_mae: 64.4322
Epoch 300/2000
1/1 [==============================] - 0s 49ms/step - loss: 7110.7852 - mae: 63.8450 - val_loss: 7554.8379 - val_mae: 64.4027
Epoch 301/2000
1/1 [==============================] - 0s 68ms/step - loss: 7109.0435 - mae: 63.8594 - val_loss: 7551.7441 - val_mae: 64.3926
Epoch 302/2000
1/1 [==============================] - 0s 76ms/step - loss: 7107.7065 - mae: 63.8696 - val_loss: 7549.1963 - val_mae: 64.3999
Epoch 303/2000
1/1 [==============================] - 0s 38ms/step - loss: 7106.2563 - mae: 63.8699 - val_loss: 7547.2041 - val_mae: 64.3884
Epoch 304/2000
1/1 [==============================] - 0s 39ms/step - loss: 7104.4561 - mae: 63.8588 - val_loss: 7545.7324 - val_mae: 64.3595
Epoch 305/2000
1/1 [==============================] - 0s 46ms/step - loss: 7102.3247 - mae: 63.8369 - val_loss: 7544.6860 - val_mae: 64.3249
Epoch 306/2000
1/1 [==============================] - 0s 69ms/step - loss: 7100.0859 - mae: 63.8071 - val_loss: 7543.8882 - val_mae: 64.3203
Epoch 307/2000
1/1 [==============================] - 0s 77ms/step - loss: 7097.9849 - mae: 63.7737 - val_loss: 7543.0791 - val_mae: 64.3149
Epoch 308/2000
1/1 [==============================] - 0s 51ms/step - loss: 7096.1069 - mae: 63.7413 - val_loss: 7541.9805 - val_mae: 64.3067
Epoch 309/2000
1/1 [==============================] - 0s 68ms/step - loss: 7094.3501 - mae: 63.7137 - val_loss: 7540.3623 - val_mae: 64.2943
Epoch 310/2000
1/1 [==============================] - 0s 76ms/step - loss: 7092.5283 - mae: 63.6937 - val_loss: 7538.1245 - val_mae: 64.2773
Epoch 311/2000
1/1 [==============================] - 0s 52ms/step - loss: 7090.5283 - mae: 63.6822 - val_loss: 7535.3364 - val_mae: 64.2562
Epoch 312/2000
1/1 [==============================] - 0s 36ms/step - loss: 7088.3750 - mae: 63.6782 - val_loss: 7532.1943 - val_mae: 64.2321
Epoch 313/2000
1/1 [==============================] - 0s 31ms/step - loss: 7086.1958 - mae: 63.6794 - val_loss: 7528.9570 - val_mae: 64.2068
Epoch 314/2000
1/1 [==============================] - 0s 32ms/step - loss: 7084.1060 - mae: 63.6823 - val_loss: 7525.8540 - val_mae: 64.1829
Epoch 315/2000
1/1 [==============================] - 0s 34ms/step - loss: 7082.1133 - mae: 63.6833 - val_loss: 7523.0420 - val_mae: 64.1842
Epoch 316/2000
1/1 [==============================] - 0s 40ms/step - loss: 7080.1274 - mae: 63.6792 - val_loss: 7520.5889 - val_mae: 64.1745
Epoch 317/2000
1/1 [==============================] - 0s 37ms/step - loss: 7078.0425 - mae: 63.6682 - val_loss: 7518.4883 - val_mae: 64.1534
Epoch 318/2000
1/1 [==============================] - 0s 63ms/step - loss: 7075.8311 - mae: 63.6503 - val_loss: 7516.6680 - val_mae: 64.1235
Epoch 319/2000
1/1 [==============================] - 0s 39ms/step - loss: 7073.5513 - mae: 63.6270 - val_loss: 7514.9907 - val_mae: 64.1005
Epoch 320/2000
1/1 [==============================] - 0s 37ms/step - loss: 7071.2920 - mae: 63.6010 - val_loss: 7513.2769 - val_mae: 64.0880
Epoch 321/2000
1/1 [==============================] - 0s 50ms/step - loss: 7069.0835 - mae: 63.5753 - val_loss: 7511.3452 - val_mae: 64.0735
```

```
Epoch 322/2000
1/1 [==============================] - 0s 70ms/step - loss: 7066.8896 - mae: 63.5528 - val_loss: 7509.0664 - val_mae: 64.0563
Epoch 323/2000
1/1 [==============================] - 0s 57ms/step - loss: 7064.6436 - mae: 63.5352 - val_loss: 7506.4077 - val_mae: 64.0360
Epoch 324/2000
1/1 [==============================] - 0s 76ms/step - loss: 7062.3149 - mae: 63.5227 - val_loss: 7503.4390 - val_mae: 64.0131
Epoch 325/2000
1/1 [==============================] - 0s 53ms/step - loss: 7059.9272 - mae: 63.5146 - val_loss: 7500.3066 - val_mae: 63.9911
Epoch 326/2000
1/1 [==============================] - 0s 48ms/step - loss: 7057.5347 - mae: 63.5086 - val_loss: 7497.1714 - val_mae: 63.9900
Epoch 327/2000
1/1 [==============================] - 0s 44ms/step - loss: 7055.1587 - mae: 63.5024 - val_loss: 7494.1689 - val_mae: 63.9846
Epoch 328/2000
1/1 [==============================] - 0s 34ms/step - loss: 7052.7769 - mae: 63.4934 - val_loss: 7491.3730 - val_mae: 63.9724
Epoch 329/2000
1/1 [==============================] - 0s 46ms/step - loss: 7050.3486 - mae: 63.4801 - val_loss: 7488.7988 - val_mae: 63.9528
Epoch 330/2000
1/1 [==============================] - 0s 40ms/step - loss: 7047.8555 - mae: 63.4623 - val_loss: 7486.3931 - val_mae: 63.9272
Epoch 331/2000
1/1 [==============================] - 0s 44ms/step - loss: 7045.3159 - mae: 63.4408 - val_loss: 7484.0601 - val_mae: 63.8987
Epoch 332/2000
1/1 [==============================] - 0s 51ms/step - loss: 7042.7622 - mae: 63.4174 - val_loss: 7481.6714 - val_mae: 63.8708
Epoch 333/2000
1/1 [==============================] - 0s 33ms/step - loss: 7040.2061 - mae: 63.3943 - val_loss: 7479.1079 - val_mae: 63.8467
Epoch 334/2000
1/1 [==============================] - 0s 41ms/step - loss: 7037.6284 - mae: 63.3734 - val_loss: 7476.2979 - val_mae: 63.8280
Epoch 335/2000
1/1 [==============================] - 0s 47ms/step - loss: 7035.0044 - mae: 63.3558 - val_loss: 7473.2397 - val_mae: 63.8149
Epoch 336/2000
1/1 [==============================] - 0s 44ms/step - loss: 7032.3296 - mae: 63.3415 - val_loss: 7470.0039 - val_mae: 63.8055
Epoch 337/2000
1/1 [==============================] - 0s 36ms/step - loss: 7029.6196 - mae: 63.3294 - val_loss: 7466.6997 - val_mae: 63.7970
Epoch 338/2000
1/1 [==============================] - 0s 33ms/step - loss: 7026.8931 - mae: 63.3177 - val_loss: 7463.4336 - val_mae: 63.7864
Epoch 339/2000
1/1 [==============================] - 0s 59ms/step - loss: 7024.1460 - mae: 63.3047 - val_loss: 7460.2803 - val_mae: 63.7715
Epoch 340/2000
1/1 [==============================] - 0s 35ms/step - loss: 7021.3628 - mae: 63.2890 - val_loss: 7457.2588 - val_mae: 63.7514
Epoch 341/2000
1/1 [==============================] - 0s 30ms/step - loss: 7018.5337 - mae: 63.2701 - val_loss: 7454.3428 - val_mae: 63.7271
Epoch 342/2000
1/1 [==============================] - 0s 37ms/step - loss: 7015.6616 - mae: 63.2484 - val_loss: 7451.4570 - val_mae: 63.7005
Epoch 343/2000
1/1 [==============================] - 0s 36ms/step - loss: 7012.7612 - mae: 63.2253 - val_loss: 7448.5122 - val_mae: 63.6745
Epoch 344/2000
1/1 [==============================] - 0s 44ms/step - loss: 7009.8350 - mae: 63.2025 - val_loss: 7445.4229 - val_mae: 63.6512
Epoch 345/2000
1/1 [==============================] - 0s 43ms/step - loss: 7006.8765 - mae: 63.1812 - val_loss: 7442.1479 - val_mae: 63.6317
Epoch 346/2000
1/1 [==============================] - 0s 46ms/step - loss: 7003.8740 - mae: 63.1622 - val_loss: 7438.7031 - val_mae: 63.6156
Epoch 347/2000
1/1 [==============================] - 0s 41ms/step - loss: 7000.8291 - mae: 63.1451 - val_loss: 7435.1504 - val_mae: 63.6013
Epoch 348/2000
1/1 [==============================] - 0s 51ms/step - loss: 6997.7495 - mae: 63.1291 - val_loss: 7431.5698 - val_mae: 63.5864
Epoch 349/2000
1/1 [==============================] - 0s 45ms/step - loss: 6994.6396 - mae: 63.1126 - val_loss: 7428.0317 - val_mae: 63.5690
Epoch 350/2000
1/1 [==============================] - 0s 37ms/step - loss: 6991.4937 - mae: 63.0945 - val_loss: 7424.5664 - val_mae: 63.5479
Epoch 351/2000
1/1 [==============================] - 0s 39ms/step - loss: 6988.3037 - mae: 63.0740 - val_loss: 7421.1660 - val_mae: 63.5235
Epoch 352/2000
1/1 [==============================] - 0s 35ms/step - loss: 6985.0713 - mae: 63.0514 - val_loss: 7417.7783 - val_mae: 63.4971
Epoch 353/2000
1/1 [==============================] - 0s 31ms/step - loss: 6981.8013 - mae: 63.0275 - val_loss: 7414.3384 - val_mae: 63.4708
Epoch 354/2000
1/1 [==============================] - 0s 35ms/step - loss: 6978.4961 - mae: 63.0036 - val_loss: 7410.7832 - val_mae: 63.4463
Epoch 355/2000
1/1 [==============================] - 0s 32ms/step - loss: 6975.1519 - mae: 62.9806 - val_loss: 7407.0835 - val_mae: 63.4243
Epoch 356/2000
1/1 [==============================] - 0s 31ms/step - loss: 6971.7622 - mae: 62.9592 - val_loss: 7403.2549 - val_mae: 63.4046
Epoch 357/2000
1/1 [==============================] - 0s 30ms/step - loss: 6968.3306 - mae: 62.9389 - val_loss: 7399.3452 - val_mae: 63.3857
Epoch 358/2000
1/1 [==============================] - 0s 43ms/step - loss: 6964.8569 - mae: 62.9191 - val_loss: 7395.4150 - val_mae: 63.3659
Epoch 359/2000
1/1 [==============================] - 0s 48ms/step - loss: 6961.3467 - mae: 62.8986 - val_loss: 7391.5098 - val_mae: 63.3437
Epoch 360/2000
1/1 [==============================] - 0s 43ms/step - loss: 6957.7915 - mae: 62.8766 - val_loss: 7387.6387 - val_mae: 63.3187
Epoch 361/2000
1/1 [==============================] - 0s 55ms/step - loss: 6954.1919 - mae: 62.8527 - val_loss: 7383.7798 - val_mae: 63.2916
Epoch 362/2000
1/1 [==============================] - 0s 44ms/step - loss: 6950.5479 - mae: 62.8275 - val_loss: 7379.8818 - val_mae: 63.2639
Epoch 363/2000
1/1 [==============================] - 0s 54ms/step - loss: 6946.8604 - mae: 62.8017 - val_loss: 7375.8994 - val_mae: 63.2371
Epoch 364/2000
1/1 [==============================] - 0s 49ms/step - loss: 6943.1313 - mae: 62.7764 - val_loss: 7371.7983 - val_mae: 63.2120
Epoch 365/2000
1/1 [==============================] - 0s 47ms/step - loss: 6939.3550 - mae: 62.7521 - val_loss: 7367.5869 - val_mae: 63.1885
Epoch 366/2000
1/1 [==============================] - 0s 57ms/step - loss: 6935.5322 - mae: 62.7286 - val_loss: 7363.2944 - val_mae: 63.1655
Epoch 367/2000
1/1 [==============================] - 0s 40ms/step - loss: 6931.6636 - mae: 62.7053 - val_loss: 7358.9692 - val_mae: 63.1418
Epoch 368/2000
1/1 [==============================] - 0s 46ms/step - loss: 6927.7510 - mae: 62.6815 - val_loss: 7354.6436 - val_mae: 63.1163
Epoch 369/2000
1/1 [==============================] - 0s 76ms/step - loss: 6923.7900 - mae: 62.6564 - val_loss: 7350.3228 - val_mae: 63.0886
Epoch 370/2000
1/1 [==============================] - 0s 74ms/step - loss: 6919.7817 - mae: 62.6299 - val_loss: 7345.9854 - val_mae: 63.0595
Epoch 371/2000
1/1 [==============================] - 0s 54ms/step - loss: 6915.7256 - mae: 62.6024 - val_loss: 7341.5947 - val_mae: 63.0301
Epoch 372/2000
1/1 [==============================] - 0s 32ms/step - loss: 6911.6216 - mae: 62.5746 - val_loss: 7337.1152 - val_mae: 63.0013
Epoch 373/2000
1/1 [==============================] - 0s 48ms/step - loss: 6907.4697 - mae: 62.5471 - val_loss: 7332.5332 - val_mae: 62.9738
Epoch 374/2000
1/1 [==============================] - 0s 39ms/step - loss: 6903.2671 - mae: 62.5203 - val_loss: 7327.8599 - val_mae: 62.9471
Epoch 375/2000
```

```
1/1 [==============================] - 0s 31ms/step - loss: 6899.0132 - mae: 62.4938 - val_loss: 7323.1240 - val_mae: 62.9203
Epoch 376/2000
1/1 [==============================] - 0s 31ms/step - loss: 6894.7109 - mae: 62.4671 - val_loss: 7318.3604 - val_mae: 62.8923
Epoch 377/2000
1/1 [==============================] - 0s 38ms/step - loss: 6890.3564 - mae: 62.4396 - val_loss: 7313.5820 - val_mae: 62.8626
Epoch 378/2000
1/1 [==============================] - 0s 35ms/step - loss: 6885.9497 - mae: 62.4109 - val_loss: 7308.7793 - val_mae: 62.8314
Epoch 379/2000
1/1 [==============================] - 0s 31ms/step - loss: 6881.4912 - mae: 62.3812 - val_loss: 7303.9268 - val_mae: 62.7996
Epoch 380/2000
1/1 [==============================] - 0s 33ms/step - loss: 6876.9800 - mae: 62.3510 - val_loss: 7298.9985 - val_mae: 62.7681
Epoch 381/2000
1/1 [==============================] - 0s 33ms/step - loss: 6872.4165 - mae: 62.3208 - val_loss: 7293.9756 - val_mae: 62.7373
Epoch 382/2000
1/1 [==============================] - 0s 32ms/step - loss: 6867.7959 - mae: 62.2910 - val_loss: 7288.8652 - val_mae: 62.7071
Epoch 383/2000
1/1 [==============================] - 0s 32ms/step - loss: 6863.1226 - mae: 62.2613 - val_loss: 7280.9180 - val_mae: 62.6613
Epoch 384/2000
1/1 [==============================] - 0s 44ms/step - loss: 6855.8018 - mae: 62.2150 - val_loss: 7274.6992 - val_mae: 62.6476
Epoch 385/2000
1/1 [==============================] - 0s 57ms/step - loss: 6850.6938 - mae: 62.1943 - val_loss: 7269.5029 - val_mae: 62.5932
Epoch 386/2000
1/1 [==============================] - 0s 39ms/step - loss: 6845.3540 - mae: 62.1484 - val_loss: 7263.9912 - val_mae: 62.5423
Epoch 387/2000
1/1 [==============================] - 0s 71ms/step - loss: 6839.8999 - mae: 62.1042 - val_loss: 7258.0508 - val_mae: 62.4597
Epoch 388/2000
1/1 [==============================] - 0s 58ms/step - loss: 6833.5718 - mae: 62.0382 - val_loss: 7251.3584 - val_mae: 62.4330
Epoch 389/2000
1/1 [==============================] - 0s 50ms/step - loss: 6827.6753 - mae: 62.0080 - val_loss: 7243.4419 - val_mae: 62.4408
Epoch 390/2000
1/1 [==============================] - 0s 37ms/step - loss: 6821.5913 - mae: 61.9984 - val_loss: 7235.9629 - val_mae: 62.4295
Epoch 391/2000
1/1 [==============================] - 0s 43ms/step - loss: 6815.6118 - mae: 61.9767 - val_loss: 7229.7109 - val_mae: 62.3657
Epoch 392/2000
1/1 [==============================] - 0s 31ms/step - loss: 6809.1885 - mae: 61.9226 - val_loss: 7223.9580 - val_mae: 62.2788
Epoch 393/2000
1/1 [==============================] - 0s 31ms/step - loss: 6802.7500 - mae: 61.8539 - val_loss: 7217.1724 - val_mae: 62.2206
Epoch 394/2000
1/1 [==============================] - 0s 31ms/step - loss: 6796.2075 - mae: 61.8025 - val_loss: 7208.9541 - val_mae: 62.2033
Epoch 395/2000
1/1 [==============================] - 0s 35ms/step - loss: 6789.2974 - mae: 61.7756 - val_loss: 7200.4707 - val_mae: 62.1906
Epoch 396/2000
1/1 [==============================] - 0s 31ms/step - loss: 6782.4097 - mae: 61.7511 - val_loss: 7192.7979 - val_mae: 62.1408
Epoch 397/2000
1/1 [==============================] - 0s 30ms/step - loss: 6775.2886 - mae: 61.7035 - val_loss: 7185.7969 - val_mae: 62.0584
Epoch 398/2000
1/1 [==============================] - 0s 30ms/step - loss: 6767.9575 - mae: 61.6356 - val_loss: 7178.3071 - val_mae: 61.9870
Epoch 399/2000
1/1 [==============================] - 0s 45ms/step - loss: 6760.5869 - mae: 61.5741 - val_loss: 7169.5776 - val_mae: 61.9513
Epoch 400/2000
1/1 [==============================] - 0s 53ms/step - loss: 6752.9033 - mae: 61.5339 - val_loss: 7160.3315 - val_mae: 61.9281
Epoch 401/2000
1/1 [==============================] - 0s 42ms/step - loss: 6745.1274 - mae: 61.5009 - val_loss: 7151.6143 - val_mae: 61.8772
Epoch 402/2000
1/1 [==============================] - 0s 51ms/step - loss: 6737.1797 - mae: 61.4506 - val_loss: 7143.4707 - val_mae: 61.7957
Epoch 403/2000
1/1 [==============================] - 0s 53ms/step - loss: 6729.0054 - mae: 61.3811 - val_loss: 7134.9355 - val_mae: 61.7214
Epoch 404/2000
1/1 [==============================] - 0s 42ms/step - loss: 6720.7437 - mae: 61.3156 - val_loss: 7125.3545 - val_mae: 61.6774
Epoch 405/2000
1/1 [==============================] - 0s 48ms/step - loss: 6712.2119 - mae: 61.2682 - val_loss: 7115.3643 - val_mae: 61.6417
Epoch 406/2000
1/1 [==============================] - 0s 55ms/step - loss: 6703.5615 - mae: 61.2253 - val_loss: 7105.8296 - val_mae: 61.5792
Epoch 407/2000
1/1 [==============================] - 0s 45ms/step - loss: 6694.7095 - mae: 61.1657 - val_loss: 7096.6260 - val_mae: 61.4941
Epoch 408/2000
1/1 [==============================] - 0s 51ms/step - loss: 6685.6719 - mae: 61.0918 - val_loss: 7086.8496 - val_mae: 61.4229
Epoch 409/2000
1/1 [==============================] - 0s 34ms/step - loss: 6676.4810 - mae: 61.0258 - val_loss: 7076.2334 - val_mae: 61.3759
Epoch 410/2000
1/1 [==============================] - 0s 44ms/step - loss: 6667.0562 - mae: 60.9742 - val_loss: 7065.5347 - val_mae: 61.3238
Epoch 411/2000
1/1 [==============================] - 0s 72ms/step - loss: 6657.4951 - mae: 60.9191 - val_loss: 7055.2524 - val_mae: 61.2440
Epoch 412/2000
1/1 [==============================] - 0s 60ms/step - loss: 6647.7056 - mae: 60.8465 - val_loss: 7044.8711 - val_mae: 61.1586
Epoch 413/2000
1/1 [==============================] - 0s 59ms/step - loss: 6637.7656 - mae: 60.7700 - val_loss: 7033.7358 - val_mae: 61.0948
Epoch 414/2000
1/1 [==============================] - 0s 51ms/step - loss: 6627.6040 - mae: 60.7063 - val_loss: 7022.1738 - val_mae: 61.0398
Epoch 415/2000
1/1 [==============================] - 0s 67ms/step - loss: 6617.2690 - mae: 60.6474 - val_loss: 7010.8618 - val_mae: 60.9637
Epoch 416/2000
1/1 [==============================] - 0s 53ms/step - loss: 6606.7334 - mae: 60.5751 - val_loss: 6999.6348 - val_mae: 60.8729
Epoch 417/2000
1/1 [==============================] - 0s 39ms/step - loss: 6596.0107 - mae: 60.4933 - val_loss: 6987.8281 - val_mae: 60.7974
Epoch 418/2000
1/1 [==============================] - 0s 56ms/step - loss: 6585.0903 - mae: 60.4202 - val_loss: 6975.5093 - val_mae: 60.7347
Epoch 419/2000
1/1 [==============================] - 0s 45ms/step - loss: 6573.9731 - mae: 60.3546 - val_loss: 6963.2949 - val_mae: 60.6561
Epoch 420/2000
1/1 [==============================] - 0s 33ms/step - loss: 6562.6616 - mae: 60.2786 - val_loss: 6951.2178 - val_mae: 60.5625
Epoch 421/2000
1/1 [==============================] - 0s 35ms/step - loss: 6551.1538 - mae: 60.1924 - val_loss: 6938.6738 - val_mae: 60.4815
Epoch 422/2000
1/1 [==============================] - 0s 31ms/step - loss: 6539.4463 - mae: 60.1131 - val_loss: 6925.6675 - val_mae: 60.4124
Epoch 423/2000
1/1 [==============================] - 0s 31ms/step - loss: 6527.5381 - mae: 60.0403 - val_loss: 6912.7158 - val_mae: 60.3283
Epoch 424/2000
1/1 [==============================] - 0s 31ms/step - loss: 6515.4297 - mae: 59.9578 - val_loss: 6899.7617 - val_mae: 60.2314
Epoch 425/2000
1/1 [==============================] - 0s 32ms/step - loss: 6503.1240 - mae: 59.8670 - val_loss: 6886.3359 - val_mae: 60.1472
Epoch 426/2000
1/1 [==============================] - 0s 40ms/step - loss: 6490.6108 - mae: 59.7832 - val_loss: 6872.5576 - val_mae: 60.0697
Epoch 427/2000
1/1 [==============================] - 0s 48ms/step - loss: 6477.8999 - mae: 59.7029 - val_loss: 6858.8330 - val_mae: 59.9758
Epoch 428/2000
1/1 [==============================] - 0s 43ms/step - loss: 6464.9810 - mae: 59.6120 - val_loss: 6844.5684 - val_mae: 59.8810
```

```
Epoch 429/2000
1/1 [==============================] - 0s 34ms/step - loss: 6451.5962 - mae: 59.5193 - val_loss: 6830.2441 - val_mae: 59.7850
Epoch 430/2000
1/1 [==============================] - 0s 41ms/step - loss: 6438.1475 - mae: 59.4256 - val_loss: 6815.5225 - val_mae: 59.6944
Epoch 431/2000
1/1 [==============================] - 0s 70ms/step - loss: 6424.4302 - mae: 59.3345 - val_loss: 6800.5918 - val_mae: 59.5974
Epoch 432/2000
1/1 [==============================] - 0s 52ms/step - loss: 6410.4463 - mae: 59.2386 - val_loss: 6785.4595 - val_mae: 59.4930
Epoch 433/2000
1/1 [==============================] - 0s 69ms/step - loss: 6396.1914 - mae: 59.1375 - val_loss: 6769.9404 - val_mae: 59.3931
Epoch 434/2000
1/1 [==============================] - 0s 74ms/step - loss: 6381.6626 - mae: 59.0383 - val_loss: 6754.1118 - val_mae: 59.2928
Epoch 435/2000
1/1 [==============================] - 0s 52ms/step - loss: 6366.8594 - mae: 58.9381 - val_loss: 6738.0957 - val_mae: 59.1828
Epoch 436/2000
1/1 [==============================] - 0s 32ms/step - loss: 6351.7734 - mae: 58.8311 - val_loss: 6721.7651 - val_mae: 59.0717
Epoch 437/2000
1/1 [==============================] - 0s 37ms/step - loss: 6336.4312 - mae: 58.7233 - val_loss: 6705.0400 - val_mae: 58.9663
Epoch 438/2000
1/1 [==============================] - 0s 51ms/step - loss: 6320.8081 - mae: 58.6182 - val_loss: 6688.0996 - val_mae: 58.8521
Epoch 439/2000
1/1 [==============================] - 0s 37ms/step - loss: 6304.8984 - mae: 58.5068 - val_loss: 6670.8857 - val_mae: 58.7330
Epoch 440/2000
1/1 [==============================] - 0s 31ms/step - loss: 6288.7026 - mae: 58.3917 - val_loss: 6653.2896 - val_mae: 58.6194
Epoch 441/2000
1/1 [==============================] - 0s 38ms/step - loss: 6272.2217 - mae: 58.2791 - val_loss: 6635.4399 - val_mae: 58.4992
Epoch 442/2000
1/1 [==============================] - 0s 31ms/step - loss: 6255.4521 - mae: 58.1616 - val_loss: 6617.3232 - val_mae: 58.3733
Epoch 443/2000
1/1 [==============================] - 0s 35ms/step - loss: 6238.3945 - mae: 58.0397 - val_loss: 6598.8428 - val_mae: 58.2520
Epoch 444/2000
1/1 [==============================] - 0s 59ms/step - loss: 6221.0479 - mae: 57.9198 - val_loss: 6580.1011 - val_mae: 58.1243
Epoch 445/2000
1/1 [==============================] - 0s 50ms/step - loss: 6203.4131 - mae: 57.7952 - val_loss: 6561.0801 - val_mae: 57.9918
Epoch 446/2000
1/1 [==============================] - 0s 33ms/step - loss: 6185.4878 - mae: 57.6667 - val_loss: 6541.7222 - val_mae: 57.8633
Epoch 447/2000
1/1 [==============================] - 0s 42ms/step - loss: 6167.2769 - mae: 57.5396 - val_loss: 6522.1064 - val_mae: 57.7269
Epoch 448/2000
1/1 [==============================] - 0s 48ms/step - loss: 6148.7769 - mae: 57.4069 - val_loss: 6502.1899 - val_mae: 57.5891
Epoch 449/2000
1/1 [==============================] - 0s 65ms/step - loss: 6129.9897 - mae: 57.2725 - val_loss: 6481.9897 - val_mae: 57.4538
Epoch 450/2000
1/1 [==============================] - 0s 36ms/step - loss: 6110.9414 - mae: 57.1382 - val_loss: 6461.5513 - val_mae: 57.3032
Epoch 451/2000
1/1 [==============================] - 0s 38ms/step - loss: 6091.6118 - mae: 56.9958 - val_loss: 6440.7466 - val_mae: 57.1696
Epoch 452/2000
1/1 [==============================] - 0s 38ms/step - loss: 6072.0737 - mae: 56.8777 - val_loss: 6419.7109 - val_mae: 57.0301
Epoch 453/2000
1/1 [==============================] - 0s 34ms/step - loss: 6052.1533 - mae: 56.7530 - val_loss: 6398.5039 - val_mae: 56.8440
Epoch 454/2000
1/1 [==============================] - 0s 37ms/step - loss: 6032.0659 - mae: 56.5881 - val_loss: 6376.9116 - val_mae: 56.7388
Epoch 455/2000
1/1 [==============================] - 0s 54ms/step - loss: 6011.7031 - mae: 56.4947 - val_loss: 6355.1816 - val_mae: 56.5429
Epoch 456/2000
1/1 [==============================] - 0s 75ms/step - loss: 5991.0981 - mae: 56.3213 - val_loss: 6333.1665 - val_mae: 56.4181
Epoch 457/2000
1/1 [==============================] - 0s 54ms/step - loss: 5970.2354 - mae: 56.2106 - val_loss: 6310.8911 - val_mae: 56.2429
Epoch 458/2000
1/1 [==============================] - 0s 56ms/step - loss: 5949.1235 - mae: 56.0556 - val_loss: 6288.3643 - val_mae: 56.0829
Epoch 459/2000
1/1 [==============================] - 0s 50ms/step - loss: 5927.7578 - mae: 55.9141 - val_loss: 6265.6074 - val_mae: 55.9300
Epoch 460/2000
1/1 [==============================] - 0s 36ms/step - loss: 5906.1367 - mae: 55.7789 - val_loss: 6242.5010 - val_mae: 55.7382
Epoch 461/2000
1/1 [==============================] - 0s 31ms/step - loss: 5884.2690 - mae: 55.6093 - val_loss: 6219.3887 - val_mae: 55.6070
Epoch 462/2000
1/1 [==============================] - 0s 71ms/step - loss: 5862.1729 - mae: 55.4933 - val_loss: 6195.6699 - val_mae: 55.3769
Epoch 463/2000
1/1 [==============================] - 0s 38ms/step - loss: 5841.6382 - mae: 55.3143 - val_loss: 6180.3594 - val_mae: 55.6146
Epoch 464/2000
1/1 [==============================] - 0s 34ms/step - loss: 5831.8213 - mae: 55.5036 - val_loss: 6154.0503 - val_mae: 54.7602
Epoch 465/2000
1/1 [==============================] - 0s 31ms/step - loss: 5809.0820 - mae: 54.8391 - val_loss: 6131.6592 - val_mae: 54.8104
Epoch 466/2000
1/1 [==============================] - 0s 31ms/step - loss: 5780.6709 - mae: 54.7891 - val_loss: 6119.3564 - val_mae: 55.1394
Epoch 467/2000
1/1 [==============================] - 0s 31ms/step - loss: 5772.1641 - mae: 55.0855 - val_loss: 6091.5698 - val_mae: 54.6155
Epoch 468/2000
1/1 [==============================] - 0s 47ms/step - loss: 5740.6489 - mae: 54.6171 - val_loss: 6072.3511 - val_mae: 54.1736
Epoch 469/2000
1/1 [==============================] - 0s 55ms/step - loss: 5731.3325 - mae: 54.3221 - val_loss: 6053.4468 - val_mae: 54.4560
Epoch 470/2000
1/1 [==============================] - 0s 40ms/step - loss: 5703.6284 - mae: 54.4762 - val_loss: 6036.9072 - val_mae: 54.4423
Epoch 471/2000
1/1 [==============================] - 0s 56ms/step - loss: 5689.4526 - mae: 54.4649 - val_loss: 6010.7607 - val_mae: 53.8635
Epoch 472/2000
1/1 [==============================] - 0s 35ms/step - loss: 5666.9766 - mae: 53.9471 - val_loss: 5990.5693 - val_mae: 53.7093
Epoch 473/2000
1/1 [==============================] - 0s 38ms/step - loss: 5647.8896 - mae: 53.8108 - val_loss: 5976.4644 - val_mae: 53.9633
Epoch 474/2000
1/1 [==============================] - 0s 34ms/step - loss: 5630.4116 - mae: 54.0372 - val_loss: 5953.0527 - val_mae: 53.6772
Epoch 475/2000
1/1 [==============================] - 0s 51ms/step - loss: 5606.8325 - mae: 53.7822 - val_loss: 5929.8442 - val_mae: 53.1932
Epoch 476/2000
1/1 [==============================] - 0s 53ms/step - loss: 5592.4790 - mae: 53.3945 - val_loss: 5911.2812 - val_mae: 53.2913
Epoch 477/2000
1/1 [==============================] - 0s 58ms/step - loss: 5567.1406 - mae: 53.4364 - val_loss: 5895.8599 - val_mae: 53.3368
Epoch 478/2000
1/1 [==============================] - 0s 36ms/step - loss: 5552.0156 - mae: 53.4747 - val_loss: 5869.3203 - val_mae: 52.8827
Epoch 479/2000
1/1 [==============================] - 0s 34ms/step - loss: 5528.7241 - mae: 53.0703 - val_loss: 5848.2075 - val_mae: 52.6475
Epoch 480/2000
1/1 [==============================] - 0s 39ms/step - loss: 5510.9595 - mae: 52.8598 - val_loss: 5832.8906 - val_mae: 52.7952
Epoch 481/2000
1/1 [==============================] - 0s 39ms/step - loss: 5490.4897 - mae: 52.9887 - val_loss: 5811.1982 - val_mae: 52.5905
Epoch 482/2000
```

```
1/1 [==============================] - 0s 36ms/step - loss: 5469.6050 - mae: 52.8052 - val_loss: 5786.2646 - val_mae: 52.1703
Epoch 483/2000
1/1 [==============================] - 0s 36ms/step - loss: 5451.5649 - mae: 52.4301 - val_loss: 5767.7129 - val_mae: 52.1690
Epoch 484/2000
1/1 [==============================] - 0s 36ms/step - loss: 5428.8687 - mae: 52.4274 - val_loss: 5751.3916 - val_mae: 52.1992
Epoch 485/2000
1/1 [==============================] - 0s 46ms/step - loss: 5411.1641 - mae: 52.4382 - val_loss: 5725.0034 - val_mae: 51.8358
Epoch 486/2000
1/1 [==============================] - 0s 53ms/step - loss: 5389.1147 - mae: 52.0958 - val_loss: 5703.5420 - val_mae: 51.6980
Epoch 487/2000
1/1 [==============================] - 0s 60ms/step - loss: 5369.4478 - mae: 51.9355 - val_loss: 5688.1030 - val_mae: 51.9680
Epoch 488/2000
1/1 [==============================] - 0s 77ms/step - loss: 5349.5508 - mae: 52.0224 - val_loss: 5664.1743 - val_mae: 51.7365
Epoch 489/2000
1/1 [==============================] - 0s 42ms/step - loss: 5327.6919 - mae: 51.7951 - val_loss: 5639.9834 - val_mae: 51.4191
Epoch 490/2000
1/1 [==============================] - 0s 38ms/step - loss: 5308.7319 - mae: 51.5234 - val_loss: 5623.3091 - val_mae: 51.7366
Epoch 491/2000
1/1 [==============================] - 0s 47ms/step - loss: 5287.0000 - mae: 51.5717 - val_loss: 5602.4131 - val_mae: 51.7089
Epoch 492/2000
1/1 [==============================] - 0s 42ms/step - loss: 5266.4478 - mae: 51.4448 - val_loss: 5576.4946 - val_mae: 51.3281
Epoch 493/2000
1/1 [==============================] - 0s 41ms/step - loss: 5246.4312 - mae: 51.1385 - val_loss: 5558.3945 - val_mae: 51.5304
Epoch 494/2000
1/1 [==============================] - 0s 51ms/step - loss: 5224.4844 - mae: 51.1262 - val_loss: 5539.2451 - val_mae: 51.6117
Epoch 495/2000
1/1 [==============================] - 0s 45ms/step - loss: 5204.2847 - mae: 51.0518 - val_loss: 5512.7090 - val_mae: 51.2433
Epoch 496/2000
1/1 [==============================] - 0s 46ms/step - loss: 5183.4189 - mae: 50.7493 - val_loss: 5493.6729 - val_mae: 51.3685
Epoch 497/2000
1/1 [==============================] - 0s 37ms/step - loss: 5161.6338 - mae: 50.6954 - val_loss: 5474.9971 - val_mae: 51.4776
Epoch 498/2000
1/1 [==============================] - 0s 53ms/step - loss: 5141.1953 - mae: 50.6325 - val_loss: 5448.3374 - val_mae: 51.1375
Epoch 499/2000
1/1 [==============================] - 0s 61ms/step - loss: 5119.9971 - mae: 50.3417 - val_loss: 5429.1597 - val_mae: 51.2443
Epoch 500/2000
1/1 [==============================] - 0s 48ms/step - loss: 5098.2031 - mae: 50.2760 - val_loss: 5409.9517 - val_mae: 51.3230
Epoch 501/2000
1/1 [==============================] - 0s 46ms/step - loss: 5077.3774 - mae: 50.1952 - val_loss: 5383.3496 - val_mae: 51.0108
Epoch 502/2000
1/1 [==============================] - 0s 32ms/step - loss: 5056.1484 - mae: 49.9159 - val_loss: 5364.9033 - val_mae: 51.1483
Epoch 503/2000
1/1 [==============================] - 0s 30ms/step - loss: 5034.2485 - mae: 49.8633 - val_loss: 5344.0410 - val_mae: 51.1440
Epoch 504/2000
1/1 [==============================] - 0s 33ms/step - loss: 5012.9365 - mae: 49.7381 - val_loss: 5318.0664 - val_mae: 50.8825
Epoch 505/2000
1/1 [==============================] - 0s 37ms/step - loss: 4991.7568 - mae: 49.4820 - val_loss: 5300.8369 - val_mae: 51.0655
Epoch 506/2000
1/1 [==============================] - 0s 42ms/step - loss: 4969.9346 - mae: 49.4663 - val_loss: 5277.0684 - val_mae: 50.9297
Epoch 507/2000
1/1 [==============================] - 0s 48ms/step - loss: 4948.0869 - mae: 49.2916 - val_loss: 5253.3071 - val_mae: 50.7910
Epoch 508/2000
1/1 [==============================] - 0s 39ms/step - loss: 4926.6553 - mae: 49.1218 - val_loss: 5236.1094 - val_mae: 50.9544
Epoch 509/2000
1/1 [==============================] - 0s 34ms/step - loss: 4905.1304 - mae: 49.1334 - val_loss: 5209.4829 - val_mae: 50.6980
Epoch 510/2000
1/1 [==============================] - 0s 56ms/step - loss: 4883.2100 - mae: 48.9077 - val_loss: 5190.0254 - val_mae: 50.7617
Epoch 511/2000
1/1 [==============================] - 0s 47ms/step - loss: 4861.2153 - mae: 48.8619 - val_loss: 5168.8057 - val_mae: 50.7422
Epoch 512/2000
1/1 [==============================] - 0s 33ms/step - loss: 4839.4463 - mae: 48.7687 - val_loss: 5143.4746 - val_mae: 50.5488
Epoch 513/2000
1/1 [==============================] - 0s 31ms/step - loss: 4817.7778 - mae: 48.5874 - val_loss: 5126.6274 - val_mae: 50.7078
Epoch 514/2000
1/1 [==============================] - 0s 30ms/step - loss: 4795.9634 - mae: 48.5830 - val_loss: 5099.5820 - val_mae: 50.4544
Epoch 515/2000
1/1 [==============================] - 0s 31ms/step - loss: 4773.9536 - mae: 48.3764 - val_loss: 5081.6421 - val_mae: 50.5649
Epoch 516/2000
1/1 [==============================] - 0s 40ms/step - loss: 4751.8560 - mae: 48.3317 - val_loss: 5057.3325 - val_mae: 50.4244
Epoch 517/2000
1/1 [==============================] - 0s 33ms/step - loss: 4729.7778 - mae: 48.1665 - val_loss: 5035.8340 - val_mae: 50.3914
Epoch 518/2000
1/1 [==============================] - 0s 39ms/step - loss: 4707.7466 - mae: 48.0610 - val_loss: 5015.4033 - val_mae: 50.3957
Epoch 519/2000
1/1 [==============================] - 0s 43ms/step - loss: 4685.7573 - mae: 47.9757 - val_loss: 4990.2944 - val_mae: 50.2274
Epoch 520/2000
1/1 [==============================] - 0s 49ms/step - loss: 4663.7969 - mae: 47.8476 - val_loss: 4973.5073 - val_mae: 50.3571
Epoch 521/2000
1/1 [==============================] - 0s 50ms/step - loss: 4641.8755 - mae: 47.8272 - val_loss: 4944.5732 - val_mae: 50.0544
Epoch 522/2000
1/1 [==============================] - 0s 54ms/step - loss: 4620.0703 - mae: 47.6754 - val_loss: 4933.1060 - val_mae: 50.3530
Epoch 523/2000
1/1 [==============================] - 0s 36ms/step - loss: 4598.6323 - mae: 47.6998 - val_loss: 4896.7725 - val_mae: 49.7897
Epoch 524/2000
1/1 [==============================] - 0s 44ms/step - loss: 4578.0552 - mae: 47.5015 - val_loss: 4899.1616 - val_mae: 50.4987
Epoch 525/2000
1/1 [==============================] - 0s 34ms/step - loss: 4559.3413 - mae: 47.6625 - val_loss: 4845.8584 - val_mae: 49.3217
Epoch 526/2000
1/1 [==============================] - 0s 33ms/step - loss: 4544.3726 - mae: 47.3296 - val_loss: 4877.9893 - val_mae: 50.8541
Epoch 527/2000
1/1 [==============================] - 0s 41ms/step - loss: 4533.6211 - mae: 47.7523 - val_loss: 4798.6191 - val_mae: 48.8810
Epoch 528/2000
1/1 [==============================] - 0s 36ms/step - loss: 4517.9277 - mae: 47.1607 - val_loss: 4830.4453 - val_mae: 50.6026
Epoch 529/2000
1/1 [==============================] - 0s 38ms/step - loss: 4484.8569 - mae: 47.4803 - val_loss: 4774.5415 - val_mae: 49.6439
Epoch 530/2000
1/1 [==============================] - 0s 33ms/step - loss: 4449.1138 - mae: 46.9865 - val_loss: 4746.9380 - val_mae: 49.3703
Epoch 531/2000
1/1 [==============================] - 0s 31ms/step - loss: 4433.6655 - mae: 46.9049 - val_loss: 4773.4678 - val_mae: 50.6793
Epoch 532/2000
1/1 [==============================] - 0s 32ms/step - loss: 4425.1084 - mae: 47.2311 - val_loss: 4702.2695 - val_mae: 49.1890
Epoch 533/2000
1/1 [==============================] - 0s 53ms/step - loss: 4399.9453 - mae: 46.7390 - val_loss: 4707.1079 - val_mae: 50.0707
Epoch 534/2000
1/1 [==============================] - 0s 63ms/step - loss: 4368.2593 - mae: 46.6757 - val_loss: 4697.0864 - val_mae: 50.3231
Epoch 535/2000
1/1 [==============================] - 0s 75ms/step - loss: 4351.7798 - mae: 46.7213 - val_loss: 4643.1650 - val_mae: 49.2477
```

```
Epoch 536/2000
1/1 [==============================] - 0s 46ms/step - loss: 4340.1143 - mae: 46.4870 - val_loss: 4665.5303 - val_mae: 50.5067
Epoch 537/2000
1/1 [==============================] - 0s 36ms/step - loss: 4315.6865 - mae: 46.6254 - val_loss: 4621.2573 - val_mae: 49.8904
Epoch 538/2000
1/1 [==============================] - 0s 39ms/step - loss: 4288.3687 - mae: 46.3138 - val_loss: 4592.9863 - val_mae: 49.6149
Epoch 539/2000
1/1 [==============================] - 0s 29ms/step - loss: 4272.3301 - mae: 46.2312 - val_loss: 4611.7451 - val_mae: 50.6100
Epoch 540/2000
1/1 [==============================] - 0s 31ms/step - loss: 4258.0767 - mae: 46.3805 - val_loss: 4553.1704 - val_mae: 49.5881
Epoch 541/2000
1/1 [==============================] - 0s 54ms/step - loss: 4234.6431 - mae: 46.0615 - val_loss: 4551.7095 - val_mae: 50.1198
Epoch 542/2000
1/1 [==============================] - 0s 52ms/step - loss: 4210.0757 - mae: 45.9721 - val_loss: 4543.8921 - val_mae: 50.3936
Epoch 543/2000
1/1 [==============================] - 0s 67ms/step - loss: 4193.2236 - mae: 45.9478 - val_loss: 4495.3101 - val_mae: 49.5901
Epoch 544/2000
1/1 [==============================] - 0s 34ms/step - loss: 4178.0186 - mae: 45.8092 - val_loss: 4514.0186 - val_mae: 50.5711
Epoch 545/2000
1/1 [==============================] - 0s 38ms/step - loss: 4157.4736 - mae: 45.8452 - val_loss: 4468.6069 - val_mae: 49.9414
Epoch 546/2000
1/1 [==============================] - 0s 42ms/step - loss: 4133.7368 - mae: 45.6292 - val_loss: 4451.9180 - val_mae: 50.0012
Epoch 547/2000
1/1 [==============================] - 0s 33ms/step - loss: 4114.2471 - mae: 45.5420 - val_loss: 4456.8516 - val_mae: 50.5549
Epoch 548/2000
1/1 [==============================] - 0s 31ms/step - loss: 4098.5122 - mae: 45.5256 - val_loss: 4405.4790 - val_mae: 49.7462
Epoch 549/2000
1/1 [==============================] - 0s 30ms/step - loss: 4080.6226 - mae: 45.3694 - val_loss: 4417.5049 - val_mae: 50.5087
Epoch 550/2000
1/1 [==============================] - 0s 50ms/step - loss: 4059.0801 - mae: 45.2908 - val_loss: 4383.5439 - val_mae: 50.1588
Epoch 551/2000
1/1 [==============================] - 0s 50ms/step - loss: 4037.8831 - mae: 45.1905 - val_loss: 4361.0859 - val_mae: 50.0576
Epoch 552/2000
1/1 [==============================] - 0s 43ms/step - loss: 4019.8191 - mae: 45.1030 - val_loss: 4366.9492 - val_mae: 50.5991
Epoch 553/2000
1/1 [==============================] - 0s 41ms/step - loss: 4003.2546 - mae: 45.0299 - val_loss: 4318.2407 - val_mae: 49.8911
Epoch 554/2000
1/1 [==============================] - 0s 38ms/step - loss: 3985.4011 - mae: 44.9286 - val_loss: 4332.9629 - val_mae: 50.6413
Epoch 555/2000
1/1 [==============================] - 0s 62ms/step - loss: 3966.0881 - mae: 44.8443 - val_loss: 4289.5361 - val_mae: 50.0844
Epoch 556/2000
1/1 [==============================] - 0s 59ms/step - loss: 3945.6746 - mae: 44.7470 - val_loss: 4284.4746 - val_mae: 50.3794
Epoch 557/2000
1/1 [==============================] - 0s 63ms/step - loss: 3925.9702 - mae: 44.6548 - val_loss: 4270.2568 - val_mae: 50.4539
Epoch 558/2000
1/1 [==============================] - 0s 60ms/step - loss: 3907.8066 - mae: 44.5641 - val_loss: 4237.4023 - val_mae: 50.1148
Epoch 559/2000
1/1 [==============================] - 0s 72ms/step - loss: 3890.6704 - mae: 44.4766 - val_loss: 4247.6978 - val_mae: 50.7012
Epoch 560/2000
1/1 [==============================] - 0s 61ms/step - loss: 3873.6277 - mae: 44.4146 - val_loss: 4198.7417 - val_mae: 50.0273
Epoch 561/2000
1/1 [==============================] - 0s 44ms/step - loss: 3856.0681 - mae: 44.3343 - val_loss: 4216.5425 - val_mae: 50.7641
Epoch 562/2000
1/1 [==============================] - 0s 55ms/step - loss: 3837.8667 - mae: 44.2739 - val_loss: 4167.0000 - val_mae: 50.0969
Epoch 563/2000
1/1 [==============================] - 0s 60ms/step - loss: 3819.2175 - mae: 44.1932 - val_loss: 4179.3706 - val_mae: 50.7072
Epoch 564/2000
1/1 [==============================] - 0s 51ms/step - loss: 3800.4458 - mae: 44.1305 - val_loss: 4139.1309 - val_mae: 50.2390
Epoch 565/2000
1/1 [==============================] - 0s 50ms/step - loss: 3781.8240 - mae: 44.0520 - val_loss: 4141.0366 - val_mae: 50.6194
Epoch 566/2000
1/1 [==============================] - 0s 38ms/step - loss: 3763.4766 - mae: 43.9854 - val_loss: 4111.9438 - val_mae: 50.3749
Epoch 567/2000
1/1 [==============================] - 0s 36ms/step - loss: 3745.4116 - mae: 43.9094 - val_loss: 4104.6709 - val_mae: 50.5593
Epoch 568/2000
1/1 [==============================] - 0s 49ms/step - loss: 3727.5708 - mae: 43.8392 - val_loss: 4083.6973 - val_mae: 50.4716
Epoch 569/2000
1/1 [==============================] - 0s 42ms/step - loss: 3709.8977 - mae: 43.7647 - val_loss: 4070.6814 - val_mae: 50.5359
Epoch 570/2000
1/1 [==============================] - 0s 44ms/step - loss: 3692.3452 - mae: 43.6919 - val_loss: 4054.5562 - val_mae: 50.5375
Epoch 571/2000
1/1 [==============================] - 0s 33ms/step - loss: 3674.8882 - mae: 43.6180 - val_loss: 4037.9983 - val_mae: 50.5287
Epoch 572/2000
1/1 [==============================] - 0s 30ms/step - loss: 3657.5396 - mae: 43.5439 - val_loss: 4024.7407 - val_mae: 50.5793
Epoch 573/2000
1/1 [==============================] - 0s 37ms/step - loss: 3640.4146 - mae: 43.4732 - val_loss: 4006.3013 - val_mae: 50.5310
Epoch 574/2000
1/1 [==============================] - 0s 33ms/step - loss: 3623.3918 - mae: 43.4005 - val_loss: 3996.9727 - val_mae: 50.6476
Epoch 575/2000
1/1 [==============================] - 0s 48ms/step - loss: 3607.0425 - mae: 43.3327 - val_loss: 3966.6785 - val_mae: 50.3723
Epoch 576/2000
1/1 [==============================] - 0s 35ms/step - loss: 3591.5659 - mae: 43.2569 - val_loss: 3984.9553 - val_mae: 50.9657
Epoch 577/2000
1/1 [==============================] - 0s 31ms/step - loss: 3577.8618 - mae: 43.2017 - val_loss: 3914.4341 - val_mae: 49.9115
Epoch 578/2000
1/1 [==============================] - 0s 51ms/step - loss: 3570.4094 - mae: 43.1075 - val_loss: 4021.0676 - val_mae: 51.8855
Epoch 579/2000
1/1 [==============================] - 0s 63ms/step - loss: 3582.6384 - mae: 43.7195 - val_loss: 3846.6819 - val_mae: 48.6355
Epoch 580/2000
1/1 [==============================] - 0s 57ms/step - loss: 3633.1658 - mae: 43.1340 - val_loss: 4107.6187 - val_mae: 53.1159
Epoch 581/2000
1/1 [==============================] - 0s 42ms/step - loss: 3666.0027 - mae: 44.7082 - val_loss: 3834.4734 - val_mae: 49.2984
Epoch 582/2000
1/1 [==============================] - 0s 34ms/step - loss: 3546.8315 - mae: 42.8311 - val_loss: 3852.1470 - val_mae: 50.1070
Epoch 583/2000
1/1 [==============================] - 0s 30ms/step - loss: 3490.1685 - mae: 42.7830 - val_loss: 4023.0793 - val_mae: 52.6679
Epoch 584/2000
1/1 [==============================] - 0s 31ms/step - loss: 3564.5872 - mae: 44.0519 - val_loss: 3800.9512 - val_mae: 49.4902
Epoch 585/2000
1/1 [==============================] - 0s 27ms/step - loss: 3494.1411 - mae: 42.6460 - val_loss: 3815.4902 - val_mae: 50.1532
Epoch 586/2000
1/1 [==============================] - 0s 33ms/step - loss: 3447.9988 - mae: 42.5962 - val_loss: 3967.0752 - val_mae: 52.4710
Epoch 587/2000
1/1 [==============================] - 0s 35ms/step - loss: 3499.1489 - mae: 43.6495 - val_loss: 3785.1763 - val_mae: 50.0391
Epoch 588/2000
1/1 [==============================] - 0s 29ms/step - loss: 3426.0261 - mae: 42.4701 - val_loss: 3766.8394 - val_mae: 49.9031
Epoch 589/2000
```

```
1/1 [==============================] - 0s 28ms/step - loss: 3419.3264 - mae: 42.4056 - val_loss: 3908.7283 - val_mae: 52.2236
Epoch 590/2000
1/1 [==============================] - 0s 28ms/step - loss: 3434.8152 - mae: 43.2044 - val_loss: 3782.9082 - val_mae: 50.6852
Epoch 591/2000
1/1 [==============================] - 0s 36ms/step - loss: 3371.3420 - mae: 42.2984 - val_loss: 3722.4849 - val_mae: 49.7012
Epoch 592/2000
1/1 [==============================] - 0s 40ms/step - loss: 3393.4456 - mae: 42.2172 - val_loss: 3843.1628 - val_mae: 51.8622
Epoch 593/2000
1/1 [==============================] - 0s 35ms/step - loss: 3370.0261 - mae: 42.6561 - val_loss: 3787.0413 - val_mae: 51.2794
Epoch 594/2000
1/1 [==============================] - 0s 36ms/step - loss: 3335.6570 - mae: 42.2518 - val_loss: 3690.1084 - val_mae: 49.7579
Epoch 595/2000
1/1 [==============================] - 0s 36ms/step - loss: 3354.5430 - mae: 42.0360 - val_loss: 3773.0605 - val_mae: 51.3935
Epoch 596/2000
1/1 [==============================] - 0s 32ms/step - loss: 3312.1360 - mae: 42.1768 - val_loss: 3783.6494 - val_mae: 51.6742
Epoch 597/2000
1/1 [==============================] - 0s 32ms/step - loss: 3307.9119 - mae: 42.2138 - val_loss: 3669.8242 - val_mae: 50.0524
Epoch 598/2000
1/1 [==============================] - 0s 36ms/step - loss: 3303.8516 - mae: 41.8612 - val_loss: 3711.1113 - val_mae: 50.9710
Epoch 599/2000
1/1 [==============================] - 0s 44ms/step - loss: 3269.1714 - mae: 41.8665 - val_loss: 3763.3948 - val_mae: 51.8173
Epoch 600/2000
1/1 [==============================] - 0s 39ms/step - loss: 3274.6926 - mae: 42.1128 - val_loss: 3659.0161 - val_mae: 50.4626
Epoch 601/2000
1/1 [==============================] - 0s 36ms/step - loss: 3253.3997 - mae: 41.6881 - val_loss: 3663.0764 - val_mae: 50.7095
Epoch 602/2000
1/1 [==============================] - 0s 30ms/step - loss: 3235.9575 - mae: 41.6320 - val_loss: 3732.4316 - val_mae: 51.8137
Epoch 603/2000
1/1 [==============================] - 0s 33ms/step - loss: 3236.4458 - mae: 41.9193 - val_loss: 3648.8115 - val_mae: 50.8079
Epoch 604/2000
1/1 [==============================] - 0s 42ms/step - loss: 3211.1836 - mae: 41.5302 - val_loss: 3626.4944 - val_mae: 50.6077
Epoch 605/2000
1/1 [==============================] - 0s 34ms/step - loss: 3203.7107 - mae: 41.4468 - val_loss: 3693.7778 - val_mae: 51.7027
Epoch 606/2000
1/1 [==============================] - 0s 36ms/step - loss: 3195.7598 - mae: 41.7130 - val_loss: 3636.7205 - val_mae: 51.0722
Epoch 607/2000
1/1 [==============================] - 0s 28ms/step - loss: 3174.3816 - mae: 41.4470 - val_loss: 3598.7354 - val_mae: 50.6349
Epoch 608/2000
1/1 [==============================] - 0s 27ms/step - loss: 3169.4211 - mae: 41.2631 - val_loss: 3655.0972 - val_mae: 51.5755
Epoch 609/2000
1/1 [==============================] - 0s 28ms/step - loss: 3157.0520 - mae: 41.5023 - val_loss: 3619.5620 - val_mae: 51.2304
Epoch 610/2000
1/1 [==============================] - 0s 29ms/step - loss: 3140.8884 - mae: 41.3317 - val_loss: 3573.1113 - val_mae: 50.6783
Epoch 611/2000
1/1 [==============================] - 0s 29ms/step - loss: 3135.5918 - mae: 41.0922 - val_loss: 3623.6001 - val_mae: 51.5237
Epoch 612/2000
1/1 [==============================] - 0s 29ms/step - loss: 3122.0847 - mae: 41.3186 - val_loss: 3599.3750 - val_mae: 51.3249
Epoch 613/2000
1/1 [==============================] - 0s 39ms/step - loss: 3108.5481 - mae: 41.1972 - val_loss: 3550.6145 - val_mae: 50.7516
Epoch 614/2000
1/1 [==============================] - 0s 35ms/step - loss: 3102.4727 - mae: 40.9509 - val_loss: 3591.2422 - val_mae: 51.4465
Epoch 615/2000
1/1 [==============================] - 0s 50ms/step - loss: 3088.2539 - mae: 41.1274 - val_loss: 3580.7744 - val_mae: 51.4216
Epoch 616/2000
1/1 [==============================] - 0s 43ms/step - loss: 3077.2991 - mae: 41.0638 - val_loss: 3530.9683 - val_mae: 50.8476
Epoch 617/2000
1/1 [==============================] - 0s 38ms/step - loss: 3069.8223 - mae: 40.8170 - val_loss: 3563.6484 - val_mae: 51.4159
Epoch 618/2000
1/1 [==============================] - 0s 33ms/step - loss: 3056.2231 - mae: 40.9806 - val_loss: 3559.9185 - val_mae: 51.4723
Epoch 619/2000
1/1 [==============================] - 0s 33ms/step - loss: 3046.3794 - mae: 40.9640 - val_loss: 3512.8508 - val_mae: 50.9450
Epoch 620/2000
1/1 [==============================] - 0s 32ms/step - loss: 3038.0833 - mae: 40.7347 - val_loss: 3540.0815 - val_mae: 51.4227
Epoch 621/2000
1/1 [==============================] - 0s 32ms/step - loss: 3025.4983 - mae: 40.8719 - val_loss: 3538.1687 - val_mae: 51.4967
Epoch 622/2000
1/1 [==============================] - 0s 48ms/step - loss: 3016.0291 - mae: 40.8621 - val_loss: 3495.4358 - val_mae: 51.0326
Epoch 623/2000
1/1 [==============================] - 0s 36ms/step - loss: 3007.8354 - mae: 40.6573 - val_loss: 3525.0359 - val_mae: 51.5221
Epoch 624/2000
1/1 [==============================] - 0s 67ms/step - loss: 2996.4504 - mae: 40.7979 - val_loss: 3510.7883 - val_mae: 51.4367
Epoch 625/2000
1/1 [==============================] - 0s 36ms/step - loss: 2986.1909 - mae: 40.7302 - val_loss: 3479.1780 - val_mae: 51.1181
Epoch 626/2000
1/1 [==============================] - 0s 41ms/step - loss: 2978.6074 - mae: 40.5791 - val_loss: 3511.6990 - val_mae: 51.6254
Epoch 627/2000
1/1 [==============================] - 0s 41ms/step - loss: 2968.7170 - mae: 40.7259 - val_loss: 3483.9077 - val_mae: 51.3690
Epoch 628/2000
1/1 [==============================] - 0s 31ms/step - loss: 2958.0503 - mae: 40.5961 - val_loss: 3470.0366 - val_mae: 51.2801
Epoch 629/2000
1/1 [==============================] - 0s 35ms/step - loss: 2949.2913 - mae: 40.5267 - val_loss: 3492.7271 - val_mae: 51.6460
Epoch 630/2000
1/1 [==============================] - 0s 55ms/step - loss: 2940.9900 - mae: 40.6227 - val_loss: 3458.1465 - val_mae: 51.3020
Epoch 631/2000
1/1 [==============================] - 0s 44ms/step - loss: 2931.1272 - mae: 40.4601 - val_loss: 3457.9922 - val_mae: 51.3839
Epoch 632/2000
1/1 [==============================] - 0s 31ms/step - loss: 2921.8965 - mae: 40.4531 - val_loss: 3472.9658 - val_mae: 51.6443
Epoch 633/2000
1/1 [==============================] - 0s 29ms/step - loss: 2913.9207 - mae: 40.5113 - val_loss: 3439.2236 - val_mae: 51.3089
Epoch 634/2000
1/1 [==============================] - 0s 27ms/step - loss: 2904.9705 - mae: 40.3521 - val_loss: 3448.4526 - val_mae: 51.5010
Epoch 635/2000
1/1 [==============================] - 0s 27ms/step - loss: 2895.7014 - mae: 40.3859 - val_loss: 3451.8235 - val_mae: 51.6140
Epoch 636/2000
1/1 [==============================] - 0s 28ms/step - loss: 2887.5789 - mae: 40.3918 - val_loss: 3422.8059 - val_mae: 51.3338
Epoch 637/2000
1/1 [==============================] - 0s 27ms/step - loss: 2879.9175 - mae: 40.2557 - val_loss: 3439.9585 - val_mae: 51.6134
Epoch 638/2000
1/1 [==============================] - 0s 27ms/step - loss: 2871.4712 - mae: 40.3246 - val_loss: 3429.9746 - val_mae: 51.5634
Epoch 639/2000
1/1 [==============================] - 0s 29ms/step - loss: 2863.4045 - mae: 40.2730 - val_loss: 3412.1245 - val_mae: 51.4164
Epoch 640/2000
1/1 [==============================] - 0s 33ms/step - loss: 2856.0466 - mae: 40.1862 - val_loss: 3429.9819 - val_mae: 51.6933
Epoch 641/2000
1/1 [==============================] - 0s 39ms/step - loss: 2848.4167 - mae: 40.2546 - val_loss: 3409.2285 - val_mae: 51.5139
Epoch 642/2000
1/1 [==============================] - 0s 41ms/step - loss: 2840.4622 - mae: 40.1563 - val_loss: 3406.3674 - val_mae: 51.5429
```

```
Epoch 643/2000
1/1 [==============================] - 0s 37ms/step - loss: 2832.9355 - mae: 40.1343 - val_loss: 3416.1782 - val_mae: 51.7165
Epoch 644/2000
1/1 [==============================] - 0s 40ms/step - loss: 2825.8269 - mae: 40.1657 - val_loss: 3392.5120 - val_mae: 51.5005
Epoch 645/2000
1/1 [==============================] - 0s 35ms/step - loss: 2818.5183 - mae: 40.0543 - val_loss: 3403.3186 - val_mae: 51.6842
Epoch 646/2000
1/1 [==============================] - 0s 33ms/step - loss: 2811.0308 - mae: 40.0894 - val_loss: 3397.6577 - val_mae: 51.6749
Epoch 647/2000
1/1 [==============================] - 0s 37ms/step - loss: 2803.8606 - mae: 40.0538 - val_loss: 3383.9585 - val_mae: 51.5716
Epoch 648/2000
1/1 [==============================] - 0s 54ms/step - loss: 2797.0122 - mae: 39.9837 - val_loss: 3397.0076 - val_mae: 51.7729
Epoch 649/2000
1/1 [==============================] - 0s 59ms/step - loss: 2790.1174 - mae: 40.0253 - val_loss: 3379.6396 - val_mae: 51.6277
Epoch 650/2000
1/1 [==============================] - 0s 58ms/step - loss: 2783.1184 - mae: 39.9398 - val_loss: 3381.6953 - val_mae: 51.7014
Epoch 651/2000
1/1 [==============================] - 0s 61ms/step - loss: 2776.2747 - mae: 39.9348 - val_loss: 3384.0051 - val_mae: 51.7752
Epoch 652/2000
1/1 [==============================] - 0s 62ms/step - loss: 2769.7122 - mae: 39.9298 - val_loss: 3368.4954 - val_mae: 51.6483
Epoch 653/2000
1/1 [==============================] - 0s 45ms/step - loss: 2763.2527 - mae: 39.8513 - val_loss: 3379.6357 - val_mae: 51.8182
Epoch 654/2000
1/1 [==============================] - 0s 59ms/step - loss: 2756.7483 - mae: 39.8818 - val_loss: 3367.3799 - val_mae: 51.7268
Epoch 655/2000
1/1 [==============================] - 0s 57ms/step - loss: 2750.2830 - mae: 39.8169 - val_loss: 3366.3896 - val_mae: 51.7590
Epoch 656/2000
1/1 [==============================] - 0s 59ms/step - loss: 2743.9949 - mae: 39.7973 - val_loss: 3369.9722 - val_mae: 51.8396
Epoch 657/2000
1/1 [==============================] - 0s 61ms/step - loss: 2737.8911 - mae: 39.7956 - val_loss: 3356.4028 - val_mae: 51.7311
Epoch 658/2000
1/1 [==============================] - 0s 59ms/step - loss: 2731.8672 - mae: 39.7247 - val_loss: 3365.9614 - val_mae: 51.8744
Epoch 659/2000
1/1 [==============================] - 0s 49ms/step - loss: 2725.8542 - mae: 39.7461 - val_loss: 3354.6401 - val_mae: 51.7894
Epoch 660/2000
1/1 [==============================] - 0s 44ms/step - loss: 2719.8933 - mae: 39.6840 - val_loss: 3355.9197 - val_mae: 51.8399
Epoch 661/2000
1/1 [==============================] - 0s 34ms/step - loss: 2714.0520 - mae: 39.6716 - val_loss: 3356.2029 - val_mae: 51.8781
Epoch 662/2000
1/1 [==============================] - 0s 29ms/step - loss: 2708.3491 - mae: 39.6548 - val_loss: 3346.8105 - val_mae: 51.8114
Epoch 663/2000
1/1 [==============================] - 0s 28ms/step - loss: 2702.7537 - mae: 39.5996 - val_loss: 3354.7383 - val_mae: 51.9289
Epoch 664/2000
1/1 [==============================] - 0s 35ms/step - loss: 2697.2195 - mae: 39.6122 - val_loss: 3342.6450 - val_mae: 51.8321
Epoch 665/2000
1/1 [==============================] - 0s 36ms/step - loss: 2691.7527 - mae: 39.5474 - val_loss: 3349.9292 - val_mae: 51.9400
Epoch 666/2000
1/1 [==============================] - 0s 34ms/step - loss: 2686.4341 - mae: 39.5564 - val_loss: 3340.1836 - val_mae: 51.8669
Epoch 667/2000
1/1 [==============================] - 0s 30ms/step - loss: 2681.1890 - mae: 39.4999 - val_loss: 3343.7949 - val_mae: 51.9335
Epoch 668/2000
1/1 [==============================] - 0s 28ms/step - loss: 2676.0183 - mae: 39.4984 - val_loss: 3339.8638 - val_mae: 51.9199
Epoch 669/2000
1/1 [==============================] - 0s 35ms/step - loss: 2670.9380 - mae: 39.4780 - val_loss: 3337.2466 - val_mae: 51.9191
Epoch 670/2000
1/1 [==============================] - 0s 61ms/step - loss: 2665.9490 - mae: 39.4627 - val_loss: 3339.4592 - val_mae: 51.9675
Epoch 671/2000
1/1 [==============================] - 0s 39ms/step - loss: 2661.0432 - mae: 39.4673 - val_loss: 3331.9683 - val_mae: 51.9145
Epoch 672/2000
1/1 [==============================] - 0s 65ms/step - loss: 2656.2266 - mae: 39.4310 - val_loss: 3339.1216 - val_mae: 52.0116
Epoch 673/2000
1/1 [==============================] - 0s 74ms/step - loss: 2651.5608 - mae: 39.4550 - val_loss: 3325.9214 - val_mae: 51.8985
Epoch 674/2000
1/1 [==============================] - 0s 72ms/step - loss: 2646.9766 - mae: 39.3936 - val_loss: 3338.6978 - val_mae: 52.0508
Epoch 675/2000
1/1 [==============================] - 0s 46ms/step - loss: 2642.4534 - mae: 39.4406 - val_loss: 3321.6675 - val_mae: 51.8978
Epoch 676/2000
1/1 [==============================] - 0s 39ms/step - loss: 2637.9941 - mae: 39.3628 - val_loss: 3337.3408 - val_mae: 52.0770
Epoch 677/2000
1/1 [==============================] - 0s 64ms/step - loss: 2633.5964 - mae: 39.4209 - val_loss: 3318.2241 - val_mae: 51.9024
Epoch 678/2000
1/1 [==============================] - 0s 59ms/step - loss: 2629.2642 - mae: 39.3341 - val_loss: 3336.1660 - val_mae: 52.1016
Epoch 679/2000
1/1 [==============================] - 0s 62ms/step - loss: 2625.0054 - mae: 39.4004 - val_loss: 3314.3767 - val_mae: 51.8998
Epoch 680/2000
1/1 [==============================] - 0s 42ms/step - loss: 2620.8286 - mae: 39.3022 - val_loss: 3336.4668 - val_mae: 52.1374
Epoch 681/2000
1/1 [==============================] - 0s 35ms/step - loss: 2616.7466 - mae: 39.3840 - val_loss: 3308.7478 - val_mae: 51.8760
Epoch 682/2000
1/1 [==============================] - 0s 34ms/step - loss: 2612.7856 - mae: 39.2612 - val_loss: 3339.9116 - val_mae: 52.2002
Epoch 683/2000
1/1 [==============================] - 0s 47ms/step - loss: 2608.9966 - mae: 39.3958 - val_loss: 3299.2139 - val_mae: 51.8092
Epoch 684/2000
1/1 [==============================] - 0s 43ms/step - loss: 2605.4749 - mae: 39.2106 - val_loss: 3349.9338 - val_mae: 52.3209
Epoch 685/2000
1/1 [==============================] - 0s 49ms/step - loss: 2602.4106 - mae: 39.4503 - val_loss: 3281.7900 - val_mae: 51.6564
Epoch 686/2000
1/1 [==============================] - 0s 59ms/step - loss: 2600.1897 - mae: 39.1359 - val_loss: 3373.8723 - val_mae: 52.5607
Epoch 687/2000
1/1 [==============================] - 0s 48ms/step - loss: 2599.5859 - mae: 39.5591 - val_loss: 3249.5620 - val_mae: 51.3326
Epoch 688/2000
1/1 [==============================] - 0s 56ms/step - loss: 2602.0767 - mae: 39.1360 - val_loss: 3426.0249 - val_mae: 53.0223
Epoch 689/2000
1/1 [==============================] - 0s 63ms/step - loss: 2609.9441 - mae: 39.7694 - val_loss: 3199.2146 - val_mae: 50.7570
Epoch 690/2000
1/1 [==============================] - 0s 58ms/step - loss: 2625.1145 - mae: 39.6185 - val_loss: 3496.5015 - val_mae: 53.6814
Epoch 691/2000
1/1 [==============================] - 0s 61ms/step - loss: 2639.2417 - mae: 40.0518 - val_loss: 3172.4194 - val_mae: 50.4332
Epoch 692/2000
1/1 [==============================] - 0s 40ms/step - loss: 2642.0447 - mae: 39.8673 - val_loss: 3444.9585 - val_mae: 53.1959
Epoch 693/2000
1/1 [==============================] - 0s 30ms/step - loss: 2604.9575 - mae: 39.8284 - val_loss: 3271.2385 - val_mae: 51.6401
Epoch 694/2000
1/1 [==============================] - 0s 31ms/step - loss: 2572.1914 - mae: 39.0993 - val_loss: 3277.0522 - val_mae: 51.7089
Epoch 695/2000
1/1 [==============================] - 0s 43ms/step - loss: 2567.5513 - mae: 39.1352 - val_loss: 3422.4414 - val_mae: 53.0437
Epoch 696/2000
```

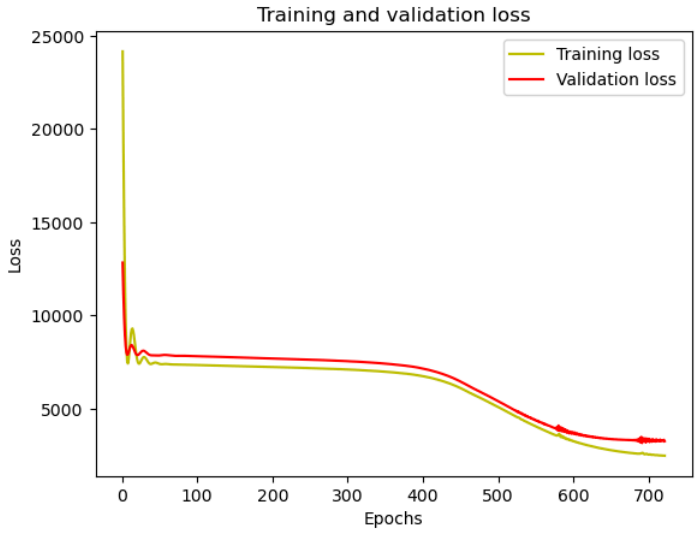
```
1/1 [==============================] - 0s 42ms/step - loss: 2585.4902 - mae: 39.7328 - val_loss: 3195.3879 - val_mae: 50.8119
Epoch 697/2000
1/1 [==============================] - 0s 41ms/step - loss: 2596.8752 - mae: 39.4903 - val_loss: 3410.5620 - val_mae: 52.9864
Epoch 698/2000
1/1 [==============================] - 0s 35ms/step - loss: 2574.6199 - mae: 39.6792 - val_loss: 3285.6523 - val_mae: 51.8236
Epoch 699/2000
1/1 [==============================] - 0s 57ms/step - loss: 2553.3008 - mae: 39.2120 - val_loss: 3265.6323 - val_mae: 51.6279
Epoch 700/2000
1/1 [==============================] - 0s 60ms/step - loss: 2553.5132 - mae: 39.1557 - val_loss: 3400.6038 - val_mae: 52.9902
Epoch 701/2000
1/1 [==============================] - 0s 60ms/step - loss: 2561.9453 - mae: 39.6297 - val_loss: 3224.9888 - val_mae: 51.2069
Epoch 702/2000
1/1 [==============================] - 0s 59ms/step - loss: 2560.7361 - mae: 39.2249 - val_loss: 3357.1257 - val_mae: 52.5222
Epoch 703/2000
1/1 [==============================] - 0s 59ms/step - loss: 2544.3730 - mae: 39.4623 - val_loss: 3327.7385 - val_mae: 52.2400
Epoch 704/2000
1/1 [==============================] - 0s 40ms/step - loss: 2537.3562 - mae: 39.3494 - val_loss: 3244.0933 - val_mae: 51.4308
Epoch 705/2000
1/1 [==============================] - 0s 64ms/step - loss: 2543.4304 - mae: 39.1690 - val_loss: 3384.2607 - val_mae: 52.9852
Epoch 706/2000
1/1 [==============================] - 0s 59ms/step - loss: 2542.1184 - mae: 39.5497 - val_loss: 3258.5337 - val_mae: 51.5874
Epoch 707/2000
1/1 [==============================] - 0s 62ms/step - loss: 2533.3108 - mae: 39.1401 - val_loss: 3313.9348 - val_mae: 52.1451
Epoch 708/2000
1/1 [==============================] - 0s 43ms/step - loss: 2524.7070 - mae: 39.2550 - val_loss: 3342.4619 - val_mae: 52.5655
Epoch 709/2000
1/1 [==============================] - 0s 32ms/step - loss: 2524.4871 - mae: 39.3706 - val_loss: 3248.5742 - val_mae: 51.4940
Epoch 710/2000
1/1 [==============================] - 0s 28ms/step - loss: 2527.1726 - mae: 39.1475 - val_loss: 3368.5017 - val_mae: 52.9718
Epoch 711/2000
1/1 [==============================] - 0s 33ms/step - loss: 2523.9944 - mae: 39.4652 - val_loss: 3269.1548 - val_mae: 51.7017
Epoch 712/2000
1/1 [==============================] - 0s 59ms/step - loss: 2516.6248 - mae: 39.0835 - val_loss: 3311.1704 - val_mae: 52.2960
Epoch 713/2000
1/1 [==============================] - 0s 41ms/step - loss: 2510.8455 - mae: 39.2216 - val_loss: 3330.7190 - val_mae: 52.5926
Epoch 714/2000
1/1 [==============================] - 0s 63ms/step - loss: 2509.4263 - mae: 39.2977 - val_loss: 3261.7476 - val_mae: 51.6713
Epoch 715/2000
1/1 [==============================] - 0s 36ms/step - loss: 2509.7339 - mae: 39.0868 - val_loss: 3355.5476 - val_mae: 52.9801
Epoch 716/2000
1/1 [==============================] - 0s 41ms/step - loss: 2507.8931 - mae: 39.3853 - val_loss: 3268.3494 - val_mae: 51.8403
Epoch 717/2000
1/1 [==============================] - 0s 31ms/step - loss: 2503.1069 - mae: 39.0619 - val_loss: 3321.4861 - val_mae: 52.6071
Epoch 718/2000
1/1 [==============================] - 0s 28ms/step - loss: 2498.1106 - mae: 39.2342 - val_loss: 3311.0205 - val_mae: 52.5011
Epoch 719/2000
1/1 [==============================] - 0s 53ms/step - loss: 2494.9744 - mae: 39.1836 - val_loss: 3278.8862 - val_mae: 52.0940
Epoch 720/2000
1/1 [==============================] - 0s 43ms/step - loss: 2493.7104 - mae: 39.0388 - val_loss: 3341.0999 - val_mae: 52.9569
Epoch 721/2000
1/1 [==============================] - ETA: 0s - loss: 2492.4771 - mae: 39.2916Restoring model weights from the end of the best epoch: 691.
1/1 [==============================] - 0s 67ms/step - loss: 2492.4771 - mae: 39.2916 - val_loss: 3269.4683 - val_mae: 52.0274
Epoch 721: early stopping
```

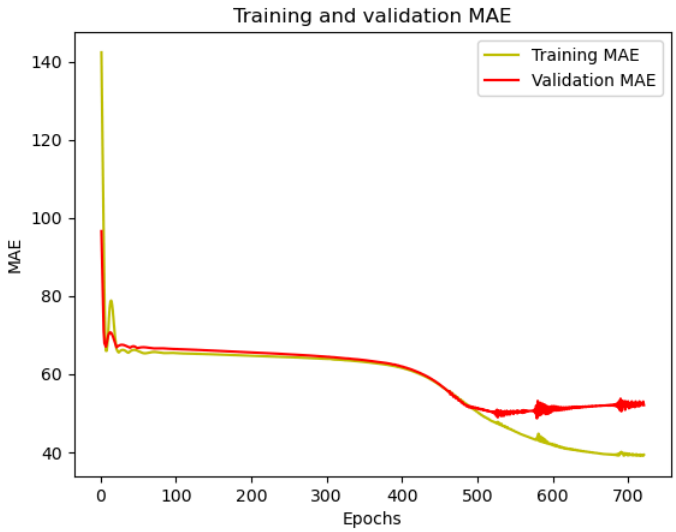
In [14]:

```
# plot the training and validation accuracy and loss at each epoch

loss = history.history['loss']
val_loss = history.history['val_loss']
epochs = range(1, len(loss) + 1)
plt.plot (epochs, loss, 'y', label = 'Training loss')
plt.plot (epochs, val_loss, 'r', label='Validation loss')
plt.title('Training and validation loss')
plt.xlabel ('Epochs')
plt.ylabel('Loss')
plt.legend()
plt.show()

acc = history.history['mae']
val_acc = history.history['val_mae']
plt.plot (epochs, acc, 'y', label = 'Training MAE')
plt.plot (epochs, val_acc, 'r', label='Validation MAE')
plt.title('Training and validation MAE')
plt.xlabel ('Epochs')
plt.ylabel('MAE')
plt.legend()
plt.show()
```





In [15]:
```
# Runs model with its current weights on the training and testing data

y_train_pred = model.predict(X_train_scaled)
y_test_pred = model.predict(X_test_scaled)

# X_test - input de teste
# X_train - input de treino

# y_test_pred - output de teste previsto
# y test - output de teste real

# Calculates and prints r2 score of training and testing data
print('R2 score train:', r2_score(y_train, y_train_pred))
print('R2 score test:', r2_score(y_test, y_test_pred))

r2nn = r2_score(y_test, y_test_pred)
r2nn
```

```
2/2 [==============================] - 0s 3ms/step
1/1 [==============================] - 0s 17ms/step
R2 score train: 0.3551114677934428
R2 score test: 0.4941453457434887
```

Out[15]:
```
0.4941453457434887
```

In [16]:
```
# Predict on test data

predictions = model.predict(X_test_scaled[:])
print("Predicted values are: ", predictions[:5])
print("Real values are: ", y_test[:5])
```

```
1/1 [==============================] - 0s 18ms/step
Predicted values are:  [[176.88853]
 [ 90.40711]
 [ 89.02615]
 [117.5611 ]
 [171.00327]]
Real values are:  [[140.12471655]
 [ 70.72562358]
 [ 60.10204082]
 [ 61.02040816]
 [174.77324263]]
```

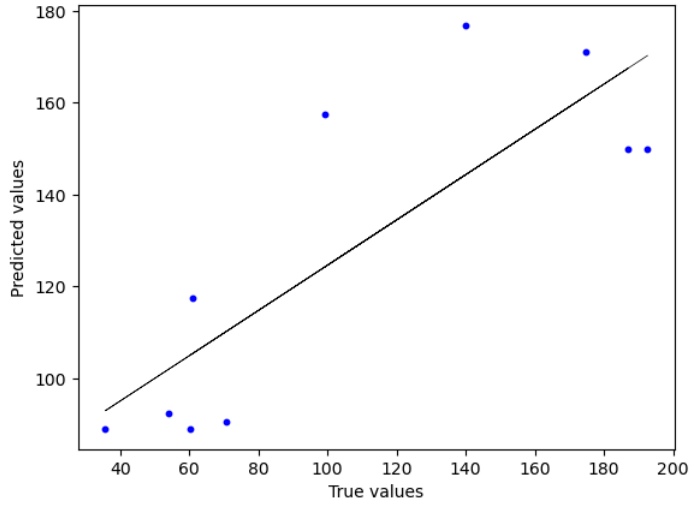
In [17]:
```
x = y_test.flatten()
y = y_test_pred.flatten()

#create scatterplot
plt.scatter(x, y, s=10, color='b')
plt.xlabel('True values')
plt.ylabel('Predicted values')

#calculate equation for trendline
z = np.polyfit(x, y, 1)
p = np.poly1d(z)

#add trendline to plot
plt.plot(x, p(x), color='k', linewidth=0.5)
```

Out[17]:
```
[<matplotlib.lines.Line2D at 0x1fd9a337d30>]
```



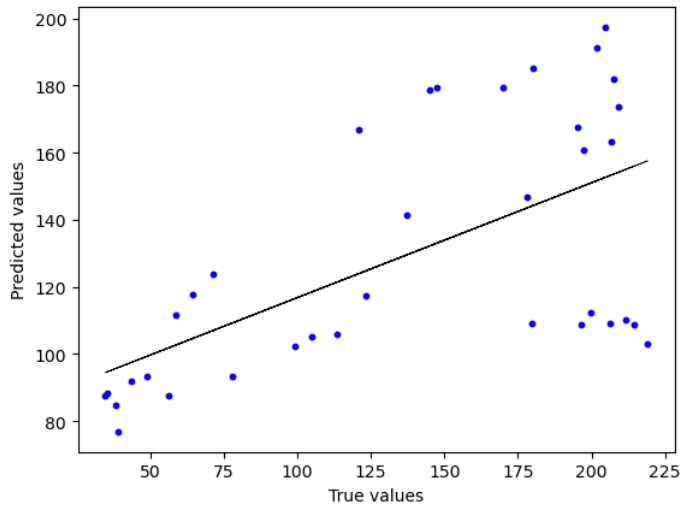
In [18]:
```
x = y_train.flatten()
y = y_train_pred.flatten()

#create scatterplot
plt.scatter(x, y, s=10, color='b')
plt.xlabel('True values')
plt.ylabel('Predicted values')

#calculate equation for trendline
z = np.polyfit(x, y, 1)
p = np.poly1d(z)

#add trendline to plot
plt.plot(x, p(x), color='k', linewidth=0.5)
```

Out[18]:
```
[<matplotlib.lines.Line2D at 0x1fd9a2ef310>]
```



APPENDIX 5 (b)

In [42]:
```
import numpy as np
import pandas as pd
import seaborn as sns
from matplotlib import pyplot as plt

df = pd.read_excel('dataset.artigoCBM,WUFIelab.tipo.slope.xlsx')
df
```

Out[42]:

	Material	Type	Slope	Temperature [°C]	Relative Humidity [%]	Δtmax [°C]	Humidity [kg/m³]	ΔT [°C]
0	1	1	1	6.99619	53.7301	2.376	233.649250	1.929128
1	1	1	1	6.99619	53.7301	2.376	221.900300	2.376436
2	1	1	2	6.99619	53.7301	2.376	164.249420	2.317941
3	1	1	2	6.99619	53.7301	2.376	145.193510	2.256899
4	1	1	2	6.99619	53.7301	2.376	137.497590	2.198631
...	...	...	...	...	...	...	...	...
5798	5	2	2	15.00000	80.0000	1.310	99.240363	0.850000
5799	5	2	2	15.00000	80.0000	1.310	71.292517	0.450000
5800	5	2	2	15.00000	80.0000	1.310	64.535147	0.380000
5801	5	2	2	15.00000	80.0000	1.310	61.020408	0.380000
5802	5	2	2	15.00000	80.0000	1.310	58.741497	0.310000

5803 rows × 8 columns

In [43]:
```
from keras.models import Model
from keras.layers import Dense, Input
from sklearn.model_selection import cross_val_score
from sklearn.model_selection import KFold
from sklearn.pipeline import Pipeline
from sklearn.model_selection import train_test_split
from sklearn.metrics import r2_score
from tensorflow.keras.callbacks import EarlyStopping


# SEPARAR INPUTS DOS OUTPUTS

X = df.drop(['Δtmax [°C]', 'Humidity [kg/m³]'], axis=1)
y = df.drop(['Material', 'Type', 'Slope', 'Temperature [°C]', 'Relative Humidity [%]', 'ΔT [°C]', 'Δtmax [°C]'], axis=1)
y = y.values

# número de dados de treinamento
m = X.shape[0]

X_train, X_test, y_train, y_test = train_test_split(X, y, test_size = 0.2, random_state=42, shuffle=True)

# Scale data, otherwise model will fail
# Standardize features by removing the mean and scaling to unit variance
from sklearn.preprocessing import MinMaxScaler
scaler = MinMaxScaler()
scaler.fit(X)

X_train_scaled = scaler.transform(X_train)
X_test_scaled = scaler.transform(X_test)


# Define the model
# Experiment with deeper and wider networks

#Start defining the input tensor:
inpTensor = Input(shape= (6,))

#create the layers and pass them the input tensor to get the output tensor:
hidden1Out = Dense(128, activation='relu')(inpTensor)
hidden2Out = Dense(64, activation='relu')(hidden1Out)
hidden3Out = Dense(64, activation='relu')(hidden2Out)
finalOut = Dense(1, activation='relu')(hidden3Out)

#define the model's start and end points
model = Model(inpTensor,finalOut)

model.compile(loss='mean_squared_error', optimizer='adam', metrics=['mae'])


# Apply the EarlyStopping function to prevent overfitting
# Train the model

monitor = EarlyStopping(monitor='val_loss', min_delta=1e-3, patience=20, verbose=1, restore_best_weights=True)

history = model.fit(X_train_scaled, y_train, validation_split=0.1, epochs=500, callbacks=[monitor], verbose=1)
```

```
Epoch 1/500
131/131 [==============================] - 2s 6ms/step - loss: 8440.3945 - mae: 68.8029 - val_loss: 4826.4209 - val_mae: 55.4504
Epoch 2/500
131/131 [==============================] - 0s 3ms/step - loss: 4575.4409 - mae: 54.2969 - val_loss: 3746.0151 - val_mae: 49.0241
Epoch 3/500
131/131 [==============================] - 0s 3ms/step - loss: 3810.5691 - mae: 49.3838 - val_loss: 3151.2534 - val_mae: 45.1549
Epoch 4/500
131/131 [==============================] - 0s 3ms/step - loss: 3306.2705 - mae: 45.7772 - val_loss: 2718.3362 - val_mae: 41.9065
Epoch 5/500
131/131 [==============================] - 0s 3ms/step - loss: 2838.8289 - mae: 41.8192 - val_loss: 2305.7095 - val_mae: 37.1837
Epoch 6/500
131/131 [==============================] - 0s 3ms/step - loss: 2357.5398 - mae: 37.3450 - val_loss: 1890.8857 - val_mae: 33.8577
Epoch 7/500
131/131 [==============================] - 0s 3ms/step - loss: 1750.9963 - mae: 31.5951 - val_loss: 1301.6721 - val_mae: 27.0996
Epoch 8/500
131/131 [==============================] - 0s 3ms/step - loss: 1093.0839 - mae: 24.3019 - val_loss: 780.2002 - val_mae: 20.6593
Epoch 9/500
131/131 [==============================] - 0s 3ms/step - loss: 638.9203 - mae: 17.6584 - val_loss: 537.1631 - val_mae: 14.9750
Epoch 10/500
131/131 [==============================] - 0s 3ms/step - loss: 459.5332 - mae: 13.6931 - val_loss: 459.1964 - val_mae: 13.2982
Epoch 11/500
131/131 [==============================] - 0s 2ms/step - loss: 390.4783 - mae: 12.2608 - val_loss: 380.1147 - val_mae: 11.3045
Epoch 12/500
131/131 [==============================] - 0s 3ms/step - loss: 345.2585 - mae: 11.1292 - val_loss: 339.9416 - val_mae: 10.6272
Epoch 13/500
131/131 [==============================] - 0s 3ms/step - loss: 300.5996 - mae: 10.2441 - val_loss: 306.5977 - val_mae: 10.7535
Epoch 14/500
131/131 [==============================] - 0s 3ms/step - loss: 266.7432 - mae: 9.6183 - val_loss: 279.2474 - val_mae: 9.9468
Epoch 15/500
131/131 [==============================] - 0s 3ms/step - loss: 251.6301 - mae: 9.4528 - val_loss: 263.4547 - val_mae: 9.4291
Epoch 16/500
131/131 [==============================] - 0s 3ms/step - loss: 234.6590 - mae: 9.1237 - val_loss: 243.4284 - val_mae: 9.1567
Epoch 17/500
131/131 [==============================] - 0s 3ms/step - loss: 222.8684 - mae: 8.9301 - val_loss: 229.4786 - val_mae: 9.0269
Epoch 18/500
131/131 [==============================] - 0s 4ms/step - loss: 209.3368 - mae: 8.7597 - val_loss: 233.4622 - val_mae: 8.7252
Epoch 19/500
131/131 [==============================] - 0s 3ms/step - loss: 201.4293 - mae: 8.4429 - val_loss: 245.5542 - val_mae: 9.8024
Epoch 20/500
131/131 [==============================] - 0s 4ms/step - loss: 189.6549 - mae: 8.2170 - val_loss: 210.0661 - val_mae: 8.8777
Epoch 21/500
131/131 [==============================] - 0s 3ms/step - loss: 188.6866 - mae: 8.3925 - val_loss: 195.0467 - val_mae: 8.1270
Epoch 22/500
131/131 [==============================] - 0s 3ms/step - loss: 185.8609 - mae: 8.1433 - val_loss: 190.1331 - val_mae: 7.5752
Epoch 23/500
131/131 [==============================] - 0s 3ms/step - loss: 171.5596 - mae: 7.6809 - val_loss: 183.7727 - val_mae: 8.1873
Epoch 24/500
131/131 [==============================] - 0s 3ms/step - loss: 168.8255 - mae: 7.6240 - val_loss: 194.4464 - val_mae: 8.3618
Epoch 25/500
131/131 [==============================] - 0s 4ms/step - loss: 162.2195 - mae: 7.5203 - val_loss: 191.8165 - val_mae: 8.1909
Epoch 26/500
131/131 [==============================] - 0s 3ms/step - loss: 161.5096 - mae: 7.4484 - val_loss: 178.9339 - val_mae: 7.9415
Epoch 27/500
131/131 [==============================] - 0s 3ms/step - loss: 156.4267 - mae: 7.2441 - val_loss: 173.3089 - val_mae: 7.2844
Epoch 28/500
131/131 [==============================] - 0s 3ms/step - loss: 152.6293 - mae: 7.0804 - val_loss: 163.5638 - val_mae: 7.2375
Epoch 29/500
131/131 [==============================] - 0s 3ms/step - loss: 150.6701 - mae: 7.1687 - val_loss: 179.1341 - val_mae: 7.3812
Epoch 30/500
131/131 [==============================] - 0s 4ms/step - loss: 146.7748 - mae: 6.8779 - val_loss: 198.8650 - val_mae: 8.7849
Epoch 31/500
131/131 [==============================] - 0s 4ms/step - loss: 145.5995 - mae: 6.8601 - val_loss: 175.7451 - val_mae: 7.5624
Epoch 32/500
131/131 [==============================] - 0s 3ms/step - loss: 146.9226 - mae: 6.9638 - val_loss: 163.1801 - val_mae: 6.8655
Epoch 33/500
131/131 [==============================] - 0s 3ms/step - loss: 140.5288 - mae: 6.7427 - val_loss: 158.2098 - val_mae: 6.7160
Epoch 34/500
131/131 [==============================] - 0s 3ms/step - loss: 138.5514 - mae: 6.5240 - val_loss: 158.2760 - val_mae: 7.1709
Epoch 35/500
131/131 [==============================] - 0s 3ms/step - loss: 153.0136 - mae: 7.2800 - val_loss: 158.5318 - val_mae: 6.3218
Epoch 36/500
131/131 [==============================] - 0s 3ms/step - loss: 137.9640 - mae: 6.4193 - val_loss: 158.5277 - val_mae: 6.5580
Epoch 37/500
131/131 [==============================] - 0s 3ms/step - loss: 132.1338 - mae: 6.2797 - val_loss: 148.2290 - val_mae: 6.2725
Epoch 38/500
131/131 [==============================] - 0s 3ms/step - loss: 139.6030 - mae: 6.7296 - val_loss: 181.0798 - val_mae: 8.1242
Epoch 39/500
131/131 [==============================] - 1s 7ms/step - loss: 140.0569 - mae: 6.7437 - val_loss: 148.4725 - val_mae: 6.4040
Epoch 40/500
131/131 [==============================] - 0s 3ms/step - loss: 137.5583 - mae: 6.6819 - val_loss: 160.6129 - val_mae: 7.1908
Epoch 41/500
131/131 [==============================] - 0s 3ms/step - loss: 129.9152 - mae: 6.3021 - val_loss: 178.9584 - val_mae: 7.5273
Epoch 42/500
131/131 [==============================] - 0s 3ms/step - loss: 127.1095 - mae: 6.1974 - val_loss: 138.4517 - val_mae: 6.0396
Epoch 43/500
131/131 [==============================] - 0s 3ms/step - loss: 127.9401 - mae: 6.2669 - val_loss: 186.6998 - val_mae: 8.7463
Epoch 44/500
131/131 [==============================] - 0s 3ms/step - loss: 123.4021 - mae: 5.9907 - val_loss: 136.0961 - val_mae: 5.8622
Epoch 45/500
131/131 [==============================] - 0s 3ms/step - loss: 129.8539 - mae: 6.3548 - val_loss: 150.8076 - val_mae: 6.5179
Epoch 46/500
131/131 [==============================] - 0s 3ms/step - loss: 123.5853 - mae: 6.0382 - val_loss: 148.5047 - val_mae: 6.9251
Epoch 47/500
131/131 [==============================] - 0s 3ms/step - loss: 116.4671 - mae: 5.9127 - val_loss: 157.3894 - val_mae: 6.5552
Epoch 48/500
131/131 [==============================] - 0s 3ms/step - loss: 121.9231 - mae: 5.9647 - val_loss: 143.4189 - val_mae: 6.1018
Epoch 49/500
131/131 [==============================] - 0s 3ms/step - loss: 114.6770 - mae: 5.7386 - val_loss: 131.6657 - val_mae: 5.6512
Epoch 50/500
131/131 [==============================] - 0s 2ms/step - loss: 110.5726 - mae: 5.5250 - val_loss: 148.9255 - val_mae: 7.5705
Epoch 51/500
131/131 [==============================] - 0s 3ms/step - loss: 109.0808 - mae: 5.4935 - val_loss: 145.2735 - val_mae: 6.7122
Epoch 52/500
131/131 [==============================] - 0s 3ms/step - loss: 109.7647 - mae: 5.6709 - val_loss: 126.2857 - val_mae: 5.5957
Epoch 53/500
131/131 [==============================] - 0s 2ms/step - loss: 110.5685 - mae: 5.6950 - val_loss: 125.5088 - val_mae: 5.7947
Epoch 54/500
```

```
131/131 [==============================] - 0s 3ms/step - loss: 111.2203 - mae: 5.9009 - val_loss: 146.3950 - val_mae: 6.5299
Epoch 55/500
131/131 [==============================] - 0s 3ms/step - loss: 103.2777 - mae: 5.3342 - val_loss: 122.5276 - val_mae: 5.2690
Epoch 56/500
131/131 [==============================] - 0s 3ms/step - loss: 107.0579 - mae: 5.5778 - val_loss: 128.3210 - val_mae: 6.1381
Epoch 57/500
131/131 [==============================] - 0s 3ms/step - loss: 101.1550 - mae: 5.4000 - val_loss: 118.1801 - val_mae: 5.8843
Epoch 58/500
131/131 [==============================] - 0s 2ms/step - loss: 97.6658 - mae: 5.2379 - val_loss: 118.4924 - val_mae: 5.8421
Epoch 59/500
131/131 [==============================] - 0s 2ms/step - loss: 108.1667 - mae: 5.7143 - val_loss: 126.3116 - val_mae: 5.9417
Epoch 60/500
131/131 [==============================] - 0s 2ms/step - loss: 104.2361 - mae: 5.5751 - val_loss: 124.9584 - val_mae: 5.6028
Epoch 61/500
131/131 [==============================] - 0s 3ms/step - loss: 99.7979 - mae: 5.4602 - val_loss: 119.0119 - val_mae: 4.9234
Epoch 62/500
131/131 [==============================] - 0s 2ms/step - loss: 105.0084 - mae: 5.7487 - val_loss: 118.7017 - val_mae: 6.2921
Epoch 63/500
131/131 [==============================] - 0s 2ms/step - loss: 95.9352 - mae: 5.3060 - val_loss: 115.1557 - val_mae: 6.0799
Epoch 64/500
131/131 [==============================] - 0s 3ms/step - loss: 96.3767 - mae: 5.1453 - val_loss: 116.1426 - val_mae: 5.1999
Epoch 65/500
131/131 [==============================] - 0s 2ms/step - loss: 95.5610 - mae: 5.1622 - val_loss: 128.0952 - val_mae: 6.7026
Epoch 66/500
131/131 [==============================] - 0s 2ms/step - loss: 94.3764 - mae: 5.4045 - val_loss: 129.4532 - val_mae: 6.3827
Epoch 67/500
131/131 [==============================] - 0s 2ms/step - loss: 91.1327 - mae: 5.0629 - val_loss: 128.4302 - val_mae: 6.8446
Epoch 68/500
131/131 [==============================] - 0s 2ms/step - loss: 90.9135 - mae: 5.2104 - val_loss: 126.6326 - val_mae: 5.2890
Epoch 69/500
131/131 [==============================] - 0s 2ms/step - loss: 85.3238 - mae: 4.8446 - val_loss: 95.6703 - val_mae: 4.8014
Epoch 70/500
131/131 [==============================] - 0s 3ms/step - loss: 87.9751 - mae: 5.0531 - val_loss: 115.4645 - val_mae: 5.6114
Epoch 71/500
131/131 [==============================] - 0s 3ms/step - loss: 89.9349 - mae: 5.2186 - val_loss: 104.0086 - val_mae: 4.8663
Epoch 72/500
131/131 [==============================] - 0s 2ms/step - loss: 95.9199 - mae: 5.4379 - val_loss: 100.2377 - val_mae: 5.0025
Epoch 73/500
131/131 [==============================] - 0s 3ms/step - loss: 89.3956 - mae: 5.2504 - val_loss: 98.3615 - val_mae: 5.6593
Epoch 74/500
131/131 [==============================] - 0s 3ms/step - loss: 83.4368 - mae: 4.8520 - val_loss: 93.2258 - val_mae: 5.1641
Epoch 75/500
131/131 [==============================] - 0s 3ms/step - loss: 88.1023 - mae: 5.1790 - val_loss: 88.1397 - val_mae: 4.3409
Epoch 76/500
131/131 [==============================] - 0s 3ms/step - loss: 87.1509 - mae: 5.2177 - val_loss: 133.2141 - val_mae: 6.7150
Epoch 77/500
131/131 [==============================] - 0s 4ms/step - loss: 81.0416 - mae: 4.9060 - val_loss: 80.3072 - val_mae: 4.6724
Epoch 78/500
131/131 [==============================] - 0s 3ms/step - loss: 77.2347 - mae: 4.6510 - val_loss: 83.1695 - val_mae: 4.6973
Epoch 79/500
131/131 [==============================] - 0s 3ms/step - loss: 78.3424 - mae: 4.6378 - val_loss: 102.5075 - val_mae: 5.4542
Epoch 80/500
131/131 [==============================] - 0s 3ms/step - loss: 77.3099 - mae: 4.7461 - val_loss: 93.0310 - val_mae: 5.5957
Epoch 81/500
131/131 [==============================] - 0s 3ms/step - loss: 74.5452 - mae: 4.6393 - val_loss: 78.5791 - val_mae: 4.5014
Epoch 82/500
131/131 [==============================] - 0s 3ms/step - loss: 77.2270 - mae: 4.6426 - val_loss: 82.0879 - val_mae: 4.7356
Epoch 83/500
131/131 [==============================] - 0s 3ms/step - loss: 71.1526 - mae: 4.4199 - val_loss: 104.9215 - val_mae: 5.2202
Epoch 84/500
131/131 [==============================] - 0s 3ms/step - loss: 72.8295 - mae: 4.6524 - val_loss: 84.7700 - val_mae: 4.5807
Epoch 85/500
131/131 [==============================] - 0s 3ms/step - loss: 71.8370 - mae: 4.4953 - val_loss: 78.2897 - val_mae: 4.8205
Epoch 86/500
131/131 [==============================] - 0s 3ms/step - loss: 70.5575 - mae: 4.4557 - val_loss: 74.6829 - val_mae: 4.8630
Epoch 87/500
131/131 [==============================] - 0s 3ms/step - loss: 77.5516 - mae: 4.9787 - val_loss: 107.2497 - val_mae: 6.6161
Epoch 88/500
131/131 [==============================] - 0s 3ms/step - loss: 71.1238 - mae: 4.6402 - val_loss: 79.2601 - val_mae: 4.7365
Epoch 89/500
131/131 [==============================] - 0s 3ms/step - loss: 66.9834 - mae: 4.4076 - val_loss: 98.3140 - val_mae: 5.2943
Epoch 90/500
131/131 [==============================] - 0s 3ms/step - loss: 71.7895 - mae: 4.5385 - val_loss: 73.3713 - val_mae: 4.3241
Epoch 91/500
131/131 [==============================] - 0s 3ms/step - loss: 67.9905 - mae: 4.3974 - val_loss: 67.5011 - val_mae: 4.3256
Epoch 92/500
131/131 [==============================] - 0s 3ms/step - loss: 73.4484 - mae: 4.6616 - val_loss: 70.4672 - val_mae: 4.2029
Epoch 93/500
131/131 [==============================] - 0s 3ms/step - loss: 64.6974 - mae: 4.2321 - val_loss: 78.1031 - val_mae: 5.2773
Epoch 94/500
131/131 [==============================] - 0s 3ms/step - loss: 68.7311 - mae: 4.3892 - val_loss: 67.5708 - val_mae: 4.5287
Epoch 95/500
131/131 [==============================] - 0s 3ms/step - loss: 69.7953 - mae: 4.5712 - val_loss: 70.3875 - val_mae: 4.1446
Epoch 96/500
131/131 [==============================] - 0s 3ms/step - loss: 65.1624 - mae: 4.3649 - val_loss: 67.4939 - val_mae: 4.2118
Epoch 97/500
131/131 [==============================] - 0s 3ms/step - loss: 64.0811 - mae: 4.3846 - val_loss: 61.9442 - val_mae: 4.6592
Epoch 98/500
131/131 [==============================] - 0s 3ms/step - loss: 68.1257 - mae: 4.5656 - val_loss: 81.6773 - val_mae: 4.2040
Epoch 99/500
131/131 [==============================] - 0s 3ms/step - loss: 62.5483 - mae: 4.1556 - val_loss: 61.5659 - val_mae: 3.9247
Epoch 100/500
131/131 [==============================] - 0s 3ms/step - loss: 63.7297 - mae: 4.3515 - val_loss: 71.8243 - val_mae: 4.4250
Epoch 101/500
131/131 [==============================] - 0s 3ms/step - loss: 56.7938 - mae: 4.0029 - val_loss: 87.3034 - val_mae: 5.4818
Epoch 102/500
131/131 [==============================] - 0s 3ms/step - loss: 64.4536 - mae: 4.3838 - val_loss: 79.5600 - val_mae: 4.4100
Epoch 103/500
131/131 [==============================] - 0s 3ms/step - loss: 62.5432 - mae: 4.2365 - val_loss: 57.5649 - val_mae: 4.1759
Epoch 104/500
131/131 [==============================] - 0s 3ms/step - loss: 60.8327 - mae: 4.3226 - val_loss: 72.7828 - val_mae: 4.6905
Epoch 105/500
131/131 [==============================] - 0s 3ms/step - loss: 60.2939 - mae: 4.2352 - val_loss: 60.2787 - val_mae: 4.2654
Epoch 106/500
131/131 [==============================] - 0s 2ms/step - loss: 60.9988 - mae: 4.2926 - val_loss: 65.6329 - val_mae: 3.6723
Epoch 107/500
131/131 [==============================] - 0s 3ms/step - loss: 62.6310 - mae: 4.4171 - val_loss: 66.4652 - val_mae: 4.4739
```

```
Epoch 108/500
131/131 [==============================] - 0s 4ms/step - loss: 64.2512 - mae: 4.4327 - val_loss: 59.3723 - val_mae: 4.0629
Epoch 109/500
131/131 [==============================] - 0s 3ms/step - loss: 56.2952 - mae: 3.9717 - val_loss: 54.1987 - val_mae: 3.8537
Epoch 110/500
131/131 [==============================] - 0s 3ms/step - loss: 59.5133 - mae: 4.3001 - val_loss: 59.1952 - val_mae: 3.8228
Epoch 111/500
131/131 [==============================] - 0s 3ms/step - loss: 60.5693 - mae: 4.2500 - val_loss: 70.8716 - val_mae: 5.1598
Epoch 112/500
131/131 [==============================] - 0s 3ms/step - loss: 56.4093 - mae: 3.9894 - val_loss: 55.5290 - val_mae: 3.8698
Epoch 113/500
131/131 [==============================] - 0s 3ms/step - loss: 49.8792 - mae: 3.7816 - val_loss: 58.6887 - val_mae: 4.3543
Epoch 114/500
131/131 [==============================] - 0s 2ms/step - loss: 59.6699 - mae: 4.2282 - val_loss: 59.2514 - val_mae: 4.1097
Epoch 115/500
131/131 [==============================] - 0s 3ms/step - loss: 53.4611 - mae: 3.9541 - val_loss: 67.3461 - val_mae: 4.5425
Epoch 116/500
131/131 [==============================] - 0s 3ms/step - loss: 53.0491 - mae: 3.9502 - val_loss: 72.7238 - val_mae: 3.9289
Epoch 117/500
131/131 [==============================] - 0s 3ms/step - loss: 49.3376 - mae: 3.7506 - val_loss: 57.9825 - val_mae: 4.1099
Epoch 118/500
131/131 [==============================] - 0s 3ms/step - loss: 48.7754 - mae: 3.6774 - val_loss: 59.7078 - val_mae: 4.1477
Epoch 119/500
131/131 [==============================] - 0s 3ms/step - loss: 52.8203 - mae: 3.9014 - val_loss: 61.8961 - val_mae: 4.0356
Epoch 120/500
131/131 [==============================] - 0s 2ms/step - loss: 56.8455 - mae: 4.2465 - val_loss: 58.3019 - val_mae: 4.2329
Epoch 121/500
131/131 [==============================] - 0s 3ms/step - loss: 56.1891 - mae: 4.0208 - val_loss: 52.5884 - val_mae: 4.3281
Epoch 122/500
131/131 [==============================] - 0s 3ms/step - loss: 53.2759 - mae: 3.9077 - val_loss: 63.0636 - val_mae: 3.6872
Epoch 123/500
131/131 [==============================] - 0s 3ms/step - loss: 49.1119 - mae: 3.6330 - val_loss: 45.4064 - val_mae: 3.8293
Epoch 124/500
131/131 [==============================] - 0s 3ms/step - loss: 46.6070 - mae: 3.6975 - val_loss: 62.4503 - val_mae: 4.2191
Epoch 125/500
131/131 [==============================] - 0s 3ms/step - loss: 46.6069 - mae: 3.6565 - val_loss: 62.3413 - val_mae: 4.5773
Epoch 126/500
131/131 [==============================] - 0s 3ms/step - loss: 51.3666 - mae: 3.8329 - val_loss: 81.0923 - val_mae: 6.1345
Epoch 127/500
131/131 [==============================] - 0s 3ms/step - loss: 61.0432 - mae: 4.5284 - val_loss: 74.3269 - val_mae: 5.1098
Epoch 128/500
131/131 [==============================] - 0s 4ms/step - loss: 45.0043 - mae: 3.5839 - val_loss: 55.1736 - val_mae: 3.7344
Epoch 129/500
131/131 [==============================] - 0s 3ms/step - loss: 45.6118 - mae: 3.6681 - val_loss: 50.8446 - val_mae: 3.1977
Epoch 130/500
131/131 [==============================] - 0s 3ms/step - loss: 50.1428 - mae: 3.8215 - val_loss: 48.0233 - val_mae: 3.5681
Epoch 131/500
131/131 [==============================] - 0s 3ms/step - loss: 46.7136 - mae: 3.5396 - val_loss: 53.9756 - val_mae: 3.8101
Epoch 132/500
131/131 [==============================] - 0s 3ms/step - loss: 54.1132 - mae: 4.1168 - val_loss: 53.8797 - val_mae: 4.1808
Epoch 133/500
131/131 [==============================] - 0s 3ms/step - loss: 51.5582 - mae: 3.9477 - val_loss: 92.0029 - val_mae: 5.7573
Epoch 134/500
131/131 [==============================] - 0s 3ms/step - loss: 51.9562 - mae: 4.0058 - val_loss: 52.5469 - val_mae: 3.7216
Epoch 135/500
131/131 [==============================] - 0s 3ms/step - loss: 49.7162 - mae: 3.7753 - val_loss: 44.1791 - val_mae: 3.6395
Epoch 136/500
131/131 [==============================] - 0s 3ms/step - loss: 44.9165 - mae: 3.5146 - val_loss: 49.7694 - val_mae: 3.6737
Epoch 137/500
131/131 [==============================] - 0s 3ms/step - loss: 42.5080 - mae: 3.4445 - val_loss: 47.5984 - val_mae: 3.4898
Epoch 138/500
131/131 [==============================] - 0s 3ms/step - loss: 42.0561 - mae: 3.5502 - val_loss: 43.1336 - val_mae: 3.0853
Epoch 139/500
131/131 [==============================] - 0s 3ms/step - loss: 42.5348 - mae: 3.4384 - val_loss: 46.8212 - val_mae: 3.4090
Epoch 140/500
131/131 [==============================] - 0s 3ms/step - loss: 41.8616 - mae: 3.5189 - val_loss: 47.3073 - val_mae: 3.3915
Epoch 141/500
131/131 [==============================] - 0s 3ms/step - loss: 41.3083 - mae: 3.3817 - val_loss: 41.2488 - val_mae: 3.4188
Epoch 142/500
131/131 [==============================] - 0s 3ms/step - loss: 44.9066 - mae: 3.5078 - val_loss: 40.6241 - val_mae: 3.3926
Epoch 143/500
131/131 [==============================] - 0s 3ms/step - loss: 37.8564 - mae: 3.1955 - val_loss: 41.0333 - val_mae: 3.2552
Epoch 144/500
131/131 [==============================] - 0s 3ms/step - loss: 45.7198 - mae: 3.6719 - val_loss: 73.4613 - val_mae: 4.0095
Epoch 145/500
131/131 [==============================] - 0s 3ms/step - loss: 48.4480 - mae: 3.7822 - val_loss: 44.6025 - val_mae: 3.3043
Epoch 146/500
131/131 [==============================] - 0s 3ms/step - loss: 43.9696 - mae: 3.6727 - val_loss: 56.6129 - val_mae: 3.9036
Epoch 147/500
131/131 [==============================] - 0s 4ms/step - loss: 44.2101 - mae: 3.7158 - val_loss: 55.0440 - val_mae: 4.4424
Epoch 148/500
131/131 [==============================] - 0s 3ms/step - loss: 46.5841 - mae: 3.6777 - val_loss: 61.7215 - val_mae: 3.4097
Epoch 149/500
131/131 [==============================] - 1s 4ms/step - loss: 40.5031 - mae: 3.4384 - val_loss: 46.8209 - val_mae: 3.7415
Epoch 150/500
131/131 [==============================] - 0s 3ms/step - loss: 45.0516 - mae: 3.8626 - val_loss: 52.1444 - val_mae: 3.6421
Epoch 151/500
131/131 [==============================] - 0s 3ms/step - loss: 40.4060 - mae: 3.5187 - val_loss: 45.4659 - val_mae: 4.0442
Epoch 152/500
131/131 [==============================] - 0s 3ms/step - loss: 44.3985 - mae: 3.7130 - val_loss: 48.1257 - val_mae: 3.5201
Epoch 153/500
131/131 [==============================] - 0s 3ms/step - loss: 44.9008 - mae: 3.7330 - val_loss: 39.6152 - val_mae: 3.3690
Epoch 154/500
131/131 [==============================] - 0s 3ms/step - loss: 39.7444 - mae: 3.4146 - val_loss: 66.9679 - val_mae: 4.8122
Epoch 155/500
131/131 [==============================] - 0s 3ms/step - loss: 38.2201 - mae: 3.2903 - val_loss: 63.7511 - val_mae: 4.6415
Epoch 156/500
131/131 [==============================] - 0s 3ms/step - loss: 40.8300 - mae: 3.3519 - val_loss: 46.8867 - val_mae: 3.9593
Epoch 157/500
131/131 [==============================] - 0s 3ms/step - loss: 36.2944 - mae: 3.1812 - val_loss: 55.5194 - val_mae: 3.6946
Epoch 158/500
131/131 [==============================] - 0s 3ms/step - loss: 40.1884 - mae: 3.4589 - val_loss: 56.2997 - val_mae: 4.3864
Epoch 159/500
131/131 [==============================] - 0s 3ms/step - loss: 35.6328 - mae: 3.2268 - val_loss: 38.3414 - val_mae: 3.2610
Epoch 160/500
131/131 [==============================] - 0s 3ms/step - loss: 40.9533 - mae: 3.6327 - val_loss: 42.2345 - val_mae: 3.6239
Epoch 161/500
```

```
131/131 [==============================] - 0s 4ms/step - loss: 41.6221 - mae: 3.5838 - val_loss: 40.8169 - val_mae: 3.2016
Epoch 162/500
131/131 [==============================] - 1s 4ms/step - loss: 37.6522 - mae: 3.3441 - val_loss: 41.8569 - val_mae: 3.4915
Epoch 163/500
131/131 [==============================] - 0s 3ms/step - loss: 43.3594 - mae: 3.5625 - val_loss: 69.3342 - val_mae: 4.7578
Epoch 164/500
131/131 [==============================] - 0s 3ms/step - loss: 44.3127 - mae: 3.8526 - val_loss: 39.7908 - val_mae: 3.5216
Epoch 165/500
131/131 [==============================] - 0s 3ms/step - loss: 34.6573 - mae: 3.1233 - val_loss: 46.4642 - val_mae: 4.0671
Epoch 166/500
131/131 [==============================] - 0s 3ms/step - loss: 36.6328 - mae: 3.0629 - val_loss: 47.7876 - val_mae: 3.8916
Epoch 167/500
131/131 [==============================] - 0s 3ms/step - loss: 39.9454 - mae: 3.5180 - val_loss: 55.3878 - val_mae: 4.5499
Epoch 168/500
131/131 [==============================] - 0s 3ms/step - loss: 40.4523 - mae: 3.5064 - val_loss: 37.4858 - val_mae: 3.1055
Epoch 169/500
131/131 [==============================] - 1s 4ms/step - loss: 36.9042 - mae: 3.2800 - val_loss: 67.1864 - val_mae: 5.0650
Epoch 170/500
131/131 [==============================] - 0s 3ms/step - loss: 40.6075 - mae: 3.4725 - val_loss: 55.4098 - val_mae: 4.0321
Epoch 171/500
131/131 [==============================] - 1s 4ms/step - loss: 37.6428 - mae: 3.2672 - val_loss: 35.6250 - val_mae: 3.1053
Epoch 172/500
131/131 [==============================] - 1s 4ms/step - loss: 31.6817 - mae: 3.0162 - val_loss: 71.9779 - val_mae: 4.4627
Epoch 173/500
131/131 [==============================] - 0s 4ms/step - loss: 33.3385 - mae: 3.1206 - val_loss: 38.3932 - val_mae: 3.6354
Epoch 174/500
131/131 [==============================] - 0s 3ms/step - loss: 41.9753 - mae: 3.6894 - val_loss: 45.6674 - val_mae: 4.1952
Epoch 175/500
131/131 [==============================] - 0s 3ms/step - loss: 37.4875 - mae: 3.2841 - val_loss: 35.2251 - val_mae: 3.1263
Epoch 176/500
131/131 [==============================] - 0s 3ms/step - loss: 33.2927 - mae: 3.1099 - val_loss: 41.6247 - val_mae: 3.3987
Epoch 177/500
131/131 [==============================] - 0s 3ms/step - loss: 34.2124 - mae: 3.1422 - val_loss: 36.4153 - val_mae: 3.1754
Epoch 178/500
131/131 [==============================] - 0s 3ms/step - loss: 38.1101 - mae: 3.3321 - val_loss: 57.4059 - val_mae: 5.0873
Epoch 179/500
131/131 [==============================] - 0s 4ms/step - loss: 38.0266 - mae: 3.4480 - val_loss: 60.0490 - val_mae: 4.1418
Epoch 180/500
131/131 [==============================] - 0s 3ms/step - loss: 42.3044 - mae: 3.7373 - val_loss: 36.8871 - val_mae: 3.1576
Epoch 181/500
131/131 [==============================] - 1s 4ms/step - loss: 31.7747 - mae: 3.0639 - val_loss: 35.0959 - val_mae: 3.1577
Epoch 182/500
131/131 [==============================] - 1s 4ms/step - loss: 32.4118 - mae: 2.8953 - val_loss: 49.8207 - val_mae: 3.9664
Epoch 183/500
131/131 [==============================] - 0s 3ms/step - loss: 35.7116 - mae: 3.3327 - val_loss: 33.5122 - val_mae: 3.2742
Epoch 184/500
131/131 [==============================] - 0s 3ms/step - loss: 32.2392 - mae: 3.0309 - val_loss: 39.1484 - val_mae: 3.3475
Epoch 185/500
131/131 [==============================] - 0s 3ms/step - loss: 30.7773 - mae: 2.9496 - val_loss: 52.0691 - val_mae: 4.3094
Epoch 186/500
131/131 [==============================] - 0s 3ms/step - loss: 31.5352 - mae: 2.9837 - val_loss: 33.7752 - val_mae: 3.2120
Epoch 187/500
131/131 [==============================] - 0s 3ms/step - loss: 36.0459 - mae: 3.4230 - val_loss: 35.8030 - val_mae: 3.8562
Epoch 188/500
131/131 [==============================] - 0s 3ms/step - loss: 29.8487 - mae: 2.9678 - val_loss: 38.2561 - val_mae: 2.9214
Epoch 189/500
131/131 [==============================] - 0s 3ms/step - loss: 33.5862 - mae: 3.0838 - val_loss: 30.9401 - val_mae: 3.2730
Epoch 190/500
131/131 [==============================] - 0s 3ms/step - loss: 30.7871 - mae: 2.9884 - val_loss: 42.7484 - val_mae: 3.3204
Epoch 191/500
131/131 [==============================] - 0s 3ms/step - loss: 29.8260 - mae: 2.9235 - val_loss: 30.8424 - val_mae: 2.8521
Epoch 192/500
131/131 [==============================] - 0s 4ms/step - loss: 31.9654 - mae: 3.0029 - val_loss: 34.4768 - val_mae: 3.2790
Epoch 193/500
131/131 [==============================] - 0s 3ms/step - loss: 32.8256 - mae: 3.1724 - val_loss: 49.7555 - val_mae: 4.7676
Epoch 194/500
131/131 [==============================] - 0s 3ms/step - loss: 31.7176 - mae: 3.0804 - val_loss: 34.0686 - val_mae: 3.1865
Epoch 195/500
131/131 [==============================] - 0s 3ms/step - loss: 33.6157 - mae: 3.3206 - val_loss: 34.1663 - val_mae: 3.3343
Epoch 196/500
131/131 [==============================] - 0s 3ms/step - loss: 30.6975 - mae: 3.0377 - val_loss: 86.1363 - val_mae: 5.8606
Epoch 197/500
131/131 [==============================] - 0s 3ms/step - loss: 32.7354 - mae: 3.2174 - val_loss: 30.5702 - val_mae: 3.2540
Epoch 198/500
131/131 [==============================] - 0s 3ms/step - loss: 32.2492 - mae: 3.0176 - val_loss: 36.7959 - val_mae: 3.5379
Epoch 199/500
131/131 [==============================] - 0s 3ms/step - loss: 35.1360 - mae: 3.4212 - val_loss: 30.7285 - val_mae: 2.7270
Epoch 200/500
131/131 [==============================] - 0s 3ms/step - loss: 34.1353 - mae: 3.1212 - val_loss: 31.5428 - val_mae: 2.7033
Epoch 201/500
131/131 [==============================] - 0s 3ms/step - loss: 32.3124 - mae: 3.1042 - val_loss: 37.9818 - val_mae: 3.5136
Epoch 202/500
131/131 [==============================] - 0s 3ms/step - loss: 34.4559 - mae: 3.1172 - val_loss: 34.0572 - val_mae: 3.0715
Epoch 203/500
131/131 [==============================] - 0s 3ms/step - loss: 30.8221 - mae: 3.1042 - val_loss: 44.1869 - val_mae: 4.4242
Epoch 204/500
131/131 [==============================] - 0s 3ms/step - loss: 32.2385 - mae: 3.0175 - val_loss: 32.3950 - val_mae: 2.9760
Epoch 205/500
131/131 [==============================] - 0s 3ms/step - loss: 29.1435 - mae: 2.8331 - val_loss: 28.0743 - val_mae: 2.8427
Epoch 206/500
131/131 [==============================] - 0s 3ms/step - loss: 29.3651 - mae: 2.8996 - val_loss: 33.2874 - val_mae: 3.0098
Epoch 207/500
131/131 [==============================] - 0s 3ms/step - loss: 33.4931 - mae: 3.2179 - val_loss: 28.2057 - val_mae: 2.8282
Epoch 208/500
131/131 [==============================] - 0s 3ms/step - loss: 33.5635 - mae: 3.1691 - val_loss: 40.7417 - val_mae: 3.3376
Epoch 209/500
131/131 [==============================] - 0s 3ms/step - loss: 34.0962 - mae: 3.1885 - val_loss: 36.0634 - val_mae: 3.3214
Epoch 210/500
131/131 [==============================] - 1s 4ms/step - loss: 29.0222 - mae: 2.9679 - val_loss: 40.8846 - val_mae: 4.1324
Epoch 211/500
131/131 [==============================] - 0s 3ms/step - loss: 26.4678 - mae: 2.8644 - val_loss: 35.7460 - val_mae: 3.2077
Epoch 212/500
131/131 [==============================] - 0s 3ms/step - loss: 29.2439 - mae: 2.9174 - val_loss: 80.8507 - val_mae: 5.6884
Epoch 213/500
131/131 [==============================] - 0s 3ms/step - loss: 36.1099 - mae: 3.3993 - val_loss: 33.5207 - val_mae: 3.3397
Epoch 214/500
131/131 [==============================] - 0s 3ms/step - loss: 23.8157 - mae: 2.5909 - val_loss: 45.7504 - val_mae: 3.4981
```

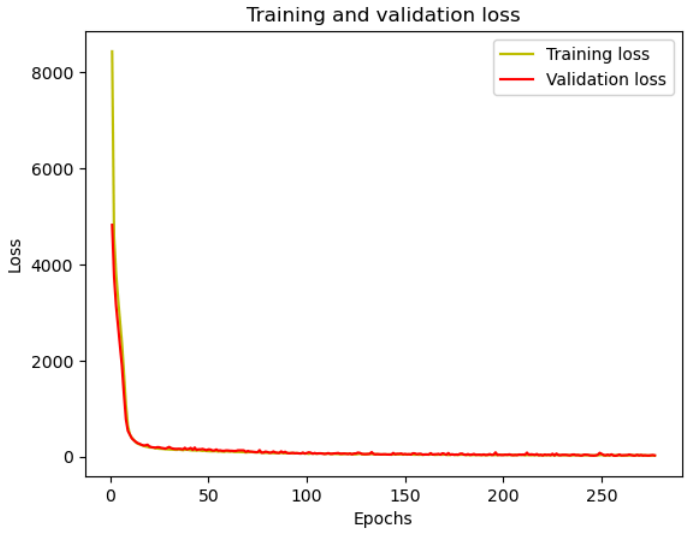
```
Epoch 215/500
131/131 [==============================] - 0s 3ms/step - loss: 29.7334 - mae: 2.9867 - val_loss: 41.1121 - val_mae: 3.5104
Epoch 216/500
131/131 [==============================] - 0s 3ms/step - loss: 30.8701 - mae: 3.1299 - val_loss: 31.2484 - val_mae: 2.7878
Epoch 217/500
131/131 [==============================] - 0s 3ms/step - loss: 30.1435 - mae: 3.0358 - val_loss: 51.0669 - val_mae: 4.1604
Epoch 218/500
131/131 [==============================] - 0s 3ms/step - loss: 30.5663 - mae: 3.0616 - val_loss: 25.1039 - val_mae: 2.8570
Epoch 219/500
131/131 [==============================] - 0s 3ms/step - loss: 26.5044 - mae: 2.7921 - val_loss: 37.3857 - val_mae: 3.1621
Epoch 220/500
131/131 [==============================] - 0s 3ms/step - loss: 25.3236 - mae: 2.7212 - val_loss: 21.6314 - val_mae: 2.5980
Epoch 221/500
131/131 [==============================] - 0s 3ms/step - loss: 26.3041 - mae: 2.7800 - val_loss: 41.3369 - val_mae: 3.0462
Epoch 222/500
131/131 [==============================] - 0s 3ms/step - loss: 30.2534 - mae: 3.0994 - val_loss: 30.3035 - val_mae: 3.5929
Epoch 223/500
131/131 [==============================] - 0s 3ms/step - loss: 29.7664 - mae: 3.1966 - val_loss: 37.9316 - val_mae: 4.1215
Epoch 224/500
131/131 [==============================] - 0s 3ms/step - loss: 24.7674 - mae: 2.6090 - val_loss: 27.5074 - val_mae: 2.8681
Epoch 225/500
131/131 [==============================] - 1s 4ms/step - loss: 31.8525 - mae: 3.1102 - val_loss: 56.5381 - val_mae: 5.0968
Epoch 226/500
131/131 [==============================] - 0s 3ms/step - loss: 23.6977 - mae: 2.6230 - val_loss: 21.0835 - val_mae: 2.3659
Epoch 227/500
131/131 [==============================] - 0s 3ms/step - loss: 30.7914 - mae: 3.0521 - val_loss: 60.6228 - val_mae: 4.0489
Epoch 228/500
131/131 [==============================] - 0s 3ms/step - loss: 33.4259 - mae: 3.3450 - val_loss: 27.9015 - val_mae: 2.9117
Epoch 229/500
131/131 [==============================] - 0s 3ms/step - loss: 27.7338 - mae: 2.8158 - val_loss: 26.9125 - val_mae: 2.9841
Epoch 230/500
131/131 [==============================] - 0s 3ms/step - loss: 26.2140 - mae: 2.7655 - val_loss: 35.1262 - val_mae: 2.8632
Epoch 231/500
131/131 [==============================] - 0s 3ms/step - loss: 25.7624 - mae: 2.7595 - val_loss: 35.5762 - val_mae: 3.3973
Epoch 232/500
131/131 [==============================] - 0s 3ms/step - loss: 26.4859 - mae: 2.7070 - val_loss: 34.5299 - val_mae: 3.3159
Epoch 233/500
131/131 [==============================] - 0s 3ms/step - loss: 28.9558 - mae: 2.8825 - val_loss: 26.6294 - val_mae: 2.9433
Epoch 234/500
131/131 [==============================] - 0s 3ms/step - loss: 24.6818 - mae: 2.6637 - val_loss: 24.1622 - val_mae: 2.6793
Epoch 235/500
131/131 [==============================] - 0s 3ms/step - loss: 25.9251 - mae: 2.7367 - val_loss: 38.7588 - val_mae: 3.6265
Epoch 236/500
131/131 [==============================] - 0s 3ms/step - loss: 25.4836 - mae: 2.8171 - val_loss: 41.3487 - val_mae: 3.5943
Epoch 237/500
131/131 [==============================] - 0s 3ms/step - loss: 34.4274 - mae: 3.2725 - val_loss: 24.7617 - val_mae: 2.5253
Epoch 238/500
131/131 [==============================] - 0s 3ms/step - loss: 23.1934 - mae: 2.6572 - val_loss: 34.1346 - val_mae: 3.5532
Epoch 239/500
131/131 [==============================] - 0s 3ms/step - loss: 25.8386 - mae: 2.8003 - val_loss: 21.8687 - val_mae: 2.6339
Epoch 240/500
131/131 [==============================] - 0s 3ms/step - loss: 22.3122 - mae: 2.5512 - val_loss: 22.3173 - val_mae: 2.5643
Epoch 241/500
131/131 [==============================] - 0s 3ms/step - loss: 26.2072 - mae: 2.8314 - val_loss: 37.7506 - val_mae: 3.7044
Epoch 242/500
131/131 [==============================] - 0s 3ms/step - loss: 25.1744 - mae: 2.7808 - val_loss: 37.2126 - val_mae: 3.2791
Epoch 243/500
131/131 [==============================] - 0s 3ms/step - loss: 30.1577 - mae: 3.2061 - val_loss: 33.6782 - val_mae: 2.8651
Epoch 244/500
131/131 [==============================] - 0s 4ms/step - loss: 22.4484 - mae: 2.6915 - val_loss: 24.5333 - val_mae: 2.3977
Epoch 245/500
131/131 [==============================] - 0s 3ms/step - loss: 23.0218 - mae: 2.5138 - val_loss: 20.8421 - val_mae: 2.4812
Epoch 246/500
131/131 [==============================] - 0s 3ms/step - loss: 25.9169 - mae: 2.8556 - val_loss: 19.0838 - val_mae: 2.3866
Epoch 247/500
131/131 [==============================] - 0s 3ms/step - loss: 23.3482 - mae: 2.6454 - val_loss: 22.9208 - val_mae: 2.3237
Epoch 248/500
131/131 [==============================] - 0s 3ms/step - loss: 26.0697 - mae: 2.7016 - val_loss: 34.7782 - val_mae: 3.3805
Epoch 249/500
131/131 [==============================] - 0s 3ms/step - loss: 28.4104 - mae: 2.8785 - val_loss: 76.1839 - val_mae: 5.5948
Epoch 250/500
131/131 [==============================] - 0s 3ms/step - loss: 35.7330 - mae: 3.3904 - val_loss: 54.3825 - val_mae: 4.6118
Epoch 251/500
131/131 [==============================] - 0s 3ms/step - loss: 21.8006 - mae: 2.4990 - val_loss: 31.3455 - val_mae: 2.9301
Epoch 252/500
131/131 [==============================] - 0s 3ms/step - loss: 22.9069 - mae: 2.7251 - val_loss: 23.5269 - val_mae: 3.0548
Epoch 253/500
131/131 [==============================] - 0s 3ms/step - loss: 24.0026 - mae: 2.7038 - val_loss: 38.8571 - val_mae: 3.8985
Epoch 254/500
131/131 [==============================] - 0s 3ms/step - loss: 21.3308 - mae: 2.4774 - val_loss: 24.9163 - val_mae: 2.4726
Epoch 255/500
131/131 [==============================] - 0s 3ms/step - loss: 33.8001 - mae: 3.0346 - val_loss: 44.5243 - val_mae: 4.1635
Epoch 256/500
131/131 [==============================] - 0s 3ms/step - loss: 27.7929 - mae: 3.0155 - val_loss: 19.5135 - val_mae: 2.2794
Epoch 257/500
131/131 [==============================] - 0s 3ms/step - loss: 22.2139 - mae: 2.5589 - val_loss: 17.0483 - val_mae: 2.1722
Epoch 258/500
131/131 [==============================] - 0s 2ms/step - loss: 31.7831 - mae: 3.0783 - val_loss: 21.8875 - val_mae: 2.8488
Epoch 259/500
131/131 [==============================] - 0s 3ms/step - loss: 23.8521 - mae: 2.6149 - val_loss: 41.3840 - val_mae: 3.7477
Epoch 260/500
131/131 [==============================] - 0s 2ms/step - loss: 19.0396 - mae: 2.4374 - val_loss: 24.3349 - val_mae: 2.3998
Epoch 261/500
131/131 [==============================] - 0s 2ms/step - loss: 21.5951 - mae: 2.5557 - val_loss: 26.4826 - val_mae: 3.0456
Epoch 262/500
131/131 [==============================] - 0s 3ms/step - loss: 21.7022 - mae: 2.4876 - val_loss: 27.2967 - val_mae: 3.2166
Epoch 263/500
131/131 [==============================] - 0s 3ms/step - loss: 24.2432 - mae: 2.7680 - val_loss: 28.0178 - val_mae: 3.5408
Epoch 264/500
131/131 [==============================] - 0s 3ms/step - loss: 22.3767 - mae: 2.5348 - val_loss: 40.9132 - val_mae: 3.6381
Epoch 265/500
131/131 [==============================] - 0s 3ms/step - loss: 26.7808 - mae: 2.8900 - val_loss: 30.1286 - val_mae: 3.1949
Epoch 266/500
131/131 [==============================] - 0s 3ms/step - loss: 27.8005 - mae: 2.9911 - val_loss: 20.3232 - val_mae: 2.4439
Epoch 267/500
131/131 [==============================] - 0s 3ms/step - loss: 21.8444 - mae: 2.6119 - val_loss: 20.1253 - val_mae: 2.8212
Epoch 268/500
```

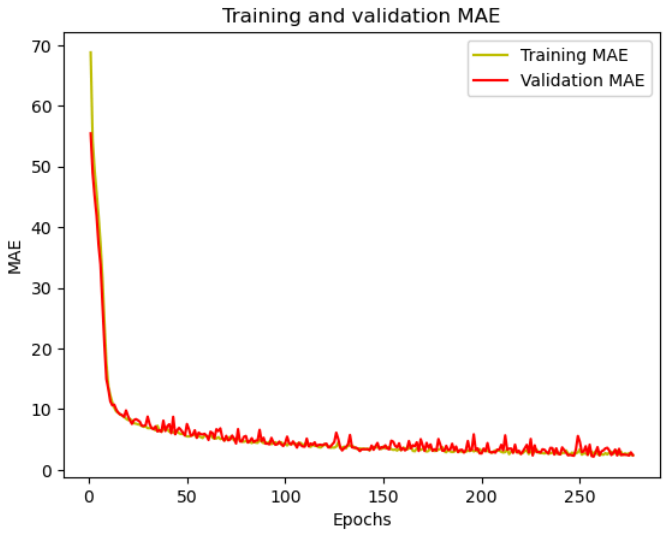
```
131/131 [==============================] - 0s 3ms/step - loss: 26.4282 - mae: 2.8359 - val_loss: 36.1628 - val_mae: 3.3496
Epoch 269/500
131/131 [==============================] - 0s 3ms/step - loss: 30.4655 - mae: 3.1689 - val_loss: 19.4939 - val_mae: 2.3716
Epoch 270/500
131/131 [==============================] - 0s 4ms/step - loss: 22.1899 - mae: 2.5098 - val_loss: 33.4812 - val_mae: 3.4741
Epoch 271/500
131/131 [==============================] - 0s 3ms/step - loss: 28.0238 - mae: 2.9791 - val_loss: 18.3887 - val_mae: 2.4173
Epoch 272/500
131/131 [==============================] - 0s 3ms/step - loss: 22.3804 - mae: 2.4361 - val_loss: 25.3690 - val_mae: 2.5527
Epoch 273/500
131/131 [==============================] - 0s 3ms/step - loss: 22.4794 - mae: 2.7257 - val_loss: 20.5445 - val_mae: 2.4836
Epoch 274/500
131/131 [==============================] - 0s 3ms/step - loss: 22.3689 - mae: 2.5737 - val_loss: 19.8581 - val_mae: 2.4669
Epoch 275/500
131/131 [==============================] - 0s 3ms/step - loss: 24.3000 - mae: 2.7270 - val_loss: 24.0710 - val_mae: 2.3604
Epoch 276/500
131/131 [==============================] - 0s 3ms/step - loss: 20.2777 - mae: 2.4588 - val_loss: 30.5420 - val_mae: 2.8865
Epoch 277/500
118/131 [==========================>...] - ETA: 0s - loss: 18.4868 - mae: 2.4309Restoring model weights from the end of the best epoch: 257.
131/131 [==============================] - 0s 3ms/step - loss: 18.3358 - mae: 2.4321 - val_loss: 22.5105 - val_mae: 2.4073
Epoch 277: early stopping
```

In [44]:
```
# plot the training and validation accuracy and loss at each epoch

loss = history.history['loss']
val_loss = history.history['val_loss']
epochs = range(1, len(loss) + 1)
plt.plot (epochs, loss, 'y', label = 'Training loss')
plt.plot (epochs, val_loss, 'r', label='Validation loss')
plt.title('Training and validation loss')
plt.xlabel ('Epochs')
plt.ylabel('Loss')
plt.legend()
plt.show()

acc = history.history['mae']
val_acc = history.history['val_mae']
plt.plot (epochs, acc, 'y', label = 'Training MAE')
plt.plot (epochs, val_acc, 'r', label='Validation MAE')
plt.title('Training and validation MAE')
plt.xlabel ('Epochs')
plt.ylabel('MAE')
plt.legend()
plt.show()
```





In [45]:
```
# Runs model with its current weights on the training and testing data

y_train_pred = model.predict(X_train_scaled)
y_test_pred = model.predict(X_test_scaled)
```

```
# X_test - input de teste
# X_train - input de treino

# y_test_pred - output de teste previsto
# y test - output de teste real

# Calculates and prints r2 score of training and testing data
print('R2 score train:', r2_score(y_train, y_train_pred))
print('R2 score test:', r2_score(y_test, y_test_pred))

r2nn = r2_score(y_test, y_test_pred)
r2nn
```

```
146/146 [==============================] - 0s 2ms/step
37/37 [==============================] - 0s 2ms/step
R2 score train: 0.9970621900647444
R2 score test: 0.9959561017383082
```

Out[45]:
```
0.9959561017383082
```

In [46]:
```
# Predict on test data

predictions = model.predict(X_test_scaled[:])
print("Predicted values are: ", predictions[:5])
print("Real values are: ", y_test[:5])
```

```
37/37 [==============================] - 0s 2ms/step
Predicted values are:  [[ 27.29742 ]
 [ 84.00268 ]
 [ 68.65811 ]
 [215.21413 ]
 [114.059845]]
Real values are:  [[ 27.331945]
 [ 85.007767]
 [ 71.608025]
 [217.3111  ]
 [112.35448 ]]
```

In [47]:
```
# Predict on new data
testando = [5, 2, 2, 15.0, 80.0, 0.31]
testando = np.array(testando)
testando= testando.reshape(1, -1)
testandonormalizado = scaler.transform(testando)

predictions2 = model.predict(testandonormalizado)
print("Predicted: ", predictions2)
print("Real value: Humidade = 58,74 kg/m³")
```

```
1/1 [==============================] - 0s 37ms/step
Predicted:  [[50.06875]]
Real value: Humidade = 58,74 kg/m³
C:\ProgramData\Anaconda3\lib\site-packages\sklearn\base.py:450: UserWarning: X does not have valid feature names, but MinMaxScaler was fitted with feature names
  warnings.warn(
```

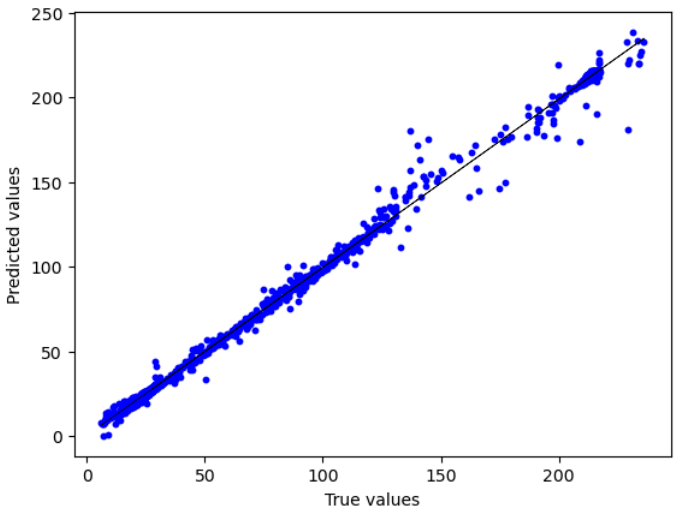
In [48]:
```
x = y_test.flatten()
y = y_test_pred.flatten()

#create scatterplot
plt.scatter(x, y, s=10, color='b')
plt.xlabel('True values')
plt.ylabel('Predicted values')

#calculate equation for trendline
z = np.polyfit(x, y, 1)
p = np.poly1d(z)

#add trendline to plot
plt.plot(x, p(x), color='k', linewidth=0.5)
```

Out[48]:
```
[<matplotlib.lines.Line2D at 0x2da97083b80>]
```



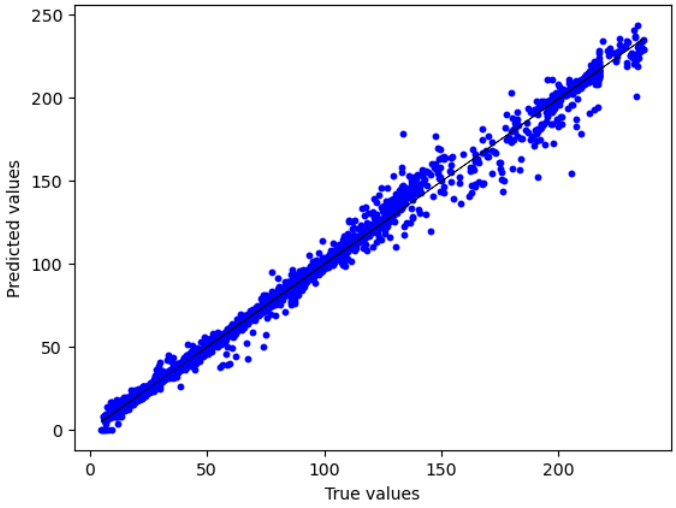
In [49]:
```
x = y_train.flatten()
y = y_train_pred.flatten()

#create scatterplot
plt.scatter(x, y, s=10, color='b')
plt.xlabel('True values')
plt.ylabel('Predicted values')
```

```
#calculate equation for trendline
z = np.polyfit(x, y, 1)
p = np.poly1d(z)

#add trendline to plot
plt.plot(x, p(x), color='k', linewidth=0.5)
```

Out[49]:
```
[<matplotlib.lines.Line2D at 0x2da96f61250>]
```



In [50]:
```
model.save('C://Users//Leticia Carvalho//Documents//humiditytheone.keras')
```

APPENDIX 6 (a)

In [9]:
```
import pandas as pd
import numpy as np

# Carregar a planilha
file_path = "imagemtermica.xlsx"  # Substitua pelo caminho correto
image = pd.read_excel(file_path, header=None)

# Exibir a matriz para o usuário selecionar a temperatura da região seca
print("Matriz de Temperatura da Imagem:")
print(image)

# Solicitar a entrada do usuário para a temperatura da região seca
while True:
    try:
        dry_region_temp = float(input("Digite a temperatura da região seca: "))
        break
    except ValueError:
        print("Entrada inválida. Digite um número válido.")

# Criar a nova imagem com a diferença entre a temperatura seca e os valores individuais das células
new_image = dry_region_temp - image

# Ajustar valores negativos para zero
new_image[new_image < 0] = 0

# Salvar o novo arquivo como Excel
output_path = "nova_imagem.xlsx"
new_image_df = pd.DataFrame(new_image)
new_image_df.to_excel(output_path, header=False, index=False)

print(f"Arquivo salvo em: {output_path}")
```

```
Matriz de Temperatura da Imagem:
        0       1       2       3       4       5       6       7       8   \
0    29.470  29.470  29.460  29.465  29.485  29.515  29.530  29.525  29.480
1    29.510  29.535  29.470  29.414  29.444  29.505  29.505  29.500  29.510
2    29.600  29.590  29.490  29.424  29.490  29.570  29.510  29.449  29.490
3    29.671  29.621  29.510  29.449  29.530  29.611  29.520  29.429  29.480
4    29.641  29.600  29.480  29.399  29.439  29.520  29.475  29.444  29.520
..      ...     ...     ...     ...     ...     ...     ...     ...     ...
162  26.533  26.497  26.394  26.301  26.280  26.321  26.342  26.363  26.327
163  26.456  26.440  26.352  26.275  26.285  26.327  26.280  26.270  26.337
164  26.316  26.358  26.363  26.342  26.316  26.285  26.218  26.213  26.301
165  26.177  26.259  26.363  26.399  26.332  26.233  26.187  26.213  26.275
166  26.068  26.171  26.280  26.316  26.270  26.197  26.187  26.223  26.265

         9   ...      18      19      20      21      22      23      24  \
0    29.475  ...  29.550  29.545  29.606  29.671  29.676  29.646  29.616
1    29.550  ...  29.575  29.600  29.641  29.671  29.671  29.631  29.560
2    29.580  ...  29.590  29.611  29.631  29.641  29.651  29.621  29.520
3    29.585  ...  29.600  29.606  29.595  29.606  29.646  29.646  29.555
4    29.600  ...  29.600  29.616  29.585  29.580  29.646  29.691  29.651
..      ...  ...     ...     ...     ...     ...     ...     ...     ...
162  26.347  ...  26.528  26.543  26.409  26.311  26.358  26.476  26.502
163  26.440  ...  26.409  26.471  26.389  26.311  26.347  26.430  26.461
164  26.404  ...  26.363  26.368  26.389  26.394  26.316  26.270  26.332
165  26.316  ...  26.347  26.270  26.389  26.482  26.321  26.156  26.218
166  26.254  ...  26.285  26.197  26.342  26.476  26.352  26.177  26.166

         25      26      27
0    29.595  29.595  29.611
1    29.540  29.600  29.666
2    29.475  29.555  29.656
3    29.480  29.505  29.575
4    29.560  29.475  29.449
..      ...     ...     ...
162  26.497  26.543  26.533
163  26.456  26.440  26.399
164  26.409  26.383  26.327
165  26.347  26.332  26.290
166  26.233  26.213  26.213

[167 rows x 28 columns]
Digite a temperatura da região seca: 29.5
Arquivo salvo em: nova_imagem.xlsx
```

In [ ]:

APPENDIX 6 (b)

In [12]:
```
import pandas as pd
import numpy as np
import matplotlib.pyplot as plt
from tensorflow.keras.models import load_model
from sklearn.preprocessing import MinMaxScaler


# Passo 1: Importar a imagem em formato Excel (.xlsx)
file_path = 'nova_imagem2.xlsx'
image = pd.read_excel(file_path, header=None)

# Extrair valores de ΔT [°C] da imagem
delta_T_values = image.values.flatten()  # Converter para uma array 1D
```

In [13]:
```
# Importar o arquivo de treinamento para ajustar o MinMaxScaler
train_data_path = 'dataset.artigoCBM,WUFIelab.tipo.slope.xlsx'  # Substitua pelo caminho do arquivo de treinamento
train_data = pd.read_excel(train_data_path)

# Separar as colunas de características (features) que foram usadas para treinar o modelo
features = ['Material', 'Type', 'Slope', 'Temperature [°C]', 'Relative Humidity [%]', 'ΔT [°C]']

# Passo 3: Ajustar o MinMaxScaler aos dados de treinamento
scaler = MinMaxScaler()
train_data_scaled = scaler.fit_transform(train_data[features])
```

In [14]:
```
# Passo 2: Definir outros inputs do modelo
material = 5.0  # Exemplo de material
type_value = 2.0   # Exemplo de tipo
slope = 2.0           # Exemplo de inclinação
temperature_C = 15.0   # Exemplo de temperatura em Celsius
relative_humidity_percent = 60.0  # Exemplo de umidade relativa em %

# Passo 3: Criar um DataFrame com todos os inputs
data = {
    'Material': [material] * len(delta_T_values),
    'Type': [type_value] * len(delta_T_values),
    'Slope': [slope] * len(delta_T_values),
    'Temperature [°C]': [temperature_C] * len(delta_T_values),
    'Relative Humidity [%]': [relative_humidity_percent] * len(delta_T_values),
    'ΔT [°C]': delta_T_values
}

input_df = pd.DataFrame(data)
input_df
```

Out[14]:

	Material	Type	Slope	Temperature [°C]	Relative Humidity [%]	ΔT [°C]
0	5.0	2.0	2.0	15.0	60.0	0.0240
1	5.0	2.0	2.0	15.0	60.0	0.0240
2	5.0	2.0	2.0	15.0	60.0	0.0320
3	5.0	2.0	2.0	15.0	60.0	0.0280
4	5.0	2.0	2.0	15.0	60.0	0.0120
...	...	...	...	...	...	...
4671	5.0	2.0	2.0	15.0	60.0	2.6584
4672	5.0	2.0	2.0	15.0	60.0	2.6672
4673	5.0	2.0	2.0	15.0	60.0	2.6136
4674	5.0	2.0	2.0	15.0	60.0	2.6296
4675	5.0	2.0	2.0	15.0	60.0	2.6296

4676 rows × 6 columns

In [15]:
```
# Passo 7: Aplicar o scaler aos novos dados de entrada
input_scaled = scaler.transform(input_df)
```

In [16]:
```
# Passo 4: Carregar o modelo de rede neural
model_path = 'C://Users//Leticia Carvalho//Documents//humiditytheone.keras'
model = load_model(model_path)
```

In [17]:
```
# Passo 5: Converter os valores de temperatura para umidade
humidity_predictions = model.predict(input_scaled)


humi = pd.DataFrame(humidity_predictions)
humi[0]
```

Out[17]:
```
147/147 [==============================] - 0s 1ms/step
0        19.735870
1        19.735870
2        21.508909
3        20.622389
4        17.087872
           ...
4671    238.255020
4672    238.698563
4673    235.997025
4674    236.803421
4675    236.803421
Name: 0, Length: 4676, dtype: float32
```

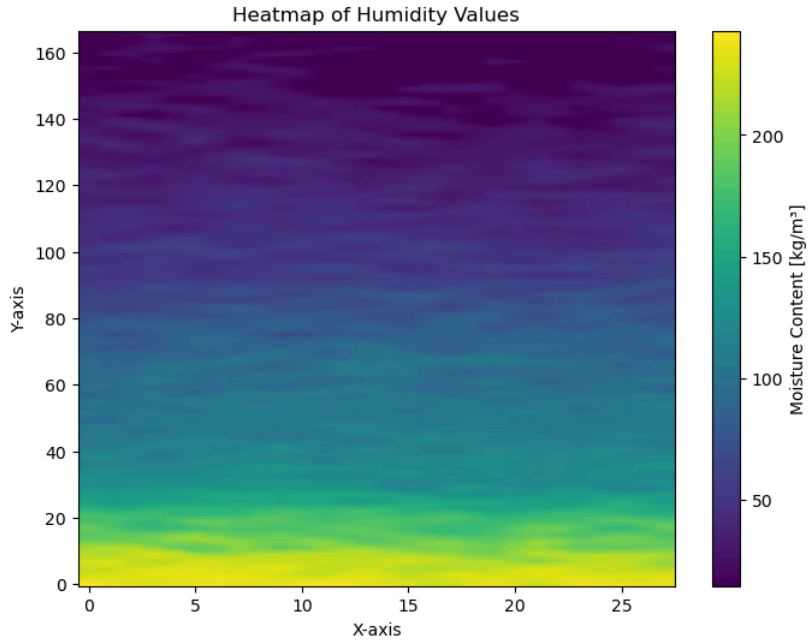
In [18]:
```
# Transformar a umidade prevista em uma matriz da mesma forma que a imagem original
humidity_image = humidity_predictions.reshape(image.shape)

# Garantir que os maiores valores fiquem na base da imagem
humidity_image = np.flipud(humidity_image)
```

Loading [MathJax]/jax/output/CommonHTML/fonts/TeX/fontdata.js

```
# Passo 10: Criar o mapa de calor com base nos valores reais de umidade
```

```
plt.figure(figsize=(8, 6))
plt.imshow(humidity_image, cmap='viridis', aspect='auto', origin='lower')  # Definir origin='lower' para inverter o eixo Y
plt.colorbar(label='Moisture Content [kg/m³]')  # Adicionar barra de cores
plt.title('Heatmap of Humidity Values')
plt.xlabel('X-axis')
plt.ylabel('Y-axis')
plt.show()
```



In [44]:

In [ ]:

In [ ]:

In [ ]:

Loading [MathJax]/jax/output/CommonHTML/fonts/TeX/fontdata.js

APPENDIX 7

In [11]:
```
#Ler os inputs wcap, wfree, td, t

import numpy as np
import pandas as pd
import seaborn as sns
from matplotlib import pyplot as plt
from sklearn.metrics import r2_score


df = pd.read_excel('inputs-taxaevaporacao-2560WUFI.xlsx')
df
```

Out[11]:

	wcap	wcrit	wequil	td	d	A	V	stage	tf
0	202	96.7	14.04	32	0.02	0.04	0.0008	1	147

In [12]:
```
wcap = df['wcap']
wcrit = df['wcrit']
wequil = df['wequil']
wequil = wequil[0]
td = df['td']
d = df['d']
stage = df['stage']
stage = stage[0]
tf = df['tf']
tf = tf[0]
evap = (wcap - wcrit) * d / td
evap = evap[0]
#evap2 = evap - evap * ((ΔT1-ΔT2)/ΔT1)
#evap2 = evap2[0]
wcap = wcap[0]
wcrit = wcrit[0]
td = td[0]

print (wcap, wcrit, td)
```

```
202 96.7 32
```

In [13]:
```
x1, y1 = 0.00001, wcap
x2, y2 = td, wcrit

# Calculando a inclinação (m) e o intercepto (c)
m = (y2 - y1) / (x2 - x1)
c = y1 - m * x1

print(f"A equação da reta é: y = {m:.2f}x + {c:.2f}")

# Definindo os coeficientes da função exponencial
z1, w1 = td, wcrit
z2, w2 = tf, wequil

# Encontrando b a partir dos pontos

b = np.log(w2/w1) / (z2-z1)

# Encontrando a usando o valor de b e um dos pontos
a = w1 / np.exp(b * z1)

print(f"Coeficientes calculados: a = {a:.6f}, b = {b:.6f}")


'''# Definindo o intervalo de x para ambos os gráficos
x_values = np.linspace(0, 150, 100)'''

# Definindo o intervalo de x para a reta (somente até o ponto de encontro)
x_values_line = np.linspace(-2, 32, 150)

# Definindo o intervalo de x para a exponencial (somente a partir do ponto de encontro)
x_values_exp = np.linspace(32, 400, 500)



# Calculando os valores da função exponencial
y_exp = a * np.exp(b * x_values_exp)

# Calculando os valores da reta
y_line = m * x_values_line + c

# Criando o gráfico
plt.figure(figsize=(10, 6))

'''# Plotando a função exponencial
plt.plot(x_values, y_exp, label=fr'Exponencial: $y = {a:.4f} \cdot e^{{{b:.4f}x}}$', color='blue')

# Plotando a reta
plt.plot(x_values, y_line, label=f'Reta: y = {m:.2f}x + {c:.2f}', color='green')
'''

# Plotando a reta (até x = 8)
plt.plot(x_values_line, y_line, label=f'First drying phase: y = {m:.2f}x + {c:.2f}', color='green')


# Plotando a função exponencial (a partir de x = 8)
plt.plot(x_values_exp, y_exp, label=fr'Second drying phase: $y = {a:.4f} \cdot e^{{{b:.4f}x}}$', color='blue')



# Destacando o ponto em comum (8, 179)
plt.scatter([td], [wcrit], color='red', zorder=5, label='Common point (td, wcrit)', s=200)

# Pontos adicionais fornecidos
pontos_x = np.array([0.00,3.00,6.00,20.00,25.00,29.00,32.00,34.00,35.00,36.00,37.00,38.00,39.00,40.00,41.00,42.00,43.00,44.00,45.00,46.00,47.00,48.00,
pontos_y = np.array([202.00,190.89,180.74,134.20,118.22,105.79,96.70,90.89,88.09,85.38,82.77,80.35,78.07,75.92,73.87,71.93,70.07,68.30,66.62,65.02,63
```

```
# Plotando os pontos adicionais
plt.scatter(pontos_x, pontos_y, color='red', zorder=5, label='Simulation', s=50)

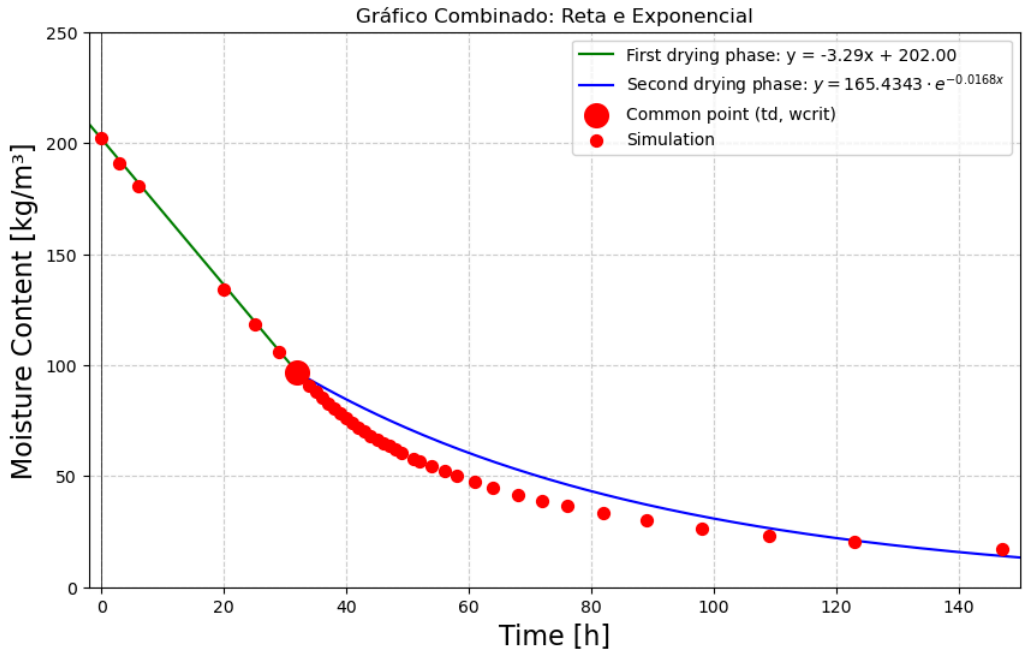


# Ajustando os limites dos eixos
plt.xlim(-2, 150)  # Intervalo para o eixo x de -2 a 150
plt.ylim(0, 250)   # Intervalo para o eixo y de 250 a 0 (invertido)


# Adicionando rótulos e título
plt.xlabel('Time [h]', fontsize = 16)
plt.ylabel('Moisture Content [kg/m³]',fontsize = 16)
plt.title('Gráfico Combinado: Reta e Exponencial')
plt.axhline(0, color='black', linewidth=0.5)
plt.axvline(0, color='black', linewidth=0.5)
plt.grid(True, linestyle='--', alpha=0.6)
plt.legend()

# Exibindo o gráfico
plt.show()
```

```
A equação da reta é: y = -3.29x + 202.00
Coeficientes calculados: a = 165.434317, b = -0.016780
```



In [15]:
```
# Separando os pontos conforme as fases
pontos_x_line = pontos_x[pontos_x <= td]  # Pontos na fase linear
pontos_y_line = pontos_y[pontos_x <= td]

pontos_x_exp = pontos_x[pontos_x > td]  # Pontos na fase exponencial
pontos_y_exp = pontos_y[pontos_x > td]

# Calculando os valores previstos pelo algoritmo
y_pred_line = m * pontos_x_line + c  # Fase linear
y_pred_exp = a * np.exp(b * pontos_x_exp)  # Fase exponencial

# Concatenando previsões e reais para cálculo geral de R²
pontos_x_all = np.concatenate([pontos_x_line, pontos_x_exp])
pontos_y_all = np.concatenate([pontos_y_line, pontos_y_exp])
y_pred_all = np.concatenate([y_pred_line, y_pred_exp])

# Cálculo do coeficiente de determinação R²
r2_total = r2_score(pontos_y_all, y_pred_all)

# Exibir os valores de R²

print(f"R² geral: {r2_total:.4f}")
```

```
R² geral: 0.9591
```

In [ ]:

In [ ]:

In [ ]:

In [ ]:

In [ ]:

In [ ]:

In [ ]:

In [26]:
```
#Ler os inputs wcap, wfree, td, t

import numpy as np
import pandas as pd
import seaborn as sns
from matplotlib import pyplot as plt
from sklearn.metrics import r2_score


df = pd.read_excel('inputs-taxaevaporacao-2560.xlsx')
df
```

Out[26]:

	wcap	wcrit	wequil	td	d	A	V	stage	tf
0	219	179	38.8	8	0.02	0.04	0.0008	1	144

In [27]:
```
wcap = df['wcap']
wcrit = df['wcrit']
wequil = df['wequil']
wequil = wequil[0]
td = df['td']
d = df['d']
stage = df['stage']
stage = stage[0]
tf = df['tf']
tf = tf[0]
evap = (wcap - wcrit) * d / td
evap = evap[0]
#evap2 = evap - evap * ((ΔT1-ΔT2)/ΔT1)
#evap2 = evap2[0]
wcap = wcap[0]
wcrit = wcrit[0]
td = td[0]

print (wcap, wcrit, td)
```

```
219 179 8
```

In [28]:
```
x1, y1 = 0.00001, wcap
x2, y2 = td, wcrit

# Calculando a inclinação (m) e o intercepto (c)
m = (y2 - y1) / (x2 - x1)
c = y1 - m * x1

print(f"A equação da reta é: y = {m:.2f}x + {c:.2f}")

# Definindo os coeficientes da função exponencial
z1, w1 = td, wcrit
z2, w2 = tf, wequil

# Encontrando b a partir dos pontos

b = np.log(w2/w1) / (z2-z1)

# Encontrando a usando o valor de b e um dos pontos
a = w1 / np.exp(b * z1)

print(f"Coeficientes calculados: a = {a:.6f}, b = {b:.6f}")


'''# Definindo o intervalo de x para ambos os gráficos
x_values = np.linspace(0, 150, 100)'''

# Definindo o intervalo de x para a reta (somente até o ponto de encontro)
x_values_line = np.linspace(-2, 8, 500)

# Definindo o intervalo de x para a exponencial (somente a partir do ponto de encontro)
x_values_exp = np.linspace(8, 150, 500)



# Calculando os valores da função exponencial
y_exp = a * np.exp(b * x_values_exp)

# Calculando os valores da reta
y_line = m * x_values_line + c

# Criando o gráfico
plt.figure(figsize=(10, 6))

'''# Plotando a função exponencial
plt.plot(x_values, y_exp, label=fr'Exponencial: $y = {a:.4f} \cdot e^{{{b:.4f}x}}$', color='blue')

# Plotando a reta
plt.plot(x_values, y_line, label=f'Reta: y = {m:.2f}x + {c:.2f}', color='green')
'''

# Plotando a reta (até x = 8)
plt.plot(x_values_line, y_line, label=f'First drying phase: y = {m:.2f}x + {c:.2f}', color='green')


# Plotando a função exponencial (a partir de x = 8)
plt.plot(x_values_exp, y_exp, label=fr'Second drying phase: $y = {a:.4f} \cdot e^{{{b:.4f}x}}$', color='blue')



# Destacando o ponto em comum (8, 179)
plt.scatter([td], [wcrit], color='red', zorder=5, label='Commom point (td, wcrit)', s=200)

# Pontos adicionais fornecidos
pontos_x = np.array([0, 0.5, 1, 2, 4, 7.5, 24, 28, 31, 48, 56, 72, 79, 144])
pontos_y = np.array([219, 214.63, 211.47, 206.39, 196.41, 179.61, 113.41, 104.77, 99.27, 77.72, 70.73, 60.1, 56.2, 38.81])
# Plotando os pontos adicionais
```

Loading [MathJax]/jax/output/CommonHTML/fonts/TeX/fontdata.js

```
plt.scatter(pontos_x, pontos_y, color='red', zorder=5, label='Laboratory tests', s=50)

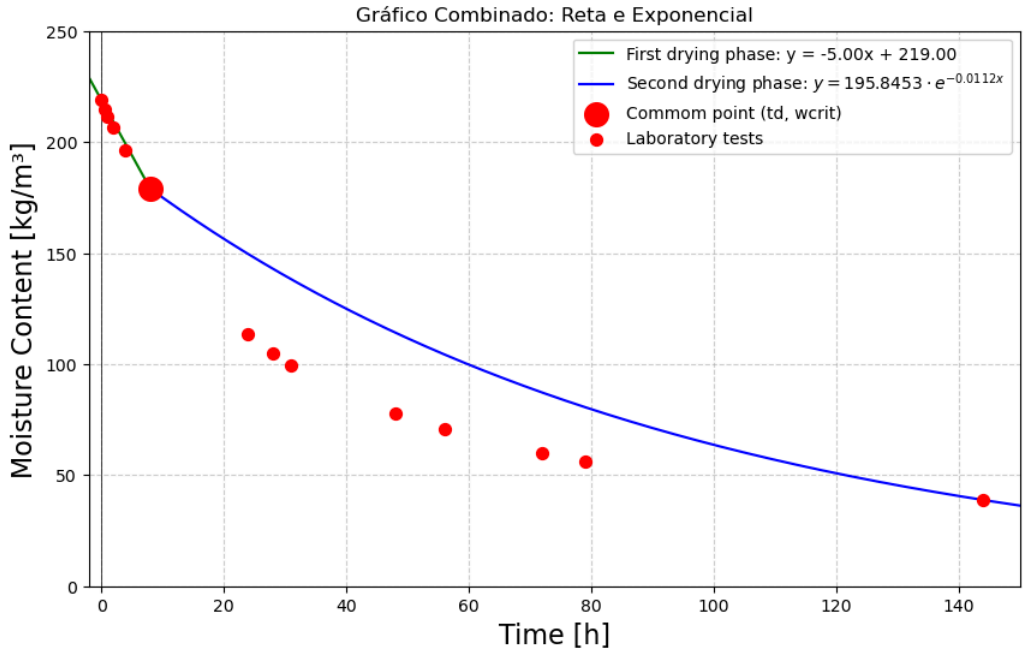


# Ajustando os limites dos eixos
plt.xlim(-2, 150)  # Intervalo para o eixo x de -2 a 150
plt.ylim(0, 250)   # Intervalo para o eixo y de 250 a 0 (invertido)


# Adicionando rótulos e título
plt.xlabel('Time [h]', fontsize = 16)
plt.ylabel('Moisture Content [kg/m³]',fontsize = 16)
plt.title('Gráfico Combinado: Reta e Exponencial')
plt.axhline(0, color='black', linewidth=0.5)
plt.axvline(0, color='black', linewidth=0.5)
plt.grid(True, linestyle='--', alpha=0.6)
plt.legend()

# Exibindo o gráfico
plt.show()
```

```
A equação da reta é: y = -5.00x + 219.00
Coeficientes calculados: a = 195.845279, b = -0.011242
```



In [30]:
```
# Separando os pontos conforme as fases
pontos_x_line = pontos_x[pontos_x <= td]  # Pontos na fase linear
pontos_y_line = pontos_y[pontos_x <= td]

pontos_x_exp = pontos_x[pontos_x > td]  # Pontos na fase exponencial
pontos_y_exp = pontos_y[pontos_x > td]

# Calculando os valores previstos pelo algoritmo
y_pred_line = m * pontos_x_line + c  # Fase linear
y_pred_exp = a * np.exp(b * pontos_x_exp)  # Fase exponencial

# Concatenando previsões e reais para cálculo geral de R²
pontos_x_all = np.concatenate([pontos_x_line, pontos_x_exp])
pontos_y_all = np.concatenate([pontos_y_line, pontos_y_exp])
y_pred_all = np.concatenate([y_pred_line, y_pred_exp])

# Cálculo do coeficiente de determinação R²

r2_total = r2_score(pontos_y_all, y_pred_all)

# Exibir os valores de R²

print(f"R² geral: {r2_total:.4f}")
```

```
R² geral: 0.8676
```

In [ ]:
In [ ]:
In [ ]:
In [ ]:
In [ ]:
In [ ]:
In [ ]:
In [ ]:
In [ ]:

Loading [MathJax]/jax/output/CommonHTML/fonts/TeX/fontdata.js

In [7]:
```
#Ler os inputs wcap, wfree, td, t

import numpy as np
import pandas as pd
import seaborn as sns
from matplotlib import pyplot as plt
from sklearn.metrics import r2_score


df = pd.read_excel('inputs-taxaevaporacao-2070.xlsx')
df
```

Out[7]:

	wcap	wcrit	wequil	td	d	A	V	stage	tf
0	199	123	34.69	30	0.02	0.04	0.0008	1	336

In [8]:
```
wcap = df['wcap']
wcrit = df['wcrit']
wequil = df['wequil']
wequil = wequil[0]
td = df['td']
d = df['d']
stage = df['stage']
stage = stage[0]
tf = df['tf']
tf = tf[0]
evap = (wcap - wcrit) * d / td
evap = evap[0]
#evap2 = evap - evap * ((ΔT1-ΔT2)/ΔT1)
#evap2 = evap2[0]
wcap = wcap[0]
wcrit = wcrit[0]
td = td[0]

print (wcap, wcrit, td)
```

```
199 123 30
```

In [9]:
```
x1, y1 = 0.00001, wcap
x2, y2 = td, wcrit

# Calculando a inclinação (m) e o intercepto (c)
m = (y2 - y1) / (x2 - x1)
c = y1 - m * x1

print(f"A equação da reta é: y = {m:.2f}x + {c:.2f}")

# Definindo os coeficientes da função exponencial
z1, w1 = td, wcrit
z2, w2 = tf, wequil

# Encontrando b a partir dos pontos

b = np.log(w2/w1) / (z2-z1)

# Encontrando a usando o valor de b e um dos pontos
a = w1 / np.exp(b * z1)

print(f"Coeficientes calculados: a = {a:.6f}, b = {b:.6f}")


'''# Definindo o intervalo de x para ambos os gráficos
x_values = np.linspace(0, 150, 100)'''

# Definindo o intervalo de x para a reta (somente até o ponto de encontro)
x_values_line = np.linspace(-2, 30, 500)

# Definindo o intervalo de x para a exponencial (somente a partir do ponto de encontro)
x_values_exp = np.linspace(30, 400, 500)



# Calculando os valores da função exponencial
y_exp = a * np.exp(b * x_values_exp)

# Calculando os valores da reta
y_line = m * x_values_line + c

# Criando o gráfico
plt.figure(figsize=(10, 6))

'''# Plotando a função exponencial
plt.plot(x_values, y_exp, label=fr'Exponencial: $y = {a:.4f} \cdot e^{{{b:.4f}x}}$', color='blue')

# Plotando a reta
plt.plot(x_values, y_line, label=f'Reta: y = {m:.2f}x + {c:.2f}', color='green')
'''

# Plotando a reta (até x = 8)
plt.plot(x_values_line, y_line, label=f'First drying phase: y = {m:.2f}x + {c:.2f}', color='green')


# Plotando a função exponencial (a partir de x = 8)
plt.plot(x_values_exp, y_exp, label=fr'Second drying phase: $y = {a:.4f} \cdot e^{{{b:.4f}x}}$', color='blue')



# Destacando o ponto em comum (8, 179)
plt.scatter([td], [wcrit], color='red', zorder=5, label='Commom point (td, wcrit)', s=100)

# Pontos adicionais fornecidos
pontos_x = np.array([0,0.5,1,2,4,7.5,24,30,96,102,120,146,196,268,311,336])
pontos_y = np.array([199.88,197.18,195.33,192.63,186.98,177.98,137.15,123.13,56.26,54.10,48.80,43.48,38.16,35.70,35.16,34.69])

# Plotando os pontos adicionais
```

```
plt.scatter(pontos_x, pontos_y, color='red', zorder=5, label='Laboratory tests', s=50)

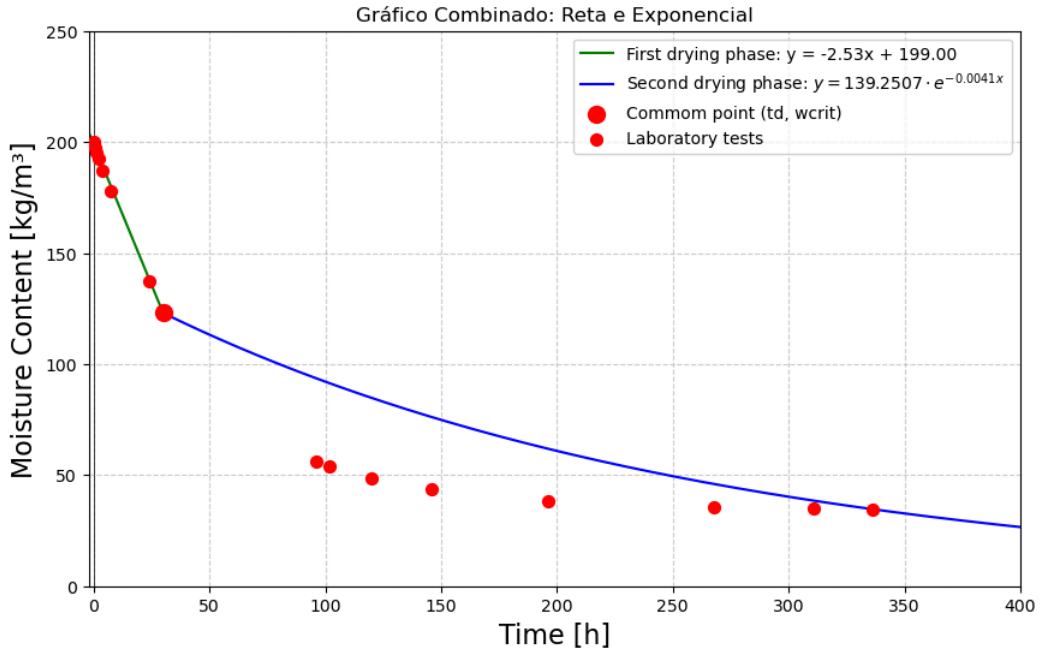


# Ajustando os limites dos eixos
plt.xlim(-2, 400)  # Intervalo para o eixo x de -2 a 150
plt.ylim(0, 250)   # Intervalo para o eixo y de 250 a 0 (invertido)


# Adicionando rótulos e título
plt.xlabel('Time [h]',fontsize = 16)
plt.ylabel('Moisture Content [kg/m³]', fontsize = 16)
plt.title('Gráfico Combinado: Reta e Exponencial')
plt.axhline(0, color='black', linewidth=0.5)
plt.axvline(0, color='black', linewidth=0.5)
plt.grid(True, linestyle='--', alpha=0.6)
plt.legend()

# Exibindo o gráfico
plt.show()
```

```
A equação da reta é: y = -2.53x + 199.00
Coeficientes calculados: a = 139.250687, b = -0.004136
```



In [11]:
```
# Separando os pontos conforme as fases
pontos_x_line = pontos_x[pontos_x <= td]  # Pontos na fase linear
pontos_y_line = pontos_y[pontos_x <= td]

pontos_x_exp = pontos_x[pontos_x > td]  # Pontos na fase exponencial
pontos_y_exp = pontos_y[pontos_x > td]

# Calculando os valores previstos pelo algoritmo
y_pred_line = m * pontos_x_line + c  # Fase linear
y_pred_exp = a * np.exp(b * pontos_x_exp)  # Fase exponencial

# Concatenando previsões e reais para cálculo geral de R²
pontos_x_all = np.concatenate([pontos_x_line, pontos_x_exp])
pontos_y_all = np.concatenate([pontos_y_line, pontos_y_exp])
y_pred_all = np.concatenate([y_pred_line, y_pred_exp])

# Cálculo do coeficiente de determinação R²

r2_total = r2_score(pontos_y_all, y_pred_all)

# Exibir os valores de R²

print(f"R² geral: {r2_total:.4f}")
```

```
R² geral: 0.9246
```

In [ ]:

In [ ]:

In [ ]:

In [ ]:

In [ ]:

In [ ]:

In [ ]:

In [ ]:

In [5]:
```
#Ler os inputs wcap, wfree, td, t

import numpy as np
import pandas as pd
import seaborn as sns
from matplotlib import pyplot as plt
from sklearn.metrics import r2_score


df = pd.read_excel('inputs-taxaevaporacao-1580.xlsx')
df
```

Out[5]:

	wcap	wcrit	wequil	td	d	A	V	stage	tf
0	209	140	58.74	52	0.02	0.04	0.0008	1	310

In [6]:
```
wcap = df['wcap']
wcrit = df['wcrit']
wequil = df['wequil']
wequil = wequil[0]
td = df['td']
d = df['d']
stage = df['stage']
stage = stage[0]
tf = df['tf']
tf = tf[0]
evap = (wcap - wcrit) * d / td
evap = evap[0]
#evap2 = evap - evap * ((ΔT1-ΔT2)/ΔT1)
#evap2 = evap2[0]
wcap = wcap[0]
wcrit = wcrit[0]
td = td[0]

print (wcap, wcrit, td)
```

```
209 140 52
```

In [7]:
```
x1, y1 = 0.00001, wcap
x2, y2 = td, wcrit

# Calculando a inclinação (m) e o intercepto (c)
m = (y2 - y1) / (x2 - x1)
c = y1 - m * x1

print(f"A equação da reta é: y = {m:.2f}x + {c:.2f}")

# Definindo os coeficientes da função exponencial
z1, w1 = td, wcrit
z2, w2 = tf, wequil

# Encontrando b a partir dos pontos

b = np.log(w2/w1) / (z2-z1)

# Encontrando a usando o valor de b e um dos pontos
a = w1 / np.exp(b * z1)

print(f"Coeficientes calculados: a = {a:.6f}, b = {b:.6f}")


'''# Definindo o intervalo de x para ambos os gráficos
x_values = np.linspace(0, 150, 100)'''

# Definindo o intervalo de x para a reta (somente até o ponto de encontro)
x_values_line = np.linspace(-2, 52, 500)

# Definindo o intervalo de x para a exponencial (somente a partir do ponto de encontro)
x_values_exp = np.linspace(52, 400, 500)



# Calculando os valores da função exponencial
y_exp = a * np.exp(b * x_values_exp)

# Calculando os valores da reta
y_line = m * x_values_line + c

# Criando o gráfico
plt.figure(figsize=(10, 6))

'''# Plotando a função exponencial
plt.plot(x_values, y_exp, label=fr'Exponencial: $y = {a:.4f} \cdot e^{{{b:.4f}x}}$', color='blue')

# Plotando a reta
plt.plot(x_values, y_line, label=f'Reta: y = {m:.2f}x + {c:.2f}', color='green')
'''

# Plotando a reta (até x = 8)
plt.plot(x_values_line, y_line, label=f'First drying phase: y = {m:.2f}x + {c:.2f}', color='green')


# Plotando a função exponencial (a partir de x = 8)
plt.plot(x_values_exp, y_exp, label=fr'Second drying phase: $y = {a:.4f} \cdot e^{{{b:.4f}x}}$', color='blue')



# Destacando o ponto em comum (8, 179)
plt.scatter([td], [wcrit], color='red', zorder=5, label='Commom point (td, wcrit)', s=200)

# Pontos adicionais fornecidos
pontos_x = np.array([0,0.5,1,2,4,20,24,28,46,48,52,70,94,168,216,262,310])
pontos_y = np.array([209.00, 207.59,206.88,204.55,201.81,180.31,174.77,169.95,147.47,144.88,140.12,120.71,99.24,71.29,64.54,61.02,58.74])
# Plotando os pontos adicionais
```

Loading [MathJax]/jax/output/CommonHTML/fonts/TeX/fontdata.js

```
plt.scatter(pontos_x, pontos_y, color='red', zorder=5, label='Laboratory tests', s=50)

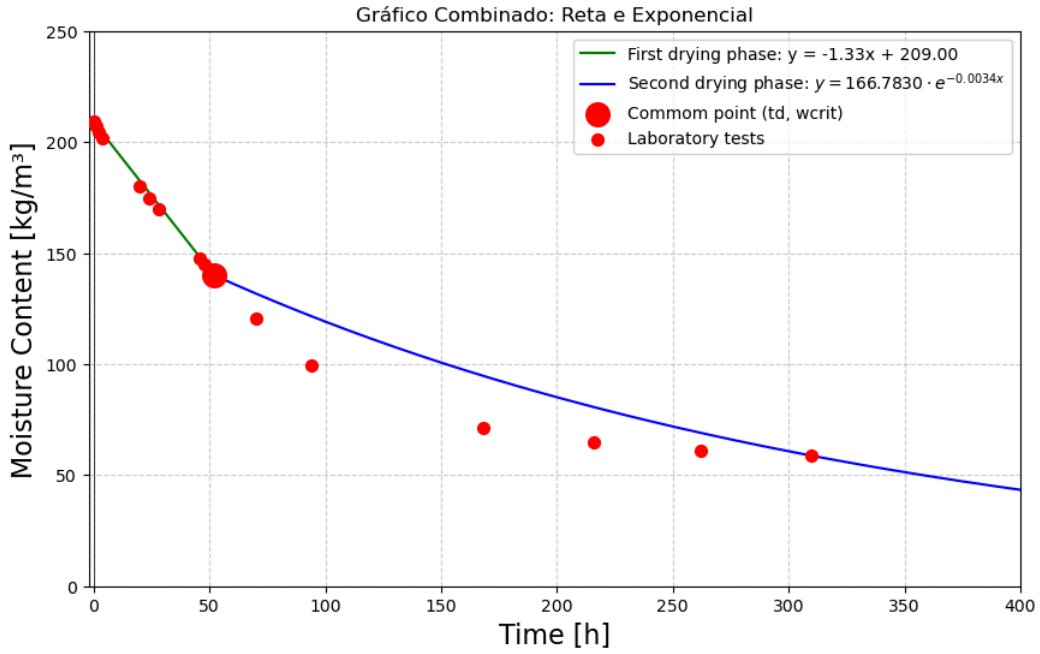


# Ajustando os limites dos eixos
plt.xlim(-2, 400)  # Intervalo para o eixo x de -2 a 150
plt.ylim(0, 250)   # Intervalo para o eixo y de 250 a 0 (invertido)


# Adicionando rótulos e título
plt.xlabel('Time [h]', fontsize = 16)
plt.ylabel('Moisture Content [kg/m³]', fontsize = 16)
plt.title('Gráfico Combinado: Reta e Exponencial')
plt.axhline(0, color='black', linewidth=0.5)
plt.axvline(0, color='black', linewidth=0.5)
plt.grid(True, linestyle='--', alpha=0.6)
plt.legend()

# Exibindo o gráfico
plt.show()
```

```
A equação da reta é: y = -1.33x + 209.00
Coeficientes calculados: a = 166.782950, b = -0.003366
```



In [9]:
```
# Separando os pontos conforme as fases
pontos_x_line = pontos_x[pontos_x <= td]  # Pontos na fase linear
pontos_y_line = pontos_y[pontos_x <= td]

pontos_x_exp = pontos_x[pontos_x > td]  # Pontos na fase exponencial
pontos_y_exp = pontos_y[pontos_x > td]

# Calculando os valores previstos pelo algoritmo
y_pred_line = m * pontos_x_line + c  # Fase linear
y_pred_exp = a * np.exp(b * pontos_x_exp)  # Fase exponencial

# Concatenando previsões e reais para cálculo geral de R²
pontos_x_all = np.concatenate([pontos_x_line, pontos_x_exp])
pontos_y_all = np.concatenate([pontos_y_line, pontos_y_exp])
y_pred_all = np.concatenate([y_pred_line, y_pred_exp])

# Cálculo do coeficiente de determinação R²

r2_total = r2_score(pontos_y_all, y_pred_all)

# Exibir os valores de R²

print(f"R² geral: {r2_total:.4f}")
```

```
R² geral: 0.9700
```

In [ ]:
In [ ]:
In [ ]:
In [ ]:
In [ ]:
In [ ]:
In [ ]:
In [ ]:

Loading [MathJax]/jax/output/CommonHTML/fonts/TeX/fontdata.js

APPENDIX 8

Case	Time	T	HR	Moisture content [kg/m³]	ΔT [°C]
A	0.00	20.00	70.00	202.00	0.00
A	3.00	20.00	70.00	195.40	1.75
A	7.00	20.00	70.00	187.27	1.81
A	31.00	20.00	70.00	139.34	1.77
A	38.00	20.00	70.00	125.83	1.72
A	45.00	20.00	70.00	112.71	1.68
A	51.00	20.00	70.00	101.79	1.63
A	57.00	20.00	70.00	91.18	1.59
A	61.00	20.00	70.00	84.31	1.55
A	63.00	20.00	70.00	81.01	1.50
A	65.00	20.00	70.00	77.80	1.46
A	67.00	20.00	70.00	74.71	1.41
A	69.00	20.00	70.00	71.75	1.35
A	70.00	20.00	70.00	70.32	1.32
A	71.00	20.00	70.00	68.93	1.29
A	72.00	20.00	70.00	67.60	1.23
A	73.00	20.00	70.00	66.33	1.18
A	74.00	20.00	70.00	65.12	1.13
A	75.00	20.00	70.00	63.94	1.09
A	76.00	20.00	70.00	62.81	1.05
A	77.00	20.00	70.00	61.72	1.01
A	79.00	20.00	70.00	59.65	0.94
A	80.00	20.00	70.00	58.66	0.91
A	82.00	20.00	70.00	56.77	0.86
A	84.00	20.00	70.00	54.98	0.81
A	86.00	20.00	70.00	53.30	0.77
A	88.00	20.00	70.00	51.70	0.72
A	90.00	20.00	70.00	50.18	0.69
A	93.00	20.00	70.00	48.06	0.63
A	96.00	20.00	70.00	46.10	0.58
A	99.00	20.00	70.00	44.29	0.54
A	102.00	20.00	70.00	42.61	0.50
A	106.00	20.00	70.00	40.56	0.45
A	110.00	20.00	70.00	38.69	0.41
A	115.00	20.00	70.00	36.58	0.37
A	121.00	20.00	70.00	34.34	0.32
A	128.00	20.00	70.00	32.06	0.27
A	137.00	20.00	70.00	29.58	0.23
A	148.00	20.00	70.00	27.10	0.18
A	161.00	20.00	70.00	24.81	0.14
A	178.00	20.00	70.00	22.68	0.09
A	206.00	20.00	70.00	20.59	0.05
A	2928.00	20.00	70.00	18.20	0.00
B	0.00	25.00	60.00	202.00	0.00
B	3.00	25.00	60.00	190.89	2.92
B	6.00	25.00	60.00	180.74	3.00

B	20.00	25.00	60.00	134.20	2.92
B	25.00	25.00	60.00	118.22	2.85
B	29.00	25.00	60.00	105.79	2.78
B	32.00	25.00	60.00	96.70	2.73
B	34.00	25.00	60.00	90.89	2.62
B	35.00	25.00	60.00	88.09	2.56
B	36.00	25.00	60.00	85.38	2.49
B	37.00	25.00	60.00	82.77	2.40
B	38.00	25.00	60.00	80.35	2.26
B	39.00	25.00	60.00	78.07	2.13
B	40.00	25.00	60.00	75.92	2.01
B	41.00	25.00	60.00	73.87	1.90
B	42.00	25.00	60.00	71.93	1.81
B	43.00	25.00	60.00	70.07	1.72
B	44.00	25.00	60.00	68.30	1.64
B	45.00	25.00	60.00	66.62	1.56
B	46.00	25.00	60.00	65.02	1.48
B	47.00	25.00	60.00	63.49	1.41
B	48.00	25.00	60.00	62.02	1.35
B	49.00	25.00	60.00	60.62	1.29
B	51.00	25.00	60.00	57.98	1.19
B	52.00	25.00	60.00	56.73	1.14
B	54.00	25.00	60.00	54.38	1.06
B	56.00	25.00	60.00	52.19	0.98
B	58.00	25.00	60.00	50.15	0.92
B	61.00	25.00	60.00	47.33	0.83
B	64.00	25.00	60.00	44.76	0.75
B	68.00	25.00	60.00	41.67	0.67
B	72.00	25.00	60.00	38.91	0.59
B	76.00	25.00	60.00	36.44	0.53
B	82.00	25.00	60.00	33.18	0.45
B	89.00	25.00	60.00	29.95	0.38
B	98.00	25.00	60.00	26.54	0.30
B	109.00	25.00	60.00	23.26	0.23
B	123.00	25.00	60.00	20.28	0.15
B	147.00	25.00	60.00	17.29	0.07
B	2928.00	25.00	60.00	14.04	0.00
C	0.00	15.00	80.00	202.00	0.00
C	3.00	15.00	80.00	198.59	0.92
C	7.00	15.00	80.00	194.33	0.95
C	44.00	15.00	80.00	155.68	0.93
C	66.00	15.00	80.00	133.31	0.91
C	75.00	15.00	80.00	124.46	0.88
C	85.00	15.00	80.00	114.91	0.86
C	94.00	15.00	80.00	106.57	0.83
C	103.00	15.00	80.00	98.46	0.81
C	113.00	15.00	80.00	89.72	0.79

C	122.00	15.00	80.00	82.11	0.76
C	131.00	15.00	80.00	74.73	0.74
C	135.00	15.00	80.00	71.58	0.71
C	138.00	15.00	80.00	69.29	0.69
C	142.00	15.00	80.00	66.34	0.67
C	146.00	15.00	80.00	63.51	0.64
C	149.00	15.00	80.00	61.46	0.62
C	152.00	15.00	80.00	59.50	0.60
C	155.00	15.00	80.00	57.61	0.57
C	158.00	15.00	80.00	55.79	0.55
C	161.00	15.00	80.00	54.05	0.53
C	165.00	15.00	80.00	51.85	0.50
C	166.00	15.00	80.00	51.33	0.48
C	168.00	15.00	80.00	50.34	0.46
C	171.00	15.00	80.00	48.93	0.42
C	173.00	15.00	80.00	48.04	0.41
C	176.00	15.00	80.00	46.78	0.38
C	179.00	15.00	80.00	45.59	0.36
C	183.00	15.00	80.00	44.11	0.33
C	187.00	15.00	80.00	42.74	0.31
C	191.00	15.00	80.00	41.46	0.29
C	196.00	15.00	80.00	39.99	0.26
C	202.00	15.00	80.00	38.37	0.24
C	208.00	15.00	80.00	36.91	0.21
C	215.00	15.00	80.00	35.38	0.19
C	224.00	15.00	80.00	33.64	0.17
C	234.00	15.00	80.00	31.97	0.14
C	245.00	15.00	80.00	30.40	0.12
C	260.00	15.00	80.00	28.64	0.10
C	278.00	15.00	80.00	27.00	0.07
C	302.00	15.00	80.00	25.45	0.05
C	342.00	15.00	80.00	23.93	0.02
C	2928.00	15.00	80.00	22.36	0.00
1	0.00	7.00	53.73	202.00	0.00
1	4.00	7.00	53.73	195.35	1.42
1	8.00	7.00	53.73	188.94	1.45
1	45.00	7.00	53.73	130.48	1.41
1	59.00	7.00	53.73	109.21	1.37
1	69.00	7.00	53.73	94.46	1.34
1	74.00	7.00	53.73	87.27	1.31
1	78.00	7.00	53.73	81.73	1.26
1	80.00	7.00	53.73	79.05	1.23
1	82.00	7.00	53.73	76.45	1.20
1	83.00	7.00	53.73	75.20	1.17
1	84.00	7.00	53.73	73.99	1.13
1	85.00	7.00	53.73	72.83	1.09
1	86.00	7.00	53.73	71.70	1.06

1	87.00	7.00	53.73	70.61	1.02
1	89.00	7.00	53.73	68.52	0.97
1	90.00	7.00	53.73	67.51	0.94
1	91.00	7.00	53.73	66.54	0.91
1	93.00	7.00	53.73	64.66	0.86
1	94.00	7.00	53.73	63.77	0.84
1	96.00	7.00	53.73	62.06	0.79
1	97.00	7.00	53.73	61.24	0.77
1	99.00	7.00	53.73	59.67	0.72
1	101.00	7.00	53.73	58.18	0.68
1	103.00	7.00	53.73	56.77	0.65
1	105.00	7.00	53.73	55.42	0.62
1	108.00	7.00	53.73	53.52	0.58
1	111.00	7.00	53.73	51.74	0.54
1	114.00	7.00	53.73	50.07	0.51
1	117.00	7.00	53.73	48.49	0.48
1	122.00	7.00	53.73	46.07	0.43
1	126.00	7.00	53.73	44.29	0.40
1	132.00	7.00	53.73	41.84	0.36
1	138.00	7.00	53.73	39.63	0.33
1	145.00	7.00	53.73	37.31	0.29
1	154.00	7.00	53.73	34.67	0.25
1	164.00	7.00	53.73	32.11	0.22
1	177.00	7.00	53.73	29.29	0.18
1	193.00	7.00	53.73	26.41	0.15
1	215.00	7.00	53.73	23.31	0.11
1	246.00	7.00	53.73	20.18	0.07
1	306.00	7.00	53.73	16.62	0.04
1	2928.00	7.00	53.73	12.34	0.00
2	0.00	16.21	79.67	202.00	0.00
2	3.00	16.21	79.67	198.30	0.99
2	7.00	16.21	79.67	193.71	1.03
2	42.00	16.21	79.67	154.28	1.00
2	61.00	16.21	79.67	133.43	0.98
2	70.00	16.21	79.67	123.88	0.95
2	79.00	16.21	79.67	114.61	0.92
2	88.00	16.21	79.67	105.61	0.90
2	96.00	16.21	79.67	97.85	0.87
2	105.00	16.21	79.67	89.36	0.85
2	114.00	16.21	79.67	81.15	0.82
2	121.00	16.21	79.67	74.96	0.80
2	125.00	16.21	79.67	71.57	0.77
2	128.00	16.21	79.67	69.11	0.74
2	131.00	16.21	79.67	66.73	0.72
2	135.00	16.21	79.67	63.67	0.69
2	138.00	16.21	79.67	61.48	0.66
2	140.00	16.21	79.67	60.07	0.65

2	143.00	16.21	79.67	58.02	0.62
2	146.00	16.21	79.67	56.07	0.59
2	149.00	16.21	79.67	54.20	0.57
2	151.00	16.21	79.67	53.00	0.55
2	153.00	16.21	79.67	51.88	0.52
2	155.00	16.21	79.67	50.81	0.49
2	157.00	16.21	79.67	49.79	0.46
2	160.00	16.21	79.67	48.35	0.43
2	162.00	16.21	79.67	47.45	0.41
2	165.00	16.21	79.67	46.16	0.39
2	169.00	16.21	79.67	44.55	0.36
2	173.00	16.21	79.67	43.07	0.33
2	177.00	16.21	79.67	41.70	0.31
2	182.00	16.21	79.67	40.11	0.28
2	187.00	16.21	79.67	38.67	0.26
2	193.00	16.21	79.67	37.09	0.23
2	200.00	16.21	79.67	35.44	0.21
2	208.00	16.21	79.67	33.77	0.18
2	217.00	16.21	79.67	32.13	0.16
2	229.00	16.21	79.67	30.28	0.13
2	243.00	16.21	79.67	28.52	0.10
2	260.00	16.21	79.67	26.85	0.08
2	282.00	16.21	79.67	25.31	0.05
2	321.00	16.21	79.67	23.71	0.03
2	2928.00	16.21	79.67	22.22	0.00
3	0.00	7.86	75.70	202.00	0.00
3	4.00	7.86	75.70	198.34	0.78
3	8.00	7.86	75.70	194.81	0.80
3	64.00	7.86	75.70	146.34	0.78
3	84.00	7.86	75.70	129.49	0.76
3	98.00	7.86	75.70	118.07	0.74
3	112.00	7.86	75.70	106.99	0.72
3	125.00	7.86	75.70	97.00	0.70
3	138.00	7.86	75.70	87.31	0.68
3	151.00	7.86	75.70	77.91	0.66
3	158.00	7.86	75.70	73.00	0.64
3	162.00	7.86	75.70	70.30	0.62
3	167.00	7.86	75.70	67.03	0.60
3	171.00	7.86	75.70	64.49	0.58
3	175.00	7.86	75.70	62.05	0.56
3	179.00	7.86	75.70	59.70	0.54
3	182.00	7.86	75.70	58.01	0.52
3	186.00	7.86	75.70	55.83	0.50
3	188.00	7.86	75.70	54.79	0.48
3	190.00	7.86	75.70	53.79	0.46
3	192.00	7.86	75.70	52.84	0.44
3	194.00	7.86	75.70	51.93	0.42

3	197.00	7.86	75.70	50.63	0.40
3	200.00	7.86	75.70	49.40	0.38
3	203.00	7.86	75.70	48.22	0.36
3	206.00	7.86	75.70	47.11	0.34
3	210.00	7.86	75.70	45.71	0.32
3	214.00	7.86	75.70	44.39	0.30
3	219.00	7.86	75.70	42.84	0.28
3	224.00	7.86	75.70	41.41	0.26
3	230.00	7.86	75.70	39.81	0.24
3	236.00	7.86	75.70	38.35	0.22
3	243.00	7.86	75.70	36.77	0.20
3	251.00	7.86	75.70	35.14	0.18
3	261.00	7.86	75.70	33.32	0.16
3	271.00	7.86	75.70	31.72	0.14
3	282.00	7.86	75.70	30.18	0.12
3	296.00	7.86	75.70	28.53	0.10
3	313.00	7.86	75.70	26.88	0.08
3	334.00	7.86	75.70	25.30	0.06
3	362.00	7.86	75.70	23.80	0.04
3	411.00	7.86	75.70	22.24	0.02
3	2928.00	7.86	75.70	20.57	0.00
4	0.00	9.75	83.06	202.00	0.00
4	4.00	9.75	83.06	199.15	0.61
4	8.00	9.75	83.06	196.42	0.62
4	56.00	9.75	83.06	164.22	0.60
4	99.00	9.75	83.06	136.17	0.58
4	112.00	9.75	83.06	127.96	0.57
4	125.00	9.75	83.06	119.99	0.55
4	138.00	9.75	83.06	112.24	0.54
4	151.00	9.75	83.06	104.72	0.52
4	164.00	9.75	83.06	97.41	0.51
4	178.00	9.75	83.06	89.80	0.49
4	191.00	9.75	83.06	82.95	0.48
4	205.00	9.75	83.06	75.82	0.46
4	218.00	9.75	83.06	69.41	0.45
4	223.00	9.75	83.06	67.04	0.43
4	229.00	9.75	83.06	64.31	0.41
4	234.00	9.75	83.06	62.11	0.40
4	240.00	9.75	83.06	59.56	0.39
4	246.00	9.75	83.06	57.12	0.37
4	251.00	9.75	83.06	55.18	0.35
4	256.00	9.75	83.06	53.32	0.34
4	261.00	9.75	83.06	51.54	0.32
4	266.00	9.75	83.06	49.85	0.31
4	271.00	9.75	83.06	48.23	0.29
4	277.00	9.75	83.06	46.40	0.28
4	282.00	9.75	83.06	44.95	0.26

4	285.00	9.75	83.06	44.13	0.25
4	289.00	9.75	83.06	43.11	0.23
4	293.00	9.75	83.06	42.16	0.22
4	298.00	9.75	83.06	41.05	0.20
4	303.00	9.75	83.06	40.02	0.19
4	309.00	9.75	83.06	38.88	0.17
4	316.00	9.75	83.06	37.66	0.15
4	324.00	9.75	83.06	36.40	0.14
4	333.00	9.75	83.06	35.13	0.12
4	344.00	9.75	83.06	33.77	0.11
4	356.00	9.75	83.06	32.48	0.09
4	371.00	9.75	83.06	31.11	0.08
4	389.00	9.75	83.06	29.77	0.06
4	412.00	9.75	83.06	28.43	0.05
4	442.00	9.75	83.06	27.19	0.03
4	492.00	9.75	83.06	25.98	0.02
4	2928.00	9.75	83.06	24.73	0.00
5	0.00	16.78	64.61	202.00	0.00
5	3.00	16.78	64.61	195.34	1.78
5	7.00	16.78	64.61	187.07	1.85
5	32.00	16.78	64.61	136.21	1.81
5	40.00	16.78	64.61	120.52	1.76
5	47.00	16.78	64.61	107.18	1.71
5	54.00	16.78	64.61	94.23	1.67
5	58.00	16.78	64.61	87.04	1.62
5	60.00	16.78	64.61	83.56	1.58
5	62.00	16.78	64.61	80.19	1.54
5	64.00	16.78	64.61	76.94	1.48
5	66.00	16.78	64.61	73.83	1.42
5	67.00	16.78	64.61	72.35	1.37
5	68.00	16.78	64.61	70.94	1.32
5	69.00	16.78	64.61	69.59	1.26
5	70.00	16.78	64.61	68.30	1.21
5	71.00	16.78	64.61	67.05	1.16
5	72.00	16.78	64.61	65.84	1.12
5	73.00	16.78	64.61	64.68	1.08
5	75.00	16.78	64.61	62.46	1.01
5	76.00	16.78	64.61	61.40	0.98
5	78.00	16.78	64.61	59.38	0.92
5	80.00	16.78	64.61	57.47	0.87
5	81.00	16.78	64.61	56.56	0.84
5	83.00	16.78	64.61	54.82	0.79
5	85.00	16.78	64.61	53.19	0.74
5	87.00	16.78	64.61	51.65	0.70
5	90.00	16.78	64.61	49.49	0.65
5	93.00	16.78	64.61	47.50	0.60
5	96.00	16.78	64.61	45.65	0.55

5	99.00	16.78	64.61	43.93	0.51
5	103.00	16.78	64.61	41.82	0.47
5	108.00	16.78	64.61	39.44	0.42
5	113.00	16.78	64.61	37.30	0.37
5	120.00	16.78	64.61	34.65	0.32
5	127.00	16.78	64.61	32.34	0.28
5	137.00	16.78	64.61	29.54	0.23
5	148.00	16.78	64.61	27.01	0.19
5	163.00	16.78	64.61	24.29	0.14
5	183.00	16.78	64.61	21.71	0.09
5	217.00	16.78	64.61	19.13	0.05
5	2928.00	16.78	64.61	15.96	0.00
6	0.00	14.98	70.42	202.00	0.00
6	3.00	14.98	70.42	196.94	1.36
6	7.00	14.98	70.42	190.63	1.41
6	41.00	14.98	70.42	137.94	1.38
6	49.00	14.98	70.42	125.96	1.35
6	58.00	14.98	70.42	112.84	1.31
6	66.00	14.98	70.42	101.52	1.28
6	74.00	14.98	70.42	90.52	1.24
6	80.00	14.98	70.42	82.50	1.21
6	83.00	14.98	70.42	78.64	1.17
6	86.00	14.98	70.42	74.91	1.13
6	88.00	14.98	70.42	72.51	1.10
6	90.00	14.98	70.42	70.18	1.07
6	92.00	14.98	70.42	67.94	1.03
6	94.00	14.98	70.42	65.77	0.99
6	95.00	14.98	70.42	64.74	0.96
6	96.00	14.98	70.42	63.75	0.93
6	97.00	14.98	70.42	62.79	0.89
6	99.00	14.98	70.42	60.96	0.84
6	100.00	14.98	70.42	60.09	0.81
6	101.00	14.98	70.42	59.24	0.79
6	103.00	14.98	70.42	57.62	0.74
6	105.00	14.98	70.42	56.07	0.71
6	107.00	14.98	70.42	54.60	0.67
6	109.00	14.98	70.42	53.21	0.64
6	112.00	14.98	70.42	51.23	0.60
6	114.00	14.98	70.42	49.98	0.57
6	117.00	14.98	70.42	48.21	0.53
6	120.00	14.98	70.42	46.55	0.50
6	124.00	14.98	70.42	44.50	0.46
6	127.00	14.98	70.42	43.09	0.43
6	131.00	14.98	70.42	41.33	0.39
6	136.00	14.98	70.42	39.33	0.35
6	141.00	14.98	70.42	37.52	0.32
6	147.00	14.98	70.42	35.57	0.28

6	154.00	14.98	70.42	33.55	0.25
6	163.00	14.98	70.42	31.30	0.21
6	173.00	14.98	70.42	29.19	0.18
6	185.00	14.98	70.42	27.09	0.14
6	201.00	14.98	70.42	24.90	0.11
6	222.00	14.98	70.42	22.85	0.07
6	257.00	14.98	70.42	20.83	0.04
6	2928.00	14.98	70.42	18.37	0.00
7	0.00	22.59	55.79	202.00	0.00
7	3.00	22.59	55.79	190.94	2.93
7	6.00	22.59	55.79	180.77	3.02
7	20.00	22.59	55.79	134.07	2.94
7	26.00	22.59	55.79	114.84	2.86
7	30.00	22.59	55.79	102.39	2.79
7	32.00	22.59	55.79	96.33	2.74
7	34.00	22.59	55.79	90.52	2.63
7	35.00	22.59	55.79	87.74	2.56
7	36.00	22.59	55.79	85.07	2.47
7	37.00	22.59	55.79	82.59	2.32
7	38.00	22.59	55.79	80.26	2.18
7	39.00	22.59	55.79	78.06	2.06
7	40.00	22.59	55.79	75.96	1.95
7	41.00	22.59	55.79	73.97	1.86
7	42.00	22.59	55.79	72.08	1.76
7	43.00	22.59	55.79	70.28	1.67
7	44.00	22.59	55.79	68.58	1.58
7	45.00	22.59	55.79	66.95	1.51
7	46.00	22.59	55.79	65.40	1.44
7	47.00	22.59	55.79	63.91	1.37
7	49.00	22.59	55.79	61.12	1.26
7	50.00	22.59	55.79	59.81	1.21
7	52.00	22.59	55.79	57.33	1.12
7	54.00	22.59	55.79	55.02	1.04
7	56.00	22.59	55.79	52.86	0.97
7	58.00	22.59	55.79	50.85	0.91
7	61.00	22.59	55.79	48.05	0.82
7	64.00	22.59	55.79	45.50	0.75
7	67.00	22.59	55.79	43.16	0.69
7	72.00	22.59	55.79	39.66	0.60
7	77.00	22.59	55.79	36.59	0.52
7	83.00	22.59	55.79	33.38	0.45
7	90.00	22.59	55.79	30.16	0.38
7	100.00	22.59	55.79	26.37	0.30
7	112.00	22.59	55.79	22.82	0.22
7	127.00	22.59	55.79	19.62	0.15
7	154.00	22.59	55.79	16.21	0.08
7	2928.00	22.59	55.79	12.90	0.00

8	0.00	17.50	72.73	202.00	0.00
8	3.00	17.50	72.73	196.70	1.42
8	7.00	17.50	72.73	190.12	1.47
8	38.00	17.50	72.73	140.11	1.43
8	46.00	17.50	72.73	127.63	1.40
8	54.00	17.50	72.73	115.50	1.36
8	62.00	17.50	72.73	103.73	1.32
8	69.00	17.50	72.73	93.73	1.29
8	76.00	17.50	72.73	84.04	1.25
8	79.00	17.50	72.73	80.01	1.22
8	82.00	17.50	72.73	76.13	1.17
8	84.00	17.50	72.73	73.62	1.14
8	86.00	17.50	72.73	71.19	1.11
8	88.00	17.50	72.73	68.84	1.07
8	90.00	17.50	72.73	66.58	1.03
8	92.00	17.50	72.73	64.41	0.99
8	93.00	17.50	72.73	63.38	0.96
8	94.00	17.50	72.73	62.38	0.93
8	95.00	17.50	72.73	61.42	0.89
8	97.00	17.50	72.73	59.59	0.83
8	98.00	17.50	72.73	58.72	0.81
8	100.00	17.50	72.73	57.06	0.76
8	101.00	17.50	72.73	56.26	0.74
8	103.00	17.50	72.73	54.72	0.70
8	105.00	17.50	72.73	53.27	0.66
8	107.00	17.50	72.73	51.89	0.63
8	110.00	17.50	72.73	49.93	0.59
8	113.00	17.50	72.73	48.11	0.55
8	116.00	17.50	72.73	46.41	0.51
8	123.00	17.50	72.73	42.83	0.44
8	127.00	17.50	72.73	41.02	0.40
8	131.00	17.50	72.73	39.36	0.37
8	136.00	17.50	72.73	37.47	0.33
8	142.00	17.50	72.73	35.44	0.29
8	148.00	17.50	72.73	33.64	0.26
8	156.00	17.50	72.73	31.55	0.22
8	166.00	17.50	72.73	29.33	0.18
8	177.00	17.50	72.73	27.33	0.15
8	192.00	17.50	72.73	25.19	0.11
8	211.00	17.50	72.73	23.27	0.07
8	242.00	17.50	72.73	21.41	0.04
8	2928.00	17.50	72.73	19.34	0.00
9	0.00	24.49	60.79	202.00	0.00
9	3.00	24.49	60.79	191.35	2.80
9	6.00	24.49	60.79	181.61	2.88
9	21.00	24.49	60.79	133.79	2.80
9	26.00	24.49	60.79	118.47	2.73

9	30.00	24.49	60.79	106.54	2.67
9	34.00	24.49	60.79	94.94	2.59
9	36.00	24.49	60.79	89.41	2.50
9	37.00	24.49	60.79	86.75	2.44
9	38.00	24.49	60.79	84.18	2.37
9	39.00	24.49	60.79	81.69	2.29
9	40.00	24.49	60.79	79.37	2.16
9	41.00	24.49	60.79	77.19	2.03
9	42.00	24.49	60.79	75.13	1.92
9	43.00	24.49	60.79	73.17	1.82
9	44.00	24.49	60.79	71.30	1.73
9	45.00	24.49	60.79	69.52	1.65
9	46.00	24.49	60.79	67.81	1.58
9	47.00	24.49	60.79	66.19	1.51
9	48.00	24.49	60.79	64.63	1.44
9	49.00	24.49	60.79	63.15	1.37
9	50.00	24.49	60.79	61.73	1.31
9	52.00	24.49	60.79	59.06	1.20
9	53.00	24.49	60.79	57.80	1.16
9	55.00	24.49	60.79	55.43	1.07
9	57.00	24.49	60.79	53.22	0.99
9	59.00	24.49	60.79	51.16	0.92
9	61.00	24.49	60.79	49.24	0.86
9	64.00	24.49	60.79	46.57	0.78
9	67.00	24.49	60.79	44.13	0.71
9	70.00	24.49	60.79	41.90	0.65
9	74.00	24.49	60.79	39.20	0.58
9	79.00	24.49	60.79	36.21	0.51
9	85.00	24.49	60.79	33.10	0.43
9	92.00	24.49	60.79	30.00	0.36
9	101.00	24.49	60.79	26.70	0.29
9	113.00	24.49	60.79	23.29	0.21
9	127.00	24.49	60.79	20.46	0.14
9	151.00	24.49	60.79	17.60	0.07
9	2928.00	24.49	60.79	14.37	0.00
10	0.00	9.33	84.62	202.00	0.00
10	4.00	9.33	84.62	199.48	0.54
10	8.00	9.33	84.62	197.06	0.55
10	57.00	9.33	84.62	167.91	0.53
10	106.00	9.33	84.62	139.60	0.52
10	123.00	9.33	84.62	130.05	0.50
10	136.00	9.33	84.62	122.97	0.49
10	149.00	9.33	84.62	116.09	0.48
10	163.00	9.33	84.62	108.89	0.46
10	177.00	9.33	84.62	101.92	0.45
10	191.00	9.33	84.62	95.15	0.44
10	206.00	9.33	84.62	88.14	0.42

10	221.00	9.33	84.62	81.37	0.41
10	235.00	9.33	84.62	75.25	0.40
10	251.00	9.33	84.62	68.51	0.38
10	258.00	9.33	84.62	65.68	0.37
10	263.00	9.33	84.62	63.73	0.36
10	270.00	9.33	84.62	61.10	0.34
10	276.00	9.33	84.62	58.94	0.33
10	283.00	9.33	84.62	56.52	0.31
10	289.00	9.33	84.62	54.54	0.30
10	295.00	9.33	84.62	52.64	0.29
10	301.00	9.33	84.62	50.84	0.27
10	307.00	9.33	84.62	49.13	0.26
10	313.00	9.33	84.62	47.50	0.25
10	320.00	9.33	84.62	45.71	0.23
10	326.00	9.33	84.62	44.26	0.22
10	333.00	9.33	84.62	42.67	0.21
10	339.00	9.33	84.62	41.39	0.19
10	343.00	9.33	84.62	40.62	0.18
10	348.00	9.33	84.62	39.71	0.16
10	354.00	9.33	84.62	38.70	0.15
10	361.00	9.33	84.62	37.63	0.14
10	369.00	9.33	84.62	36.52	0.12
10	378.00	9.33	84.62	35.40	0.11
10	389.00	9.33	84.62	34.19	0.10
10	402.00	9.33	84.62	32.95	0.08
10	417.00	9.33	84.62	31.74	0.07
10	435.00	9.33	84.62	30.55	0.05
10	459.00	9.33	84.62	29.31	0.04
10	491.00	9.33	84.62	28.14	0.03
10	542.00	9.33	84.62	27.04	0.01
10	2928.00	9.33	84.62	25.93	0.00
11	0.00	15.12	80.95	202.00	0.00
11	3.00	15.12	80.95	198.73	0.88
11	7.00	15.12	80.95	194.65	0.91
11	44.00	15.12	80.95	157.64	0.89
11	68.00	15.12	80.95	134.26	0.87
11	77.00	15.12	80.95	125.79	0.85
11	87.00	15.12	80.95	116.64	0.82
11	96.00	15.12	80.95	108.64	0.80
11	106.00	15.12	80.95	100.01	0.78
11	115.00	15.12	80.95	92.48	0.75
11	125.00	15.12	80.95	84.38	0.73
11	134.00	15.12	80.95	77.32	0.71
11	141.00	15.12	80.95	72.00	0.68
11	144.00	15.12	80.95	69.81	0.66
11	148.00	15.12	80.95	66.99	0.64
11	152.00	15.12	80.95	64.27	0.62

11	156.00	15.12	80.95	61.65	0.59
11	159.00	15.12	80.95	59.77	0.57
11	162.00	15.12	80.95	57.96	0.55
11	166.00	15.12	80.95	55.65	0.52
11	169.00	15.12	80.95	54.00	0.50
11	172.00	15.12	80.95	52.42	0.48
11	176.00	15.12	80.95	50.40	0.45
11	178.00	15.12	80.95	49.46	0.43
11	180.00	15.12	80.95	48.57	0.41
11	182.00	15.12	80.95	47.72	0.39
11	185.00	15.12	80.95	46.51	0.37
11	188.00	15.12	80.95	45.37	0.34
11	192.00	15.12	80.95	43.95	0.32
11	196.00	15.12	80.95	42.63	0.30
11	200.00	15.12	80.95	41.41	0.27
11	205.00	15.12	80.95	39.99	0.25
11	211.00	15.12	80.95	38.45	0.23
11	217.00	15.12	80.95	37.05	0.21
11	224.00	15.12	80.95	35.58	0.18
11	233.00	15.12	80.95	33.91	0.16
11	243.00	15.12	80.95	32.30	0.14
11	255.00	15.12	80.95	30.68	0.11
11	269.00	15.12	80.95	29.11	0.09
11	287.00	15.12	80.95	27.53	0.07
11	311.00	15.12	80.95	26.04	0.05
11	351.00	15.12	80.95	24.58	0.02
11	2928.00	15.12	80.95	23.09	0.00
12	0.00	6.00	87.22	202.00	0.00
12	4.00	6.00	87.22	200.28	0.37
12	8.00	6.00	87.22	198.62	0.38
12	67.00	6.00	87.22	174.55	0.37
12	126.00	6.00	87.22	151.16	0.36
12	171.00	6.00	87.22	133.77	0.35
12	187.00	6.00	87.22	127.79	0.34
12	204.00	6.00	87.22	121.62	0.33
12	221.00	6.00	87.22	115.63	0.32
12	238.00	6.00	87.22	109.81	0.31
12	256.00	6.00	87.22	103.84	0.30
12	275.00	6.00	87.22	97.74	0.29
12	294.00	6.00	87.22	91.84	0.28
12	313.00	6.00	87.22	86.15	0.27
12	333.00	6.00	87.22	80.36	0.26
12	353.00	6.00	87.22	74.78	0.25
12	374.00	6.00	87.22	69.14	0.24
12	394.00	6.00	87.22	63.97	0.23
12	402.00	6.00	87.22	62.00	0.23
12	411.00	6.00	87.22	59.87	0.22

12	420.00	6.00	87.22	57.83	0.21
12	429.00	6.00	87.22	55.88	0.20
12	439.00	6.00	87.22	53.81	0.19
12	450.00	6.00	87.22	51.65	0.18
12	459.00	6.00	87.22	49.97	0.17
12	469.00	6.00	87.22	48.20	0.16
12	479.00	6.00	87.22	46.55	0.15
12	489.00	6.00	87.22	44.99	0.14
12	499.00	6.00	87.22	43.54	0.13
12	510.00	6.00	87.22	42.05	0.12
12	522.00	6.00	87.22	40.54	0.11
12	535.00	6.00	87.22	39.04	0.10
12	549.00	6.00	87.22	37.56	0.09
12	564.00	6.00	87.22	36.13	0.08
12	572.00	6.00	87.22	35.45	0.08
12	584.00	6.00	87.22	34.55	0.07
12	598.00	6.00	87.22	33.64	0.06
12	615.00	6.00	87.22	32.70	0.05
12	637.00	6.00	87.22	31.70	0.04
12	665.00	6.00	87.22	30.72	0.03
12	705.00	6.00	87.22	29.72	0.02
12	766.00	6.00	87.22	28.82	0.01
12	2928.00	6.00	87.22	27.94	0.00
13	0.00	11.56	88.08	202.00	0.00
13	3.00	11.56	88.08	200.31	0.46
13	7.00	11.56	88.08	198.20	0.48
13	50.00	11.56	88.08	175.81	0.46
13	93.00	11.56	88.08	154.06	0.45
13	131.00	11.56	88.08	135.36	0.44
13	143.00	11.56	88.08	129.64	0.43
13	155.00	11.56	88.08	124.08	0.42
13	168.00	11.56	88.08	118.24	0.40
13	181.00	11.56	88.08	112.57	0.39
13	194.00	11.56	88.08	107.08	0.38
13	207.00	11.56	88.08	101.75	0.37
13	221.00	11.56	88.08	96.21	0.36
13	235.00	11.56	88.08	90.85	0.35
13	250.00	11.56	88.08	85.31	0.33
13	265.00	11.56	88.08	79.97	0.32
13	280.00	11.56	88.08	74.84	0.31
13	296.00	11.56	88.08	69.57	0.30
13	312.00	11.56	88.08	64.50	0.29
13	318.00	11.56	88.08	62.69	0.27
13	325.00	11.56	88.08	60.66	0.26
13	332.00	11.56	88.08	58.73	0.25
13	340.00	11.56	88.08	56.62	0.24
13	348.00	11.56	88.08	54.63	0.23

13	356.00	11.56	88.08	52.73	0.21
13	365.00	11.56	88.08	50.70	0.20
13	372.00	11.56	88.08	49.22	0.19
13	380.00	11.56	88.08	47.62	0.18
13	389.00	11.56	88.08	45.95	0.17
13	398.00	11.56	88.08	44.39	0.15
13	407.00	11.56	88.08	42.95	0.14
13	417.00	11.56	88.08	41.47	0.13
13	429.00	11.56	88.08	39.86	0.12
13	441.00	11.56	88.08	38.40	0.11
13	455.00	11.56	88.08	36.88	0.09
13	471.00	11.56	88.08	35.35	0.08
13	482.00	11.56	88.08	34.43	0.07
13	495.00	11.56	88.08	33.52	0.06
13	513.00	11.56	88.08	32.49	0.05
13	536.00	11.56	88.08	31.47	0.04
13	568.00	11.56	88.08	30.46	0.02
13	620.00	11.56	88.08	29.47	0.01
13	2928.00	11.56	88.08	28.61	0.00
14	0.00	21.11	71.44	202.00	0.00
14	3.00	21.11	71.44	195.38	1.75
14	6.00	21.11	71.44	189.28	1.81
14	31.00	21.11	71.44	139.40	1.76
14	38.00	21.11	71.44	125.93	1.72
14	44.00	21.11	71.44	114.70	1.67
14	50.00	21.11	71.44	103.79	1.63
14	56.00	21.11	71.44	93.18	1.58
14	61.00	21.11	71.44	84.61	1.54
14	63.00	21.11	71.44	81.31	1.50
14	65.00	21.11	71.44	78.12	1.45
14	67.00	21.11	71.44	75.02	1.40
14	69.00	21.11	71.44	72.06	1.35
14	70.00	21.11	71.44	70.62	1.32
14	72.00	21.11	71.44	67.86	1.26
14	73.00	21.11	71.44	66.56	1.21
14	74.00	21.11	71.44	65.31	1.16
14	75.00	21.11	71.44	64.11	1.11
14	76.00	21.11	71.44	62.96	1.07
14	77.00	21.11	71.44	61.86	1.03
14	78.00	21.11	71.44	60.79	0.99
14	79.00	21.11	71.44	59.75	0.96
14	81.00	21.11	71.44	57.78	0.90
14	82.00	21.11	71.44	56.84	0.87
14	84.00	21.11	71.44	55.04	0.82
14	86.00	21.11	71.44	53.34	0.77
14	88.00	21.11	71.44	51.74	0.73
14	91.00	21.11	71.44	49.48	0.67

14	93.00	21.11	71.44	48.08	0.64
14	96.00	21.11	71.44	46.09	0.59
14	99.00	21.11	71.44	44.26	0.54
14	102.00	21.11	71.44	42.57	0.50
14	106.00	21.11	71.44	40.49	0.45
14	111.00	21.11	71.44	38.17	0.40
14	116.00	21.11	71.44	36.10	0.36
14	121.00	21.11	71.44	34.25	0.32
14	128.00	21.11	71.44	31.98	0.27
14	137.00	21.11	71.44	29.51	0.23
14	147.00	21.11	71.44	27.26	0.18
14	160.00	21.11	71.44	24.97	0.14
14	176.00	21.11	71.44	22.97	0.09
14	203.00	21.11	71.44	20.96	0.05
14	2928.00	21.11	71.44	18.80	0.00
15	0.00	5.25	63.16	202.00	0.00
15	4.00	5.25	63.16	197.25	1.02
15	8.00	5.25	63.16	192.66	1.04
15	59.00	5.25	63.16	135.02	1.01
15	74.00	5.25	63.16	118.64	0.99
15	89.00	5.25	63.16	102.74	0.96
15	102.00	5.25	63.16	89.37	0.94
15	110.00	5.25	63.16	81.35	0.91
15	115.00	5.25	63.16	76.52	0.88
15	118.00	5.25	63.16	73.71	0.86
15	121.00	5.25	63.16	70.99	0.84
15	124.00	5.25	63.16	68.35	0.81
15	126.00	5.25	63.16	66.65	0.79
15	128.00	5.25	63.16	65.04	0.74
15	129.00	5.25	63.16	64.26	0.72
15	130.00	5.25	63.16	63.51	0.71
15	132.00	5.25	63.16	62.06	0.67
15	133.00	5.25	63.16	61.36	0.66
15	135.00	5.25	63.16	60.00	0.63
15	137.00	5.25	63.16	58.69	0.60
15	140.00	5.25	63.16	56.83	0.57
15	142.00	5.25	63.16	55.65	0.55
15	145.00	5.25	63.16	53.95	0.52
15	147.00	5.25	63.16	52.87	0.50
15	150.00	5.25	63.16	51.34	0.47
15	153.00	5.25	63.16	49.89	0.44
15	156.00	5.25	63.16	48.53	0.42
15	159.00	5.25	63.16	47.24	0.39
15	163.00	5.25	63.16	45.63	0.36
15	167.00	5.25	63.16	44.13	0.34
15	172.00	5.25	63.16	42.38	0.31
15	178.00	5.25	63.16	40.47	0.28

15	184.00	5.25	63.16	38.73	0.26
15	191.00	5.25	63.16	36.88	0.23
15	199.00	5.25	63.16	34.98	0.21
15	209.00	5.25	63.16	32.88	0.18
15	220.00	5.25	63.16	30.86	0.16
15	235.00	5.25	63.16	28.53	0.13
15	252.00	5.25	63.16	26.36	0.10
15	276.00	5.25	63.16	23.96	0.08
15	308.00	5.25	63.16	21.68	0.05
15	369.00	5.25	63.16	19.11	0.03
15	2928.00	5.25	63.16	15.35	0.00
16	0.00	14.25	74.01	202.00	0.00
16	3.00	14.25	74.01	197.73	1.15
16	7.00	14.25	74.01	192.39	1.20
16	46.00	14.25	74.01	141.32	1.17
16	56.00	14.25	74.01	128.63	1.14
16	66.00	14.25	74.01	116.31	1.11
16	75.00	14.25	74.01	105.55	1.08
16	84.00	14.25	74.01	95.10	1.05
16	92.00	14.25	74.01	86.08	1.02
16	102.00	14.25	74.01	75.26	0.96
16	105.00	14.25	74.01	72.20	0.93
16	108.00	14.25	74.01	69.25	0.90
16	110.00	14.25	74.01	67.34	0.87
16	113.00	14.25	74.01	64.59	0.83
16	115.00	14.25	74.01	62.82	0.81
16	117.00	14.25	74.01	61.12	0.78
16	119.00	14.25	74.01	59.50	0.74
16	120.00	14.25	74.01	58.73	0.72
16	121.00	14.25	74.01	57.98	0.70
16	123.00	14.25	74.01	56.55	0.66
16	125.00	14.25	74.01	55.19	0.62
16	127.00	14.25	74.01	53.89	0.59
16	129.00	14.25	74.01	52.66	0.56
16	131.00	14.25	74.01	51.48	0.54
16	134.00	14.25	74.01	49.81	0.50
16	136.00	14.25	74.01	48.75	0.48
16	140.00	14.25	74.01	46.76	0.45
16	143.00	14.25	74.01	45.37	0.42
16	147.00	14.25	74.01	43.63	0.39
16	151.00	14.25	74.01	42.02	0.36
16	156.00	14.25	74.01	40.15	0.33
16	162.00	14.25	74.01	38.12	0.30
16	167.00	14.25	74.01	36.59	0.27
16	174.00	14.25	74.01	34.67	0.24
16	181.00	14.25	74.01	32.97	0.21
16	190.00	14.25	74.01	31.07	0.18

16	201.00	14.25	74.01	29.10	0.15
16	214.00	14.25	74.01	27.19	0.12
16	230.00	14.25	74.01	25.34	0.09
16	252.00	14.25	74.01	23.54	0.06
16	288.00	14.25	74.01	21.80	0.03
16	2928.00	14.25	74.01	19.87	0.00
17	0.00	20.16	50.36	202.00	0.00
17	3.00	20.16	50.36	190.90	2.96
17	7.00	20.16	50.36	177.19	3.06
17	21.00	20.16	50.36	130.04	2.98
17	26.00	20.16	50.36	113.82	2.91
17	30.00	20.16	50.36	101.17	2.85
17	32.00	20.16	50.36	95.09	2.76
17	33.00	20.16	50.36	92.16	2.70
17	34.00	20.16	50.36	89.32	2.62
17	35.00	20.16	50.36	86.65	2.49
17	36.00	20.16	50.36	84.16	2.34
17	37.00	20.16	50.36	81.81	2.21
17	38.00	20.16	50.36	79.58	2.09
17	39.00	20.16	50.36	77.48	1.97
17	40.00	20.16	50.36	75.49	1.86
17	41.00	20.16	50.36	73.60	1.76
17	42.00	20.16	50.36	71.81	1.67
17	43.00	20.16	50.36	70.11	1.59
17	44.00	20.16	50.36	68.49	1.51
17	45.00	20.16	50.36	66.93	1.44
17	46.00	20.16	50.36	65.44	1.38
17	47.00	20.16	50.36	64.01	1.32
17	49.00	20.16	50.36	61.32	1.22
17	51.00	20.16	50.36	58.81	1.13
17	52.00	20.16	50.36	57.63	1.09
17	55.00	20.16	50.36	54.31	0.98
17	57.00	20.16	50.36	52.26	0.92
17	60.00	20.16	50.36	49.43	0.84
17	63.00	20.16	50.36	46.83	0.76
17	67.00	20.16	50.36	43.69	0.68
17	71.00	20.16	50.36	40.87	0.61
17	76.00	20.16	50.36	37.71	0.54
17	83.00	20.16	50.36	33.88	0.46
17	91.00	20.16	50.36	30.19	0.38
17	101.00	20.16	50.36	26.37	0.30
17	114.00	20.16	50.36	22.47	0.23
17	131.00	20.16	50.36	18.79	0.15
17	161.00	20.16	50.36	14.96	0.08
17	2928.00	20.16	50.36	11.43	0.00
18	0.00	13.50	89.03	202.00	0.00
18	3.00	13.50	89.03	200.27	0.46

18	7.00	13.50	89.03	198.12	0.48
18	46.00	13.50	89.03	177.45	0.47
18	84.00	13.50	89.03	157.88	0.46
18	123.00	13.50	89.03	138.36	0.45
18	137.00	13.50	89.03	131.55	0.44
18	148.00	13.50	89.03	126.36	0.42
18	160.00	13.50	89.03	120.86	0.41
18	171.00	13.50	89.03	115.98	0.40
18	183.00	13.50	89.03	110.81	0.39
18	195.00	13.50	89.03	105.80	0.38
18	208.00	13.50	89.03	100.55	0.36
18	221.00	13.50	89.03	95.49	0.35
18	234.00	13.50	89.03	90.59	0.34
18	248.00	13.50	89.03	85.51	0.33
18	262.00	13.50	89.03	80.62	0.31
18	277.00	13.50	89.03	75.59	0.30
18	292.00	13.50	89.03	70.75	0.29
18	308.00	13.50	89.03	65.82	0.28
18	318.00	13.50	89.03	62.85	0.27
18	325.00	13.50	89.03	60.88	0.25
18	332.00	13.50	89.03	59.01	0.24
18	339.00	13.50	89.03	57.23	0.23
18	347.00	13.50	89.03	55.30	0.22
18	355.00	13.50	89.03	53.47	0.21
18	364.00	13.50	89.03	51.52	0.19
18	374.00	13.50	89.03	49.50	0.18
18	381.00	13.50	89.03	48.18	0.17
18	390.00	13.50	89.03	46.59	0.16
18	400.00	13.50	89.03	44.96	0.14
18	410.00	13.50	89.03	43.46	0.13
18	420.00	13.50	89.03	42.09	0.12
18	432.00	13.50	89.03	40.60	0.11
18	446.00	13.50	89.03	39.05	0.10
18	461.00	13.50	89.03	37.58	0.08
18	478.00	13.50	89.03	36.15	0.07
18	498.00	13.50	89.03	34.72	0.06
18	524.00	13.50	89.03	33.20	0.05
18	546.00	13.50	89.03	32.18	0.04
18	577.00	13.50	89.03	31.19	0.02
18	629.00	13.50	89.03	30.21	0.01
18	2928.00	13.50	89.03	29.34	0.00
19	0.00	21.74	65.92	202.00	0.00
19	3.00	21.74	65.92	193.85	2.16
19	6.00	21.74	65.92	186.33	2.23
19	26.00	21.74	65.92	137.15	2.17
19	32.00	21.74	65.92	122.93	2.12
19	38.00	21.74	65.92	109.11	2.06

19	43.00	21.74	65.92	97.92	2.01
19	47.00	21.74	65.92	89.22	1.95
19	49.00	21.74	65.92	85.04	1.89
19	51.00	21.74	65.92	81.02	1.83
19	52.00	21.74	65.92	79.08	1.78
19	53.00	21.74	65.92	77.19	1.74
19	54.00	21.74	65.92	75.35	1.69
19	55.00	21.74	65.92	73.59	1.63
19	56.00	21.74	65.92	71.93	1.55
19	57.00	21.74	65.92	70.35	1.47
19	58.00	21.74	65.92	68.84	1.41
19	59.00	21.74	65.92	67.39	1.35
19	60.00	21.74	65.92	66.00	1.29
19	61.00	21.74	65.92	64.66	1.24
19	63.00	21.74	65.92	62.12	1.15
19	64.00	21.74	65.92	60.91	1.11
19	65.00	21.74	65.92	59.75	1.07
19	67.00	21.74	65.92	57.53	1.00
19	69.00	21.74	65.92	55.47	0.93
19	70.00	21.74	65.92	54.49	0.90
19	74.00	21.74	65.92	50.88	0.79
19	77.00	21.74	65.92	48.45	0.72
19	79.00	21.74	65.92	46.95	0.68
19	83.00	21.74	65.92	44.18	0.60
19	86.00	21.74	65.92	42.30	0.56
19	90.00	21.74	65.92	40.00	0.50
19	95.00	21.74	65.92	37.43	0.44
19	100.00	21.74	65.92	35.14	0.39
19	107.00	21.74	65.92	32.36	0.33
19	115.00	21.74	65.92	29.66	0.28
19	125.00	21.74	65.92	26.89	0.22
19	137.00	21.74	65.92	24.28	0.17
19	153.00	21.74	65.92	21.78	0.11
19	179.00	21.74	65.92	19.37	0.06
19	2928.00	21.74	65.92	16.50	0.00
20	0.00	10.79	78.12	202.00	0.00
20	4.00	10.79	78.12	198.09	0.83
20	8.00	10.79	78.12	194.36	0.84
20	55.00	10.79	78.12	151.22	0.82
20	77.00	10.79	78.12	131.56	0.80
20	89.00	10.79	78.12	121.19	0.78
20	100.00	10.79	78.12	111.95	0.76
20	112.00	10.79	78.12	102.16	0.74
20	123.00	10.79	78.12	93.45	0.72
20	135.00	10.79	78.12	84.24	0.69
20	146.00	10.79	78.12	76.07	0.67
20	151.00	10.79	78.12	72.47	0.65

20	156.00	10.79	78.12	69.00	0.63
20	160.00	10.79	78.12	66.33	0.61
20	164.00	10.79	78.12	63.74	0.59
20	168.00	10.79	78.12	61.26	0.57
20	171.00	10.79	78.12	59.46	0.55
20	175.00	10.79	78.12	57.16	0.52
20	178.00	10.79	78.12	55.51	0.50
20	181.00	10.79	78.12	53.91	0.49
20	184.00	10.79	78.12	52.40	0.46
20	185.00	10.79	78.12	51.92	0.45
20	188.00	10.79	78.12	50.54	0.42
20	190.00	10.79	78.12	49.67	0.40
20	193.00	10.79	78.12	48.43	0.38
20	196.00	10.79	78.12	47.26	0.36
20	199.00	10.79	78.12	46.14	0.34
20	203.00	10.79	78.12	44.75	0.32
20	207.00	10.79	78.12	43.44	0.30
20	212.00	10.79	78.12	41.92	0.27
20	217.00	10.79	78.12	40.52	0.25
20	223.00	10.79	78.12	38.96	0.23
20	229.00	10.79	78.12	37.54	0.21
20	236.00	10.79	78.12	36.03	0.19
20	245.00	10.79	78.12	34.30	0.17
20	254.00	10.79	78.12	32.76	0.15
20	266.00	10.79	78.12	30.98	0.13
20	280.00	10.79	78.12	29.22	0.10
20	296.00	10.79	78.12	27.57	0.08
20	316.00	10.79	78.12	25.96	0.06
20	342.00	10.79	78.12	24.48	0.04
20	386.00	10.79	78.12	23.02	0.02
20	2928.00	10.79	78.12	21.58	0.00
21	0.00	8.88	60.46	202.00	0.00
21	4.00	8.88	60.46	195.65	1.35
21	8.00	8.88	60.46	189.55	1.38
21	45.00	8.88	60.46	133.96	1.34
21	57.00	8.88	60.46	116.57	1.31
21	68.00	8.88	60.46	101.09	1.27
21	78.00	8.88	60.46	87.43	1.24
21	81.00	8.88	60.46	83.46	1.21
21	85.00	8.88	60.46	78.34	1.17
21	87.00	8.88	60.46	75.87	1.14
21	89.00	8.88	60.46	73.47	1.10
21	91.00	8.88	60.46	71.17	1.06
21	92.00	8.88	60.46	70.07	1.02
21	93.00	8.88	60.46	69.02	0.99
21	94.00	8.88	60.46	67.99	0.96
21	95.00	8.88	60.46	67.00	0.93

21	96.00	8.88	60.46	66.04	0.90
21	98.00	8.88	60.46	64.19	0.85
21	99.00	8.88	60.46	63.30	0.83
21	101.00	8.88	60.46	61.58	0.79
21	103.00	8.88	60.46	59.95	0.75
21	105.00	8.88	60.46	58.40	0.71
21	106.00	8.88	60.46	57.65	0.70
21	108.00	8.88	60.46	56.22	0.66
21	110.00	8.88	60.46	54.86	0.63
21	113.00	8.88	60.46	52.94	0.58
21	115.00	8.88	60.46	51.73	0.55
21	118.00	8.88	60.46	50.02	0.52
21	121.00	8.88	60.46	48.42	0.48
21	125.00	8.88	60.46	46.43	0.45
21	129.00	8.88	60.46	44.60	0.41
21	133.00	8.88	60.46	42.90	0.38
21	139.00	8.88	60.46	40.57	0.34
21	145.00	8.88	60.46	38.48	0.31
21	152.00	8.88	60.46	36.28	0.27
21	160.00	8.88	60.46	34.06	0.24
21	170.00	8.88	60.46	31.64	0.21
21	182.00	8.88	60.46	29.16	0.17
21	197.00	8.88	60.46	26.60	0.14
21	218.00	8.88	60.46	23.81	0.10
21	245.00	8.88	60.46	21.24	0.07
21	297.00	8.88	60.46	18.30	0.03
21	2928.00	8.88	60.46	14.23	0.00
22	0.00	12.09	66.77	202.00	0.00
22	3.00	12.09	66.77	197.14	1.32
22	7.00	12.09	66.77	191.02	1.37
22	43.00	12.09	66.77	136.91	1.34
22	53.00	12.09	66.77	122.39	1.31
22	63.00	12.09	66.77	108.28	1.27
22	72.00	12.09	66.77	95.95	1.24
22	81.00	12.09	66.77	84.00	1.20
22	84.00	12.09	66.77	80.17	1.17
22	87.00	12.09	66.77	76.45	1.13
22	89.00	12.09	66.77	74.05	1.10
22	91.00	12.09	66.77	71.72	1.07
22	93.00	12.09	66.77	69.46	1.04
22	95.00	12.09	66.77	67.30	0.99
22	96.00	12.09	66.77	66.28	0.96
22	97.00	12.09	66.77	65.29	0.92
22	98.00	12.09	66.77	64.33	0.89
22	99.00	12.09	66.77	63.40	0.87
22	101.00	12.09	66.77	61.62	0.82
22	102.00	12.09	66.77	60.77	0.79

22	104.00	12.09	66.77	59.13	0.75
22	106.00	12.09	66.77	57.57	0.72
22	108.00	12.09	66.77	56.09	0.68
22	110.00	12.09	66.77	54.67	0.65
22	112.00	12.09	66.77	53.31	0.62
22	115.00	12.09	66.77	51.39	0.58
22	117.00	12.09	66.77	50.18	0.55
22	120.00	12.09	66.77	48.47	0.51
22	123.00	12.09	66.77	46.88	0.48
22	126.00	12.09	66.77	45.38	0.45
22	130.00	12.09	66.77	43.54	0.41
22	134.00	12.09	66.77	41.83	0.38
22	139.00	12.09	66.77	39.88	0.35
22	145.00	12.09	66.77	37.77	0.31
22	151.00	12.09	66.77	35.87	0.28
22	159.00	12.09	66.77	33.63	0.24
22	168.00	12.09	66.77	31.45	0.21
22	179.00	12.09	66.77	29.18	0.17
22	193.00	12.09	66.77	26.80	0.14
22	211.00	12.09	66.77	24.42	0.10
22	234.00	12.09	66.77	22.24	0.07
22	276.00	12.09	66.77	19.89	0.03
22	2928.00	12.09	66.77	16.86	0.00
23	0.00	20.71	52.18	202.00	0.00
23	3.00	20.71	52.18	191.03	2.92
23	7.00	20.71	52.18	177.50	3.02
23	21.00	20.71	52.18	130.98	2.94
23	26.00	20.71	52.18	114.97	2.87
23	31.00	20.71	52.18	99.42	2.79
23	33.00	20.71	52.18	93.48	2.69
23	34.00	20.71	52.18	90.62	2.63
23	35.00	20.71	52.18	87.86	2.55
23	36.00	20.71	52.18	85.28	2.41
23	37.00	20.71	52.18	82.86	2.27
23	38.00	20.71	52.18	80.57	2.14
23	39.00	20.71	52.18	78.40	2.03
23	40.00	20.71	52.18	76.34	1.92
23	41.00	20.71	52.18	74.40	1.82
23	42.00	20.71	52.18	72.55	1.72
23	43.00	20.71	52.18	70.80	1.63
23	44.00	20.71	52.18	69.13	1.55
23	45.00	20.71	52.18	67.54	1.48
23	46.00	20.71	52.18	66.01	1.41
23	47.00	20.71	52.18	64.55	1.35
23	48.00	20.71	52.18	63.15	1.30
23	50.00	20.71	52.18	60.50	1.20
23	51.00	20.71	52.18	59.25	1.15

23	53.00	20.71	52.18	56.89	1.07
23	55.00	20.71	52.18	54.67	1.00
23	58.00	20.71	52.18	51.62	0.90
23	61.00	20.71	52.18	48.83	0.82
23	64.00	20.71	52.18	46.29	0.75
23	68.00	20.71	52.18	43.20	0.67
23	72.00	20.71	52.18	40.43	0.60
23	77.00	20.71	52.18	37.33	0.53
23	83.00	20.71	52.18	34.08	0.46
23	91.00	20.71	52.18	30.37	0.38
23	101.00	20.71	52.18	26.56	0.30
23	114.00	20.71	52.18	22.68	0.23
23	131.00	20.71	52.18	19.05	0.15
23	160.00	20.71	52.18	15.40	0.08
23	2928.00	20.71	52.18	11.92	0.00
24	0.00	18.29	54.33	202.00	0.00
24	3.00	18.29	54.33	192.70	2.49
24	7.00	18.29	54.33	181.16	2.58
24	24.00	18.29	54.33	132.90	2.52
24	31.00	18.29	54.33	113.78	2.45
24	36.00	18.29	54.33	100.52	2.39
24	39.00	18.29	54.33	92.81	2.32
24	40.00	18.29	54.33	90.32	2.28
24	41.00	18.29	54.33	87.89	2.23
24	42.00	18.29	54.33	85.53	2.18
24	43.00	18.29	54.33	83.26	2.10
24	44.00	18.29	54.33	81.13	1.99
24	45.00	18.29	54.33	79.12	1.89
24	46.00	18.29	54.33	77.20	1.79
24	47.00	18.29	54.33	75.37	1.71
24	48.00	18.29	54.33	73.62	1.63
24	49.00	18.29	54.33	71.95	1.56
24	50.00	18.29	54.33	70.35	1.49
24	51.00	18.29	54.33	68.83	1.42
24	52.00	18.29	54.33	67.38	1.35
24	53.00	18.29	54.33	65.98	1.30
24	54.00	18.29	54.33	64.64	1.24
24	56.00	18.29	54.33	62.12	1.15
24	57.00	18.29	54.33	60.93	1.10
24	59.00	18.29	54.33	58.66	1.03
24	61.00	18.29	54.33	56.55	0.96
24	63.00	18.29	54.33	54.57	0.90
24	65.00	18.29	54.33	52.71	0.84
24	68.00	18.29	54.33	50.11	0.77
24	71.00	18.29	54.33	47.72	0.71
24	74.00	18.29	54.33	45.52	0.65
24	78.00	18.29	54.33	42.84	0.59

24	83.00	18.29	54.33	39.84	0.52
24	89.00	18.29	54.33	36.66	0.45
24	96.00	18.29	54.33	33.45	0.39
24	104.00	18.29	54.33	30.30	0.33
24	115.00	18.29	54.33	26.73	0.26
24	129.00	18.29	54.33	23.16	0.19
24	148.00	18.29	54.33	19.68	0.13
24	181.00	18.29	54.33	16.14	0.06
24	2928.00	18.29	54.33	12.51	0.00
25	0.00	23.18	84.90	202.00	0.00
25	3.00	23.18	84.90	198.18	1.00
25	6.00	23.18	84.90	194.69	1.03
25	31.00	23.18	84.90	166.16	1.01
25	56.00	23.18	84.90	138.47	0.98
25	63.00	23.18	84.90	130.96	0.95
25	69.00	23.18	84.90	124.70	0.93
25	76.00	23.18	84.90	117.60	0.90
25	83.00	23.18	84.90	110.71	0.88
25	90.00	23.18	84.90	104.02	0.85
25	97.00	23.18	84.90	97.54	0.83
25	104.00	23.18	84.90	91.27	0.80
25	112.00	23.18	84.90	84.34	0.77
25	119.00	23.18	84.90	78.50	0.75
25	126.00	23.18	84.90	72.84	0.72
25	130.00	23.18	84.90	69.72	0.70
25	133.00	23.18	84.90	67.48	0.67
25	137.00	23.18	84.90	64.62	0.64
25	140.00	23.18	84.90	62.56	0.62
25	143.00	23.18	84.90	60.58	0.60
25	147.00	23.18	84.90	58.05	0.57
25	150.00	23.18	84.90	56.25	0.54
25	153.00	23.18	84.90	54.53	0.52
25	156.00	23.18	84.90	52.89	0.49
25	160.00	23.18	84.90	50.83	0.46
25	163.00	23.18	84.90	49.37	0.44
25	167.00	23.18	84.90	47.52	0.41
25	171.00	23.18	84.90	45.79	0.39
25	175.00	23.18	84.90	44.18	0.36
25	177.00	23.18	84.90	43.43	0.34
25	180.00	23.18	84.90	42.39	0.31
25	184.00	23.18	84.90	41.10	0.28
25	188.00	23.18	84.90	39.92	0.26
25	193.00	23.18	84.90	38.58	0.23
25	199.00	23.18	84.90	37.15	0.21
25	206.00	23.18	84.90	35.68	0.18
25	214.00	23.18	84.90	34.22	0.15
25	223.00	23.18	84.90	32.83	0.13

25	235.00	23.18	84.90	31.31	0.10
25	249.00	23.18	84.90	29.92	0.08
25	269.00	23.18	84.90	28.50	0.05
25	298.00	23.18	84.90	27.30	0.03
25	2928.00	23.18	84.90	26.15	0.00
26	0.00	18.53	77.95	202.00	0.00
26	3.00	18.53	77.95	197.49	1.20
26	7.00	18.53	77.95	191.93	1.24
26	38.00	18.53	77.95	149.63	1.21
26	51.00	18.53	77.95	132.35	1.18
26	59.00	18.53	77.95	122.07	1.15
26	67.00	18.53	77.95	112.09	1.12
26	75.00	18.53	77.95	102.41	1.09
26	82.00	18.53	77.95	94.19	1.06
26	89.00	18.53	77.95	86.20	1.03
26	96.00	18.53	77.95	78.46	1.00
26	99.00	18.53	77.95	75.25	0.97
26	102.00	18.53	77.95	72.16	0.93
26	105.00	18.53	77.95	69.18	0.90
26	108.00	18.53	77.95	66.31	0.87
26	110.00	18.53	77.95	64.47	0.84
26	112.00	18.53	77.95	62.69	0.81
26	115.00	18.53	77.95	60.13	0.77
26	117.00	18.53	77.95	58.50	0.74
26	119.00	18.53	77.95	56.93	0.72
26	121.00	18.53	77.95	55.45	0.67
26	122.00	18.53	77.95	54.75	0.65
26	124.00	18.53	77.95	53.40	0.61
26	125.00	18.53	77.95	52.76	0.60
26	127.00	18.53	77.95	51.52	0.57
26	130.00	18.53	77.95	49.77	0.52
26	132.00	18.53	77.95	48.68	0.50
26	135.00	18.53	77.95	47.12	0.47
26	138.00	18.53	77.95	45.67	0.44
26	142.00	18.53	77.95	43.87	0.40
26	145.00	18.53	77.95	42.62	0.38
26	150.00	18.53	77.95	40.69	0.34
26	154.00	18.53	77.95	39.28	0.31
26	160.00	18.53	77.95	37.35	0.28
26	166.00	18.53	77.95	35.63	0.25
26	174.00	18.53	77.95	33.60	0.22
26	182.00	18.53	77.95	31.84	0.19
26	193.00	18.53	77.95	29.78	0.15
26	205.00	18.53	77.95	27.94	0.12
26	220.00	18.53	77.95	26.15	0.09
26	239.00	18.53	77.95	24.55	0.06
26	270.00	18.53	77.95	23.01	0.03

26	2928.00	18.53	77.95	21.51	0.00
27	0.00	12.46	67.72	202.00	0.00
27	3.00	12.46	67.72	197.18	1.30
27	7.00	12.46	67.72	191.12	1.36
27	43.00	12.46	67.72	137.54	1.33
27	53.00	12.46	67.72	123.16	1.29
27	63.00	12.46	67.72	109.19	1.26
27	72.00	12.46	67.72	96.98	1.23
27	81.00	12.46	67.72	85.14	1.19
27	85.00	12.46	67.72	80.06	1.15
27	87.00	12.46	67.72	77.60	1.13
27	90.00	12.46	67.72	74.02	1.09
27	92.00	12.46	67.72	71.71	1.06
27	94.00	12.46	67.72	69.47	1.03
27	96.00	12.46	67.72	67.32	0.99
27	97.00	12.46	67.72	66.29	0.96
27	98.00	12.46	67.72	65.29	0.93
27	99.00	12.46	67.72	64.33	0.90
27	101.00	12.46	67.72	62.50	0.84
27	102.00	12.46	67.72	61.63	0.82
27	104.00	12.46	67.72	59.94	0.77
27	105.00	12.46	67.72	59.14	0.75
27	107.00	12.46	67.72	57.58	0.71
27	109.00	12.46	67.72	56.10	0.68
27	111.00	12.46	67.72	54.68	0.65
27	113.00	12.46	67.72	53.33	0.62
27	116.00	12.46	67.72	51.41	0.58
27	119.00	12.46	67.72	49.62	0.54
27	122.00	12.46	67.72	47.94	0.50
27	125.00	12.46	67.72	46.38	0.47
27	128.00	12.46	67.72	44.91	0.44
27	132.00	12.46	67.72	43.10	0.41
27	136.00	12.46	67.72	41.43	0.37
27	141.00	12.46	67.72	39.51	0.34
27	146.00	12.46	67.72	37.77	0.31
27	153.00	12.46	67.72	35.58	0.27
27	160.00	12.46	67.72	33.64	0.24
27	169.00	12.46	67.72	31.47	0.21
27	180.00	12.46	67.72	29.21	0.17
27	194.00	12.46	67.72	26.85	0.14
27	211.00	12.46	67.72	24.61	0.10
27	235.00	12.46	67.72	22.36	0.07
27	275.00	12.46	67.72	20.14	0.03
27	2928.00	12.46	67.72	17.25	0.00
28	0.00	7.51	69.53	202.00	0.00
28	4.00	7.51	69.53	197.50	0.96
28	8.00	7.51	69.53	193.16	0.98

28	60.00	7.51	69.53	137.72	0.96
28	74.00	7.51	69.53	123.30	0.93
28	87.00	7.51	69.53	110.28	0.91
28	100.00	7.51	69.53	97.64	0.88
28	112.00	7.51	69.53	86.31	0.86
28	121.00	7.51	69.53	78.06	0.83
28	125.00	7.51	69.53	74.54	0.81
28	129.00	7.51	69.53	71.12	0.78
28	132.00	7.51	69.53	68.64	0.76
28	135.00	7.51	69.53	66.23	0.74
28	138.00	7.51	69.53	63.91	0.71
28	140.00	7.51	69.53	62.41	0.69
28	142.00	7.51	69.53	60.98	0.66
28	143.00	7.51	69.53	60.30	0.64
28	145.00	7.51	69.53	58.98	0.61
28	147.00	7.51	69.53	57.72	0.58
28	148.00	7.51	69.53	57.11	0.57
28	150.00	7.51	69.53	55.93	0.54
28	153.00	7.51	69.53	54.25	0.51
28	155.00	7.51	69.53	53.18	0.49
28	158.00	7.51	69.53	51.65	0.47
28	161.00	7.51	69.53	50.20	0.44
28	164.00	7.51	69.53	48.82	0.42
28	168.00	7.51	69.53	47.09	0.39
28	172.00	7.51	69.53	45.46	0.37
28	176.00	7.51	69.53	43.94	0.34
28	180.00	7.51	69.53	42.53	0.32
28	185.00	7.51	69.53	40.89	0.29
28	190.00	7.51	69.53	39.38	0.27
28	196.00	7.51	69.53	37.72	0.25
28	203.00	7.51	69.53	35.97	0.22
28	211.00	7.51	69.53	34.18	0.20
28	220.00	7.51	69.53	32.39	0.17
28	231.00	7.51	69.53	30.50	0.15
28	244.00	7.51	69.53	28.59	0.12
28	261.00	7.51	69.53	26.54	0.10
28	282.00	7.51	69.53	24.58	0.07
28	310.00	7.51	69.53	22.70	0.05
28	361.00	7.51	69.53	20.68	0.02
28	2928.00	7.51	69.53	18.00	0.00
29	0.00	24.32	57.63	202.00	0.00
29	3.00	24.32	57.63	190.56	3.02
29	6.00	24.32	57.63	180.08	3.10
29	19.00	24.32	57.63	135.43	3.03
29	24.00	24.32	57.63	118.88	2.95
29	29.00	24.32	57.63	102.84	2.87
29	31.00	24.32	57.63	96.60	2.81

29	33.00	24.32	57.63	90.63	2.70
29	34.00	24.32	57.63	87.77	2.62
29	35.00	24.32	57.63	85.02	2.54
29	36.00	24.32	57.63	82.46	2.39
29	37.00	24.32	57.63	80.06	2.25
29	38.00	24.32	57.63	77.79	2.12
29	39.00	24.32	57.63	75.65	2.00
29	40.00	24.32	57.63	73.60	1.90
29	41.00	24.32	57.63	71.66	1.80
29	42.00	24.32	57.63	69.82	1.71
29	43.00	24.32	57.63	68.07	1.62
29	44.00	24.32	57.63	66.41	1.54
29	45.00	24.32	57.63	64.82	1.47
29	46.00	24.32	57.63	63.30	1.40
29	47.00	24.32	57.63	61.84	1.34
29	49.00	24.32	57.63	59.11	1.23
29	50.00	24.32	57.63	57.82	1.18
29	52.00	24.32	57.63	55.39	1.09
29	54.00	24.32	57.63	53.12	1.02
29	56.00	24.32	57.63	51.01	0.95
29	59.00	24.32	57.63	48.09	0.86
29	62.00	24.32	57.63	45.44	0.78
29	66.00	24.32	57.63	42.25	0.69
29	70.00	24.32	57.63	39.40	0.61
29	74.00	24.32	57.63	36.85	0.55
29	80.00	24.32	57.63	33.48	0.47
29	87.00	24.32	57.63	30.13	0.39
29	96.00	24.32	57.63	26.58	0.31
29	108.00	24.32	57.63	22.90	0.23
29	122.00	24.32	57.63	19.82	0.16
29	147.00	24.32	57.63	16.60	0.08
29	2928.00	24.32	57.63	13.40	0.00
30	0.00	19.60	59.25	202.00	0.00
30	3.00	19.60	59.25	193.16	2.35
30	7.00	19.60	59.25	182.25	2.44
30	25.00	19.60	59.25	133.95	2.37
30	31.00	19.60	59.25	118.44	2.32
30	37.00	19.60	59.25	103.36	2.25
30	41.00	19.60	59.25	93.59	2.20
30	43.00	19.60	59.25	88.89	2.14
30	45.00	19.60	59.25	84.37	2.05
30	46.00	19.60	59.25	82.20	2.00
30	47.00	19.60	59.25	80.10	1.94
30	48.00	19.60	59.25	78.13	1.84
30	49.00	19.60	59.25	76.26	1.75
30	50.00	19.60	59.25	74.48	1.66
30	51.00	19.60	59.25	72.78	1.59

30	52.00	19.60	59.25	71.15	1.52
30	53.00	19.60	59.25	69.58	1.45
30	54.00	19.60	59.25	68.08	1.40
30	55.00	19.60	59.25	66.64	1.34
30	56.00	19.60	59.25	65.26	1.28
30	57.00	19.60	59.25	63.93	1.23
30	58.00	19.60	59.25	62.66	1.18
30	60.00	19.60	59.25	60.26	1.09
30	61.00	19.60	59.25	59.12	1.05
30	63.00	19.60	59.25	56.97	0.98
30	65.00	19.60	59.25	54.96	0.91
30	67.00	19.60	59.25	53.07	0.85
30	69.00	19.60	59.25	51.29	0.80
30	72.00	19.60	59.25	48.82	0.73
30	75.00	19.60	59.25	46.55	0.67
30	79.00	19.60	59.25	43.79	0.60
30	83.00	19.60	59.25	41.31	0.54
30	87.00	19.60	59.25	39.05	0.49
30	93.00	19.60	59.25	36.04	0.43
30	100.00	19.60	59.25	33.00	0.36
30	108.00	19.60	59.25	30.03	0.31
30	119.00	19.60	59.25	26.68	0.24
30	132.00	19.60	59.25	23.58	0.18
30	150.00	19.60	59.25	20.49	0.12
30	181.00	19.60	59.25	17.39	0.06
30	2928.00	19.60	59.25	13.84	0.00

APPENDIX 9

In [1]:

```python
import pandas as pd
import matplotlib.pyplot as plt
import ipywidgets as widgets
from IPython.display import display

# Carregar o dataset
file_path = "Dataset.time.xlsx"  # Atualize o caminho do arquivo conforme necessário
df = pd.read_excel(file_path, sheet_name="Planilha1")

# Obter valores únicos de Tar e Hrar
tar_values = sorted(df["Tar"].unique())
hrar_values = sorted(df["Hrar"].unique())

# Criar widgets interativos
tar_dropdown = widgets.Dropdown(options=tar_values, description="Tar (°C):")
hrar_dropdown = widgets.Dropdown(options=hrar_values, description="Hrar (%):")

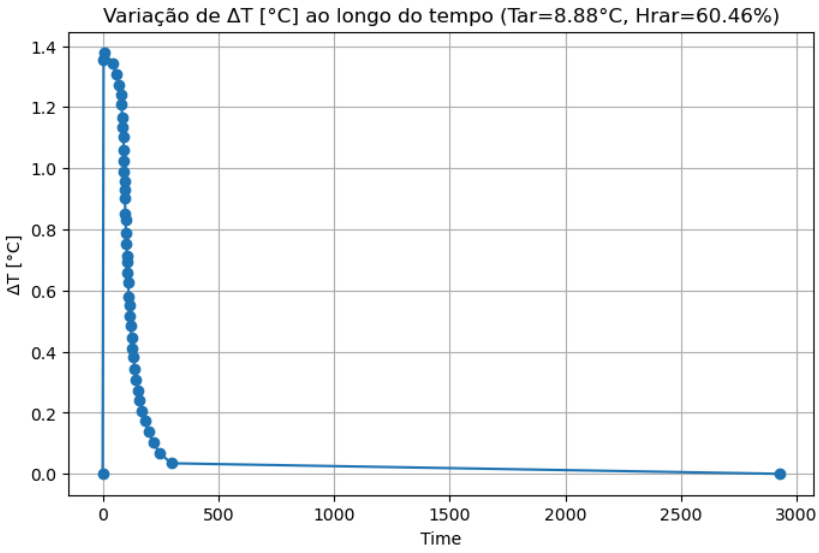
def update_plot(tar, hrar):
    df_filtered = df[(df["Tar"] == tar) & (df["Hrar"] == hrar)]

    plt.figure(figsize=(8, 5))
    plt.plot(df_filtered["Time"], df_filtered["ΔT [°C]"], marker='o', linestyle='-')
    plt.xlabel("Time")
    plt.ylabel("ΔT [°C]")
    plt.title(f"Variação de ΔT [°C] ao longo do tempo (Tar={tar}°C, Hrar={hrar}%)")
    plt.grid(True)
    plt.show()

# Criar interatividade
display(widgets.interactive(update_plot, tar=tar_dropdown, hrar=hrar_dropdown))
```

Tar (°C): 8.88

Hrar (%): 60.46



In [ ]:

```python
```